THE MINIATURE TWO PHASE INDUCTION MOTOR AS AN ELEMENT OF AN

ALTERNATING CURRENT SERVOSYSTEM.

Presented by John Ward for the degree of Doctor of Philosophy,

University of Aston in Birmingham,

February, 1974.

SUMMARY.

After an introduction in which the suitability of this particular machine for servosystem application is explained and its specification of performance outlined, reasons are put forward for the use of its resistance and metric tensors as a mathematical representation of the machine in system simulation. A complete analysis is then formulated for the machine covering true dynamic and steady state operation and extended to include the effects of space harmonics in the machine's magnetomotive force waveform.

From this analysis the mathematical model, in the form of the metric and resistance tensors, is derived. New methods of calculating the elements of these tensors are proposed and also a practical method, employing a new locus diagram for the induction motor, for measuring these elements. For the determination of this locus diagram and for eventually corroborating the predicted performance of the machine with its measured performance, a special dynamometer is designed and made and suitable measuring techniques evolved.

As a result of the interpretation of the new locus diagram for a test motor, an improved representation of the rotor of the miniature induction motor is discovered and a new method of determining the effective airgap, which differs from the mechanical dimension due to the effects of machining stresses in the core material, is found. A mathematical model incorporating these improvements and derived from the locus diagram is presented. This model is compared with that obtained from the design data and is then used to predict the full range of performance, both steady state and dynamic, of the test motor.

By comparing the measured performance with the predicted performance the efficacy of the model obtained from the locus diagram is established and, thereby, that of the model determined by calculation in the design stages. This comparison serves also to ratify the method of analysis used.

The study ends with a brief catalogue of future work consequent upon that of this investigation.

DEDICATION

To the lasting memories of my father,

JOHN W. WARD.

and of my original supervisor,

JAMES R. HENDERSON.

Acknowledgements.

The author wishes to acknowledge the helpful criticisms given during the course of this work by Dr. B.L.Adkins and the encouragement given in the final stages of its presentation by Professor J.E.Flood.

He also expresses gratitude to his colleagues in Industry and in the University for their willingess to chat and to his wife,family and friends for their forbearance and inspiration.

To Dr.W.J.Gibbs he records posthumous thanks for invaluable guidance in the methods of engineering research.

CONTENTS

THE MINIATURE TWO PHASE INDUCTION MOTOR AS AN ELEMENT OF AN ALTERNATING CURRENT SERVOSYSTEM.

Introduction.

Over the past twenty years there has been widescale application of automatic closed loop control systems in both heavy and instrument engineering.

These control systems can be considered as consisting basically of an input station, error detector, amplifier, motor and controlled load as indicated in fig. (1.1). In this system the error detector compares the output conditions of either load position or load velocity with the input conditions; then feeds - via the amplifier - a signal, related to the error between the output and the input, into the motor coupled to load thereby causing it to drive until the error is reduced to a minimum, ideally zero.

In all cases the features of the system which are of paramount importance are (a) sensitivity, (b) stability, (c) response, (d) reliability, and it is essential that these factors should be correctly estimated in the system design stage. It is emphasized that the system of fig. (1.1) is a basic one. In practice, however, phase advance networks and integral and derivative feed backs are added to enhance the system response and stability. But the elementary concept is sufficient for it to be realized that the assessment of the performance of any control system, in respect of the features just listed, necessitates a knowledge of the behaviour of each of the system elements, not in isolation but in relationship to the system as a whole and, furthermore, covering true dynamic conditions of operation.

It is apparent then that "performance curves" of the elements taken under conditions not identical to those obtaining in the actual system, will be of limited use. The use of an analogue, in which each element is represented by an equivalent electrical network, is one possible way of obtaining information concerning the response and stability of the proposed system. But this presupposes that the various elements are all representable in this way under all conditions of operation and this may or may not be the case.

An alternative approach is to represent the system mathematically. This requires that each element be described by a mathematical model accurate for all conditions of operation. One way in which this approach has been used is that of determining individual transfer functions, relating the input to the output of each of the elements,and using these to obtain the overall transfer function.

This use of transfer function analysis assumes that the individual transfer functions can be dependably obtained in the design stages and that they are independent of the system,both of which assumptions are violated in certain cases. It is concluded,therefore,that some other form of mathematical model is required which does not depend upon violable assumptions. It is thought that the impedance tensor might fulfil these requirements,at the same time enabling use to be made of the methods of tensor analysis in the study of the system. It should be noted that the term "impedance tensor" is here used as a collective term signifying the resistance and the metric tensor.

For this approach to be possible,it is obviously necessary to be able to construct the impedance tensor from design details. Since the components of this tensor consist of the element's inductances,resistances, friction coefficient and moment of inertia,the efficacy of the tensor depends entirely upon the methods of calculation employed in estimating the element parameters.

So far as machine elements are concerned,their calculation outside servosystem application is a science which has been established for many years. The techniques involved are the results of successive comparisons of test results on actual machines with those predicted in the design stages using estimated parameters,the methods of calculation then being adjusted, often empirically, to achieve better compatibility. The tests used for these comparisons were usually only steady state performance and the range of machine covered by this design development process did not include miniature machines. Consequently, the methods of calculation currently used for parameter estimation cannot be directly applied to the miniature machine in the context of control systems for both of the above reasons. It is, therefore, necessary, for servosystem application, to formulate a design process for miniature machines efficacious for both steady state and dynamic performance, but it is not feasible to have to wait until a prolonged exercise of modification has been completed before a successful process is obtained.

Restricting our attention to the particular machine with which this thesis is primarily concerned, namely the squirrel cage induction motor, present design methods have as their basis the per phase equivalent circuit of the machine. It is clearly shown by W.J.Gibbs [20] that this equivalent circuit is really a representation of the more fundamental impedance tensor limited to the condition of constant operating speed, for with this limitation the impedance tensor can be made into a single array symmetrical about its main diagonal. Under dynamic conditions of operation, i.e. variable speed, the impedance tensor cannot be made into a single array and consequently, under these conditions, the equivalent circuit has no existence; it is for this reason that no attempt should ever be made to calculate the dynamic performance of an induction motor using the equivalent circuit directly. However, if the parameters of the equivalent circuit are accurately known, then as shown in the thesis, the components of the impedance tensor can, with the exception of the friction coefficient and the rotor moment of inertia, be determined from them in terms of the transformation ratio between the stator and the rotor.

The concept of a transformation ratio is, in the case of a squirrel cage motor, a difficult one and providing only the external, as opposed to the internal, characteristics of the machine are required, the components of the impedance tensor can be expressed in terms of the circuit parameters alone, without invalidating any subsequent determination of the machine's dynamic performance. A great deal of work has already been done, principally by Kron,(21) on the analysis of electrical machine performance in terms of the impedance tensor. The work is, however, somewhat difficult to follow, is not practically proven and does not include the effect of space harmonics in the magnetmotive force waveform, although Kron does mention the possibility of so doing. A comprehensive performance analysis is included in this thesis which extends Kron's work to embrace space harmonics, establishes the truth of the statement made above concerning the equivalent circuit parameters and also the relationship between these and the components of the impedance tensor. Hence, the design for dynamic performance can still be based on the per phase equivalent circuit if used correctly.

A simple corroboration of a measured steady state speed/torque curve with one obtained using design estimated equivalent circuit parameters is, however, not sufficient to establish the correctness of the estimated parameters for use in constructing the impedance tensor. It is demonstrated in the analysis of performance given herein, that although, as already stated, the calculated dynamic performance is not influenced by using referred values of parameters, it is greatly influenced by the values of the parameters in relationship to each other. Having established this, the problem remaining is that of obtaining sufficiently accurate values for the circuit paramaters.

To this end, in this thesis a new locus diagram is introduced for the induction motor. This is the input impedance per unit frequency locus. From the theoretical analysis of this locus diagram, it is clear that it is not possible, using steady state characteristics alone, to determine absolute values for the parameters. In order to be able to assign definite values of resistance and inductance it is necessary to calculate one of the parameters, other than the stator winding resistance, from the design details.

The cores of these miniature machines are usually of nickel-iron alloy in the annealed state. The permeability of these alloys is dependent upon the state of anneal, and any mechanical strain to which the material may be subjected subsequent to the annealing process, results in a drastic reduction in local permeability. Since the bore surfaces of these machines are ground and lapped/honed to finish size, the effective magnetic airgap is likely to be much greater than the mechanical gap would indicate; this likelihood has never been taken account of in the design process but is both confirmed and accounted for in this investigation. Consequently, if a parameter is to be estimated for the purpose of measuring the other parameters, as suggested above, it must be one of the most dependable and one of the least affected by the dimension of the magnetic airgap.

Using the per unit frequency impedance locus, a new semi-empirical method of determining the stator leakage inductance is presented. In this method the actual value of the magnetic airgap is obtained from the locus diagram using the expression for the stator total self inductance as a function of the gap dimension. In this way a more accurate set of equivalent circuit parameters is obtained than has hitherto been possible.

Alongside this a set of methods, some of them original, is put forward for the calculation of these parameters from the details of the machine. This set of methods constitutes the design process which will yield the accurate mathematical model of the miniature induction motor required for servosystem application. The methods used are of a fundamental nature and make minimum use of empirical factors. They are fully given in the thesis so that the influences of the various quantities in the miniature machine can be appreciated since some of these influences are quite different from those in larger machines. This process is presented as an entity. Where it differs from the more usual process and the contribution made to the science, thereby, is pointed out in the particular chapter of the thesis dealing with it.

With these methods the parameters, and therefrom the impedance tensor, of a test machine are calculated from its details. The same machine is then subjected to a constant current,variable frequency test to obtain its per unit frequency impedance locus.It is at this stage that the investigation indicates that the usually accepted form of the equivalent circuit of the induction motor does not hold for the miniature machine.

A new circuit configuration is put forward for this machine and the interpretation and analysis of the impedance per unit frequency locus are revised accordingly. The parameters of this circuit and the corresponding impedance tensor for the machine are again determined and a comparison made between these and those obtained by calculation from the design details to establish the degree of compatibility between the two tensors and between the corresponding parameters. A method of obtaining the parameters of the new form of equivalent circuit ,and consequently the impedance tensor of the machine,from design details is then proposed.

Following this the steady state performance and the dynamic performance of the machine are measured experimentally and also calculated using the performance analysis given and the impedance tensor constructed from the measured parameters;the two sets of characteristics are then compared.

In order to be able clearly to prove the bases of the methods of analysis,measurement and design and to avoid confusion of influences, the machine chosen as test machine has a two pole stator winding for which the harmonic content of the magnetomotive force wave is negligible. Nevertheless,the modifications to the design calculations and to the interpretation of the impedance locus to allow for space harmonics are presented.

It is submitted that if the calculated components of the impedance tensor of the machine without space harmonics have a good degree of compatibility with its measured components,and if the measured characteristics compare favourably with the calculated characteristics,then it is reasonable to take the method of machine analysis,the methods of estimation and of measurement of the machine parameters and the new form of the equivalent circuit as ratified. In addition, use of the design calculations, as indicated, to obtain the tensor components for the space harmonics would be justified and extended application to other machines of the methods of measurement and calculation would be warranted.

This may seem to be somewhat overambitious. Indeed the scope of the investigation was overwhelming in prospect and a great deal of thought was given to determine whether or not any part could be left out as being already proven or unnecessary. The lack of verified information in the methods of measurement, design, analysis and prediction of overall performance made it quite obvious that omission of any part of the work would invalidate the remainder, the remarks being restricted of course to the realm of the miniature machine.

As a result, whilst the thesis is primarily concerned with a particular machine, it is envisaged that the investigation will provide a general basis for the design, analysis and testing of miniature machines for dynamic operation in instrument servosystems. The dimensions of this type of machine are within the range 0.5" to 2.5" outside diameter with a corresponding axial length of approximately 0.75" to 3.0". Their sizes are usually quoted in terms of their outside diameter to the nearest 0.1", taking this as the unit; thus a 1.5" outside diameter machine would be designated size 15. The use of these machines is now so widespread that this method of specification which originated in America is internationally accepted. This serves to indicate the timeliness and importance of the investigation which whilst being of an academic nature is not intended entirely as such. It was realized at the onset, as a result of personal experiences by the author in this field, that an engineering contribution to the industry was called for; it is intended that this thesis should make such a contribution in addition to its academic content.

It need hardly be stressed that the efficacy of this contribution, both engineering and academic, hinges on the dependability of the measurements made during the investigation. For this reason this aspect is given particular attention. Whilst the testing of large, medium and small machines has been carried out for many years and suitable measuring equipment has been devized for steady state work, the same cannot be said for dynamic work in this range and cannot be said for either steady state or dynamic work in the miniature range. Consequently, any study of miniature machines must be preceded by the design, manufacture and proving of a dynamometer capable of measuring steady and dynamic torques of a comparatively low order, speeds, currents and voltages. Such a development and proving of measuring equipment and techniques is also a part of this project. It is further submitted that the techniques evolved and the equipment designed and used are essential for the measurement of the performance of miniature machines.

To summarize, the objects of this investigation into the miniature squirrel cage induction motor are, for the machine with balanced stator windings:

1) To formulate a complete analysis for the machine covering true dynamic and steady state performance.
2) To formulate fundamental design calculations and apply them to a test machine.
3) To design and construct a precision dynamometer capable of measuring the true performance of the machine, overall, and to establish the techniques of measurement.
4) To measure the performance of a test machine, overall.
5) To devize a way of measuring and to obtain by direct measurement the impedance tensor of the machine under test.
6) To construct the impedance tensor of the test machine from the design calculations and compare this with the measured impedance tensor.
7) To calculate the performance of the test machine using the measured impedance tensor.
8) To compare the measured and calculated performances.

Thereby,

practically to confirm the method of analysis and the methods of calculation and measurement, used herein, for the parameters of the machine and its performance.

As a contribution to the knowledge of electrical machines the thesis presents:

1) An extension of the general mathematical analysis to include the effect of space harmonics in the magnetomotive force waveform.
2) An improved process of design for the miniature squirrel cage induction motor, capable of yielding a mathematical model accurate under all conditions of operation.
3) A method of obtaining the mathematical model from the design details of the machine.
4) A valid method of obtaining the same mathematical model by direct measurement on the machine itself.
5) A ratified method of using this model.
6) Accurate methods and equipment for measuring the overall performance of miniature machines.
7) A new mathematical model for the miniature induction motor.

The current programme of future work provides similar investigations for the other miniature electrical machines used in instrument servosystems.

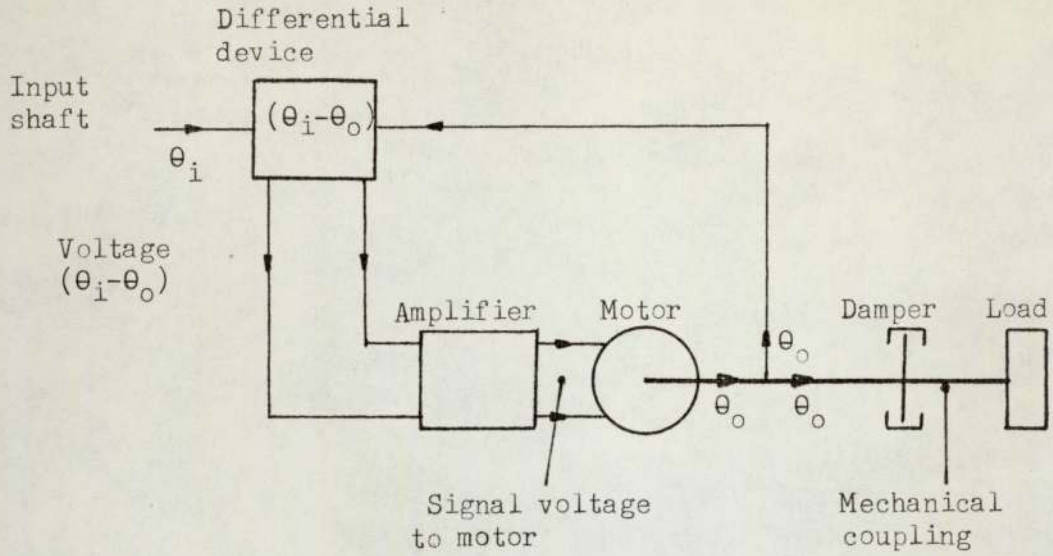

FIG.(1.1). BLOCK DIAGRAM OF ELEMENTARY POSITION CONTROL SYSTEM.

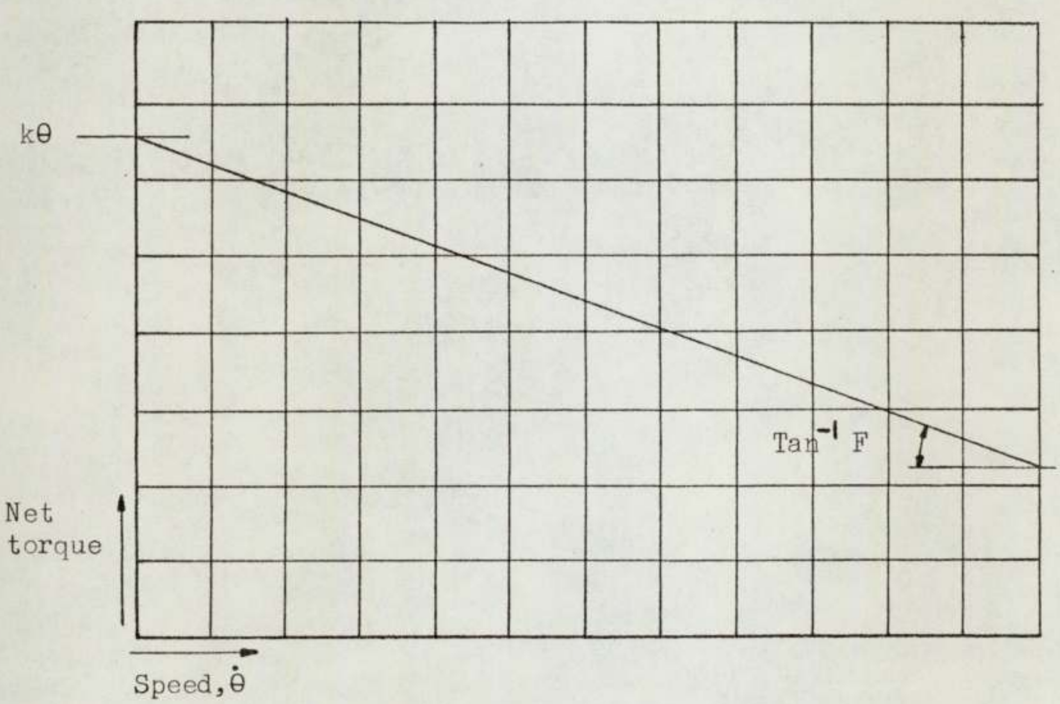

FIG.(1.2). TORQUE versus SPEED CHARACTERISTIC FOR IDEAL MOTOR/DAMPER COMBINATION.

CHAPTER I.

Prelude.

1) Review.

Before proceeding with a detailed investigation into the use of a machine for a particular purpose it is essential to have a clear concept of why this machine was chosen to fulfil this role in the first place. To this end refer to fig. (1.1) and let the following relationships be assumed for the various components with the system operating as a position control:[1]

Differential, output proportional to $(\theta_i - \theta_o)$

Amplifier, output proportional to input, fixed gain.

Motor, output torque proportional to signal voltage and independent of speed,

i.e. torque $= k\theta$

where $\theta = (\theta_i - \theta_o)$ and k is a constant.

Damper, damping torque proportional to load velocity,

i.e. torque $= F\dot{\theta}_o$

where F is a constant.

With these simplifying assumptions the equation of motion of the system will be $k\theta = J\ddot{\theta}_o + F\dot{\theta}_o$

where J is the moment of inertia of the load and drive.

Hence, $k\theta = J(\ddot{\theta}_i - \ddot{\theta}) + F(\dot{\theta}_i - \dot{\theta})$

giving $J\ddot{\theta} + F\dot{\theta} + k\theta = J\ddot{\theta}_i + F\dot{\theta}_i$

The solution to this equation for a step change ω_i in θ_i is given by

$$\theta = \frac{F}{k}\omega_i + A_1\varepsilon^{p_1 t} + A_2\varepsilon^{p_2 t}$$

where A_1 and A_2 are constants and

$$p_1 = -\frac{F}{2J} + \frac{F - 4Jk}{2J}$$

$$p_2 = -\frac{F}{2J} - \frac{F - 4Jk}{2J}$$

This means that for the best compromise between rate of response and stability, the condition $0 \ll F^2 < 4Jk$ should obtain.

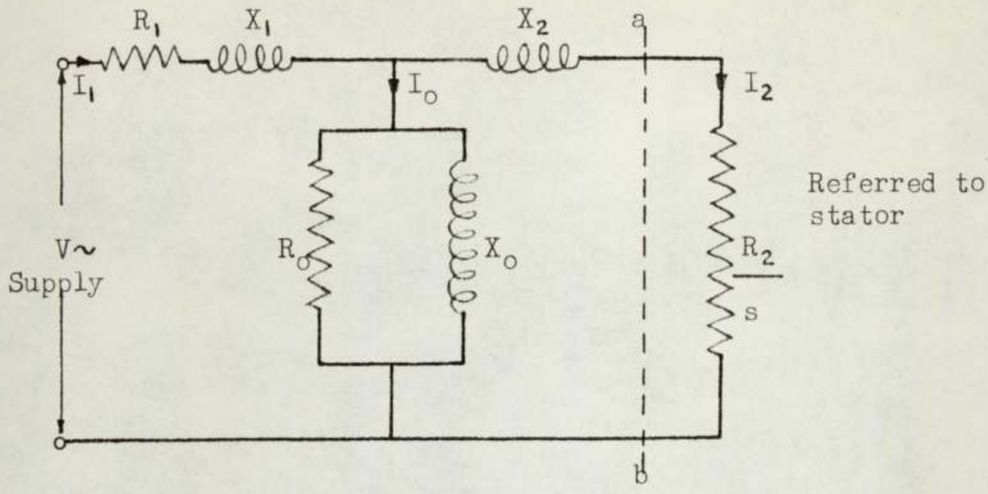

R_1 stator resistance. X_1 stator leakage reactance.
R_2 rotor resistance. X_2 rotor leakage reactance.
R_0 magnetising resistance. X_0 magnetising reactance.
s rotor slip.

FIG.(1.3).CONVENTIONAL EQUIVALENT CIRCUIT per PHASE OF BALANCED POLYPHASE INDUCTION MOTOR.

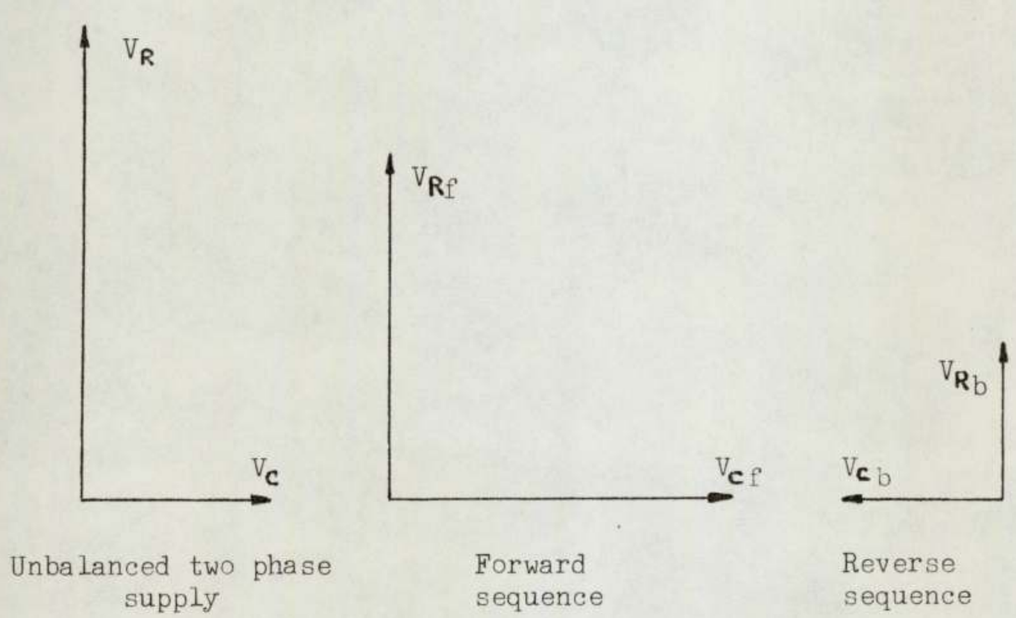

FIG.(1.4). RESOLUTION OF UNBALANCED VOLTAGE SUPPLY.

Grouping the motor torque and damping torque together, the net output torque is given by ($k\theta - F\dot{\theta}_0$) which, if the motor torque is independent of speed as stated, will give output torque as a function of speed as shown in fig. (1.2).

Hence, if a motor exhibited such a torque/speed characteristic without being coupled to a damper and had a linear torque/voltage characteristic it could be used in a control system without a damper and would render the system stable with good response providing that the statement $0 \ll F^2 < 4Jk$ was satisfied.

In fig. (1.3) is given the equivalent circuit per phase of a polyphase induction motor where it is assumed that both time and space harmonics are negligible. Sectioning this circuit at ab and applying Thevenin's theorem gives, neglecting iron loss,

$$I_2 = \frac{V_{ab}}{Z_{th} + \frac{R_2}{s}} \qquad (1.1)$$

where,

$$V_{ab} = \frac{V}{R_1 + j(X_1 + X_0)} jX_0 = KV \qquad (1.2)$$

$$Z_{th} = Z_{source} + R_{ab} + jX_{ab}$$

$$= Z_{source} + \frac{(R_1 + jX_1)jX_0}{R_1 + j(X_1 + X_0)} + jX_2 \qquad (1.3)$$

whence, the developed torque at any value s of rotor slip is given by

$$T = \frac{m}{\omega_S} \frac{(KV)^2}{(R_{source} + R_{ab} + \frac{R_2}{s})^2 + (X_{source} + X_{ab})^2} \frac{R_2}{s} \qquad (1.4)$$

where m is the number of phases for which the motor is wound and ω_S is its synchronous speed.

Consider now a balanced two phase machine operating from an unbalanced two phase supply. If the machine can be taken as being magnetically linear, it is permissible to resolve the unbalanced voltage system into two balanced systems of opposite phase sequence; determine the operation of the machine subjected in turn to each of these two systems and finally combine the results to obtain the actual performance on the unbalanced supply.[2]

Referring to fig. (1.4),

$$V_R = V_{R_f} + V_{R_b} \qquad V_C = V_{C_f} + V_{C_b}$$

$$V_R + jV_C = V_{R_f} + V_{R_b} + j(V_{C_f} + V_{C_b})$$

$$= V_{R_f} + V_{R_b} + V_{R_f} - V_{R_b}$$

$$= 2V_{R_f}$$

$$\left|V_{R_f}\right| = V_f = \tfrac{1}{2}\left|V_R + jV_C\right| = \frac{|V_R| + |V_C|}{2} \tag{1.5}$$

Similarly,

$$V_R - jV_C = V_{R_f} + V_{R_b} - V_{R_f} + V_{R_b}$$

whence,

$$\left|V_{R_b}\right| = V_b = \tfrac{1}{2}\left|V_R - jV_C\right| = \frac{|V_R| - |V_C|}{2} \tag{1.6}$$

In determining the torque developed by each of these systems it must be borne in mind that for any given rotor velocity, ω_r, the slip will assume two different values, one for the forward sequence and one for the reverse sequence system.

Thus, for the forward sequence,

$$s_f = \frac{\omega_s - \omega_r}{\omega_s} = 1 - \frac{\omega_r}{\omega_s} \tag{1.7}$$

and for the reverse sequence,

$$s_b = \frac{\omega_s - (-\omega_r)}{\omega_s} = 1 + \frac{\omega_r}{\omega_s} = 2 - s_f \tag{1.8}$$

Furthermore, it must also be observed that the source impedance could have different values for the two sequences. For simplicity, however, it will be assumed that this impedance is negligible in both instances, equation (1.4) then becoming,

$$T = \frac{m}{\omega_s} \frac{(KV)^2}{(R_{ab} + \frac{R}{s})^2 + X_{ab}^2} \frac{R_2}{s} \tag{1.9}$$

Consequently, if a torque versus slip characteristic for balanced supply voltage V volts covering slip range 0 to 2.0 is available then by equations (1.5), (1.6) and (1.9) the forward and reverse sequence torques will be given by

$$T_f = \left(\frac{V_f}{V}\right)^2 T_{s_f} \quad \text{and} \quad T_b = \left(\frac{V_b}{V}\right)^2 T_{s_b}, \text{ respectively}$$

where, T_{s_f} is the torque developed at slip s_f and T_{s_b} is the torque developed at $(2 - s_f)$ obtained from the torque versus slip curve.

The net torque is, therefore,

$$T_n = T_f - T_b, \text{ forward.}$$

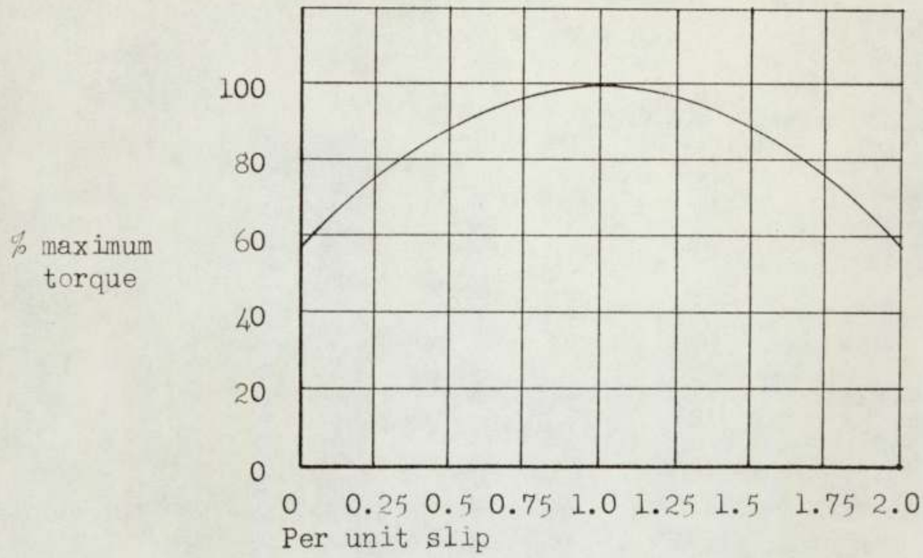

FIG.(1.5). SYMMETRICAL,TORQUE versus SLIP CHARACTERISTIC.

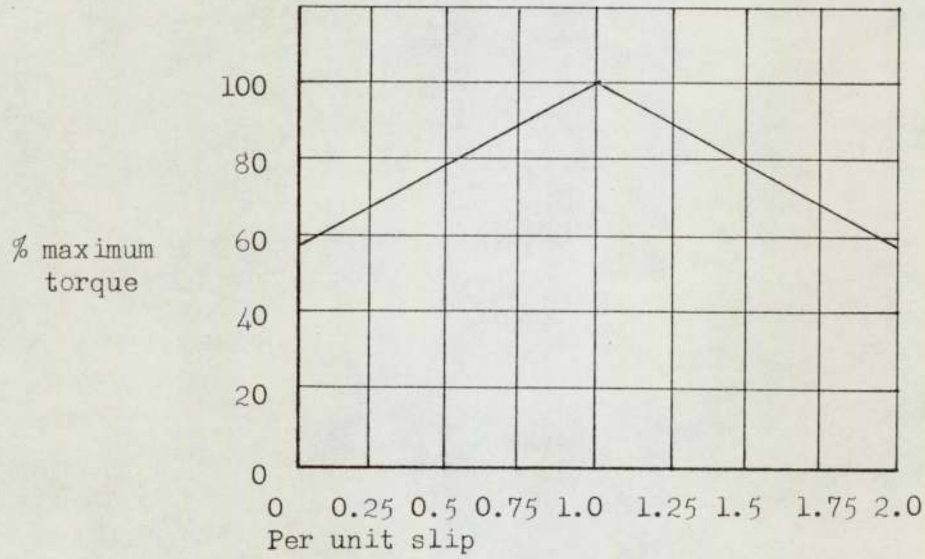

FIG.(1.6). SYMMETRICAL & LINEAR,TORQUE versus SLIP CHARACTERISTIC

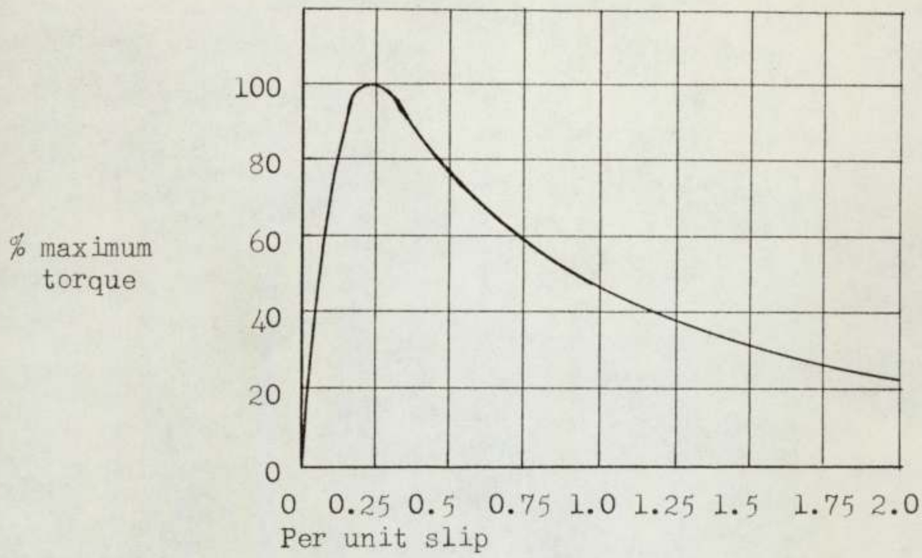

FIG.(1.7). CUSTOMARY ,TORQUE versus SLIP CHARACTERISTIC.

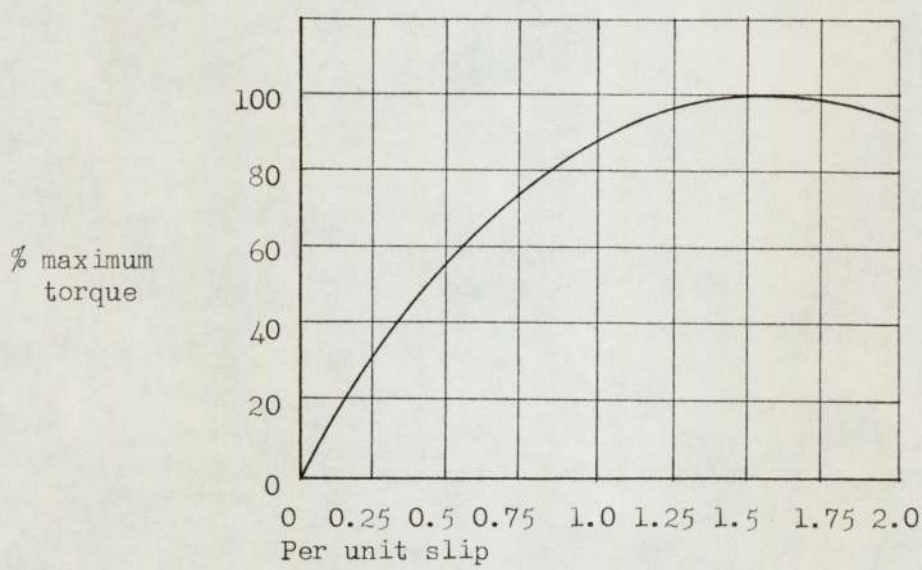

FIG.(1.8). TORQUE versus SLIP CHARACTERISTIC FOR HIGH RESISTANCE ROTOR.

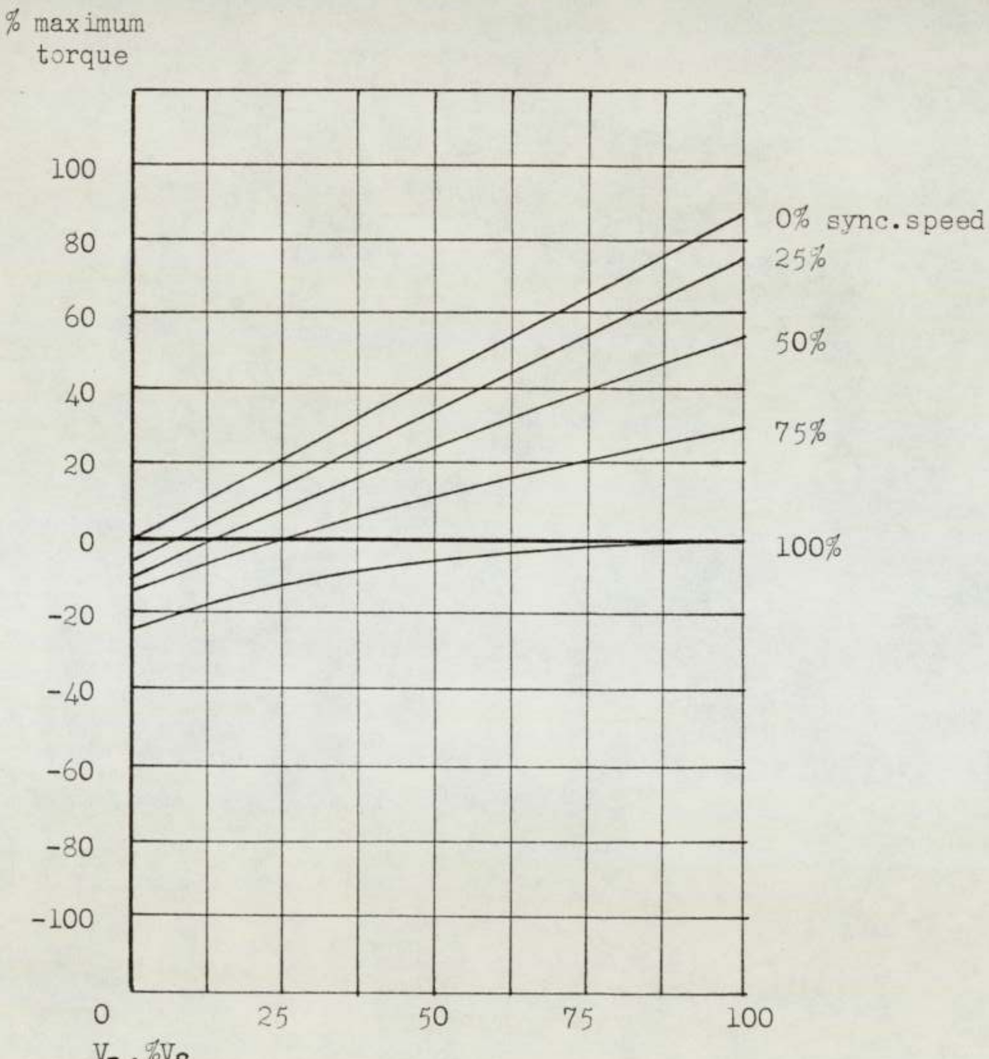

FIG.(1.9). TORQUE versus VOLTAGE CHARACTERISTIC, CONSTANT SPEED.

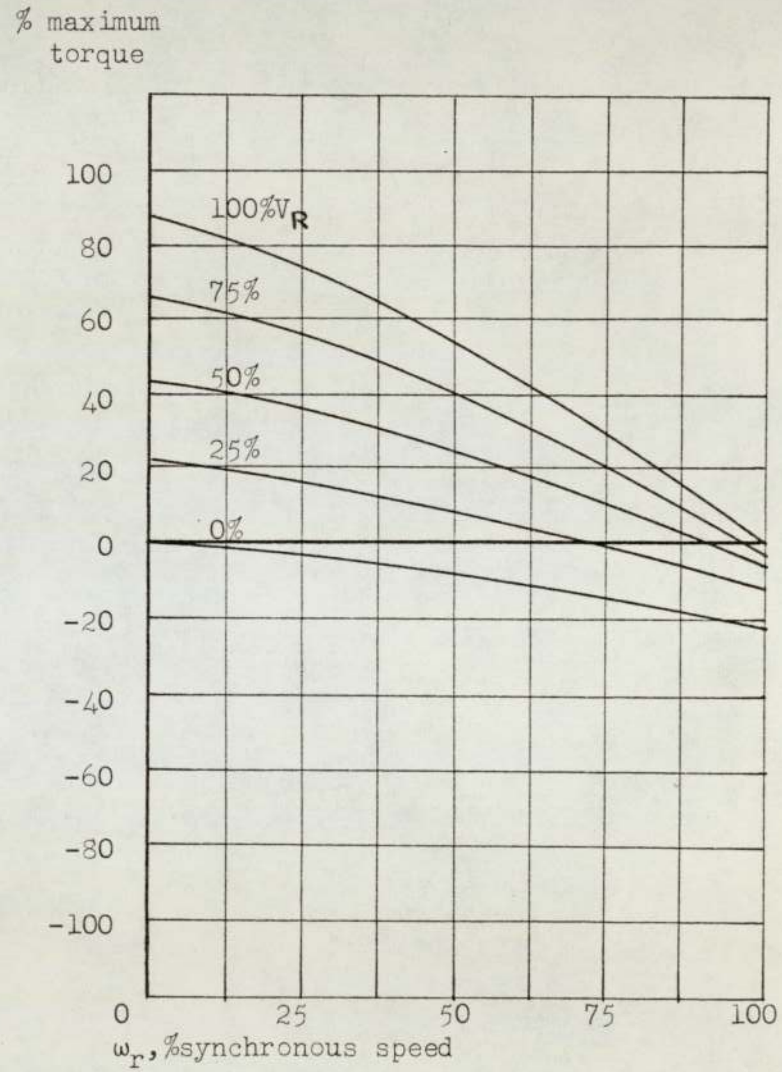

FIG.(1.10). TORQUE versus SPEED CHARACTERISTIC, CONSTANT VOLTAGE.

i.e. $$T_n = \frac{1}{V^2}\left(T_{s_f}V_f^2 - T_{s_b}V_b^2 \right) \qquad (1.10)$$

Substituting equations (1.5) & (1.6) in equation (1.10),

$$T_n = \frac{1}{4V^2}\left[T_{s_f}(V_R + V_c)^2 - T_{s_b}(V_R - V_c)^2 \right]$$

$$= \frac{1}{4V^2}\left[2(T_{s_f} + T_{s_b})V_R V_c + (T_{s_f} - T_{s_b})(V_R^2 + V_c^2) \right] \qquad (1.11)$$

Examination of this result reveals that if one of the phase voltages, say V_R, is held constant the net torque will be made up of a component directly proportional to V_c and the sum of the sequence torques and another component varying as (V_c^2 + constant) and the difference of the sequence torques, for a given rotor speed. Hence the value of the net torque for a particular value of V_c is governed by the shape of the balanced voltage torque versus slip curve about the 1.0 slip ordinate [(3)]. For a curve symmetrically disposed about this ordinate as in fig. (1.5), equation (1.11) reduces to

$$T_n = T_{s_f} \times \frac{V_c}{V_R}$$

giving the direct torque versus voltage relationship specified in the elementary control system. If in addition this curve could be made linear as in fig. (1.6), then not only would the above be obtained but also the linear torque versus speed relationship for the ideal motor/damper combination.

The torque versus slip characteristic, fig. (1.7), usually associated with the squirrel cage induction motor would obviously be unsuitable but by making the rotor resistance very high a balanced voltage curve such as fig. (1.8) is obtained which results in the unbalanced voltage characteristics of torque versus voltage, constant speed and torque versus speed, constant voltage illustrated in figs. (1.9) & (1.10), respectively. It will be seen that these are approximately linear as required but that for a particular speed there is a minimum of voltage below which the machine torque reverses and that for a particular voltage there is a maximum of speed above which the torque again reverses.

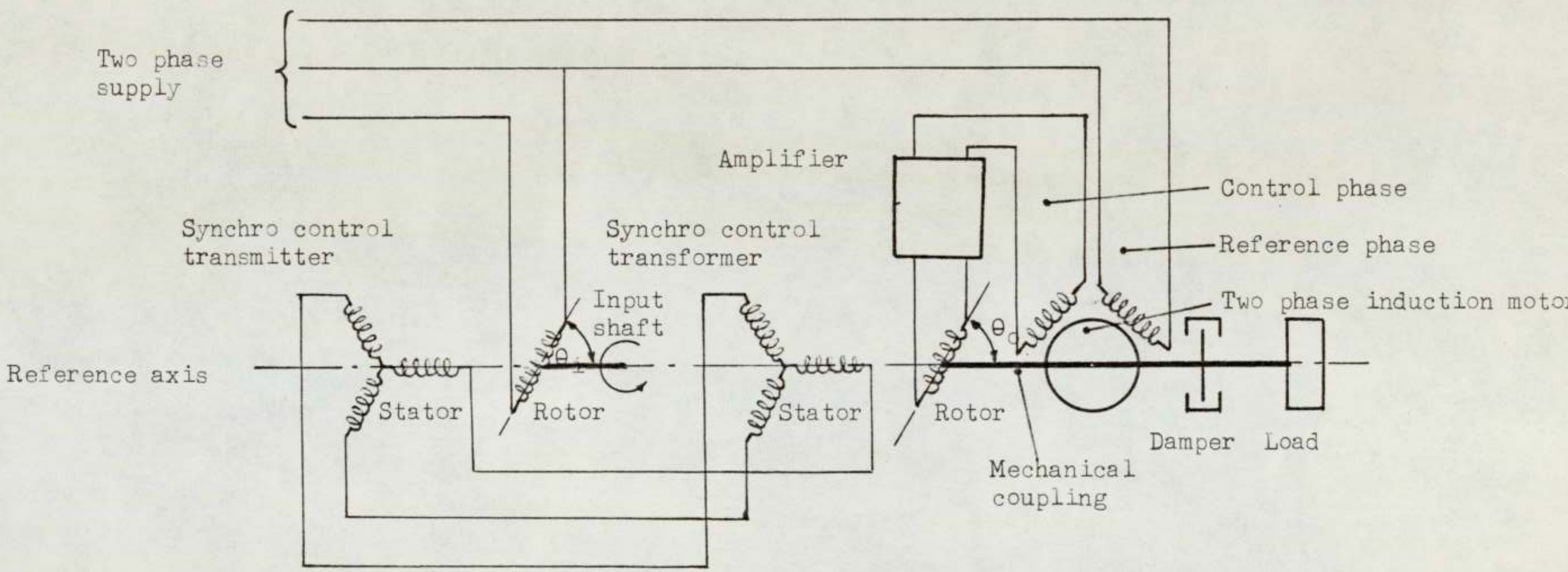

FIG.(1.11). ELEMENTARY POSITION CONTROL SYSTEM UTILISING TWO PHASE INDUCTION MOTOR & CONTROL SYNCHRO LINK.

Since, when used as a servomotor the machine is effectively error fed, these limitations of voltage and speed are acceptable. Indeed in an actual system when, after driving to nullify a system error the motor speed would not, due to mechanical inertia, reduce to zero at the same time as the controlling voltage, the negative torque thereby developed would help to bring the system to rest quickly and prevent the machine operating as a single phase motor.

To test for stability of operation, the values of k and F used in the equation of motion of the elementary system must be obtained. If the characteristics given in figs. (1.9) & (1.10) are assumed linear and so drawn, these values are given as $k = a \dfrac{\delta T_n}{\delta V_c}$ and $F = \dfrac{\delta T_n}{\delta \omega_r}$ where a is the error sensing constant in volts per radian. Since the family of lines are, in each case, nonparallel, the maximum value of F and the minimum value of k must be taken.

Accepting that the condition of stability can be satisfied, one further condition needs to be investigated. To comply with the condition, torque = $k\theta$, stated earlier, the motor developed torque must reverse when θ goes negative. For the two phase induction motor this means that negative θ must constitute a phase reversal. This can be brought about in the error detecting link [(4)].

It appears, therefore, that this high rotor resistance squirrel cage machine in having properties approaching those of the ideal combination of motor and brake also fulfils the requirements of a basic control system. These features together with its mechanical simplicity and freedom from sliding contacts with their inherent stiction, friction and electrical noise have resulted in the wide application of this machine as the motor element in instrument servomechanisms; fig. (1.11) illustrates an elementary control system utilizing this drive.

It should be noted at this stage that error control of the amplitude of one of the phase voltages is not the only way in which the two phase induction motor can be operated in a servomechanism. It is also possible to use the error to control the electrical angle between the two phase voltages, keeping their magnitudes fixed. This aspect was originally dealt with by Steinhacker and Mésèrve (5) who claimed that by using this method of control, the motor was prevented from developing any appreciable torques arising from voltage noise. Although this might seem to be a great advantage over the voltage amplitude control method, it is offset by the fact that in the former both phases are always fully excited as opposed to only the reference phase being always fully excited in the latter. Therefore, the heat dissipation and power consumption in the phase angle control arrangement will be almost double what they would be in an equivalent voltage amplitude control system. As both of these quantities are almost invariably required to be minimised in an instrument servomechanism, phase angle control is deemed impractical in the majority of cases and is ,therefore, not further considered in this thesis.

It should be appreciated that the foregoing appraisal of the machine is an oversimplification, being based entirely on the steady state performance of a magnetically linear machine completely free from time and space harmonics and supplied from sources of negligible impedance. As was pointed out earlier, the only really valid assessment of an element of a servosystem is that which is made with the element associated with its parent system and under true general conditions of operation. Consequently, having seen the reason for the original choice for the machine as a servomotor it now becomes necessary, in view of the ever more exacting dynamical application of control mechanisms, to examine critically the existing methods, and their development, for dynamic appraisal of the performance of the motor, in the correct context, and in its actual as opposed to its ideal harmonic free form.

2) Literature Survey.

The first main contribution to this field of study was made by Koopman (2) in his paper on the operating characteristics of the two phase servomotor published in 1949. In this paper he carried out an analysis of the simplified machine but took into account the effect of its source impedances. Whilst dealing extensively with steady state performance and providing, thereby, the basis of a great deal of subsequent work by others, he made only brief mention of the application of his methods to the "transient analysis of control systems." He stated that the important quantities in the transient performance of a servomotor were its torque per unit control voltage and its internal damping expressed as the reciprocal of the slope of the speed/torque curve. Having shown, earlier in the paper, the torque/control voltage relationship to be almost linear, he went on to investigate the damping as a function of control voltage and as a function speed. His results showed that these functions were non-linear for both zero and finite source impedance. From this he concluded that the performances of systems employing this machine could not be described by linear differential equations and took the matter no further other than to suggest that the performance of a system be "bracketed" by taking maximum and minimum values of the damping. Whatever the possibilities of using this bracket may be, the basic criticism is that in using steady state curves to obtain the torque per unit voltage figure and the damping factor, the electrical transients of the machine itself are ignored.

Hopkin (6) used Koopman's steady state analysis as the foundation for his work on the transient response of the two phase induction motor. He recognized the presence of the electrical transients but, having mentioned the publications of Stanley (7) in which were derived, for the polyphase induction motor, a set of non-linear differential equations describing these electrical transients, he developed a linear equation of performance having variable coefficients which required not only the assumption that the electrical transients were negligibly small, but that the machine had a linear torque/speed curve with gradient independent of voltage and was fed from sources of low impedance. Thus, to extend Koopman's work to a tangible transient analysis, Hopkin found it necessary to impose extra constraints on the machine. The formal solution to his equation was given as

$$\omega_r = \varepsilon^{-\int\left[D\left[V_C^2(t) + V_R^2\right] + 2b\omega_s\right]dt} \times \int \frac{DV_C(t)V_R - a}{J}\,\varepsilon^{\int\left[\frac{D\left[V_C^2(t) + V_R^2\right] + 2b\omega_s}{2\omega_s J}\right]dt} . dt$$

where a and b are the coefficients of coulomb and viscous friction for the load, respectively, in the equation $T_l = (a + b\omega_r)$, and where D is the constant relating the motor torque to speed and balanced supply voltage in the equation $T_m = DV^2(1 - \omega_r/\omega_s)$.

For a step input of voltage this reduces to

$$\omega_r = \omega_{rs}(1 - \varepsilon^{-\frac{t}{T}}) \quad \text{exactly}$$

for a speed range $-\omega_s$ to $+\omega_s$, where ω_{rs} is the steady state speed given by

$$\omega_{rs} = \frac{2\omega_s(DV_R V_C - a)}{D(V_R^2 + V_C^2) + 2b\omega_s}$$

and T is an effective time constant given by

$$T = \frac{2\omega_s J}{D(V_R^2 + V_C^2) + 2b\omega_s}$$

Hopkin compared the results of these expressions of ω_{rs} and T for an actual machine with values obtained from measured speed/time curves for various amplitudes of step input voltage. The comparison indicated errors of 13% in T and -1% in ω_{rs} at $V_C = V_R$ and errors of -36% in T and -16% in ω_{rs} at $V_C = 20\% \, V_R$. It is not possible to be specific about the meaning of these errors since no indication was given in the paper of the methods of measurement used.

The same equation of performance was used to obtain the steady state response to a sinusoidally modulated control signal. The solution to the equation was, in this case, not exact and was based on the assumption that the sinusoidally varying amplitude of the control field voltage was small. It was concluded that, under these conditions, the frequency response of the machine was of the same form as that of a single time constant, linear system. A comparison between the calculated and measured values of the phase relationship between the input signal and the output velocity, indicated an error of approximately 0% at a modulation frequency of 1.0Hz. increasing to approximately 20%, based on the measured figure, at a modulation frequency of 6.0Hz. Hopkin claimed that these discrepancies were due to his having neglected the electrical time delays in the motor and suggested that the equation of performance should take the form

$$\omega_r = \omega_{rs}(1 - C_1 \varepsilon^{-\frac{t}{T}} + C_2 \varepsilon^{-\frac{t}{0.005}})$$

in which the latter term represents the electrical delays.

At the same time as Hopkin published his work, Brown[8] presented a paper quoting, as a result of extending the work of Nichols and Sobczyk,[9] a Laplace transfer function of the form

$$KG(s) = \frac{H}{s(s + 1/T_1)} \quad ,$$

in which H is the gain constant, T_1 is the mechanical time constant of the system and s is the Laplace variable, to describe the transient behaviour of the two phase motor. This again states that the motor effectively behaves as a single time constant system. From experimental observations, Brown also deduced that the above transfer function was oversimplified and should be replaced by

$$KG(s) = \frac{H}{s(1 + 1/T_1)(s + 1/T_2)}$$

where T_2 is the electrical time constant.

On the premise that in the simplified machine the effects of the stator resistance and leakage inductance could be discounted, he proceeded to determine this fuller form of transfer function, observing that, in the terms of the Laplace variable, the transformation of the velocity function for a step input of voltage gives the same result as the division of the transformation of the position function by the transformation of the input voltage. He, therefore, set about obtaining a torque equation for the motor and solving this for the velocity function. The basis of his method was to use assumed expressions for the stator voltages and deduce corresponding expressions for flux density, induced voltage and hence current in an element of the rotor. The torque on the element he then took as the product of flux and current and integrated this round the rotor to give total torque. The final equation for the instantaneous velocity of the rotor he gave as

$$\omega_r = \omega_{rs} + M_1 \varepsilon^{-\frac{F}{J}t} + M_2 \varepsilon^{-\frac{R_r}{L_r}t}$$

in which R_r and L_r are the resistance and inductance of an element of the rotor and M_1 and M_2 are constants to be determined in terms of ω_{rs} from the assumed initial conditions of zero velocity and acceleration. It will be seen that this equation is of the same type as that finally suggested by Hopkin. Brown obtained the Laplace transfer function corresponding to the above velocity function as

$$KG(s) = \frac{\omega_{rs}}{V_c} \frac{1/T_1 T_2}{s(s + 1/T_1)(s + 1/T_2)},$$

where $T = -\frac{J}{F}$ and $T = -\frac{L_r}{R_r}$, and proceeded to compare the frequency response measured on an actual motor with that predicted for the same machine using the above function. To do this he took the ratio L_r/R_r as the ratio of the rotor leakage inductance to the effective rotor resistance in the equivalent circuit referred to the stator and obtained its value from a measured steady state speed/torque curve by utilizing the steady state torque equation in terms of R_2 and L_2, stator quantities being assumed negligible. It should be noted that the steady state torque equation as derived by Brown is dimensionally incorrect in that the rotor radius appears to have been omitted. Fortunately the equation was used twice in a simultaneous solution for two steady speeds with the result that the omission had no effect. This comparison revealed that at low frequencies, 0.3Hz., the errors in amplitude and phase were -25% and 3%, and at the higher frequencies, 5Hz., -30% and 0%, respectively, based on the experimental figures, for $V_C = 40\% V_R$. Compared with Hopkin's results, the figures just quoted show some improvement in the phase relationship but are unsatisfactory from the point of view of amplitude response. Nevertheless, it was in this paper that the idea of obtaining a transfer function for the motor which included its own electrical delays was first put forward thereby setting the pattern for much of the future work in that subsequent contributions, by different authors, were aimed at obtaining more representative transfer functions by using improved mathematical equations to describe the machine's behaviour.

Thus, in a paper published the following year, Sadovskii (10) used the differential equations obtained by Stanley for the polyphase induction motor. It should be noted that, in formulating these equations, Stanley had assumed a simplified machine so that this is implicit in Sadovskii's work although he did not specifically say so. The equations give, in axes stationary with respect to the stator, the relationships between the applied voltage, the current and the rate of change of flux linkages, and between the torque, the current and the flux linkages. By making substitution for the current from the voltage relationship and neglecting leakage fluxes, Sadovskii stated the torque equation in terms of the rotor angular velocity, ω, the rotor resistance, r, the stator phase flux linkages, ψ_α and ψ_β and their time rate of change as

$$T = \frac{1}{r}\left(\psi_\alpha \frac{d\psi_\beta}{dt} - \psi_\beta \frac{d\psi_\alpha}{dt} - \omega(\psi_\alpha^2 + \psi_\beta^2)\right).$$

Taking the stator resistance to be negligible, he related the rate of change of the stator flux linkages directly to the applied voltages and obtained the flux linkages by integration. The results of these operations were substituted in the torque equation. The actual voltage expressions used by Sadovskii were

$$U_\alpha = U_0 \cos\omega_0 t, \qquad \text{reference phase}$$

and

$$U_\beta = a\cos(\Omega t + \emptyset)\cos(\omega_0 t + \gamma), \qquad \text{control phase}$$

where ω_0 is the angular frequency of the supply. The latter equation describes the control phase voltage as being either amplitude or phase modulated. To obtain a manageable equation for the electromagnetic torque, in terms of these voltages, he found it necessary to ignore all terms in $2\omega_0$ and to assume the value of ψ_β, the control phase flux linkages, to be negligibly small in comparison with ψ_α, the reference phase flux linkages; these two simplifications are not justifiable and neither is that of assuming negligible leakage fluxes. His resulting equation for torque is

$$T = \frac{1}{r}\left[\frac{U_o a}{2(\omega_o^2 - \Omega^2)}\sin(\ t + \emptyset)\cos\gamma - \frac{U_o a}{2\omega_o}\left(1 + \frac{\omega_o}{\omega_o^2 - \Omega^2}\right)\frac{\cos(\Omega t + \emptyset)}{\sin\gamma}\right] - \frac{U_o^2\omega}{2\omega_o} \ .$$

Equating this to the mechanical torque requirements and relating the output conditions to the input conditions, a machine transfer function was derived. No experimental corroboration for this function was given in the paper.

Some three years after the publication of Sadovskii's work, Stein and Thaler[34] reported the results of their investigation into the non-linearity of the two phase servomotor. Unfortunately their investigation was concerned only with the non-linearity of the steady state torque/speed curves as illustrated in fig.(1.10). The effects of the electrical time delays were, therefore, excluded so that their paper offered little in the way of advancement.

In the same year, however, Titov,[11] again using the basic differential equations, in axes stationary with respect to the stator, for the simplified machine, developed an expression for the torque generated by the two phase motor on the assumption of negligible e.m.f. due to the rotation of the rotor. Although this is an improvement on Sadovskii it cannot be accepted as a generally valid premise since it limits the performance of the system to conditions of zero speed. Notwithstanding, by neglecting the double frequency terms, as Sadovskii had done, Titov calculated an expression for the transfer function of the motor which included the time constants T_c of the stator winding, T_p of the rotor winding and T_1 of the mechanical system. He then showed that this transfer function could be simplified if $T_p < T_c$ and if the product of the total self inductances of the stator and the rotor was equal to the square of the mutual inductance between the stator and the rotor; the latter implies negligible leakage inductance for both components. Again, neither of these is a valid assumption. Taking this simplified form of the transfer function, he further demonstrated that if T_c tended to zero the function degenerated into the one given by Sobczyk and alternatively if T_c tended to infinity the function became that as presented by Sadovskii. He then went on to analyse the use of his own simplification in various systems. Thus, this paper summarizes a lot of the previous work in the Russian school.

In 1958, Mikhail and Fett (12) also applied the results of Stanley's analysis and developed a linear differential equation with variable coefficients relating the instantaneous values of the motor speed and its stator phase currents, the forms of the latter as functions of time being assumed to be known. This is obviously a very limiting assumption and apart from its exclusion of the electrical/time characteristics of the stator winding, is untenable in general practice. On this basis they proceeded to evaluate the transfer function for the machine fed with a modulated control current. No practical evidence of the efficacy of their result was given and their mathematical approach, and consequently the validity of their conclusion, was questioned by Padegs in the ensuing discussion.

A notable departure from the trend of previous workers, with the exception of Koopman, was made by Kutvinov (13) who, whilst yet again employing the differential equations of Stanley, as stated by Sadovskii, included in his ultimate equation for torque the effects of the motor source impedances. His equations of performance were generalized for any motor supply circuit by use of the equivalent generator theorem and embraced the electrical/time properties of both the stator and the rotor. In obtaining a solution, however, he stated that the ratio of the rotor actual speed to the synchronous speed would always be less than unity. For instantaneous speeds during general dynamic operation this is not so since, as shown by Shubenko, (14) the rotor speed can overshoot synchronous speed. The method of solution does, therefore, anticipate an invalid result.

During the years 1960 and 1961, Vlasov (15, 16, 17) published three papers all dealing with the transfer functions of alternating current servomechanisms. The first of these was of a more general nature than the other two and is of the most consequence. In this paper he analysed a basic form of a section of a control system comprising an ideal modulator coupled to a linear passive quadripole in turn coupled to an ideal phase detector, obtaining finally an overall system transfer function.

In most of its applications, the two phase servomotor is controlled by means of a synchro link. This combination falls into the general category analysed by Vlasov . By applying the results of his analysis to this particular, taking Sadovskii's work as the basis for mathematically describing the motor, he showed quite clearly that the overall transfer function of the arrangement could not be obtained as the product of the individual transfer functions of the system elements. Consequently, the whole notion of transfer function analysis is, for systems employing the alternating current induction servomotor, thrown into doubt. This inevitably indicates that the transfer function is not an ideal mathematical model for this element. However, in his doctoral thesis, presented in 1964, Law[18] claimed, as a result of a largely experimental investigation, that "the transfer function calculation closely approximates the speed transient as determined by the computer representation in the most stringent case, that of zero external inertia." In fact his results show a poor correspondence in the first few milliseconds of operation, a period of great importance in dynamic performance. This he stated to be due to the neglect of electrical time delays in the transfer function; he had indeed used a single time constant function, assumed negligible source impedance and no additional circuit elements. This is surprising since the major part of his thesis was concerned with the effects of source impedance on the response of the alternating current servomotor. It is concluded that his claim cannot be taken seriously and in no way diminishes the validity of Vlasov's exposition.

Recognizing the fact that it is due to its own non-linearity that the induction servomotor cannot be represented by a general transfer function, Wilson[19] proposed that the motor always operated at speeds close to zero at which the torque could be taken as the instantaneous stalled torque and, further, that the stator currents could be considered to be governed by the standstill impedances of the stator windings. On these premises he was able to determine a general transfer function. His assumption, however, precludes the effects of rotational voltages in the machine and cannot, therefore, be accepted as a generallity.

It is concluded from this survey that work aimed at obtaining a rigorous transfer function for the induction servomotor cannot yield a satisfactory result and is in any case, as already pointed out, not a valid way of modelling the element. A mathematical model is, however, essential to enable system performance to be predicted in the design stages. Sensibly, this model should be available from the design calculations of the machine itself else how can its performance be optimized other than by trial and error?

Now it has been observed that the induction servomotor finds most of its applications in instrument servomechanisms and falls, therefore, mainly into the class of miniature machines. It does, by virtue of its smallness, very often contain a large harmonic content in its magnetomotive force as a function of space. Indeed, in the miniature range, motors exist which have only one slot per pole per phase in their stator winding resulting in a completely rectangular magnetomotive force waveform in space. The fact that these machines are designed to be magnetically unsaturated excludes internally generated time harmonics other than those caused by the magnetomotive force space function. The mathematical model, to be effective, must then include representation of the space harmonics. In the work so far, no attempt has been made to fulfil this requirement, it appears, ab initio, to have been overlooked. Furthermore, neither has there been any attempt to ratify the design calculations through dynamic performance or to extend them and their ratification to the space harmonics in the miniature machine.

It is at this stage that the present study commences and seeks, through the curriculum detailed in the introduction, both to establish a valid mathematical model and to improve, extend and ratify the design calculations for the miniature two phase induction servomotor.

CHAPTER II.

Method of Analysis.

3) The Tensor Approach.

The equation of voltage for a rotating coil situated in a time varying magnetic field can be written as

$$e = Ri + p\phi + \psi p\theta \qquad \text{(motor principle)}$$

where R is the winding resistance, ϕ is the winding flux linkages, ψ is the winding flux conductors, p being the differential operator. In index notation this equation can be written as a tensor equation applicable to all coils as

$$e_m = R_{mn} i^n + p\phi_m + \psi_m p\theta$$

in which e is taken as a covariant tensor and i as a contravariant tensor as is customary. From the definition of inductance ϕ_m can be written as $L_{mn} i^n$ so that, if for simplicity magnetic linearity and constant inductance are assumed, $p\phi_m$ can be written as $L_{mn} p i^n$, L being taken as a general coefficient of inductance including self and mutual. In similarity let ψ_m be written as $G_{mn} i^n$ in which the tensor G_{mn} is defined by the statement. The voltage equation now becomes

$$e_m = R_{mn} i^n + L_{mn} p i^n + G_{mn} p\theta i^n.$$

If the term $p\theta$ is assumed to be a single entity, i.e. constant, this voltage equation may be written

$$e_m = (R_{mn} + L_{mn} p + G_{mn} p\theta) i^n.$$

The three grouped tensors can be added to form the impedance object Z_{mn} which if written in array form for a given machine gives the familiar transient impedance matrix. If this matrix can be made symmetrical the machine may be represented by an equivalent circuit. It is apparent, therefore, that under conditions of changing speed neither the impedance matrix nor the equivalent circuit can have existence so that any attempt to use either of these devices directly in the prediction of dynamic performance must be in error.

To set up the equations of true dynamic performance, two methods of approach are possible, viz:

1) analyse the individual machine physically taking into account all relative movements of conductors, time variations of currents and mechanical inertia of rotating parts.

2) consider the machine as a system containing both electrical and gravitational energies and apply Lagrange's particle dynamics equation as generalized by Maxwell for electrical and geometrical coordinates.

Because of its individuality the former method is considered to be too restricting in an area of work where it is intended to relate dynamic performance to design for a range of machines. The latter approach is thought to be more relevant in that it is disciplinary and is, therefore, adopted in this investigation. The equation of Lagrange as generalized by Maxwell, however, is only valid for holonomic systems whereas electrical machines under dynamic conditions of operation are generally non-holonomic systems. This fact was realized by Kron (22) who took Lagrange's equation as modified by Boltzmann, Hamel and Whittaker for non-holonomic particle systems and generalized it to include electrical and geometrical coordinates for all reference systems by writing it in tensor form. It is with this equation that the subsequent analysis commences.

For any electrical machine let the following quantities be defined in non-holonomic reference axes:

1) (a) the total number of charges passing through any winding counted from a definite time,

(b) the instantaneous angular displacement of the rotor from the reference axis

as x^{α} where α may assume any value q,d,--- t for which x^{t} is θ the rotor displacement, the other indices representing different windings.

2) (a) the instantaneous current in each winding,

(b) the instantaneous angular velocity of the rotor

as $\dot{x}^{\alpha} = \dfrac{d}{dt}x^{\alpha}$.

3) (a) the instantaneous terminal voltage applied to any winding

(b) the instantaneous applied shaft torque

as e_β where β may assume any value q,d,--- t for which e_t is the applied torque T.

4) the metric tensor as $L_{\alpha\beta}$ in which L_{tt} is the mechanical inertia of the rotating parts.

5) the resistance tensor as $R_{\alpha\beta}$ in which R_{tt} is the mechanical friction to rotation.

The combined electrical and mechanical equation of dynamic performance as given by Kron in tensor form is

$$e_\beta = R_{\alpha\beta}\dot{x}^\alpha + L_{\alpha\beta}\frac{\delta\dot{x}^\alpha}{\delta t} \tag{2.1}$$

where $\frac{\delta}{\delta t}$ signifies the intrinsic derivative.

The squirrel cage induction motor is a smooth bore machine symmetrical on both sides of the air gap. It is ,therefore, convenient to choose reference axes fixed with respect to the stator and along which the magnetic axes of the two phase stator winding are directed. The rotor winding may be thought of as a polyphase winding and can, therefore,be represented by an equivalent two phase winding having magnetic axes fixed in space relative to the stator magnetic axes. For convenience the rotor axes are taken to be colinear with the stator axes. The primitive arrangement of the machine is then as shown in fig. (2.1).

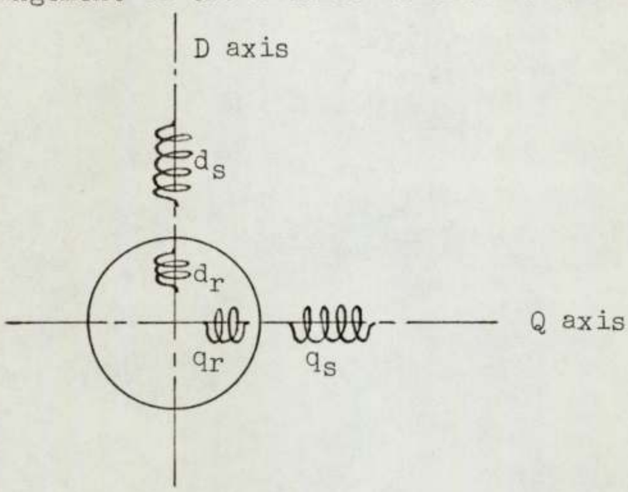

FIG. (2.1). PRIMITIVE OF TWO PHASE SQUIRREL CAGE MOTOR.

In this the presence of space harmonics in the magnetomotive force waveform is ignored but will be dealt with finally.

Although the magnetic axes of the rotor equivalent windings are fixed relative to the stator axes, the rotor conductors will have an angular velocity ω with respect to these axes and the system is, therefore, non-holonomic. Consequently equation (2.1) must be used as a basis for the formulation of the equations of dynamic performance for the machine.

The resistance tensor and the metric tensor of equation (2.1) can be written by inspection of fig. (2.1), thus

$$R_{\alpha\beta} = \begin{array}{c|ccccc} {}_{\alpha}\backslash^{\beta} & d_s & d_r & q_s & q_r & t \\ \hline d_s & R_s & & & & \\ d_r & & R_r & & & \\ q_s & & & R_s & & \\ q_r & & & & R_r & \\ t & & & & & F \end{array}$$

where F is the mechanical friction constant, s signifies stator, r signifies rotor.

$$L_{\alpha\beta} = \begin{array}{c|ccccc} {}_{\alpha}\backslash^{\beta} & d_s & d_r & q_s & q_r & t \\ \hline d_s & L_s & M & & & \\ d_r & M & L_r & & & \\ q_s & & & L_s & M & \\ q_r & & & M & L_r & \\ t & & & & & J \end{array}$$

where L is the coefficient of self inductance, M is the coefficient of mutual inductance and J the moment of inertia of the rotating parts.

Carrying out the intrinsic differentiation in equation (2.1),

$$L_{\alpha\beta}\frac{\delta\dot{x}^{\alpha}}{\delta t} = L_{\alpha\beta}\left(\frac{d\dot{x}^{\alpha}}{dt} + \Gamma^{\alpha}_{\rho\sigma}\,\dot{x}^{\rho}\dot{x}^{\sigma}\right)$$

where $\Gamma^{\alpha}_{\rho\sigma}$ is the affine connection, which in general links a tensor with its derivative, and where α,ρ,σ may assume any value q, d, --- t.

Since $L_{\alpha\beta}$ is the metric tensor, then by lowering indices

$$L_{\alpha\beta}\Gamma^{\alpha}_{\rho\sigma} = \Gamma_{\rho\sigma,\beta}$$

Hence
$$L_{\alpha\beta}\Gamma^{\alpha}_{\rho\sigma}\,\dot{x}^{\rho}\dot{x}^{\sigma} = \Gamma_{\rho\sigma,\beta}\,\dot{x}^{\rho}\dot{x}^{\sigma}$$

and by replacing dummy index ρ by α

$$L_{\alpha\beta}\Gamma^{\alpha}_{\rho\sigma}\,\dot{x}^{\rho}\dot{x}^{\sigma} = \Gamma_{\alpha\sigma,\beta}\,\dot{x}^{\alpha}\dot{x}^{\sigma}$$

where $\Gamma_{\alpha\sigma,\beta}$ is the non-holonomic Christoffel symbol and is made up of

$$\frac{1}{2}\left[\frac{\partial L_{\beta\sigma}}{\partial x^{\alpha}} + \frac{\partial L_{\beta\alpha}}{\partial x^{\sigma}} - \frac{\partial L_{\alpha\sigma}}{\partial x^{\beta}}\right] + \Omega_{\sigma\beta,\alpha} + \Omega_{\beta\alpha,\sigma} - \Omega_{\alpha\sigma,\beta}$$

where the Ω are non-holonomic geometric objects which derive from the non-holonomic transformation of a first order Christoffel symbol, [ab,c] .

In this relationship, $L_{\beta\sigma}$, $L_{\beta\alpha}$, $L_{\alpha\sigma}$ are all representations of the metric tensor which has, in this case, only constant terms. Hence the derivatives above will all be zero so that the non-holonomic Christoffel symbol reduces to

$$\Omega_{\sigma\beta,\alpha} + \Omega_{\beta\alpha,\sigma} - \Omega_{\alpha\sigma,\beta}$$

whence,

$$L_{\alpha\beta}\Gamma^{\alpha}_{\rho\sigma}\,\dot{x}^{\rho}\dot{x}^{\sigma} = (\Omega_{\sigma\beta,\alpha} + \Omega_{\beta\alpha,\sigma} - \Omega_{\alpha\sigma,\beta})\dot{x}^{\alpha}\dot{x}^{\sigma}$$

Hence the equation of performance can be written

$$e_{\beta} = R_{\alpha\beta}\dot{x}^{\alpha} + L_{\alpha\beta}\frac{d\dot{x}^{\alpha}}{dt} + (\Omega_{\sigma\beta,\alpha} + \Omega_{\beta\alpha,\sigma} - \Omega_{\alpha\sigma,\beta})\dot{x}^{\alpha}\dot{x}^{\sigma} \qquad (2.2)$$

In the final term of this equation, $(\Omega_{\alpha\sigma,\beta})\dot{x}^{\alpha}\dot{x}^{\sigma}$ must be zero since the non-holonomic object Ω is skew symmetric in its first two indices. Also, expanding the second component of this last term gives

$$\Omega_{\beta\alpha,\sigma} = \frac{L_{\sigma\gamma}}{2}\left[-\frac{\partial C^{\gamma}_{a}}{\partial x^{b}} + \frac{\partial C^{\gamma}_{b}}{\partial x^{a}}\right] C^{a}_{\alpha}C^{b}_{\beta}$$

$$= \frac{L_{\sigma\gamma}}{2}\left[C^{b}_{\beta}\frac{\partial C^{\gamma}_{b}}{\partial x^{\alpha}} - C^{a}_{\alpha}\frac{\partial C^{\gamma}_{a}}{\partial x^{\beta}}\right] \qquad (2.3)$$

in which $L_{\sigma\gamma}$ is the metric tensor and C^{γ}_{b} and C^{γ}_{a} are the non-holonomic to holonomic transformation tensor. Referring to fig. (2.2) in which is shown the primitive arrangement in the two systems of axes, let $\theta = \int \omega dt$ be the angle between the fixed and the moving axes at any instant. Since the transformation is non-holonomic to holonomic, the transformation tensor will be given by the relation between the derived variables, i.e. the currents, thus using non-tensor indices

$$i_{dr} = i_{r1}\cos\theta - i_{r2}\sin\theta$$

$$i_{qr} = i_{r1}\sin\theta + i_{r2}\cos\theta$$

Since θ is the angle between the axes moving relative to the rotor and those fixed relative to the rotor measured in the direction of rotor rotation, then θ must be reckoned as a negative angle.

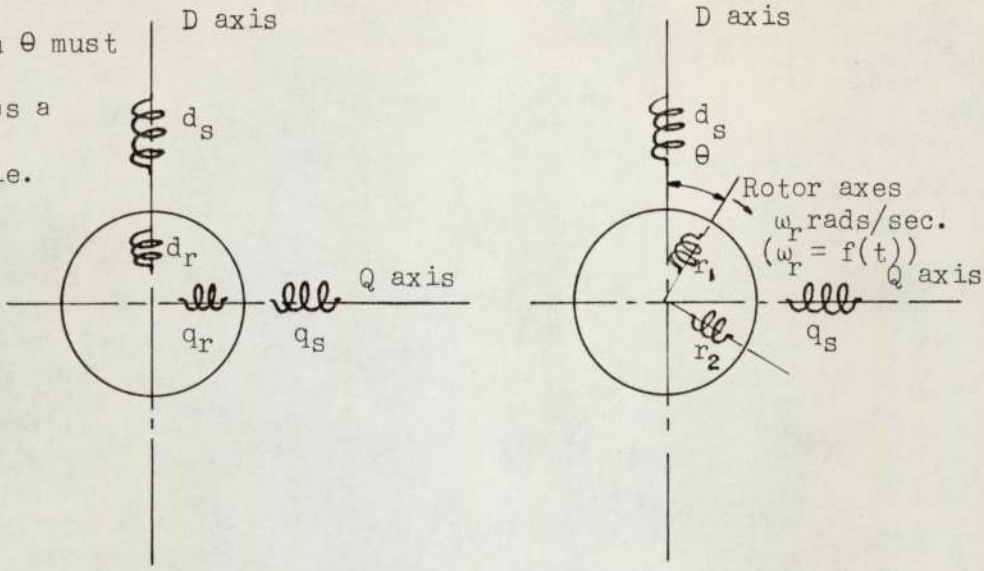

Non-holonomic. Holonomic.

FIG. (2.2). PRIMITIVE OF TWO PHASE SQUIRREL CAGE MOTOR IN TWO REFERENCE SYSTEMS.

Defining C^{γ}_{b} as $\dfrac{\partial i_{old}}{\partial i_{new}}$, i.e. $\dfrac{\partial i^{\gamma}}{\partial i^{b}}$ in the equation $i^{\gamma} = C^{\gamma}_{b} i^{b}$ and remembering that only rotor currents are affected, gives

C^{γ}_{b} =

γ \ b	d_s	r_1	q_s	r_2	t
d_s	1				
d_r		cos-θ		-sin-θ	
q_s			1		
q_r		sin-θ		cos-θ	
t					1

Since this is a function of θ, then in the expansion of $\Omega_{\beta\alpha,\sigma}$ the indices α and β must be t for the partial derivative $\dfrac{\partial C^{\gamma}_{b}}{\partial x^{\alpha}}$ and the partial derivative $\dfrac{\partial C^{\gamma}_{a}}{\partial x^{\beta}}$ to have non-zero values. For the mechanical equation of torque, both α and β take the value t simultaneously. The above derivatives therefore assume their non-zero values simultaneously and, since these are identical,

$$\left[C^{b}_{\beta} \frac{\partial C^{\gamma}_{b}}{\partial x^{\alpha}} - C^{a}_{\alpha} \frac{\partial C^{\gamma}_{a}}{\partial x^{\beta}} \right] = 0.$$

Also, for the electrical equation, α and β never take the value t.

Hence the two derivatives will always be zero so that again

$$\left[C^b_\beta \frac{\partial C^\gamma_b}{\partial x^\alpha} - C^a_\alpha \frac{\partial C^\gamma_a}{\partial x^\beta} \right] = 0$$

But, $\Omega_{\beta\alpha,\sigma}\dot{x}^\alpha\dot{x}^\sigma = \Omega_{\sigma\beta,\alpha}\dot{x}^\alpha\dot{x}^\sigma$ since α and σ are dummy indices.

Hence $\Omega_{\beta\alpha,\sigma}$ must be set to $\Omega_{\sigma\beta,\alpha}$ in the general equation of performance which then reduces to

$$e_\beta = R_{\alpha\beta}\dot{x}^\alpha + L_{\alpha\beta}\frac{d\dot{x}^\alpha}{dt} + 2(\Omega_{\sigma\beta,\alpha})\dot{x}^\alpha\dot{x}^\sigma \tag{2.4}$$

Expanding the remaining non-holonomic object in this equation gives,

$$2\Omega_{\sigma\beta,\alpha} = L_{\alpha\gamma}\left[\frac{\partial C^\gamma_c}{\partial x^b} - \frac{\partial C^\gamma_b}{\partial x^c}\right] C^b_\beta C^c_\sigma$$

$$= L_{\alpha\gamma}\left[C^c_\sigma \frac{\partial C^\gamma_c}{\partial x^\beta} - C^b_\beta \frac{\partial C^\gamma_b}{\partial x^\sigma}\right]$$

Again the derivatives can only have non-zero values when β or σ assume the value t giving x^β and x^σ as θ.

Differentiating the transformation tensor C^γ_c with respect to θ gives,

γ \ c	d_s	r_1	q_s	r_2	t
d_s					
d_r		$-\sin\theta$		$\cos\theta$	
q_s					
q_r		$-\cos\theta$		$-\sin\theta$	
t					

Hence when β takes the value t the product $C^c_\sigma \dfrac{\partial C^\gamma_c}{\partial x^\beta}$ is given by

σ \ c	d_s	r_1	q_s	r_2	t
d_s	1				
d_r		$\cos-\theta$		$-\sin-\theta$	
q_s			1		
q_r		$\sin-\theta$		$\cos-\theta$	
t					1

γ \ c	d_s	r_1	q_s	r_2	t
d_s					
d_r		$-\sin\theta$		$\cos\theta$	
q_s					
q_r		$-\cos\theta$		$-\sin\theta$	
t					

in which C^c_σ is obtained as the inverse of C^σ_c identical to that of C^γ_b.

$$\text{i.e.}\quad C^c_\sigma \frac{\partial C^\gamma_c}{\partial x^\beta} = \begin{array}{c|ccccc} {}_\gamma\backslash^\sigma & d_s & d_r & q_s & q_r & t \\ \hline d_s & & & & & \\ d_r & & & & 1 & \\ q_s & & & & & \\ q_r & & -1 & & & \\ t & & & & & \end{array} = A^\gamma_\sigma$$

Furthermore, with β set at t, $\Omega_{\sigma\beta,\alpha}$ will only have a non-zero value when $\sigma \neq t$. Under these conditions the derivative $\dfrac{\partial C^\gamma_b}{\partial x^\sigma}$ will always be zero and the remaining non-holonomic object $\Omega_{\sigma\beta,\alpha}$ reduces to $\frac{L_{\alpha\gamma}}{2} A^\gamma_\sigma \dot{x}^\alpha \dot{x}^\sigma$. Since α and β do not take the value t independently, then with β set at t α must also have this value and the equation of performance is then, as stated earlier, the mechanical equation of torque. Hence from equation (2.4)

$$e_t = R_{tt}\dot{x}^t + L_{tt}\frac{d\dot{x}^t}{dt} + L_{\alpha\gamma}A^\gamma_\sigma \dot{x}^\alpha \dot{x}^\sigma.$$

$$= R_{tt}\dot{x}^t + L_{tt}\frac{d\dot{x}^t}{dt} + G_{\alpha\sigma}\dot{x}^\alpha \dot{x}^\sigma,$$

$$\text{where } G_{\alpha\sigma} = L_{\alpha\gamma}A^\gamma_\sigma$$

Replacing dummy index σ by β ,

$$e_t = R_{tt}\dot{x}^t + L_{tt}\frac{d\dot{x}^t}{dt} + G_{\alpha\beta}\dot{x}^\alpha \dot{x}^\beta, \qquad (2.5)$$

in which

$$G_{\alpha\beta} = \begin{array}{c|ccccc} {}_\alpha\backslash^\gamma & d_s & d_r & q_s & q_r & t \\ \hline d_s & L_s & M & & & \\ d_r & M & L_r & & & \\ q_s & & & L_s & M & \\ q_r & & & M & L_r & \\ t & & & & & J \end{array} \cdot \begin{array}{c|ccccc} {}_\gamma\backslash^\beta & d_s & d_r & q_s & q_r & t \\ \hline d_s & & & & & \\ d_r & & & & 1 & \\ q_s & & & & & \\ q_r & & -1 & & & \\ t & & & & & \end{array}$$

$$= \begin{array}{c|ccccc} {}_\alpha\backslash^\beta & d_s & d_r & q_s & q_r & t \\ \hline d_s & & & & M & \\ d_r & & & & L_r & \\ q_s & & -M & & & \\ q_r & & -L_r & & & \\ t & & & & & \end{array} \qquad (2.6)$$

This form of the $G_{\alpha\beta}$ array, which is the transpose of the more usual form, results from the use of tensor as opposed to matrix multiplication.

On the other hand, when σ assumes the value t $\left[C^c_\sigma \frac{\partial C^\gamma_c}{\partial x^\beta} - C^b_\beta \frac{\partial C^\gamma_b}{\partial x^\sigma} \right]$ will only have a non-zero value when $\beta \neq t$ for then the derivative $\frac{\partial C^\gamma_c}{\partial x^\beta}$ is always zero and the non-holonomic object is simply $-L_{\alpha\gamma} C^b_\beta \frac{\partial C^\gamma_b}{\partial x^t} \dot{x}^\alpha \dot{x}^t$. For this condition the equation of performance becomes the voltage equation so that from equation (2.4)

$$e_\beta = R_{\alpha\beta}\dot{x}^\alpha + L_{\alpha\beta}\frac{d\dot{x}^\alpha}{dt} - L_{\alpha\gamma}C^b_\beta\frac{\partial C^\gamma_b}{\partial x^t}\dot{x}^\alpha\dot{x}^t$$

Since $L_{\alpha\gamma}C^b_\beta \frac{\partial C^\gamma_b}{\partial x^t}$ will be the same as $L_{\alpha\gamma} C^c_\sigma \frac{\partial C^\gamma_c}{\partial x^t}$ already obtained as $G_{\alpha\beta}$ then the voltage equation can be written

$$e_\beta = R_{\alpha\beta}\dot{x}^\alpha + L_{\alpha\beta}\frac{d\dot{x}^\alpha}{dt} - G_{\alpha\beta}\dot{x}^\alpha\dot{x}^t \qquad (2.7)$$

Hence the equations of dynamic performance are now formulated in terms of the tensors $R_{\alpha\beta}$, $L_{\alpha\beta}$ and $G_{\alpha\beta}$. It remains to relate these to the actual machine so that they may be calculated to enable the dynamic performance to be predicted. It is proposed to obtain this relationship by means of the equivalent circuit.

Under steady state conditions assume the rotor to be stationary and the applied voltages to be balanced. Since $\dot{x}^t$ is zero, the voltage equation (2.7) reduces to

$$e_\beta = R_{\alpha\beta}\dot{x}^\alpha + L_{\alpha\beta}\frac{d\dot{x}^\alpha}{dt}$$

$$= (R_{\alpha\beta} + L_{\alpha\beta}p)i^\alpha$$

where p is the differential operator.

Assuming the current to be a sinusoidal function of time p may be replaced by $j\omega$, ω being the angular frequency of supply, so that

$$e_\beta = (R_{\alpha\beta} + j\omega L_{\alpha\beta})i^\alpha = Z_{\alpha\beta}i^\alpha$$

where $Z_{\alpha\beta}$ is the summation of the two tensors $R_{\alpha\beta}$ and $j\omega L_{\alpha\beta}$ restricting the index range to q,d, i.e. excluding t.

$$Z_{\alpha\beta} = \begin{array}{c|cccc} \alpha \backslash \beta & d_s & d_r & q_s & q_r \\ \hline d_s & j\omega L_s & j\omega M & & \\ d_r & j\omega M & j\omega L_r & & \\ q_s & & & j\omega L_s & j\omega M \\ q_r & & & j\omega M & j\omega L_r \end{array} + \begin{array}{c|cccc} \alpha \backslash \beta & d_s & d_r & q_s & q_r \\ \hline d_s & R_s & & & \\ d_r & & R_r & & \\ q_s & & & R_s & \\ q_r & & & & R_r \end{array}$$

$$\text{i.e.}\quad Z_{\alpha\beta} = \begin{array}{c|c|c|c|c|} {}_{\alpha}\diagdown^{\beta} & d_s & d_r & q_s & q_r \\ \hline d_s & R_s + j\omega L_s & j\omega M & & \\ \hline d_r & j\omega M & R_r + j\omega L_r & & \\ \hline q_s & & & R_s + j\omega L_s & j\omega M \\ \hline q_r & & & j\omega M & R_r + j\omega L_r \\ \hline \end{array}$$

Since this tensor in matrix form is symmetrical about its main diagonal, the equivalent circuit may be drawn immediately and is given in fig.(2.3) in which $M = k\sqrt{L_s L_r}$,k being the coupling coefficient between the stator and the rotor. Since $|v_{ds}| = |v_{qs}|$ for balanced supply voltages and since the circuit is symmetrical about the common connection,then v_{ds} and v_{qs} can be considered to be acting independently on the same circuit, i.e. the "per phase" equivalent circuit can be drawn as in fig.(2.4). Let the inductance of the stator winding due to its own leakage flux be l_s and that of the rotor winding due to its own leakage flux be l_r. Fig.(2.4) may then be redrawn as in fig.(2.5). If the effective transformation ratio stator/rotor is u then $j\omega(L_r - l_r)u^2 = j\omega(L_s - l_s)$ so that transforming all the rotor quantities the equivalent circuit becomes that of fig.(2.6) which,so far as the values of voltage,current, power and power factor are concerned,may be taken as the circuit of fig.(2.7) which is the usual per phase equivalent circuit of the polyphase induction motor referred to the stator.

Hence,if the parameters of this circuit can be determined and the value of u estimated,then the values of R_r ,R_s ,M ,L_r and L_s can be obtained and the tensors $R_{\alpha\beta}$,$L_{\alpha\beta}$ and $G_{\alpha\beta}$ constructed. Alternatively, if calculations are to be limited to external as opposed to internal properties of the machine,the tensors may be constructed in terms of the referred values of R_r ,l_r and M which in the usual representation of the equivalent circuit are R_2 ,L_2 and L_0; R_s and l_s being then R_1 and L_1 respectively.

That the construction of the tensors in terms of these referred values does not invalidate the calculation of machine performance using them, is most easily seen by expanding equations (2.5) and (2.7) after substitution of the $R_{\alpha\beta}$, $L_{\alpha\beta}$ and $G_{\alpha\beta}$ tensors.

Thus, equation (2.5) gives

$$T_a = F\dot{\theta} + J\ddot{\theta} + M(i_{qs}i_{dr} - i_{ds}i_{qr})$$

where T_a is the applied shaft torque,

and equation (2.7) gives

$$e_{ds} = R_s i_{ds} + L_s p i_{ds} + M p i_{dr}$$

$$e_{dr} = R_r i_{dr} + M p i_{ds} + L_r p i_{dr} - M p i_{qs} - L_r p i_{qr}$$

$$e_{qs} = R_s i_{qs} + L_s p i_{qs} + M p i_{qr}$$

$$e_{qr} = R_r i_{qr} + M p i_{qs} + L_r p i_{qr} + M p i_{ds} + L_r p i_{dr}$$

Reference to fig.(2.7) shows that for a transformation ratio u ,

M becomes Mu

R_r " " $R_r u^2$

L_r " " $L_r u^2$

i_{dr}" " i_{dr}/u

i_{qr}" " i_{qr}/u

the other quantities remaining unchanged.

Hence, by substitution of these referred values in the torque and voltage equations above, it is seen that e_{ds} and e_{qs} are unaltered, e_{dr} and e_{qr} become $e_{dr}u$ and $e_{qr}u$, respectively. But, in the squirrel cage motor both e_{dr} and e_{qr} are zero so that their equations are effectively unchanged. This means that i_{qs} and i_{ds} will still be the same as also will be the equation for T_a. Consequently, the overall calculated performance is unaffected by the use of the referred values.

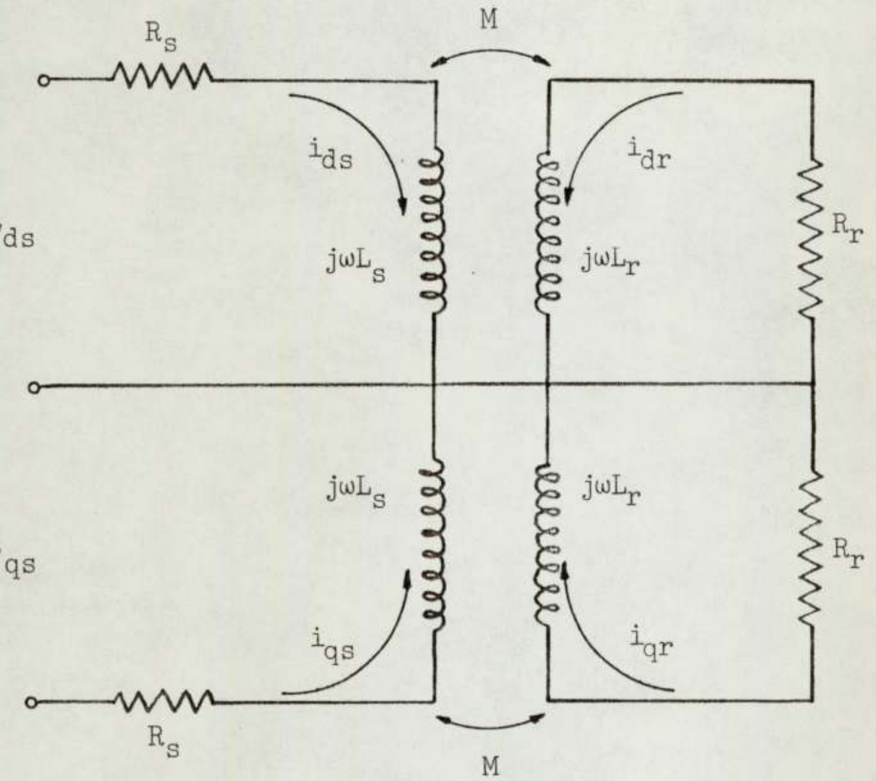

FIG. (2.3). EQUIVALENT CIRCUIT FOR IMPEDANCE TENSOR $Z_{\alpha\beta}$.

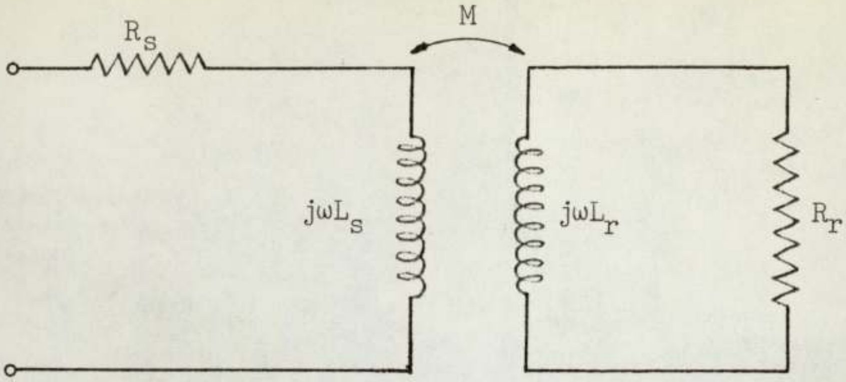

FIG. (2.4). PER PHASE EQUIVALENT CIRCUIT FOR IMPEDANCE TENSOR $Z_{\alpha\beta}$

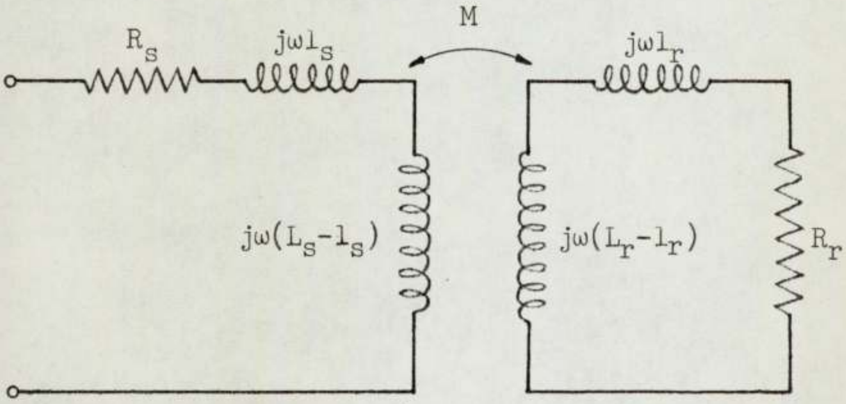

FIG. (2.5). CIRCUIT OF FIG. (2.4) MODIFIED TO INCLUDE LEAKAGE INDUCTANCES.

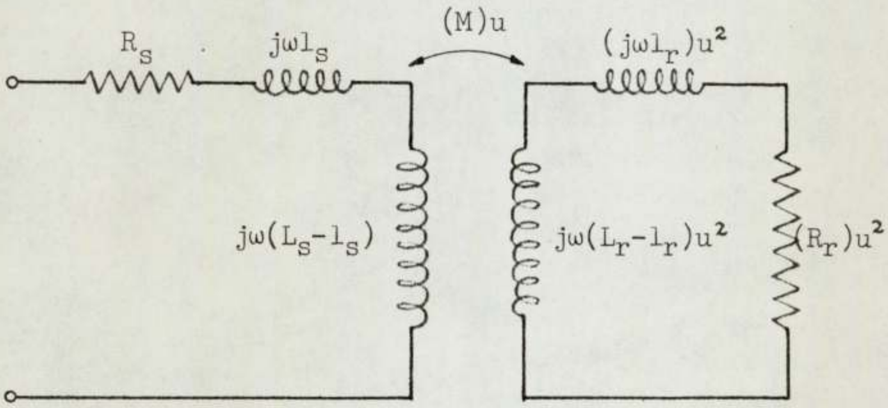

FIG. (2.6). CIRCUIT OF FIG. (2.5) WITH TRANSFORMED ROTOR PARAMETERS.

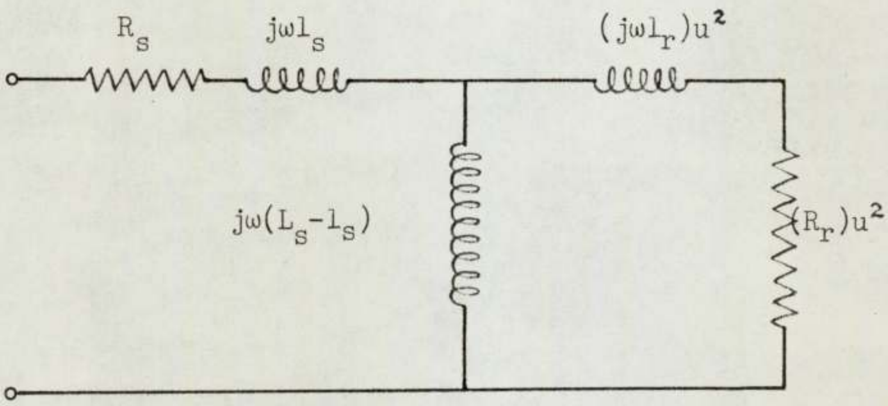

FIG. (2.7). FINAL FORM OF PER PHASE EQUIVALENT CIRCUIT WITH LEAKAGE AND MAGNETISING INDUCTANCES.

Effect of space harmonics:

If the machine is such that the stator magnetomotive force wave contains appreciable harmonic components, the foregoing analysis still holds in principle but requires extending to include their effects. Kron in his work on tensor analysis[22] only mentions the possibility of including space harmonics but offers no contribution as to the manner of handling them. In his book on the equivalent circuits of electrical machinery[23], however, he does deal with space harmonics but on the assumption that each harmonic can be considered as operating in a separate machine all of which may be subsequently interconnected. Since the harmonics are, in fact, all generated by the same winding this assumption is, in the author's opinion untenable. In addition, for the squirrel cage rotor he considers each bar as a separate pole phase group capable of causing a harmonic flux which subsequently affects the stator conditions. As the rotor slots are almost invariably skewed this seems to be an unnecessary complication, for the effect of the skew will be to make the rotor appear more like a homogeneous component, from the stator point of view, than it would were the slots not skewed. On these grounds, the rotor magnetomotive force wave can be assumed to be identical to that of the stator. This being so, each harmonic component of the stator magnetomotive force wave can, if the machine is magnetically linear, be treated separately remembering that they are all generated by the same winding as already observed; the actual harmonic content can, of course, be determined by a simple Fourrier analysis of the stator waveform obtainable from the design details of the machine. The need for the machine to be magnetically linear is realized in the case of the miniature induction motor for servosystem application since they are so designed.

The non-holonomic primitive of fig.(2.1) is representative of an actual machine having any number of pole pairs. The effect of the number of pole pairs becomes evident in the transformation from non-holonomic to holonomic axes, fig.(2.2), for in these axes the angle θ between the D and Q axes and the rotor axes must be interpreted as an electrical angle $P_n\theta$, where P_n is the number of pole pairs and θ is the mechanical angle through which the rotor axes are transformed, when setting up the relationships between the currents in the two systems. If Kron's assumption,(23) that harmonic fluxes having different numbers of pole pairs do not interact, is accepted, then in the primitive model each harmonic could be represented by a separate pair of rotor coils having no mutual coupling with any other pair of rotor coils. This is, however, untenable and unnecessary.

Thus, consider a machine whose stator magnetomotive force wave has a fundamental, third and fifth harmonic component. The non-holonomic primitive model of this machine will be as shown in fig.(2.8); it consists of three coexisting primitive forms, one for each component of the magnetomotive force. All coils on the same axis are mutually coupled.

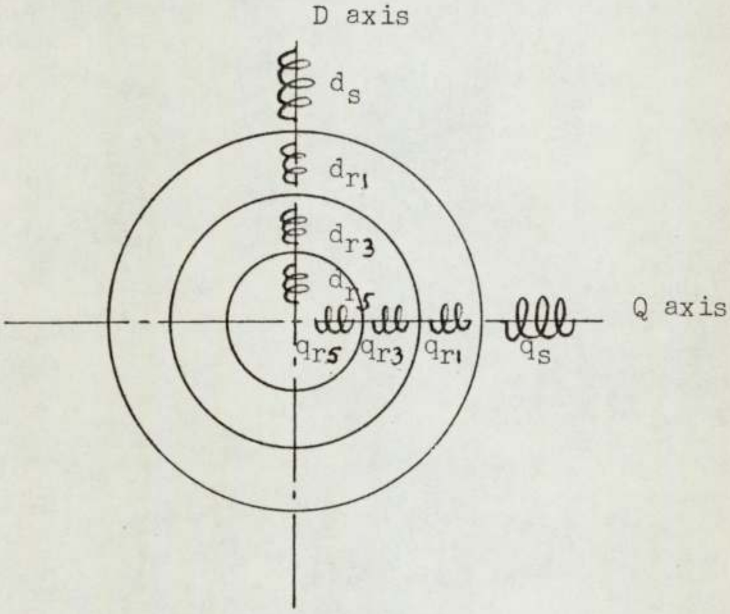

FIG. (2.8). NON-HOLONOMIC PRIMITIVE OF MACHINE WITH SPACE HARMONICS.

The corresponding holonomic primitive is given in fig.(2.9) in which it is seen that the angles between the D,Q axes and the various rotor coils are electrical and, therefore, functions of the number of poles in the particular harmonic field, and that cognizance is taken of the fact that some harmonic fields are contrarotating.(24) In the rotor coil designation the first number in the suffix relates to the order of the harmonic, the second to the rotor axis. With these models established, the foregoing analysis of the machine without harmonics may be followed and the resistance tensor and metric tensor written by inspection as,

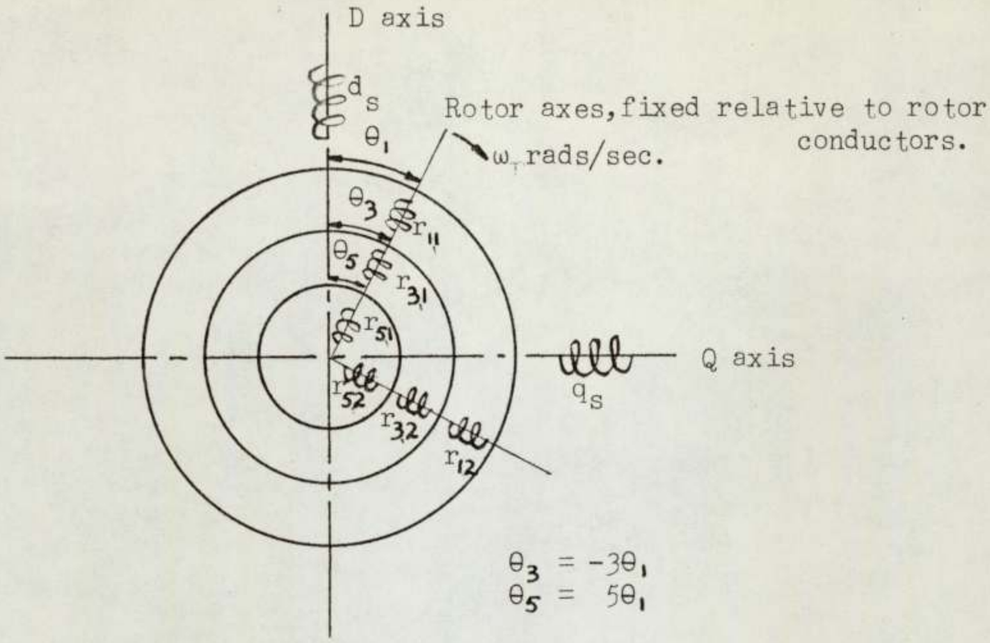

FIG. (2.9). HOLONOMIC PRIMITIVE OF MACHINE WITH SPACE HARMONICS.

$R_{\alpha\beta} =$

$\alpha \backslash \beta$	d_s	d_{r1}	d_{r3}	d_{r5}	q_s	q_{r1}	q_{r3}	q_{r5}	t
d_s	R_s								
d_{r1}		R_{r1}							
d_{r3}			R_{r3}						
d_{r5}				R_{r5}					
q_s					R_s				
q_{r1}						R_{r1}			
q_{r3}							R_{r3}		
q_{r5}								R_{r5}	
t									F

$L_{\alpha\beta} =$

$\alpha \backslash \beta$	d_s	d_{r1}	d_{r3}	d_{r5}	q_s	q_{r1}	q_{r3}	q_{r5}	t
d_s	L_s	M_1	M_3	M_5					
d_{r1}	M_1	L_{r1}	M_{13}	M_{15}					
d_{r3}	M_3	M_{31}	L_{r3}	M_{35}					
d_{r5}	M_5	M_{51}	M_{53}	L_{r5}					
q_s					L_s	M_1	M_3	M_5	
q_{r1}					M_1	L_{r1}	M_{13}	M_{15}	
q_{r3}					M_3	M_{31}	L_{r3}	M_{35}	
q_{r5}					M_5	M_{51}	M_{53}	L_{r5}	
t									J

From fig.(2.9), the relationships between the derived variables, i.e. the currents, using non-tensor indices are

$$i_{dr1} = i_{r11}\cos\theta_1 - i_{r12}\sin\theta_1$$

$$i_{qr1} = i_{r11}\sin\theta_1 + i_{r12}\cos\theta_1$$

$$i_{dr3} = i_{r31}\cos3\theta_1 + i_{r32}\sin3\theta_1$$

$$i_{qr3} = i_{r32}\cos3\theta_1 - i_{r31}\sin3\theta_1$$

$$i_{dr5} = i_{r51}\cos5\theta_1 - i_{r52}\sin5\theta_1$$

$$i_{qr5} = i_{r51}\sin5\theta + i_{r52}\sin5\theta_1$$

from which the transformation tensor C_b^{γ} given by $\dfrac{\partial i^{\gamma}}{\partial i^{b}}$ in the equation $i^{\gamma} = C_b^{\gamma} i^{b}$ is obtained, again remembering that θ_1 must be reckoned negative (page 35), as

$$C_b^{\gamma} = \begin{array}{c|ccccccccc} {}_{\gamma}\diagdown^{b} & d_s & r11 & r31 & r51 & q_s & r12 & r32 & r52 & t \\ \hline d_s & 1 & & & & & & & & \\ d_{r1} & & \cos\theta_1 & & & & \sin\theta_1 & & & \\ d_{r3} & & & \cos3\theta_1 & & & & \bar{\sin}3\theta_1 & & \\ d_{r5} & & & & \cos5\theta_1 & & & & \sin5\theta_1 & \\ q_s & & & & & 1 & & & & \\ q_{r1} & & \bar{\sin}\theta_1 & & & & \cos\theta_1 & & & \\ q_{r3} & & & \sin3\theta_1 & & & & \cos3\theta_1 & & \\ q_{r5} & & & & \bar{\sin}5\theta_1 & & & & \cos5\theta_1 & \\ t & & & & & & & & & 1 \end{array}$$

Since this is again simply a function of the mechanical angle θ_1 between the D,Q axes and the axes fixed relative to the rotor conductors, equation (2.4) will still apply and the non-holonomic object contained, therein, will again reduce to $L_{\alpha\gamma} A_{\sigma}^{\gamma}\dot{x}^{\alpha}\dot{x}^{\sigma}$ where $A_{\sigma}^{\gamma} = C_{\sigma}^{c}\dfrac{\partial C_c^{\gamma}}{\partial x^{\beta}}$.
When β takes the value t, x^{β} is the angle θ_1 mechanical being in this sense the angle of transformation from non-holonomic to holonomic axes. The partial differentiation of C_c^{γ} involved in obtaining A_{σ}^{γ} is, therefore, with respect to this mechanical angle and not the electrical ones. Carrying out this differentiation, remembering that C_c^{γ} is of the same form as C_b^{γ} gives,

$\frac{\partial}{\partial \theta} C_c^{\gamma} =$

$\gamma \backslash c$	d_s	r_{11}	r_{31}	r_{51}	q_s	r_{12}	r_{32}	r_{52}	t
d_s									
d_{r1}		$-\sin\theta_1$				$\cos\theta_1$			
d_{r3}			$-3\sin 3\theta_1$				$-3\cos 3\theta_1$		
d_{r5}				$-5\sin 5\theta_1$				$5\cos 5\theta_1$	
q_s									
q_{r1}		$-\cos\theta_1$				$-\sin\theta_1$			
q_{r3}			$3\cos 3\theta_1$				$-3\sin 3\theta_1$		
q_{r5}				$-5\cos 5\theta_1$				$-5\sin 5\theta_1$	
t									

The tensor C_{σ}^{c} is the inverse of the tensor C_{c}^{σ} identical to C_{b}^{γ} .By taking C_{b}^{γ} as a two rowed,doubly compounded tensor the inverse C_{σ}^{c} is obtained as

$C_{\sigma}^{c} =$

$\sigma \backslash c$	d_s	r_{11}	r_{31}	r_{51}	q_s	r_{12}	r_{32}	r_{52}	t
d_s	1								
d_{r1}		$\cos\theta_1$				$\sin\theta_1$			
d_{r3}			$\cos 3\theta_1$				$-\sin 3\theta_1$		
d_{r5}				$\cos 5\theta_1$				$\sin 5\theta_1$	
q_s					1				
q_{r1}		$-\sin\theta_1$				$\cos\theta_1$			
q_{r3}			$\sin 3\theta_1$				$\cos 3\theta_1$		
q_{r5}				$-\sin 5\theta_1$				$\cos 5\theta_1$	
t									1

Hence,forming the product of the two tensors above,

$A_{\sigma}^{\gamma} =$

$\gamma \backslash \sigma$	d_s	d_{r1}	d_{r3}	d_{r5}	q_s	q_{r1}	q_{r3}	q_{r5}	t
d_s									
d_{r1}						1			
d_{r3}							-3		
d_{r5}								5	
q_s									
q_{r1}		-1							
q_{r3}			3						
q_{r5}				-5					
t									

from which the torque tensor $G_{\alpha\beta}$ as the product $L_{\alpha\gamma}A^{\gamma}_{\sigma}$,replacing the dummy index σ by β becomes

$G_{\alpha\beta} =$

$\alpha \backslash \beta$	d_s	d_{r1}	d_{r3}	d_{r5}	q_s	q_{r1}	q_{r3}	q_{r5}	t
d_s						M_1	$-3M_3$	$5M_5$	
d_{r1}						L_{r1}	$-3M_{13}$	$5M_{15}$	
d_{r3}						M_{31}	$-3L_{r3}$	$5M_{35}$	
d_{r5}						M_{51}	$-3M_{53}$	$5L_{r5}$	
q_s		$-M_1$	$3M_3$	$-5M_5$					
q_{r1}		$-L_{r1}$	$3M_{13}$	$-5M_{15}$					
q_{r3}		$-M_{31}$	$3L_{r3}$	$-5M_{35}$					
q_{r5}		$-M_{51}$	$3M_{53}$	$5L_{r5}$					
t									

The tensors $R_{\alpha\beta}$,$L_{\alpha\beta}$ and $G_{\alpha\beta}$ may be substituted in equations (2.5)and (2.7) to give the required equations of dynamic performance for the machine with space harmonics. As before,it is now proposed to relate the three tensors to the actual machine through an equivalent circuit.

Thus,under steady state conditions with the rotor stationary and balanced applied voltages,the tensor $Z_{\alpha\beta}$ may again be obtained by summing the tensors $R_{\alpha\beta}$ and $j\omega L_{\alpha\beta}$and excluding the index t giving,

$Z_{\alpha\beta} =$

α \ β	d_s	d_{r1}	d_{r3}	d_{r5}	q_s	q_{r1}	q_{r3}	q_{r5}
d_s	$R_s + j\omega L_s$	$j\omega M_1$	$j\omega M_3$	$j\omega M_5$				
d_{r1}	$j\omega M_1$	$R_{r1} + j\omega L_{r1}$	$j\omega M_{13}$	$j\omega M_{15}$				
d_{r3}	$j\omega M_3$	$j\omega M_{31}$	$R_{r3} + j\omega L_{r3}$	$j\omega M_{35}$				
d_{r5}	$j\omega M_5$	$j\omega M_{51}$	$j\omega M_{53}$	$R_{r5} + j\omega L_{r5}$				
q_s					$R_s + j\omega L_s$	$j\omega M_1$	$j\omega M_3$	$j\omega M_5$
q_{r1}					$j\omega M_1$	$R_{r1} + j\omega L_{r1}$	$j\omega M_{13}$	$j\omega M_{15}$
q_{r3}					$j\omega M_3$	$j\omega M_{31}$	$R_{r3} + j\omega L_{r3}$	$j\omega M_{35}$
q_{r5}					$j\omega M_5$	$j\omega M_{51}$	$j\omega M_{53}$	$R_{r5} + j\omega L_{r5}$

Since this tensor is symmetrical about its main diagonal, it may be represented as an equivalent circuit, fig. (2.10), which corresponds to that of fig. (2.4).

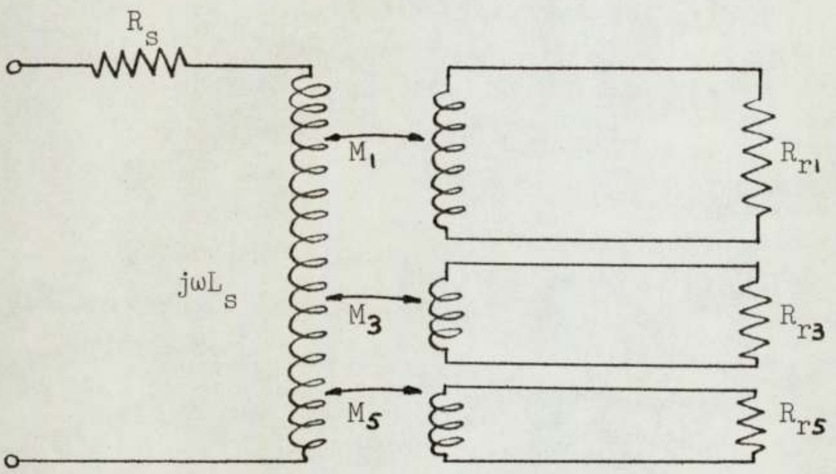

FIG. (2.10). PER PHASE EQUIVALENT CIRCUIT FOR IMPEDANCE TENSOR $Z_{\alpha\beta}$ FOR MACHINE WITH SPACE HARMONICS.

By the same process as that applied to the circuit of fig. (2.4), this circuit can, assuming the stator leakage inductance to have the same value for all the harmonics since it is a function of the geometry and the machine is unsaturated, be reduced to that shown in fig. (2.11), corresponding to fig. (2.7), in which u_1, u_3 and u_5 are the harmonic transformation ratios. In so doing it is assumed that the coupling between the rotor coils on a given axis is ideal (see appendix B).

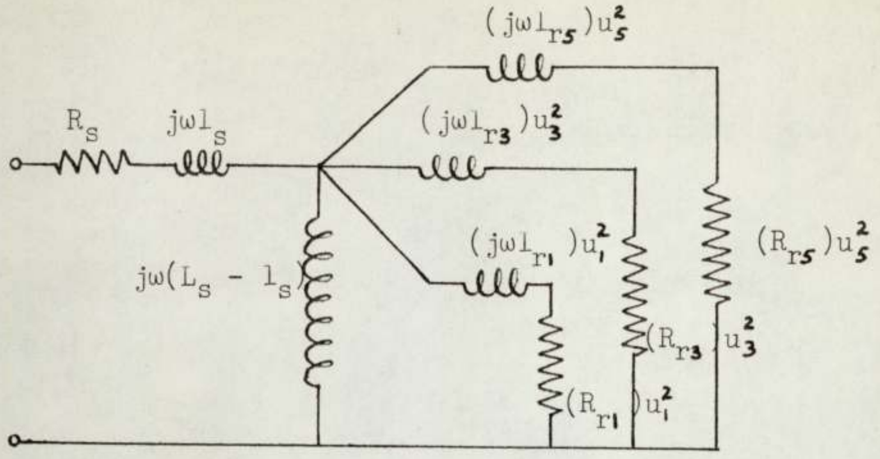

FIG. (2.11). FINAL FORM OF PER PHASE EQUIVALENT CIRCUIT WITH LEAKAGE AND MAGNETISING INDUCTANCES FOR MACHINE WITH SPACE HARMONICS.

As for the machine without harmonics, if the parameters of this circuit can be determined and the values of u_1, u_3, and u_5 estimated then the values of $R_s, R_{r1}, R_{r3}, R_{r5}, L_s, L_{r1}, L_{r3}, L_{r5}$ can be obtained and the resistance, metric and torque tensors constructed. Alternatively, for external calculations only, the referred values of the parameters may be used to construct the tensors as already explained.

It should be noted that in this equivalent circuit the total rotor power is the torque in synchronous watts per phase. To obtain the torque in Newton-metres each harmonic component of the rotor power must be divided by its own synchronous speed, bearing in mind the direction of rotation of the particular harmonic field.

This equivalent circuit differs from that proposed by Alger (36) in that he starts by representing each harmonic by a separate magnetizing reactance all of which are connected in series across the phase supply. Such a representation is not acceptable since it does not recognize the fact that all the harmonic fields are produced by one and the same current in one winding. Furthermore, with such a representation it is not possible to construct the metric tensor since a group of series connected mutual inductances on the stator side, which are presupposed by the series connected magnetizing reactances, cannot be interpreted in terms of the primitive machine. It would appear that to commence the construction of an equivalent circuit from the concept of the fictitious magnetizing reactance is an unsound practice.

CHAPTER III.

Design Procedure and Measuring Equipment.

4) Design of Test Machine, General Design Procedure.

The design of an electrical machine is usually carried out to meet a particular performance specification. The procedure can be broken down into five main sections, viz:

a) Tentative proportioning of the machine.

b) Calculation of machine parameters.

c) Calculation of machine performance using estimated parameters.

d) Comparison of calculated performance with specified performance.

e) Adjustment of machine proportions if necessary.

It was shown in the last chapter that the design of the induction motor to meet a dynamic specification can be based on the steady state equivalent circuit parameters, since the components of the impedance tensor, which is required in order to be able to calculate dynamic performance, can mostly be derived from these. The procedure will obviously remain as given above. The main differences between design for steady state and design for dynamic performances will occur in sections (c) and (e). The change in section (c) has been dealt with in chapter II; this present section deals with the essence of section (e).

In order to be able to make an effective adjustment of machine dimensions from the point of view of machine performance, it is necessary to know in what way the change of dimension will influence performance. Since this performance is calculated in terms of the impedance tensor, which is in turn related to the equivalent circuit parameters of the machine, to know the influence of a dimension on performance breaks down into knowing the influence of that dimension on the parameters and the influence of the parameters on performance. This latter influence can be obtained from the analysis given in chapter II so that attention will now be restricted to the former of these influences.

The influence of a machine dimension on parameters is best seen in the calculation of the parameters in terms of the dimensions. Various methods have, over the years, been developed for carrying out these estimations but only for a limited range of machine size and performance. The range of size did not include the miniature machine and the range of performance did not properly include dynamic performance. Thus, in the case of the induction motor, the fact that the estimated parameters might predict a correct steady state performance does not prove that these parameter values are correct in themselves. For these reasons the methods of calculation at present available cannot be assumed to apply to the design of a miniature machine to meet a dynamic specification. Consequently, the estimation of the parameters of the miniature machine must be approached fundamentally.

This investigation is limited to the polyphase induction motor and, although in the overall programme of work it is intended to examine machines having 2, 6 and 8 poles, only the two pole machine is considered here. The frame chosen is size 15. The machine was designed for operation from a 115 volt/phase, 400Hz., 2 phase supply to meet a steady state specification. In this case then, the parameters are calculated from already fixed dimensions, the influences of the machine dimensions on the parameters should nevertheless be apparent. The subject of this section is the formulation of these methods of calculation for the miniature induction motor; the construction of the impedance tensor is given in chapter VI, section 21. The parameters to be calculated are the stator winding resistance R_1, the rotor winding resistance referred to the stator R_2, the magnetising inductance referred to the stator L_0, the stator leakage inductance L_1, and the rotor leakage inductance referred to the stator L_2.

The principal quantity in any rotating electrical machine is the mutual, or in machine parlance, the airgap flux since it is through the mechanism of this that energy is transferred from the stator to the rotor and hence transformed from electrical to mechanical energy or vice-versa.

Whether the machine's performance is calculated in terms of this flux and the component currents or in terms of the parameters and the currents is a matter of choice and convenience and ,as should by now be apparent, the author's choice is that of analysis in terms of the impedance tensor because of its generality and the ease with which it handles the problem of varying speed. The commencement, therefore, of any design must be a statement of the mutual coupling, in whatever terms suit, between the stator and the rotor. In most squirrel cage induction motors it is assumed that the space function of the resultant magnetomotive force giving rise to the airgap flux is, if magnetic saturation is ignored, sinusoidal. This is because the stator winding has a sufficient number of slots to enable the designer to make the stator magnetomotive force a sinusoidal function of space and because the squirrel cage rotor has a sufficient number of bars for it to be able to generate a magnetomotive force which, as a function of space, is dictated by the stator magnetomotive force. The design of the machine is then carried through in terms of the peak space value and the mean space value of the airgap flux density. Obviously, for a sinusoidal space function these two values have the ratio B_{peak}/B_{mean} of 1.57. When saturation is present, as is almost always the case in the larger [25] machines, this factor changes to a smaller value. The miniature induction motor intended for servosystem application is deliberately wound to keep the flux density low in order that the torque/signal voltage characteristic shall be linear. Consequently, the value of 1.57 should be taken.

Countering this simplification, the slotting in the miniature machine is very restricted, the 8 pole size 15 having only one slot/pole/phase. This means that the stator magnetomotive force cannot be taken as a simple sinusoidal function of space. To allow for this the design procedure given herein is really founded upon aFourier analysis of this space waveform. Each component of the stator magnetomotive force is, if it is appreciable, then treated separately based on the extension to Kron's analysis presented in chapter II.

The dimensions of the test machine are given on page 57 and the stator and rotor lamination and slot details are shown in figs.(3.1)&(3.2), respectively. Because the machine was already wound, the calculations do not commence with an assumed gap flux density, as would be the case if the winding were to be decided upon, but with the determination of the stator winding resistance. The formula used for this is empirical and is based on previous experience. Following this the electric loading diagram is constructed and the stator magnetomotive force distribution obtained as the space integral of this loading. This is done for two extreme cases of excitation and in each case the Fourier analysis of the magnetomotive force waveform is obtained.

The winding factor for the stator is then determined in the usual manner; it could equally well have been calculated from the Fourier coefficients. Since the waveform analyses indicated that, for this machine, the harmonic content was negligible the winding factor for the fundamental only is calculated. The same remark applies to the ensuing calculations but for those parameters which change for space harmonics, the methods of calculation used are designed to enable the harmonic parameter values to be obtained by the same method.

The next item to be estimated was the rotor winding resistance per phase referred to the stator. The method used here is based on one given in Trickey's[26] paper but is made more general and more fundamental in order to elucidate dimensional sensitivity and to allow extension to harmonic rotor resistances since, as shown in chapter II, the rotor resistance is one of the parameters which changes with harmonic order; this extension is given at the end of the section. Taken as a whole, this method is a contribution to the existing knowledge.

Another departure from existing techniques is the determination of the magnetising inductance per phase referred to the stator. Since, in the equivalent circuitthis inductance is made common to all branches of the rotor circuit, it need only be obtained for the fundamental component of the magnetomotive force. Because of the magnetic linearity of the machine this value is independent of the airgap flux and use is made of this fact. In addition, in determining the effective gap length, Binns's [27] work on doubly slotted structures was applied.

The estimation of the stator leakage inductance is of paramount importance in this work, as will be apparent ultimately. It was decided that the usual approaches based on the slot leakage flux for a slot facing a plain iron boundary would be inadequate for this type of machine. The method put forward by Binns [27] for a double slot was investigated but was found to be in error in that Binns had taken the term $\frac{s_1' s_2'}{\delta}$ to be dimensionless whereas it obviously is not. Since the formulae given by Binns were obtained from empirical results on a given system using a curve fitting process, and were therefore true for a system of those particular dimensions, it was considered feasible to introduce a scaling factor y into the errant term so relating the dimensions of Binns's experimental system to a system of any other dimensions. This was in fact done and although Binns's work was carried out on a system representative of much larger machines, the results appear to be satisfactory for this miniature machine.

The estimation of the slot leakage permeance for the relatively large, tapered, round bottomed slot could not, it was felt, be based on existing methods using empirical or approximate curves intended for slots of quite different proportions. For this reason the slot permeance was calculated absolutely. The calculation was lengthy but gives an accurate formula which has not been presented before. In addition to this it was also felt necessary to make as accurate as possible an assessment of the overhang leakage permeance. Owing to the relatively large endwinding section, this assessment is made using an experimental flux plot in which the endwinding is represented as a distributed source. To take account of the very close proximity of the endwinding to the core, two flux plots were made, one for the endwinding opposite a stator slot and the other for the endwinding opposite a stator tooth. An average overhang permeance factor was then calculated.

The various leakage permeances are summed to give a total leakage permeance factor whereby the leakage inductance is calculated. The whole process clearly indicates the dimensional sensitivity and independence of harmonic order,as is pointed out at the end of the section,and forms another contribution to the existing knowledge.

A similar treatment is accorded to the rotor leakage permeance which is required in order to estimate the rotor leakage inductance referred to the stator. The usual procedures for obtaining this inductance from a permeance factor appear to overlook the fact that,for a squirrel cage winding there exist mutual couplings between circuits formed by various combinations of two rotor bars,which do not exist in other types of windings. This was brought to light when rotor leakage inductances calculated by conventional methods were compared with the values obtained by the experimental techniques using the impedance locus presented in this thesis;the calculated values were very much lower than the measured ones.

To overcome this,an entirely new method of calculating the rotor leakage inductance from the permeance factor is put forward. This is based on the concept of a loop current existing in the circuit formed by two adjacent rotor bars and takes fully into account the mutual couplings referred to above. To arrive at the value of this inductance referred to the stator,a similar technique to that used for the rotor resistance is employed. As in the case of the resistance,the referred rotor leakage inductance is seen to be a parameter which is very dependent upon harmonic order. The method of calculation is such that the values of the harmonic rotor leakage inductances can readily be determined,as shown at the end of the section. This estimation of the rotor leakage inductance also forms a contribution to the science of electrical machine design.

The presence of the additional mutual couplings is again manifest in the determination of the effects of rotor bar skew and has,hitherto been overlooked in this context also. The approach given herein is quite original and makes allowance for the extra couplings.

Following the notes on the changes to the mechanical arrangements of the motor to make it suitable as a test machine, are details of the modifications to the calculations of the rotor resistance and leakage inductance to obtain the harmonic parameters. The results of these modified calculations show that the harmonic parameters can be given in terms of those for the fundamental component. To do this, two new ratios, the harmonic resistance ratio and the harmonic leakage inductance ratio are presented as a further original contribution, as is also the effect of skew on these factors giving the skew modified rotor harmonic resistance and inductance ratios.

Details of test machine:

Dimensions:

Core length, l = 1.83 cms. including end cheeks.

Laminations per stack = 46 araldite bonded.

Stacking factor = 94.5%, helical stagger - one slot pitch.

Active iron length, l_o = 1.73 cms.

Stator bore finish diameter, D = 1.27 cms.

Rotor finish diameter, d = 1.2598 cms.

Radial airgap. δ = 0.05 mm.

No. stator slots, n_1 = 16.

No. rotor slots, n_2 = 25.

Stator outside diameter = 3.432 cms.

Rotor inside diameter = 4.826 mm.

No. poles, $2p_1$ = 2.

Supply frequency, f = 400 Hz.

Synchronous speed, N_s = 24,000 rev./min.

Core material:

Core magnetic flux density not to exceed 0.5 Wb/m^2.

Stator and rotor cores to be of 0.0376 mm. permalloy B.

Laminations to be annealed in a reducing atmosphere, prior to stacking, in accordance with material manufacturer's specification. All subsequent

Dimensions as punched.
All dimensions cms.
Material:
Permalloy B:

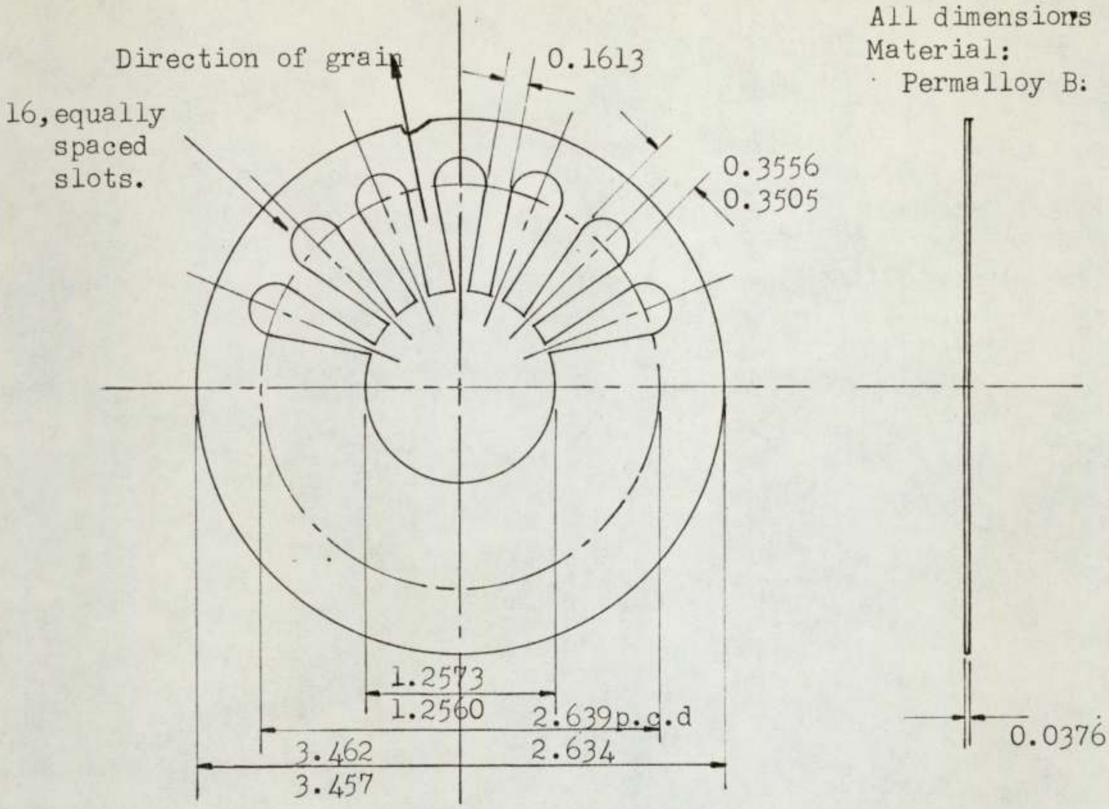

STATOR LAMINATION. SCALE, 2:1

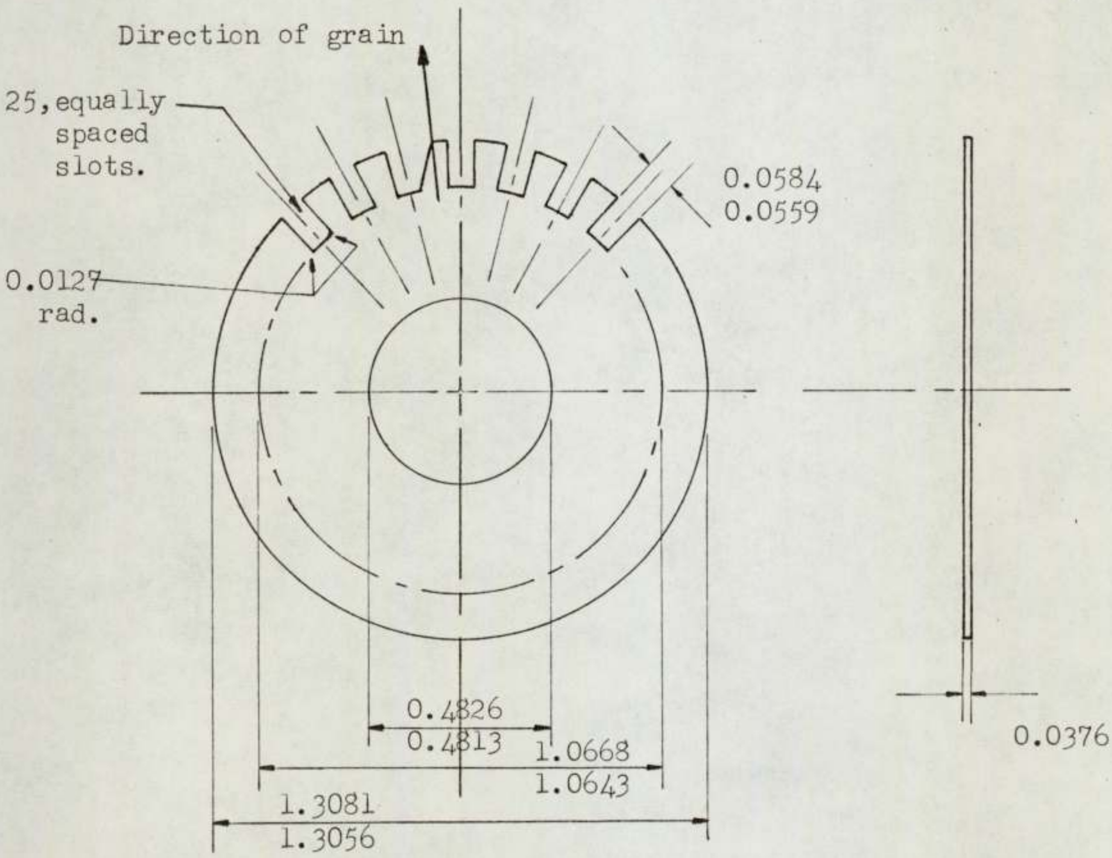

ROTOR LAMINATION. SCALE, 5:1

FIG. (3.1). STATOR AND ROTOR LAMINATIONS FOR TEST MACHINE.

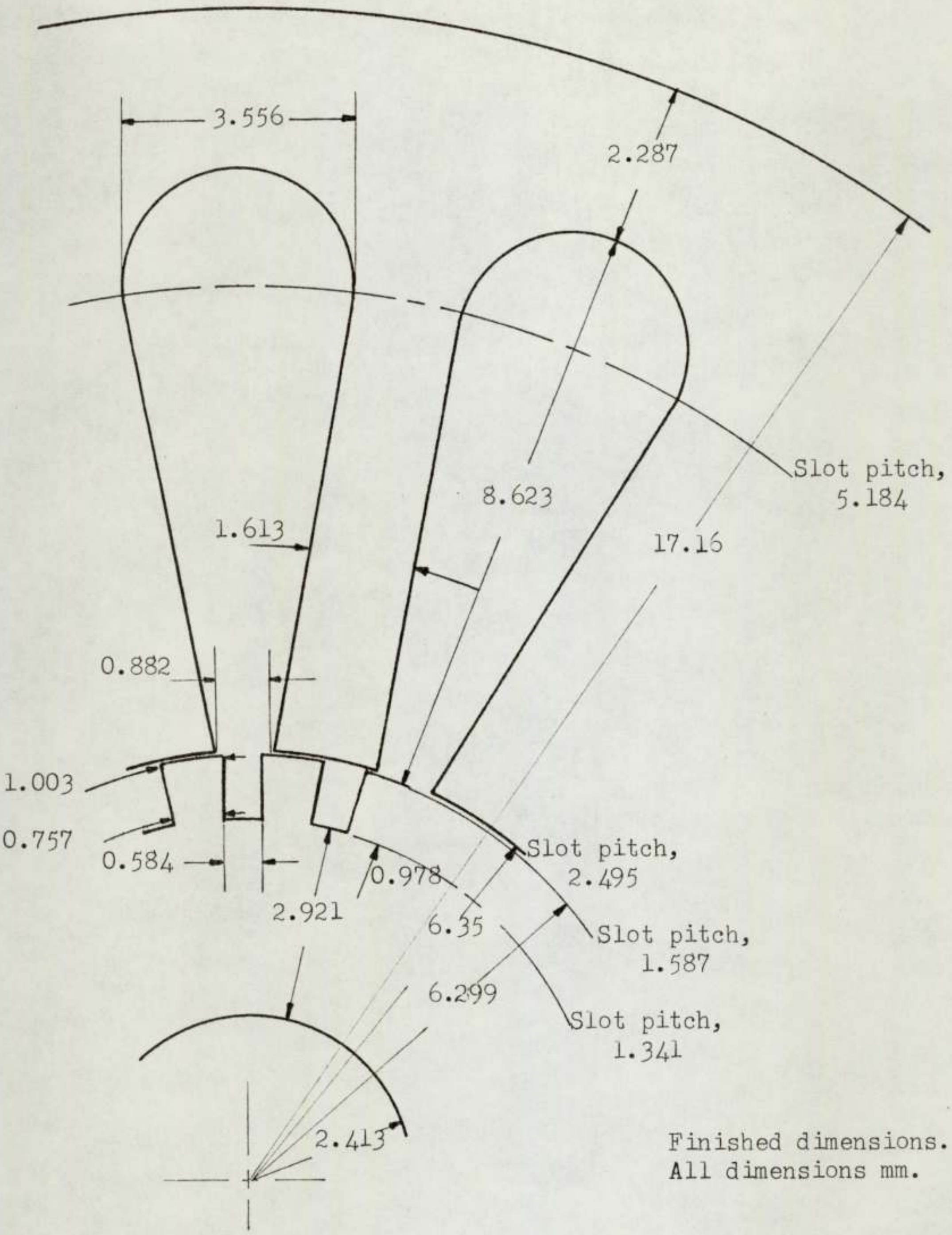

FIG. (3.2). STATOR AND ROTOR SLOT DETAIL. SCALE, 10:1.

operations to be performed with extreme care to avoid stressing or straining the annealed magnetic material.

Stator winding:

Balanced two phase. Two layer, one phase per layer, lapwound.

Reference phase voltage, V_R = 115 volts.

Control phase voltage, V_C = 0 - 115 volts.

No. slots/pole/phase, q_1 = 4

No. conductors/slot, c_1 = 176 x 2

No. conductors/phase, $2pq_1c_1$ = 2816, in series.

Coil pitch, slot 1 - slot 6 = 62.5%.

Total slot area, from fig. (3.2), = 20.2 mm.

Insulation; glass fibre wedges and end cheeks with P.T.F.E. tape slot liners and overhang wraps. Unimpregnated.

Available slot area for winding at 1/3 total area = 6.75 mm^2.

Current density = 5 amps/mm^2.

Copper section = 0.0137 mm^2 made up of 1 no. 39 s.w.g. enam.

Conductor diameter = 0.13208 insulated to 0.15494 mm.

Length of conductor, l_c = (coil throw in slot pitches x slot pitch on p.c.d.) + (2 x maximum slot width) + core length.

= 5 x 5.184 + 2 x 3.556 + 18.3

= 51.33 mm.

Length per phase, $2pq_1c_1l_c$ = 144.54 m.

$$\text{Resistance per phase } R_1 = \frac{1.561 \times 10^{-6} \times 144.54 \times 10^{2}}{0.0137 \times 10^{-2}}$$

i.e. R_1 = 164.7 ohms at 0°C.

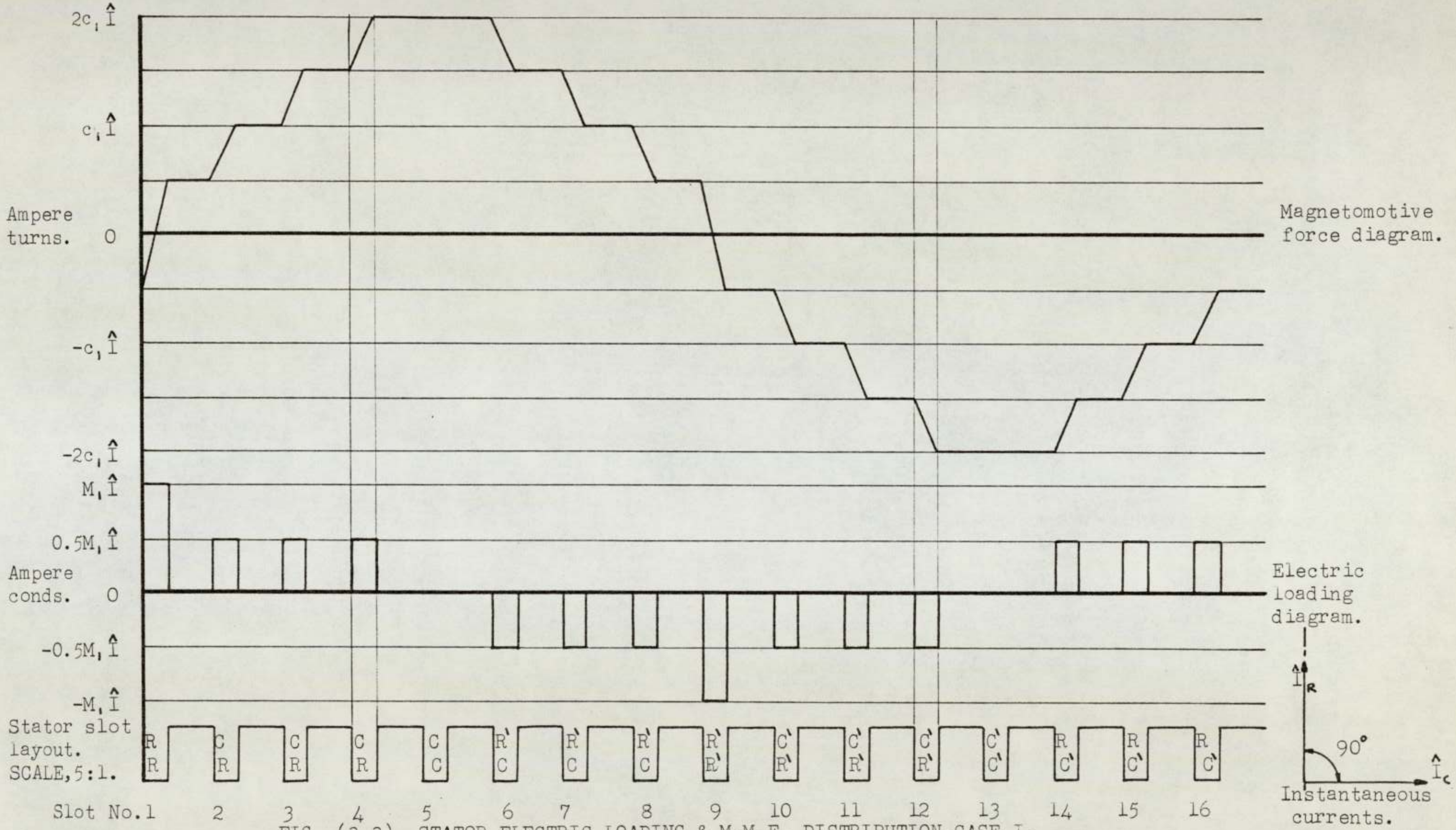

FIG. (3.3). STATOR ELECTRIC LOADING & M.M.F. DISTRIBUTION, CASE I.

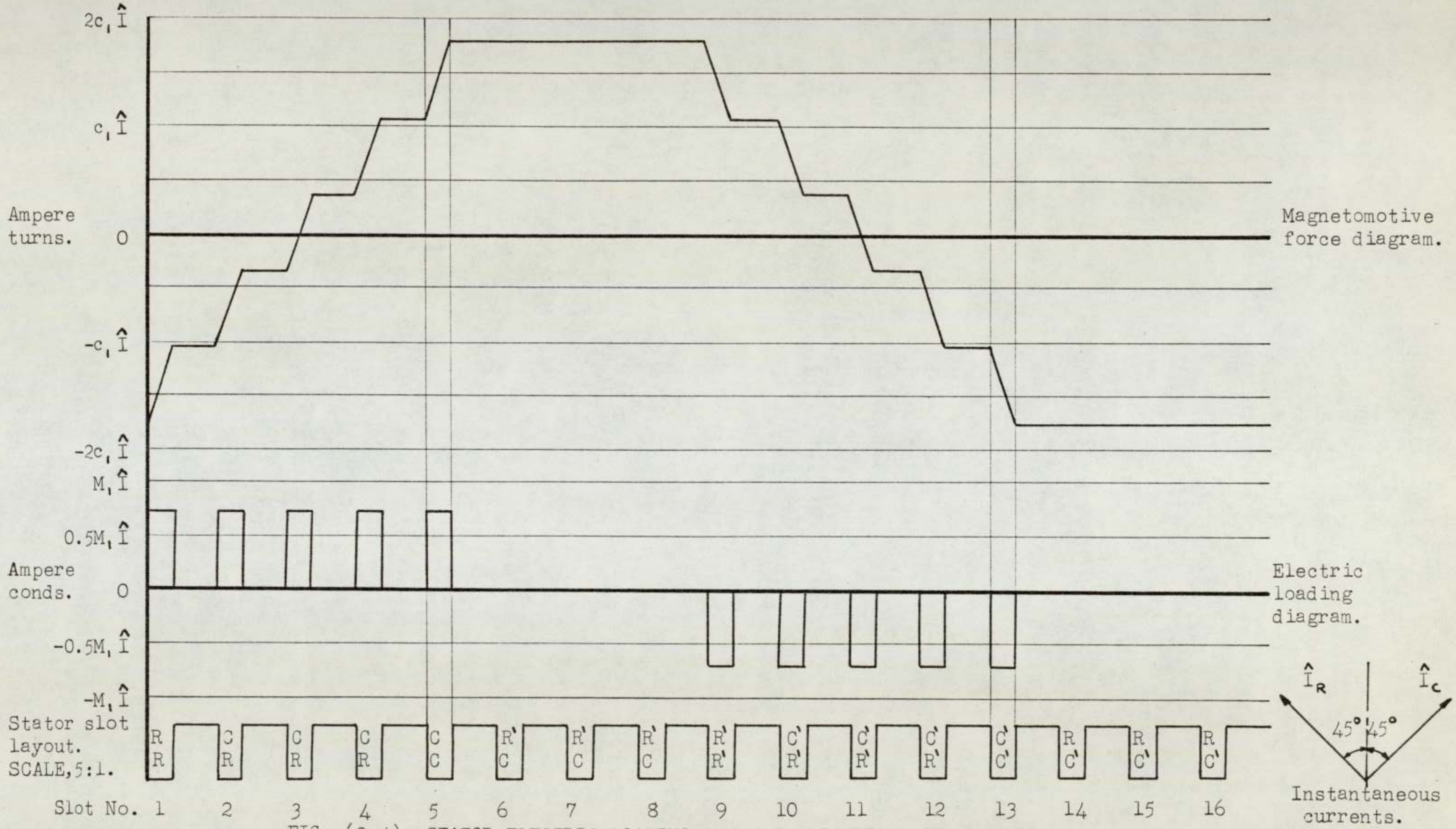

FIG. (3.4). STATOR ELECTRIC LOADING & M.M.F. DISTRIBUTION, CASE II.

Harmonic analysis of the stator magnetomotive force waves:

Consider the two extreme cases of excitation,(I) one phase current maximum,the other zero (II) both phase currents equal in magnitude. Figs. (3.3) and (3.4) give the winding distribution,electric loading and magnetomotive force diagrams for each of these cases,respectively,corresponding to the connection diagram of fig. (3.5); in these figures,R refers to the reference phase and C refers to the control phase.

In constructing the diagrams,it is assumed that the number of conductors along any radial line lying within the slot is the same at M_1 conductors per radius. The electric loading along these radii is then $M_1 I$ and zero elsewhere. The diagrams are drawn in the developed form and represent,to scale,conditions at the bore surface,the slot dimension being taken as that of its opening. The magnetomotive force diagram,which gives the magnetomotive force due to the stator winding acting along the closed path passing through the particular point on the stator periphery,is obtained by graphical integration along the stator periphery,of the electric loading curve.

The analyses of these magnetomotive force waveforms up to and including the sevevteenth harmonic,were obtained using a Stanley harmonic analyser and are given in tables (3.1) and (3.2). From these,the magnetomotive force as a function of the electrical θ round the bore of the machine is seen to be,

case (I)

$$\text{m.m.f.}_\theta = (3.85\sin\theta - 0.11\sin 3\theta + 0.19\sin 5\theta + 0.065\sin 7\theta + 0.045\sin 9\theta + 0.095\sin 11\theta - 0.035\sin 13\theta + 0.22\sin 15\theta + 0.19\sin 17\theta)0.5c_1\hat{I}.$$

case (II)

$$\text{m.m.f.}_\theta = (3.85\sin\theta + 0.10\sin 3\theta - 0.20\sin 5\theta + 0.075\sin 7\theta + 0.06\sin 9\theta - 0.09\sin 11\theta + 0.02\sin 13\theta + 0.21\sin 15\theta + 0.165\sin 17\theta)0.5c_1\hat{I}.$$

Examination of these two equations shows the fundamental to be the same in both cases at 3.85sin θ and the harmonic content to be maximum

Order of harmonic	Initial reading sin	Final reading sin	Coeff. sin	Initial reading cos	Final reading cos	Coeff. cos
1	1.983	2.368	3.850	0.341	0.341	0.000
3	1.458	1.447	- 0.110	0.418	0.418	0.000
5	1.558	1.577	0.190	0.352	0.352	0.000
7	1.593	1.606	0.065	0.259	0.259	0.000
9	1.692	1.701	0.045	0.367	0.367	0.000
11	2.005	2.024	0.095	0.434	0.432	- 0.010
13	2.102	2.095	- 0.035	0.316	0.315	0.005
15	1.784	1.828	0.220	0.397	0.392	- 0.025
17	1.867	1.905	0.190	0.440	0.438	- 0.010

All readings in cms., 1cm = $0.5c_1\hat{I}$. Trace period, 20.4cms.

TABLE (3.1). HARMONIC ANALYSIS OF STATOR M.M.F. SPACE WAVE, CASE I.

Order of harmonic	Initial reading sin	Final reading sin	Coeff. sin	Initial reading cos	Final reading cos	Coeff. cos
1	2.750	3.135	3.850	0.323	0.314	- 0.090
3	3.218	3.228	0.100	0.098	0.098	0.000
5	3.389	3.369	- 0.200	0.977	0.981	0.040
7	3.186	3.201	0.075	0.018	0.020	0.010
9	3.220	3.232	0.060	0.337	0.337	0.000
11	3.327	3.309	- 0.090	0.331	0.335	0.020
13	3.464	3.468	0.020	0.339	0.335	- 0.020
15	3.280	3.322	0.210	0.266	0.251	- 0.045
17	3.360	3.393	0.165	0.362	0.347	- 0.075

All readings in cms., 1cm = $0.5c_1\hat{I}$. Trace period, 20.4cms.

TABLE (3.2). HARMONIC ANALYSIS OF STATOR M.M.F. SPACE WAVE, CASE II.

for the fifteenth harmonic. Since the order of this is less than 6% that of the fundamental, the harmonics are not further considered. The cosine coefficients should theoretically all be zero and have been taken as such.

Stator winding connection and winding factors:

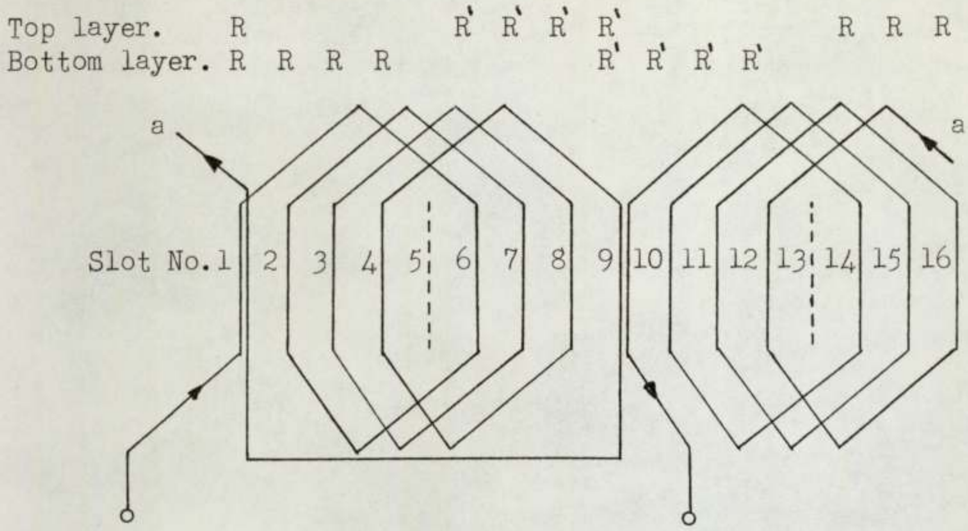

For control phase, advance by 90 elec. relative to slot number.

FIG. (3.5). STATOR CONNECTION DIAGRAM, REFERENCE PHASE ONLY.

Pitch factor:

$$\text{Pitch factor}, K_p = \cos\left[(1.0 - 0.625) \times \frac{180}{2}\right]$$

$$= \cos 33.75$$

$$= 0.833$$

Distribution factor:

$$\text{Distribution factor}, K_d = \frac{\sin \frac{360 \times 4}{16 \times 2}}{4 \sin \frac{360}{16 \times 2}}$$

$$= \frac{\sin 45}{4 \sin 11.25}$$

$$= \frac{0.7071}{4 \times 0.195}$$

$$= 0.906$$

Winding factor:

$$\text{Winding factor}, K_w = K_p K_d = 0.833 \times 0.906$$

$$\text{i.e. } K_w = 0.754$$

for space fundamental only.

Rotor winding:

Aluminium squirrel cage,centrifugally cast.

Specific resistance of cast aluminium $\rho_{al} = 2.69 \times 10^{-6}$ ohm/cm.cube at 0°C.

Temperature coefficient of cast aluminium $\alpha_{al} = 0.00445/^\circ$C in range 0 - 100°C.

Bar skew = two rotor slot pitches.

$$\text{Laminar rotation per lamination} = \frac{360 \times 2}{n_2 \times \text{rotor laminations}}$$

$$= \frac{360 \times 2}{25 \times 46}$$

$= 0.626^\circ$ (see fig. (3.6)).

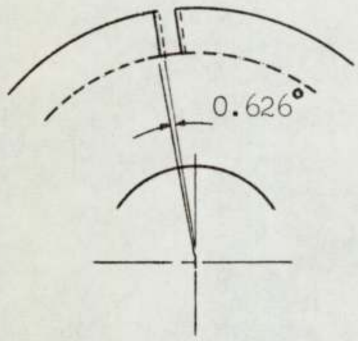

FIG. (3.6). ROTOR LAMINAR ROTATION,DUE TO SKEW.

Bar depth = 0.978 mm.

$$\text{Mean bar pitch circle radius} = \frac{\text{rotor outside dia. - bar depth}}{2}$$

$= 6.299 - 0.489$

$= 5.810$ mm.

Laminar circumferential displacement per lamination on mean bar pitch circle dia. $= 5.810 \times \dfrac{0.626 \times \pi}{180}$

$= 0.0635$ mm.

Effective bar width = 0.584 - 0.0635

= 0.5205 mm.

Effective bar section, $A_b = 0.5205 \times 0.978$

$= 0.509$ mm^2.

Rotor core length, $l_b = 1.76$ cms.

Endring section, A_r = radial depth of ring x axial depth of ring

$= 1.25 \times 1.9$

$= 2.375\ mm^2$.

Mean pitch circle of rotor bars, D_b = 2 x mean bar radius

= 2 x 5.81 mm . dia.

Determination of rotor winding resistance, R_2 :

If the space harmonics of the stator and rotor magnetomotive force waves are ignored, an ideal balance will exist between the rotor magnetomotive force and that component of the stator magnetomotive force due to the load current. Consider a set of axes travelling at synchronous speed. In these axes, the stator magnetomotive force is representable as a function of the electrical space angle θ by the expression,

$$m.m.f_{\theta} = k_1 c_1 \hat{I}_1 \sin(\theta + \alpha)$$

in which the constant k_1 is obtained from the analysis of the waveform of the stator magnetomotive force, and α is an arbitrary displacement.

Let the current density distribution in the rotor be such as to cause a load current of peak value $\hat{I}_2$ and of sinusoidal time function in the stator. The stator magnetomotive force due to this current will be $k_1 c_1 \hat{I}_2 \sin(\theta + \alpha)$. Let it further be assumed that the current density distribution in the squirrel cage rotor can be represented as part of a continuous current density distribution in a conducting sheet of resistivity ρ, the same as that of the bar material, and of uniform radial thickness T the same as that of the bars; the validity of this assumption is enhanced by the fact that the bars are skewed. Thus, for this sheet, since the current distribution will be generally rotating at slip speed $s\omega_s$ relative to the sheet, for any point ψ on the rotor the current density will be given by

$$J_{\psi} = \hat{J} f(\psi, s\omega_s t), \tag{3.0}$$

where the angles are measured in electrical radians. The instantaneous current flowing through an elemental strip of width $\frac{D_b}{2} \times \frac{\delta\psi}{p_1}$ at ψ is then

$$i_\psi = \hat{J} f(\psi, s\omega_s t) \frac{D_b \delta\psi}{2p_1} T \qquad (3.1)$$

and magnetomotive force across the air gap at this point is

$$\text{m.m.f.}_\psi = \frac{\hat{J} D_b T}{2p_1} \int_{f_0}^{\psi} f(\psi, s\omega_s t) d\psi, \text{ where } f_0 \text{ is } \psi \text{ at } f = 0.$$

This magnetomotive force is due to a homogeneous sheet. The magnetomotive force due to the squirrel cage, which can be considered as an inhomogeneous sheet, will be given by

$$\frac{V_c}{V_s}\left[\frac{\hat{J} D_b T}{2p_1} \int_{f_0}^{(\psi - s\omega_s t)} f(\psi, \cancel{s\omega_s} t) d\psi\right]$$

where V_c is the total volume of the cage, excluding endrings, and V_s is the volume of the sheet. Since both the cage and the sheet are of the same radial thickness and axial length, the ratio $\frac{V_c}{V_s}$ can be written as $\frac{\text{average slot width}}{\text{average slot pitch}}$, i.e. $\frac{s_w}{s_p}$.

Hence, since the magnetomotive force balance is ideal,

$$k_1 c_1 \hat{I}_2 \sin(\theta + \alpha) = \frac{s_w \hat{J} D_b T}{s_p 2p_1} \int_{f_0}^{\psi} f(\psi, s\omega_s t) d\psi$$

from which it is apparent that

$f(\psi, s\omega_s t) = \cos(\psi - s\omega_s t)$ where $(\psi - s\omega_s t) = (\theta + \alpha)$

and that $k_1 c_1 \hat{I}_2 = \frac{s_w \hat{J} D_b T}{s_p 2p_1}$

Equation (3.1) may, therefore, be written

$$i_\psi = \frac{\hat{J} D_b T}{2p_1} \cos(\psi - s\omega_s t)\delta\psi \qquad (3.2)$$

$$\text{where } \hat{J} = \frac{2s_p k_1 c_1 p_1 \hat{I}_2}{s_w D_b T} \tag{3.3}$$

and equation (3.0) becomes $J_\psi = \hat{J}\cos(\psi - s\omega_s t)$ (3.4)

The resistance of an elemental strip of the conducting sheet is

$$\delta R = \frac{2\rho l_b p_1}{D_b T\, \delta\psi} \text{ ohms,}$$

and the power loss in this strip will be

$$\delta W_{sh} = i_\psi^2 \delta R$$

i.e. by equation (3.2),

$$\delta W_{sh} = \frac{\hat{J}^2 D_b T\rho l_b}{2p_1}\cos^2(\psi - s\omega_s t)\delta\psi .$$

Hence, the total power dissipated in the sheet will be

$$W_{sh} = \frac{\hat{J}^2 D_b T\rho l_b}{2p_1}\int_0^{2p_1\pi}\cos^2(\psi - s\omega_s t)d\psi ,$$

i.e. $W_{sh} = 1.57\ \hat{J}^2 D_b T\rho l_b$ watts.

The power dissipated in the squirrel cage will, therefore, be

$$W_c = \frac{V_c}{V_s} W_{sh} ,$$

i.e.

$$W_c = \frac{s_w}{s_p}(1.57\ \hat{J}^2 D_b T\rho l_b) \text{ watts.} \tag{3.5}$$

For the endrings, the current flowing through the ring section at the corresponding point ψ is given by

$$i_{r\psi} = \int_{s\omega_s t}^{\psi} \frac{J_\psi T D_r}{2p_1} d\psi$$

where D_r is the effective diameter of the endring, allowing for a different distribution of current in the ring from that in the sheet.

i.e.

$$i_{r\psi} = \frac{\hat{J} T D_r}{2p_1}\int_{s\omega_s t}^{\psi}\cos(\psi - s\omega_s t)d\psi$$

i.e.

$$i_{r\psi} = \frac{\hat{J} T D_r}{2p_1}\Big[\sin(\psi - s\omega_s t)\Big]$$

This is again due to the whole sheet. Hence for the cage

$$i_{c\psi} = \frac{s_w \hat{J} T D_r}{s_p 2 p_1} \sin(\psi - s\omega_s t) \tag{3.6}$$

The resistance of an element of length $\frac{D_r \delta\psi}{2p_1}$ of the endring is

$$\delta R_r = \frac{\rho D_r \delta\psi}{2p_1 A_r}$$

The total power dissipated in the two endrings, due to the cage, will be

$$W_r = 2\left[\frac{s_w \hat{J} T D_r}{s_p 2 p_1}\right]^2 \frac{\rho D_r}{2p_1 A_r} \int_0^{2p_1\pi} \left[\sin(\psi - s\omega_s t)\right]^2 d\psi$$

$$= \frac{s_w^2 \hat{J}^2 T^2 D_r^3 \rho}{4 s_p^2 A_r p_1^3} \int_0^{2p_1\pi} \sin(\psi - s\omega_s t) d\psi$$

$$= 0.784 \frac{s_w^2 \hat{J}^2 T^2 D_r^3 \rho}{s_p^2 p_1^2 A_r} \tag{3.7}$$

From equations (3.5) and (3.7), the total power dissipated in the rotor is

$$W_2 = \hat{J}^2 \rho \left[1.57 D_b l_b T \frac{s_w}{s_p} + \frac{0.784 T^2 D_r^3 s_w^2}{p_1^2 A_r s_p^2}\right] \tag{3.8}$$

Substituting for $\hat{J}$ from equation (3.3),

$$W_2 = 6.28(p_1 k_1 c_1 \hat{I}_2)^2 \rho \left[\frac{l_b s_p}{D_b T s_w} + \frac{D_r^3}{2p_1^2 A_r D_b^2}\right]$$

But $\pi D_b T l_b \frac{s_w}{s_p}$ is the total volume of the bars, i.e. $n_2 A_b l_b$.

Hence, $$\frac{s_p}{D_b T s_w} = \frac{\pi}{n_2 A_b}$$

Substituting this in the expression derived above for W_2 gives, therefore,

$$W_2 = 6.28(p_1 k_1 c_1 \hat{I}_2)^2 \rho \left[\frac{\pi l_b}{n_2 A_b} + \frac{D_r^3}{2p_1^2 A_r D_b^2}\right]$$

i.e. in terms of the root mean square current,

$$W_2 = 39.5\rho(p_1 k_1 c_1 I_2)^2 \left[\frac{l_b}{n_2 A_b} + \frac{0.159\ D_r^3}{p_1^2 A_r D_b^2}\right] \qquad (3.9)$$

If R_2 is the actual rotor resistance per phase referred to the stator, then, $W_2 = I_2^2 R_2 m$, where m is the number of phases.

Hence, from equation (3.9)

$$R_2 = 39.5\frac{\rho}{m}(p_1 k_1 c_1)^2 \left[\frac{l_b}{n_2 A_b} + \frac{0.159\ D_r^3}{p_1^2 A_r D_b^2}\right] \qquad (3.10)$$

Let $D_r = KD_b$; the final term of equation (3.10) may then be written as $\frac{K^3 D_b}{p_1^2 A_r}$. Trickey (26) has investigated the value of the constant K as a function of the annular width of the endrings and the pole pitch. His results give a constant K_{ring} (which is K^3 in the foregoing expression) as a function of the number of poles and the ratio $\frac{ID_r}{D_b}$, where ID_r is the inside diameter of the endring; these results are given graphically in fig.(3.6'). In terms of this constant equation (3.10) becomes,

$$R_2 = 39.5\frac{\rho}{m}(p_1 k_1 c_1)^2 \left[\frac{l_b}{n_2 A_b} + \frac{0.159\ D_b\ K_{ring}}{p_1^2 A_r}\right] \qquad (3.11)$$

From the waveform analysis, $k_1 = 3.85 \times 0.5 = 1.925$.

Ratio $\frac{ID_r}{D_b} = \frac{5.049}{5.810} = 0.869$ and for this ratio, from fig.(3.6'), $K_{ring} = 0.94$.

Substituting these values and the values for the other quantities in equation (3.11) gives,

$$R_2 = 39.5\ \frac{2.69 \times 10^{-6}}{2}(1.925 \times 352)^2 \times 10 \times \left[\frac{17.6}{0.509 \times 25} + \frac{0.159 \times 11.6 \times 0.94}{2.375}\right]$$

i.e. $\underline{R_2 = 513 \text{ ohms at } 0^\circ C.}$

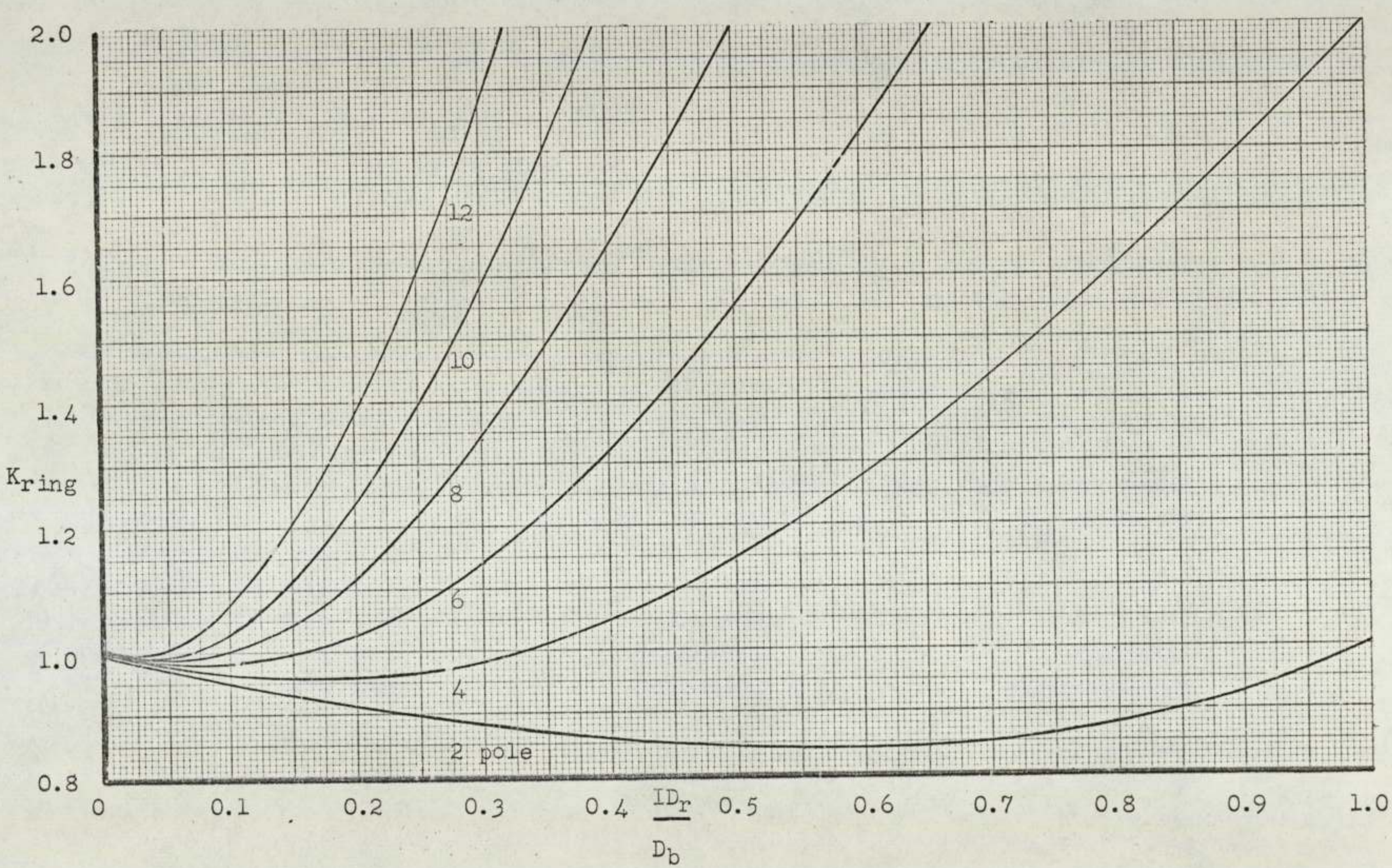

FIG. (3.6'). TRICKEY'S ENDRING COEFFICIENT.

Determination of the magnetising inductance, L_o:

This inductance is obtained as the ratio $\frac{E_o}{\omega I_o}$, where E_o is the induced e.m.f. per phase in the stator winding due to the airgap flux, I_o is the magnetising current per phase and ω is the angular frequency of supply. To do this both E_o and I_o are obtained as functions of $\emptyset$ the stator core flux; the above ratio then gives L_o independent of $\emptyset$.

Magnetising current, I_o:

From the results of the harmonic analysis of the stator magnetomotive force waves, the rotating magnetomotive force can be taken as a sinusoidal function, of amplitude $3.85 \times 0.5c_1\hat{I}$ ampere turns, of the electrical space angle θ. Hence, for a complete magnetic path passing through an arbitrary point θ, the net magnetomotive force acting at any instant of time is given by

$$\text{m.m.f.}_\theta = 2 \times 3.85 \times 0.5c_1\hat{I}_o\sin(\theta - \omega_s t),$$

where ω_s is the angular velocity of the rotating wave in electrical radians/second. In terms of the r.m.s. magnetising current per phase this becomes

$$\text{m.m.f.}_\theta = 5.44c_1 I_o\sin(\theta - \omega_s t) \text{ ampere turns.}$$

Since the machine is magnetically unsaturated, the airgap flux density at the same arbitrary point will be a similar function but of amplitude $\hat{B}$,

$$\text{i.e.} \quad B_\theta = \hat{B}\sin(\theta - \omega_s t) \text{ webers/metre}^2.$$

In determining the value of I_o from an analysis of the magnetic circuit of the machine, the calculations are carried out for the position where B_θ is a maximum, i.e. $\sin(\theta - \omega_s t) = 1$, so that the value of the magnetomotive force obtained for the teeth and the airgap will also be a maximum. Since the airgap flux density is a sinusoidal function of space, the flux densities in the cores will also be sinusoidal space functions. Hence, in determining the magnetomotive forces required for the cores, it is permissible to assume the flux densities therein to be mean values over the whole pole pitch whence,

$$\text{m.m.f.}_{\text{core}} = H \text{ for } B_{\text{mean}} \times \text{pole pitch on mean core diameter,}$$

for all conditions.

The effect of leakage flux is taken into consideration by using a leakage factor defined as the ratio $\dfrac{\text{total leakage flux}}{\text{total flux}}$. Obviously this factor can only be rigorously estimated from the equivalent circuit of the machine which, in turn, cannot be determined until the design is completed. A figure of 10% is, therefore, initially assumed for the leakage factor and verified subsequently. The factor is used progressively in increments of 2.5% proceeding inwards from the stator core. The analysis, which is made in terms of the stator flux ϕ and an effective airgap length δ_e, is carried out in tabular form in table (3.3), the total maximum value of the magnetomotive force being given as a function of ϕ and δ_e. This is then equated to the peak value for the rotating wave in order to obtain the expression for I_o.

Thus, from table (3.3) the total maximum magnetomotive force required is $\dfrac{0.087\phi}{\mu_o} + 8.6\dfrac{\delta_e\phi}{\mu_o}$ where δ_e is in millimetres. Hence, from the equation of the rotating wave,

$$5.44c_1 I_o = (0.087 + 8.6\delta_e)\frac{\phi}{\mu_o},$$

giving

$$I_o = \frac{(0.087 + 8.6\delta_e)\,\phi}{5.44c_1\mu_o} \text{ amperes.} \tag{3.12}$$

Induced e.m.f., E_o:

Consider the full pitch coil shown in radial and developed form in fig. (3.7) for a machine having p_1 pole pairs. For the airgap flux density equation as developed earlier, the mutual flux linking an elemental arc $\underline{\dfrac{r\delta\theta}{p_1}}$ at the arbitrary point θ is given by

$$\delta\phi = \hat{B}\sin(\theta - \omega_s t)l_o\frac{r\delta\theta}{p_1} \text{ weber.}$$

The flux linking the whole coil is, therefore,

$$\phi = \int_0^{\pi}\hat{B}\sin(\theta - \omega_s t)l_o\frac{rd\theta}{p_1}$$

$$= \frac{2\hat{B}l_o r}{p_1}\cos\omega_s t.$$

Hence, the induced e.m.f. for a full pitch concentrated coil of c_1 turns is

$$E = c_1\frac{d}{dt}\,\frac{2\hat{B}l_o r}{p_1}\cos\omega_s t$$

$$= \frac{1}{p_1}2\hat{B}l_o r c_1\omega_s\sin\omega_s t.$$

	Item	Area m^2	Flux Wb	$\frac{\hat{B}}{B_m}$	Flux density Wb/m^2	AT/mtere	Length m	Ampere turns
Stator	Core	$2.287 \times 1.73 \times 10^{-5}$	0.5ϕ	1.00	$\frac{0.5\phi}{3.96 \times 10^{-5}}$	$\frac{1.26\phi}{\mu_o}$	$1.6\pi \times 10^{-2}$	$\frac{0.064\phi}{\mu_o}$
	Teeth	$1.613 \times 1.73 \times 8 \times 10^{-5}$	$\phi(1 - 0.25\sigma)$	1.57	$\frac{1.57 \times 0.975\phi}{22.32 \times 10^{-5}}$	$\frac{0.686\phi}{\mu_o}$	$2 \times 8.623 \times 10^{-3}$	$\frac{1.082\phi \times 10^{-2}}{\mu_o}$
Gap		$2.495 \times 1.73 \times 8 \times 10^{-5}$	$\phi(1 - 0.50\sigma)$	1.57	$\frac{1.57 \times 0.95\phi}{34.53 \times 10^{-5}}$	$\frac{0.432\phi \times 10^{4}}{\mu_o}$	$2\delta_e \times 10^{-3}$	$\frac{8.6\phi\delta_e}{\mu_o}$
Rotor	Teeth	$\frac{1}{2}(1.003 + 0.757) \times 1.73 \times 12.5 \times 10^{-5}$	$\phi(1 - 0.75\sigma)$	1.57	$\frac{1.57 \times 0.925\phi}{19.02 \times 10^{-5}}$	$\frac{0.764\phi}{\mu_o}$	$2 \times 0.978 \times 10^{-3}$	$\frac{1.484\phi \times 10^{-3}}{\mu_o}$
	Core	$2.921 \times 1.73 \times 10^{-5}$	$0.5\phi(1 - \sigma)$	1.00	$\frac{0.90\phi \times 0.5}{5.05 \times 10^{-5}}$	$\frac{0.89\phi}{\mu_o}$	$3.87\pi \times 10^{-3}$	$\frac{1.09\phi \times 10^{-2}}{\mu_o}$

Relative permeabillity of stator and rotor iron taken as 10,000.

TABLE (3.3),MAGNETIC CIRCUIT ANALYSIS.

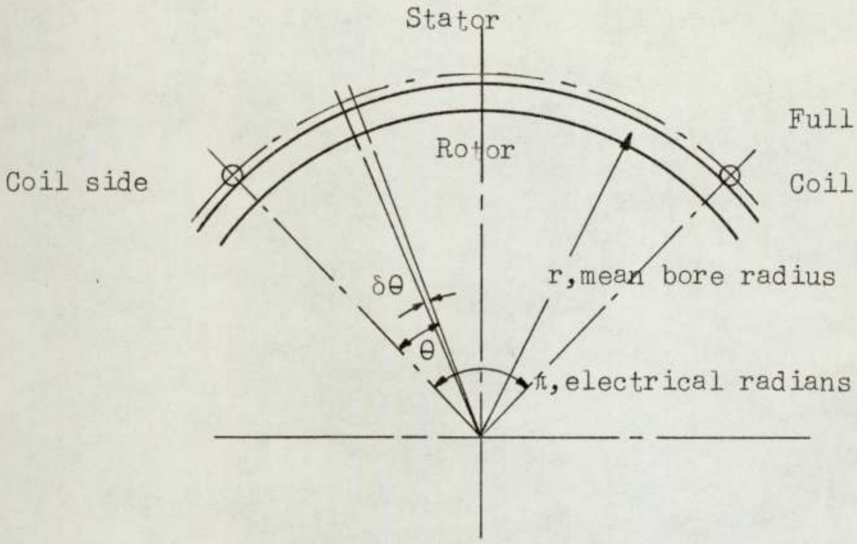

RADIAL REPRESENTATION.

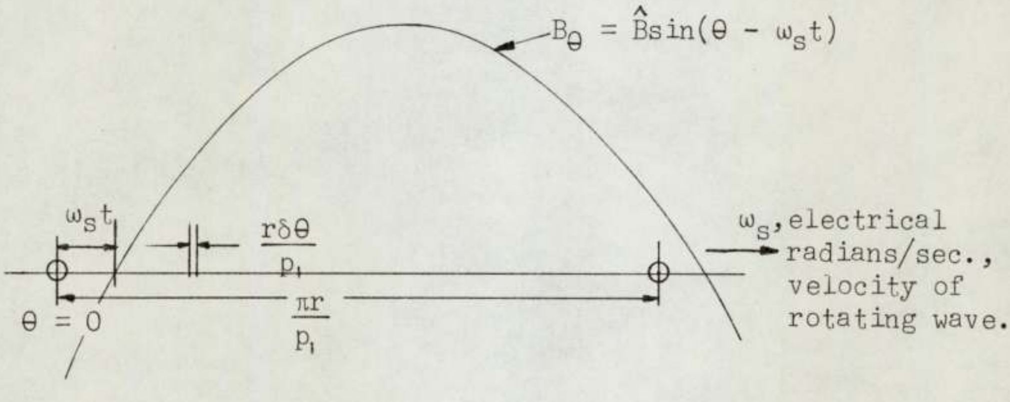

EQUIVALENT DEVELOPED REPRESENTATION.

FIG. (3.7). LAYOUT OF SINGLE FULL PITCHED COIL.

For the general case of a chorded, distributed winding having $pq_1 c_1$ turns per phase and a winding factor K_w, the induced e.m.f. per phase due to the mutual or airgap flux is then

$$E_o = \sqrt{2}\hat{B} l_o r q_1 c_1 \omega_s K_w \text{ volts r.m.s.} \qquad (3.13)$$

From the magnetic circuit analysis, for the airgap

$$\hat{B} = \frac{1.57 \times 0.95\phi}{3.453 \times 10^{-4}}$$

$$= 4.32\phi \times 10^{3} \text{ weber/metre}^{2}$$

whence $$E_o = 6.11\, K_w l_o r q_1 c_1 \phi \omega_s \times 10^{3} \text{ volts.}$$

Substituting this and the expression for I_o in the equation for L_o gives

$$L_o = \frac{3.32\, K_w l_o r q_1 c_1^2 \phi \omega_s \mu_o \times 10^{4}}{(0.087 + 8.6\delta_e)\phi\omega}$$

$$= \frac{3.32\, K_w l_o r q_1 c_1^2 \mu_o \times 10^{4}}{(0.087 + 8.6\delta_e)} \quad (\text{since } \omega = \omega_s).$$

which, for this particular machine on insertion of the specified and calculated values of the factors gives

$$L_o = \frac{1.699}{(0.087 + 8.6\delta_e)} \text{ henry.} \qquad (3.14)$$

Effective airgap length, δ_e:

Using the method developed by Binns (27) based on the work of Carter (28), for a doubly slotted structure the gap extension factor, g_c, is given by

$$g_c = \tfrac{1}{2}(g_1 g_2 + g_1 + g_2 - 1)$$

where g_1 and g_2 are the gap coefficients for each set of slots separately given by

$$g_1 = \frac{p_1'}{p_1' - s_1'\sigma_1} \text{ for the stator}$$

and $$g_2 = \frac{p_2'}{p_2' - s_2'\sigma_2} \text{ for the rotor}$$

in which σ_1 & σ_2 are Carter's coefficients, p_1' & p_2' are slot pitches at the bore surfaces and s_1' & s_2' are the slot openings for stator and rotor, respectively.

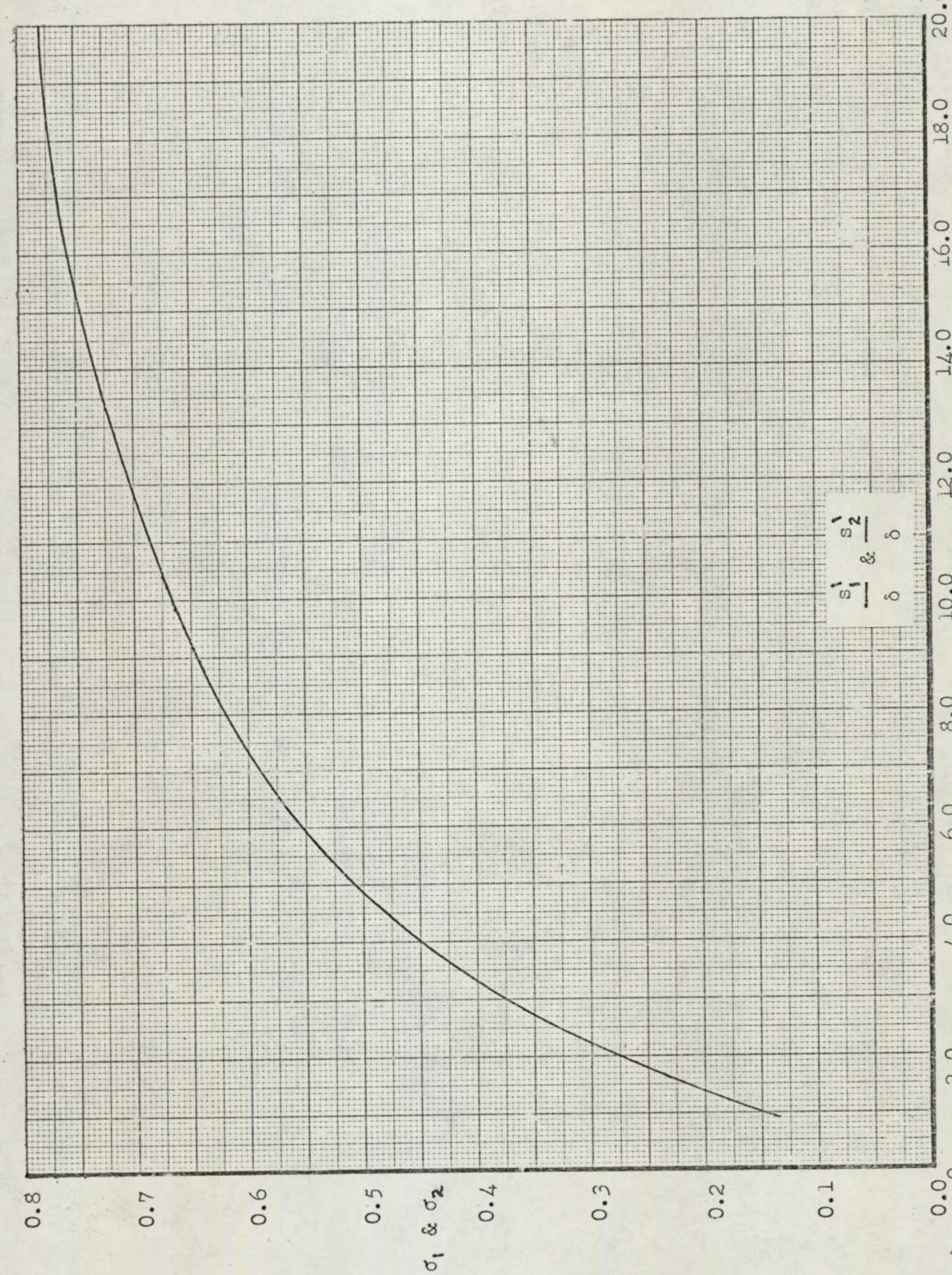

FIG. (3.8). CARTER'S GAP COEFFICIENT FOR SINGLE SLOT FACING PLANE IRON BOUNDARY.

δ_e is then given by $g_c\delta$, where δ is the actual mechanical gap length.

From fig.(3.2) and Carter's curves as in fig.(3.8),

$$\text{for } \frac{s_1'}{\delta} = \frac{0.882}{0.05} = 17.64, \quad \sigma_1 = 0.77$$

$$\text{and for } \frac{s_2'}{\delta} = \frac{0.584}{0.05} = 11.68, \quad \sigma_2 = 0.69$$

whence

$$g_1 = \frac{2.495}{2.495 - 0.882 \times 0.77} = 1.374$$

and

$$g_2 = \frac{1.587}{1.587 - 0.584 \times 0.69} = 1.340,$$

giving an overall gap extension factor

$$g_c = \tfrac{1}{2}(1.374 \times 1.340 + 1.374 + 1.340 - 1)$$
$$= 1.778.$$

The effective airgap length is, therefore, 1.778δ i.e. 1.778×0.05 or 0.0889 mm.

Substituting this value in the expression for L_0 gives

$$L_0 = \frac{1.699}{0.087 + 8.6 \times 0.0889} = 1.997 \text{ henry.}$$

Stator leakage inductance L_1:

The estimation of this quantity is based on the method developed by Binns (27) for doubly slotted structures which, although intended for much larger machines, is here assumed valid for the miniature range. In this method the leakage permeance is considered to be made up of an air gap leakage permeance Λ_{g1}, a slot leakage permeance Λ_{s1} and an overhang leakage permeance Λ_{h1}. Considering these in turn,

Λ_{g1}:

Allowing for the effect of the variable displacement between the stator slots and the rotor slots due to their different numbers, Binns defines a maximum, minimum and mean value for the air gap permeance such that

$$\Lambda_{g1} = \Lambda_{g1\,mean} = \tfrac{1}{2}(\Lambda_{g1\,min} + \Lambda_{g1\,max}) - 0.4(s_1' + s_2' - \delta)\frac{(\Lambda_{g1\,max} - \Lambda_{g1\,min})}{s_2' + t_2'}$$

$$\text{where } \Lambda_{g1\,min} = \frac{\mu_0}{\delta}\left[\frac{\delta}{3} + \frac{s_1'}{40} - \frac{s_2'}{30} - \frac{s_1' s_2'}{100y}\right]$$

$$\text{and}\ \Lambda_{g1\,max} = \frac{\mu_o}{\delta}\left[\frac{\delta}{3} + \frac{s_2'}{9} - \frac{s_1'}{6} - \frac{s_1' s_2'}{100y} + \frac{t_2'}{4}\right]$$

where y is the scaling factor required to render the term $\frac{s_1' s_2'}{\delta . y}$ dimensionless, s_1' & s_2', t_1' & t_2' are the slot openings and tooth top widths of the stator and rotor, respectively.

Hence, substituting the appropriate values from figs.(3.1) & (3.2) gives,

$$\Lambda_{g1\,min} = \frac{\mu_o}{\delta}\left[\frac{\delta}{3} + \frac{0.882 \times 10^{-3}}{40} - \frac{0.584 \times 10^{-3}}{30} - \frac{0.882 \times 0.584 \times 10^{-6}}{100 \times 10^{-3}}\right]$$

$$= \mu_o\left[0.33 - \frac{0.0022}{\delta}\right] \qquad \text{for } \delta \text{ in mm.}$$

$$\Lambda_{g1\,max} = \frac{\mu_o}{\delta}\left[\frac{\delta}{3} + \frac{0.584 \times 10^{-3}}{9} - \frac{0.882 \times 10^{-3}}{6} - \frac{0.882 \times 0.584 \times 10^{-6}}{100 \times 10^{-3}} + \frac{1.003 \times 10^{-3}}{4}\right]$$

$$= \mu_o\left[0.33 + \frac{0.163}{\delta}\right] \qquad \text{for } \delta \text{ in mm.}$$

$$\text{Whence, } \Lambda_{g1} = \mu_o\left\{\frac{1}{2}\left[0.66 + \frac{0.161}{\delta}\right] - 0.4\left[0.882 \times 10^{-3} + 0.584 \times 10^{-3} - \delta \times 10^{-3}\right] \times \left[\frac{0.165}{\delta(0.584 \times 10^{-3} + 1.003) \times 10^{-3}}\right]\right\}$$

$$\text{i.e. } \Lambda_{g1} = \mu_o\left[0.372 + \frac{0.02}{\delta}\right]$$

Substituting the value already obtained for δ this gives,

$$\Lambda_{g1} = 0.772\mu_o \qquad (3.15)$$

Λ_{s1}:

Assuming the stator slot to be wound to within 33.3% total slot depth from the bore surface, then from figs.(3.1) & (3.2) the slot may be represented as in fig.(3.9) and considered in the three sections e, c and o as shown. The m.m.f. required to drive the flux through the iron is ignored.

Section e.

Referring to fig.(3.10)

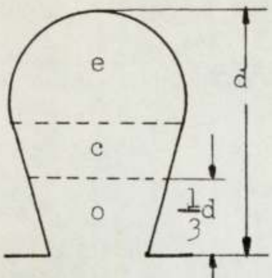

FIG. (3.9).STATOR SLOT.

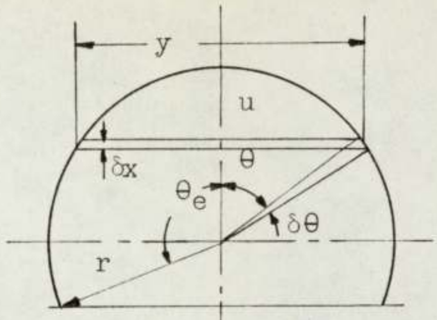

FIG. (3.10),DETAIL OF SECTION'e'.

Permeance of element $= \frac{\delta x}{y}\mu_o$ per unit length,

$$= \frac{r\delta\theta \sin\theta}{2r \sin\theta}\mu_o = \frac{\delta\theta}{2}\mu_o$$

Magnetomotive force acting on element $= \dfrac{\text{area of sector u}}{\text{total area taken by winding}} \times c_1 I,$

where I is an arbitrary current.

Area of sector u $= \frac{\pi r^2}{2\pi} \times 2\theta - r^2\sin\theta\cos\theta$

$$= r^2(\theta - \sin\theta\cos\theta).$$

Let winding area be A_w, then,

magnetomotive force acting on element $= \dfrac{r^2(\theta - \sin\theta\cos\theta)}{A_w} \times c_1 I,$

and the flux linkages/ampere/unit core length for the element will be

$$\frac{r^2(\theta - \sin\theta\cos\theta)}{A_w} \times c_1 \times \frac{\delta\theta}{2} \times \mu_o \times \text{conductors in sector u.}$$

i.e. $$\left[\frac{r^2}{A_w}(\theta - \sin\theta\cos\theta)c_1\right]^2 \frac{\delta\theta}{2} \times \mu_o$$

Hence, inductance/unit core length for complete end section

$$= 2\int_0^{\theta_e} \frac{c_1^2 r^4 \mu_o}{2A_w^2}(\theta - \sin\theta\cos\theta)^2 d\theta$$

$$= \frac{c_1^2 r^4 \mu_o}{A_w^2}\left[\frac{\theta^3}{3} + \frac{\theta\cos2\theta}{2} + \frac{\sin2\theta}{4} + \frac{\theta}{8} - \frac{\sin4\theta}{32}\right]_0^{\theta_e}$$

$$= \frac{c_1^2 r^4 \mu_o}{A_w^2}\left[\frac{\theta_e^3}{3} + \frac{\theta_e\cos2\theta_e}{2} + \frac{\sin2\theta_e}{4} + \frac{\theta_e}{8} - \frac{\sin4\theta_e}{32}\right]$$

giving a permeance factor

$$\Lambda_e = \frac{r^4\mu_o}{A_w^2}\left[\frac{\theta_e^3}{3} + \frac{\theta_e\cos 2\theta_e}{2} + \frac{\sin 2\theta_e}{4} + \frac{\theta_e}{8} - \frac{\sin 4\theta_e}{32}\right] \qquad (3.16)$$

From fig. (3.2), by measurement,

$$\theta_e = \frac{93.5}{180}\pi = 1.632 \text{ radians.}$$

$$b = 2.0 \text{ mm., } d = 8.623 \text{ mm., } r = \frac{3.556}{2} = 1.778 \text{ mm.}$$

Hence,

$$A_w = \text{slot area} - \frac{(\text{slot opening} + b)}{2} \times \frac{d}{3}$$

$$= 20.2 - \frac{(0.882 + 2)}{2} \times 2.88$$

$$= 16.05 \text{ mm}^2.,$$

$$\text{and } \Lambda_e = \frac{1.778^4\mu_o}{16.05^2}\left[\frac{1.63^3}{3} - \frac{1.632 \times 0.993}{2} - \frac{0.124}{4} - \frac{1.63}{8} - \frac{0.242}{32}\right]$$

$$= \frac{1.778^4 \times 0.726\mu_o}{16.05^2} = 0.0278\mu_o.$$

Section c.

Referring to fig. (3.11)

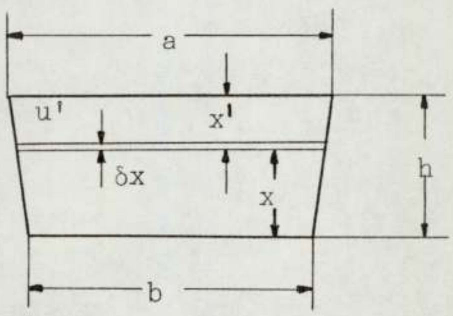

FIG. (3.11).DETAIL OF SECTION'c'.

$$\text{Permeance of element} = \frac{\delta_x}{b + (a - b)\frac{x}{h}}\mu_o.$$

$$\text{Magnetomotive force acting on element} = \frac{\text{area of sector } u' + u}{\text{total area taken by winding}} \times c_1 I.$$

Let $a = b(1 + \sigma)$, where $\sigma = \dfrac{a - b}{b}$.

The length of the element may then be written as

$$b - \left[b - b(1 + \sigma)\right]\frac{x}{h}$$

i.e. $$b(1 + \frac{\sigma x}{h})$$

The permeance of the element then becomes

$$\frac{\delta x\ \mu_o}{b(1 + \frac{\sigma x}{h})}$$

Area of sector $u' = \left[a + b(1 + \frac{\sigma x}{h})\right]\dfrac{x'}{2}$, so that if W is the area of sector u, the magnetomotive force acting on the element is

$$\left[W + \left[a + b(1 + \frac{\sigma x}{h})\right]\frac{x'}{2}\right]\frac{c_1 I}{A_w}.$$

Hence the flux linkages/ampere/unit core length for the element are

$$\left[W + \left[a + b(1 + \frac{\sigma x}{h})\right]\frac{x'}{2}\right]^2\left[\frac{c_1}{A_w}\right]^2\frac{\mu_o \delta x}{b(1 + \frac{\sigma x}{h})}$$

i.e. $$\frac{Q}{4}\left[2W + \left[a + b(1 + \frac{\sigma x}{h})\right]x'\right]^2\frac{\delta x}{b(1 + \frac{\sigma x}{h})}$$

where $Q = \left[\dfrac{c_1}{A_w}\right]^2\mu_o$,

i.e. $$\frac{Q}{4}\left[2W + \left[a + b(1 + \frac{\sigma x}{h})\right]x'\right]\left[x' + \frac{ah}{b\sigma} + \frac{2W - \frac{ha}{\sigma}}{b(1 + \frac{\sigma x}{h})}\right]\delta x$$

i.e. $$\frac{Q}{4}\left[\left[2W + \left[a + b(1 + \frac{\sigma x}{h})\right]x'\right]\left[x' + \frac{ah}{b\sigma}\right] + \left[2W - \frac{ha}{\sigma}\right]\left[x' + \frac{ah}{b\sigma} + \frac{2W - \frac{ha}{\sigma}}{b(1 + \frac{\sigma x}{h})}\right]\right]\delta x$$

i.e. $$\frac{Q}{4}\left[\left[4W + \left[a + b(1 + \frac{\sigma x}{h})\right]x' - \frac{ha}{\sigma}\right]\left[x' + \frac{ah}{b\sigma}\right] + \frac{\left[2W - \frac{ha}{\sigma}\right]^2}{b(1 + \frac{\sigma x}{h})}\right]\delta x$$

i.e. $$\frac{Q}{4}\left[\frac{b\sigma x x'^2}{h} + xx'(2a + b) + x'(4W + \frac{a^2h}{b\sigma}) + \frac{ah}{b\sigma}(4W - \frac{ah}{\sigma}) + \frac{\left[2W - \frac{ha}{\sigma}\right]^2}{b(1 + \frac{\sigma x}{h})}\right]\delta x$$

The inductance per unit core length for the complete centre section is then,

$$\frac{Q}{4}\int_0^h \left[\frac{b\sigma x x'^2}{h} + xx'(2a + b) + x'\left(4W + \frac{a^2h}{b\sigma}\right) + \frac{ah}{b\sigma}\left(4W - \frac{ah}{\sigma}\right) + \frac{\left[2W - \frac{ha}{\sigma}\right]^2}{b\left(1 + \frac{\sigma x}{h}\right)}\right] dx$$

giving a permeance factor

$$\Lambda_c = \frac{\mu_o}{4A_w^2}\left[\frac{b\sigma h^3}{12} + \frac{h^3}{6}(2a + b) + \frac{h^2}{2}\left(4W + \frac{a^2 h}{b\sigma}\right) + \frac{ah^2}{b\sigma}\left(4W - \frac{ah}{\sigma}\right) + \frac{h}{b\sigma}\left[2W - \frac{ha}{\sigma}\right]^2 \log_\varepsilon(1 + \sigma)\right] \quad (3.17)$$

To check this equation, consider a flat bottomed, parallel sided slot. In this case $W = 0$, $\sigma = 0$, $a = b$.

Substituting $W = 0$ and $\log_\varepsilon(1 + \sigma) = \sigma - \frac{\sigma^2}{2} + \frac{\sigma^3}{3} - \frac{\sigma^5}{5} + \text{--------}$ into equation (3.17) gives

$$\Lambda_c = \frac{\mu_o}{4A_w^2}\left[\frac{b\sigma h^3}{12} + \frac{h^3}{6}(2a + b) + \frac{a^2h^3}{2b\sigma} - \frac{a^2h^3}{b\sigma^2} + \frac{h^3a^2}{b\sigma^3}\left[\sigma - \frac{\sigma^2}{2} + \frac{\sigma^3}{3} - \frac{\sigma^5}{5} + \text{-------}\right]\right]$$

$$= \frac{\mu_o}{4A_w^2}\left[\frac{b\sigma h^3}{12} + \frac{h^3}{6}(2a + b) + \frac{a^2h^3}{3b} - \frac{a^2h^3\sigma^2}{5b} + \text{-------}\right]$$

Substituting $\sigma = 0$, $a = b$, $A_w = ah$ gives

$$\Lambda_c = \frac{\mu_o}{4a^2h^2}\left[ah^3 + \frac{ah^3}{3}\right] = \mu_o\frac{h}{3a}, \text{ as required.}$$

From fig.(3.2),

$$W = r^2\theta_e = 1.778^2 \times 1.632 = 5.14 \text{ mm}^2.$$

$$a = 3.50 \text{ mm.}$$

$$b = 2.0 \text{ mm.}$$

$$h = \frac{2d}{3} - r = 5.75 - 1.778 = 3.972 \text{ mm.}$$

$$\sigma = \frac{3.50 - 2.0}{2.0} = 0.75$$

$$A_w = 16.05 \text{ mm}^2.$$

Substitution of these values into equation (3.17) gives,

$$\Lambda_c = 0.784\mu_o$$

Section o.

Referring to fig.(3.12)

As for section c, permeance of element = $\dfrac{\delta x\ \mu_o}{s_1'(1 + \frac{\sigma x}{k})}$

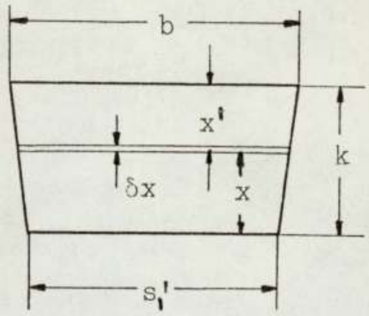

FIG. (3.12). DETAIL OF SECTION 'o'.

The magnetomotive force acting on the element is the total for the slot, i.e. $c_1 I$. Hence the flux linkages/ampere/unit core length for the element are,

$$\frac{\mu_o \delta x}{s_1'(1 + \frac{\sigma x}{k})} c_1^2$$

and the inductance/unit core length for the complete open section is,

$$\mu_o c_1^2 \int_o^k \frac{dx}{s_1'(1 + \frac{\sigma x}{k})}$$

$$\text{i.e.} \qquad \frac{\mu_o c_1^2 k}{s_1' \sigma} \log_\varepsilon(1 + \sigma)$$

giving a permeance factor

$$\Lambda_o = \frac{\mu_o k}{s_1' \sigma} \log_\varepsilon(1 + \sigma) \qquad (3.18)$$

From fig.(3.2), $k = d/3 = 2.875$, $s_1' = 0.882$

Substituting these values and that of σ into equation (3.18) gives

$$\Lambda_o = 2.44\mu_o$$

The total slot permeance factor $\Lambda_{s_1} = \Lambda_e + \Lambda_c + \Lambda_o$

Hence, $\Lambda_{s_1} = \mu_o(0.028 + 0.784 + 2.44)$

$$\text{i.e. } \Lambda_{s_1} = 3.252\mu_o$$

Λ_{h_1}:

This permeance factor is determined using two-dimensional flux plots.

Since the rotor slot is much smaller than the stator slot, it is assumed that the leakage flux is unaffected by rotor position. The stator winding outhang does, however, face either a stator slot or a stator tooth, in the extremes, depending upon the particular point on the outhang periphery at which the flux plot is studied. To allow for this two plots were made, one for each of the extreme conditions, with the intention of using the average of the two values of inductance/unit length of outhang/unit core length so obtained. The coil corners were assumed to have the same value of leakage inductance/unit length as the peripheral outhang. The actual dimensions of the outhang were obtained by measurement on the test machine.

The two flux plots referred to above were made using teledeltos paper (see fig.(3.13)) to fix the equipotentials, the flux lines being then drawn in freehand using curvilinear square techniques. These maps are given in fig.(3.14). For each of these, two regions need to be considered;

(a) outside the current carrying region, (b) inside the current carrying region, the flux linkages for each region being determined separately for an arbitrary current I and then summed to obtain the total flux linkages as a function of I from which the permeance factor may then be obtained.(29)

Thus, let T be the number of flux tubes, M the number of magnetomotive force tubes, $\emptyset_e$ the flux and $c_1 I$ the magnetomotive force for the entire field. Then the flux/tube $= \dfrac{\emptyset_e}{T}$ and in the external region, the magnetomotive force/tube $= \dfrac{c_1 I}{M}$.

Considering unit length of outhang, the permeance per rectangle of the field map is given by $\mu_o \dfrac{w}{l}$ where w is the length of the curvilinear rectangle along the equipotential and l is the length of the curvilinear rectangle along the flux line. Hence, from above for region (a) outside the conductors,

$$\frac{\emptyset_e}{T} \times \frac{M}{c_1 I} = \mu_o \frac{w}{l},$$

whence,

$$\frac{c_1 \emptyset_e}{T} = \frac{c_1^2 I \mu_o w}{lM} \tag{3.19}$$

Let the number of flux tubes in this region be T_o. Then the flux in this region will be $\dfrac{\emptyset_e T_o}{T}$ and, since this links all the conductors, the flux

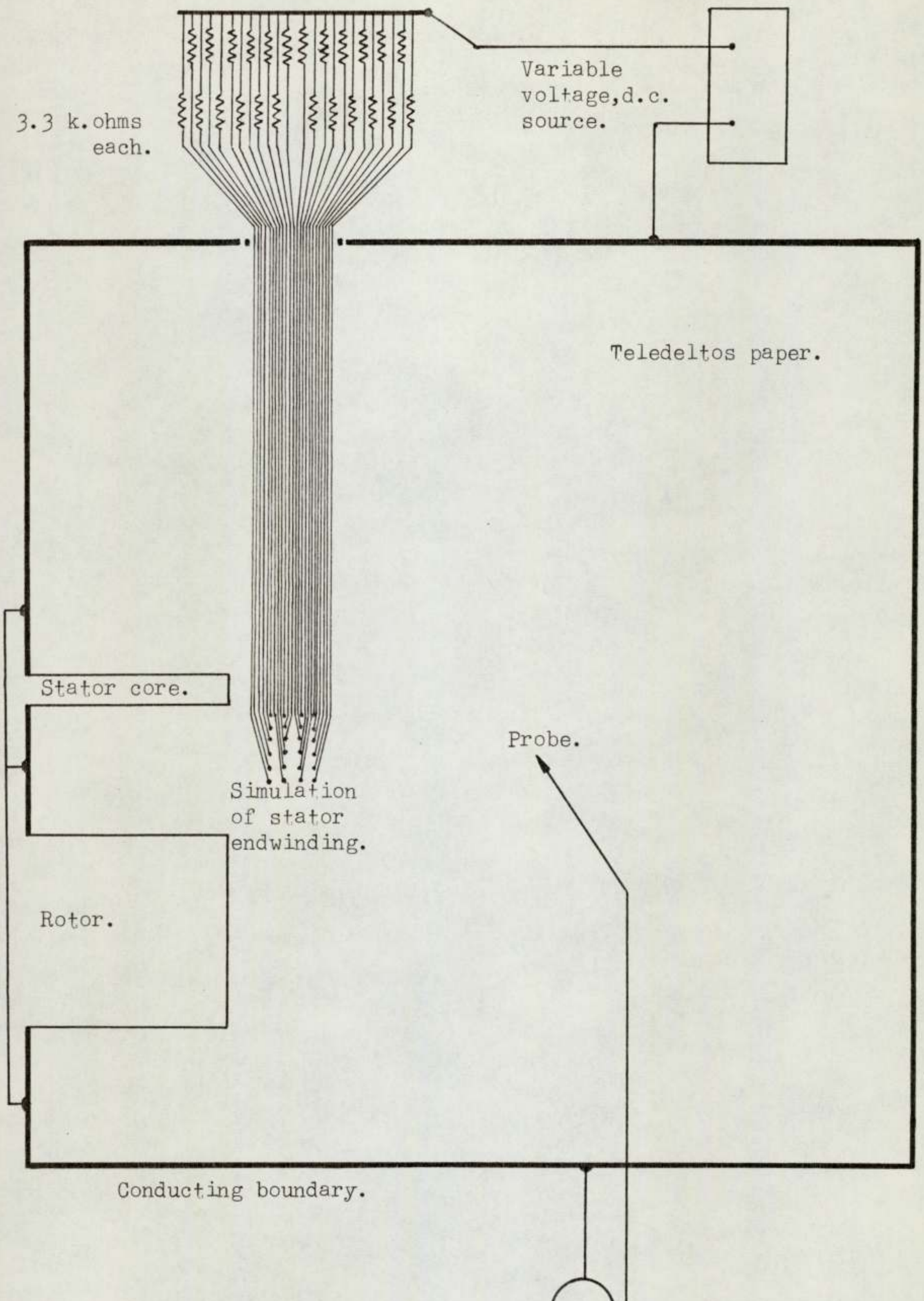

FIG. (3.13). DETERMINATION OF STATOR ENDWINDING FLUX DISTRIBUTION.
(For map 2 of fig.(3.14)).

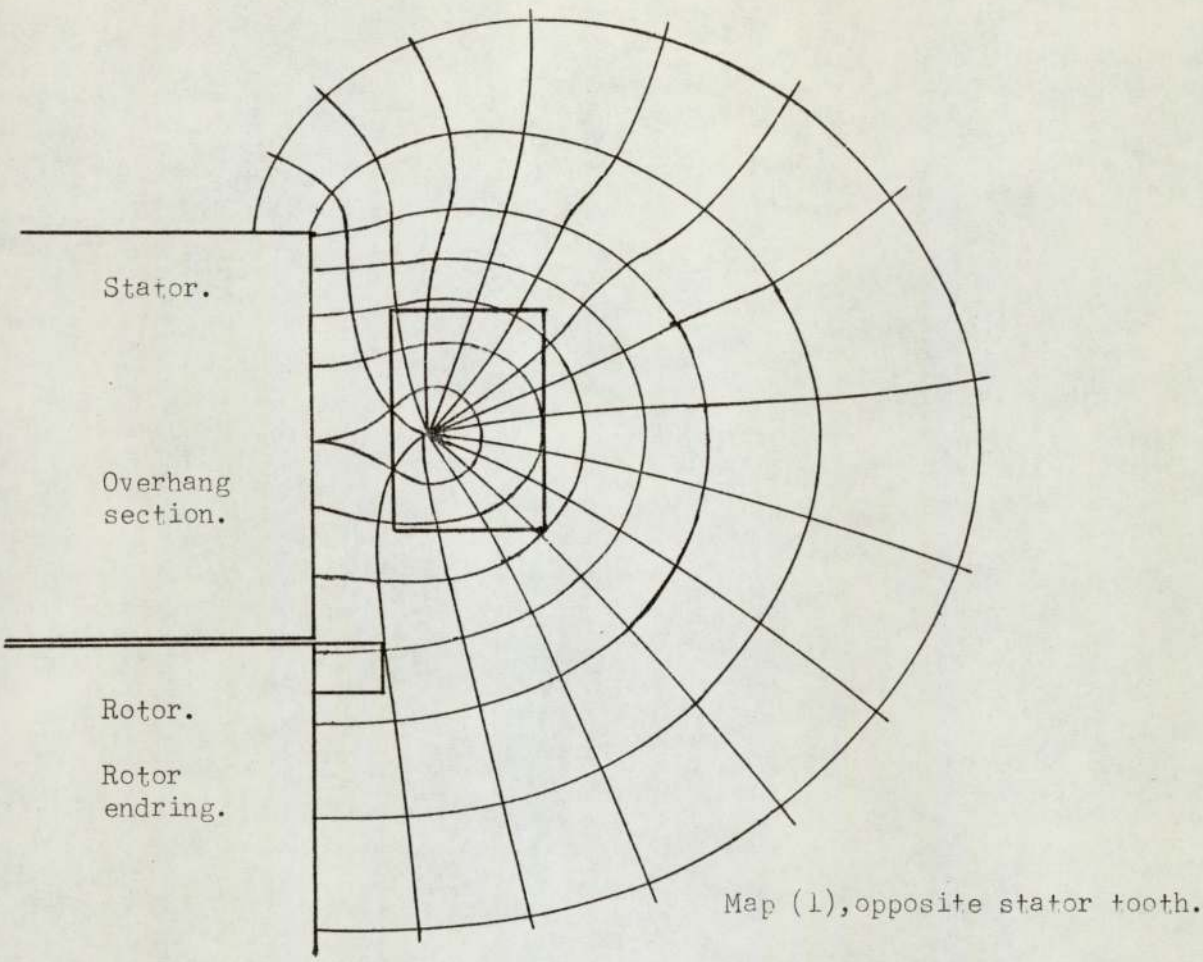

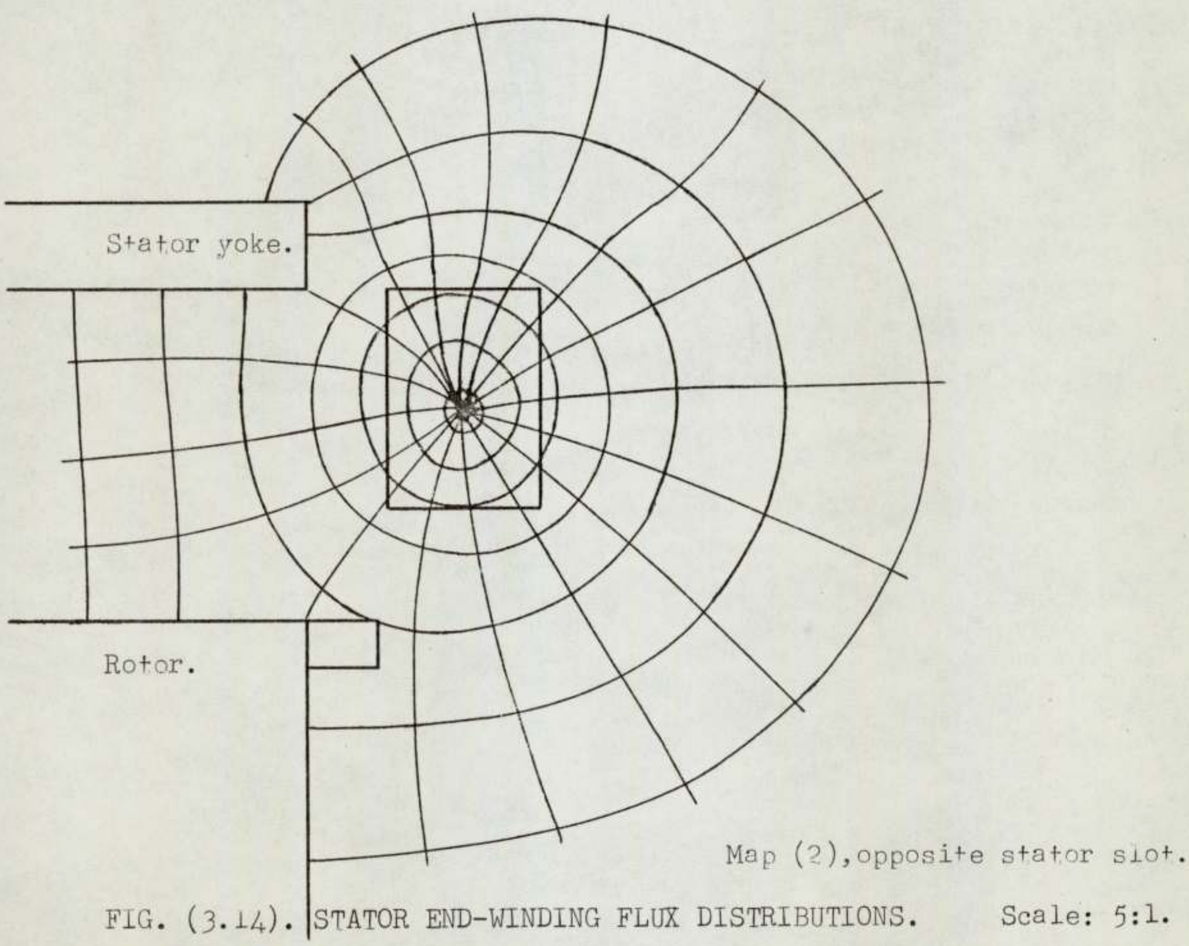

FIG. (3.14). STATOR END-WINDING FLUX DISTRIBUTIONS. Scale: 5:1.

linkages due to this flux will be $\dfrac{c_1 \phi_e T_o}{T}$. Substituting from equation (3.19) this may be written as $\dfrac{c_1^2 I \mu_o T_o}{M}$, remembering that $w = 1$ in this region since the field was mapped in curvilinear squares.

For region (b), inside the conductors, the number of conductors linked by a given flux tube can be taken to be approximately $c_1 \dfrac{a}{A}$ in which A is the total area of the conducting region and a is the area of this region enclosed by the centre line of the given flux tube. Inside this region, the continuation of the equipotential lines of region (a) cease to be equipotentials and become lines of no work. The magnetomotive force/tube now becomes approximately $\dfrac{c_1 I}{M} \times \dfrac{a'}{A'}$ where a' is the conducting area enclosed between the adjacent lines of no work from the kernel up to the mean flux line and A' is the total conducting area between the adjacent lines of no work. Hence the flux/tube is $\dfrac{c_1 I a'}{MA'} \times \mu_o \dfrac{w}{1}$.

In the external region, the flux/tube was given by the expression $\dfrac{c_1 I}{M}\mu_o$, so that for the flux/tube to be a constant at $\dfrac{\phi_e}{T}$ for the entire field

$$\frac{c_1 I}{M}\mu_o = \frac{c_1 I a'}{MA'} \times \mu_o \frac{w}{1},$$

i.e. in the conducting region $\dfrac{a'}{A'} = \dfrac{1}{w}$. The field maps were so drawn, consequently,

$$\text{flux linkages/tube} = \frac{\phi_e}{T} \times c_1 \frac{a}{A}$$

Substituting for $\dfrac{\phi_e}{T} c_1$ from equation (3.19) again remembering that $w = 1$ in the external region, the above expression may be written

$$\text{flux linkages/tube} = \frac{c_1^2 I \mu_o}{M} \times \frac{a}{A}.$$

Hence, the total flux linkages/metre length of outhang are

$$\frac{c_1^2 I \mu_o T_o}{M} + \sum \frac{c_1^2 I \mu_o a}{MA}$$

$$\text{i.e.} \quad \frac{c_1^2 I \mu_o}{M}\left[T_o + \sum \frac{a}{A}\right]$$

whence the permeance factor is given by

$$\Lambda_{h_1} = \frac{\mu_o}{M}\left[T_o + \sum\frac{a}{A}\right] x \ \frac{\text{outhang length}}{\text{core length}} \qquad (3.20)$$

From fig.(3.14), map (1), taking the field up to the inside diameter of the rotor endring,

$T_o = 2$; $M = 15$: $A = 2.05 \times 2.9 = 5.94$ cm^2., to the scale of fig.(3.14).

For paths inside the current carrying region, by planimeter,

$a_1 = 5.3$ cm^2., to the scale of fig.(3.14)

$a_2 = 2.4$ " "

$a_3 = 0.4$ " "

Hence, substituting in equation (3.20),

$$\Lambda_{h_1} = 0.225\mu_o \ x \ \frac{\text{outhang length}}{\text{core length}}.$$

From fig.(3.14), map (2),

$T_o = 2$; $M = 17$; $A = 5.94$ cm^2., to the scale of fig.(3.14).

For paths inside the current region, by planimeter,

$a_1 = 5.9$ cm^2., to the scale of fig.(3.14)

$a_2 = 3.5$ " "

$a_3 = 0.8$ " "

$a_4 = 0.05$ " "

Hence, substituting in equation (3.20),

$$\Lambda_{h_1} = 0.219\mu_o \ x \ \frac{\text{outhang length}}{\text{core length}}.$$

There is, apparently, little difference between the two extremes. However, taking the average,

$$\Lambda_{h_1} = 0.222\mu_o \ x \ \frac{\text{outhang length}}{\text{core length}}.$$

From the details of the stator winding given on page (60),

$$\frac{\text{outhang length}}{\text{core length}} = \frac{l_c - \text{core length}}{\text{core length}}$$

$$= \frac{51.33 - 18.3}{18.3}$$

$$= 1.804$$

Hence, $\Lambda_{h_1} = 0.4\mu_o$

and the total permeance factor for the stator is given by $(\Lambda_{g_1} + \Lambda_{s_1} + \Lambda_{h_1})$,

i.e. $$= \mu_o(0.77 + 3.25 + 0.4)$$

$$= 4.42\mu_o$$

For the winding arrangement used, the number of turns in the endwinding section is the same as that in the slot. The stator leakage inductance per slot per unit core length is, therefore, $4.42\mu_o c_1^2$ and the stator leakage inductance per phase is

$$L_1 = 2pq_1 c_1^2 \times 4.42\mu_o \times \text{core length}$$

$$= 2 \times 4 \times 352^2 \times 1.83 \times 10^{-2} \times 4.42 \times 4\pi \times 10^{-7}$$

i.e. $$\underline{L_1 = 0.10 \text{ henry.}}$$

Rotor leakage inductance L_2:

Using the same methods as for the stator, the rotor air gap permeance Λ_{g_2}, slot leakage permeance Λ_{s_2} and overhang permeance Λ_{h_2} are determined individually.

Λ_{g_2} :

$$\Lambda_{g_2 min} = \frac{\mu_o}{\delta}\left[\frac{\delta}{3} + \frac{s_2'}{40} - \frac{s_1'}{30} - \frac{s_1' s_2'}{100y}\right]$$

Substituting values from fig.(3.1) & fig.(3.2),

$$\Lambda_{g_2 min} = \frac{\mu_o}{\delta}\left[\frac{\delta}{3} + \frac{0.584 \times 10^{-3}}{40} - \frac{0.882 \times 10^{-3}}{30} - \frac{0.882 \times 0.584 \times 10^{-6}}{100 \times 10^{-3}}\right]$$

i.e. $$\Lambda_{g_2 min} = \left[0.33 - \frac{0.02}{\delta}\right] \qquad \text{for } \delta \text{ in mm.}$$

$$\Lambda_{g_2 max} = \frac{\mu_o}{\delta}\left[\frac{\delta}{3} + \frac{s_1'}{9} - \frac{s_2'}{6} - \frac{s_1' s_2'}{100y} + \frac{t_1'}{4}\right]$$

Substituting values from fig.(3.1) & fig.(3.2),

$$\Lambda_{g_2 max} = \left[\frac{\delta}{3} + \frac{0.882 \times 10^{-3}}{9} - \frac{0.584 \times 10^{-3}}{6} - \frac{0.882 \times 0.584 \times 10^{-6}}{100 \times 10^{-3}} + \frac{1.613 \times 10^{-3}}{4}\right]\frac{\mu_o}{\delta}$$

$$\text{i.e.} \qquad \Lambda_{g_2 max} = \left[0.33 + \frac{0.398}{\delta}\right] \qquad \text{for } \delta \text{ in mm.}$$

$$\Lambda_{g_2} = \Lambda_{g_2 mean} = \tfrac{1}{2}(\Lambda_{g_2 min} + \Lambda_{g_2 max}) - 0.4(s_1' + s_2' - \delta)\frac{(\Lambda_{g_2 max} - \Lambda_{g_2 min})}{s_1' + t_1'}$$

$$\text{i.e.}\,\Lambda_{g_2} = \mu_o\left\{\frac{1}{2}\left[0.66 + \frac{0.378}{\delta}\right] - 0.4\left[0.882 \times 10^{-3} + 0.584 \times 10^{-3} - \delta \times 10^{-3}\right] \times \left[\frac{0.418}{\delta(0.882 \times 10^{-3} + 1.613 \times 10^{-3})}\right]\right\}$$

$$\text{i.e.}\,\Lambda_{g_2} = \mu_o\left[0.397 + \frac{0.091}{\delta}\right]$$

Substituting for δ, $\quad \Lambda_{g_2} = 2.217\mu_o$ per unit core lenght of rotor.

Λ_{s_2}:

The slot is rectangular, straight sided, fully open and fully wound. Hence, from fig.(3.2),

$$\Lambda_{s_2} = \mu_o \times \frac{0.978}{3 \times 0.584}$$

i.e. $\quad \Lambda_{s_2} = 0.559\mu_o$ per unit length of rotor bar.

Allowing for skew,

$$\text{rotor bar length} = \frac{\text{rotor core length}}{\cos\alpha}$$

where α is the skew angle. For a skew of two slot pitches

$$\alpha = \tan^{-1}\left[\frac{\pi D_b \times 2/25}{\text{rotor core length}}\right]$$

$$= \tan^{-1}\left[\frac{\pi \times 5.81 \times 2 \times 2}{25 \times 17.6}\right]$$

i.e. $\quad \alpha = 9.4$ and $\cos\alpha = 0.99$

whence, $\quad \Lambda_{s_2} = 0.553\mu_o$ per unit core length.

Λ_{h_2}:

Using the same technique as that developed for the stator overhang, two flux plots were made and are given in fig.(3.15). From map (1), taking the field up to the outside diameter of the stator overhang and ignoring the current distribution in the rotor endring,

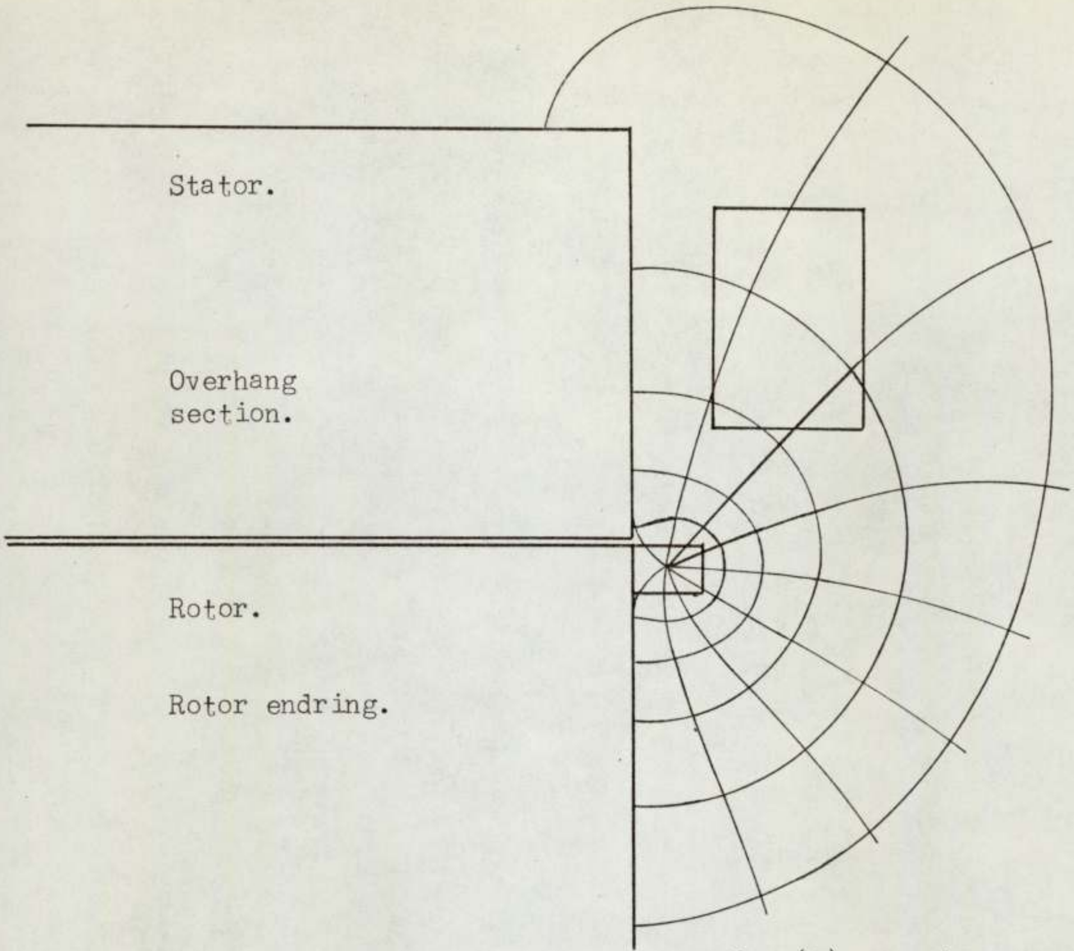

Map (1), opposite stator tooth.

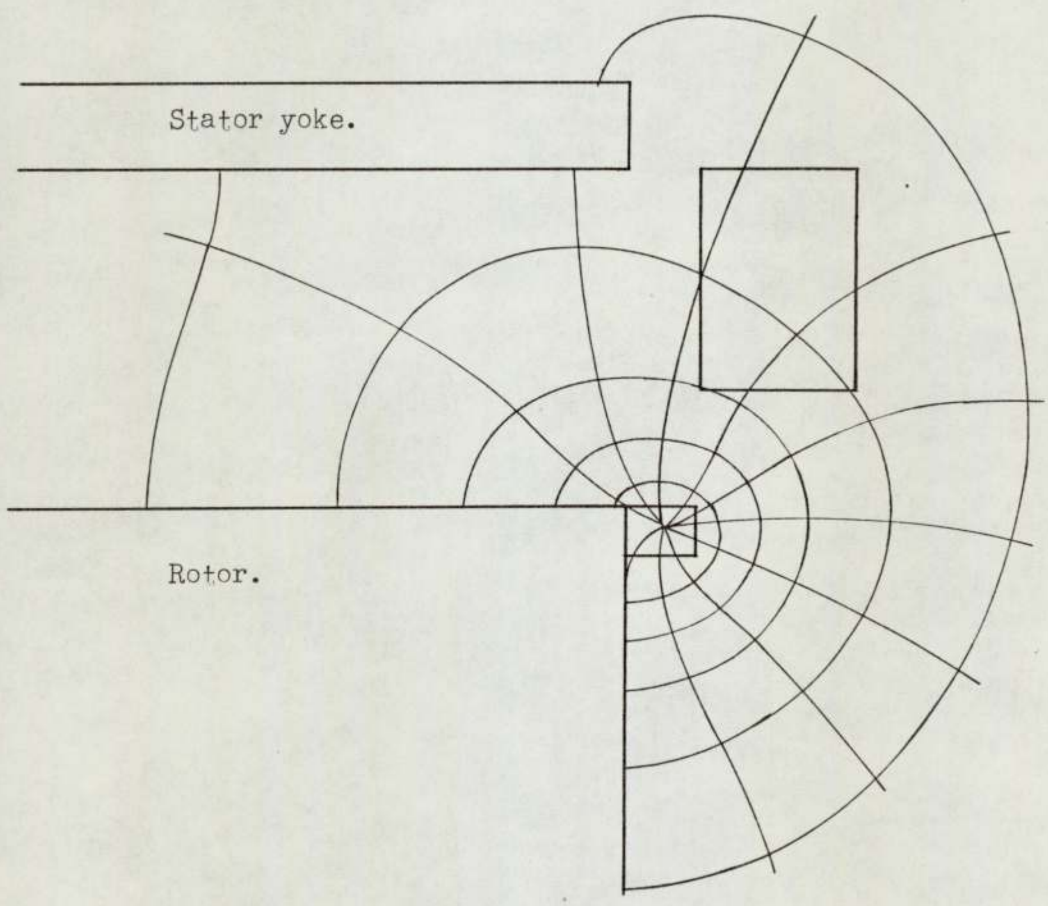

Map (2), opposite stator slot.

FIG.(3.15). ROTOR ENDRING FLUX DISTRIBUTIONS.

$$T_o = 5; \ M = 8 \ \text{giving}$$

$$\Lambda_{h_2} = \mu_o \frac{5}{8} \times \frac{\text{outhang length}}{\text{rotor core length}} .$$

From map (2) for the same conditions,

$$T_o = 5; \ M = 10 \ \text{giving}$$

$$\Lambda_{h_2} = \mu_o \frac{5}{10} \times \frac{\text{outhang length}}{\text{rotor core length}} .$$

Taking the average of these two values,

$$\Lambda_{h_2} = 0.562\mu_o \times \frac{\text{outhang length}}{\text{rotor core length}} .$$

In the determination of the resistance of the endrings, the effective diameter D_r of the rings was obtained in terms of the mean pitch circle diameter of the bars, D_b, and a coefficient K_{ring} such that $D_r = D_b K_{ring}$. Using this same value of D_r, the length of overhang between the rotor bars one slot pitch apart is

$$\frac{K_{ring} D_b \pi}{n}$$

i.e. substituting the appropriate values, rotor overhang per bar is

$$\frac{0.94 \times 11.6 \times \pi}{25} \quad \text{i.e.} \quad 1.38 \text{ mm.}$$

Hence,
$$\Lambda_{h_2} = 0.562\mu_o \times \frac{1.38}{17.6}$$

$$\text{i.e.} \ \Lambda_{h_2} = 0.044\mu_o$$

The total permeance factor for the rotor is, therefore,

$$= (\Lambda_{g_2} + \Lambda_{s_2} + \Lambda_{h_2})$$
$$= (2.217 + 0.553 + 0.044)$$

$$\text{i.e.} \ \Lambda_2 = 2.81\mu_o$$

Taking the current to be a sinusoidal function of space as in the method used for determining the referred rotor resistance, the rotor bar current is in general given by $i_{bar} = J \cos(\psi - s\omega_s t) A_b$ by equation (3.0). Considering two adjacent bars and the connecting sections of the endrings to constitute a current loop, the loop current will be given by

$$i_{loop} = \hat{J}\, A_b \left[\cos(\psi - s\omega_s t) - \cos(\,(\psi + \psi') - s\omega_s t) \right]$$

where ψ' is the bar displacement in electrical radian measure.

$$\text{i.e. } i_{loop} = 2\, A_b \hat{J} \left[\sin\tfrac{1}{2}(2\psi + \psi' - 2s\omega_s t)\sin\tfrac{1}{2}(\psi') \right]$$

$$= 2\, A_b \hat{J} \left[\sin(\psi + \psi'/2 - s\omega_s t)\sin\psi'/2 \right]$$

From equation (3.3), $$\hat{J} = \frac{2s_p k_1 c_1 p\hat{I}_2}{s_w D_b T}$$

Hence, in terms of the referred load current $\hat{I}_2$,

$$i_{loop} = \frac{2 \times 2s_p k_1 c_1 p\hat{I}_2 A_b}{s_w D_b T} \sin(\psi + \psi'/2 - s\omega_s t)\sin\psi'/2$$

so that $$I_{loop}\,(\text{r.m.s.}) = \frac{4s_p k_1 c_1 p\hat{I}_2 A_b}{\sqrt{2}\, s_w D_b T} \sin\psi'/2 \qquad (3.21)$$

Consider the leakage flux generated by the loop current in loop (1) of fig.(3.16).

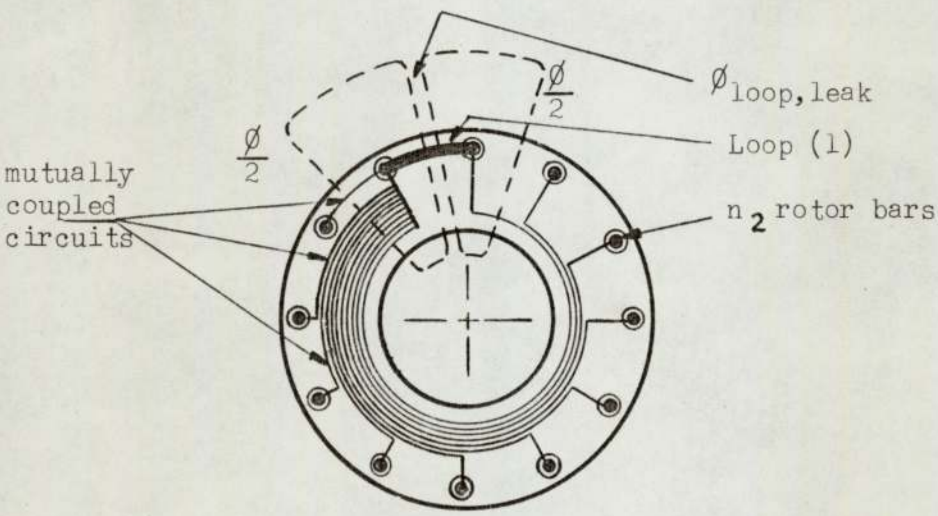

FIG. (3.16). PERTAINING TO ROTOR LEAKAGE INDUCTANCE.

The number of flux linkages associated with this flux is $(n_2 - 1)\emptyset_{loop,leak}$, by mutual coupling, and $1 \times \emptyset_{loop,leak}$ for the loop containing the current. Since the endring resistance and reactance are small compared with those of the bars, then the impedances of all the circuits coupled will be the same. In assessing this quantity it is assumed that the leakage flux path is as shown above, the flux being completely contained by the teeth adjacent to the one forming the core of the loop; this is verified by fig.(3.17).

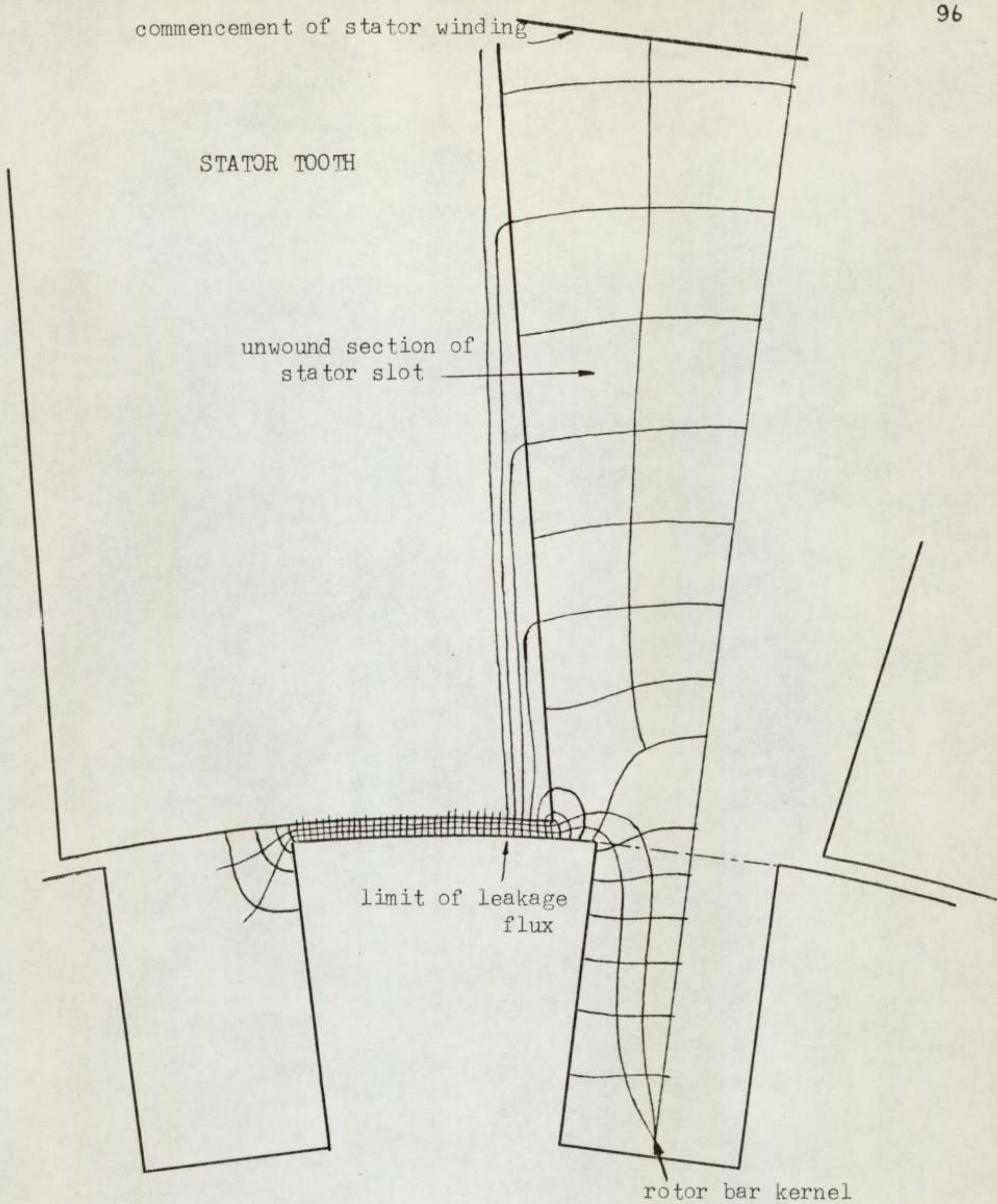

FIG.(3.17). ROTOR BAR LEAKAGE FLUX DISTRIBUTION.

In this figure a plot was made to determine the extent to which the leakage flux assocaited with one rotor bar linked the adjacent rotor bars. This was plotted for the rotor in what was considered to be the position that would give maximum inter-bar coupling.

In terms of Λ_2, the rotor permeance factor, the permeance factor for the loop made up of two adjacent rotor bars and the sections of endrings connecting them will be $2\Lambda_2$. The loop inductance is, therefore, $2\Lambda_2 l_b$ and the reactive volt-amperes for this loop for any slip s are

$$I^2_{loop} \times 2\Lambda_2 l_b \times s\omega_s,$$

i.e. by equation (3.21),

$$VAr_{loop} = 2\Lambda_2 l_b \left[\frac{4s_p k_1 c_1 p_1 \hat{I}_2 A_b}{2s_w D_b T} \sin\psi'/2 \right]^2 s\omega_s.$$

Since the mutually coupled circuits have the same impedance as the loop containing the current, then each of these circuits will have a current equal to I_{loop} induced in it. Hence, since there are as many circuits, including the primary loop, as there are bars, the total reactive volt-amperes associated with this one primary loop current are $2n_2 VAr_{loop}$ so that the total reactive volt-amperes for the entire rotor current distribution will be $n_2 \times 2n_2 VAr_{loop}$. If the rotor leakage reactance per phase referred to the stator is L_2, then equating the referred rotor reactive volt-amperes to the actual rotor reactive volt-amperes,

$$m\left[\frac{\hat{I}_2}{\sqrt{2}}\right]^2 \omega_o L_2 = 2n_2^2 VAr_{loop},$$

where ω_o is the angular frequency of the supply.

i.e. substituting from above, taking s =1.0,

$$L_2 = \frac{2n_2^2 \Lambda_2 l_b}{m} \left[\frac{4s_p k_1 c_1 A_b p_1}{s_w D_b T} \sin\psi'/2 \right]^2 \qquad (3.22)$$

From page(70),

$$\frac{1}{D_b T} \times \frac{s_p}{s_w} = \frac{\pi}{n_2 A_b}.$$

Substituting in equation (3.22),

$$L_2 = \frac{32\pi^2 \Lambda_2 l_b}{m} \left[k_1 c_1 p_1 \sin\psi'/2 \right]^2 \qquad (3.23)$$

Inserting the appropriate values this yields,

$$L_2 = 16\pi^2 \times 2.81 \times 4\pi \times 10^{-7} \times 1.76 \times 10^{-2} \times \left[1.925 \times 352 \times \sin \frac{360}{50} \right]^2$$

i.e. $L_2 = 0.071$ henry.

Effects of rotor bar skew:

Apart form the increase in rotor conductor length already allowed for, the skewing of the rotor conductors relative to the stator has the effect of reducing the mutual coupling between the stator and the rotor and is best considered from this point of view instead of that of reduced rotational voltage which will be taken care of through the terms of the $G_{\alpha\beta}$ tensor (see equations (2.6) and (2.7)).

On no load conditions, the flux in the machine will, since the overall reluctance is not affected to any extent by skew, be the same as it would be if the rotor bars were not skewed. Consequently, any changes in the equivalent circuit parameters, caused by the skew, must be restricted to the rotor branch. The change in the mutual inductance must, therefore, be caused by a change in $(L_r - l_r)$ and l_r (see fig.(2.5)). If it is assumed that the total self inductance L_r of the rotor is unaffected, then the effect of skew can be looked upon as a redistribution of the rotor mutual and leakage fluxes - not the stator fluxes.

Let the change in mutual inductance be $S_k M$, where S_k is here defined as the "skew reduction factor."

The new mutual inductance will then be given by

$$M' = M(1 - S_k)$$

From fig. (2.5),

$$\sqrt{(L_s - l_s)(L_r - l_r')} = (1 - S_k)\sqrt{(L_s - l_s)(L_r - l_r)}$$

where l_r' is the new rotor leakage inductance.

Therefore, $$(L_r - l_r') = (1 - S_k)^2(L_r - l_r).$$

Hence, in the equivalent circuit referred to the stator, since the magnetizing inductance will still remain at $(L_s - l_s)$ being insensitive to skew, as argued above, then $(L_r - l_r') \times u'^2$ must be equal to $(L_s - l_s)$ and, therefore, to $(L_r - l_r) \times u^2$.

$$\text{i.e. } u'^2 = \frac{u^2}{(1 - S_k)^2} \qquad (3.23a)$$

where u' is the new rotor/stator transformation ratio accounting for the effect of the rotor bar skew.

This means that if L_2 and R_2 are calculated from the design details as if the rotor bars were not skewed, then their values must be divided by $(1 - S_k)^2$ to allow for the skew, before insertion into the equivalent circuit or use in the construction of the impedance tensor.

Determination of the value of the skew reduction factor:

Consider one pole of the stator flux distribution and let there be q_2 rotor slots per pole, taking the nearest integer if q_2 is fractional. Fig.(3.18) shows this arrangement, with and without skew, for q_2 equal to 5.

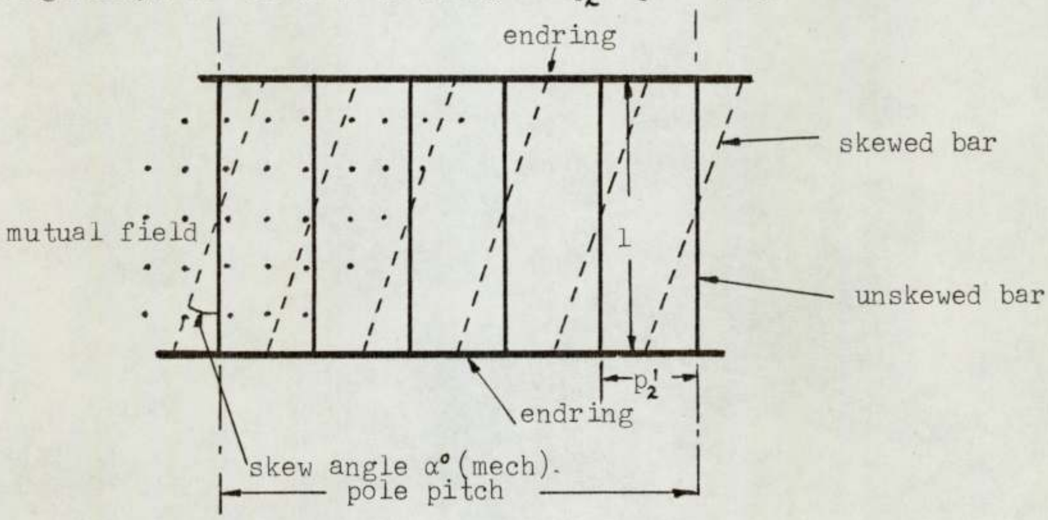

FIG. (3.18). PERTAINING TO EFFECT OF SKEW ON MUTUAL COUPLING.

Assume the flux density to be uniform over the pole face.

For no skew: Due to the nature of the squirrel cage winding, there are many more circuits linking the stator flux than is apparent at first sight. Thus, each pair of adjacent bars links the flux ϕ/q_2 where ϕ is the total flux per pole. Therefore, the flux linkages due to circuits comprising adjacent bars is $q_2(\phi/q_2)$.

Similarly, each pair of adjacent but one bars links the flux $2\phi/q_2$ and the total flux linkages due to these circuits is $(q_2 - 1) \times 2\phi/q_2$.
Likewise, each pair of adjacent but two bars links the flux $3\phi/q_2$, the total flux linkages for these circuits being $(q_2 - 2) \times 3\phi/q_2$.
In general, therefore, the total flux linkages per pole for the cage winding having q_2 slots per pole is given by

$$\phi \sum_{X=0}^{X=(q_2-1)} (q_2 - X)\frac{(X+1)}{q_2}$$

With skew: For every constituent type of bar combination, it is apparent from fig.(3.18) that the effect of skew is to reduce the total flux linkages by

$$4 \times \frac{\phi}{q_2} \times \frac{\frac{l\tan\alpha}{2} \times \frac{1}{2}}{l p_2'}$$

i.e.
$$\frac{l\tan\alpha}{q_2 p_2'}\phi$$

Since there are q_2 types of bar combination, the flux linkages per pole are, therefore, reduced by $\frac{l\tan\alpha}{p_2'}\phi$ and the new total flux linkages per pole then become

$$\left[\sum(q_2 - X)\frac{(X+1)}{q_2} - \frac{l\tan\alpha}{p_2'}\right]\phi$$

Therefore,

$$\frac{M'}{M} = 1 - \frac{q_2 l\tan\alpha}{p_2'\sum(q_2 - X)(X+1)}$$

and the change in the mutual coupling is then,

$$S_k = \frac{q_2 l\tan\alpha}{p_2'\sum(q_2 - X)(X+1)} . M \qquad (3.23b)$$

for the limits $X = 0$ to $X = (q_2 - 1)$.
In this case, substitution of the appropriate values gives $S_k = 24/364$, which is negligible.

Assessment of machine's suitability as a servomotor:

As discussed in the prelude, the basic criterion is that the peak torque of the machine should occur at a slip greater than unity.

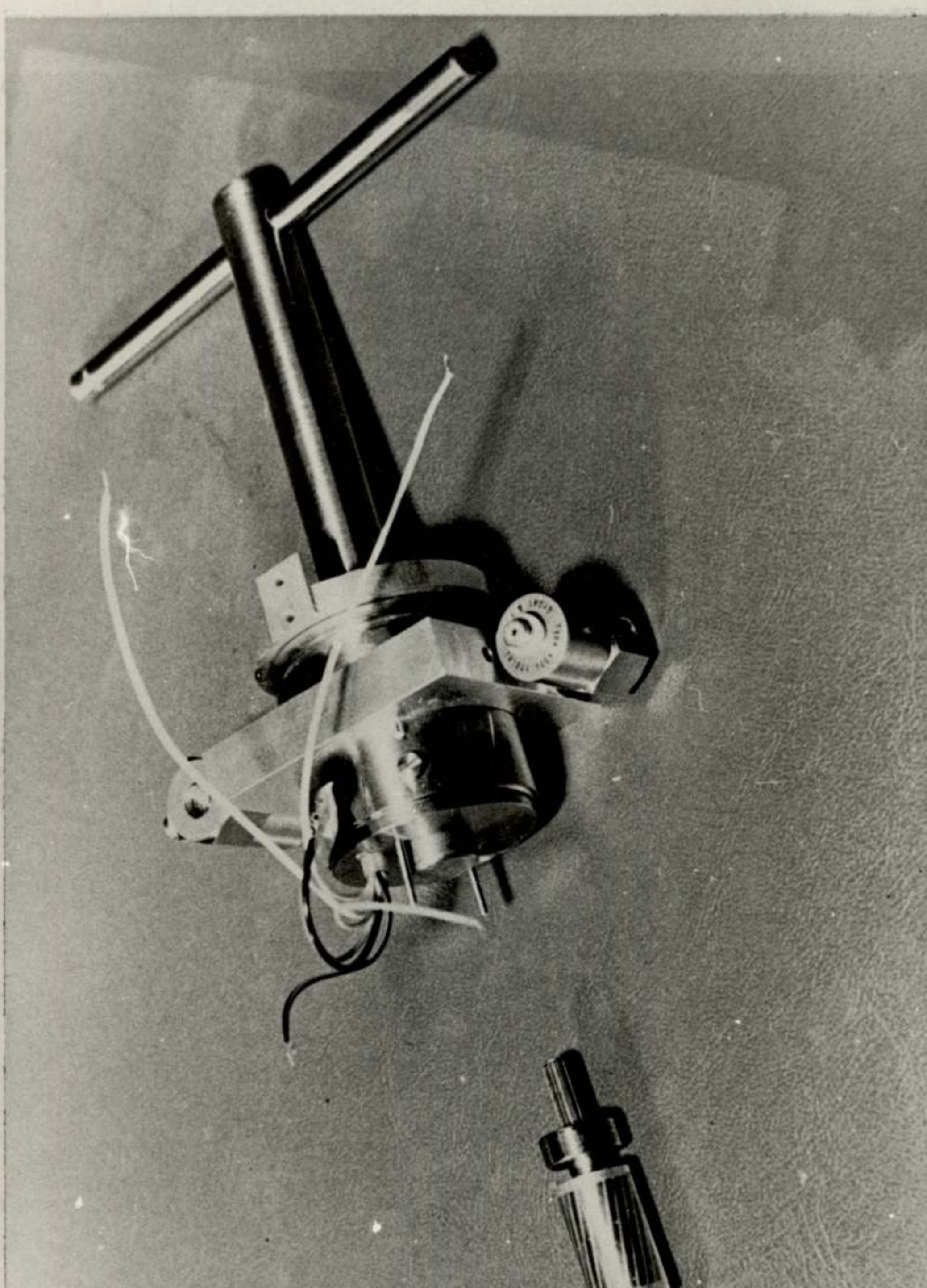

PHOTOGRAPH (3.1).USE OF ASSEMBLY MANDREL.

From the steady state analysis of the machine given in the prelude, peak torque occurs at a slip

$$s_{\hat{T}} = \left| \frac{R_2}{Z_{source} + \dfrac{(R_1 + jX_1)jX_o}{R_1 + j(X_1 + X_o)} + jX_2} \right|$$

Taking the source impedance as negligible and substituting the values calculated for the other parameters

$$s_{\hat{T}} = 1.7 \text{ pu., at } 113^\circ C$$

which is satisfactory on this criterion.

Mechanical design:

The usual method of assembly of these types of machine is described in reference (3). The mechanical arrangement adopted for this test machine is such that it is easily possible to change the stator, rotor or bearings whilst maintaining the accuracy of the air gap.

The principle used is that of mandrel assembly. The stator housing is of stainless steel and has three pairs of set screws at 120° to each other for locking the stator in position. Integral with the stator housing is the frontend bearing bracket, the back end bracket being spiggotted to the housing and held by three further set screws. The bearing registers and the stator bore are of the same diameter and machined prior to assembly. A polished mandrel with only 0.0001" diametral clearance is used to align the stator housing, the stator itself and the front end bearing bracket after which all the set screws are tightened and the mandrel removed.

Photograph no. (3.1) shows this mandrel in use. With this method of assembly, the necessity of potting the machine in araldite and through-boring as detailed in reference(3), were obviated.

Since it was intended to carry out measurements of dynamic torque on this machine, the rotor was subjected to a small axial spring load by means of an adjustable axial pressure plate on the outer race of the back end bearing, the inner race of this bearing being located against a shoulder on the rotor shaft and retained by a small circlip, whilst the outer race floats in its housing to allow for thermal expansions. This shaft end-load was found to be necessary as a result of earlier experimental work in the measurement of the dynamic performance of these small machines where axial oscillation of the rotor had been encountered and had caused spurrious results; fig.(3.18a) illustrates the use of this pressure plate.

Apart from the modifications to assembly just described, the usual methods of core and winding construction were followed.

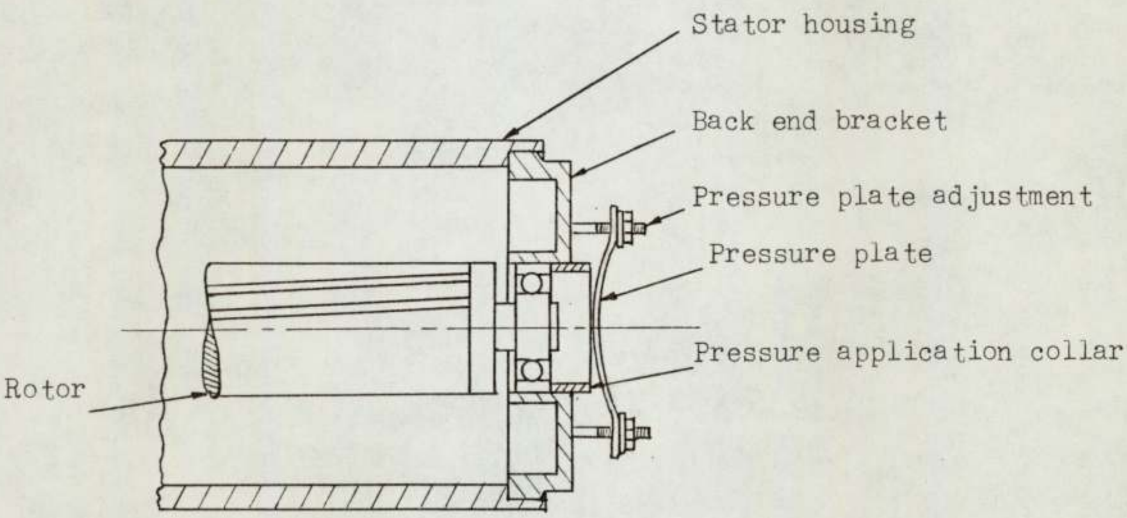

Stator core and winding omitted for clarity.

FIG. (3.18a). BACK END BEARING PRESSURE PLATE ON TEST MACHINE.

Modification to Design Calculations to Obtain Equivalent Circuit Parameters For Space Harmonics:

With the design calculations fully laid out, it is now possible to decide which of the machine parameters are affected by space harmonics, thereby corroborating the assumptions made in chapter II, and indicate the modification to the method of calculation necessary for its application to the harmonic. Taking each calculation in turn:

Stator winding resistance, R_1:

Not affected.

Rotor winding resistance, R_2:

From equation (3.11) R_2 is obviously sensitive to harmonic order. The form of this equation for a harmonic cannot, however, be obtained simply by inspection, it is necessary to retrace the development. Thus, in the expression for the stator magnetomotive force, the angles should be electrical for the particular harmonic and the correct Fourier coefficient should be used so that

$$\text{m.m.f.}_\theta = k_n c_1 \hat{I}_1 \sin(n\theta + \alpha_n)$$

Considering that each harmonic component of the stator magnetomotive force generates a particular current of sinusoidal time function in the squirrel cage rotor, then if an ideal balance is assumed for each component of the stator magnetomotive force with the corresponding component of the rotor magnetomotive force, the stator component will be given by $k_n c_1 \hat{I}_2 \sin(n\theta + \alpha_n)$.

The current density distribution in the rotor will be

$$J_{n\psi} = \hat{J}_n f(n\psi,\ s_n\omega_{s,n}t)$$

where $s_n\omega_{s,n}$ is the slip speed of the harmonic current distribution in the rotor relative the conducting sheet. Equation (3.1) becomes

$$i_{n\psi} = \hat{J}_n f(n\psi,\ s_n\omega_{s,n}t)\,\frac{D_b\ \delta\psi}{2p_n}T \qquad (3.24)$$

Consequently, the magnetomotive force across the air gap at any point ψ is

$$\frac{V_c}{V_s}\left[\frac{\hat{J}_n D_b T}{2p_n}\int_{f_o}^{\psi} f(n\psi,\ s_n\omega_{s,n}t)d\psi\right]\qquad \text{for the rotor.}$$

Whence, for the ideal magnetomotive force balance,

$$k_n c_1 \hat{I}_2 \sin(n\theta + \alpha_n) = \frac{s_w \hat{J}_n D_b T}{s_p 2p_n}\int_{f_o}^{\psi} f(n\psi,\ s_n\omega_{s,n}t)d\psi$$

from which it is apparent that

$$f(n\psi,\ s_n\omega_{s,n}t) = \cos(n\psi - s_n\omega_{s,n}t)$$

and that

$$k_n c_1 \hat{I}_2 = \frac{s_w \hat{J}_n D_b T}{s_p 2p_n}\quad .$$

The elemental harmonic rotor current is then

$$i_{n\psi} = \frac{\hat{J}_n D_b T}{2p_n}\cos(n\psi - s_n\omega_{s,n}t)\delta\psi \qquad (3.25)$$

$$\text{where}\quad \hat{J}_n = \frac{2s_p k_n c_1 p_n \hat{I}_2}{s_w D_b T} \qquad (3.26)$$

The total power dissipated in the squirrel cage by the harmonic component current will be, from equation (3.5),

$$W_{cn} = \frac{s_w}{s_p}(1.57\ \hat{J}_n^2 D_b T\rho l_b)n \quad \text{watts.} \qquad (3.27)$$

The total power dissipated in the endrings by this harmonic current is, by equation (3.7)

$$W_{rn} = 0.784\,\frac{s_w^2 \hat{J}_n^2 T^2 D_r^3 \rho}{s_p^2 p_n^2 A_r}\,n \qquad (3.28)$$

Hence, the total rotor power dissipated by the harmonic component current is

$$W_n = \hat{J}_n^2 \rho n\left[1.57\ D_b l_b T\frac{s_w}{s_p} + \frac{0.784\ T^2 D_r^3 s_w^2}{p_n^2 A_r s_p^2}\right] \qquad (3.29)$$

If $R_{2,n}$ is the actual harmonic rotor resistance referred to the stator, then

$$W_{2,n} = I_{2,n}^2 R_{2,n}\ m$$

where $I_{2,n}$ would be the stator current resulting from the harmonic current in the rotor.

Each rotor space harmonic was originally generated by a sinusoidal stator current of fundamental frequency and consequently, since the machine is magnetically linear, each rotor space harmonic will cause a sinusoidal stator current of fundamental frequency. However, the transformation from rotor to stator is not simply the inverse of the transformation from stator to rotor due to the presence of the Fourier coefficients associated with the stator winding only. Thus, if for a particular stator current the rotor current is $k_n w I_s$ where w is a simple invertible transformation ratio, the stator current caused by this rotor current will be proportional to $k_n \frac{k_n w I_s}{w}$, i.e. $k_n^2 I_s$. Hence, for a total referred rotor current I_2, the component harmonic referred currents will be given by

$$I_{2,n} = \left[\frac{k_n}{\sum k_n}\right]^2 I_2$$

Therefore,

$$W_{2,n} = \left[\frac{k_n}{\sum k_n}\right]^4 I_2^2 R_{2,n}\ m$$

and equation (3.10) then becomes

$$R_{2,n} = 39.5\ n \frac{\rho}{m} \frac{(p_n(\sum k_n)^2 c_1)^2}{k_n^2} \left[\frac{l_b}{n_2 A_b} + \frac{0.159\ D_r^3}{p_n^2 A_r D_b^2}\right] .$$

Since the value of K_{ring} is a function of the number of poles, then its value for the harmonic will be different from that for the fundamental; the actual may still be obtained from fig.(3.6'), let this be $K_{ring,n}$. The above equation for $R_{2,n}$ may then be written

$$R_{2,n} = 39.5\ n \frac{\rho}{m} \frac{(p_n(\sum k_n)^2 c_1)^2}{k_n^2} \left[\frac{l_b}{n_2 A_b} + \frac{0.159\ D_b K_{ring,n}}{p_n^2 A_r}\right] \quad (3.30)$$

In comparison with equation (3.11), the form is exactly the same except for the multiplying factor n, the order of the harmonic, and the factor $((\sum k_n)^2/k_n)^2$.

If $R_{2,1}$ is the rotor resistance for the fundamental component, then from equation (3.30)

$$R_{2,n} = R_{2,1}\left[\frac{k_1 p_n}{k_n p_1}\right]^2_n \left[\frac{\dfrac{l_b}{n_2 A_b} + \dfrac{0.159\ D_b K_{ring,n}}{p_n^2 A_r}}{\dfrac{l_b}{n_2 A_b} + \dfrac{0.159\ D_b K_{ring,1}}{p_1^2 A_r}}\right] \qquad (3.31)$$

i,e, $R_{2,n} = R_{2,1} H_{r,n}$

where $H_{r,n}$ is defined by equation (3.31) and will be called the "rotor harmonic resistance ratio."

Magnetising inductance, L_o:

In chapter II, fig. (2.11) shows that the magnetising inductance, for the equivalent circuit referred to the stator, is, on the assumption of a single valued stator leakage inductance, common to all rotor branches. Consequently, there is no need to examine L_o itself for variation due to harmonic order and immediate attention may be given to the stator leakage inductance.

Stator leakage inductance, L_1:

From the calculation of L_1, it is apparent that all the constituent permeance factors are, for the unsaturated machine, functions of the machine geometry only and are insensitive to harmonic order. In this case the stator leakage inductance must be constant. This validates the assumption made in chapter II and verifies that the magnetising inductance will assume a common value.

Rotor leakage inductance, L_2:

As for the stator leakage inductance, the constituent permeance factors are insensitive to harmonic order with the exception of the overhang leakage which is a function of K_{ring} and is, therefore a function of the number of poles. However, since, from the numerical values obtained, this is seen to be only 1.6% total permeance factor, it is assumed that its variation can be ignored and the total permeance factor taken as constant. It is in obtaining the value of the leakage referred to the stator that the effect of harmonic order is manifest. Again, following the method through, the r.m.s. loop current given by equation (3.21) will become

$$I_{loop,n} = \frac{4\, s_p k_n c_1\, p_n \hat{I}_{2,n} A_b}{\sqrt{2}\, s_w D_b T} \sin\frac{n\psi'}{2} \qquad (3.32)$$

Consequently

$$VAr_{loop,n} = 2\Lambda_2 l_b \left[\frac{4\, s_p k_n c_1\, p_n \hat{I}_{2,n} A_b}{\sqrt{2}\, s_w D_b T} \sin\frac{n\psi'}{2}\right] s_n \omega_{s,n}$$

so that if the actual rotor reactive volt-amperes are equated to the referred rotor reactive volt-amperes bearing in mind the relationship between the component harmonic referred rotor current and the total referred rotor current, already established,

$$L_{2,n} = \frac{2n_2^2\Lambda_2 l_b}{k_n^2 m}\left[\frac{4\, s_p(\Sigma k_n')^2 c_1\, A_b p_n}{s_w D_b T} \sin\frac{n\psi'}{2}\right]\frac{\omega_{s,n}}{\omega_o}$$

but $\dfrac{\omega_{s,n}}{\omega_o} = \dfrac{1}{n}$ whence equation (3.23) becomes

$$L_{2,n} = \frac{32\pi\Lambda_2 l_b}{k_n^2 mn}\left[(\Sigma k_n)^2 c_1\, p_n \sin n\psi'/2\right]^2 \qquad (3.33)$$

In comparison with equation (3.23) the form is the same except for the multiplying factor $1/n$ and the factor $((\Sigma k_n)^2/k_n)^2$. The former factor is in contrast to the factor n for the referred rotor resistance.

If $L_{2,1}$ is the rotor leakage inductance for the fundamental component then from equation (3.33)

$$L_{2,n} = L_{2,1}\left[\left[\frac{p_n k_1}{p_1 k_n}\right]\frac{\sin n\psi'/2}{\sin\psi'/2}\right]^2\frac{1}{n} \qquad (3.34)$$

i.e. $L_{2,n} = L_{2,1} H_{1,n}$

where $H_{1,n}$ is defined by equation (3.34) and will be called the

"rotor harmonic leakage inductance ratio."

The effect of rotor bar skew on harmonic parameters:

Reference to equation (3.23b), and its development, shows that the skew reduction factor is affected by the number of rotor slots per pole. For a harmonic, this must be taken as the number of slots per harmonic pole. The harmonic skew factors will, therefore, be greater than that for the fundamental; for example, in the test machine $S_{k,1} = 24/364$, $S_{k,5} = 6/10$, $S_{k,9} = 4/4$ taking q_2 as 2, $S_{k,11} = 2/1$ taking q_2 as 1. For any harmonic where $S_{k,n} \geqslant$ unity, the harmonic is, of course, rendered ineffective.

The effect on the harmonic parameters is the same as for the fundamental in that both $R_{2,n}$ and $L_{2,n}$ must be divided by $(1 - S_{k,n})^2$ if originally calculated for no rotor skew; $S_{k,n}$ is here defined as the "harmonic skew reduction factor."

Assuming that the fundamental rotor resistance and leakage inductance have been calculated to include the skew, then the above operation can conveniently be incorporated in the harmonic resistance and inductance ratios. Thus,

$$H'_{r,n} = H_{r,n}\left[\frac{1 - S_{k,1}}{1 - S_{k,n}}\right]^2 \qquad (3.35)$$

and

$$H'_{l,n} = H_{l,n}\left[\frac{1 - S_{k,1}}{1 - S_{k,n}}\right]^2 \qquad (3.36)$$

where $H'_{r,n}$ and $H'_{l,n}$ can be defined as the "skew modified rotor harmonic resistance and inductance ratios" respectively.

5) Design of Dynamometer.

To make accurate steady state and dynamic measurements on the miniature machine under investigation, it was found necessary to design and construct a suitable dynamometer, there being no such equipment on the market. To cover the characteristics of the test machine and those of other machines encompassed in the envisaged field of subsequent investigation, the dynamometer was required to meet the following basic specification:

a) To be capable of measuring steady state and dynamic torques of up to and including 50×10^{-3} Nm. over a speed range of 0-24000 r.p.m. in both directions of rotation for machines up to and including size 15.

b) To measure the gross torque developed by the machine under test.

c) To be capable of indicating irregularities in the machine's speed/torque characteristic due to the presence of m.m.f. harmonics in the machine.

Preliminary design considerations:

It was decided to adopt the conventional form of dynamometer in which the test machine is fixed to a frame carried on a pair of trunnion bearings between which the frame can rotate under the influence of the reaction torque generated on the machine's stator, this rotation being balanced by a restoring torque caused by the frame rotation itself.

Because of the low order of the torques to be measuredand because also of the sensitivity required to indicate harmonic torques, it was clear that the usual form of ball-race trunnions used to support the frame would not be suitable unless the races were of the contra-rotating type to overcome stiction. The chances of obtaining such trunnions which would at the same time generate an acceptably low drag torque were thought to be remote and although the possibilities were investigated, the idea was abandoned.

The further idea of using air-bearing trunnions was explored but was also abandoned again because of the probable generation of drag torque by the bearings.

It was finally decided to support the dynamometer on cross-flexure pivots (30) which offered several advantages, in particular,

a) being free of sliding parts, there would be complete absence of stiction,

b) within a limited rotation the relationship between torque and deflection is linear,

c) with suitable design, the pivot reeds could be insulated from the frame and supports and used as electrical leads into the servomotor so eliminating spurrious torques due to lead drag.

The necessity for the dynamometer to be capable of indicating harmonic torques in the test machine's characteristic, meant that the motor torque had to be measured at a fixed speed. That this is so is apparent on consideration of the possible shape of the speed/torque curve, for this type of machine, containing a pronounced irregularity, see fig. (3.19).

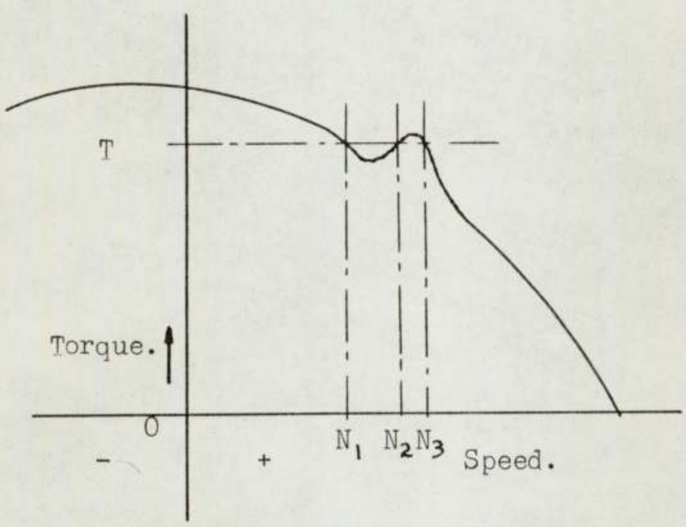

FIG. (3.19). SERVOMOTOR SPEED/TORQUE CURVE EXHIBITING PRONOUNCED HARMONIC IRREGULARITY.

In this diagram, the harmonic torque is shown as existing over a relatively wide range of speed. This is because the induction servomotor has a very high rotor resistance in order that the machine will give the required shape of speed/torque curve. It will be seen that for a given torque T, the motor could operate at any one of three different speeds stably or unstably depending upon the load characteristic. On the other hand, for a given speed N, there is only one possible value of torque. In order to obtain this type of measurement it is necessary to drive the motor under test at a predetermined speed, by means of a seperate driving motor, and measure the torque generated by the test machine at this speed. Assuming a driving motor is available the method offers the further advantage of satisfying the requirement of section (b) of the preliminary specification by adopting the following procedure for each determination:

i) With the servomotor on test unenergized, set the driving motor to a given speed and drive the servomotor at this speed noting the deflection of the dynamometer from zero.

ii) With the servomotor still being driven at the given speed, energize its windings and again note the frame deflection.

The sum of these two readings measured from zero, will then be the deflection due to the gross torque developed by the servomotor at the particular speed and excitation.

From these considerations, it was possible to sketch the tentative basic arrangement for the dynamometer, fig. (3.20), and draw up a more detailed specification for which a functional design could be executed.

Design specification:

Frame.	To be of aluminium light alloy. To be as rigid as possible, commensurate with light weight.
Cross-beam.	To be of aluminium light alloy and suitable for flange mounting motors of sizes up to and including size 15, by means of adaptor plates.
Pivots.	To be of cross-flexure type using insulated metallic reeds. Rotation to be limited to $\pm 20^\circ$ about zero. Reeds to be used as electrical leads into test motor and to be capable of generating a restoring torque of up to 25×10^{-3} Nm. per pivot.

Drive. Suitable for speed range 0-24000 r.p.m. in both directions of rotation with a minimum output torque of 70×10^{-3} Nm. at 6000 r.p.m.. Speed to be independent of load.

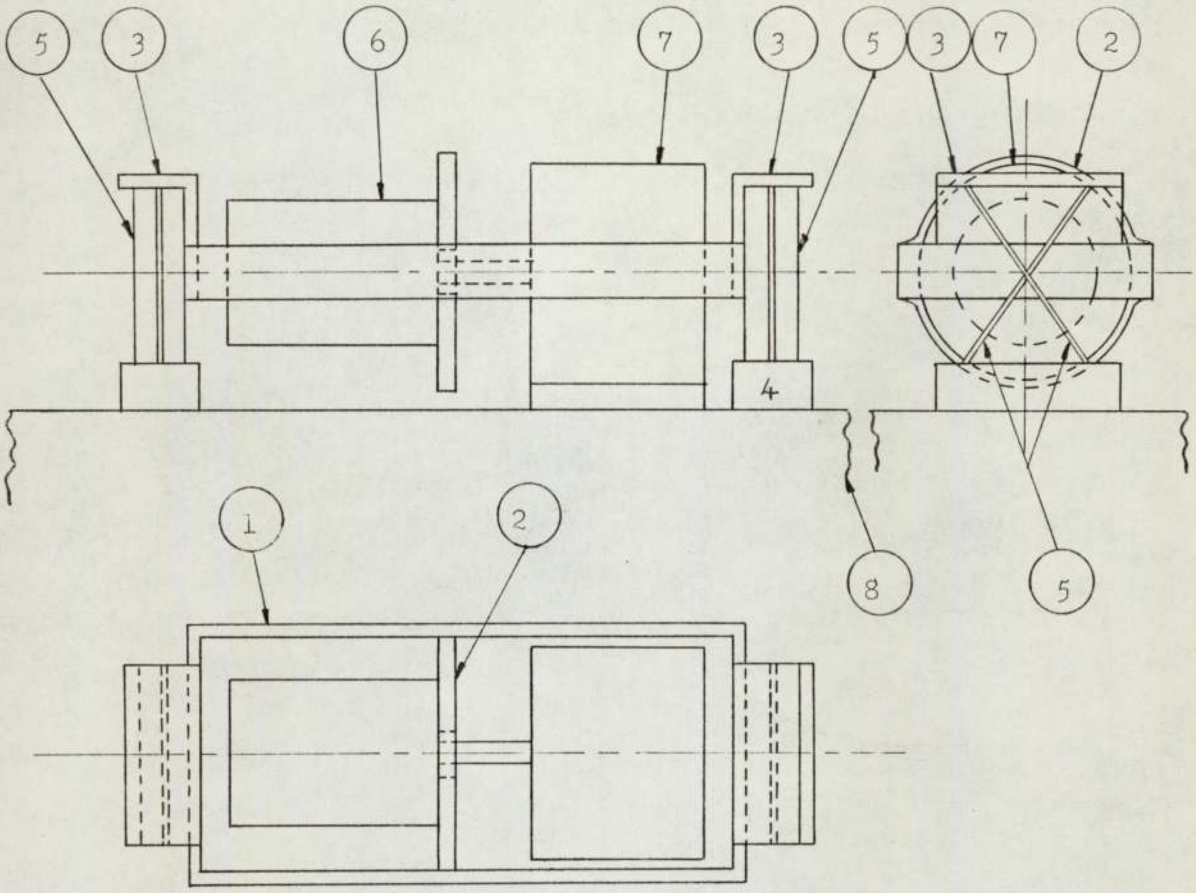

FIG. (3.20). TENTATIVE BASIC ARRANGEMENT FOR DYNAMOMETER.

Item schedule for fig.(3.20):

Item No.	Description.
1	Dynamometer frame.
2	Cross-beam for flange mounting motor under test.
3	Upper cross-flexure reed anchorage.
4	Lower cross-flexure reed anchorage.
5	Cross-flexure reeds.
6	Servomotor under test.
7	Driving motor, fixed to baseplate.
8	Baseplate.

Dynamometer frame:

Before commencing the design of the frame, further consideration was given to the type of drive to be used. The basic specification for the dynamometer requires that the instrument be capable of measuring steady state and dynamic torques. The term "dynamic torque" usually refers to the instantaneous torque developed whilst the motor is accelerating or decelerating, whereas the steady state torque is taken as the average torque over several revolutions at constant speed.

Since, at some time during the overall programme of investigation into the dynamic behaviour of these miniature machines, it was thought likely that instantaneous torque at constant speed would be of interest, it was decided to use a speed fixing motor which would generate the minimum amount of vibration and noise. This precluded the use of commutator machines and favoured the use of synchronous or induction motors. From the point of view of the speed range required, the synchronous motor would require a source the frequency of which would have to be continuously variable from zero. Furthermore, at the slow speeds, due to the time variation in its mutual flux wave, this motor would not have a constant instantaneous speed. Whilst this would not be a serious draw-back in the measurement of average steady state torque, it is inacceptable in the measurement of instantaneous steady state torque.

These observations led to the conclusion that in the speed fixing motor both the rotating field and the rotor should have as high an angular velocity as possible. The latter of these dictated the use of a stepped pulley and belt drive whilst the former favoured the use of a double fed induction motor, the low speeds being then given by the difference in the velocities of the stator and rotor rotating fields in conjunction with the step down ratio of the belt drive.

The design of this drive is dealt with in section (6). Its use dictated the final dimensions of the frame and a modification to the basic arrangement of the dynamometer. Thus, whereas in fig.(3.20) the frame encompasses the driving motor and lies in the horizontal plane, in the modified arrangement the driving motor is situated outside the frame which has been turned into the vertical plane. This allows easy access for the belt drive apart from other advantages which will become apparent.

Since the cross-flexure pivots are very sensitive to side loads, it was not possible to have the pulley on the shaft of the motor under test. Quite apart from this it would in any case be bad practice from the point of view of bearing noise in the test machine which should be avoided if a true instantaneous developed torque is to be measured. To overcome this difficulty, a driving head was interposed between the test motor and the speed fixing motor. In this way the driving head, being attached to the dynamometer bed, takes all the side load due to the belt drive and transmits a pure torque, via a dog coupling, to the test machine. Fig.(3.21) is the final general arrangement of the dynamometer and corresponds to the detailed working drawings given in the appendix. By allowing space for the driving head and arranging that the centre of gravity of the test motor coincided with the frame centre-line to ensure an equal distribution of the dead weight between the two pivots, the frame dimensions were fixed and are as shown in sheet (1) of the working drawings. This frame was made from aluminium manganese alloy. It was milled from the solid and finally stress relieved to prevent any distortion taking place during use since this would complicate the performance of the pivots.

To maintain a linear pivot performance, balance weights were included in the frame design to counter the weight of the frame pivot anchorages. The size of these weights was determined by direct weighing after the pivot anchorages had been made. The design of the frame was such that the pivot anchorages could be at the top frame edge or the bottom frame edge. This was to allow the pivots to be used either in tension or in compression at will; it had the added advantage of providing accurate location holes for the balance weights which are screwed to the frame through the vacant anchorage location holes.

ITEM No.	DESCRIPTION.
1	Bedplate.
2	Dynamometer frame.
3	Dynamometer frame supports.
4	Pivot beam.
5	Pivot reed.
6	Motor mounting flange.
7	Motor under test.
8	Driving head.
9	Driving pulley.
10	Frame balance weights.
11	Dynamometer way.
12	Driving motor.
13	Motor pulley.
14	Driving motor support.
15	Round belt drive.
16	Driving motor way.
17	Mirror.
18	Clamping bolts, etc..

FIG. (3.21). GENERAL ARRANGEMENT OF DYNAMOMETER.

SCALE: Full size.

For detailed working drawings to which the arrangement refers, see appendix.

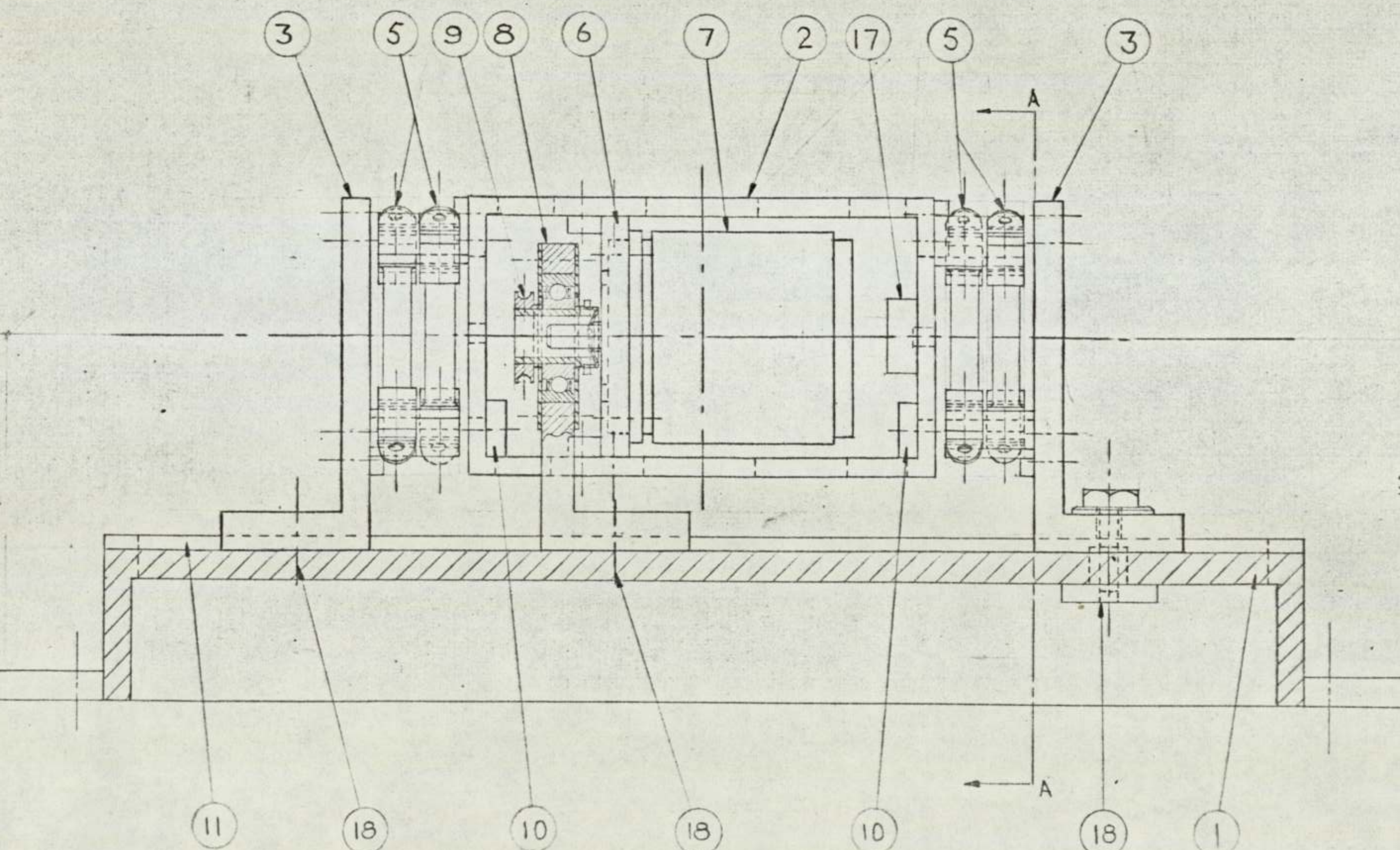

SECTION ON BB.

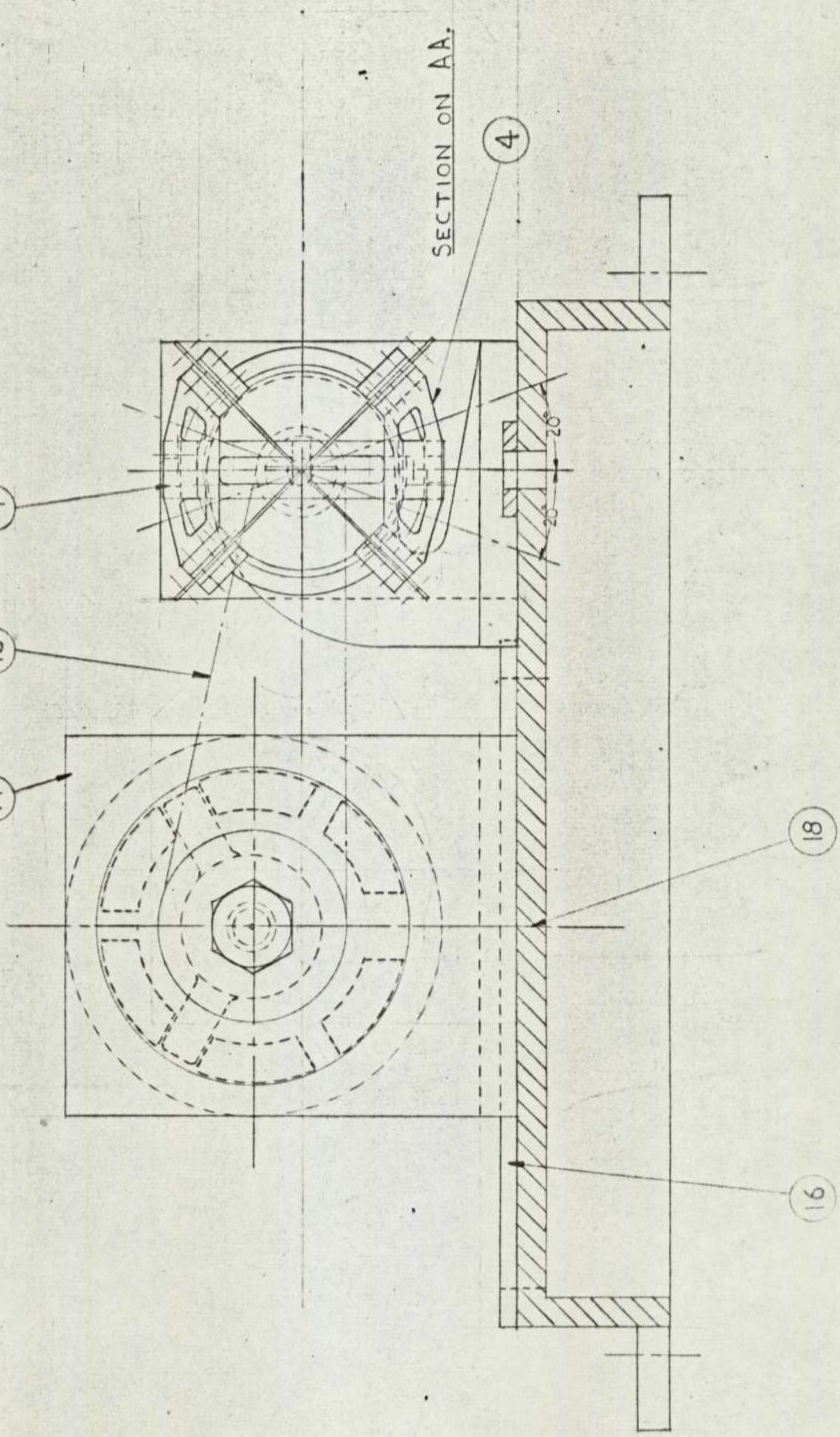
SECTION ON AA.
4
4
15
14
18
16
20
20

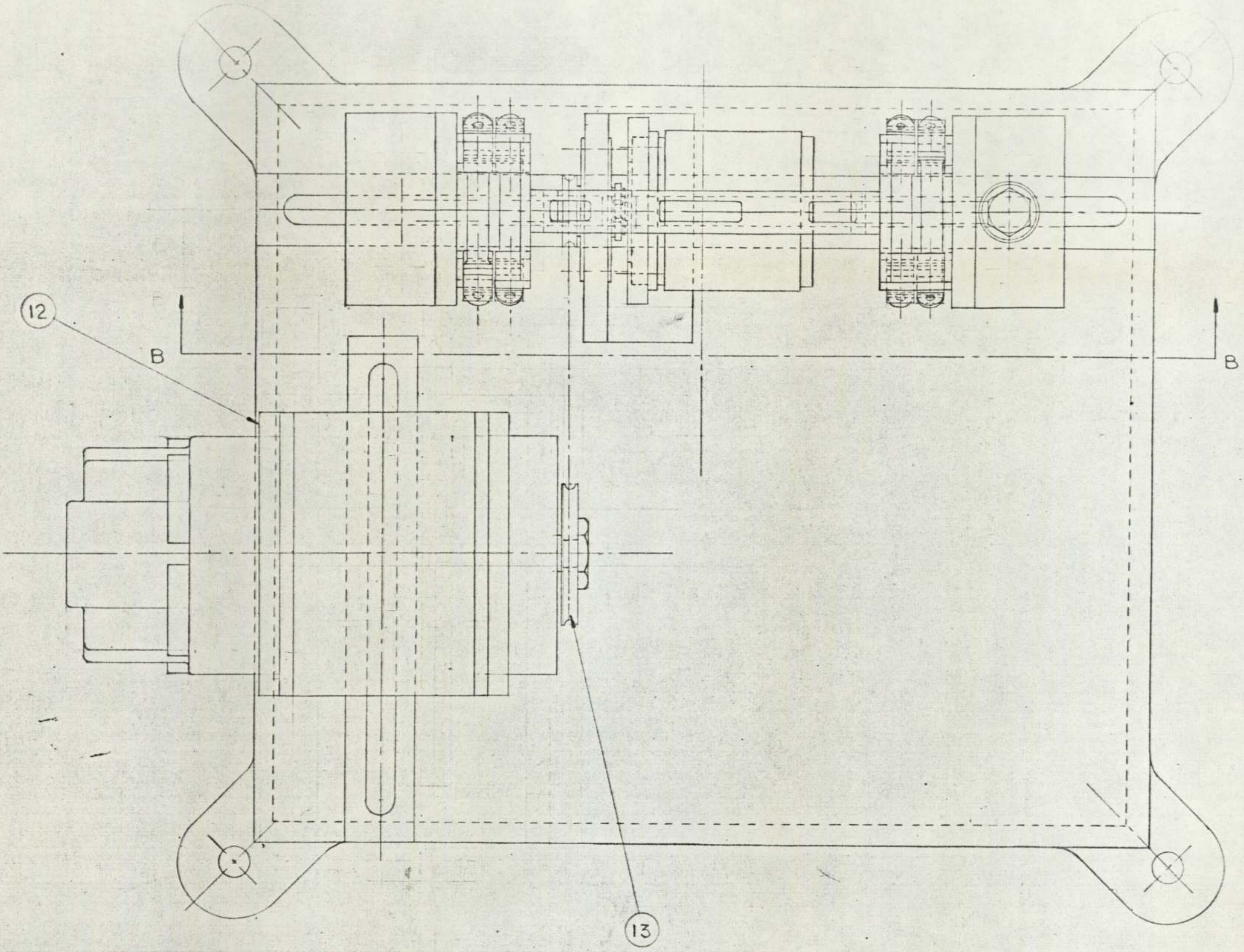

12
B
B
13

Pivot design:

The design of these cross-flexure pivots is based on the results of work carried by W.H.Wittrick and published in the Australian Journal of Scientific Research. (30) This paper deals with the analysis and design of cross-flexure pivots subjected to horizontal and/or vertical loads. It shows that the sensitivity of the pivot, expressed as deflection/ unit torque, is adversely affected by horizontal loads whereas vertical forces can be utilized to either increase or decrease the pivot stiffness depending upon whether the pivot is in compression or tension. Fig.(7) of the paper gives the relationships between the pivot stiffness KL/EI, the vertical compressive load $V_c L^2/EI$, the vertical tensile load $V_t L^2/EI$, and the horizontal load HL^2/EI for a stable pivot having a reed cross-over angle of 90°, where

K = torque/unit deflection,

L = length of pivot reed,

E = Young's modulus of pivot reed,

I = section modulus of pivot reed,

and V_c, V_t and H are the compressive, tensile and horizontally applied forces.

In this particular application, where the loading on the pivots will depend upon the weight of the motor being tested and where high sensitivity is required for low torque measurement and a correspondingly low sensitivity is required for high torque measurement, a versatile pivot system is called for. To achieve this it was decided to use three sets of reeds of the same lengths but having different sections. As it was intended to use the reeds as the electrical leads into the machine under test, the material selected for the reeds was hard drawn beryllium copper annealed for 23 minutes at 350°C having a conductivity of 27% that of refined copper and a Young's modulus of 19.5×10^6 lbs/in^2.. Bearing in mind the maximum size of motor to be tested, the length of the reeds was fixed at 1.25 ins.. The following reed sections were then examined:

	Reed section.	Section modulus ($I = bt^3/12$)
a)	0.1875" x 0.005"	0.195×10^{-8} ins^3.
b)	0.1875" x 0.010"	1.56×10^{-8} "
c)	0.1875" x 0.015"	2.70×10^{-8} "

From Wittrick's results, the characteristics relating the stiffness to the vertical compressive and vertical tensile loadings for a pivot having zero horizontal load and a 90° cross-over angle, are given in fig.(3.22). From this the torque versus vertical load characteristics for a deflection of 20° have been calculated for pivots using each of the selected reed sections in turn for 90° cross-over angle. These characteristics are tabulated in table (3.1) and shown graphically in fig.(3.23). Although the performance fell somewhat short of the specified restoring torque of 25×10^{-3} Nm. per pivot, it was taken to be satisfactory and the selected sections were, therefore, adopted. Details of the manufacture and assembly of these pivots are given on sheet (1) of the working drawings in the appendix.

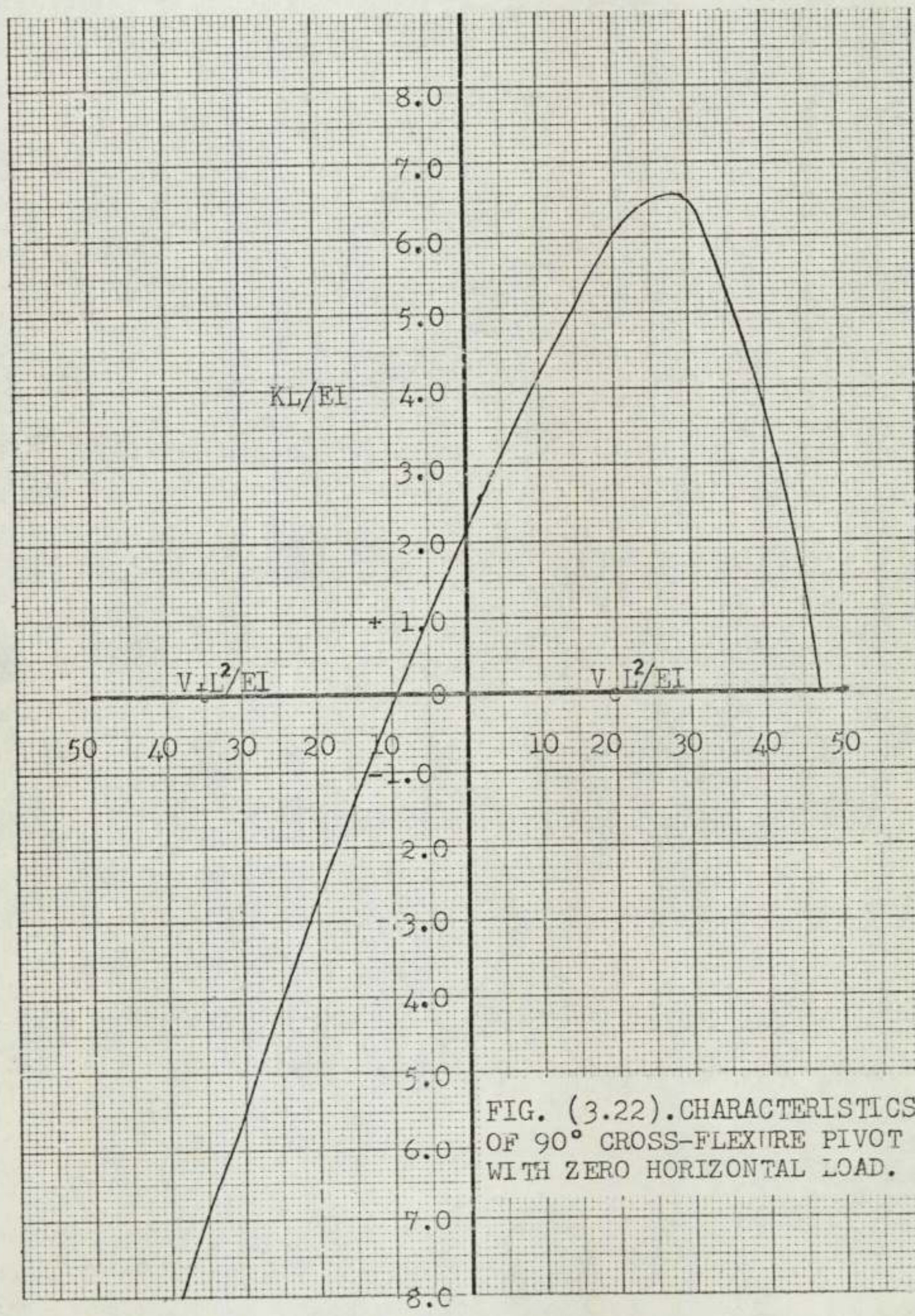

FIG. (3.22). CHARACTERISTICS OF 90° CROSS-FLEXURE PIVOT WITH ZERO HORIZONTAL LOAD.

Reed section.	a			b			c		
Vertical load, grms/pivot.	VL^2/EI	KL/EI	Torque for 20° defl'n. Nm.	VL^2/EI	KL/EI	Torque for 20° defl'n. Nm.	VL^2/EI	KL/EI	Torque for 20° defl'n. Nm.
+ 200	+ 18.10	+ 5.70	+ 34.8 x 10^{-4}	+ 2.27	+ 2.70	+ 132 x 10^{-4}	+ 1.31	+ 2.50	+ 212 x 10^{-4}
150	13.60	4.90	30.0 "	1.70	2.50	122 "	0.98	2.40	203 "
100	9.05	4.10	25.1 "	1.13	2.40	118, "	0.65	2.30	195 "
50	4.53	3.20	19.6 "	0.57	2.30	112 "	0.33	2.22	188 "
0	0.00	2.15	13.5 "	0.0	2.15	105 "	0.0	2.15	182 "
- 50	- 4.53	1.10	6.7 "	- 0.57	2.00	98 "	- 0.33	2.08	177 "
100	9.05	0.0	0.0	1.13	1.90	93 "	0.65	2.00	169 "
150	13.60	- 1.10	- 6.7 "	1.70	1.80	88 "	0.98	1.95	165 "
200	18.10	2.20	13.5 "	2.27	1.70	83 "	1.31	1.89	160 "

+ compression, - tension.
for vertical load.

TABLE (3.1). VERTICAL LOAD versus TORQUE FOR 20 DEFLECTION FOR DYNAMOMETER PIVOTS.

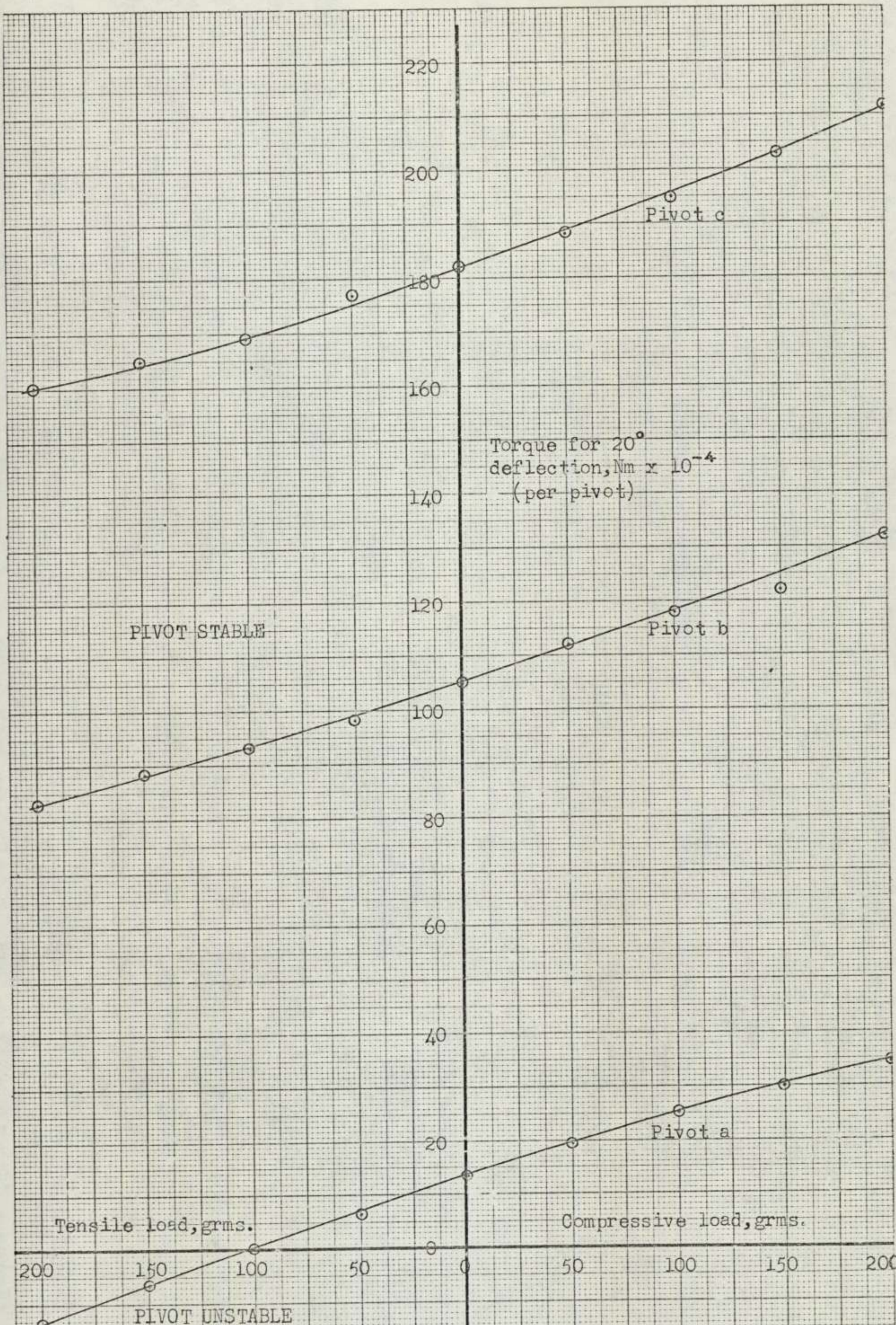

FIG. (3.23). VERTICAL LOAD versus TORQUE FOR 20° DEFLECTION FOR DYNAMOMETER PIVOTS.

Reference to fig.(3.23) shows, however, that these three sets of reeds did not cover the complete range of torque required, there being gaps between the maximum torque for pivot (a) and the minimum torque for pivot (b) and between the maximum torque for pivot (b) and the minimum torque for pivot (c). To fill these gaps two further sets of reeds were made having sections of 0.1875"x0.0075" and 0.1875"x 0.0125". The reeds were all made from 0.015" thick material, the thinner sections being obtained by milling using a stretching jig to prevent buckling; this jig is shown in photograph no.(3.2).

The pivots are carried by the dynamometer frame supports, item 3 of fig.(3.21), which are clamped to the bedplate. These supports have double pivot beam locations, identical to those on the dynamometer frame, to enable the pivots to be used in tension or compression as explained earlier.

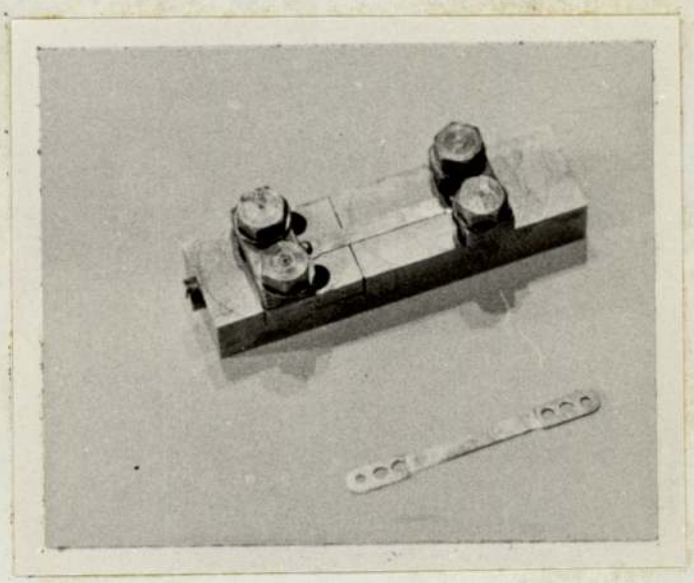

PHOTOGRAPH (3.2) STRETCHING JIG FOR PIVOT REED MILLING.

Driving head:

This consists basically of a pulley mounted on a hollow mandrel carried by an oil lubricated, high grade ball race, the one end of the mandrel forming the slotted section of a simple dog clutch. The whole of this assembly is carried by a bracket, relieved at its lower end to permit rotation of the dynamometer frame. The base of the bracket is grooved to locate, accurately, the head on the dynamometer way and is provided with a clamping screw for locking the head in position. Fig.(3.21) shows the arrangement of this driving head on the dynamometer whilst its dimensions are given on sheet (2) of the working drawings.

Baseplate:

Fig.(3.21) and sheet (2) of the drawings show the design of this base. It was cast from aluminium alloy, seasoned and its top face machined flat. The dynamometer way and driving motor way are of ground steel and are fixed to the base by screwing. These ways are precisely located at 90° to each other and give accurate alignment of the dynamometer frame supports with each other and with the driving head, and of the dynamometer as a whole with the driving motor. The base has four fixing lugs for its attachment to an absorbent bed to prevent transmission of external vibrations to the dynamometer; this precaution is of the utmost importance in the measurement of dynamic torques.

Alignment jig:

For accurate performance, the centres of rotation of the cross-flexure pivots and of the motor under test must be in precise alignment. To achieve this a special alignment jig is used. The basic design and method of use of this jig are shown in fig.(3.24) and photograph no.(3.3)

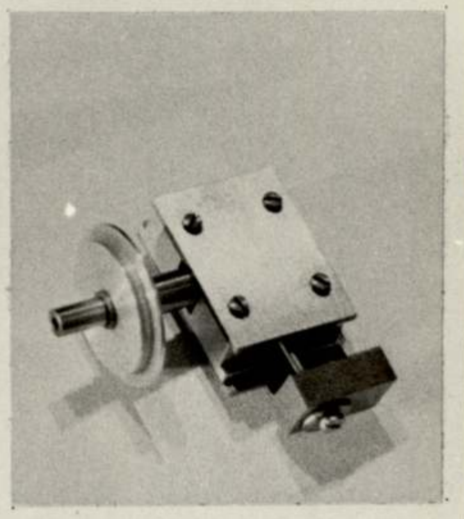

PHOTOGRAPH (3.3) DYNAMOMETER ALIGNMENT JIG.

ITEM No.	DESCRIPTION.
1	Jig body.
2	Jig/way reference plate.
3	Jig/frame clamping plate.
4	Frame/way reference block.
5	Jig/head reference mandrel.
6	Jig/frame reference flange.
7	Jig clamping screws.
2/1	Dynamometer frame.
6/1	Motor mounting flange.
8/1	Driving head.
11/1	Dynamometer way.

FIG. (3.24). DYNAMOMETER ALIGNMENT JIG.

SCALE: Full size.

See also photograph no. (3.3).

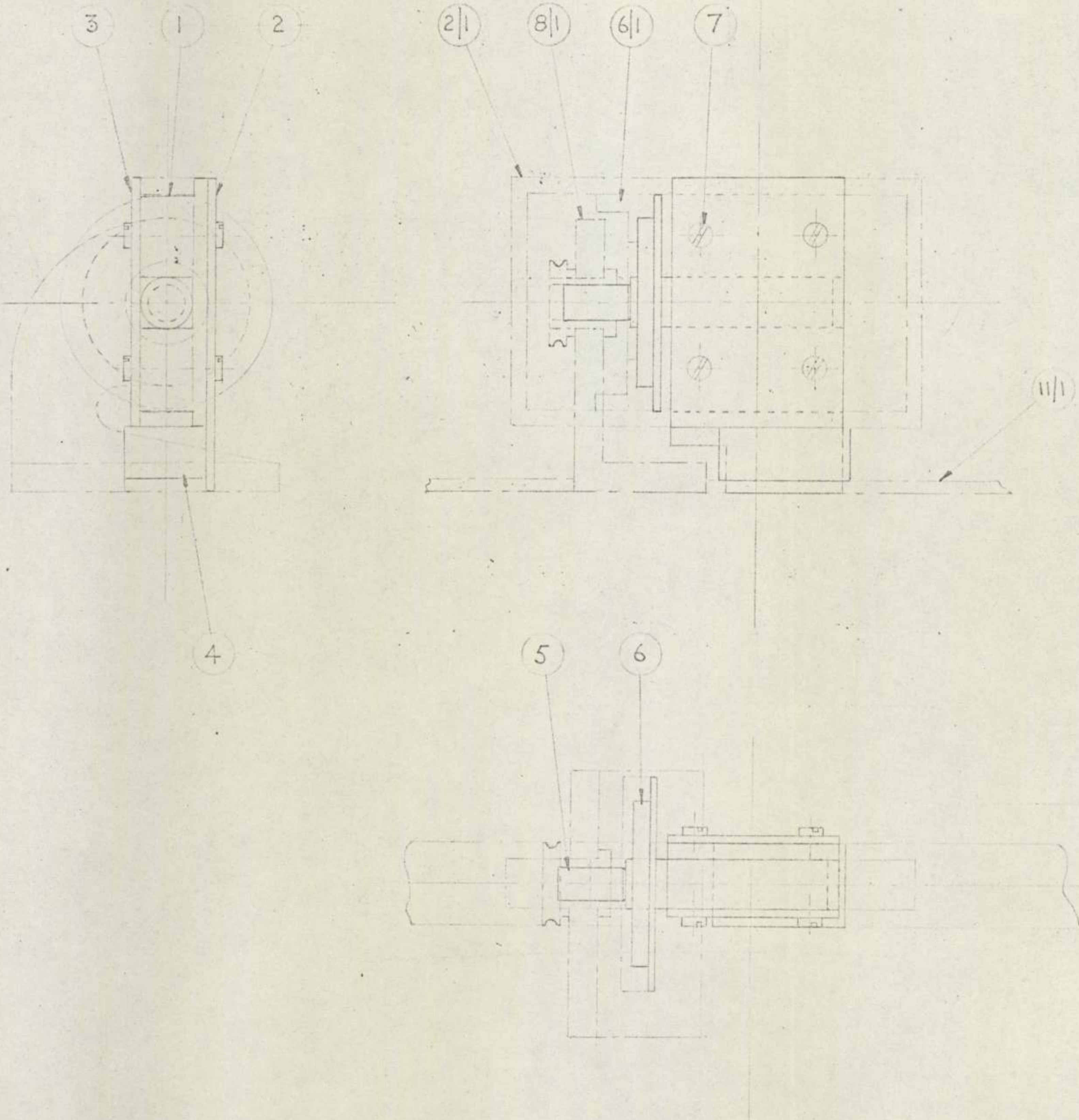

3
1
2
2|1
8|1
6|1
7
11|1
4
5
6

As will be seen, this jig consists of an aluminium alloy body made to fit snuggly inside the dynamometer frame, being located by flanges registering on the sides of the top and bottom members of the frame on one face only. This body has a slot machined in it the centreline of which coincides with the horizontal centreline of the dynamometer frame. This slot is accurately machined to locate the jig/head reference mandrel, item 5, which is retained therein by item 3, the jig/frame clamping plate. This mandrel has attached to it item 6, the jig/frame reference flange, which accurately fits the spigot recess in the motor mounting flange, 6/1; the exposed end of the jig mandrel is a sliding fit into the bore of the driving head hollow mandrel. In this way the alignment of the axes of the frame, motor mounting flange and driving head is assured. The alignment of these axes with the centres of rotation of the pivots is achieved by means of the frame/way reference block, item 4, in conjunction with item 3, the jig/way reference plate, which is fastened to the jig body by the jig clamping screws, item 7.

To use the jig, the dynamometer is assembled leaving the pivot clamping screws , driving head clamping screw and the motor mounting flange screws loose. The jig body, mandrel, reference plate, clamping plate and reference block are then firmly located and the motor mounting flange screws and the pivot clamping screws tightened. The jig is then removed by releasing its clamping screws and withdrawing the jig body, reference block and mandrel leaving the dynamometer fully lined up.

Frame damper:

To give stable conditions rapidly after a change of speed during steady state measurements, the dynamometer frame is provided with an eddy current damper. This consists of a thin aluminium vane attached to the front, i.e. the driving head, end of the frame at its centre of rotation. The vane oscillates in the field of an electromagnet, fastened to the bedplate, thereby generating a damping moment. For dynamic measurements the damper is made inoperative by de-energising the electromagnet. This damping system is clearly seen in photograph no. (3.4).

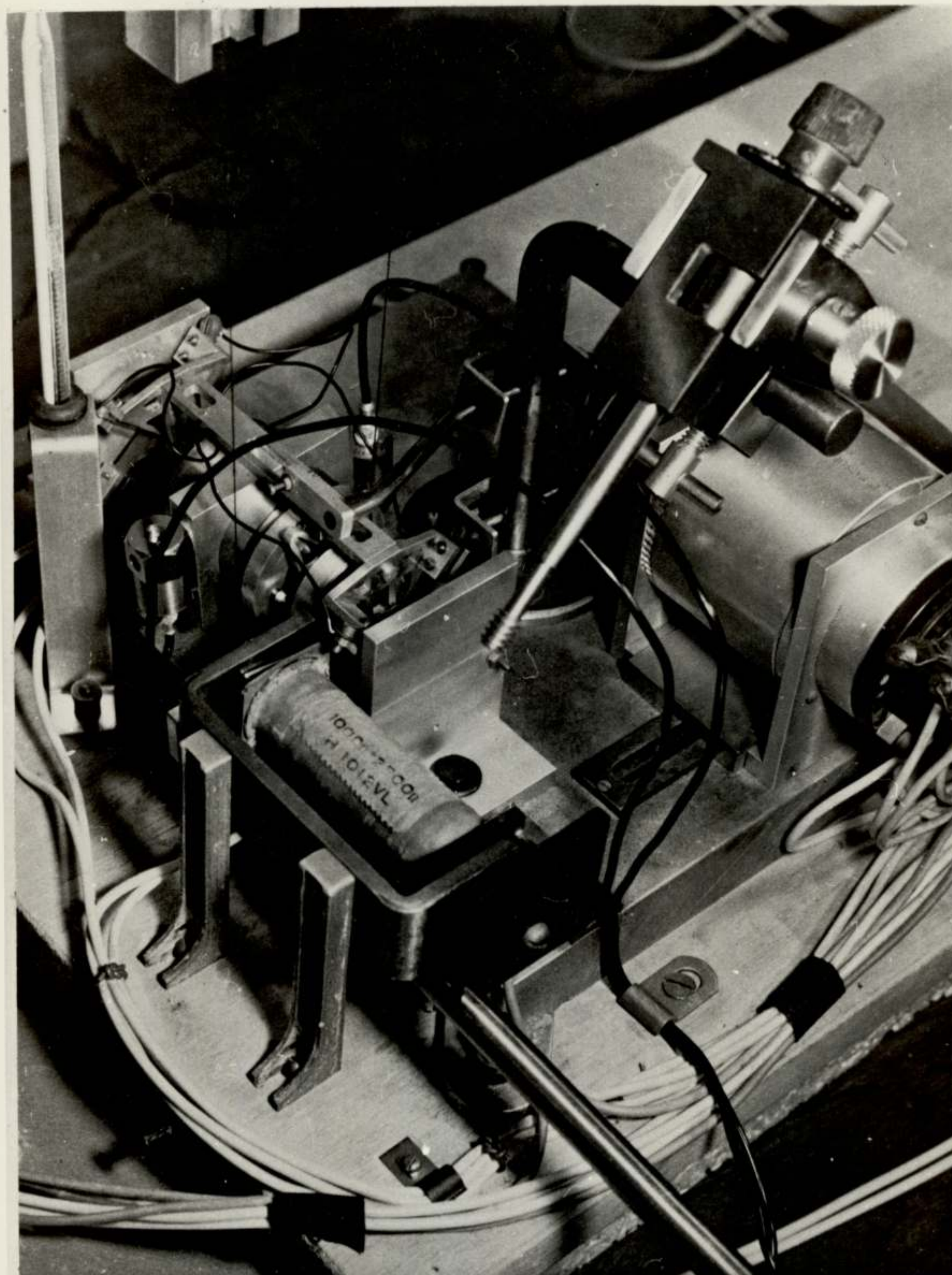

PHOTOGRAPH (3.4). GENERAL VIEW OF ASSEMBLED DYNAMOMETER.

Stalling gear:

For carrying out measurements with the test machine stalled, the dynamometer is equipped with stalling gear which consists of a 60 tooth pinion and a calibrated worm drive. The pinion locates on the splined shaft of the test motor and the worm drive is held in a clamping bracket fixed to the dynamometer bedplate. With this arrangement it is easily possible to stall the machine's rotor in any desired position. This system is also clearly visible in photograph no.(3.4).

Torque and speed registers:

These are fully described in sections (8)&(9).

6) Design of Speed Fixing Motor.

For the reasons given in section (5) it was decided to investigate the use of a double fed induction motor as the main driving motor. For a two pole machine of this type, if ω_1 is the angular frequency of the stator supply and ω_2 is the angular frequency of the rotor supply then, for the case when the stator and rotor rotating fields are in the same direction, the rotor speed would be given by $(\omega_1 - \omega_2)\frac{60}{2\pi}$, i.e. $(f_1 - f_2)60$, where f_1 and f_2 are the corresponding frequencies in Hz., and for the case when the two rotating fields are in the opposite direction the rotor speed would be given by $(f_1 + f_2)60$ r.p.m.

For this to be a working proposition the motor must always be started with the values of frequency required to give zero speed since it is effectively a synchronous machine. This is most easily achieved for the case when the two rotating fields are in the same direction for then the rotor speed is zero when $\omega_1 = \omega_2$. Hence, by having ω_1 fixed and starting with $\omega_1 = \omega_2$ the rotor would cover a speed range of zero up to a value depending upon the maximum value of ω_2, subject always to mechanical limitations.

Furthermore, successful operation also requires that the two rotating fields are correctly balanced initially and remain so throughout the entire speed range. If this is not achieved, synchronous running will be lost, the one field superseding the other so causing the machine to operate as an induction motor with a definite slip.

Before proceeding with any actual design calculationsfor such a machine, it was thought desirable to determine experimentally whether or not the scheme was a feasible one. For this purpose the stator of a 2" resolver and the rotor of a 2" induction motor were used to build a trial machine. The rotor had a three phase, star connected, distributed winding the lines of which were closed through fixed resistors mounted on the shaft. These resistors were removed and replaced by three slip-rings to which the windings were connected to form an open star. These windings had only a few turns per phase and required a low voltage excitation. It was decided, therefore, to feed them from the three phase 50 Hz. main supply via step-down transformers. The stator winding, on the other hand, being that of a voltage generator, was wound with a large number of turns per phase and required a low value of excitation current. This two phase winding was, therefore, excited by two amplifiers having a two phase decade oscillator as their signal source.

When this arrangement was tried experimentally, it was found that, having set the machine for zero speed and adjusted the amplifier gains to give zero speed (thereby assuring balance of stator and rotor fields) the motor would hold synchronism for a speed range of 0 to 3,300 r.p.m. on no load providing, at each change of frequency the amplifier gains were adjusted to maintain the field balance. The limitation on speed was due to the fact that the step change in frequency, at this maximum speed, was too large for the motor to accept without losing synchronism.

The torque generated by this machine was of the order required for the dynamometer and it appeared, that if this particular motor could be given a stator supply generating a constant current throughout an infinitely variable frequency range covering 50 to 450 Hz., it would, in fact, probably meet the required specification.

Simple measurements made on the stator winding revealed that the impedance of these was an almost linear function of frequency over the required range. This meant that the output voltage of the supply for these windings had also to be such a linear function of frequency. The most economical way of obtaining this was by using a speed controlled, low resistance alternator, although this could not be expected to cover the required range of frequency. This difficulty was overcome by using a stepped pulley on the double fed induction motor thereby restricting its rotor speed to a maximum of 6,000r.p.m.. Thus, the corresponding frequency span of the alternator was reduced to 50 - 150 Hz. and a 3:1 speed variation of this machine covered the entire speed range laid down in the specification. To give smooth running at low speeds, the pulley was also made with one step-down ratio.

The alternator used was specially designed for the purpose to the following brief specification:

Two phase, 150 volts/phase, 3.3 amps/phase, 150 Hz. at 1500 r.p.m.. It was driven by a 1.0 h.p. speed controlled d.c. motor using a d.c. tachogenerator feedback loop to regulate split-field excitation via a d.c. amplifier with a push-pull output.

The combination of this and the experimental machine gave a performance which satisfied the actual requirements and no further work was necessary on this particular aspect except that of finally engineering the system, mechanically balancing the synchronous motor rotor and providing it with bearings suitable for smooth operation at speeds of up to and including 6,000 r.p.m..

It was realized at this stage that the chief drawback to the double fed induction motor had not been encountered, i.e. instability resulting from load variation. This was fortuitous in that the rotor used, in the making of the experimental machine, had a very low resistance winding and was being supplied via step-down transformers thus giving overall low resistance rotor circuits. Consequently, the rotor windings were, themselves, also acting as damper windings, thereby rendering the machine stable. This driving motor is shown in fig. (3.21) and is also seen in photograph no. (3.4).

7) Supply System and Environment.

The design of the supply system and the instrumentation for this dynamometer are of major importance to the success of the investigation. Experience with raw supplies, varying ambient conditions, external vibration and dirty atmosphere caused the author to realize that any attempt to measure accurately the dynamic or steady state speed and torque of miniature machines without proper control of the experimental environment was wasted effort. At the onset it was clear that, apart from anything else, a basic requirement was that of stabilized supplies, and, as will be seen in fig.(3.25), with the exception of the three phase supply to the speed fixing motor, the entire system is fed through stabilizers.

As it was required to obtain an impedance per unit frequency locus for the test machine, the supply to this machine had to be of variable frequency. The usual way of achieving this, in the electrical machine world, is to use a variable speed alternator. Due to its lack of stability and limitation of frequency range, this method of supply would have been of no use in this work. However, the small power requirements of the miniature machine allow use to be made of electronic supplies. The machine is, therefore, fed from a two phase, variablefrequency oscillator via two 1 KW. a.c. amplifiers. The amplifier size was dictated by the lower end of the frequency range, since they have transformer coupled outputs, and by the extent of the range itself, since it was desired to avoid rematching during the test. The combination of the oscillator and amplifiers gave a supply frequency range with flat response from 2.0 to 1,000 Hz. with a maximum voltage of 200 volts. The voltage waveform and load current phase angles are continuously monitored by means of a cathode ray oscilloscope and a phase meter, respectively. The voltage and current are measured using thermocouple meters and the power is measured by means of a dynamometer wattmeter specially calibrated for the frequency range; this instrumentation is switched from phase to phase as shown in fig.(3.25).

For dynamic testing it was necessary to be able to switch on one phase (the motor control phase) at any point in its waveform. To achieve this an oscilloscope with X-amplifier output terminals was used.

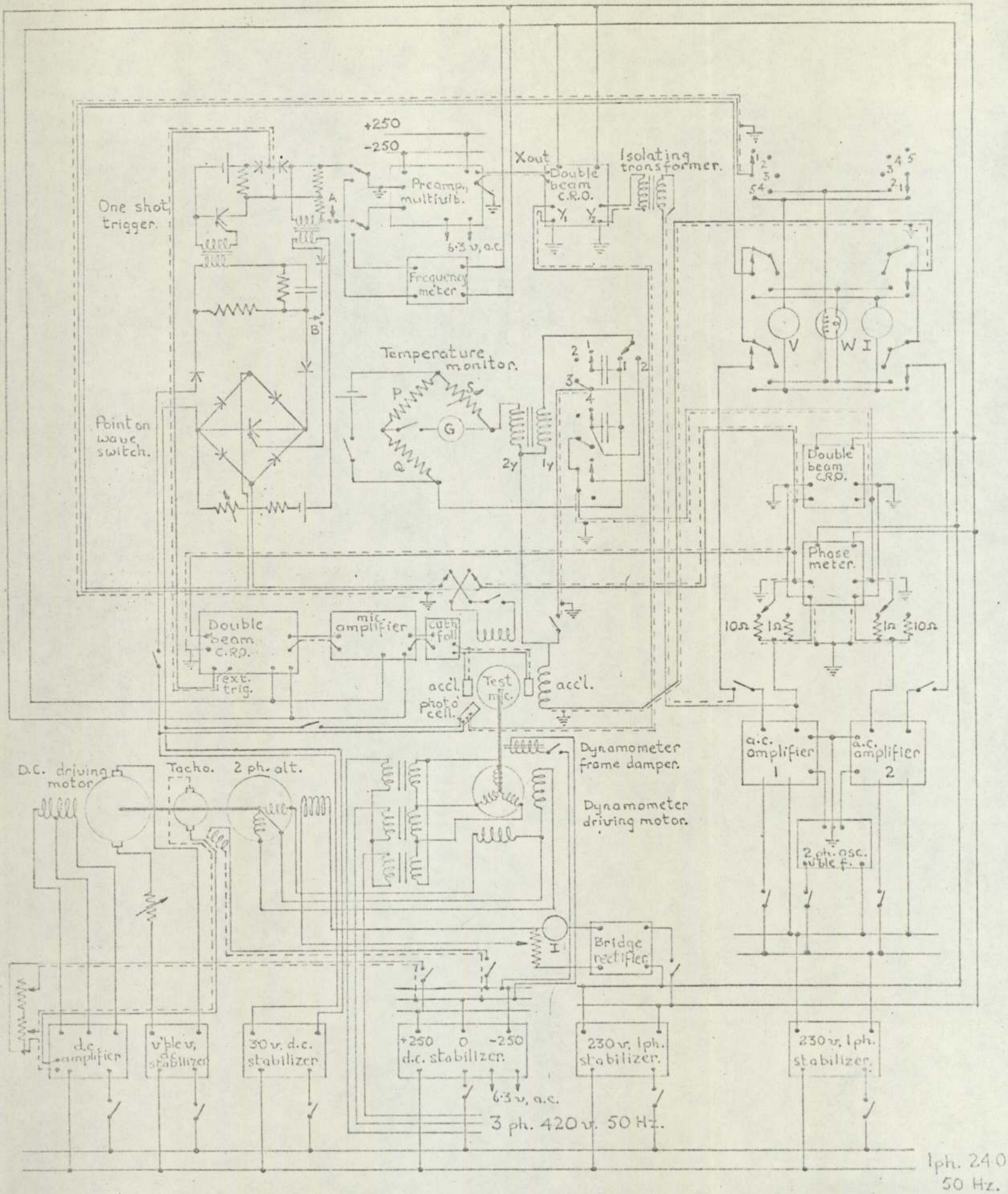

FIG. (3.25). COMPLETE CIRCUIT DIAGRAM OF DYNAMOMETER SUPPLY SYSTEM AND INSTRUMENTATION.

By displaying the control voltage and triggering the oscilloscope from the input signal,a time-base fly-back pulse is available at the X-amplifier output at the point in time at which the oscilloscope trace is extinguished and,therefore,at the point in time corresponding to the final instantaneous value of the voltage displayed. By varying the triggering level,this final voltage can be made to be that for any desired point on the control voltage waveform,within the limits of the oscilloscope triggering characteristics. A feature of this method is the visible indication given of the actual point on the supply voltage waveform at which the pulse is generated.

The time-base pulse is fed into a preamplifier and multivibrator to suitably shape it. It is then fed to the external trigger input of a recording oscilloscope and also to a pulse transformer,the latter converting it from a high level voltage pulse into a current pulse. In this form it is used to fire a silicon controlled rectifier connected in a bridge switch circuit provided with an ancillary holding current circuit energized from a 30 volt d.c. supply. This switch closes the supply to the control phase of the motor under test.

The holding current of this switch is transformer coupled to a trigger bias circuit controlled by another silicon controlled rectifier, also provided with an ancillary holding current circuit. Initiation of the holding current of the switch circuit rectifier,causes a pulse in the trigger bias circuit which fires its rectifier. This bias circuit is connected,via buffer diodes,to the recording oscilloscope trigger input. With the rectifier in the conducting mode,a negative bias voltage is applied to the trigger input which prevents further triggering of the oscilloscope, subsequent to its having been triggered by the supply voltage initiation pulse. This "one shot" trigger circuit for the recording oscilloscope is clearly indicated in fig.(3.25);this device is essential for recording dynamic performance and,in this form,is quite novel.

The supply to the dynamometer speed fixing motor rotor is taken from the three phase mains via step-down transformers. Ideally this should also come through stabilizers but economics prevented this. The stator supply, as explained earlier, had to be two phase, variable frequency with continuous control and an output impedance proportional to the frequency. This is derived from an alternator driven by a speed regulated d.c.motor, the speed control being effected by variation of the tachogenerator reference voltage taken from a stabilized d.c. supply via a potential divider.

So far as environmental conditions are concerned, the whole of the equipment was housed in a pressurized room in order to keep the ingress of dust and grit to a minimum. This is very necessary since the presence of even a small piece of foreign matter in the bearings of either the test machine or the speed fixing motor can cause erroneous measurements. The room was also temperature controlled and, in addition, the dynamometer itself was provided with a perspex cover to shield it from draughts, so minimizing variations in ambient temperature; the temperature sensitivity of these miniature machines demands this precaution. To reduce the possibility of spurious torque signals due to external vibrations, the dynamometer assembly was constructed on a bed of expanded polystyrene, of approximately $2\frac{1}{2}$" thickness. With these conditions it was felt that the experimental results would be dependable.

8) Torque Register.

For the purpose of this investigation, it was necessary to measure both steady state and dynamic torques. These are measured by two independent methods.

The characteristic of the cross-flexure pivots is that their rotation is directly proportional to the torque applied to them over a limited range. The pivots were designed to be within this limited range and the above property was, therefore, utilized as a measure of applied steady torque by calibrating the dynamometer rotation against known applied torques. The rotation of the dynamometer frame was measured by means of an optical lever, using the small mirror, item 17 of fig.(3.21), at the rear of the dynamometer frame.

For measuring the dynamic torque, it was decided to use the angular acceleration of the test motor stator and dynamometer frame assembly. The analysis of this method of measurement is given in chapter IV, section (11) which deals with the dynamometer calibration overall. Obviously, the basic requirement is an accurate indication of the angular acceleration. To obtain this, two Bruel and Kjaer matched accelerometers are mounted in tandem on a yoke secured to the motor stator (see fig.(3.26)& photograph no.(3.4)). The mounting is such that, with the dynamometer in the position of zero torque, both transducers have their maximum sensitivity in the vertical direction but reversed with respect to each other. Thus, with their outputs connected in parallel, any vertical oscillation of the dynamometer frame causes zero resultant accelerometer voltage. Similarly, although the signal voltage in this direction is low in any case, any horizontal swing of the frame will also cause zero signal. Hence, the only movement which will generate a net accelerometer voltage is a rotational acceleration of the dynamometer frame. That this method is effective is demonstrated by the calibration given in section (11). The net output voltage of the accelerometers is fed into a Bruel and Kjaer cathode follower, to present them with a very high impedance load, and thence into a Bruel and Kjaer microphone amplifier. The output of this amplifier is recorded on the recording oscilloscope using the one-shot trigger. The dynamic torque is thus indirectly obtained as a function of time from the photograph of the oscilloscope trace. With a knowledge of the inertias of the moving parts, the actual torque is obtainable from this trace by calculation.

The reason for measuring the torque on the stator assembly is simply that, to be sure that the dynamic characteristic obtained was actually that of the motor and not, incidentally, of a coupled load, the dynamic performance was measured with the machine on no load. Consequently, no rotor mounted device was acceptable. The more usual method of using a pressure transducer under one of the motor feet with the motor "solidly" mounted, is considered, by the author, to be unreliable, since the signal obtained by this means must contain an amount due to irrotational stator vibration. As explained, the method presented herein renders the measurement insensitive to such vibrations and was, in fact, designed for this purpose. It does, of course, depend on the dynamic characteristics of the cross-flexure pivots, but as will be seen in section (11), these are quite suitable and do not indeed interfere with the measurement in this case.

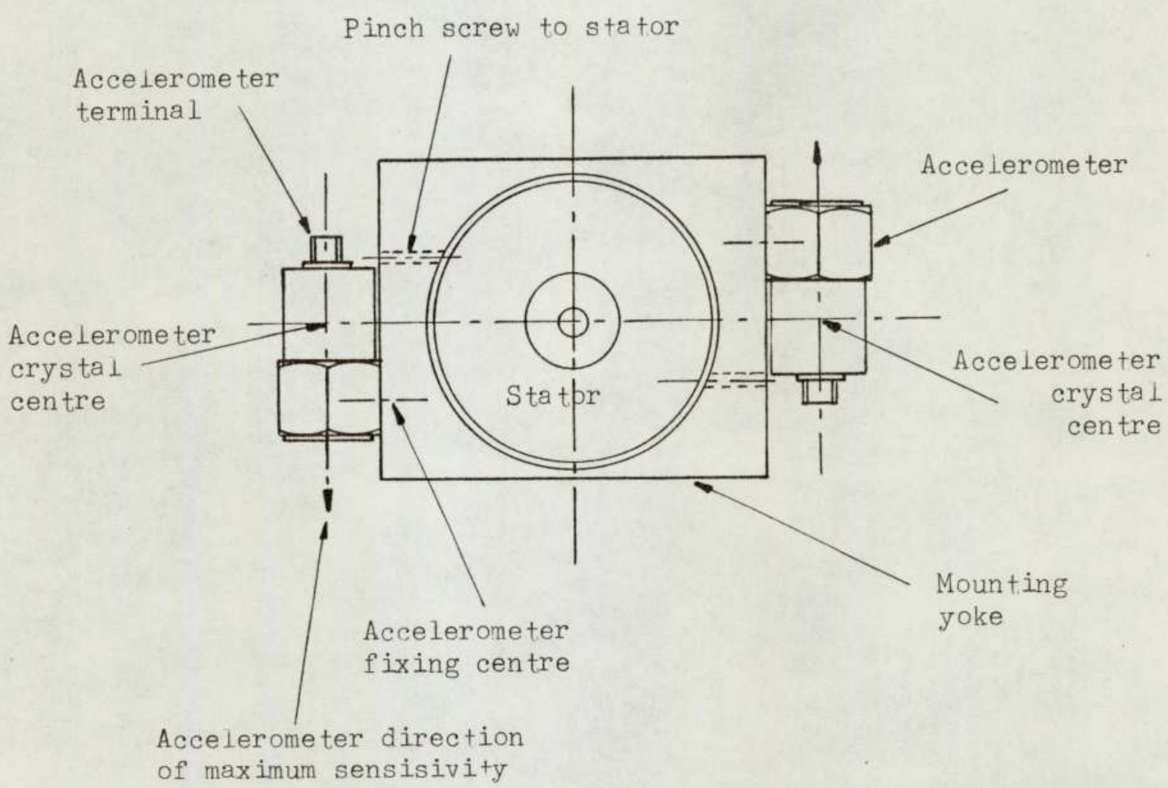

FIG. (3.26). TANDEM ACCELEROMETER & YOKE ASSEMBLY.

9) Speed Register.

As for the torque register, the equipment is capable of measuring both steady state and dynamic values. Although in this particular investigation the dynamic speed was not required, the method of its measurement is indicated.

For monitoring the steady state speed, a digital frequency meter is used, in an inverted mode, to count the number of cycles of the output of its own crystal oscillator between two consecutive gating pulses. These pulses are obtained from a photoelectric cell, activated by a black radial stripe on a polished disc mounted on the dynamometer driving head pulley. A great deal of experimental work was done in arriving at the correct dimensions of the stripe for maximum signal from the photoelectric cell at very slow speeds, and a definite response at the high speeds. The slightest judder on the waveform of this pulse is enough to cause the counter to gate, so giving a spurious result. In order to reduce the risk of spurious gating and to ensure that the gating signal seen by the counter was always of the same shape, independent of the motor speed, the output of the photoelectric cell is fed into the same oscilloscope, with the X-amplifier output, as that used for controlling the point on wave switching circuit. As in the point on wave switching system, the time-base fly-back pulse triggers the multivibrator, the output of which is used as the gating pulse. In this way a visible indication is given, not only of the photoelectric cell output pulse, but of the point on that pulse at which the counter is gated; indeed, control of the oscilloscope triggering level allows adjustment of this point. It should be appreciated that for accurate measurement of speed, great care is necessary in the generation of this gating pulse.

The instantaneous value of dynamic speed is most easily obtained by integration of the net accelerometer output voltage/time characteristic. This can be done graphically using the recorded trace. For these miniature machines the usual method of using a tachogenerator coupled to the machine under test is not feasible, since the tachometer itself loads the machine.

In any case, there is great doubt in the author's mind about the use of tachogenerators for dynamic speed measurement, since the generator will have an electrical time characteristic of the same order as that of the test machine, in which case, without some very sophisticated calibration, assessment of the dynamic speed of the test machine will be impossible. Since the frequency characteristics of the accelerometers, used in this proposed method, are flat up to 45 KHz., which should easily cover the frequency spectrum of the electrical machine's behaviour, it is contended that this method is a valid one.

10) Temperature Register.

As will be seen from the design calculations, the winding resistances of these miniature machines are relatively high. Consequently, their performances are very temperature sensitive. It is, therefore, essential that all measurements be carried out at the same temperature. The actual method of doing this is dealt with in chapter IV, section (12). The machine temperature is measured indirectly by measuring the stator winding resistance to a small, injected, direct current by means of a Wheatstone bridge circuit. This circuitry is adequately shown in fig. (3.25) and is taken from a report on the measurement of temperature rise by the method of superposition. (35) This has been found, by experience, to be the most satisfactory form of temperature measurement for this size of machine. The fixing of external thermometers is deemed impracticable as is the use of external thermocouples, the latter because of lead drag which must be kept to a minimum. Indeed, the only lead drag to which the dynamometer frame is subjected is that of the accelerometer leads, which was unavoidable.

The complete layout of the dynamometer bench and supplies may be seen in photographs nos. (3.5), (3.6), (3.7) & (3.8) in addition to photograph no. (3.4) already referred to.

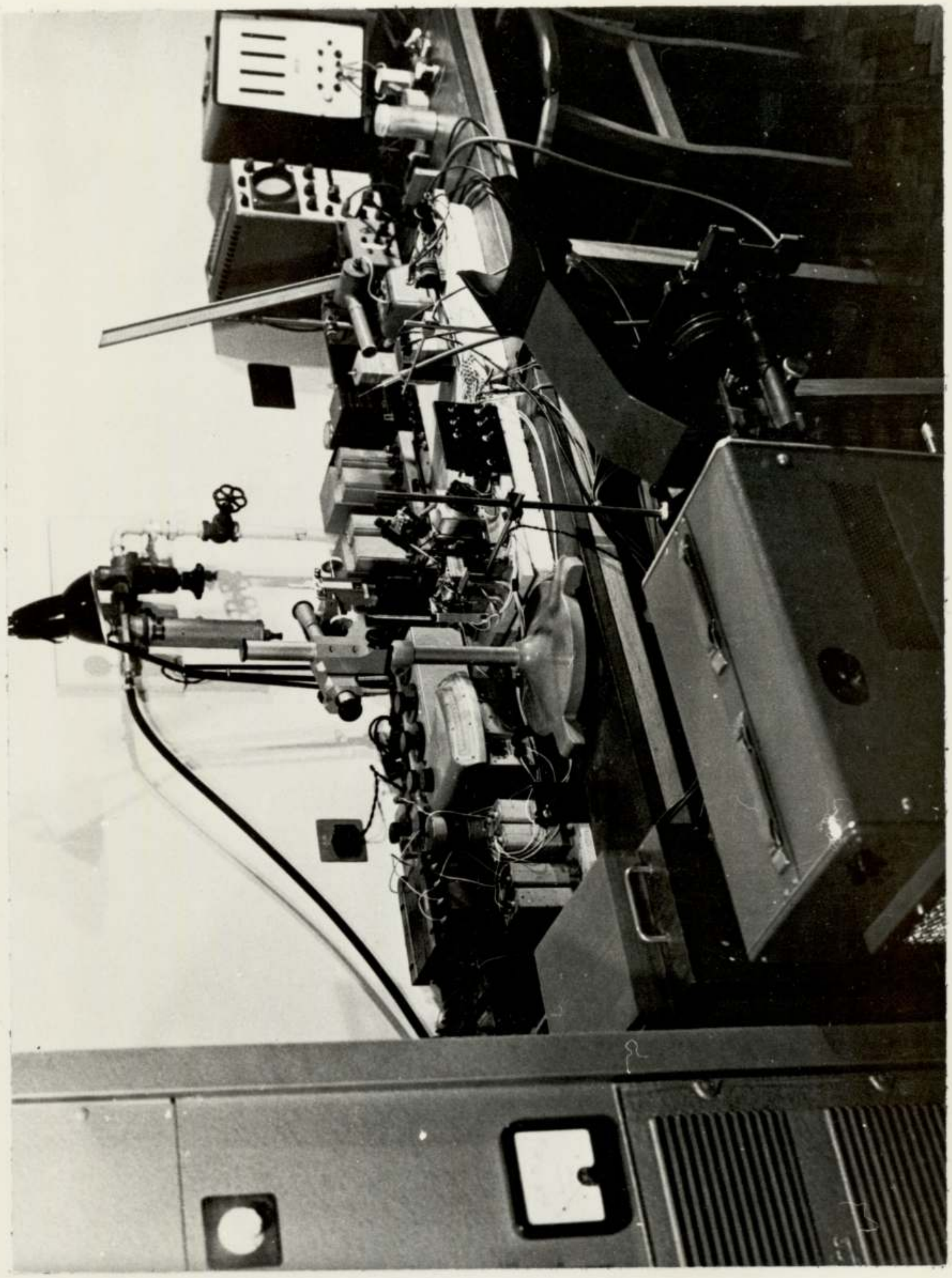

PHOTOGRAPH (3.5) COMPLETE DYNAMOMETER BENCH LAYOUT.

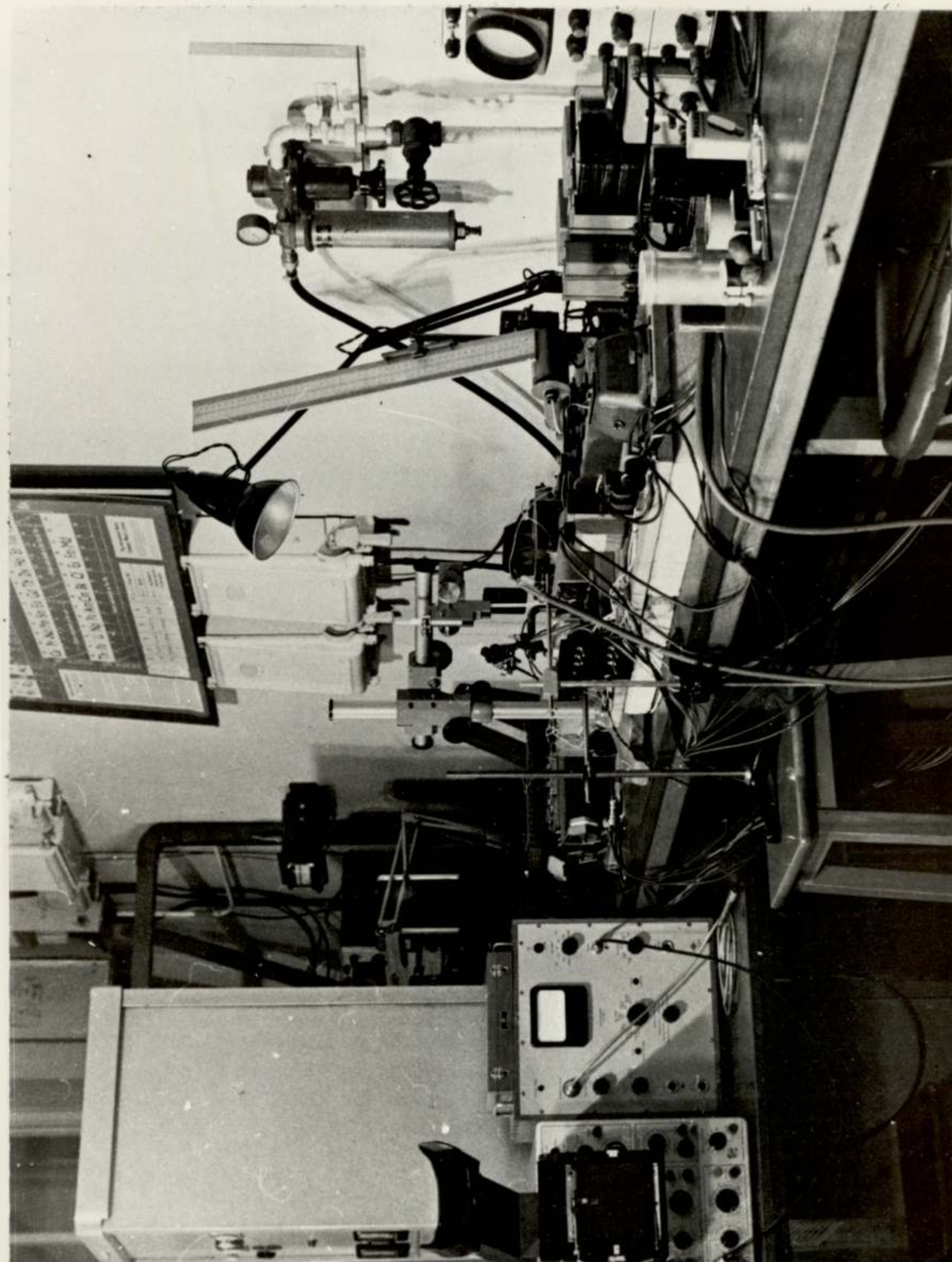

PHOTOGRAPH (3.6) COMPLETE DYNAMOMETER BENCH LAYOUT.

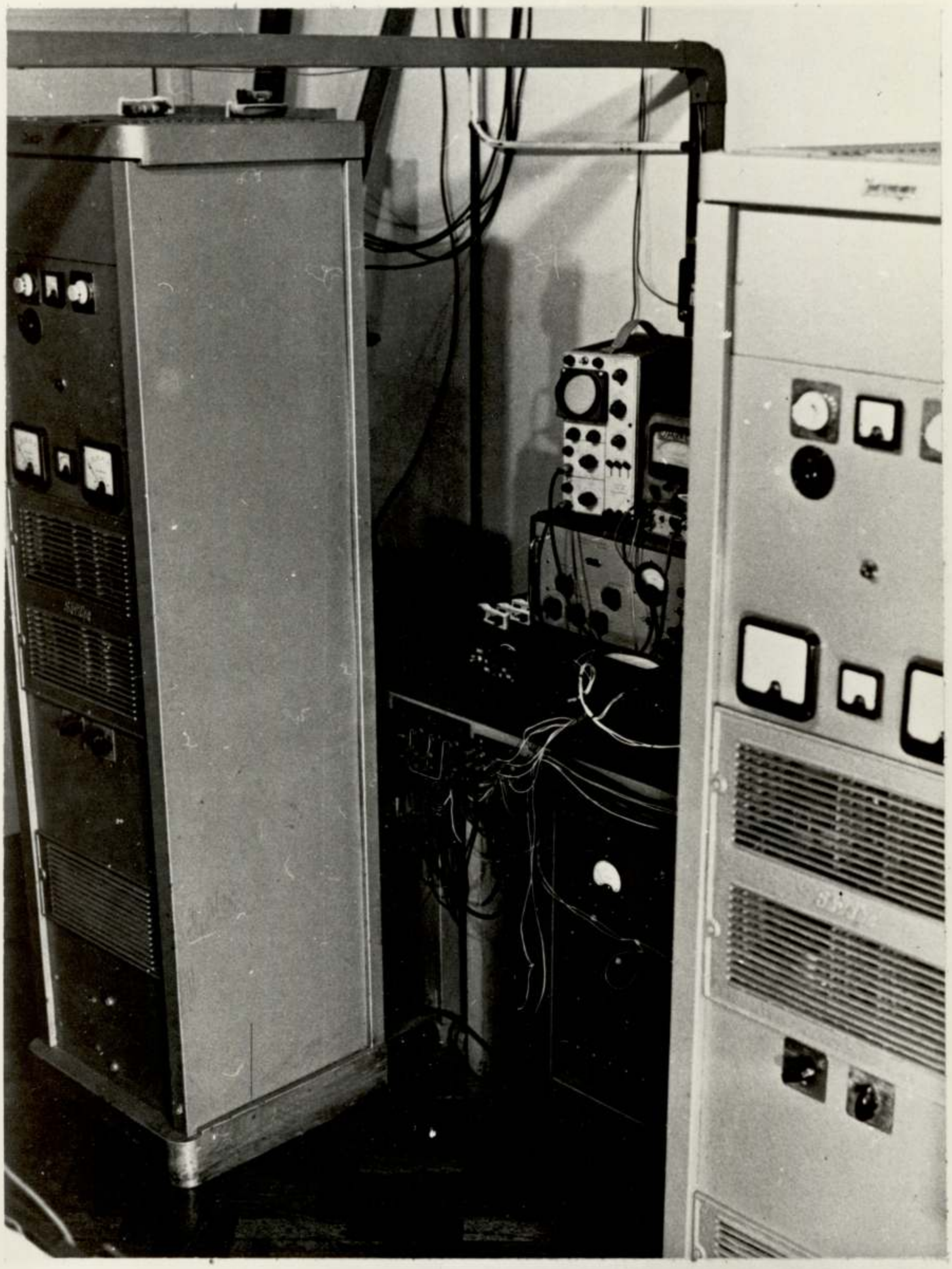

PHOTOGRAPH (3.7) TWO PHASE,A.C.,VARIABLE FREQUENCY,ELECTRONIC SUPPLY.

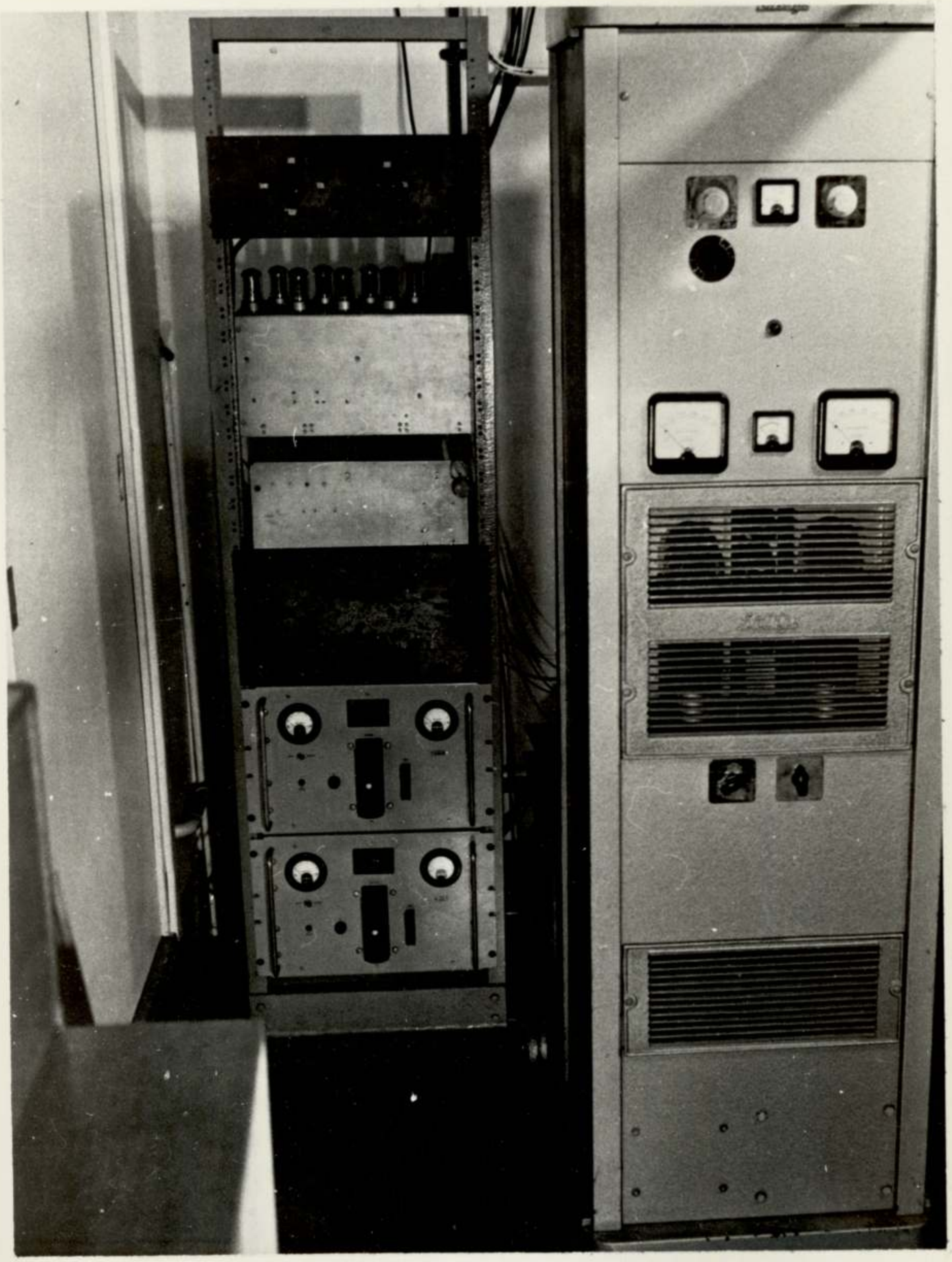

PHOTOGRAPH (3.8) RACK MOUNTED, A.C. STABILIZERS & D.C. AMPLIFIER.

CHAPTER IV.

Performance of Test Machine.

11) Dynamometer Calibration.

Static:

With the test machine and the accelerometer assembly fixed into the dynamometer frame, a light torque beam was fastened to the splined shaft of the test motor such that the beam would contact opposite sides of the upper and lower members of the dynamometer frame, simultaneously. The motor shaft was coupled to the driving head by means of the dog coupling. By applying tangential loads, using a thread and weight pan, to the driving head pulley, pure torques were applied to the dynamometer frame via the dog coupling and beam, the dead weight being completely taken by the driving head. The rotation, measured as the deflection in cms. on the optical lever scale, was plotted against the applied torque for both clockwise and anticlockwise rotation of the frame. This calibration was repeated several times and the results are given in fig.(4.1).

Dynamic:

For this calibration, the test machine and accelerometer assembly are fixed into the dynamometer frame as for the static calibration but with the beam removed and the motor uncoupled from the driving head. A pure mechanical torque was applied to the frame by means of the apparatus illustrated in fig.(4.2). This consisted of a heavy microscope swan-neck stand having course horizontal and fine vertical rack and pinion adjustment. Two miniature ball-races, acting as pulleys, were carried on a cross-arm fixed to the vertical slide of the swan-neck stand. A third miniature ball-race, carried by an independent arm, was used as the lower pulley. The tensioning loop was of cotton with an insert of unspun silk lying between the two upper pulleys.

By raising the vertical slide, so tensioning the loop to any desired

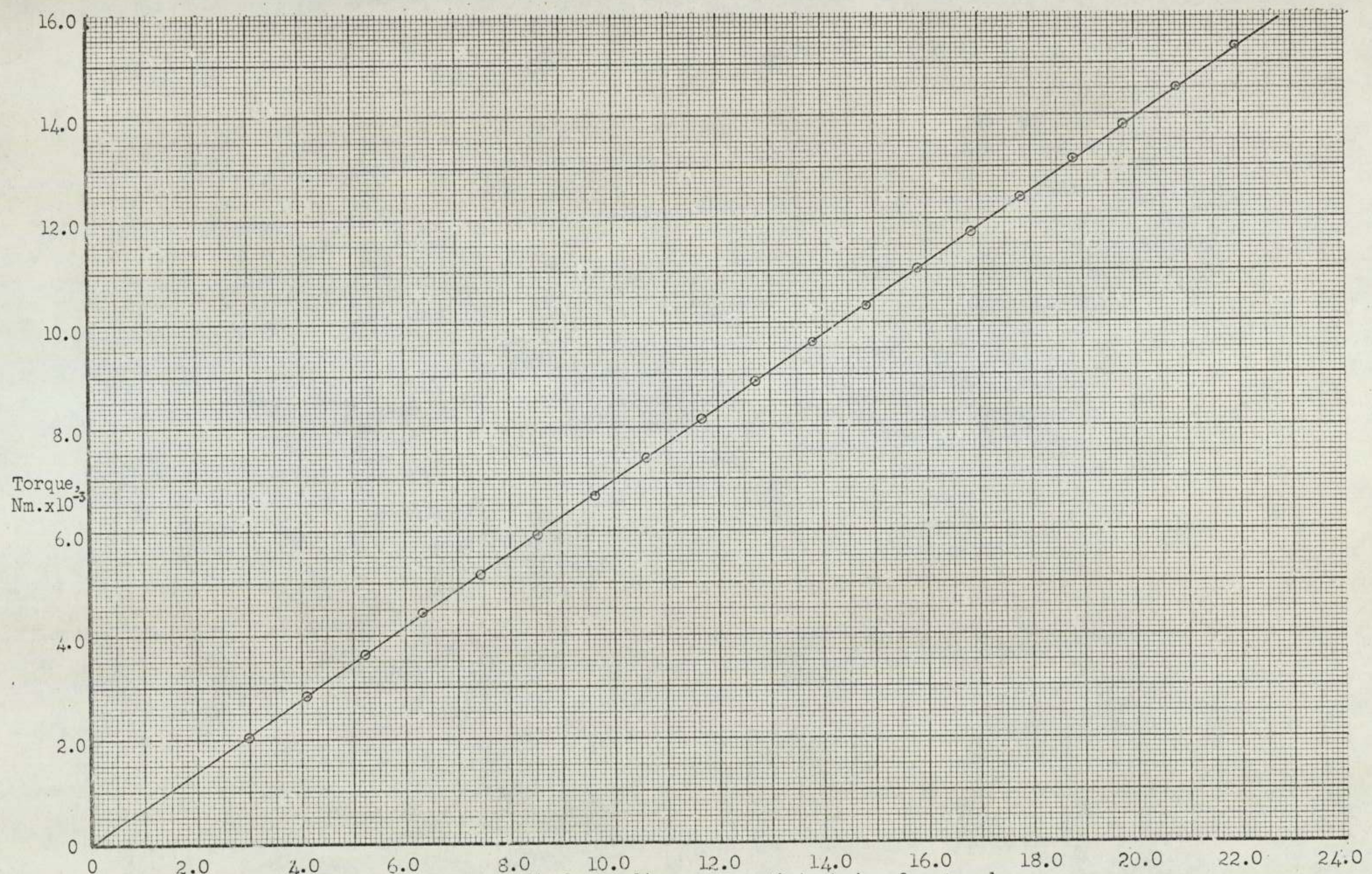

FIG. (4.1). STATIC CALIBRATION OF DYNAMOMETER.

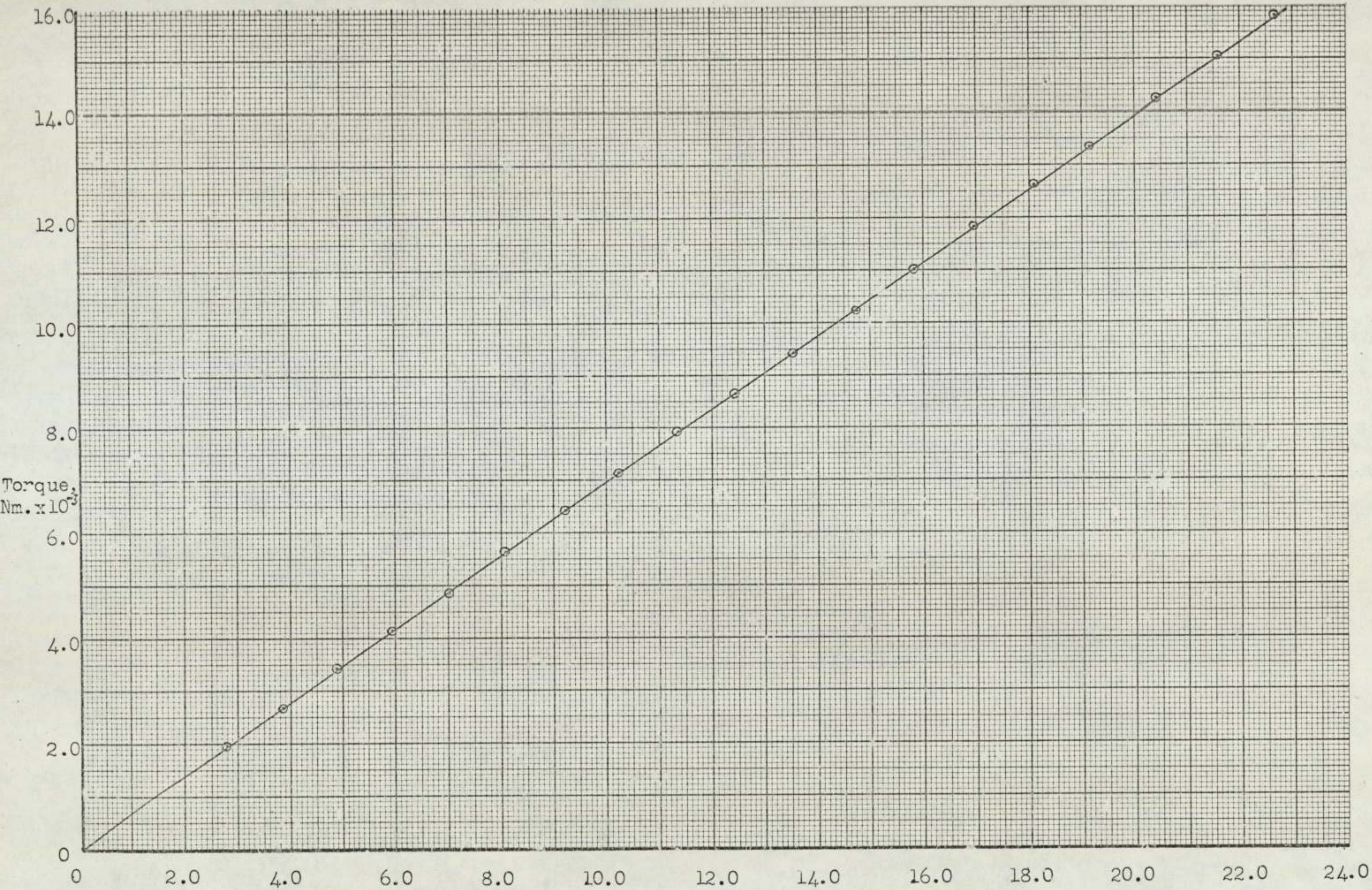

FIG.(4.1),ctd.. Scale reading, cms., clockwise front end.

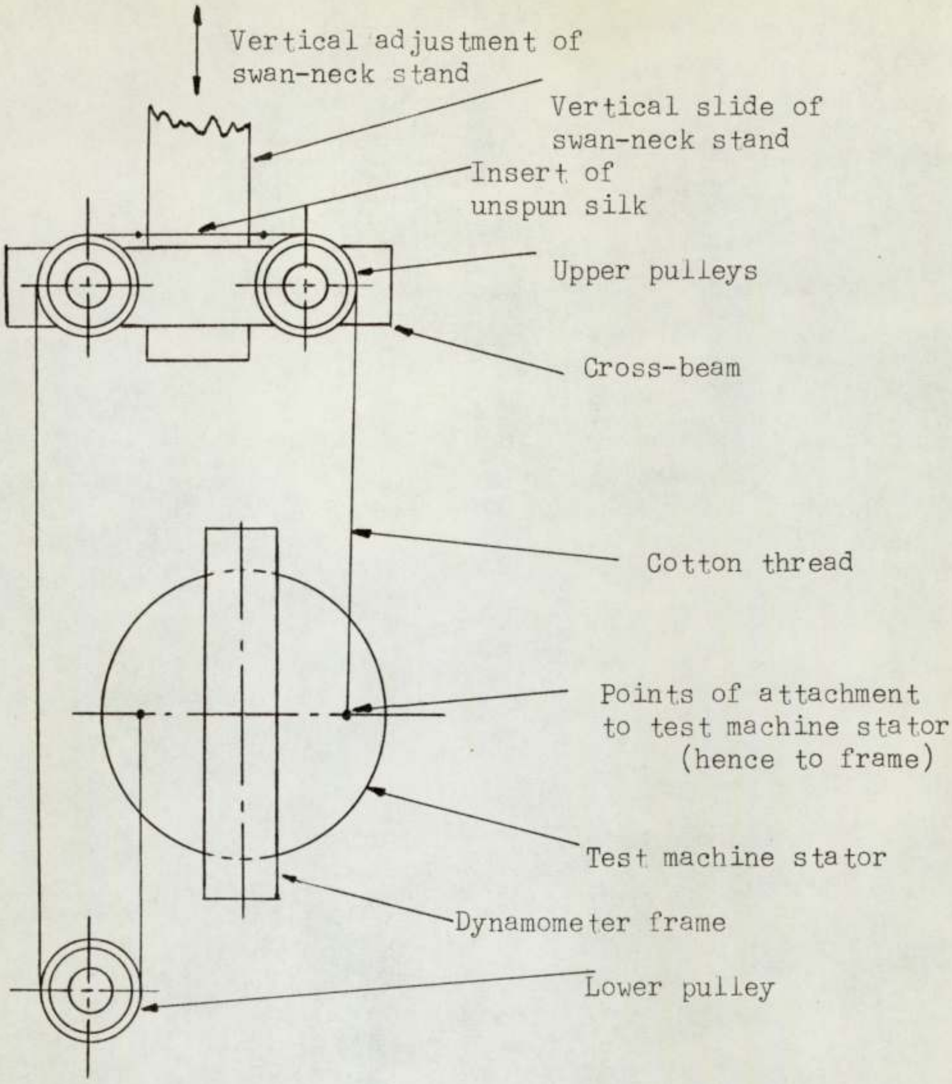

FIG. (4.2). APPARATUS FOR DYNAMIC CALIBRATION OF DYNAMOMETER.

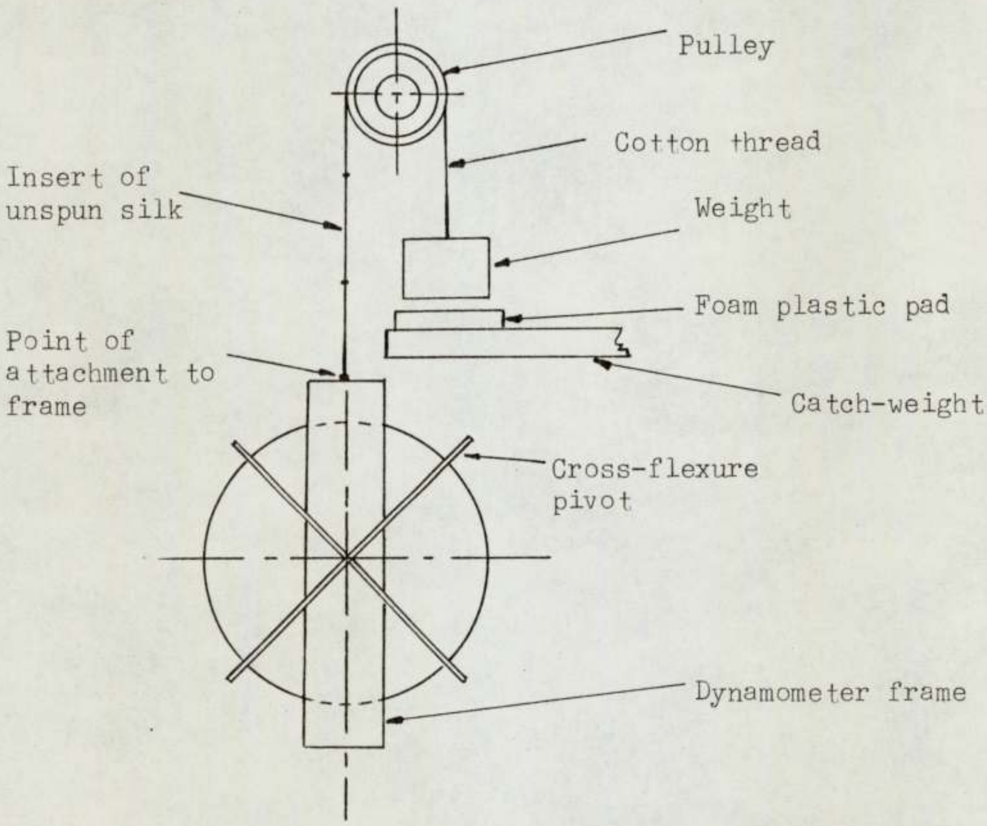

FIG. (4.6). APPARATUS FOR CHECKING VERTICAL SENSITIVITY OF DYNAMOMETER.

degree, a pure torque was applied to the dynamometer frame and the deflection of the frame recorded using the optical lever. In photographs nos. (3.4), (4.1) & (4.2) the dynamometer is shown set up for this particular calibration. With the frame so deflected, the silk insert was burned through thereby suddenly releasing the frame and subjecting the system to a step change of torque. The reason for using unspun silk as the opening link, was to avoid "stranding" noise which had been experienced when a cotton link had been used. The output voltage of the tandem accelerometers was recorded, using the recording oscilloscope. This process was repeated for several different time-base settings on the oscilloscope, to cover operating times from 2.0 secs. to 5.0 millisecs., for the same applied torque. For the first of these traces, i.e. operating time 2.0 secs., the slow time-base on the oscilloscope allowed the oscilloscope to be triggered manually before the dynamometer frame was released. By this means it was possible to decide the oscilloscope automatic trigger settings for the subsequent recordings, with the faster operating times. These traces are shown in fig. (4.3), nos. 1 to 4 inclusive.

Trace no. 1, displaying several cycles of oscillation of the frame, was enlarged pantographically, fig. (4.4), and three cycles of this analysed for fundamental, third and fifth harmonics using a Stanley harmonic analyser. The Fourier expression for the net accelerometer voltage so obtained is

$$v_a = 10.07 \sin\omega_f t + 0.02 \sin(3\omega_f t - \pi/4)$$
$$+ 0.024 \sin(5\omega_f t - \pi/4.7)$$

where ω_f is the natural frequency of oscillation of the frame. Traces nos. 2 and 3 indicate the presence of oscillations of the order of 15, 2.5 and 0.87 KHz. with magnitudes of 2.8%, 2.8% and 2.1% fundamental, respectively.

Remembering that the natural frequency of the accelerometers is of the order of 45 KHz., it is concluded that the harmonics observed above are all due to the movement of the frame itself. They are, however, sufficiently small to be neglected. The motion of the dynamometer frame is, therefore, taken as simple harmonic.

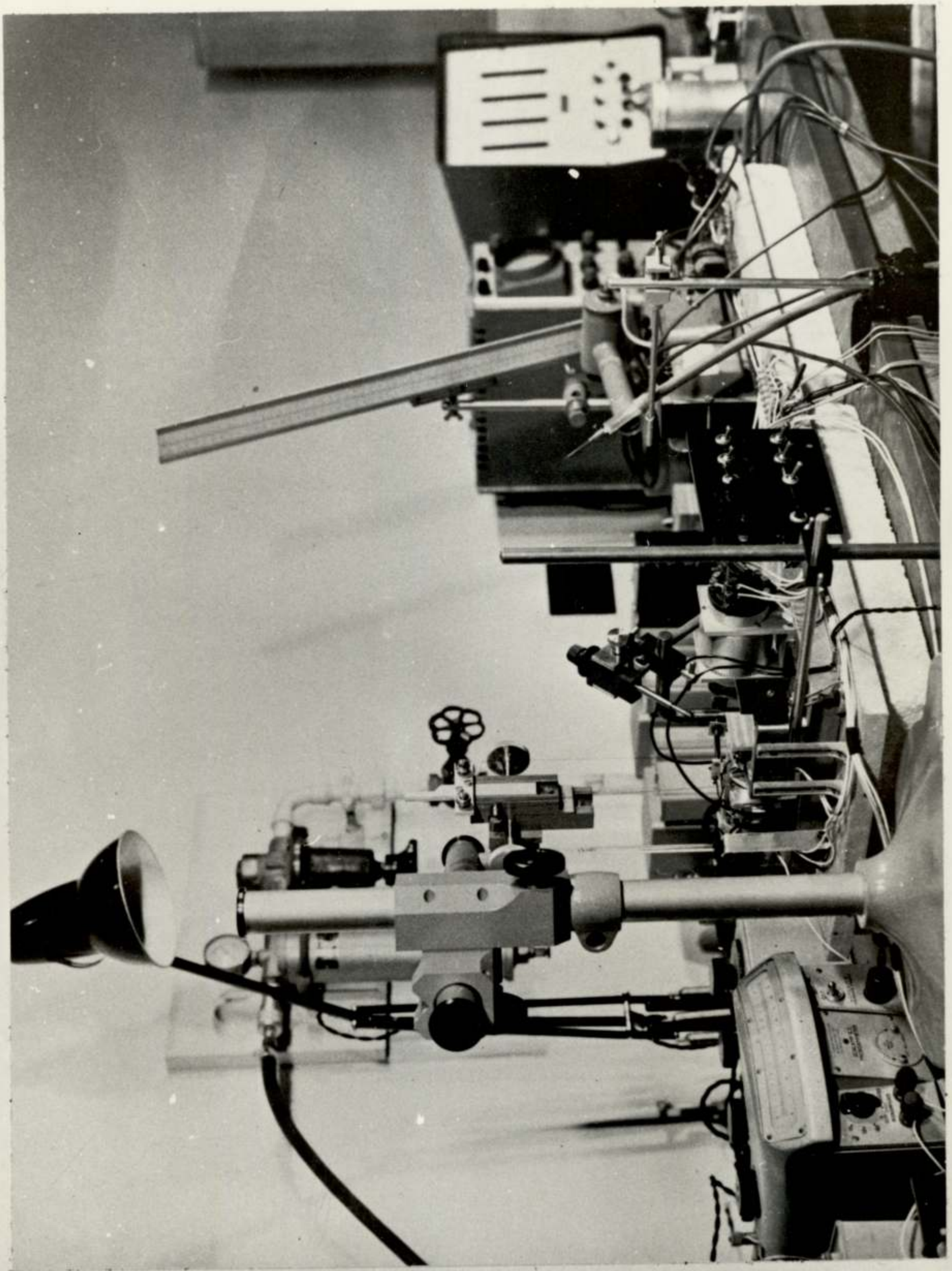

PHOTOGRAPH (4.1). DYNAMOMETER SET UP FOR DYNAMIC CALIBRATION.

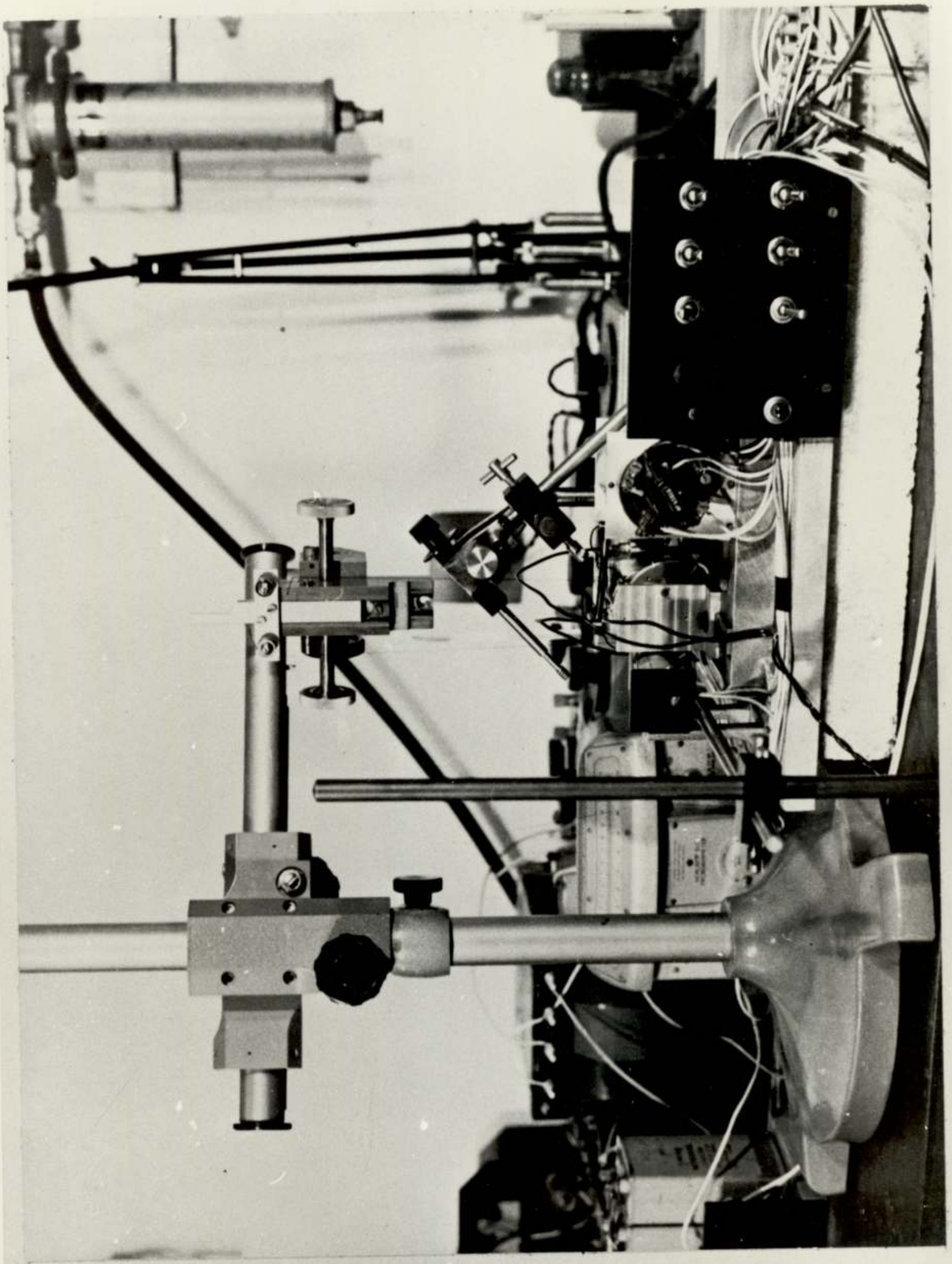

PHOTOGRAPH (4.2). DYNAMOMETER SET UP FOR DYNAMIC CALIBRATION.

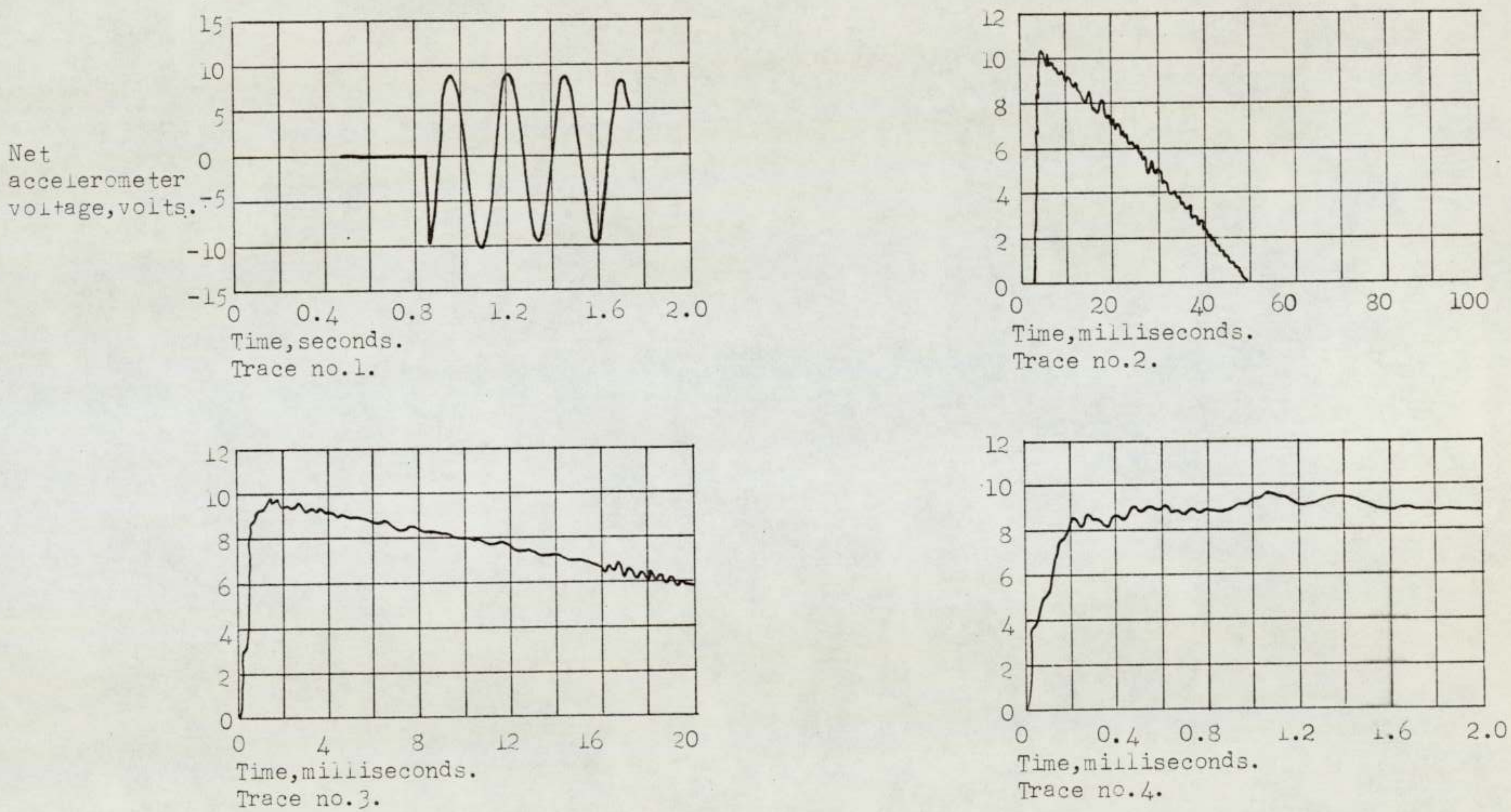

FIG.(4.3). DYNAMIC CALIBRATION OF DYNAMOMETER.

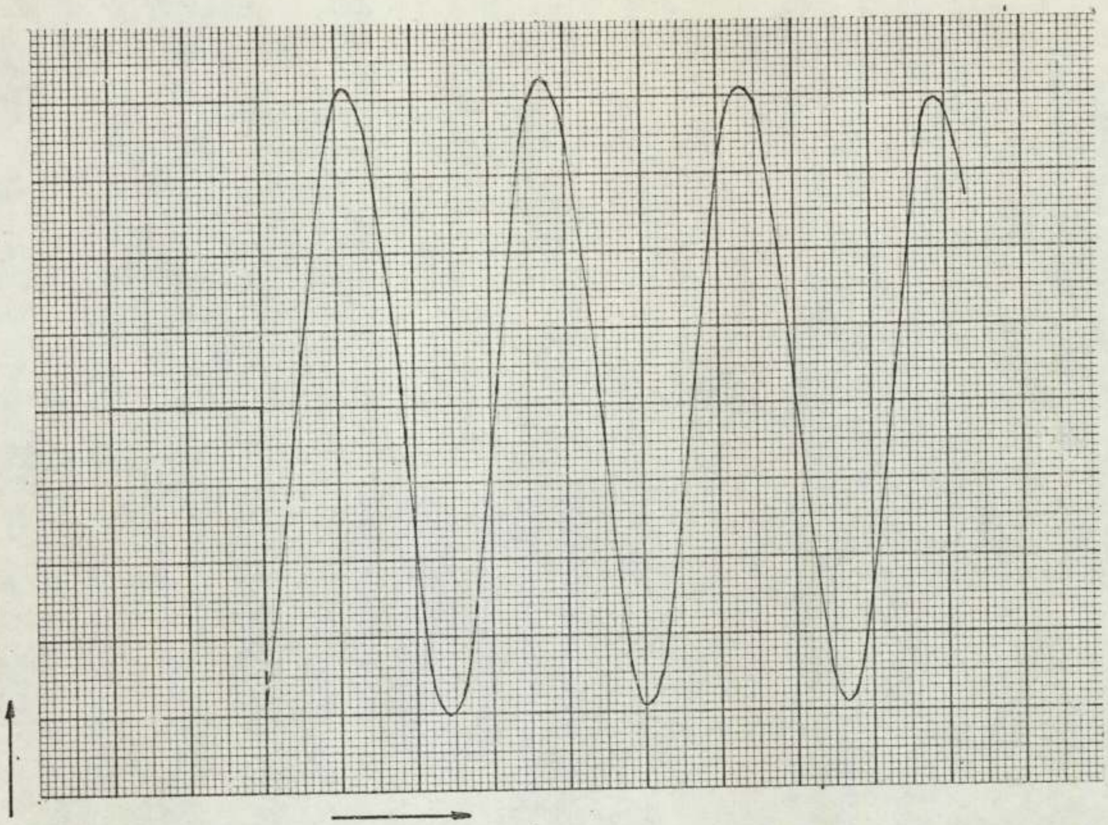

FIG.(4.4). NATURAL OSCILLATION OF DYNAMOMETER FRAME.
(Pantographic enlargement, trace no.1)

Let I_f be the total moment of inertia of the frame, accelerometer assembly and test machine and let μ_p be the control constant of the cross-flexure pivots. Taking the damping to be negligible, by virtue of the design of the dynamometer, over a period of several cycles of frame oscillation, then the equation of motion of the frame is,

$$I_f\ddot{\theta}_f + \mu_p\theta_f = 0$$

from which the period of oscillation is $2\pi\sqrt{\frac{I_f}{\mu_f}}$.

From fig.(4.3), trace no.1,

period of oscillation = 0.25 secs..

From the static calibration,

$$\text{rotation of frame} = \tfrac{1}{2}\left[\tan^{-1}\frac{\text{deflection, cms.}}{70}\right]$$

For a deflection of 20cms.,

$$\theta_f = 7.97\frac{\pi}{180}\text{ radians}$$

and for this deflection,

applied torque = 13.92×10^{-3} Nm.

for both directions of rotation.

Hence ,
$$\mu_p = \frac{13.92 \times 10^{-3} \times 180}{7.97 \times \pi} = 0.10 \text{ Nm./radian.}$$

Substitution of this value in the expression for the period of oscillation gives, on rearrangement

$$I_f = 1584 \text{ grm.cm}^2$$

In the dynamic calibration, initial deflection = 15 cms. on optical lever scale. The corresponding value of $\mu_p\theta_f$ is, from the static calibration curve, 10.44×10^{-3} Nm..

The initial acceleration of the frame assembly is, therefore, given by

$$\frac{\mu_p\theta_f}{I_f} = \frac{10.44 \times 10^{-3}}{0.1584 \times 10^{-3}} = 65.9 \text{ rads./sec.}$$

The tangential acceleration of the accelerometer is $r\ddot{\theta}_f$, where r is the mean radius of the accelerometer crystal fromthe axis of rotation. By direct measurement this distance is 2.65 cms..

Therefore, initially, $r\ddot{\theta} = 1.746 \text{ m/sec}^2$.

From the accelerometer charts, fig.(4.5), the acceleration sensitivity of the parallel accelerometers is

$$\tfrac{1}{2}(53.5 + 53.8) \text{ mV/g.}$$

i.e. 53.65 mV/g,

where $g = 9.806 \text{ m/sec}^2$.

Consequently, the initial voltage signal from the accelerometers should be

$$\frac{1.746}{9.806} \times 53.65 \text{ , i.e. } 9.53 \text{ mV..}$$

With a gain of 60 dB in the microphone amplifier, this gives an input voltage to the recording oscilloscope of 9.53 volts.

From trace no.3, the peak initial voltage signal is 9.58 volts. The rounding of the corner of this trace is assumed to be due to a certain amount of stretching in the silk insert whilst burning through. For this reason, the maximum voltage is taken.

Taking the calculated value as reference, the error between these two values is -0.525%

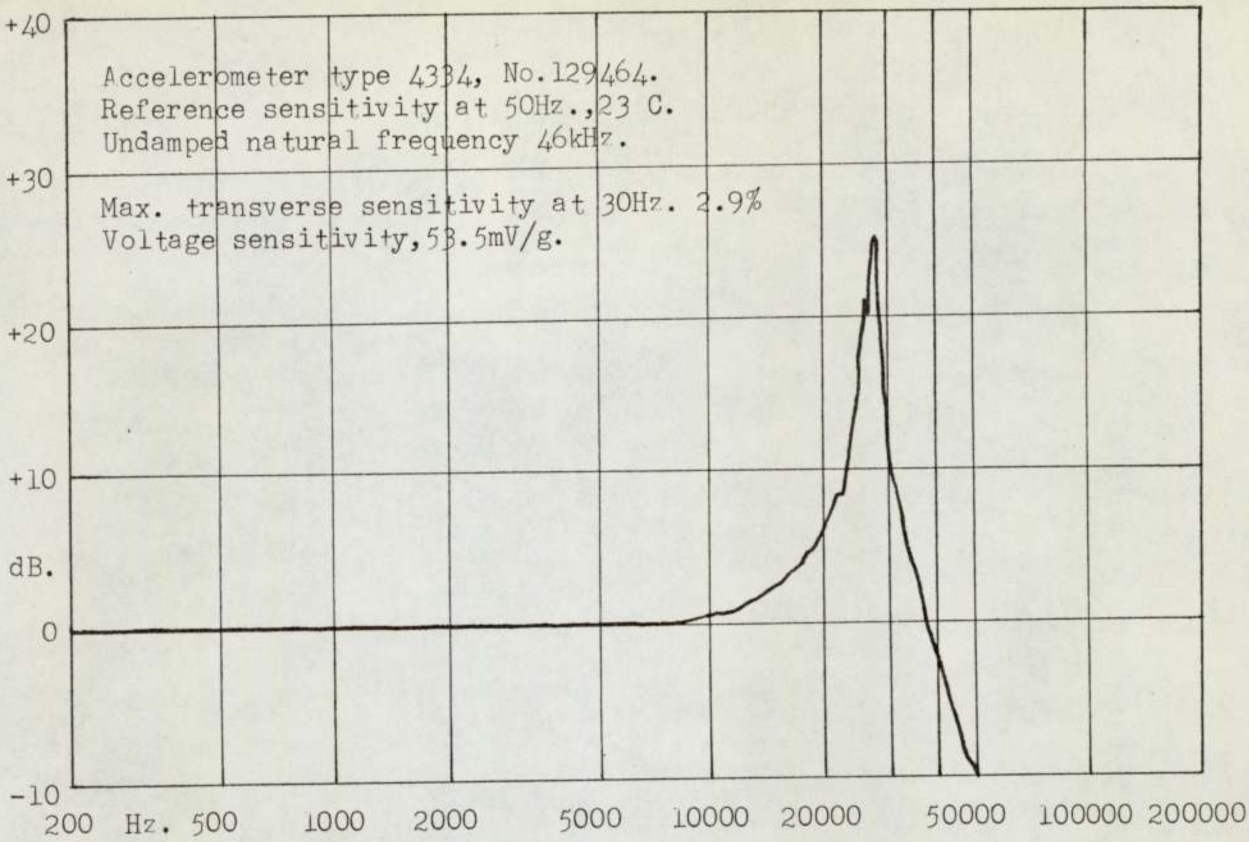

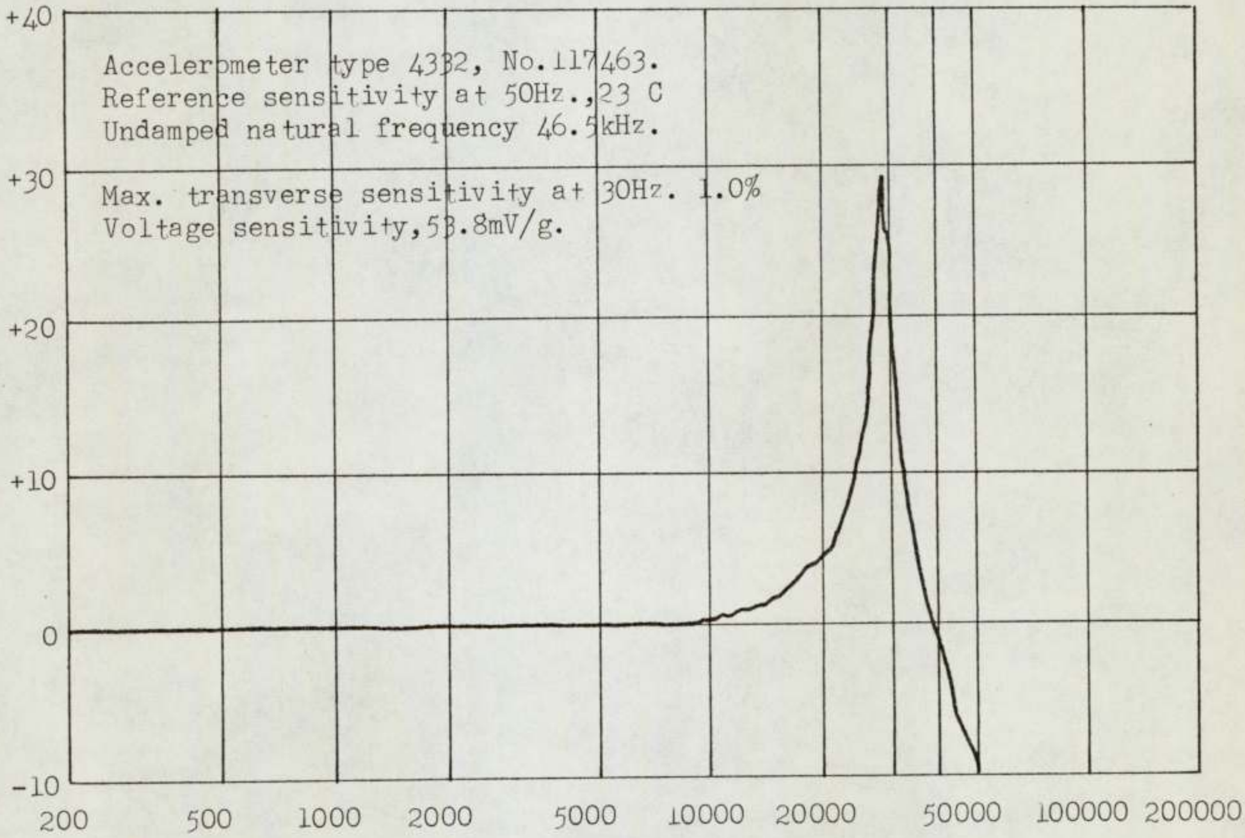

FIG.(4.5). ACCELEROMETER DETAILS & FREQUENCY RESPONSE RELATIVE TO REFERENCE SENSITIVITY.

Hence, over the period of time covered by trace no.1, the traces can be used directly with an accelerometer sensitivity of 53.65 mV/g. to give $\ddot{\theta}_f$.

$$\text{i.e.}\quad \ddot{\theta}_f = \frac{\text{Trace voltage} \times 10^{-3} \times 9.806}{53.65 \times 10^{-3} \times 2.65 \times 10^{-2}}$$

$$= \text{Trace voltage} \times 6.90 \text{ rads/sec.,}$$

for 60 dB amplifier gain. (4.1)

Furthermore, over the period of time covered by trace no.4, the frame response can be taken as being directly related to the applied torque, since over this limited period of time the frame characteristic has negligible influence, i.e. the accelerometer voltage is a direct measure of applied torque such that

$$\text{applied torque} = I_f\ddot{\theta}_f$$

$$= 0.1584 \times 10^{-3} \times \text{trace voltage} \times 6.90 .$$

$$\text{i.e. Applied torque} = \text{Trace voltage} \times 1.093 \times 10^{-3} \text{ Nm.,}$$

for 60 dB amplifier gain. (4.2)

To check that the accelerometers were insensitive to vertical oscillations of the dynamometer frame, a direct pull of 100grms. was applied, via asmall pulley, to the frame top member, as shown in fig.(4.6). Again, a strand of unspun silk was inserted in the link thread and the vertical force was suddenly removed by burning this strand. The resulting accelerometer net voltage was recorded and is given in fig.(4.7). From this it is concluded that the effect of any vertical oscillation of the dynamometer frame which might occur, can be neglected.

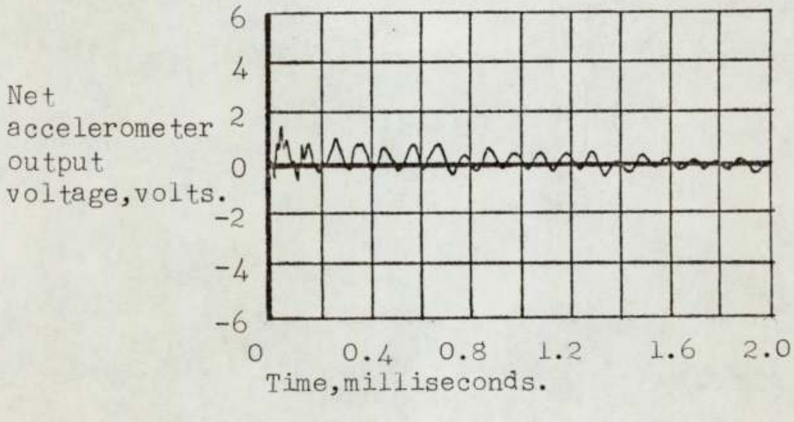

FIG.(4.7). EFFECT OF SUDDEN VERTICAL LOAD ON DYNAMOMETER FRAME.

Calibration of electrical instrumentation for variable frequency:

Since, in the course of the investigation, measurements were required over a range of supply frequency, it was necessary to check the instrumentation for variable frequency. To do this the reference phase was closed through a non-inductive fixed resistor at the motor terminals, having disconnected the latter. With a constant current of 90mA (the phase current taken by the machine when stalled) the supply frequency was varied from 20Hz to 600Hz and readings of voltage and power taken for each frequency. The difference between the wattmeter reading and the product of voltage and current, expressed as a percentage of the wattmeter reading, was plotted against supply frequency and is given in fig.(4.9). This indicates a difference of less than 1.0% and it was concluded, therefore, that the equipment could be used without correction.

Effect of source impedance on transient current:

In addition to looking into the effects of variable frequency, it was also essential to be sure that the impedances of the sources feeding the test machine would not influence the transient machine current. This was investigated by closing the control phase through a fixed resistor, as above, and initiating the control phase voltage at various points on its waveform. For each case the control phase current was recorded photographically. The traces showed that the source impedance did not affect the transient current.

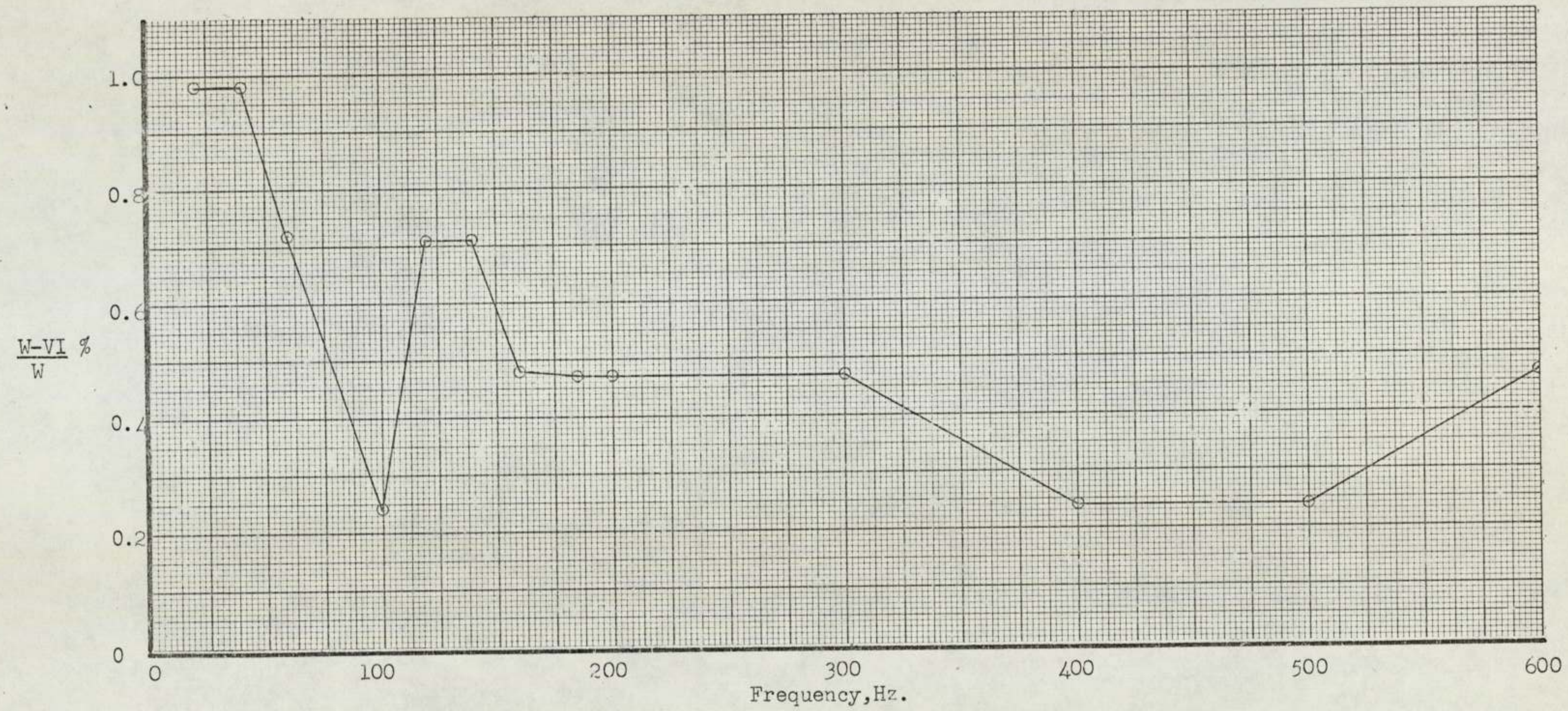

FIG.(4. 9). CALIBRATION OF INSTRUMENTATION AGAINST FREQUENCY.

12) Base temperature method of measurement.

To indicate the temperature sensitivity of the machine, the stalled performance of the motor was measured for various winding temperatures at constant current per phase and balanced excitation. To do this, the machine was thermally soaked at 90 mA per phase until a steady temperature was attained. At this temperature readings were taken of the phase voltage and power, the dynamometer deflection and the winding resistance (and hence the temperature).

The current was then reduced and the machine allowed to cool down to a lower steady temperature at which the current was restored to 90 mA and further readings taken, as quickly as possible, to prevent appreciable change in the machine's temperature during the period of measurement. Following this, the current was reduced to an even lower value and the process repeated.

The results of this test are given graphically in fig.(4.8) and cover a temperature range of approximately 40°C to 130°C; the rate of change of machine temperature near ambient made readings impossible at temperatures lower than 40°C. From these graphs it is seen that for constant current the voltage sensitivity is 0.29%/°C, the power sensitivity is 0.34%/°C and the torque sensitivity is 0.31%/°C.

Since these types of machines have an operating temperature rise of about 90°C, it will be appreciated that these sensitivities are embarassingly high. To overcome their effects the base temperature method of measurement was employed for all tests.

For this method the machine is always initially thermally soaked to a steady temperature as indicated by the bridge monitor. All measurements are then carried out at this base temperature, the machine being restored to base conditions after every reading and, as an extra precaution, the temperature is checked immediately after every set of readings. Should the temperature have altered appreciably, the readings are repeated. It is only by means such as this that dependable measurements can be obtained during the testing of miniature machines.

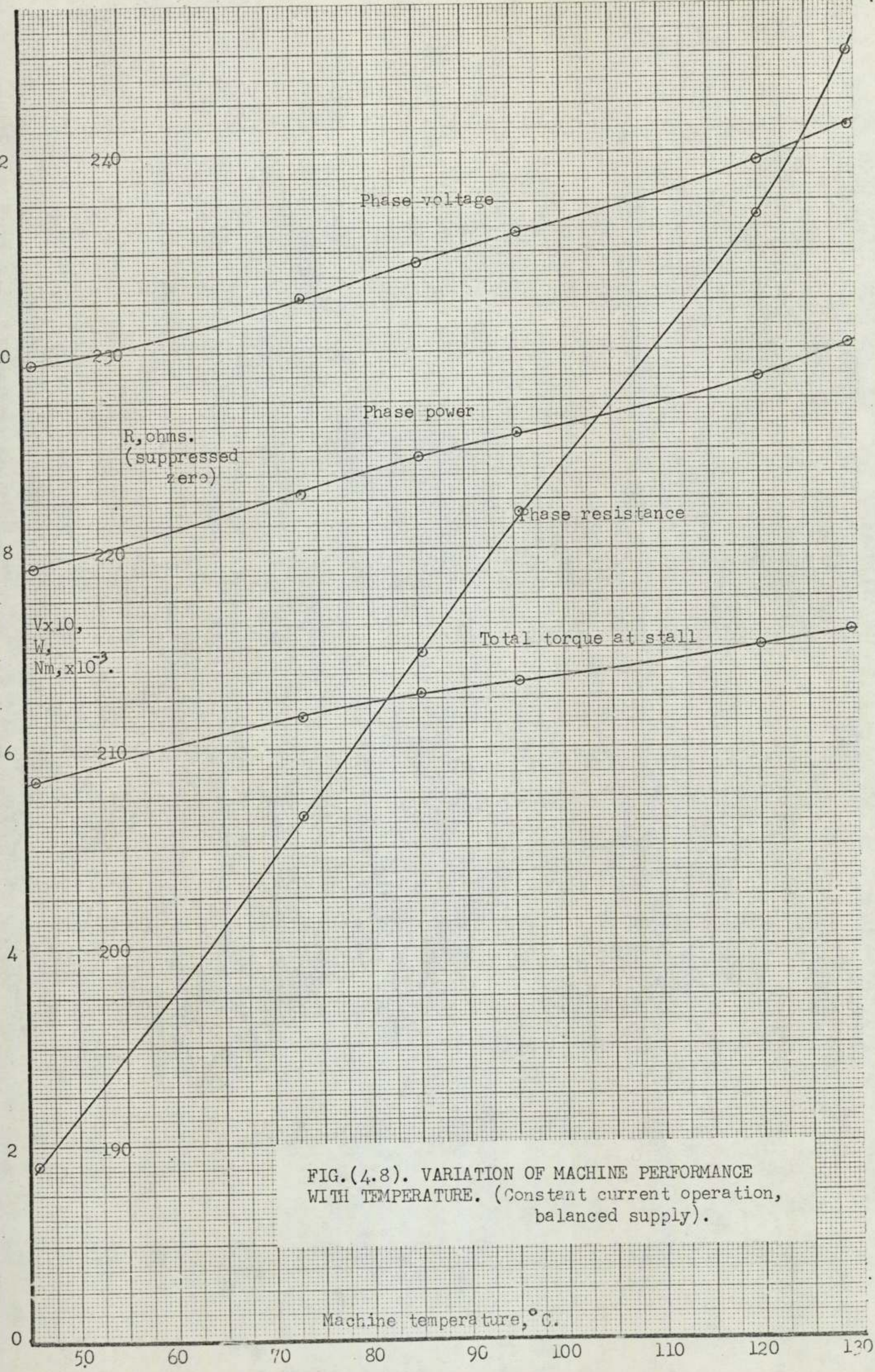

FIG.(4.8). VARIATION OF MACHINE PERFORMANCE WITH TEMPERATURE. (Constant current operation, balanced supply).

13) Steady state performance.

In measuring the pefformance of the test machine, the object was to cover as much of the complete range of servosystem requirements as possible, in order to be able subsequently to verify the method of obtaining and using the model of the machine.

Thus, in the steady state region, five sets of characteristics were obtained, using the techniques already detailed,

a) balanced rated voltage, rated frequency, variable speed for slip range 0 - 2.0,

b) unbalanced voltage, rated frequency, variable speed for slip range 0 - 1.0; reference phase set at rated voltage, control phase set at 50% rated voltage,

c) as for (b) but with control phase voltage set at zero and the winding short circuited,

d) steady speed, variable control voltage; reference phase set at rated voltage, speed set at 50% synchronous speed,

e) as for (d) but with zero speed and reference phase current held constant at rated value.

In tests (a), (b) and (c), particular care was taken in the regions of speed where the effects of space harmonics might have been apparent, in order that any such effects should not be missed. The five characteristics were all obtained at the same base temperature and all record voltage, current, power, per phase, and total developed electromagnetic torque. They are presented graphically on figs. (4.10), (4.11)&(4.12), (4.13)&(4.14), (4.15) and (4.16), respectively.

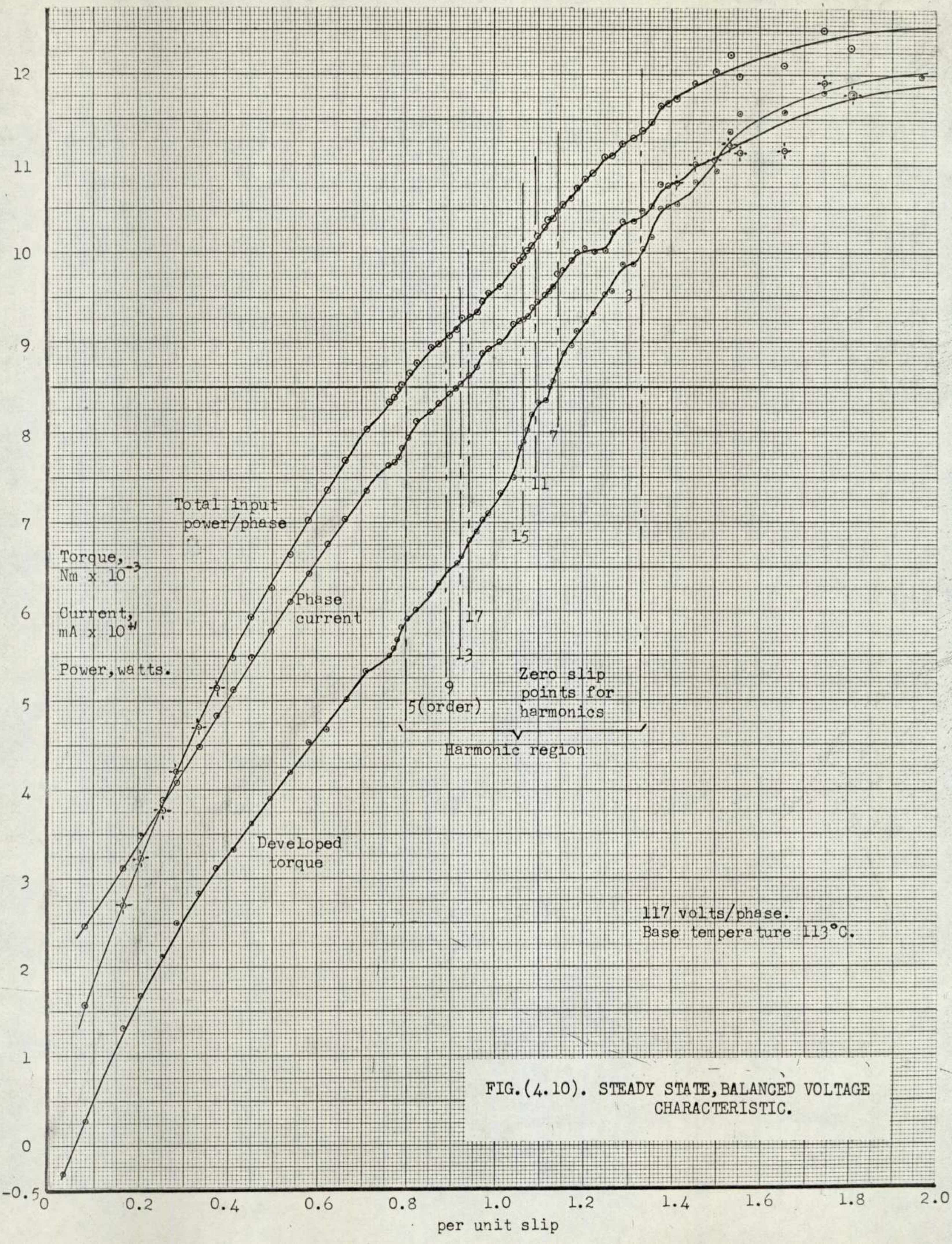

FIG.(4.10). STEADY STATE, BALANCED VOLTAGE CHARACTERISTIC.

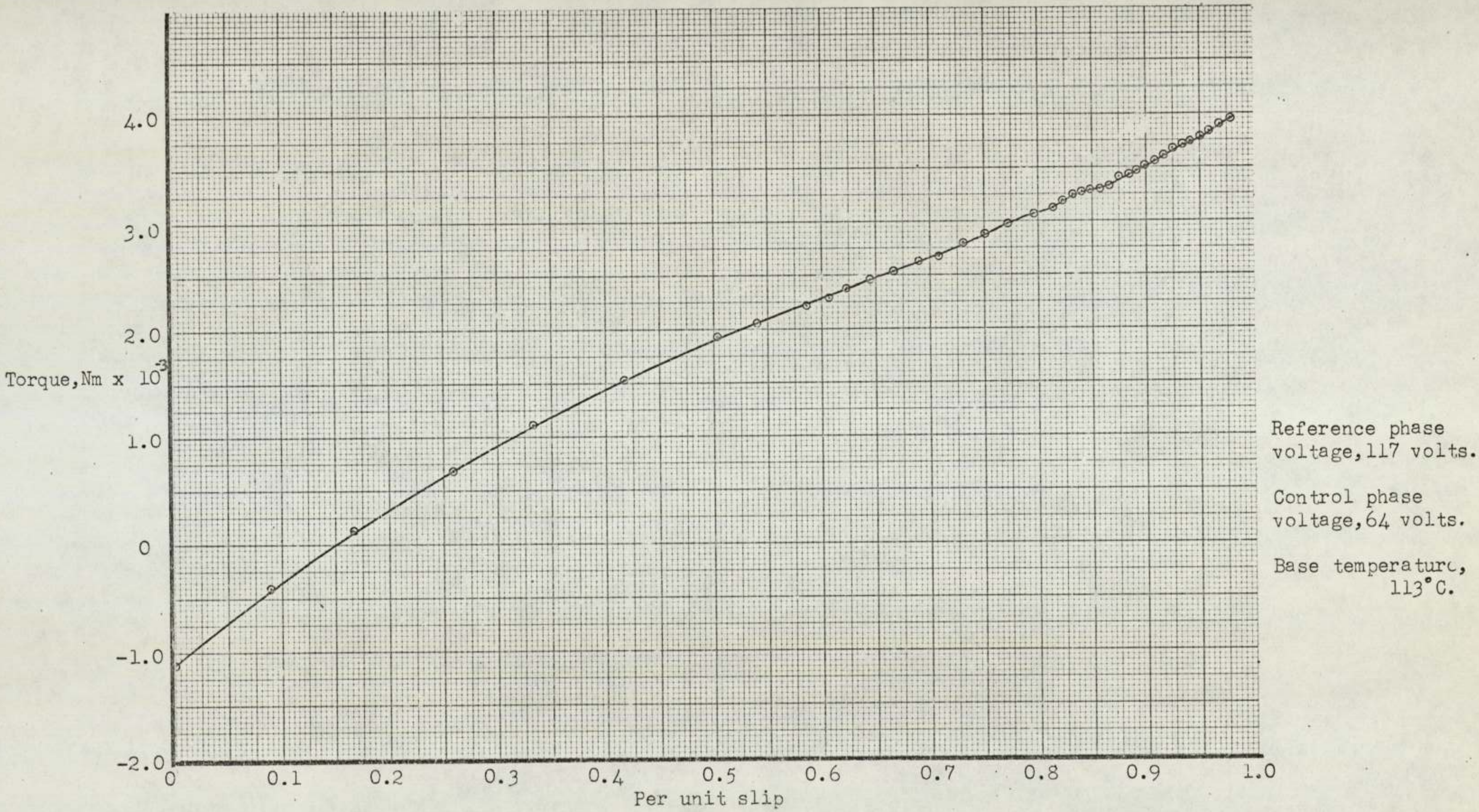

FIG.(4.11). UNBALANCED VOLTAGE, TORQUE versus SLIP CHARACTERISTIC.

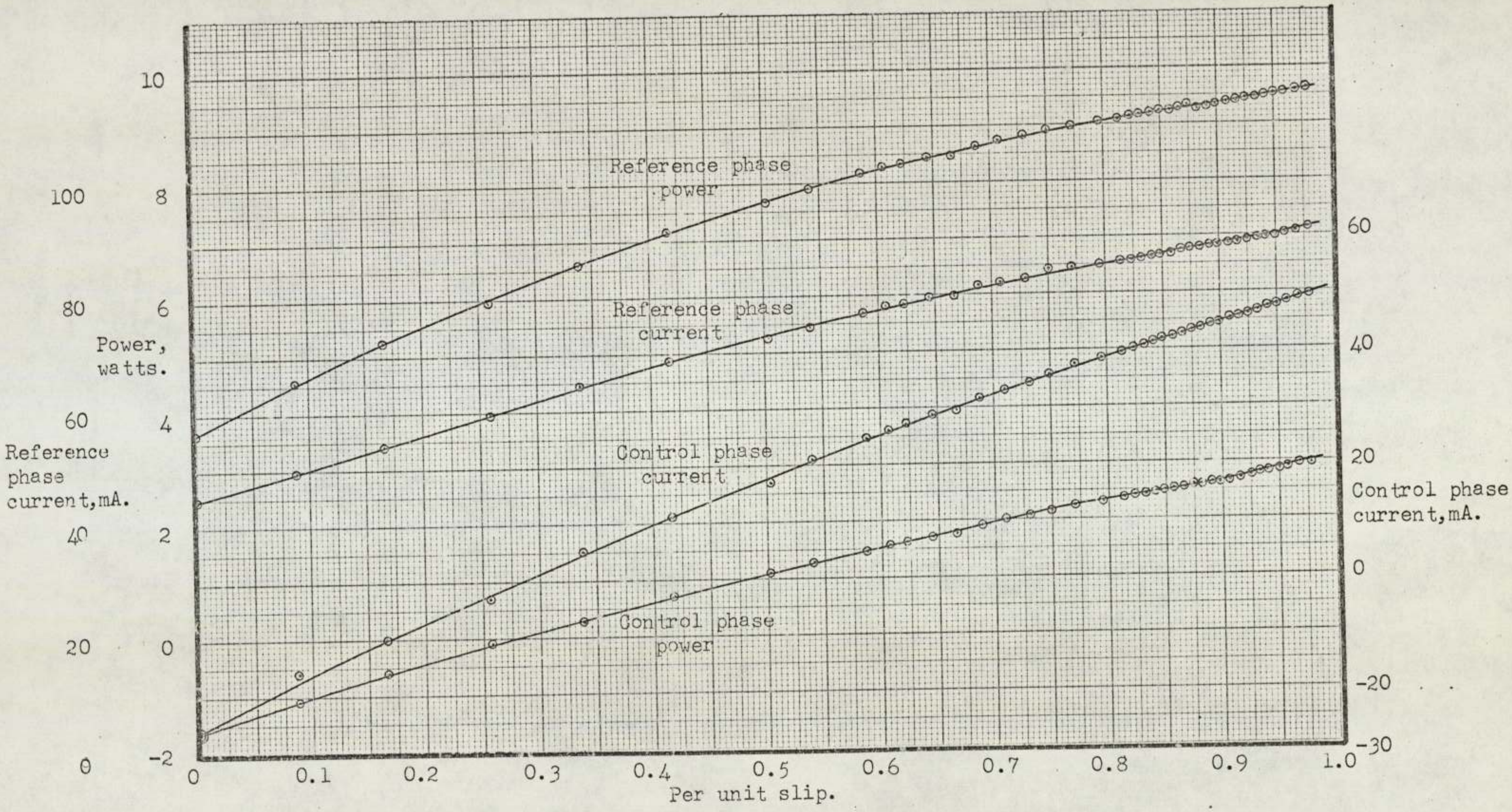

FIG.(4.12). CURRENT & POWER versus SLIP CHARACTERISTIC CORRESPONDING TO FIG.(4.11).

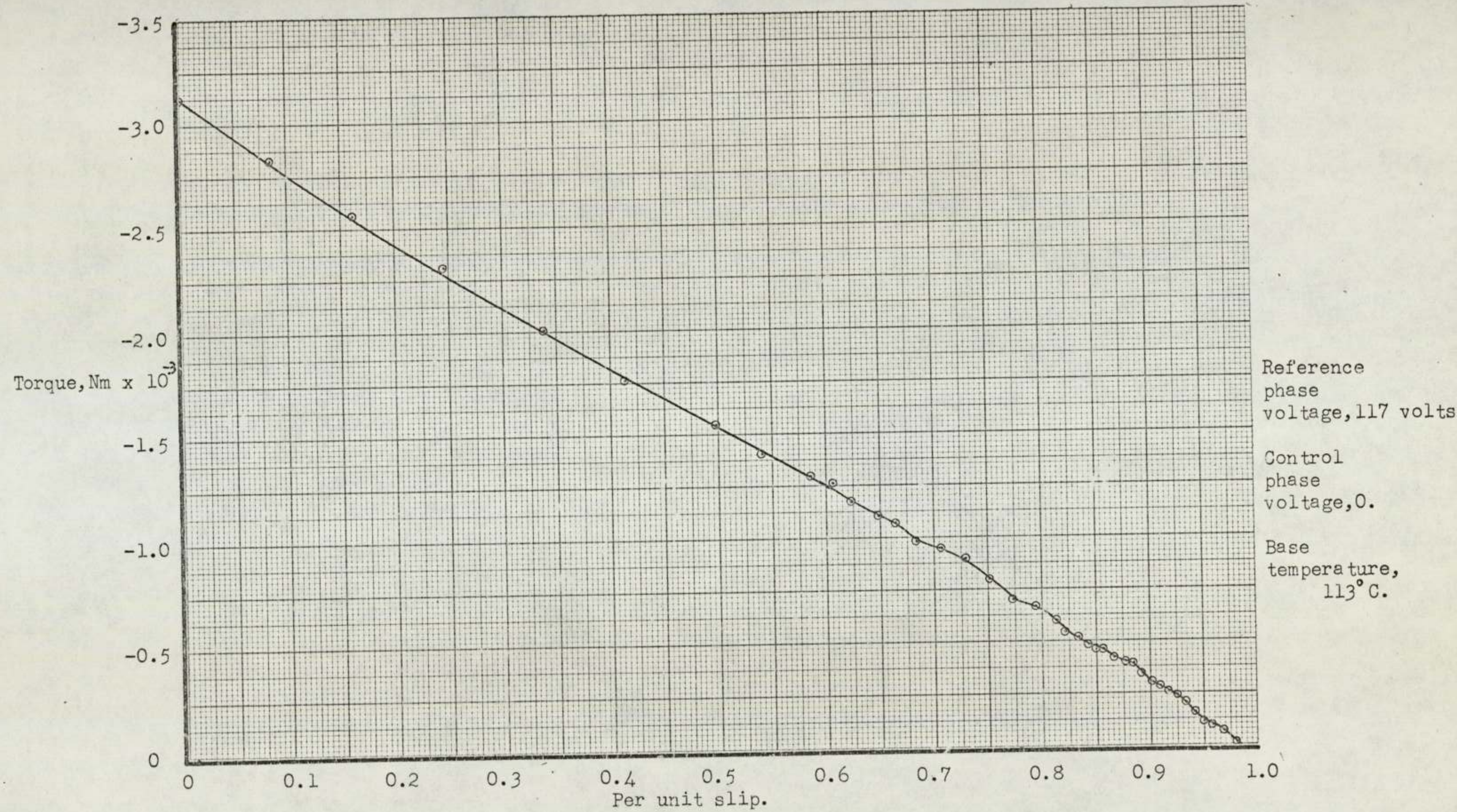

FIG.(4.13). UNBALANCED VOLTAGE, TORQUE versus SLIP CHARACTERISTIC.

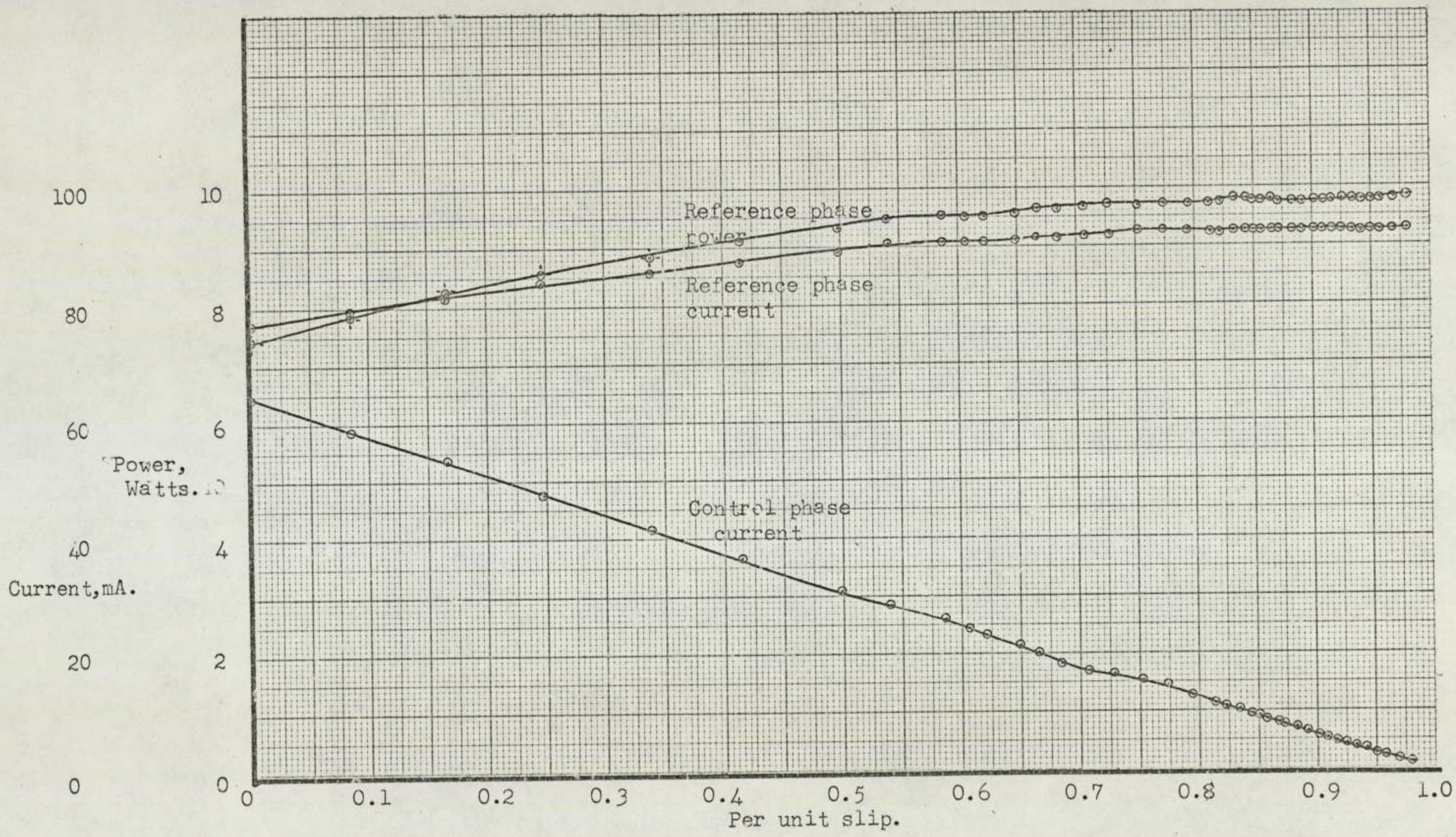

FIG.(4.14). CURRENT & POWER versus SLIP CHARACTERISTIC CORRESPONDING TO FIG.(4.13).

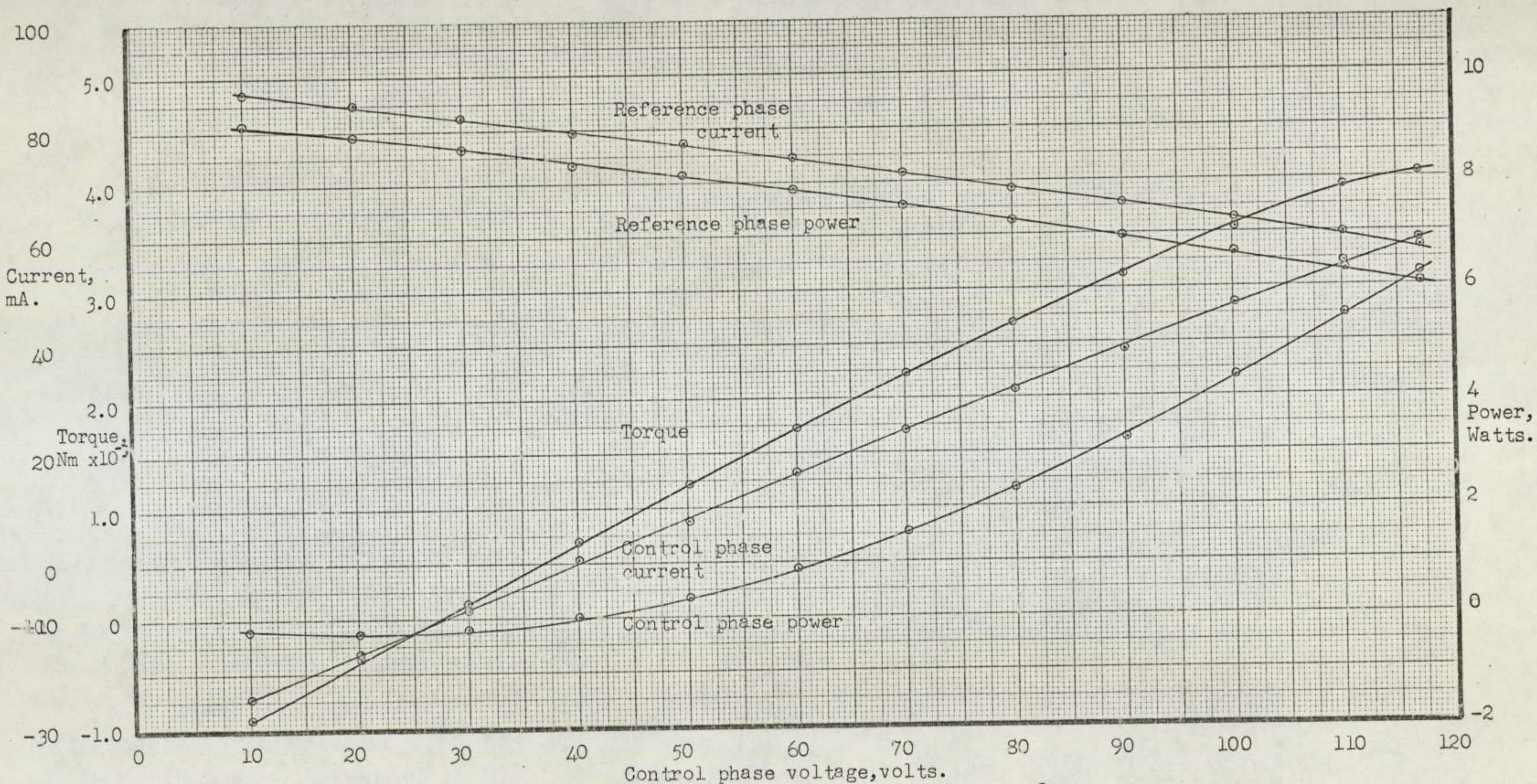

Reference phase voltage, 117 volts; speed, 12,000 r.p.m. ; base temperature, 113°C.

FIG.(4.15). STEADY SPEED, VARIABLE CONTROL VOLTAGE CHARACTERISTICS.

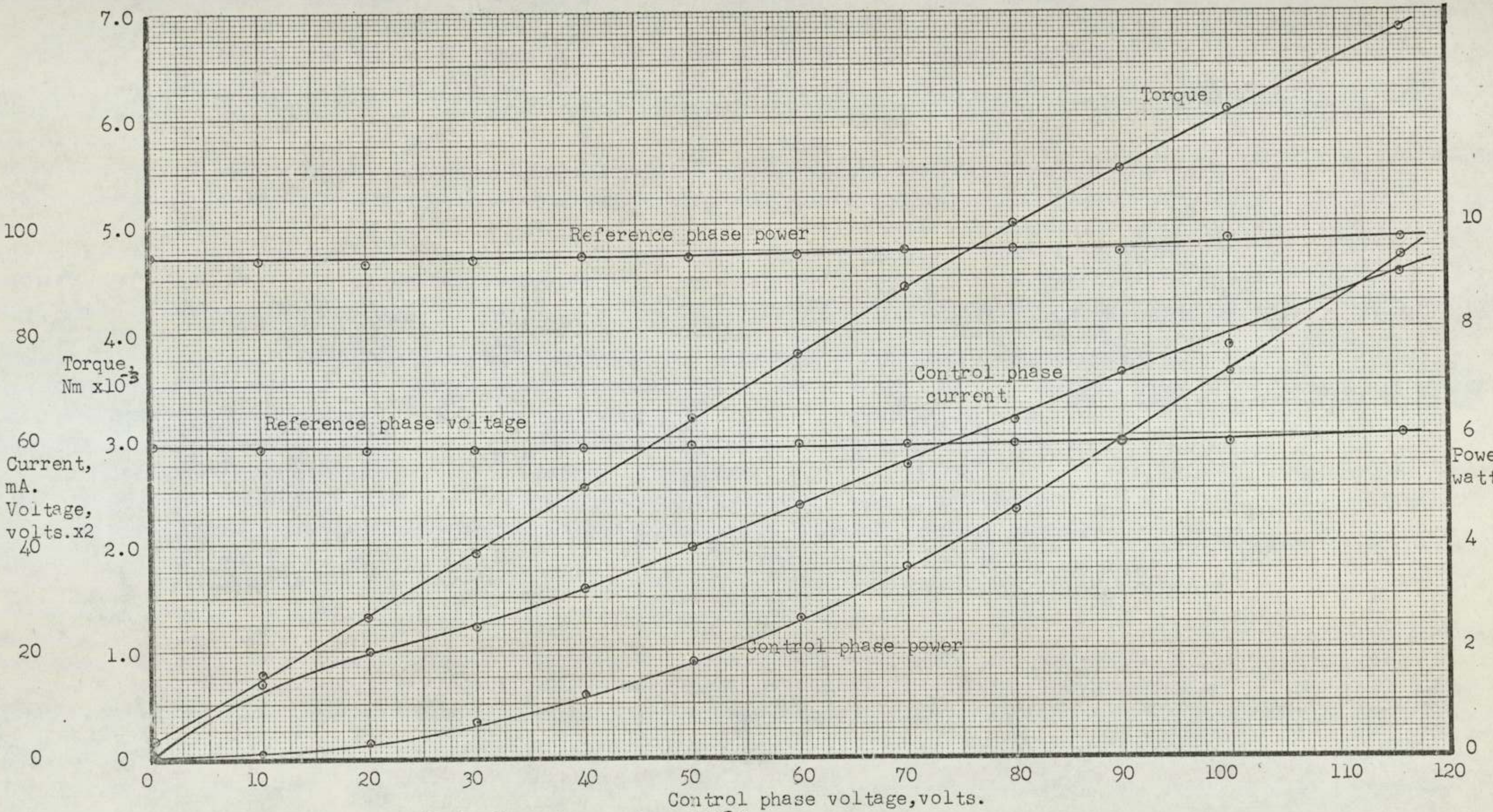

Reference phase current, 90mA ; base temperature, 113°C.

FIG.(4.16). ZERO SPEED, VARIABLE CONTROL VOLTAGE CHARACTERISTICS.

14) Dynamic performance.

The particular type of dynamic characteristic selected for measurement, was the no-load starting torque versus time characteristic for various points of voltage initiation on the control voltage waveform. This choice was made so as to be sure that the behaviour measured was solely that of the motor and did not include the behaviour of a coupled load. In all, twenty measurements were made, ten for balanced r.m.s. voltage conditions giving 90mA per phase, and ten for unbalanced conditions, the r.m.s. control voltage being approximately 50% r.m.s. reference voltage for 90mA reference phase current. In all cases the motor was maintained at the base temperature used throughout the steady state tests. For each run in the groups of ten, the reference phase was continually excited. The control phase voltage initiation point was set by means of the point on wave switch described in section 7, chapter III, the run number corresponding to the initiation point number as specified in fig.(4.17). Thus, the performance measured is that of the machine responding to a control phase stimulus. The transient control voltage, control current, reference current and net accelerometer output voltage (developed torque) were recorded photographically using the recording oscilloscope controlled by the one shot trigger, described earlier, and superimposed; the currents were measured as voltage drops across 1.9 ohm non-inductive resistors. The traces so obtained are reproduced in fig.(4.18) and fig.(4.18a) for the balanced and the unbalanced supply conditions, respectively. In addition to these, fig.(4.19) gives the net accelerometer voltage and the control phase current, with a slower time-base, for two initiation points only, on each supply; the results in this case indicate the extent of the transient period.

Since the accelerometer output voltage in fig.(4.19) exhibted, at steady speed, both low and high frequency components, relatively speaking, which make it difficult to assess the information, it was decided to examine the nature of the developed torque under no-load, steady speed conditions. Thus, with the machine on no-load and running stably, the net accelerometer output voltage was fed into a Bruel and Kjaer band pass filter set, with automatic switching, coupled to a Bruel and Kjaer level recorder so that a clear indication of the frequencies present and their relative magnitudes could be obtained. The resulting spectrograms, for the two voltage conditions used in the dynamic tests, are in fig.(4.20) and fig.(4.21); again, all measurements were carried out at base temperature.

Discussion of all of these results is deferred to the two final chapters.

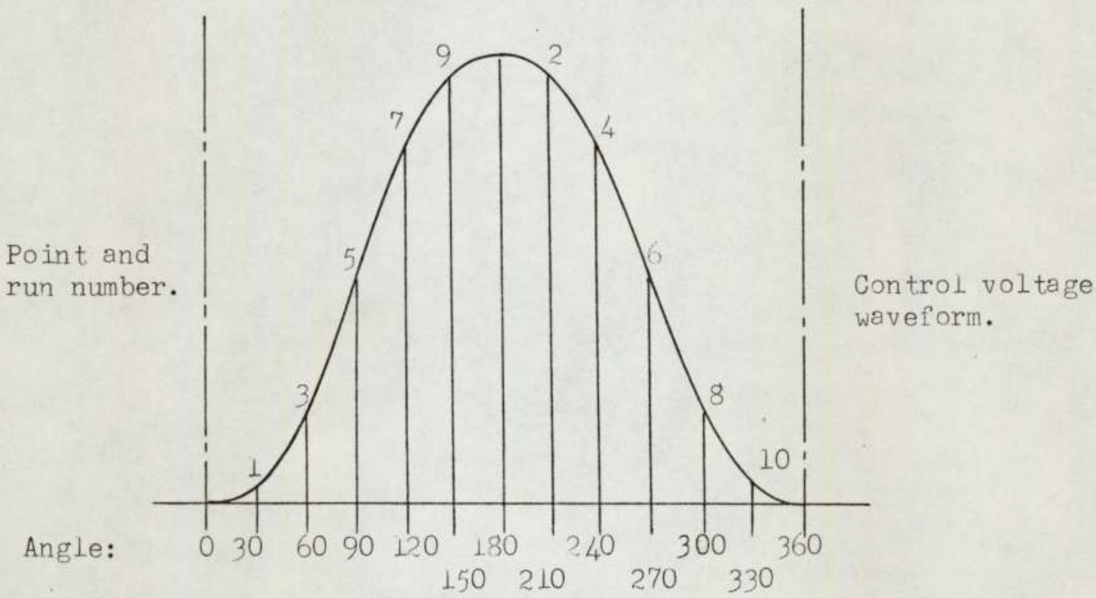

FIG.(4.17). CONTROL PHASE VOLTAGE INITIATION POINTS FOR DYNAMIC TESTS.

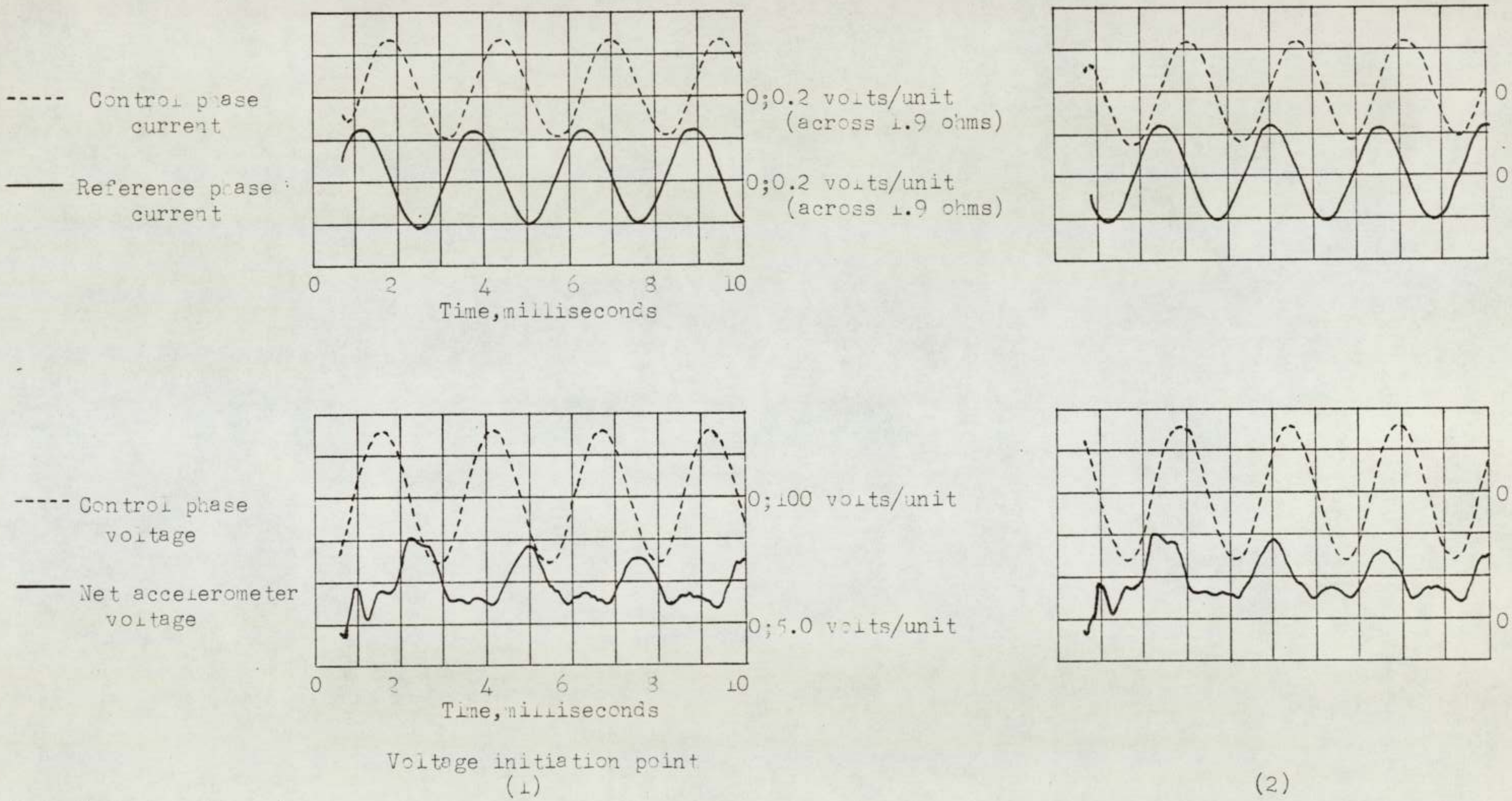

Key and scales apply to all traces in fig.(4.18).

FIG.(4.18). DYNAMIC PERFORMANCE OF TEST MACHINE ON NO-LOAD, BALANCED SUPPLY.

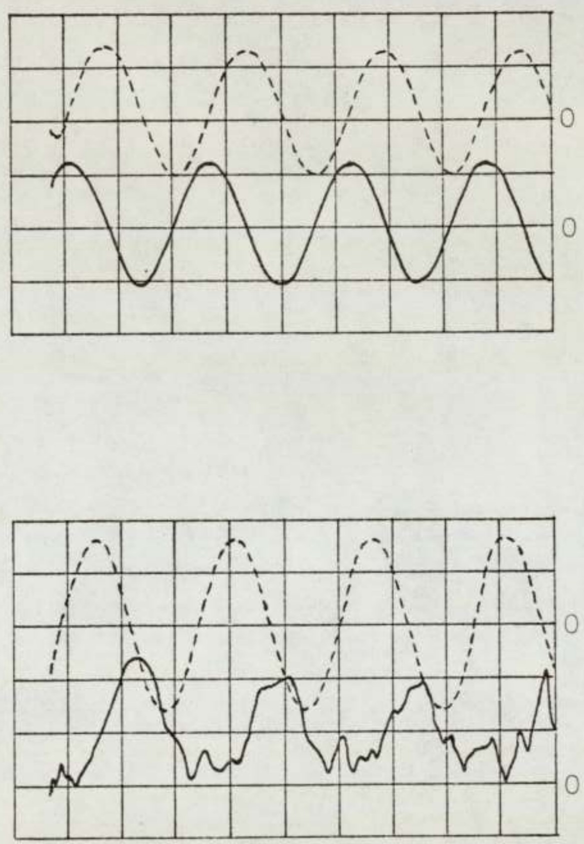

(3)

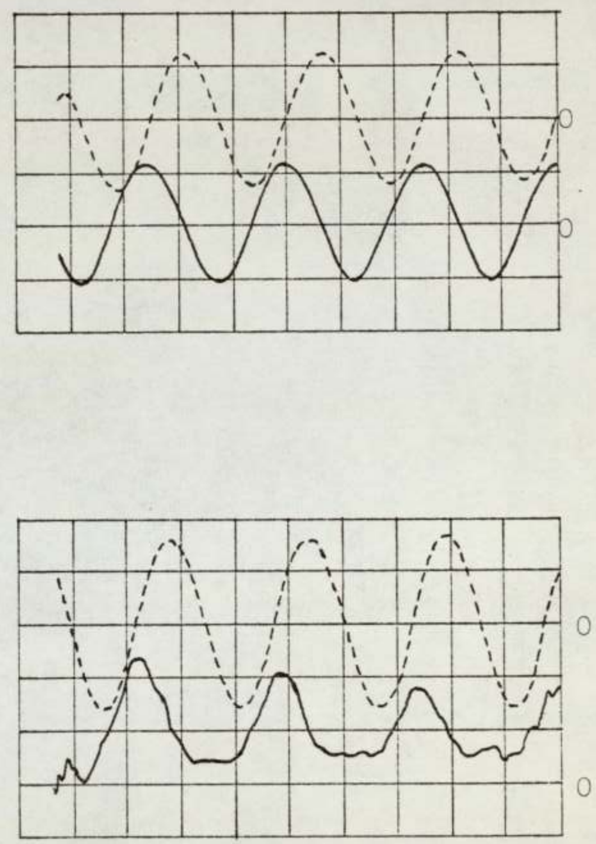

(4)

For scales and key,
see first sheet of figure.

FIG.(4.18). continued.

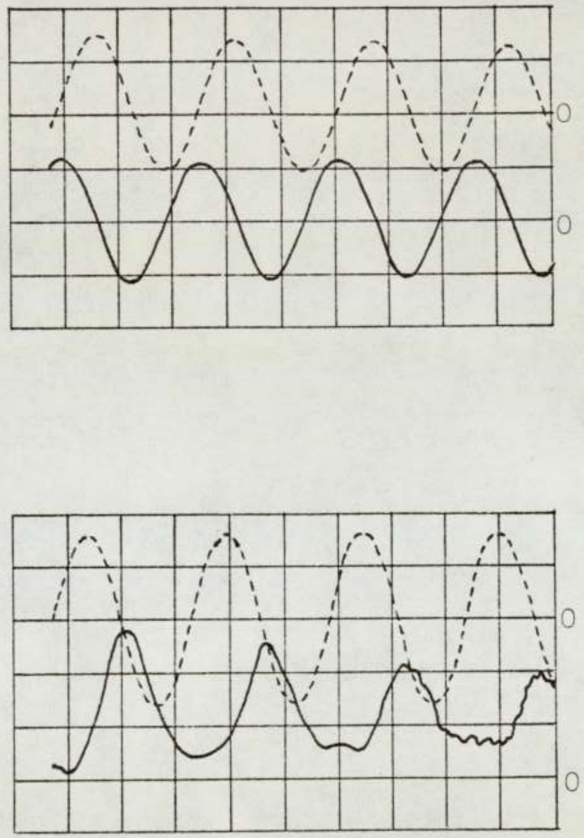

(5)

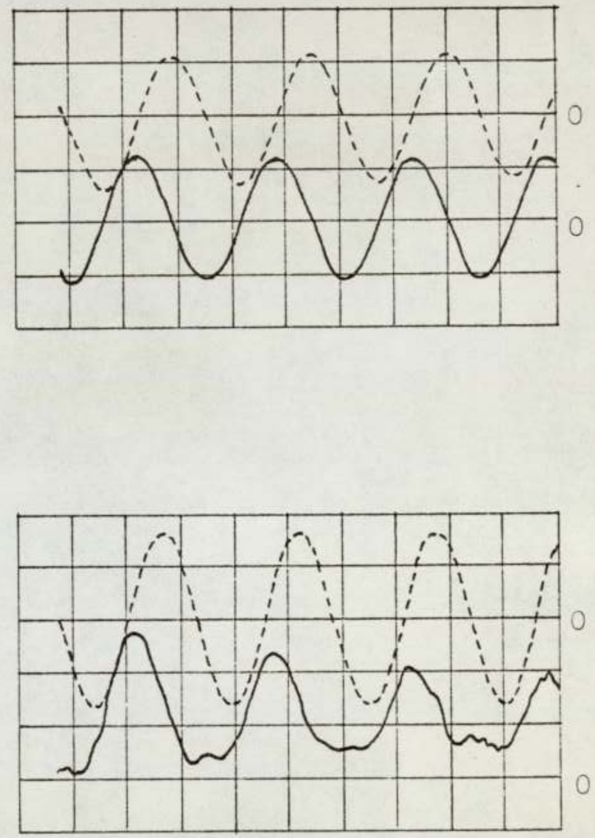

(6)

For scales and key,
see first sheet of figure.

FIG.(4.18). continued.

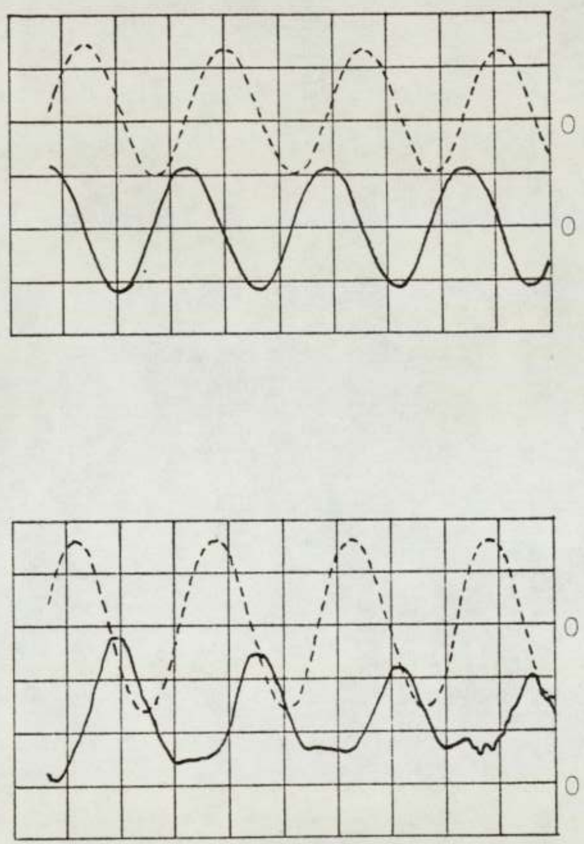

(7)

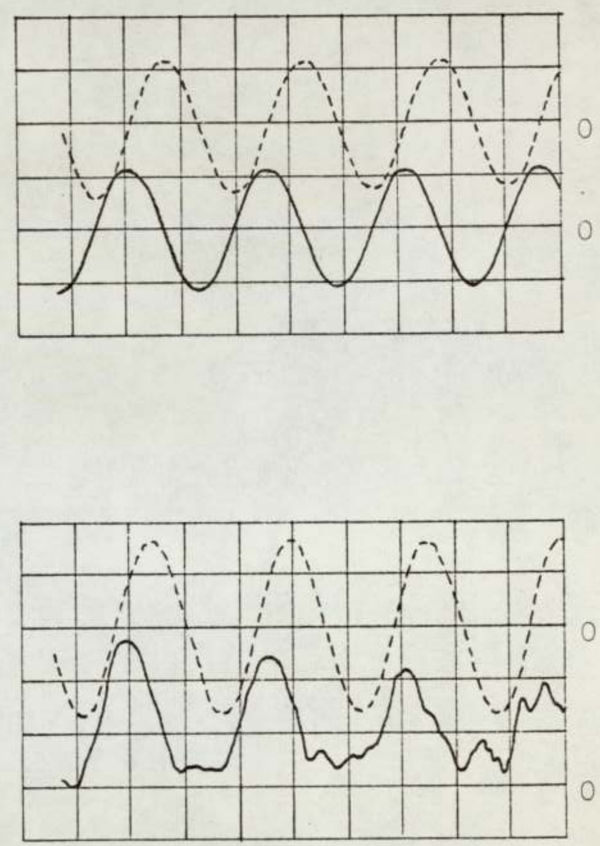

(8)

For scales and key,
see first sheet of figure.

FIG.(4.18). continued.

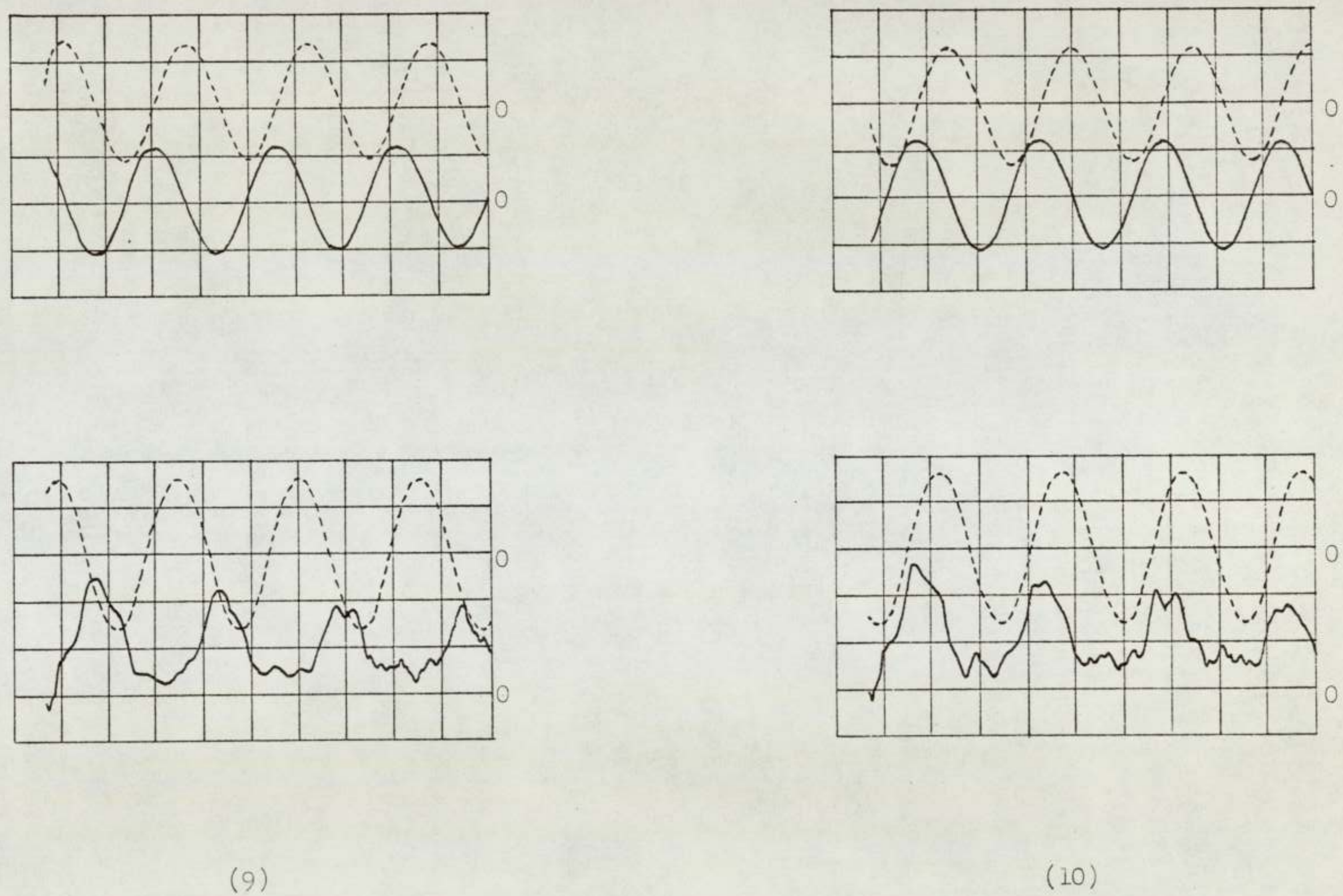

For scales and key,
see first sheet of figure.

FIG.(4.13). continued.

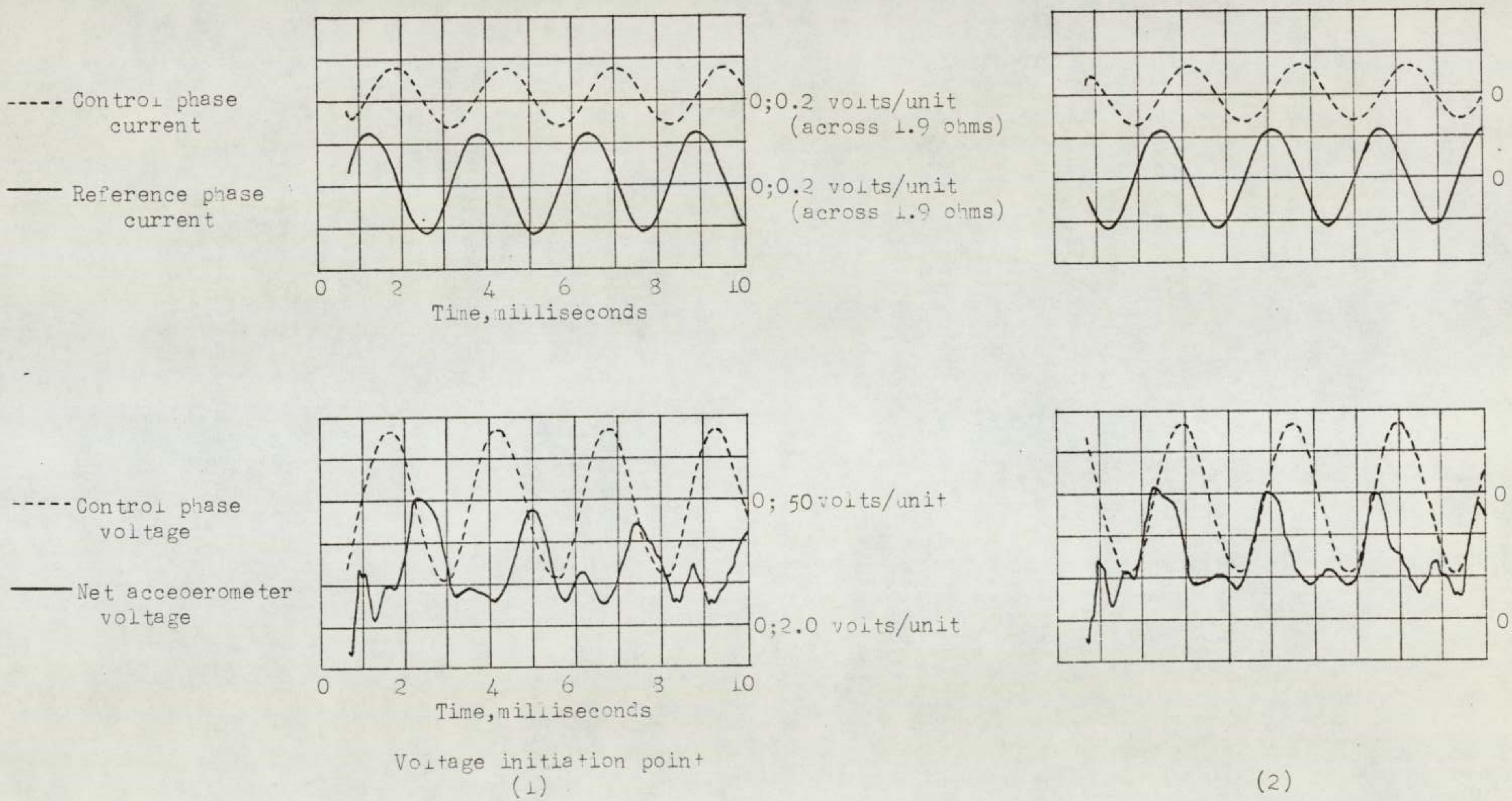

Key and scales apply to all traces in fig.(4.13a)

FIG.(4.13a). DYNAMIC PERFORMANCE OF TEST MACHINE ON NO-LOAD, UNBALANCED SUPPLY.

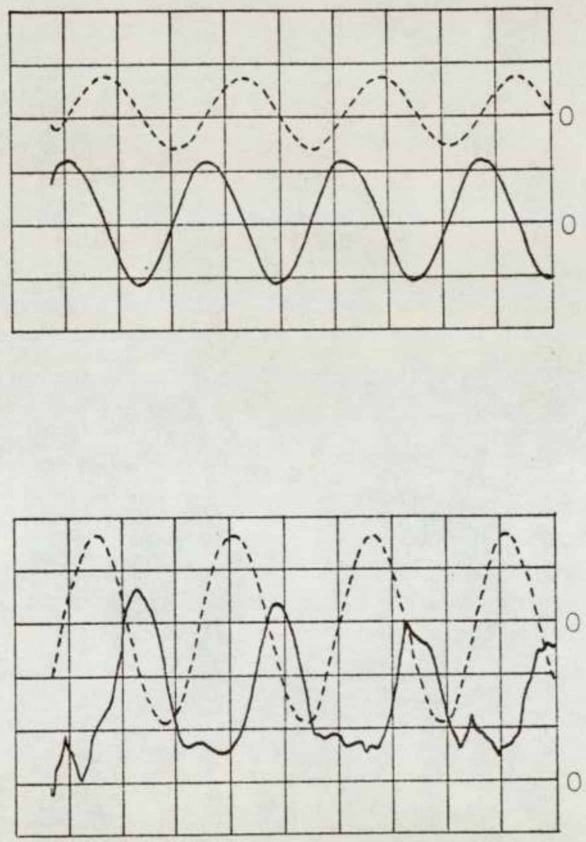

(3)

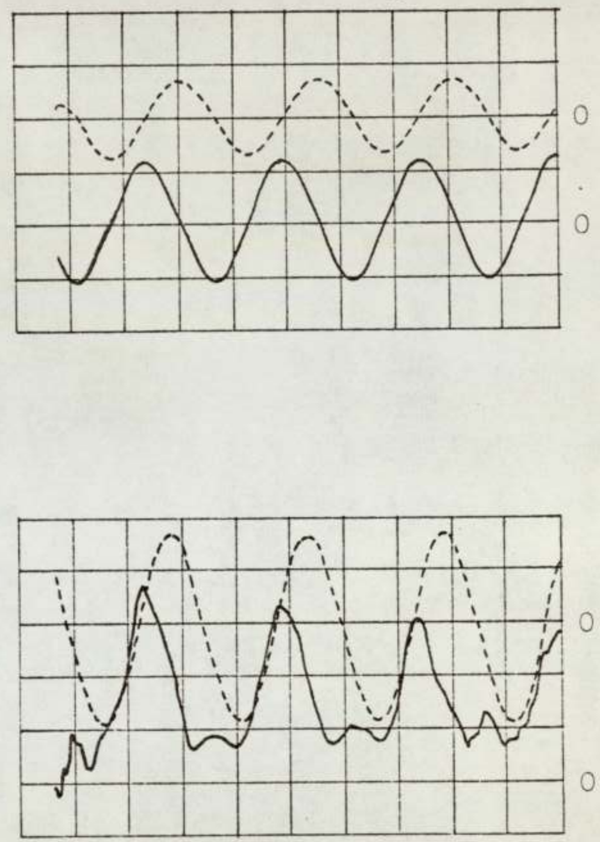

(4)

For scales and key,
see first sheet of figure.

FIG.(4.18a).continued.

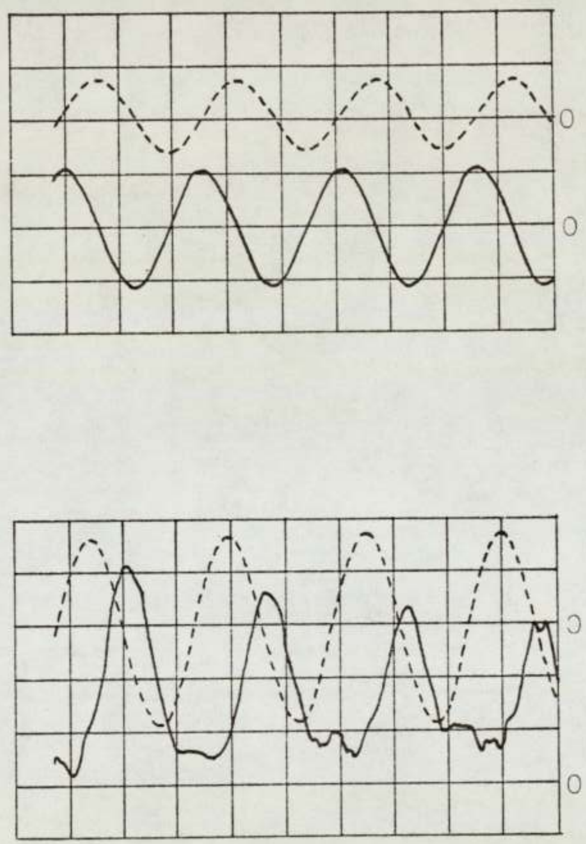

(5)

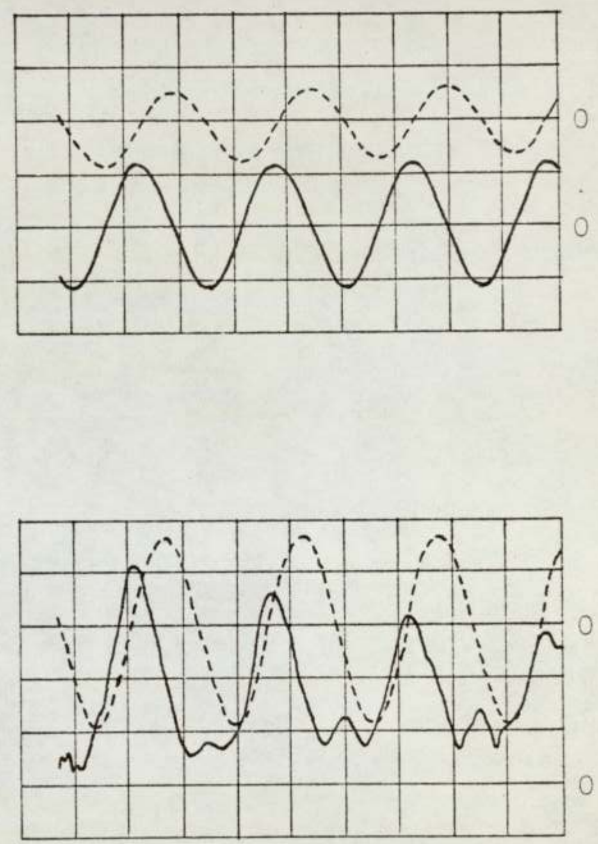

(6)

For scales and key,
see first sheet of figure.

FIG.(4.18a). continued.

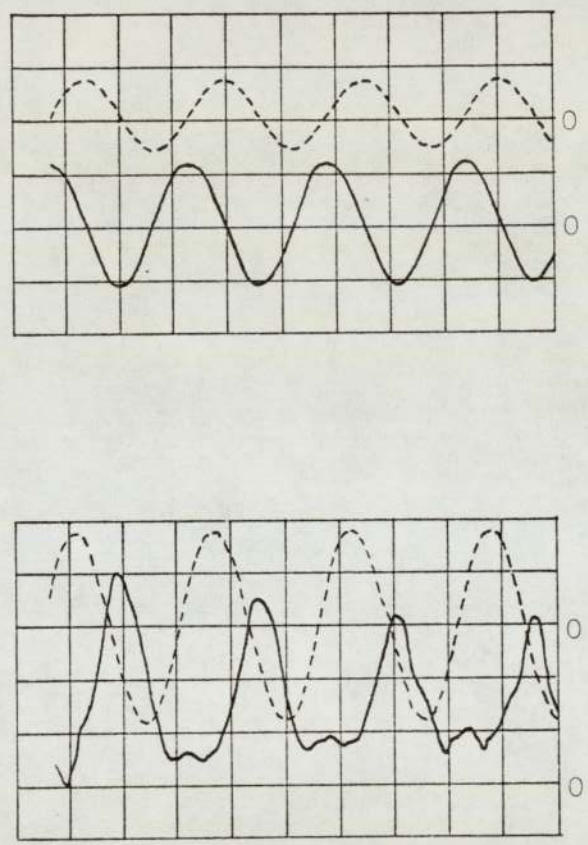

(7)

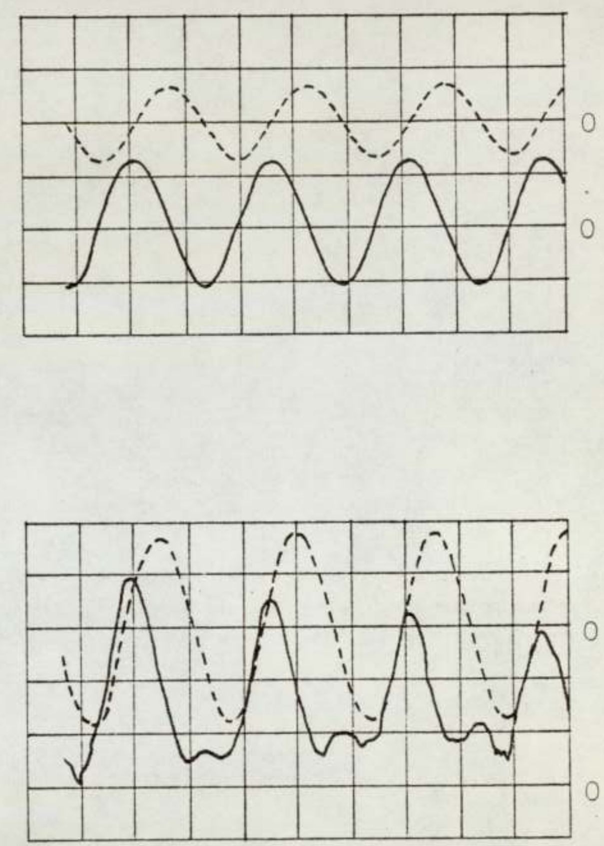

(8)

For scales and key,
see first sheet of figure.

FIG.(4.18a). continued.

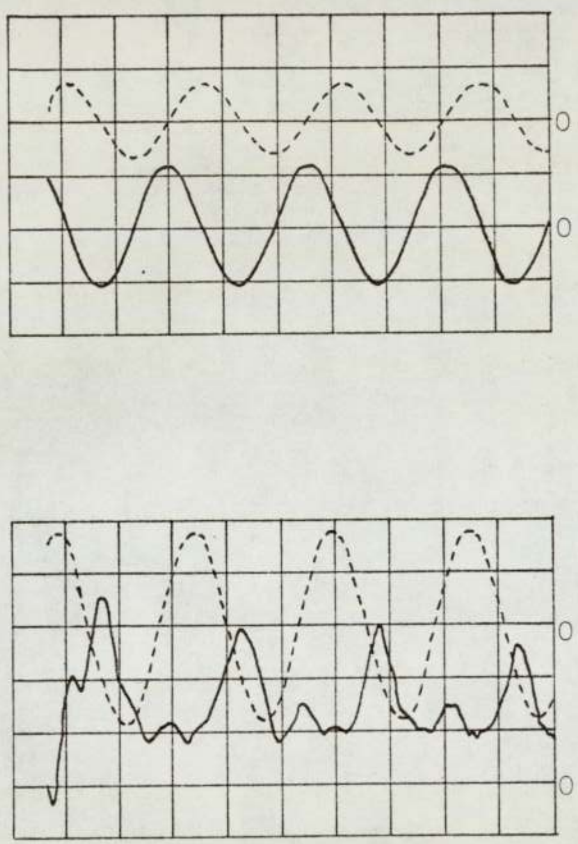

(9)

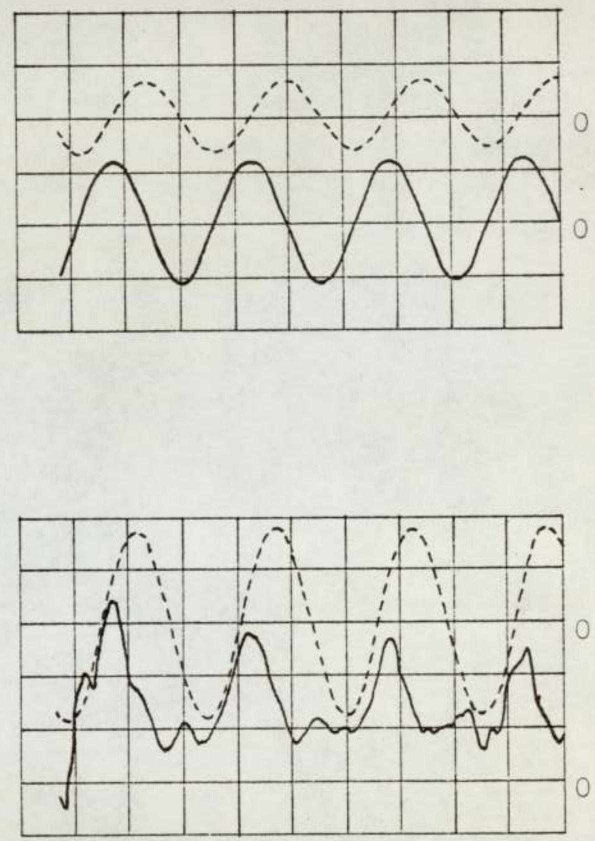

(10)

For scales and key,
see first sheet of figure.

FIG.(4.13a). continued.

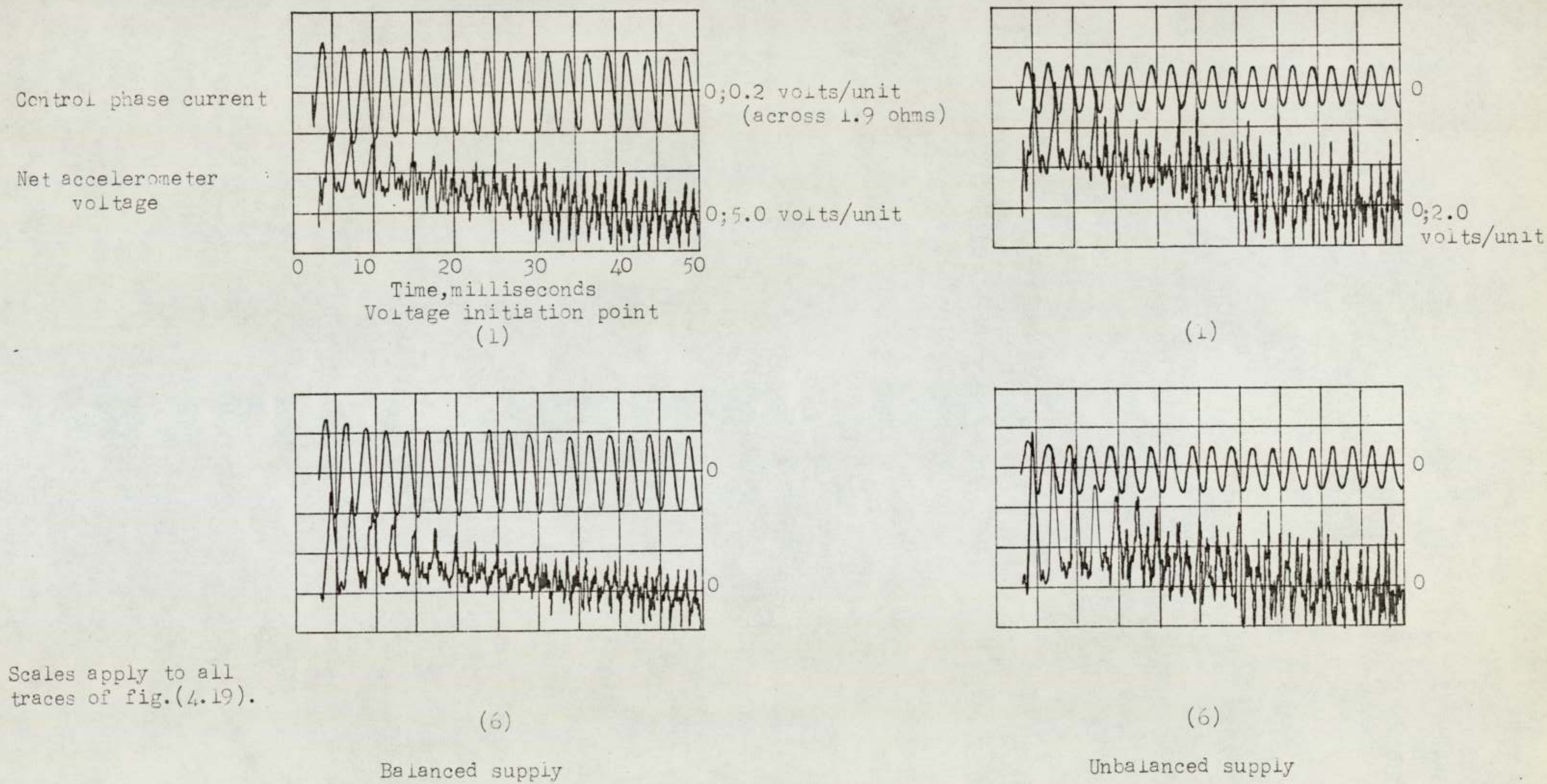

FIG.(4.19). DYNAMIC PERFORMANCE INDICATING EXTENT OF TRANSIENT PERIOD.

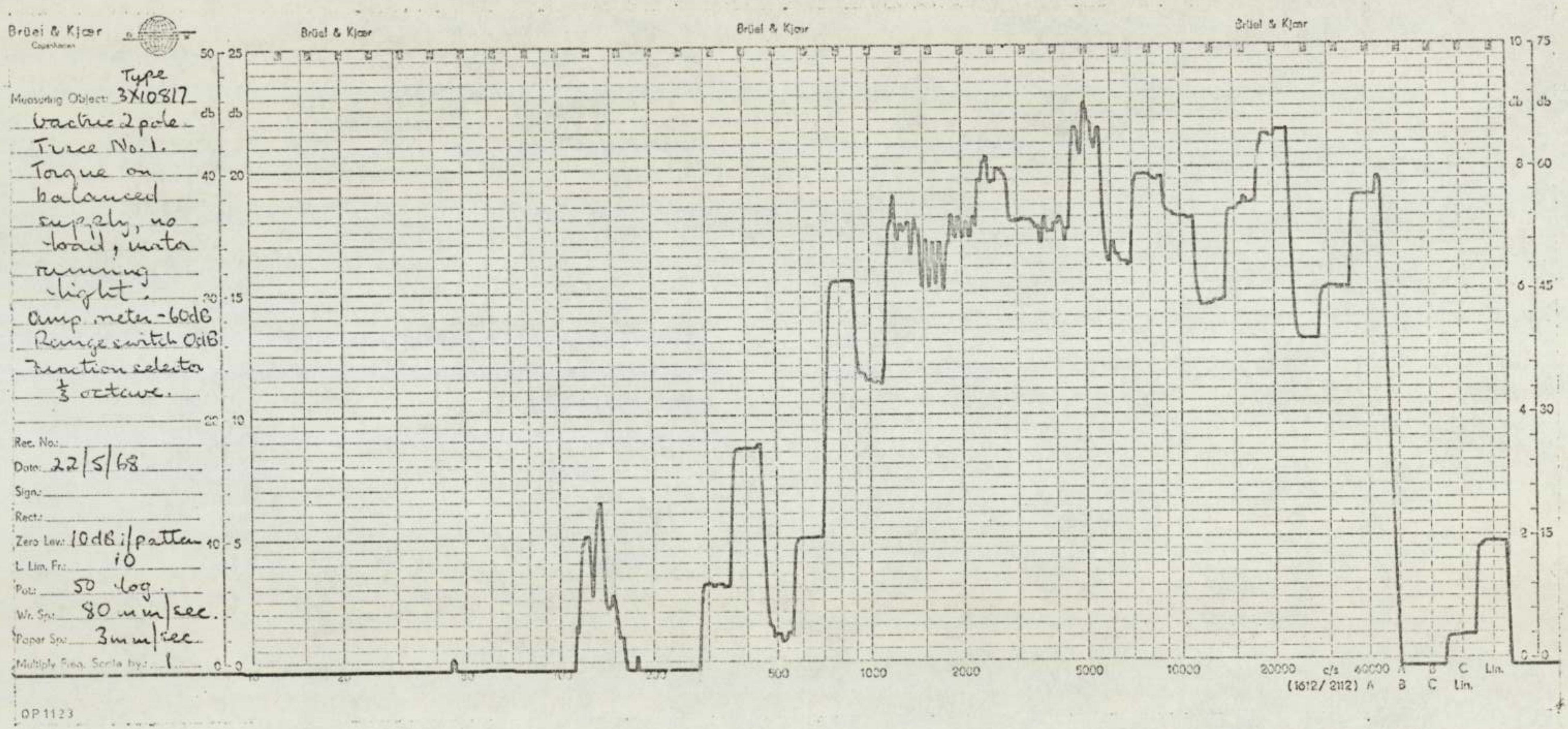

FIG.(4.20). SPECTROGRAM OF NO-LOAD NET ACCELEROMETER VOLTAGE, BALANCED SUPPLY.

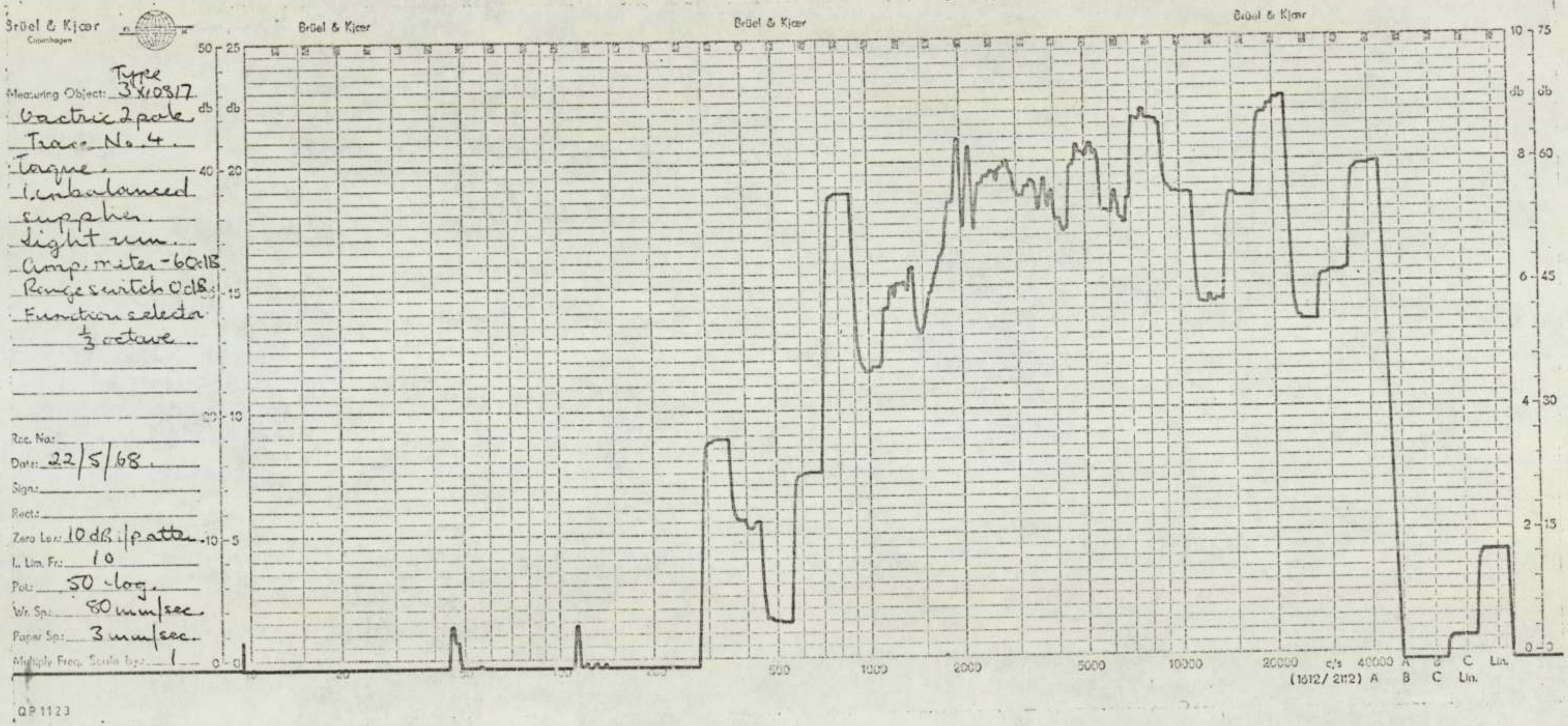

FIG. (4.21). SPECTROGRAM OF NO-LOAD NET ACCELEROMETER VOLTAGE, UNBALANCED SUPPLY.

CHAPTER V.

Measurement of the Impedance Tensor.

15) Theory of method.

For the size of machine considered in this investigation, the restriction in winding space can result in a considerable harmonic content in the spacial distribution of stator magnetomotive force. Consequently, these harmonics cannot be simply ignored and must either be shown to have little effect on the general performance of the machine or be properly taken into account. The steady state characteristics obtained for the test machine indicated little in the way of harmonic torque and to commence with it is, therefore, assumed that the harmonics may be neglected. The presence of space harmonics is considered at the end.

In the following experimental determination of the impedance tensor the starting point is taken to be the equivalent circuit per phase given in fig. (1.3) for the idealised machine. The parameters of this circuit are derived through a geometrical analysis of its impedance per unit frequency locus, this latter being obtained by means of a variable frequency test. Using these parameters the resistance tensor and the metric tensor of the motor are then constructed.

Referring to fig. (1.3), the resistance R_1 is the resistance of a multiturn winding and can, therefore, be assumed independent of frequency. The resistance R_2 is that of a squirrel cage winding which, in this type of machine, has bar dimensions giving a ratio a.c. resistance/d.c. resistance of the order of 1.01 so that this resistance may also be considered as independent of frequency. The core material used for these machines is usually low loss nickel iron alloy. Since they are designed to operate in the linear region of their magnetic circuits and because of their small size, these machines will have negligible iron loss. Hence the resistor R_0 representing this loss may be assumed infinite and omitted; reference to the design calculations carried out in chapter III will show all of these assumptions to be justified. The remaining

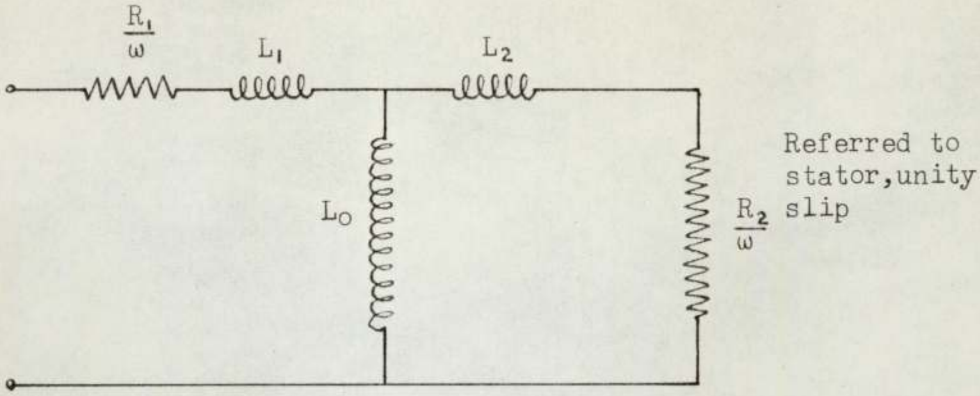

FIG.(5.1). PER UNIT FREQUENCY EQUIVALENT CIRCUIT per PHASE OF BALANCED POLYPHASE INDUCTION MOTOR.

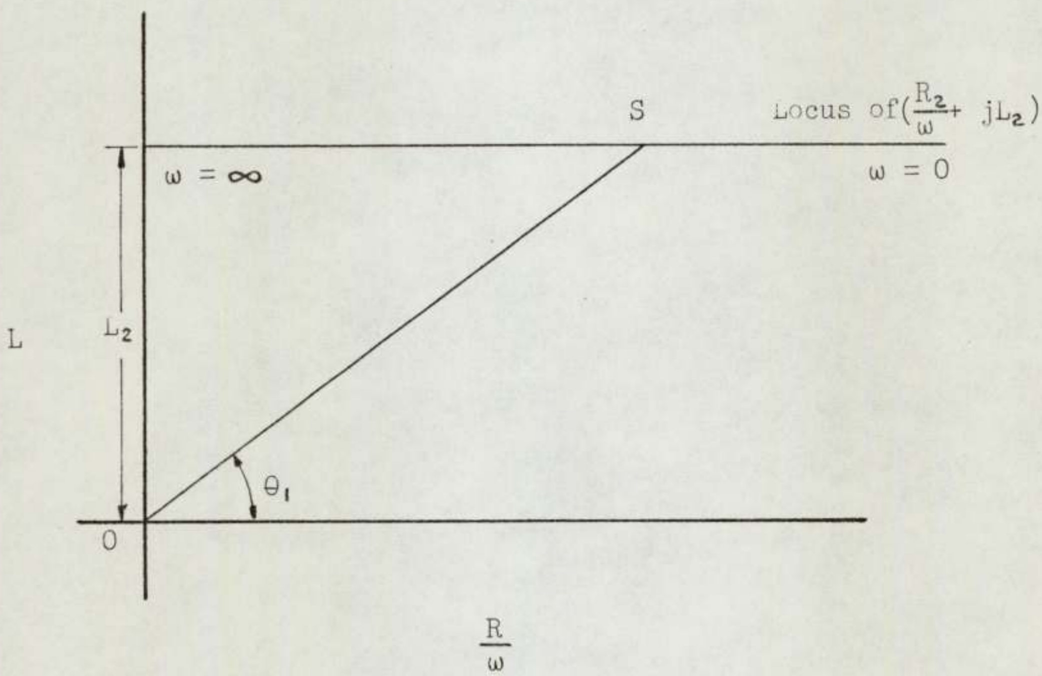

FIG.(5.2). ROTOR BRANCH, IMPEDANCE per UNIT FREQUENCY LOCUS.

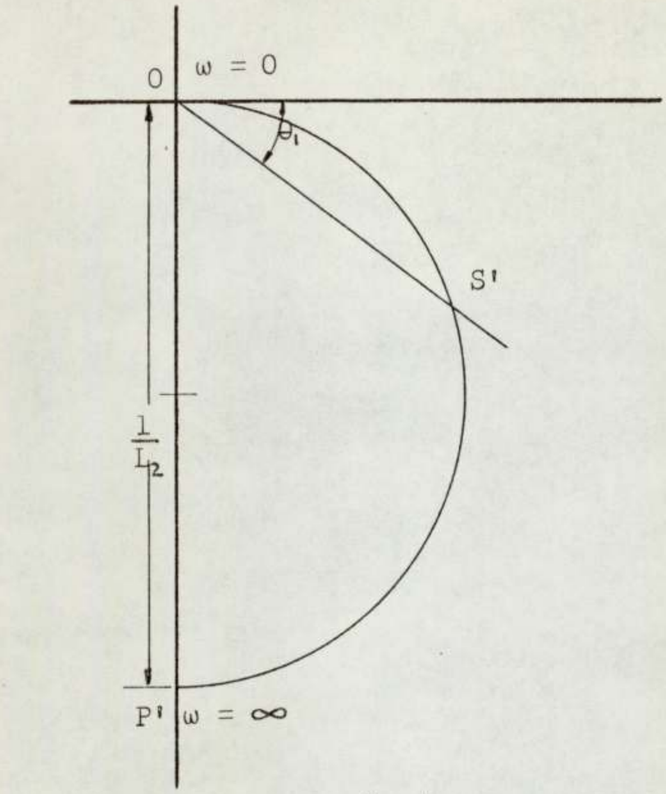

FIG.(5.3). INVERSION OF FIG.(5.2) ABOUT POINT O.

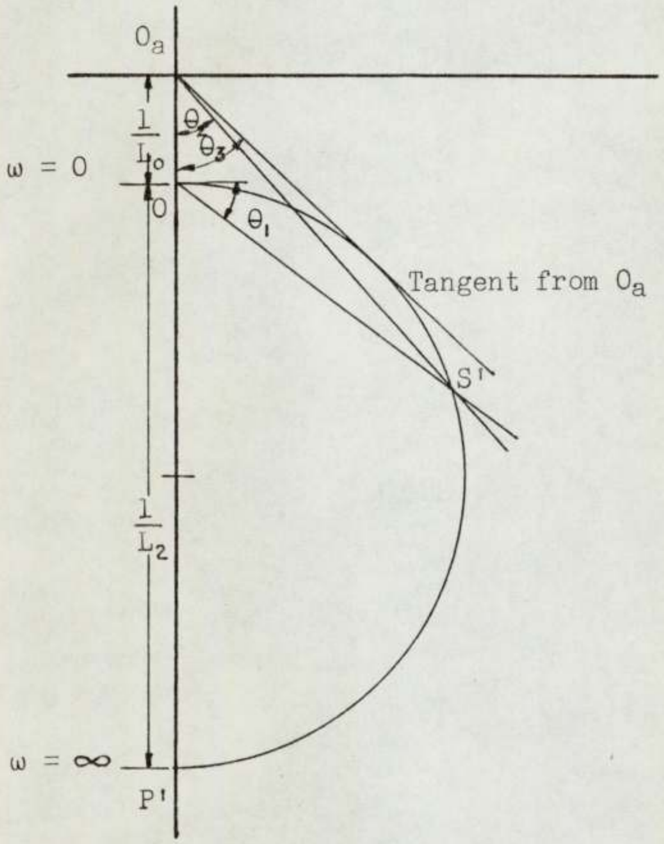

FIG.(5.4). ROTOR BRANCH & MAGNETISING BRANCH, ADMITTANCE per UNIT FREQUENCY LOCUS.

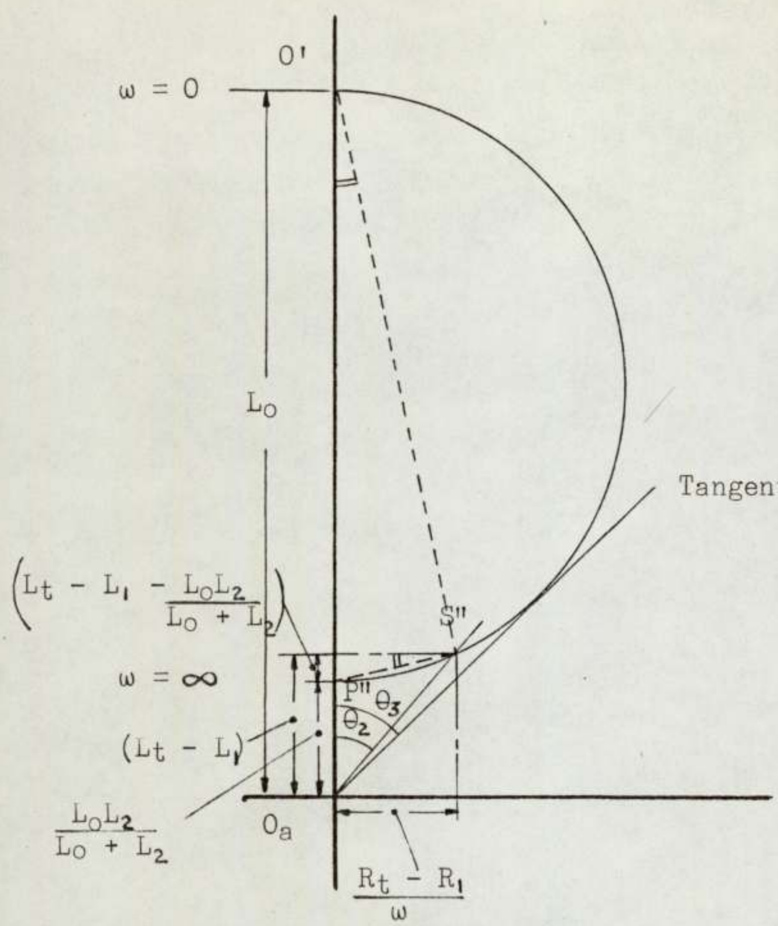

FIG.(5.5). INVERSION OF FIG.(5.4) ABOUT POINT O_a .

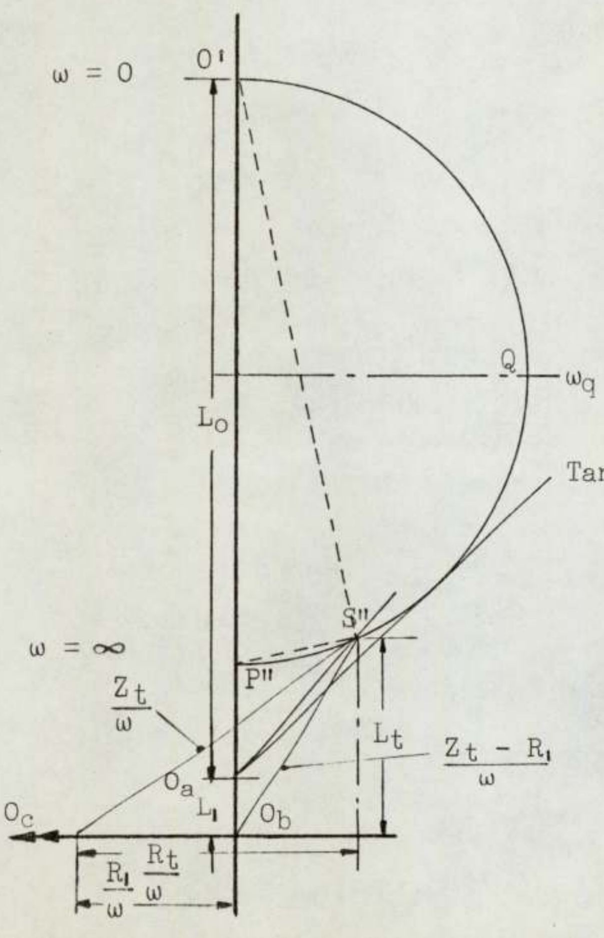

FIG.(5.6).
EQUIVALENT CIRCUIT,
IMPEDANCE per UNIT
FREQUENCY LOCUS.

parameters are all reactances and will be taken as being directly proportional to the supply frequency. Expressing the parameters in ohms per unit frequency of supply, the equivalent circuit per phase of the miniature two phase induction motor is as shown in fig. (5.1).

The total impedance of this circuit is given by $\frac{Z_t}{\omega}$ where Z_t is the true total equivalent impedance at angular frequency of supply ω radians/second. Hence,

$$\frac{Z_t}{\omega} = \frac{R_t}{\omega} + jL_t$$

where R_t is the true total equivalent resistance and L_t is the true total equivalent inductance. To obtain the theoretical locus of the vector $\frac{Z_t}{\omega}$ as ω varies from zero to infinity, consider first the rotor branch consisting of L_2 and $\frac{R_2}{\omega}$ in series for unity slip. The locus of the impedance per unit frequency vector of this section of the circuit is as shown in fig. (5.2) from which is obtained the locus of the admittance per unit frequency vector $\left[\frac{R_2}{\omega} + jL_2\right]^{-1}$ by inversion about the point O. Thus in fig. (5.3), for point S', the inverse of point S in fig. (5.2),

$$\frac{1}{Z_2} = \frac{\frac{R_2}{\omega}}{\left(\frac{R_2}{\omega}\right)^2 + L_2^2} - j\frac{L_2}{\left(\frac{R_2}{\omega}\right)^2 + L_2^2} = OQ' - OP'$$

Adding the vector $\frac{1}{L_0}$ to fig. (5.3) so moving the origin from O to O_a gives fig. (5.4). Inverting this diagram about point O_a results in fig. (5.5) wherein point S" is the inverse of point S' in fig. (5.4). Adding the vectors L_1 and $\frac{R_1}{\omega}$ in turn to fig. (5.5) moves the origin to O_c through O_b and gives finally the locus of $\frac{Z_t}{\omega}$ in which, it should be noted, the new origin O_c will move as the frequency is varied. Since the stator winding resistance R_1 is usually a known quantity and has been stated to be independent of frequency, it will be as informative to consider the locus of $\frac{Z_t - R_1}{\omega}$ as it would be to consider the locus of $\frac{Z_t}{\omega}$. In so doing, the vector representing $\frac{R_1}{\omega}$ is omitted making the fixed point O_b the origin of the diagram. In this form the locus diagram of a given motor can be constructed from the results of a locked rotor, variable frequency test. Furthermore, if this test is carried out under constant current conditions, then the abscissae $\dfrac{R_t - R_1}{\omega}$ of the locus diagram will be directly related to the torque developed by the motor.

Assuming fig. (5.6) with O_b as origin to have been obtained experimentally, the following quantities will be immediately available,

$$(L_o + L_1) = O'O_b \tag{5.1}$$

$$L_o - \frac{L_o L_2}{L_o + L_2} = \frac{L_o^2}{L_o + L_2} = O'P'' \tag{5.2}$$

From the equivalent circuit of fig. (5.1),

$$\frac{R_t - R_1}{\omega} = \text{Real}\left[\left(\frac{1}{jL_o} + \frac{1}{\frac{R_2}{\omega} + jL_2}\right)^{-1} + jL_1\right]$$

$$= \text{Real}\left[\frac{\left(\frac{R_2}{\omega} - j(L_o + L_2)\right)\left(jL_o\frac{R_2}{\omega} - L_oL_2\right)}{\left(\frac{R_2}{\omega}\right)^2 + (L_o + L_2)^2} + jL_1\right]$$

$$= \frac{L_o^2 \frac{R_2}{\omega}}{\left(\frac{R_2}{\omega}\right)^2 + (L_o + L_2)^2} \tag{5.3}$$

Hence, if at point Q in fig. (5.6) the frequency is ω_q then,

$$\frac{1}{2}\left[\frac{L_o^2}{L_o + L_2}\right] = \frac{L_o^2 \frac{R_2}{\omega_q}}{\left(\frac{R_2}{\omega_q}\right)^2 + (L_o + L_2)^2}$$

i.e. $2(L_o + L_2)L_o^2 \frac{R_2}{\omega_q} = L_o^2\left(\frac{R_2}{\omega_q}\right)^2 + L_o^2(L_o + L_2)^2$

i.e. $(L_o + L_2) = \frac{R_2}{\omega_q}$ and is the condition for maximum torque. (5.4)

For the general point S'' it is seen in fig. (5.5) that

$$\frac{P''S''}{O'S''} = \frac{L_t - L_1 - \frac{L_oL_2}{L_o + L_2}}{\frac{R_t - R_1}{\omega}}$$

i.e. $\dfrac{P''S''}{O'S''} = \dfrac{\omega_q}{\omega}$ (appendix A) (5.5)

By use of the relationship (5.5), the consistency of frequency distribution and geometry can be checked for the experimental locus diagram.

For the point S' in fig. (5.4),

$$\frac{OS'}{P'S'} = \tan \theta_1 = \frac{L_2}{R_2/\omega}$$

At the point at which O_aS' is tangent to the circle, S' and its inverse S" will occupy identical positions on the two circular loci of figs. (5.4) & (5.5), respectively. Hence, for this condition, in fig. (5.5)

$$\frac{P''S''}{O'S''} = \frac{L_2}{R_2/\omega_p}$$

where ω_p is the frequency at which OS' and, therefore, O_aS'' are tangents to their respective circles. By equation (5.5) this gives,

$$\frac{L_2}{R_2} = \frac{\omega_q}{\omega_p^2}$$

Consequently, if in fig. (5.6) the value of L_1 is estimated, the point of inversion O_a can be found giving immediately by equation (5.1), $L_o = (O'O_b - L_1)$ and by equation (5.2), $L_2 = L_o\left[\frac{L_o}{O'P''} - 1\right]$.
If a tangent is then drawn to the circle from O_a, the ratio of L_2/R_2 can be determined giving $R_2 = L_2 \frac{\omega_p^2}{\omega_q}$. Since R_1 can be measured directly, the values of all of the parameters of the equivalent circuit are known.

The values so obtained obviously depend upon the value assigned to L_1. To determine the point of inversion O_a other than by estimating L_1 would require a knowledge of the corresponding frequencies of a pair of inverse points S' and S". Then for unity constant of inversion both of these points could be inserted in fig. (5.6). A line drawn through these points and projected onto the axis of inductance would meet this axis at the required point of inversion O_a. As it stands, the only pairs of inverse points that are known are O & O' and P & P' for the two extremities of the semi-circle all of which lie on the inductance axis and cannot, therefore, be used to isolate O_a.

Using the values of the equivalent circuit parameters obtained as above and those of the rotor moment of inertia and coefficient of viscous friction measured by any suitable method, the metric tensor and resistance tensor may now be constructed.

The effect of space harmonics:

The equivalent circuit of fig.(2.11) shows that the presence of space harmonics in the magnetomotive force waveform results in several parallel branches in the rotor circuit, each branch consisting of a leakage inductance in series with an equivalent rotor resistance, both parameters having possibly different values in each branch. Taking referred values, the admittance per unit frequency locus for each of the branches will be a semicircle of diameter $1/L_{2,n}$ as shown in chain-dotted line in fig.(5.6a). The total admittance locus for the rotor circuit will be the sum of all these branch loci.

To be able to determine the shape of this locus, it is necessary to have some idea of the relative values of the harmonic leakage inductances and the harmonic resistances. These will obviously be particular for a given machine so that generalization is difficult. However, to give some indication, consider the highest order harmonic for the test machine, i.e. the fifteenth, for which, by equation (3.34) and omitting the effect of skew,

$$L_{2,15} = L_{2,1}\left[\frac{15 \times 3.85}{1 \times 0.22} \times \frac{\sin 108}{\sin 7.2}\right]^{2}\frac{1}{15}$$

$$= 3.2 \times 10^{5} L_{2,1}$$

i.e. $L_{2,15}$ is very much greater than $L_{2,1}$,

and, by equation (3.31)

$$R_{2,15} = R_{2,1}\left[\frac{15 \times 3.85}{1 \times 0.22}\right]^{2} \times 15 \times \left[\frac{1.383 + \frac{0.159 \times 11.6 K_{ring,n}}{225 \times 2.375}}{1.383 + 0.73}\right]$$

Unfortunately, the curves of fig(3.6') do not cover numbers of poles greater than 12, so that in this case $K_{ring,n}$ cannot be estimated. Examination of these curves does, however, show that for a given ratio ID_r/D_b the value of the ratio K_{ring}/p_n reduces as p_n increases so that this term will, in the case of the harmonic, be less than for the fundamental. Assume, therefore, that it may be neglected for the fifteenth order harmonic, then

$$R_{2,15} = 0.502 \times 10^{5} R_{2,1} ,$$

i.e. $R_{2,15}$ is very much greater than $R_{2,1}$. The effect of skew would be to cause further increase in both of these values.

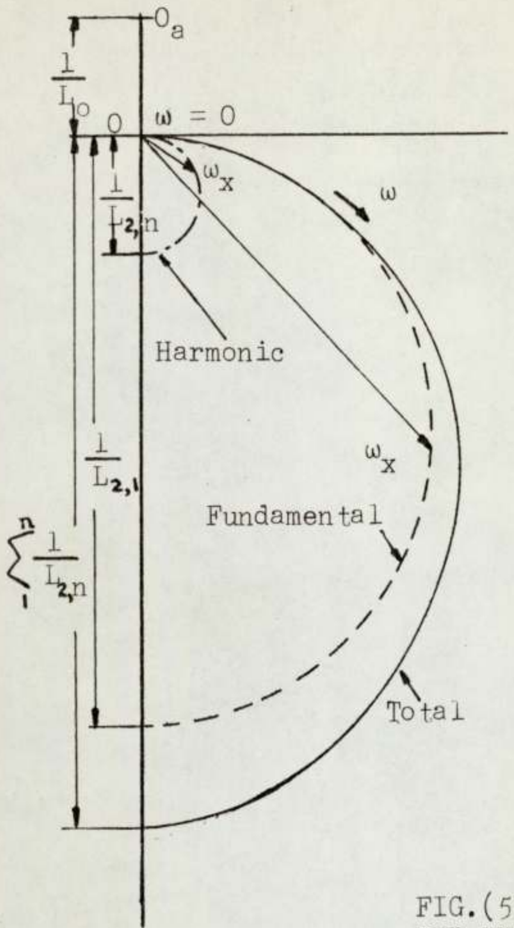

FIG.(5.6a). ROTOR TOTAL ADMITTANCE PER UNIT FREQUENCY LOCUS.

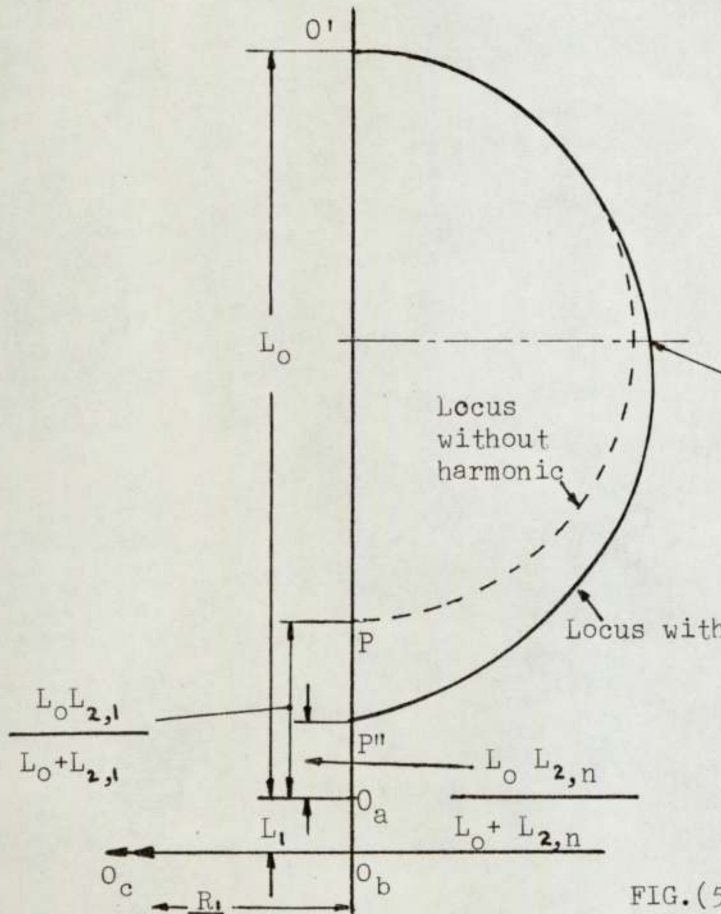

FIG.(5.6b). IMPEDANCE PER UNIT FREQUENCY LOCUS WITH SPACE HARMONIC.

It is concluded, that, in general, the harmonic parameters will be greater than those for the fundamental. Thus, in fig.(5.6a), the locus of the harmonic rotor branch is shown to be much smaller, due to the relatively large value of $L_{2,n}$, than that of the fundamental given in dotted line. The effect of the large value for $R_{2,n}$ is to cause angular displacement between the two admittance vectors for a given frequency, that for the harmonic lagging that for the fundamental in the direction of increasing frequency. The total admittance locus is shown in solid line. It is seen to be a distorted semicircle of base $\sum_{1}^{n} 1/L_{2,n}$. The addition of the magnetizing branch admittance shifts the origin from 0 to O_a as for fig.(5.4). Inversion about O_a and the addition of L_1 and R_1/ω results in the locus diagram of fig.(5.6b) corresponding to fig.(5.6).

From this it is clear that the determination of L_1 and L_o will be the same as for the machine with no space harmonics. However, the distance O_aP'' is now a function of $\sum_{1}^{n} L_{2,n}$ and L_o and, therefore, determines $\sum_{1}^{n} L_{2,n}$ and not simply L_2 as before. Reference to equation (3.34) reveals that $L_{2,n} = H_{1,n}L_{2,1}$ where $H_{1,n}$ was defined as the harmonic leakage inductance ratio for the rotor. This ratio can be dependably calculated from the design details of the machine and the Fourier analysis of its stator magnetomotive force waveform. Using this ratio

$$\sum_{1}^{n} L_{2,n} = L_{2,1}\sum_{1}^{n} H_{1,n} .$$

The rotor leakage inductance for the fundamental is then given by

$$L_{2,1} = \frac{L_o\left[\dfrac{L_o}{O'P''} - 1\right]}{\sum_{1}^{n} H_{1,n}} .$$

With $L_{2,1}$ determined, the various values of $L_{2,n}$ can be readily obtained by calculating the value of $H_{1,n}$ for each harmonic component.

To obtain the corresponding values of $R_{2,n}$, using the values as determined above, calculate the value of $\dfrac{L_o L_{2,1}}{L_o + L_{2,1}} + L_1$ and mark in the point P''' distant $\dfrac{L_o L_{2,1}}{L_o + L_{2,1}} + L_1$ from O_b. Draw in the semicircle having O'P''' as diameter and obtain the frequency, on the locus diagram with harmonics, corresponding to the midpoint of the semicircle. If it is assumed that this is the value ω_q for maximum torque for the machine without harmonics then equation (5.4) can be applied to determine the value of $R_{2,1}$. By referring to equation (3.31), it is seen that $R_{2,n} = R_{2,1} H_{r,n}$ where $H_{r,n}$ was defined as the harmonic resistance ratio for the rotor. As for the leakage inductances, this ratio can be calculated from the Fourier analysis and design information. $R_{2,n}$ may, therefore, be evaluated for each harmonic component.

With the values of $L_{2,n}$ and $R_{2,n}$ determined, the metric and resistance tensors can be constructed to include the harmonic rotor branches as established in chapter II.

If the rotor bars are skewed, the skew modified harmonic resistance and inductance ratios, defined by equations (3.35) and (3.36), must be used in the foregoing evaluations.

16) Effect of Rotor Position.

Before proceeding with the variable frequency test for the determination of the impedance per unit frequency locus,a preliminary experiment was carried out to determine the effect of rotor position on the magnitude of the developed stalled torque. To do this the rotor was stalled,via the dynamometer driving head,by means of the locking pinion and worm as described in section 5. The motor was then supplied with 115 volts/phase at 400 cycles/sec. and left to stabilise thermally. When a steady temperature,as indicated by the bridge monitor, was attained measurements were made of current and power for both phases, the phase angle between the phase currents and the developed torque for four different positions of the rotor relative to the stator,each position being displaced by 90° mechanical from the next. At the same time,the control phase current and the output voltage of the accelerometers were simultaneously displayed using a cathode ray oscilloscope and photographed,by means of the one shot trigger, for each rotor position. The movement of the rotor from one position to the other was made and measured by rotation of the locking worm.

Throughout this test the dynamometer was completely shielded to prevent intermittent cooling and disturbance by draughts. To ensure that no variation in temperature occurred the temperature of the motor was checked for all the measurements.

Following this the rotor position was varied over a range of 18° in intervals of 0.6°,this being the increment between adjacent calibrations on the locking worm control knob for the 60 toothed locking pinion. At each interval measurements were made as before with the exception of the output voltage of the accelerometers which was not recorded.

The results of this investigation are given in table (5.1) and figs. (5.7),(5.8) and (5.9).

Rotor angle °mech.	Ref. current mA.	Cont. current mA.	Ref. power Watts.	Cont. power Watts.	Phase angle °elec.	Scale cms.	Torque Nm. $\times 10^{-3}$	Trace number
0.0	85.5	87.0	9.08	9.38	93	+9.55	6.62	1
90.0	86.0	87.5	9.06	9.30	"	9.68	6.71	2
180.0	86.0	88.0	9.00	9.30	"	8.70	6.02	3
270.0	85.5	87.0	9.04	9.28	"	8.65	6.00	4
0.0	85.5	87.0	9.08	9.38	"	9.55	6.62	
0.6	85.5	87.0	9.00	9.34	"	9.65	6.69	
1.2	84.5	87.0	9.02	9.34	"	9.48	6.57	
1.8	84.5	86.5	9.00	9.32	"	9.70	6.72	
2.4	"	"	"	"	"	9.45	6.55	
3.0	"	"	"	"	"	9.60	6.67	
3.6	"	"	"	"	"	9.70	6.72	
4.2	"	"	"	"	"	9.71	6.73	
4.8	"	"	"	"	"	9.59	6.66	
5.4	"	"	"	"	"	9.71	6.73	
6.0	"	"	"	"	"	9.59	6.66	
6.6	"	"	"	"	"	9.58	6.65	
7.2	"	"	"	"	"	9.68	6.71	
7.8	"	"	"	"	"	9.90	6.87	
8.4	"	"	"	"	"	9.80	6.80	
9.0	"	"	"	"	"	9.80	6.80	
9.6	"	"	"	"	"	9.90	6.87	
10.2	"	"	"	"	"	9.70	6.72	
10.8	"	"	"	"	"	9.56	6.63	
11.4	"	"	"	"	"	9.57	6.64	
12.0	"	"	"	"	"	9.60	6.66	
12.6	"	"	"	"	"	9.60	6.66	
13.2	"	"	"	"	"	9.70	6.72	
13.8	"	"	"	"	"	10.00	6.94	CONT'D.

Rotor angle °mech.	Ref. current mA.	Cont. current mA.	Ref. power Watts.	Cont. power Watts.	Phase angle °elec.	Scale cms.	Torque Nm. $x10^{-3}$
14.4	84.5	86.5	9.00	9.32	93	+9.92	6.89
15.0	"	"	"	"	"	10.00	6.94
15.6	"	"	"	"	"	10.00	6.94
16.2	"	"	"	"	"	9.90	6.87
16.8	"	"	"	"	"	9.70	6.72
17.4	"	"	"	"	"	9.78	6.79
18.0	"	"	"	"	"	9.56	6.61

TABLE (5.1). EFFECT OF ROTOR POSITION ON DEVELOPED TORQUE.

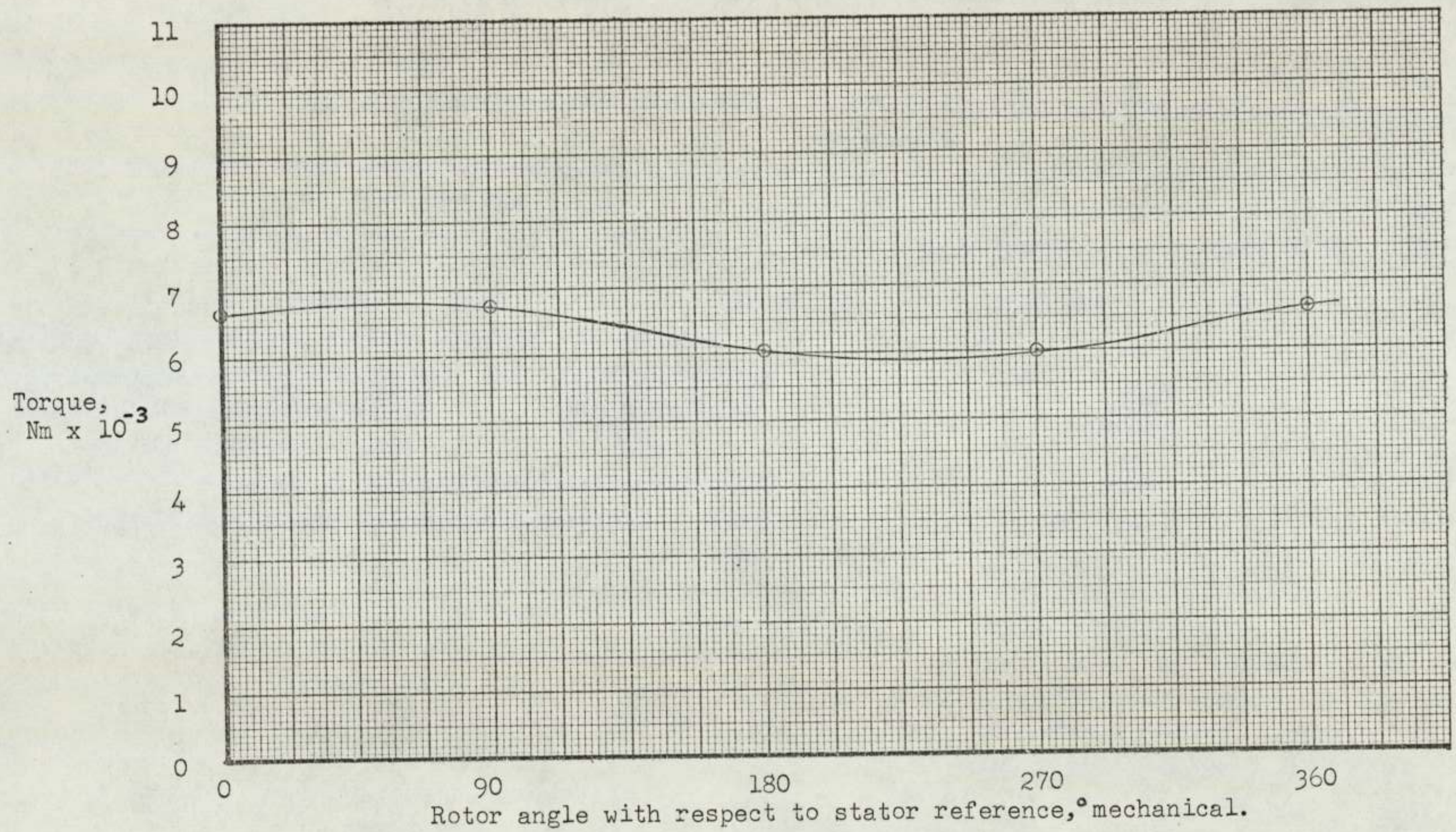

FIG. (5.7). VARIATION OF STALLED TORQUE WITH ROTOR POSITION.

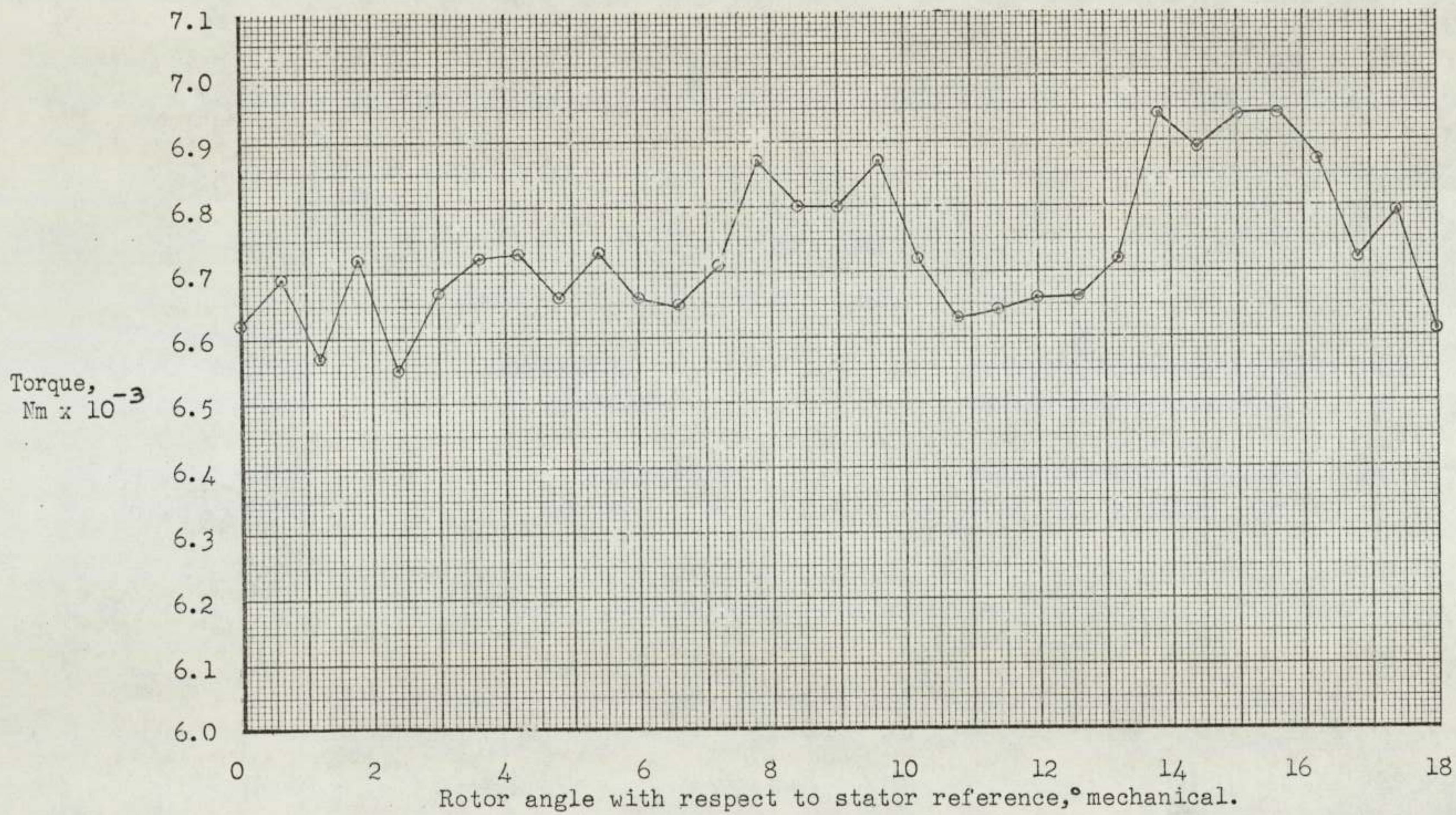

FIG. (5.8). VARIATION OF STALLED TORQUE WITH ROTOR POSITION.

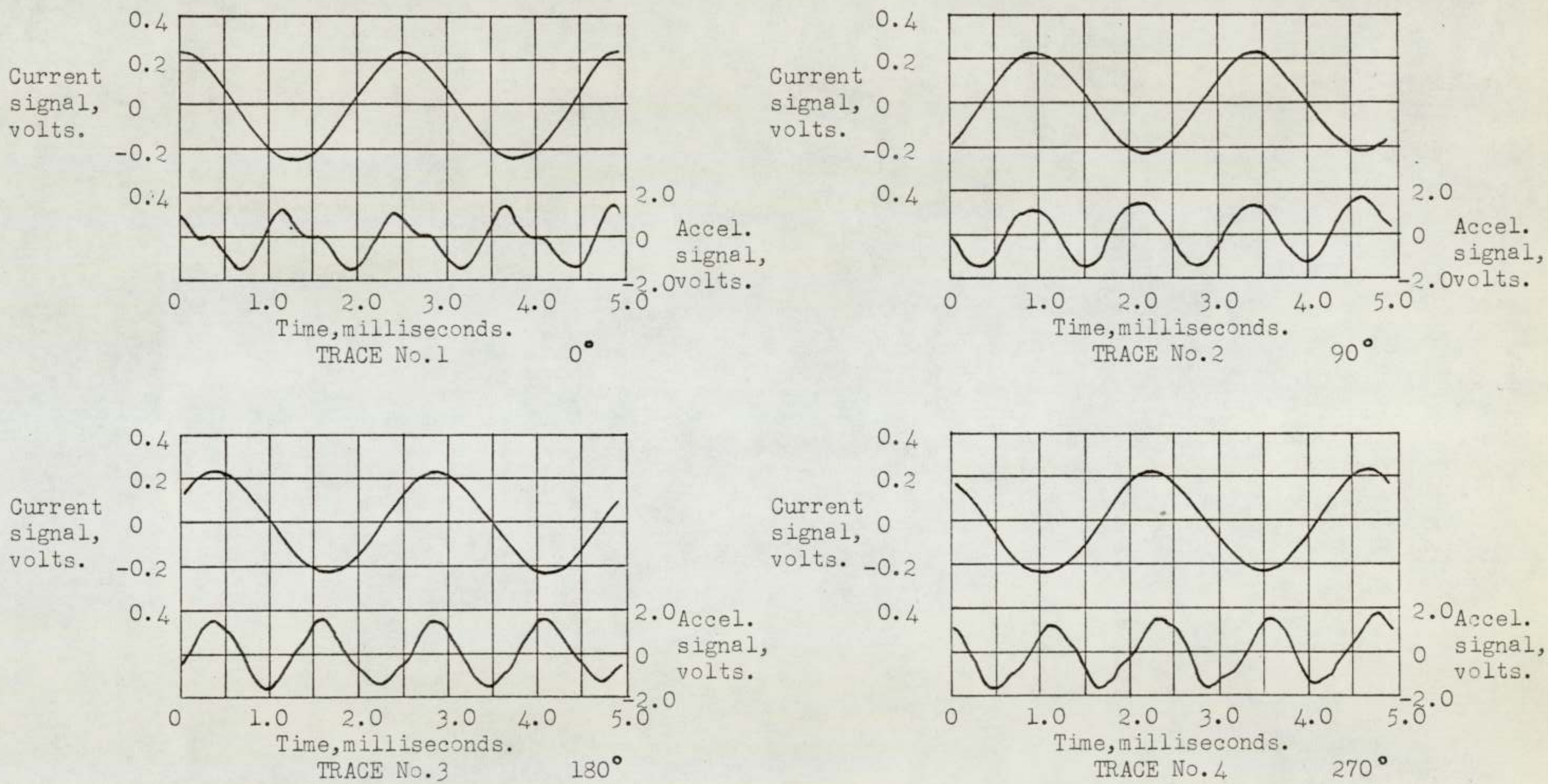

FIG. (5.9). VARIATION OF INSTANTANEOUS STALLED TORQUE WITH ROTOR POSITION.

In fig. (5.7) it is seen that the stalled torque exhibits a variation of $\pm 7\%$ about a mean value of 6.35×10^{-3} Nm. once per revolution. This variation could be due to the combined effect of magnetic dissymetries of the stator and the rotor and strongly suggests the presence of such dissymetries.

The cyclic variation of approximately $\pm 2\%$ shown in fig. (5.8) is a cogging effect which may have its origin not in the slot combination, since the rotor slots were skewed, but in differences in the electrical conductivities of the rotor bars caused by inhomogeneity of the cast aluminium of which they were made. It has been found experimentally that such differences in bar conductivity result in pronounced cogging torques in miniature induction motors.

The twice line frequency variation of the instantaneous torques of fig. (5.9) does not appear to alter greatly in magnitude throughout a complete revolution of the rotor and need not be further considered at this stage.

After examining the results of this experiment, it was decided to carry out the variable frequency test with the rotor in the position of mean torque as indicated by fig. (5.7) and to maintain this position relative to the stator throughout the test by adjusting the rotor for each stator deflection.

17) Variable Frequency Test.

With the motor assembled in the dynamometer as for the experiment of section (16), the rotor was set in the 320° position relative to the stator, this being one of the mean torque positions. The supply frequency was reduced to 5 cycles/sec. and the phase currents were both set to 90 milliamps. Keeping these currents constant, the frequency was increased in steps until a maximum was observed in the developed stalled torque. In this region the frequency increment was reduced to 2 cycles/sec. over a sufficiently wide range to give a clear indication of the frequency at which the maximum torque was occurring. The frequency was then further increased in larger increments until the torque reduced to approximately the value measured at the lower frequencies. For all frequencies the initial position of the rotor relative to the stator was maintained and measurements of the voltage and power for both phases, the phase angle between the phase currents and the developed torque were made using the base temperature method described in section (12). In addition, the control phase current and the output voltage of the accelerometers were recorded, as in section (16), over a limited range of frequency to furnish information on the developed torque as a function of time, required for the subsequent correlation of measured and predicted motor performance (chapter VIII).

The results of this experiment are given in table (5.2) and figs. (5.10), (5.11), (5.12) and (5.13). The oscillograms of control phase current and accelerometer voltage are given in figs. (5.14a)-(5.14d) but comment on these is deferred until chapter VIII.

Supply freq. Hz.	Ref. voltage Volts.	Cont. voltage Volts.	Ref. power Watts.	Cont. power Watts.	Phase angle °elec.	Bridge reading Ohms.	Winding temp. °C.	Scale cms.	Torque Nm. $\times 10^{-3}$	Trace number.	Average power per ph.	Average voltage per ph.	$W_{av}-I_1^2R_1$ Watts.	$T\omega/2$ Watts.
	Motor unenergised.					1730	21.0							
						33.1								
5	43.8 x 0.5	43.7 x 0.5	1.0 x 2.0	1.0 x 2.0	92	2343	112.5	1.65	1.12		2.0	21.87	0.114	0.0176
10	46.7	46.4	1.03	1.03	"	"	"	3.40	2.34		2.06	23.27	0.174	0.073
15	51.9	51.7	1.06	1.06	"	"	"	5.10	3.52		2.12	25.90	0.234	0.166
20	29.0 x 1.0	28.9 x 1.0	1.13	1.14	"	"	"	6.80	4.71	1	2.27	28.95	0.384	0.296
25	32.2	32.2	1.18	1.20	"	"	"	8.50	5.90		2.38	32.20	0.494	0.464
30	35.9	35.7	1.29	1.30	"	"	"	10.00	6.94		2.59	35.80	0.704	0.650
35	39.1	38.8	1.36	1.37	"	"	"	11.45	7.96		2.73	38.95	0.844	0.876
40	43.3	43.0	1.50	1.51	"	"	"	12.40	8.61	2	3.01	43.15	1.12	1.08
45	47.2	46.8	1.63	1.63	"	"	"	13.60	9.46		3.26	47.00	1.37	1.34
50	50.8	50.1	1.74	1.74	"	"	"	14.50	10.08		3.48	50.45	1.59	1.58
60	58.0	57.2	2.00	1.99	"	"	"	16.10	11.20	3	3.99	57.60	2.10	2.11
80	34.9 x 2.0	34.3 x 2.0	2.51	2.49	"	"	"	18.28	12.71	4	5.00	69.20	3.11	3.20
100	39.3	38.4	2.93	2.91	"	"	"	19.23	13.37	5	5.84	77.70	3.95	4.20
102	40.4	39.8	3.02	3.00	"	"	"	19.28	13.41		6.02	80.20		

CONT'D.

Supply freq. Hz.	Ref. voltage Volts.	Cont. voltage Volts.	Ref. power Watts.	Cont. power Watts.	Phase angle °elec.	Bridge reading Ohms.	Winding temp. °C.	Scale cms.	Torque Nm. $\times 10^{-3}$	Trace number.	Average power per ph.	Average voltage per ph.	$W_{av}-I_1^2R_1$ Watts.	$T\omega/2$ Watts.
104	40.8	40.2	3.06	3.04	"	"	"	19.35	13.47		6.10	81.00		
106	41.1	40.3	3.11	3.06	"	"	"	19.41	13.51		6.17	81.40		
108	41.7	41.1	3.15	3.13	"	"	"	19.45	13.54		6.28	82.80		
110	42.2	41.7	3.20	3.18	"	"	"	19.50	13.58		6.38	83.90		
112	42.6	42.0	3.26	3.24	"	"	"	19.55	13.62		6.50	84.60		
114	42.8	41.9	3.28	3.27	"	"	"	19.53	13.60		6.55	84.70		
116	43.5	42.8	3.35	3.30	"	"	"	19.47	13.55		6.65	86.30		
118	43.9	43.1	3.38	3.34	"	"	"	19.35	13.47		6.72	87.00		
120	44.2	43.6	3.39	3.35	"	"	"	19.30	13.43	6	6.74	87.80	4.85	5.07
140	47.2	46.7	3.70	3.68	"	"	"	18.84	13.11	7	7.38	93.90	5.49	5.77
160	49.7	48.9	3.98	3.93	"	"	"	18.20	12.67	8	7.91	98.60	6.02	6.37
180	51.4	50.8	4.17	4.14	"	"	"	17.27	12.01	9	8.31	102.20	6.42	6.80
200	53.0	52.1	4.33	4.26	"	"	"	16.48	11.46	10	8.59	105.10	6.70	7.21
250	55.6	54.9	4.58	4.54	"	"	"	14.40	10.01		9.12	110.5	7.23	7.87
300	57.7	56.9	4.75	4.71	"	"	"	12.53	8.70	11	9.46	114.6	7.57	8.21

CONT'D.

Supply freq. Hz.	Ref. voltage Volts.	Cont. voltage Volts.	Ref. power Watts.	Cont. power Watts.	Phase angle °elec.	Bridge reading Ohms.	Winding temp. °C.	Scale cms.	Torque Nm. $\times 10^{-3}$	Trace number.	Average power per ph.	Average voltage per ph.	$W_{av}-I_1^2R_1$ Watts.	$T\omega/2$ Watts.
400	24.2 x 5.0	24.0 x 5.0	5.02	5.00	"	"	"	10.20	7.08	12	10.02	120.50	8.13	8.90
500	24.9	24.4	5.15	5.12	"	"	"	8.20	5.69	13	10.27	123.25	8.38	8.95
600	26.1	25.6	5.21	5.20	"	"	"	7.07	4.90	14	10.41	129.25	8.52	9.24
700	27.2	26.5	5.30	5.31	"	"	"	6.20	4.29		10.61	134.25	8.72	9.45
800	27.7	26.8	5.33	5.32	"	"	"	5.50	3.80		10.65	136.25	8.76	9.56
900	28.9	27.8	5.35	5.34	"	"	"	5.00	3.46		10.69	141.75	8.80	9.79
1000	30.0	28.8	5.42	5.40	"	"	"	4.54	3.13		10.82	147.00	8.93	9.84

From bridge readings, winding resistance cold $= \dfrac{1730 - 33.1}{10} + 1.9 = 171.6$ ohms.

winding resistance hot, during test $= \dfrac{2343 - 33.1}{10} + 1.9 = 232.9$ ohms.

TABLE (5.2). EFFECT OF VARYING SUPPLY FREQUENCY ON LOCKED ROTOR PERFORMANCE.

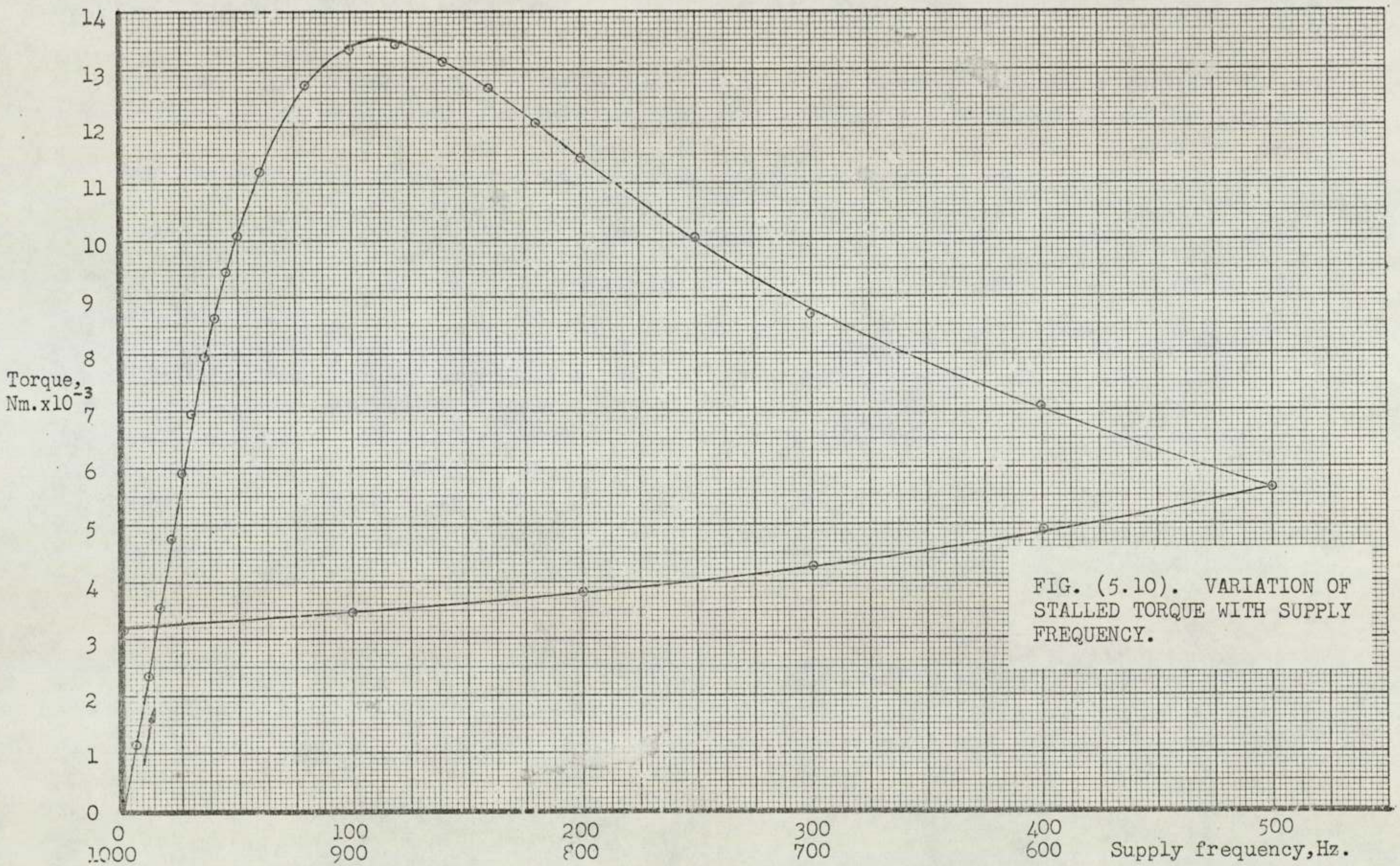

FIG. (5.10). VARIATION OF STALLED TORQUE WITH SUPPLY FREQUENCY.

FIG. (5.11). VARIATION OF STALLED TORQUE WITH SUPPLY FREQUENCY, REGION OF MAXIMUM TORQUE.

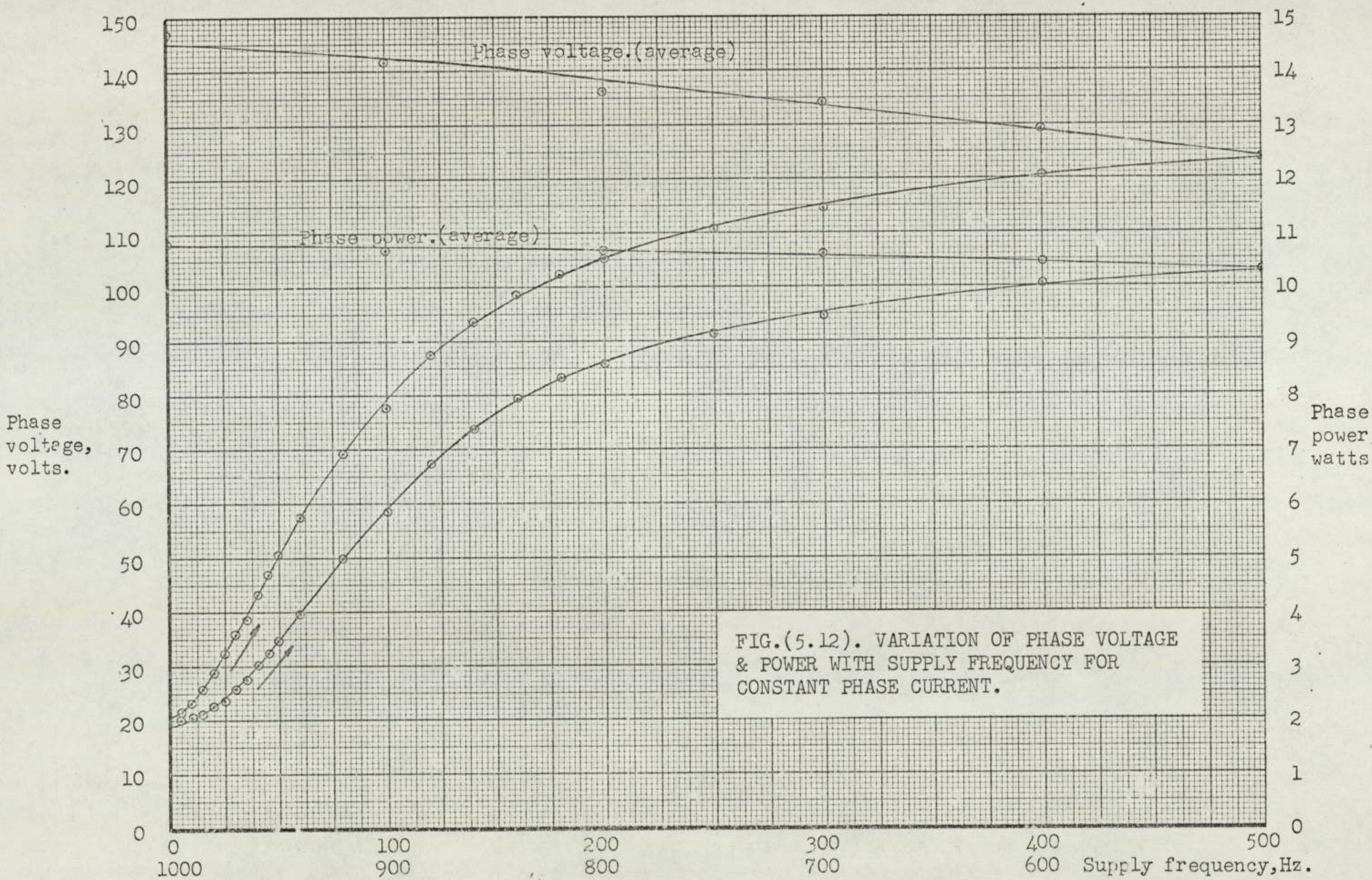

FIG.(5.12). VARIATION OF PHASE VOLTAGE & POWER WITH SUPPLY FREQUENCY FOR CONSTANT PHASE CURRENT.

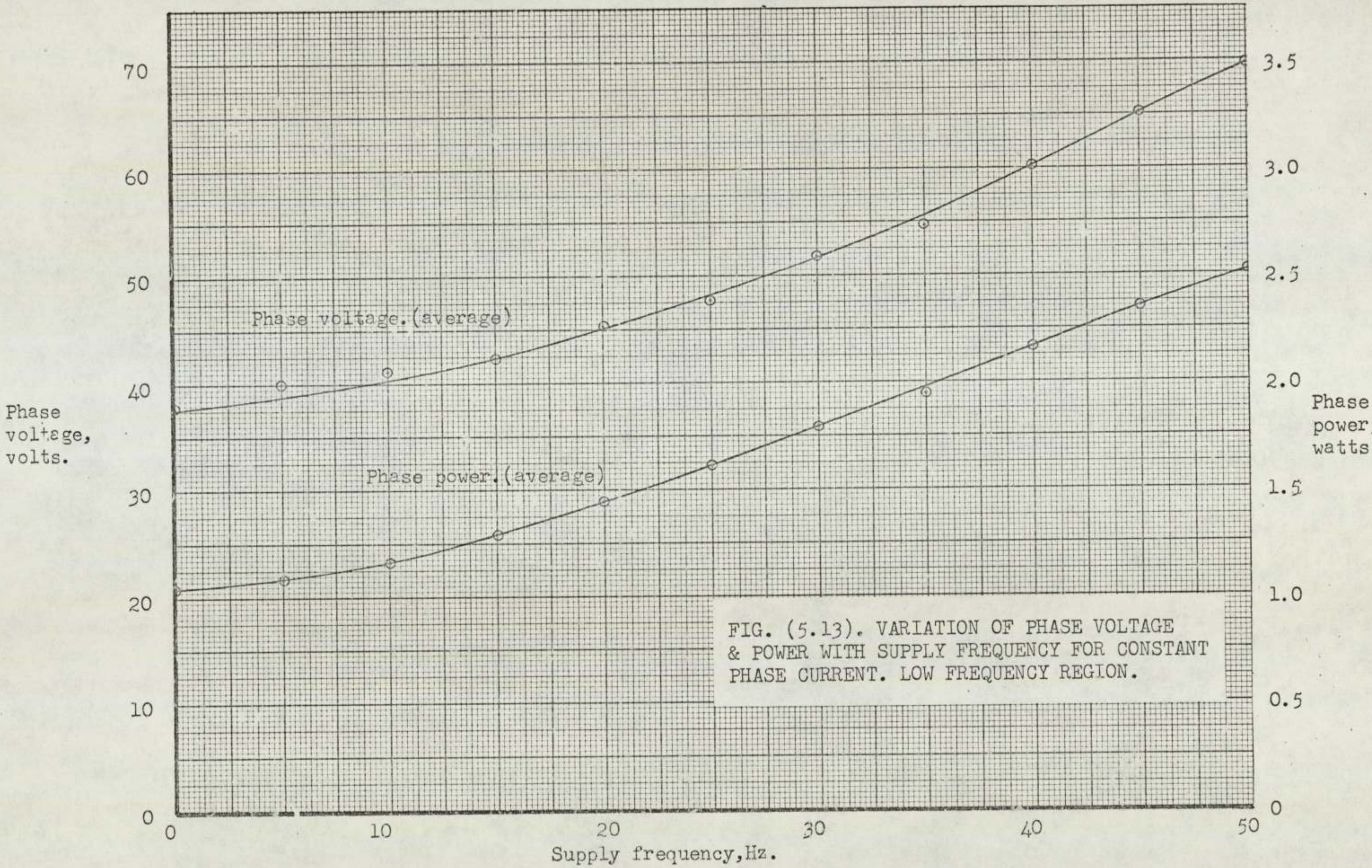

FIG. (5.13). VARIATION OF PHASE VOLTAGE & POWER WITH SUPPLY FREQUENCY FOR CONSTANT PHASE CURRENT. LOW FREQUENCY REGION.

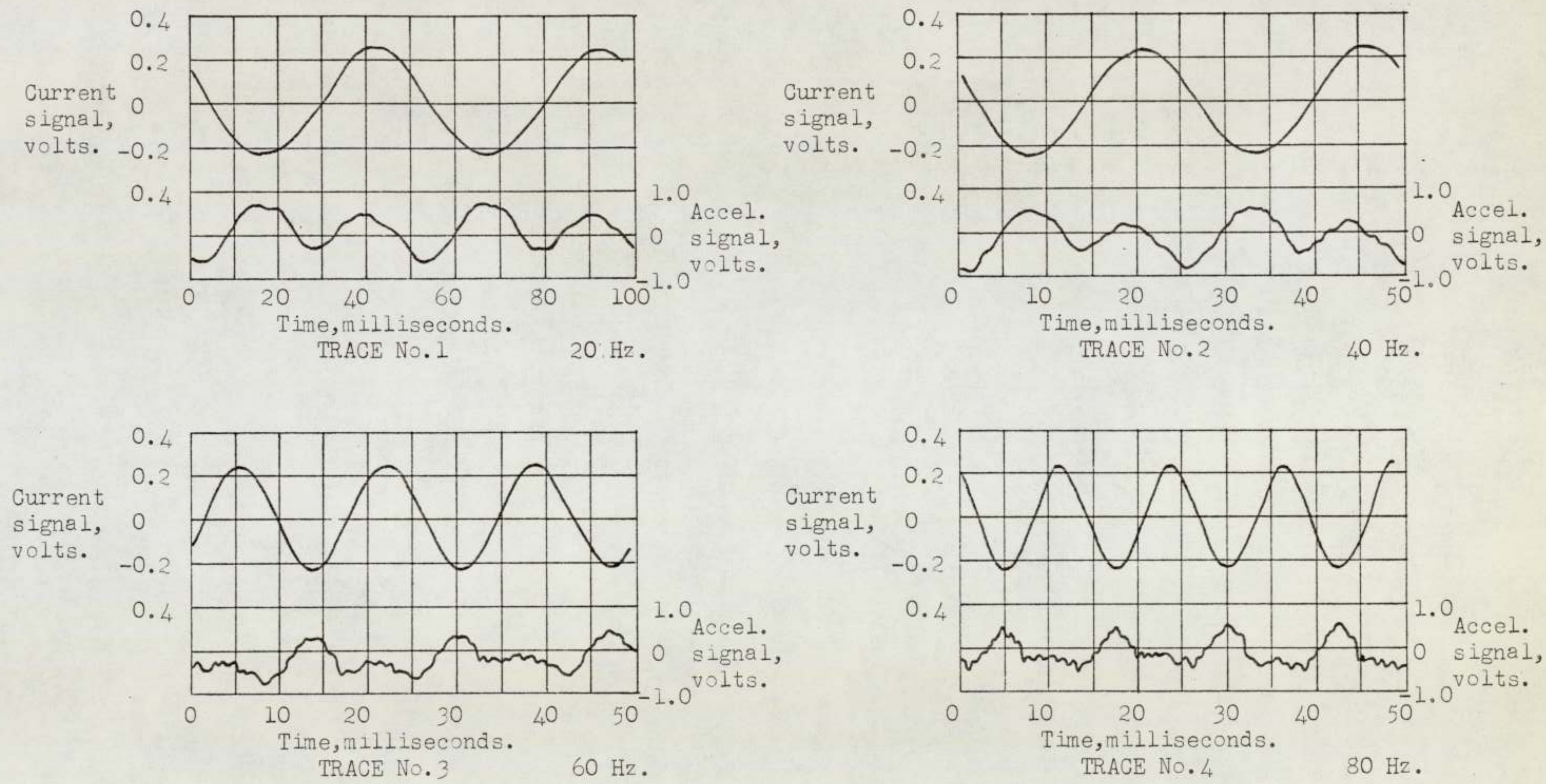

FIG. (5.14a). VARIATION OF INSTANTANEOUS STALLED TORQUE WITH SUPPLY FREQUENCY.

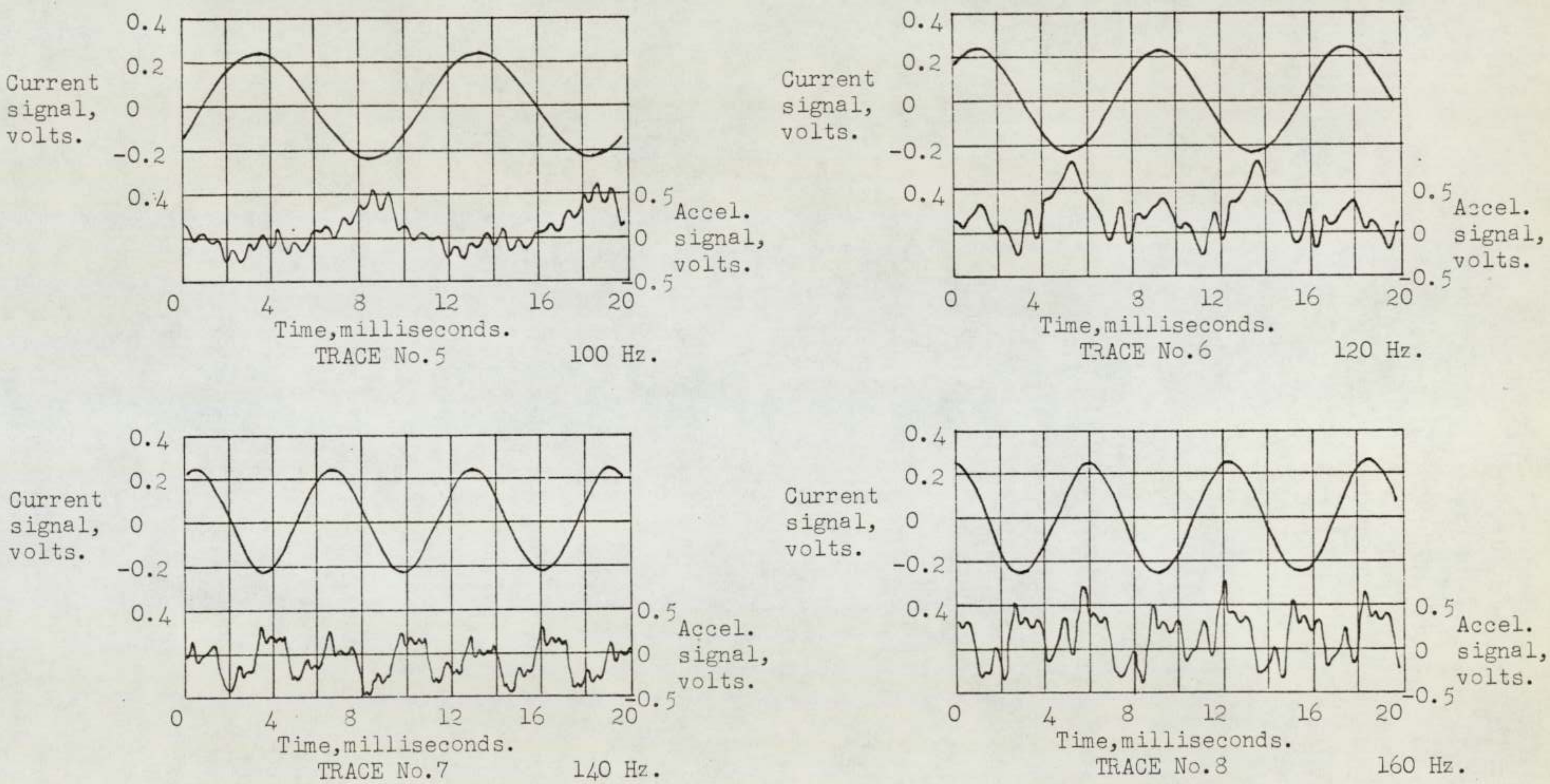

FIG. (5.14b). VARIATION OF INSTANTANEOUS STALLED TORQUE WITH SUPPLY FREQUENCY.

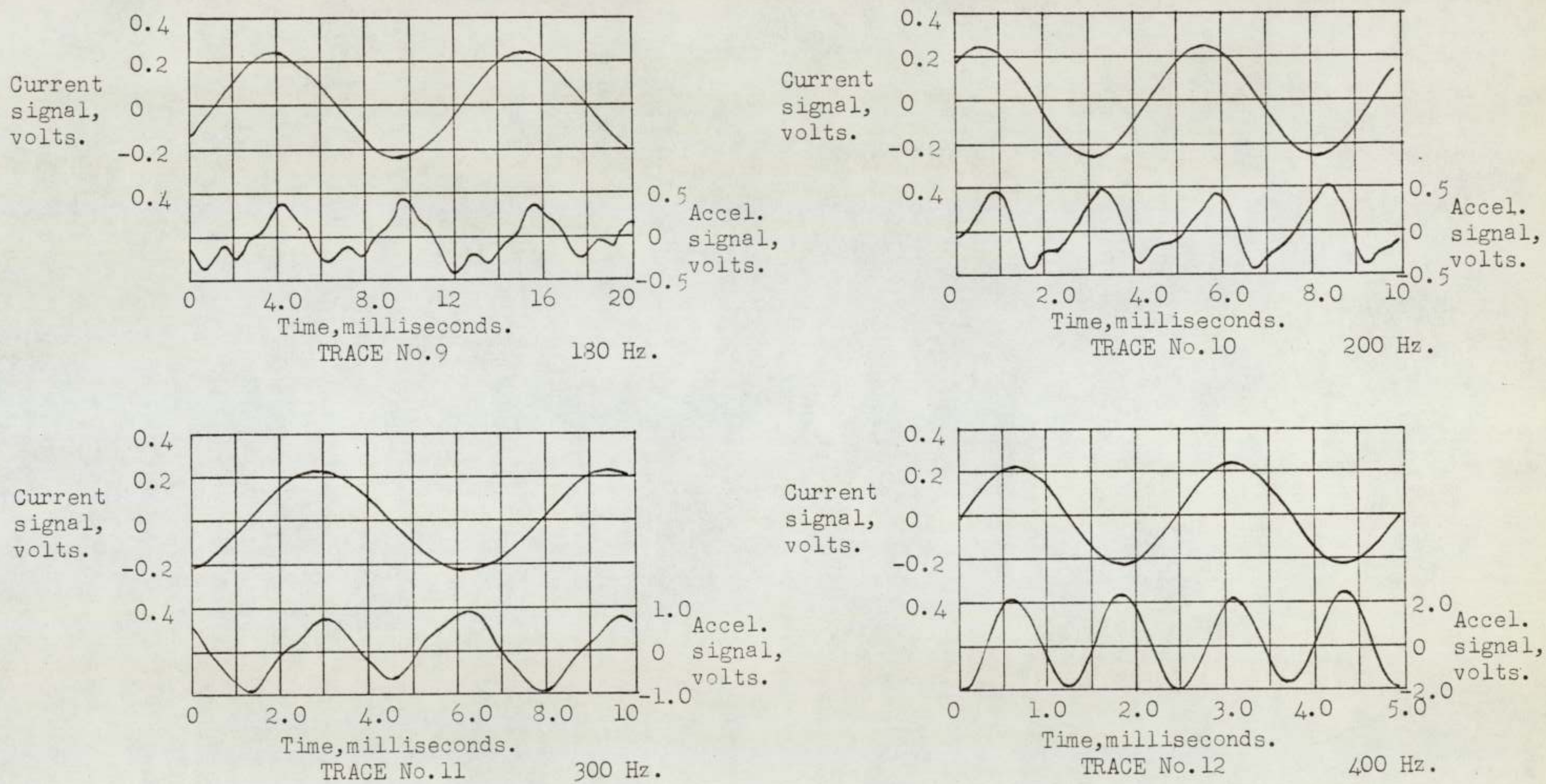

FIG. (5.14c). VARIATION OF INSTANTANEOUS STALLED TORQUE WITH SUPPLY FREQUENCY.

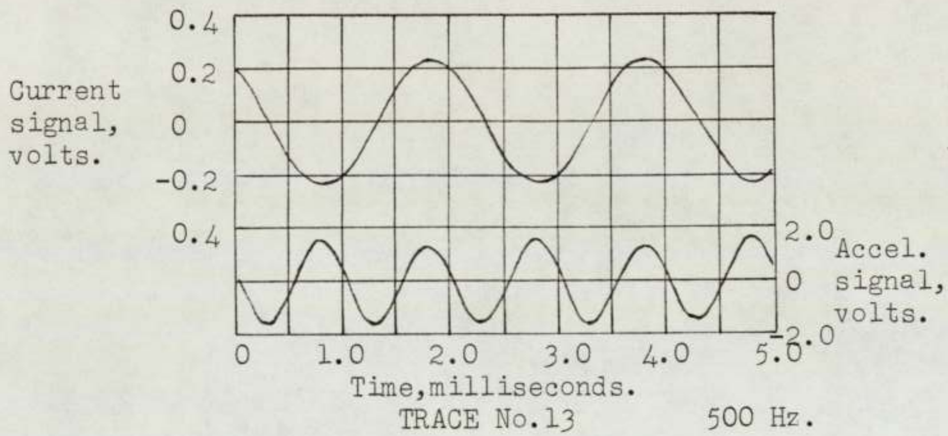

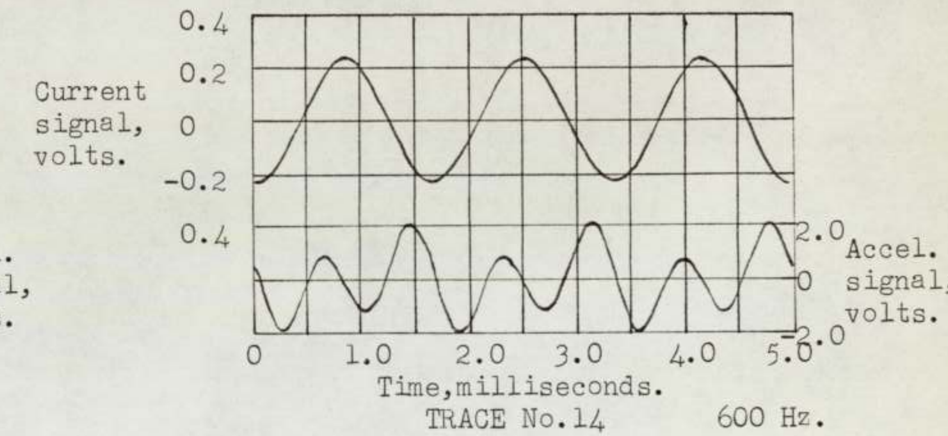

FIG. (5.14d). VARIATION OF INSTANTANEOUS STALLED TORQUE WITH SUPPLY FREQUENCY.

18) Construction of Locus Diagram.

The components of the impedance vector $\frac{Z_t}{\omega}$ can be written as

$$\frac{R_1}{\omega} + \frac{(R_t - R_1)}{\omega} \qquad \text{and} \qquad j\frac{X_t}{\omega}.$$

The quantity $(R_t - R_1)$ is the equivalent resistance of the magnetising branch and the rotor branch in parallel. Since iron loss is negligible, the power dissipated in this resistor will represent the developed torque at standstill providing stray losses are also negligible.

i.e.
$$I_1^2(R_t - R_1) = \frac{T\omega}{pm}$$

where p is the number of pole pairs and I_1 is the stator phase current, assuming balanced operation.

Hence,
$$\frac{(R_t - R_1)}{\omega} = \frac{T}{pI_1^2 m}$$

and can be obtained directly from the test results.

Alternatively, the power dissipated in the resistance $(R_t - R_1)$ can be taken as (input power)-(stator loss).

i.e. for negligible iron loss,

$$I_1^2(R_t - R_1) = W - I_1^2 R_1$$

where W is the input power per phase, again assuming balanced operation.

This gives,
$$\frac{(R_t - R_1)}{\omega} = \frac{1}{\omega}\left[\frac{W}{I_1^2} - R_1\right],$$ also directly obtainable.

Physically, these two methods of determining the value of $\frac{(R_t - R_1)}{\omega}$ amount to using either the measured torque or the measured power as a basis. To obtain an indication of the degree of compatibility between the two methods, values of $W - I_1^2 R_1$ and $\frac{T\omega}{pm}$ have been calculated in table (5.2) and plotted to a base of frequency in fig. (5.15). In these calculations the value of W was taken as the average for the two phases and the value of R_1 was obtained from the readings of the bridge monitor. Reference to this graph shows that the power equivalent of the measured torque is, with the exception of the lower frequencies, in general 8%-10%

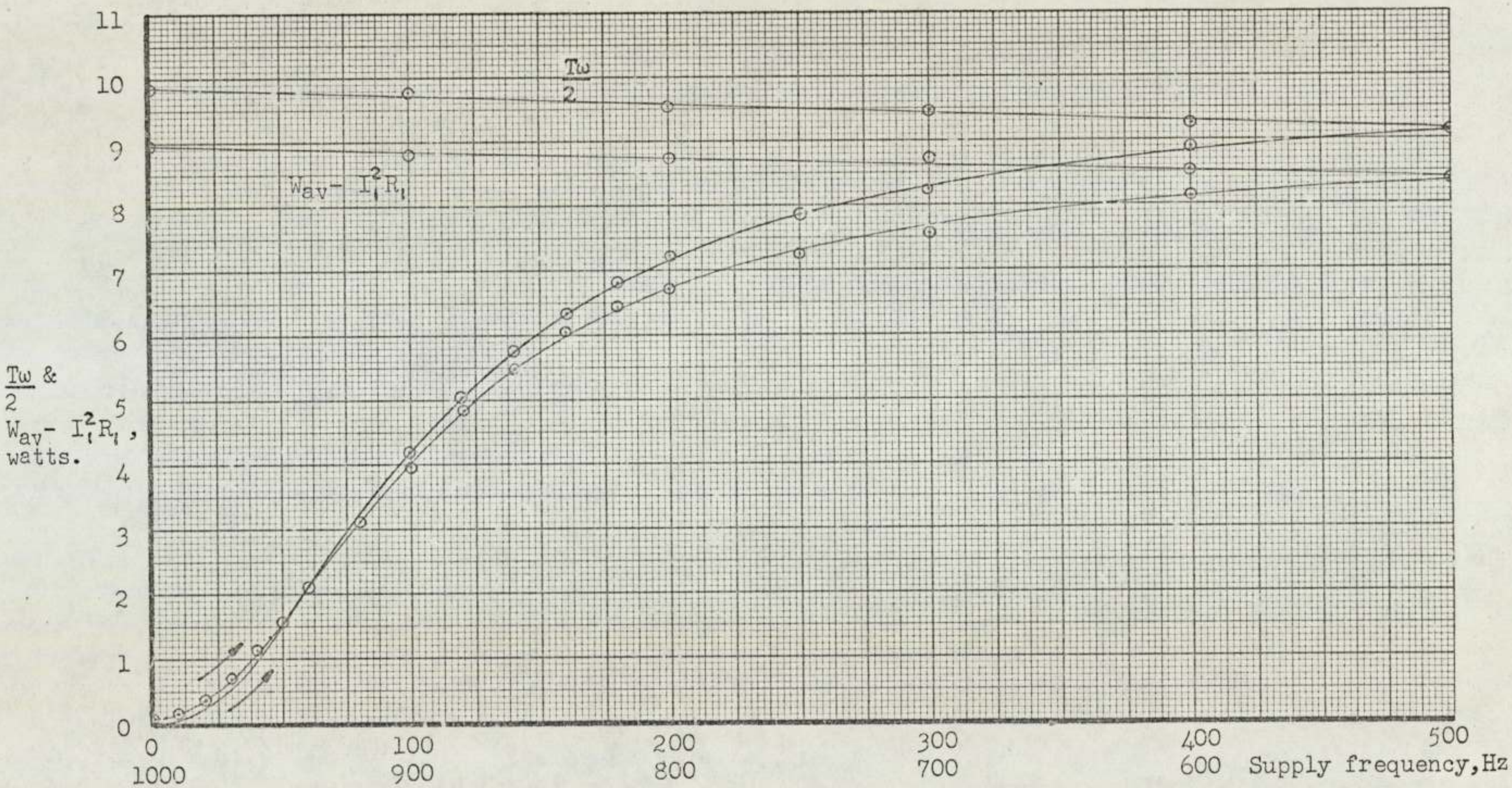

FIG. (5.15). VARIATION OF $T\omega/2$ & $W_{av} - I_1^2R_1$ WITH SUPPLY FREQUENCY UNDER STALLED CONDITIONS.

higher than the corresponding (input power)-(stator loss). This lends weight to the validity of the assumption of negligible iron and stray losses, since had these been appreciable the power equivalent of the measured torque would be lower than the corresponding (input power)-(stator loss), particularly at the higher frequencies.

This comparison of these two quantities indicates the presence of an additional torque even though the experiment was carried out with the rotor in a mean torque position, as indicated by the experiment of section (16), in an attempt to eliminate errors due to reluctance type torques. It is further observed, in fig. (5.10), that the developed torque is zero at zero frequency; this point was checked by exciting the machine with direct current. These observations lead to the conclusion that the additional torque is not of the simple reluctance type but is generated by the effects of the combined magnetic dissymetries of the stator and the rotor which are manifest only when both of these components are excited. The identification of the exact nature of these dissymetries would require further investigations and is considered in chapter IX . So far as this determination is concerned, the value of $\frac{(R_t - R_1)}{\omega}$ obtained with power as a basis is taken as the more dependable and is used in the calculation of the value of $\frac{X_t}{\omega}$ and the subsequent construction of the locus diagram.

To determine the value of $\frac{X_t}{\omega}$ the overall power factor of the equivalent circuit, at any particular frequency, is obtained as $\frac{R_t}{Z_t}$ in which $R_t = \frac{W}{I_1^2}$ and $Z_t = \frac{V}{I_1}$, W and V both being taken as average values for the two phases and read from figs. (5.12)&(5.13).

i.e. $$\cos \phi = \frac{W_{av}/I_1^2}{V_{av}/I_1}.$$

From this the corresponding value of $\sin \phi$ is derived and $\frac{X_t}{\omega}$ is then evaluated as $\frac{Z_t}{\omega}\sin \phi$. At the lower frequencies, the values of $\cos \phi$ are close to unity and those of $\sin \phi$ are close to zero. Consequently, small errors in the value of $\cos \phi$ will result in very large errors in the value of $\sin \phi$ and, therefore, of $\frac{X_t}{\omega}$. To minimise these errors as much as possible, separate graphs are drawn to cover the low frequency ranges of W_{av} and V_{av}, fig. (5.13), and the calculated values of cos ϕ are plotted against frequency, the values required for obtaining sin ϕ being then read from these graphs. In addition, $\frac{X_t}{\omega}$ and $\frac{(R_t - R_1)}{\omega}$ are drawn as functions of frequency to further minimise errors and to give ready access to their values at any frequency for the construction of the locus diagram. In all cases, as for W_{av} and V_{av}, separate graphs are drawn to cover the low frequency ranges. The calculations leading to these graphs are given in table (5.3) and the graphs themselves in figs. (5.16)-(5.19).

Even with this procedure, $\frac{X_t}{\omega}$ is limited in calculation to a minimum frequency below which the effect of instrument errors would make the values obtained liable to large inaccuracies. Thus, if a satisfactory maximum error in sin ϕ is fixed at a nominal $\pm$ 20%, then the frequency limit for a dependable result can be assessed by an analysis of the errors involved.

Wattmeter:

Instrument accuracy $\pm$0.6% F.S.D. for F.S.D. 6.0 watts.

Hence, at readings in the order of 1.0 watt, instrument error may be taken as approximately $\pm$3.6%.

Reading error, say $\pm$2%.

Total error, $\pm$5.6%.

Ammeter:

Always set at 90mA. F.S.D. 100 mA.

Instrument accuracy approximately $\pm$0.1%, from manufacturer's calibration.

Reading error, say $\pm$0.2%.

Total error, $\pm$0.3%.

Voltmeter:

Multirange meter.

Instrument accuracy, say $\pm$1% overall.

Reading error, say $\pm$1% overall.

Total error, $\pm$2%.

Hence,

total error in cos $\phi = \pm(5.6 + 0.3 + 2) = \pm 7.9\%$, say $\pm 10\%$.

Writing sin ϕ as $(1 - \cos\phi)^{\frac{1}{2}}$, then, if the value of cos ϕ in which a $\pm 10\%$ error results in a $\mp 20\%$ error in sin ϕ is y, we have,

$$0.2 = \frac{(1 - (1 - 0.1)^2 y^2)^{\frac{1}{2}} - (1 - y^2)^{\frac{1}{2}}}{(1 - y^2)^{\frac{1}{2}}}$$

$$= \frac{(1 - 0.81y^2)^{\frac{1}{2}}}{(1 - y^2)^{\frac{1}{2}}} - 1$$

which gives, $y = 0.836$.

From table (5.3), therefore, values of $\frac{X_t}{\omega}$ calculated for frequencies below 22.5 Hz. are taken as a guide only. In the graph of $\frac{X_t}{\omega}$ versus ω, the low frequency region is really a justifiable extrapolation.

The values of ω, $\frac{X_t}{\omega}$, and $\frac{(R_t - R)}{\omega}$ used in the construction of the locus diagram are given in table (5.4) and the locus diagram itself is given in fig. (5.20).

Supply freq. Hz.	Average voltage per ph. V_{av} volts.	Average power per ph. W_{av} watts.	Z_t V_{av}/I_1 ohms.	R_t W_{av}/I_1^2 ohms.	cos ϕ correct	sin ϕ	$\frac{X_t}{\omega}$ ohmsecs.	$\frac{(R_t - R_1)}{\omega}$ ohmsecs.
0	20.9	1.89	232.2	232.2	1.00	0.00		
2.5	21.2	1.90	235.6	234.6	0.995	0.100	1.500	0.114
5.0	21.8	1.93	242.2	238.3	0.985	0.172	1.325	0.175
7.5	22.5	1.97	250.0	243.2	0.971	0.239	1.267	0.220
10.0	23.3	2.01	258.9	248.1	0.954	0.300	1.235	0.243
12.5	24.5	2.05	272.2	253.1	0.934	0.357	1.236	0.258
15.0	25.7	2.11	285.6	260.5	0.912	0.410	1.241	0.293
17.5	27.2	2.18	302.2	269.1	0.890	0.458	1.257	0.330
20.0	28.7	2.24	318.9	276.5	0.868	0.496	1.257	0.347
22.5	30.4	2.32	337.8	286.4	0.848	0.530	1.265	0.379
25.0	32.2	2.40	357.8	296.3	0.829	0.559	1.272	0.404
27.5	33.9	2.48	376.7	306.2	0.813	0.582	1.268	0.431
30.0	35.8	2.57	397.8	317.3	0.799	0.601	1.267	0.448
35.0	39.4	2.77	437.8	342.0	0.781	0.625	1.242	0.496
40.0	43.2	3.01	480.0	371.6	0.774	0.633	1.208	0.552
50.0	50.3	3.48	558.9	429.6	0.769	0.639	1.136	0.626
60.0	57.4	3.99	637.8	492.6	0.772	0.636	1.079	0.688
70.0	63.8	4.50	708.9	555.6	0.784	0.621	1.000	0.733
80.0	69.3	5.00	770.0	617.3	0.802	0.598	0.915	0.764
100.0	79.3	5.90	881.1	728.4	0.830	0.558	0.782	0.788
120.0	87.4	6.74	971.1	832.1	0.857	0.515	0.662	0.794
140.0	93.4	7.39	1037.8	912.3	0.878	0.479	0.565	0.772
160.0	98.2	7.92	1091.1	977.8	0.895	0.446	0.484	0.740
180.0	102.1	8.31	1134.4	1025.9	0.904	0.428	0.429	0.701
200.0	105.3	8.62	1170.0	1064.2	0.910	0.415	0.387	0.661
250.0	111.1	9.18	1234.4	1133.3	0.918	0.397	0.312	0.573
300.0	115.1	9.54	1278.9	1177.8	0.922	0.387	0.262	0.501
350.0	118.2	9.81	1313.3	1211.1	0.923	0.385	0.230	0.444

CONT'D.

Supply freq. Hz.	Average voltage per ph. V_{av} volts.	Average power per ph. W_{av} watts.	Z_t V_{av}/I_1 ohms.	R_t W_{av}/I_1^2 ohms.	cos ϕ correct	sin ϕ	$\frac{X_t}{\omega}$ ohmsecs.	$\frac{(R_t - R_1)}{\omega}$ ohmsecs.
400.0	120.4	10.01	1337.8	1235.8	0.924	0.382	0.203	0.399
450.0	122.3	10.16	1358.9	1254.3	0.924	0.382	0.183	0.361
500.0	123.8	10.28	1375.6	1269.1	0.921	0.390	0.170	0.329
550.0	126.4	10.38	1404.4	1281.5	0.912	0.410	0.166	0.307
600.0	128.9	10.44	1432.2	1288.9	0.901	0.434	0.165	0.280
650.0	131.2	10.51	1457.8	1297.5	0.890	0.456	0.162	0.261
700.0	133.7	10.58	1485.6	1306.2	0.879	0.477	0.161	0.244
750.0	136.0	10.62	1511.1	1311.1	0.868	0.496	0.159	0.228
800.0	138.3	10.68	1536.7	1318.5	0.858	0.513	0.157	0.216
850.0	140.8	10.73	1564.4	1324.7	0.848	0.530	0.155	0.204
900.0	142.3	10.76	1582.2	1328.4	0.840	0.543	0.152	0.193
950.0	144.0	10.79	1600.0	1332.1	0.833	0.553	0.148	0.184
1000.0	145.1	10.81	1612.2	1334.6	0.828	0.561	0.144	0.175

TABLE (5.3). CALCULATION OF X_t/ω AND $(R_t - R_1)/\omega$ AS FUNCTIONS OF SUPPLY FREQUENCY.

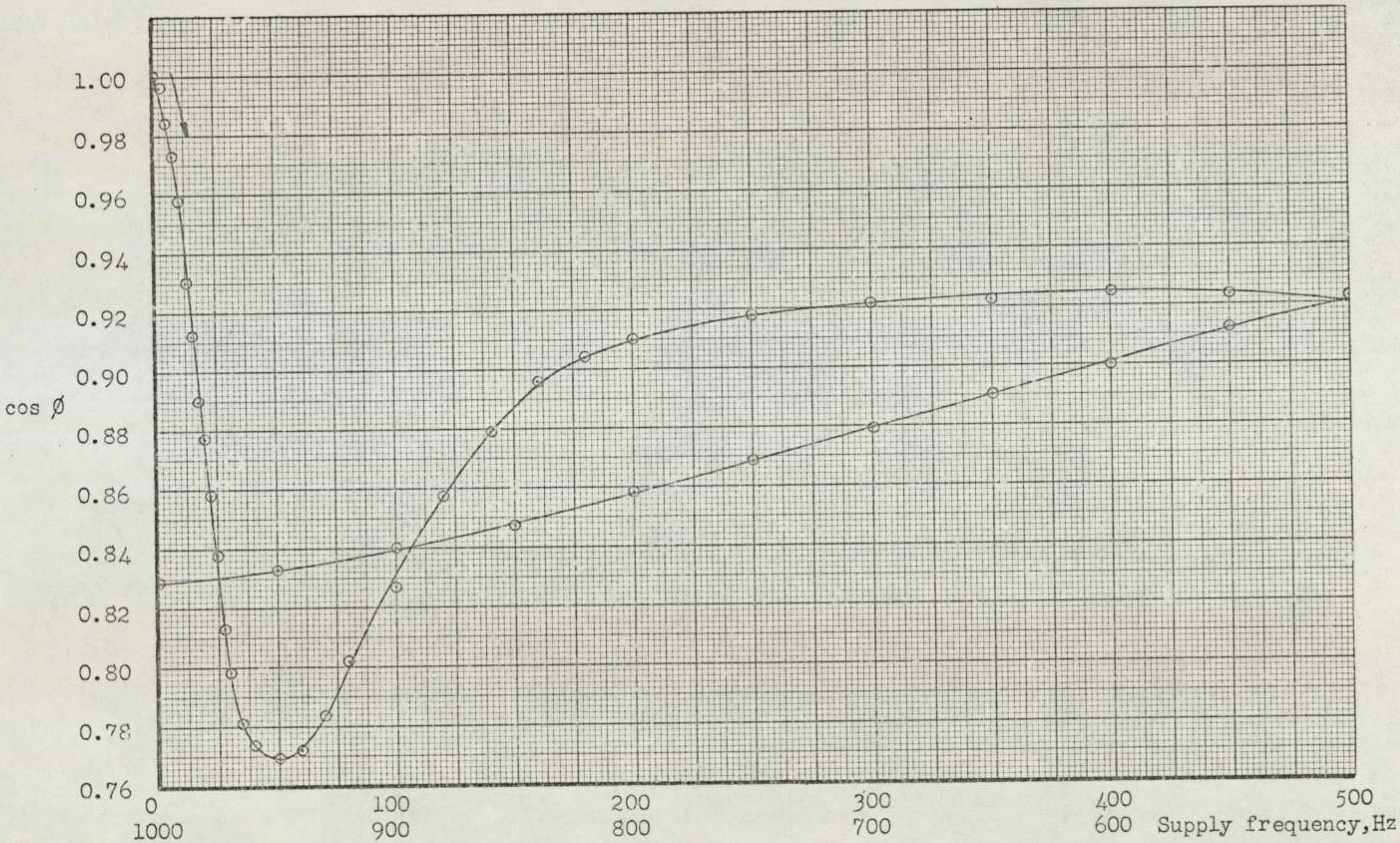

FIG. (5.16). VARIATION OF OVERALL POWER FACTOR, cos Ø, WITH SUPPLY FREQUENCY.

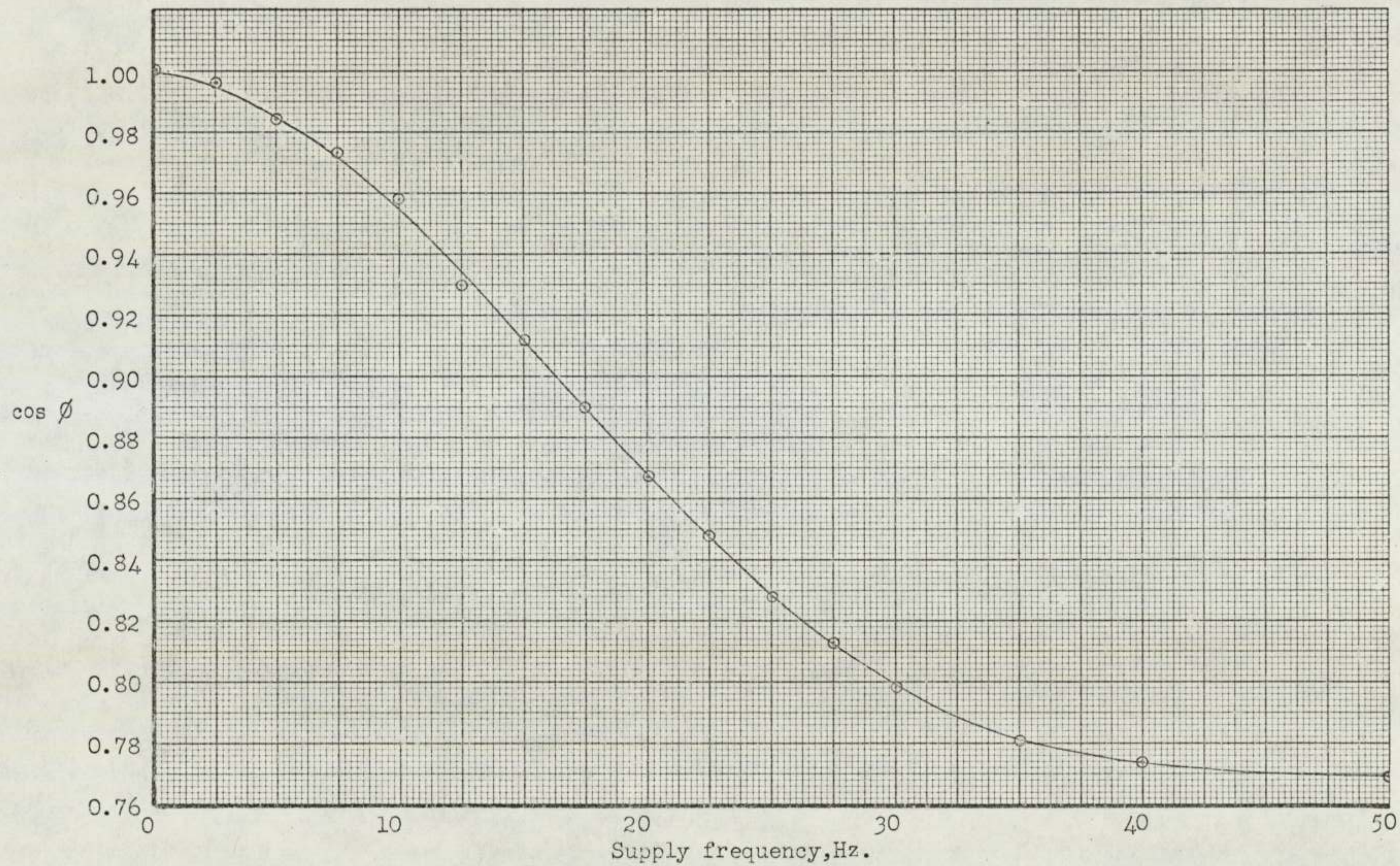

FIG. (5.17). VARIATION OF OVERALL POWER FACTOR, cos Ø, WITH SUPPLY FREQUENCY, LOW FREQUENCY REGION.

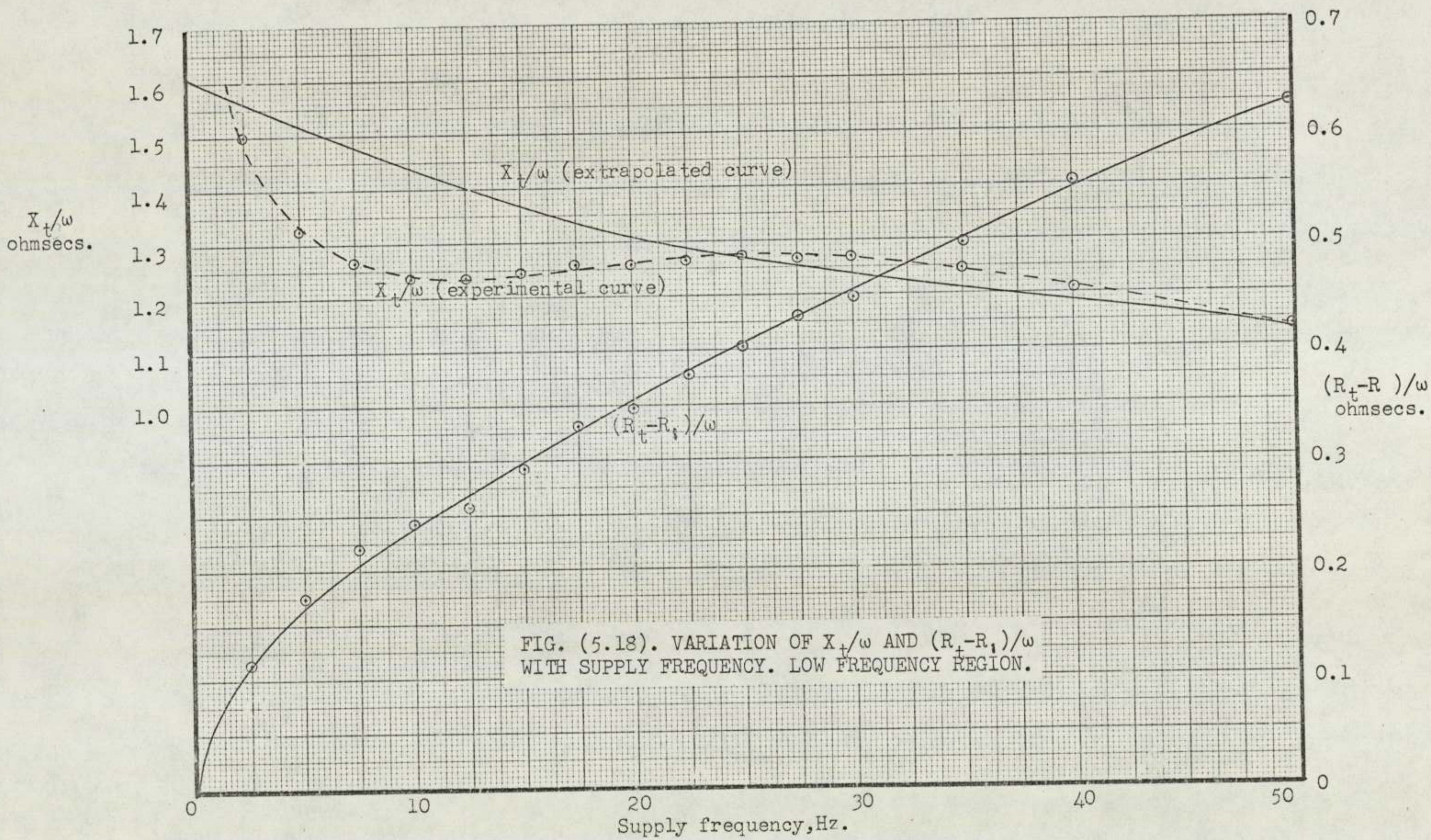

FIG. (5.18). VARIATION OF X_t/ω AND $(R_t-R_1)/\omega$ WITH SUPPLY FREQUENCY. LOW FREQUENCY REGION.

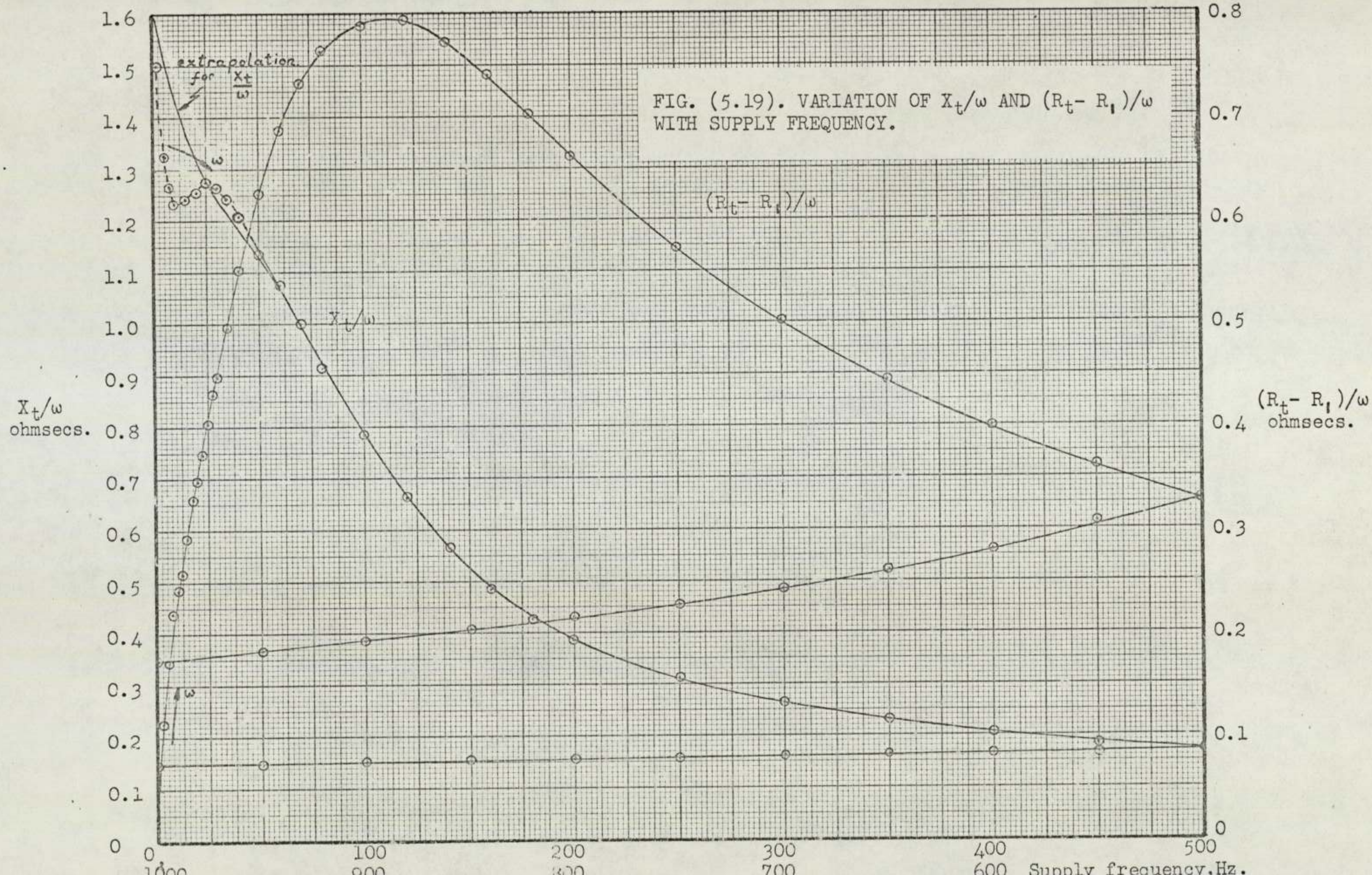

FIG. (5.19). VARIATION OF X_t/ω AND $(R_t - R_1)/\omega$ WITH SUPPLY FREQUENCY.

Supply freq. Hz.	$\frac{X_t}{\omega}$ ohmsecs.	$\frac{(R_t-R_1)}{\omega}$ ohmsecs.	Supply freq. Hz.	$\frac{X_t}{\omega}$ ohmsecs.	$\frac{(R_t-R_1)}{\omega}$ ohmsecs.	Supply freq. Hz.	$\frac{X_t}{\omega}$ ohmsecs.	$\frac{(R_t-R_1)}{\omega}$ ohmsecs.
0	1.610	0.000	62.50	1.052	0.700	206.00	0.376	0.650
1.75	1.576	0.100	68.00	1.010	0.725	234.00	0.333	0.600
4.10	1.530	0.150	75.10	0.955	0.750	263.00	0.298	0.550
7.00	1.480	0.200	87.00	0.870	0.775	300.00	0.264	0.500
10.75	1.423	0.250	95.00	0.814	0.785	344.00	0.233	0.450
15.00	1.366	0.300	102.50	0.766	0.793	400.00	0.205	0.400
19.95	1.310	0.350	112.50	0.708	0.795	467.00	0.182	0.350
24.45	1.271	0.400	120.00	0.667	0.793	555.00	0.169	0.300
29.97	1.231	0.450	132.00	0.608	0.785	677.00	0.161	0.250
35.10	1.202	0.500	143.00	0.563	0.770	868.00	0.151	0.200
40.50	1.180	0.550	154.00	0.510	0.750	1000.00	0.149	0.175
46.25	1.154	0.600	168.00	0.462	0.725			
50.60	1.120	0.650	181.00	0.427	0.700			

TABLE (5.4). PERTAINING TO CONSTRUCTION OF IMPEDANCE per UNIT FREQUENCY LOCUS DIAGRAM.

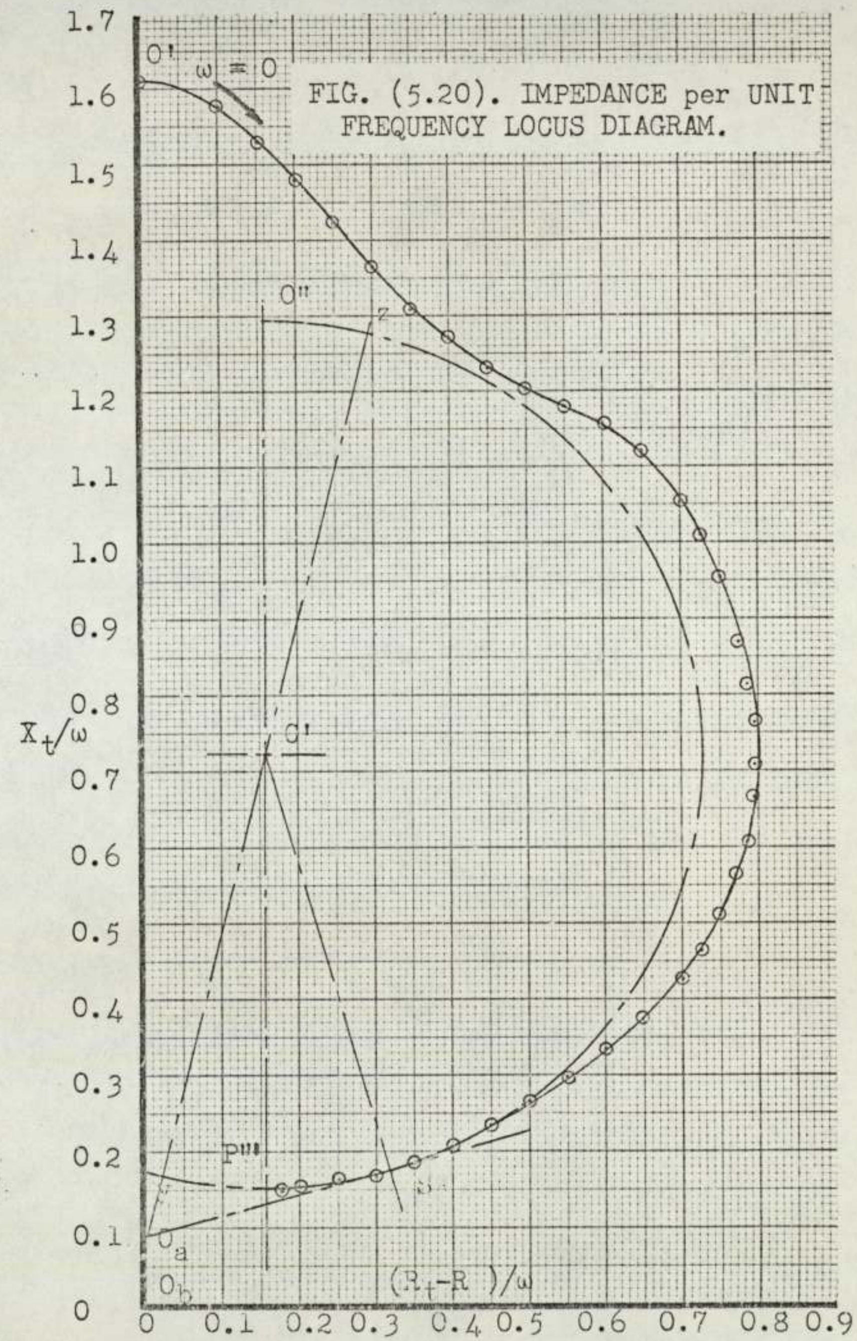

FIG. (5.20). IMPEDANCE per UNIT FREQUENCY LOCUS DIAGRAM.

19) Interpretation of Locus Diagram.

The locus diagram constructed from the results of the constant current, variable frequency test is seen to differ from that expected for the assumed form of the equivalent circuit. It appears, to a good approximation, to commence at the high frequency end as a semicircle as expected, but displaced from the vertical axis, and then run into a more indefinite curve. The general conclusion to be derived from this is that the values of the effective rotor resistance per unit frequency as given by $\frac{(R_t - R_1)}{\omega}$ are higher in proportion, compared with the effective reactance, than the equivalent circuit suggests. Since the value of R_1 is accurately known, this implies that there must be present in the true equivalent circuit another resistor or resistors in either the stator branch, the rotor branch or both.

Reference to fig.(5.15) and to the discussion thereon, shows that the measured torque figures indicate a torque greater than that expected from the synchronous watts in the rotor, and it is decided that the assumption of negligible iron loss is valid. Consequently, the lateral displacement of the locus diagram cannot be taken as being due to the presence of an equivalent iron loss resistor. The effect must, therefore, have its origins in the rotor circuit.

Remembering that the torque developed by the motor is given by $\frac{p_n(\text{rotor power})}{\omega}$ this displacement of the locus diagram must have associated with it a torque which is independent of the supply frequency in the variable frequency test and, therefore, of the rotor speed under normal operating conditions. This suggests a hysteresis torque but, as has already been pointed out, magnetic hysteresis in the core of this machine is negligible so that an appreciable torque of this nature is not feasible. Since the locus diagram has been constructed using values of equivalent resistance obtained from power measurements and not from torque measurements, this additional torque must then be the result of current paths in the rotor supplementary to those usually defined for the basic equivalent circuit.

This conclusion is substantiated by considering the general form of the experimental locus. From the semicircular nature of this diagram, it is inferred that the rotor winding resistance in series with its leakage reactance will be present in the true equivalent circuit as a separate branch, since otherwise the theoretical locus of this circuit could not demonstrate this particular form. Consequently, the displacement of the locus diagram must be caused principally by additional branches in parallel with the normal branch in the equivalent circuit and which are not harmonics.

In fig.(5.21) a possible form of modified equivalent circuit is shown in which the branch consisting of the resistor R_e carries the supplementary currents. For the torque generated by these currents to be independent of the frequency of them, the resistor R_e must be a linear function of rotor frequency. This resistor will, therefore, be more explicitly represented as $R_e s|\omega|$. The per unit frequency equivalent circuit per phase, at standstill will then be as shown in fig.(5.22).

Retracing the theoretical development of the impedance per unit frequency locus as given in figs.(5.1) - (5.6), the effect of the additional branch will first be manifest in fig.(5.4) in which, before adding the vector $\frac{1}{L_o}$, a vector $\frac{1}{R_e}$ would need to be added as shown in fig.(5.23). The inversion of this diagram about the point O_a is given in fig.(5.24) from which it is seen that the diameter of the semicircle now lies off the vertical axis as required.

Considering the extremities O' and P" of this locus, the experimental evidence of fig.(5.18) shows that at zero frequency $\frac{(R_t-R_1)}{\omega}$ is zero and $\frac{X_t}{\omega}$ has a value of 1.61 whilst at infinite frequency, by extrapolation, their values would tend to 0.1 and 0.15, respectively. This means that in fig.(5.24) the lower extremity P" is correctly located whereas the upper extremity O' should extend to the vertical axis. The fact that it does not suggests that the extra branch in the equivalent circuit should consist not simply of a single resistor $R_e s|\omega|$ proportional to the frequency, but of this and another resistor r_e, an inverse function of the rotor frequency, in series with it.

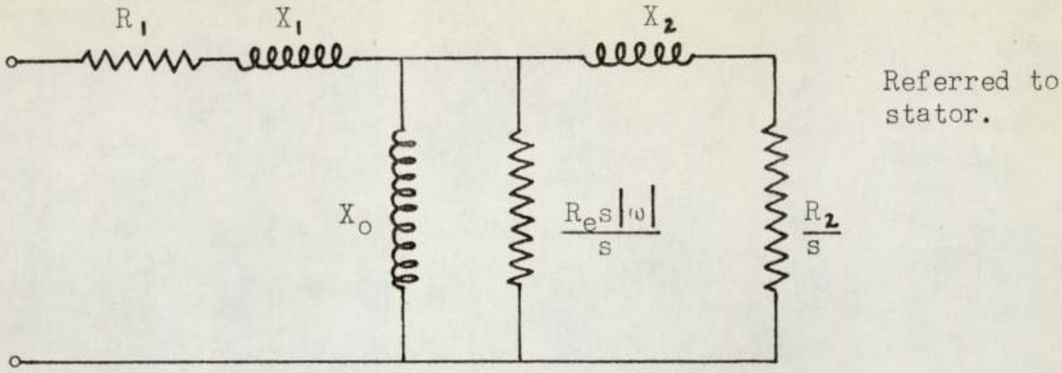

FIG. (5.21). POSSIBLE FORM OF MODIFIED EQUIVALENT CIRCUIT PER PHASE.

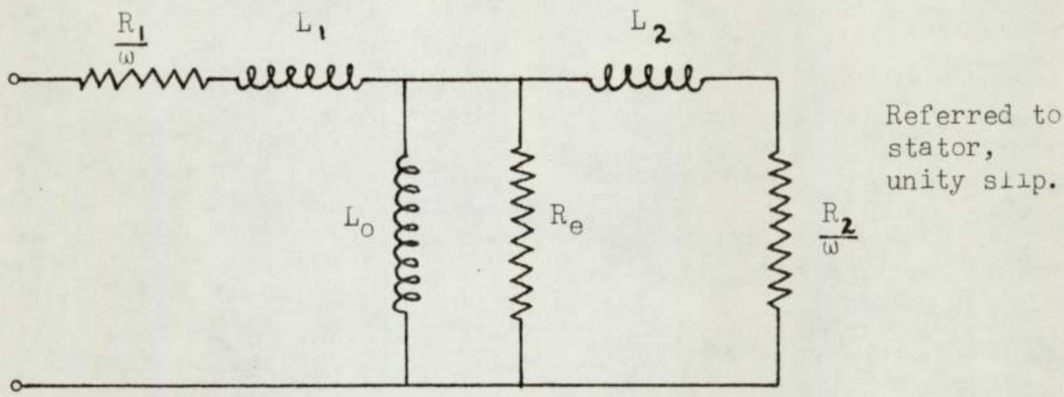

FIG. (5.22). PER UNIT FREQUENCY EQUIVALENT CIRCUIT PER PHASE CORRESPONDING TO FIG. (5.21).

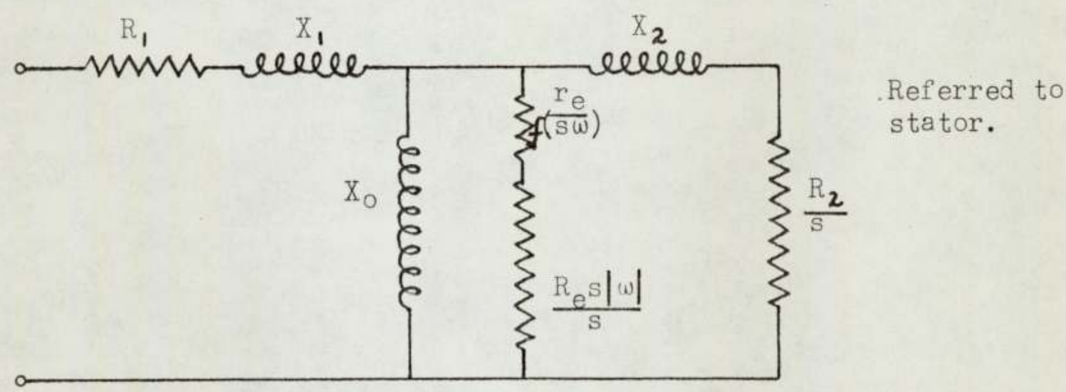

FIG.(5.27). FINAL FORM OF MODIFIED EQUIVALENT CIRCUIT PER PHASE.

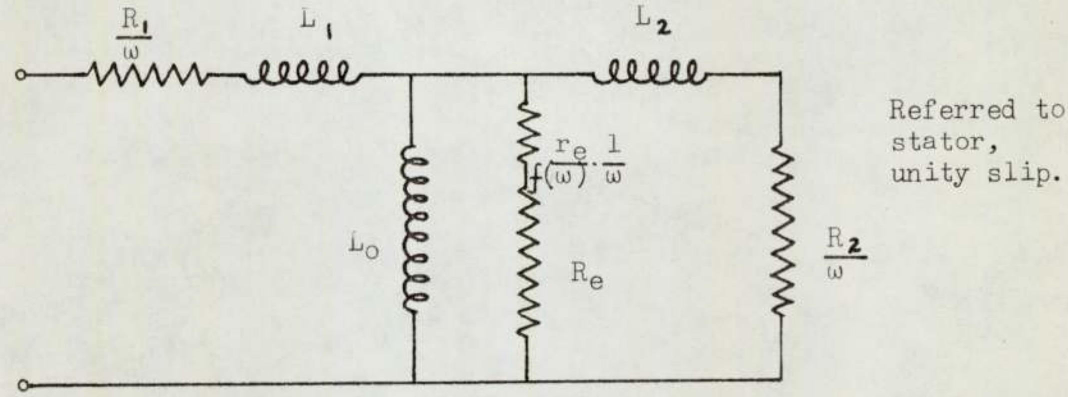

FIG. (5.28). PER UNIT FREQUENCY EQUIVALENT CIRCUIT PER PHASE CORRESPONDING TO FIG.(5.27).

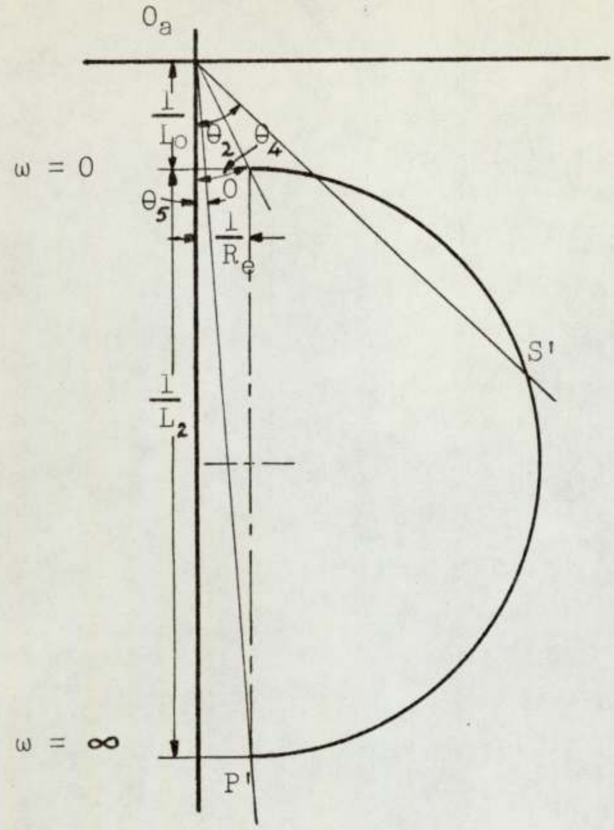

FIG. (5.23). ROTOR BRANCH & MAGNETISING BRANCH, ADMITTANCE per UNIT FREQUENCY LOCUS FOR CIRCUIT OF FIG. (5.21).

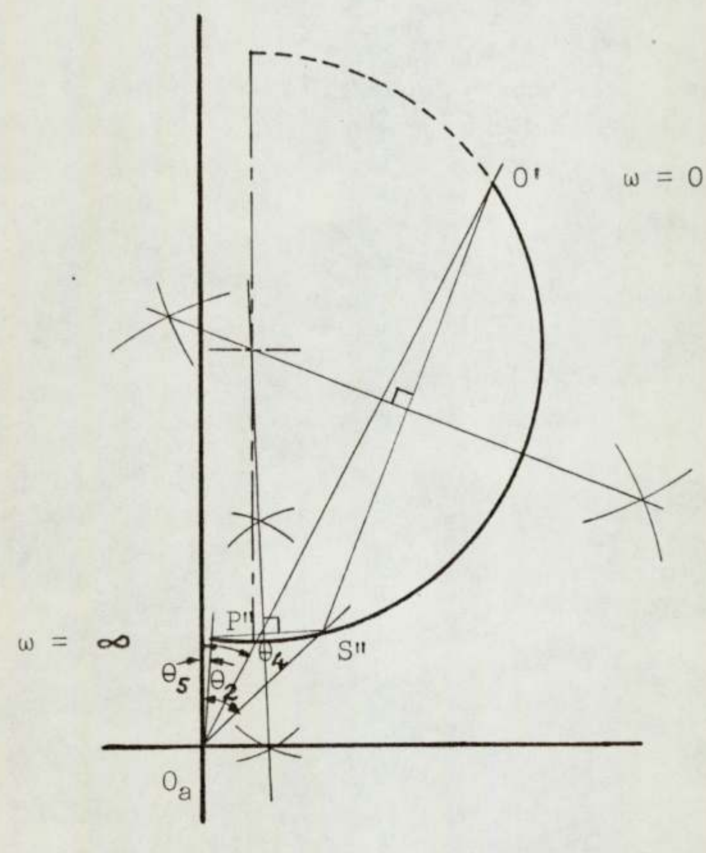

FIG. (5.24). INVERSION OF FIG. (5.23) ABOUT POINT O_a.

With this arrangement, the vector $\frac{1}{R_e}$ in fig.(5.23) will be replaced by the vector $\frac{1}{R_e + r_e/f(\omega)}$ which becomes zero at zero frequency and has, at infinite frequency, the value $\frac{1}{R_e}$ as before. This is shown diagrammatically in fig.(5.25) with the corresponding inversion about the point O_a in fig.(5.26). In this latter diagram it is seen that the extremity P″ remains in the same place as in fig.(5.24) but the extremity O′ is now on the vertical axis.

The presence of the resistor r_e will obviously cause some distortion of the semicircular locus, to a degree dependent upon the value of the ratio $\frac{r_e}{R_e}$ and the particular nature of r_e as a function of ω. That this is so can best be appreciated by writing the expression for the additional vector as $\frac{1}{R_e}\left[\frac{1}{(r_e/R_e)/f(\omega) + 1}\right]$. In this expression, the term $\frac{1}{(r_e/R_e)/f(\omega) + 1}$ modifies the original additional vector $\frac{1}{R_e}$ so that examination of this term as a function of both the frequency and the ratio $\frac{r_e}{R_e}$ will give information concerning the distortion of the locus in fig.(5.25) and, therefore, in fig.(5.26). This examination is carried out in tabular form in table (5.5) in which the value of the modifying term is calculated for various values of the ratio $\frac{r_e}{R_e}$ over a range of frequency assuming r_e to be the simple inverse r_e/ω. From this it is apparent that if the value of r_e is less than h x R_e, where h is an arbitrary constant, its effect on the locus will be negligible at frequencies above 5h Hz.

r_e/R_e	h/1000	h/100	h/10	h/1
Frequency, Hz.	Value of modifying term.			
0.00h	0.0000	0.0000	0.0000	0.0000
0.01h	0.9091	0.5000	0.0909	0.0099
0.05h	0.9804	0.8333	0.3333	0.0476
0.10h	0.9901	0.9091	0.5000	0.0909
0.50h	0.9980	0.9804	0.8333	0.3333
1.00h	0.9990	0.9901	0.9091	0.5000
5.00h	0.9998	0.9980	0.9804	0.8333

TABLE (5.5). MODIFICATION TO LOCUS DUE TO RESISTOR r_e.

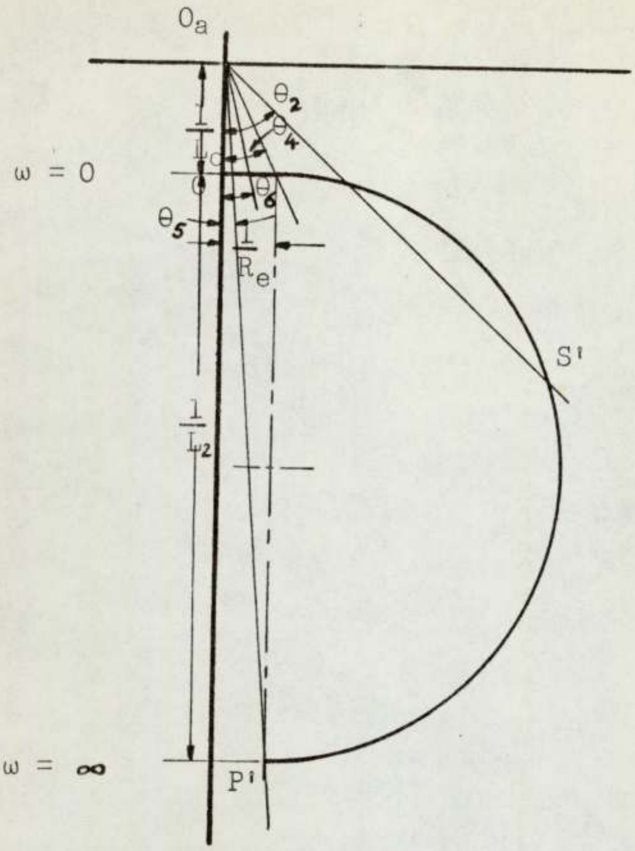

FIG. (5.25). ROTOR BRANCH & MAGNETISING BRANCH, ADMITTANCE per UNIT FREQUENCY LOCUS FOR CIRCUIT OF FIG. (5.27).

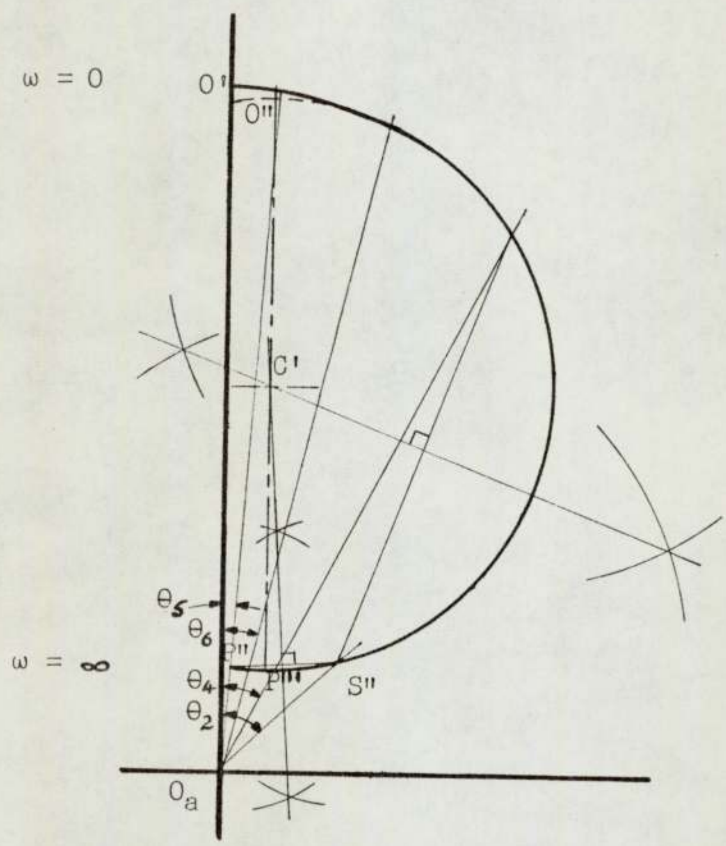

FIG. (5.26). INVERSION OF FIG. (5.25) ABOUT POINT O_a .

In constructing the locus diagram of fig.(5.25), it was assumed that the ratio $\frac{r_e}{R_e}$ was such that the distortion of the semicircle could be mostly ignored. This diagram appears, therefore, simply as a semicircle whose diameter is displaced from the vertical axis but whose upper extremity has been extended onto this axis. Reference to fig.(5.20), however, shows the distortion of the experimental locus to be quite considerable and it is, therefore, concluded that the resistor r_e is large in comparison with R_e inthis case. As a result it is to be expected that only those points, in the experimental locus, taken at the higher frequencies will lie on a semicircle. From fig.(5.26) and the arguments used in its development, it is apparent that this semicircle must be contained within the actual locus. In fig.(5.20) this semicircle has been drawn in in chain-dotted line and bears out the above statements. The other chain-dotted lines are included for use in section (20) and their relevance will be seen therein.

The final form of the modified equivalent circuit is given in fig.(5.27) and the corresponding per unit frequency equivalent circuit in fig.(5.28). It is now necessary to reconsider the analysis carried out in section(15) in order to include the additional circuit elements and to derive a method of estimating their values and their relationships to the rotor frequency.

The experimental locus diagram has the general characteristics indicated in fig.(5.26) with the addition of the vector L_1 moving the origin from point 0_a to point 0_b as explained in section (15) in relation to fig.(5.6). If the value of L_1 is estimated from design data then point 0_a can be found, as before, giving $L_0 = 0'0_b - L_1$ by equation (5.1). The distance $0_aP''$ is now no longer directly related to L_2 but if, in fig.(5.26), a line is drawn from point 0_a through the centre of the circle to cut the circle at points y and z as in fig.(5.29), and if $\frac{1}{0_a y} = 0_a z'$ and $\frac{1}{0_a z} = 0_a y'$ the points y' and z' would be diametrically opposite points on the circle of fig.(5.25) the diameter of which is $\frac{1}{L_2}$.
Hence, if in fig.(5.29) $C \times 0_a z = \frac{1}{0_a y}$, C being a constant, then $0_a z' - 0_a y'$, the diameter of the circle of fig.(5.25), will be given by

$$\frac{1}{O_a y} - \frac{1}{O_a z}, \text{i.e. } CO_a z - CO_a y.$$

$$\text{i.e. } \frac{1}{L_2} = C(O_a z - O_a y)$$

$$\text{whence, } L_2 = \frac{O_a z O_a y}{O_a z - O_a y} \qquad (5.6)$$

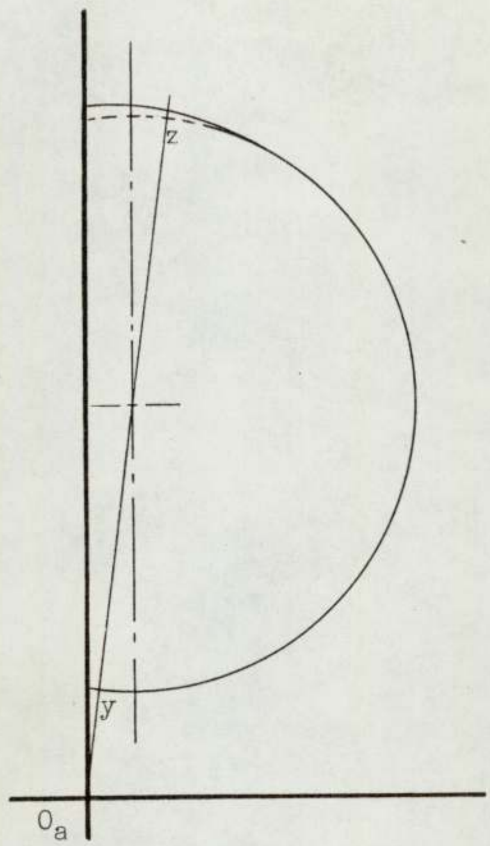

FIG. (5.29). APPERTAINING TO DETERMINATION OF L_2.

In section (15), the value of R_2 was obtained by constructing the tangent to the circle and using the derived value of L_2 in equation (5.5). Because of the non-circular extremities of the locus, the relationship of equation (5.5) no longer applies. Nevertheless, for the condition when O_aS'' in fig.(5.26) is a tangent to the circle, the line O_aS' in fig.(5.25) will also be a tangent, the points S" and S' occupying identical positions as before and occurring at the same frequency.

$$\text{Hence, } \frac{P'''S''}{O''S''} = \frac{L_2}{R_2/\omega_p}$$

Since L_2 is now known and ω_p can be obtained from fig.(5.19) in conjunction with fig.(5.20), the rotor resistance is determined as

$$R_2 = \frac{O''S'' \times L_2 \times \omega_p}{P''' S''} \tag{5.7}$$

From fig.(5.28),

$$j\left[\frac{X_t}{\omega} - L_1\right] + \frac{R_t - R_1}{\omega} = \left[\frac{1}{jL_o} + \frac{1}{R_e + r_e/f(\omega)} + \frac{1}{R_2/\omega + jL_2}\right]^{-1}$$

or, inverting,

$$\left[j\left[\frac{X_t}{\omega} - L_1\right] + \frac{R_t - R_1}{\omega}\right]^{-1} = \frac{1}{jL_o} + \frac{1}{R_e + r_e/f(\omega)} + \frac{R_2/\omega - jL_2}{(R_2/\omega)^2 + L_2^2}$$

whence,

$$R_e + r_e/f(\omega) = \left[Rl.\left[j\left[\frac{X_t}{\omega} - L_1\right] + \frac{R_t - R_1}{\omega}\right]^{-1} - \frac{R_2/\omega}{(R_2/\omega)^2 + L_2^2}\right]^{-1}$$

giving,

$$r_e/f(\omega) = \left[Rl.\left[j\left[\frac{X_t}{\omega} - L_1\right] + \frac{R_t - R_1}{\omega}\right]^{-1} - \frac{R_2/\omega}{(R_2/\omega)^2 + L_2^2}\right]^{-1} - R_e \tag{5.7a}$$

At infinite frequency $r_e/f(\omega) = 0$ and $\dfrac{R_2/\omega}{(R_2/\omega)^2 + L_2^2} = 0$ so that, from equation (5.7a),

$$R_e = \left[Rl\left[j\left[\frac{X_t}{\omega} - L_1\right] + \frac{R_t - R_1}{\omega}\right]^{-1}\right]^{-1} \tag{5.7b}$$

Since L_1 is determined and $\dfrac{X_t}{\omega}$ and $\dfrac{R_t - R_1}{\omega}$ are known as functions of ω in fig.(5.19), their values at infinite frequency being obtained by extrapolation R_e may be calculated by substitution in equation (5.7b). Also, since R_1, R_2, R_e and L_2 are now evaluated and $\dfrac{X_t}{\omega}$ and $\dfrac{R_t - R_1}{\omega}$ may be had as functions of ω, as stated above, the whole of the right hand side of equation (5.7a) can be calculated for various values of frequency thereby giving r_e as a function of ω, the actual function being obtainable by plotting $r_e/f(\omega)$ against ω and then using a curve fitting process.

20) Formulation of Impedance Tensor of Test Machine.

In section (15), the method developed for the formulation of the impedance tensor was based on an estimation of the value of the stator leakage inductance L_1 . Such an estimation was carried out in section (4) dealing with the design of the test machine. In the calculation, the value obtained for L_1 is dependent upon the value assigned to the effective air gap. This, in turn, was based upon the actual mechanical gap dimension which was implicitly assumed to be truly representative of the magnetic dimension. It was noted in section (15) that the material used for the cores of these machines is nickel iron alloy. This group of magnetic materials is used because their oxide forms a very thin protective coating. This prevents further oxidation which could cause mechanical fouling of the stator and the rotor due to the very small air gaps used. The high values of permeability of these alloys are obtained by a careful annealing process and are extremely sensitive to any subsequent mechanical strain. In the method employed for assembling these cores, the laminations are bonded together using resin bonding materials. The curing temperature of these resins is much lower than the annealing temperature of the alloys. The cores are, therefore, stacked using already annealed laminations. The subsequent machining operations carried out on the assembled cores consist of grinding and honing/lapping the bore surfaces. Whilst the handling of the laminations themselves and the machining processes are carried out with great care, it is inevitable that the magnetic material must suffer some mechanical strain at the bore surfaces. Consequently, the relation which the mechanical gap bears to the actual magnetic gap is indefinite. For this reason, any attempt to estimate the value of L_1 using the measured mechanical air gap must give a doubtful result. The following method which utilises the impedance per unit frequency locus, is aimed at overcoming this difficulty in the estimation of L_1, at the same time giving some indication of the extent of the magnetic damage at the bore surfaces.

From section (4), equation (3.14), L_0 is expressible as a function of the air gap δ thus,

$$L_0 = \frac{1.699}{0.087 + 8.6\delta_e}$$

in which, assuming the gap extension factor to be unaltered, $\delta_e = 1.778\delta$ where δ is in mm.

Also from section (4), the stator leakage permeance factor is obtained as

$$\Lambda_1 = (\Lambda_{g1} + \Lambda_{s1} + \Lambda_{h1})$$

in which Λ_{s1} and Λ_{h1} are independent of the air gap dimension and Λ_{g1} is a function of this dimension given by equation (15) as

$$\Lambda_{g1} = \mu_0 \left[0.372 + \frac{0.02}{\delta} \right].$$

Hence, as a function of the air gap δ,

$$\Lambda_1 = \mu_0 \left[0.372 + \frac{0.02}{\delta} + 3.25 + 0.4 \right]$$

giving, $$L_1 = 2pq_1 c_1^2 l \mu_0 \left[4.02 + \frac{0.02}{\delta} \right]$$

$$\text{i.e.} \; L_1 = 2 \times 4 \times 352^2 \times 1.83 \times 10^{-2} \times 4\pi \times 10^{-7} \left[4.02 + \frac{0.02}{\delta} \right]$$

$$\text{i.e.} \quad L_1 = 0.0914 + \frac{0.000455}{\delta} \qquad (5.7)$$

Hence, $(L_1 + L_0)$ as a function of δ becomes

$$(L_1 + L_0) = \frac{1.699}{0.087 + 8.6 \times 1.778\delta} + 0.0914 + \frac{0.000455}{\delta}$$

$$\text{i.e.} \quad (L_1 + L_0)(0.087 + 15.3\delta) = 1.71 + 1.4\delta + \frac{0.00004}{\delta} \qquad (5.8)$$

But from equation (5.1), fig. (5.18) and the impedance per unit frequency locus, fig. (5.20)

$$(L_1 + L_0) = 1.61 \;\text{henry}.$$

Hence, substituting in equation (5.8)

$$1.61\,(0.087 + 15.3\delta) = 1.71 + 1.4\delta + \frac{0.00004}{\delta}$$

from which, $\delta = 0.068$mm.

This represents an increase of 36% on the mechanical gap dimension. This increased figure will be defined as the magnetic gap dimension; it excludes the Carter gap extension factor.

Substituting in equation (5.7c),

$$\underline{L_1 = 0.097 \text{ henry.}}$$

whence, $$L_o = 1.61 - 0.097$$

$$\text{i.e. } \underline{L_o = 1.513 \text{ henry.}}$$

Using equation (5.6), $$L_2 = \frac{O_az \times O_ay}{O_az - O_ay}$$

and referring to figs.(5.20)&(5.29),

$$O_az = 1.215$$

$$O_ay = 0.073$$

whence, $$\underline{L_2 = 0.0775 \text{ henry.}}$$

Also from fig.(5.20),

$$P''S'' = 0.17$$

$$O''S'' = 1.128$$

$$\omega_p = 512 \text{ Hz.}$$

Therefore, by equation (5.7),

$$\underline{R_2 = 1648 \text{ ohms at } 112^\circ C.}$$

From fig.(5.19) by extrapolation,

at infinite frequency $$\frac{X_t}{\omega} = 0.14$$

and $$\frac{R_t - R_1}{\omega} = 0.15$$

Therefore, by equation (5.7b),

$$\underline{R_e = 0.280 \text{ ohms at } 112^\circ C.}$$

It is seen in fig.(5.20) that the distortion of the semicircular locus is negligible at frequencies above 300 Hz. Using fig.(5.18),(5.19) and equation (5.7a) $r_e/f(\omega)$ is calculated for various values of ω in the range 0 - 300 Hz. and plotted against ω. This graph is given in fig.(5.29a) from which, to a good degree of approximation,

$$\underline{r_e/f(\omega) = \frac{49}{\omega} + \frac{59}{+\sqrt{\omega}}}$$

The curve of this function is superimposed in fig.(5.29a) for comparison.

From table (5.2),

$$\underline{R_1 = 232.9 \text{ ohms at } 112^\circ C.}$$

By direct measurement, using the dynamometer, the friction constant was found to be negligible over the complete speed range of the test machine.

Also, by direct measurement, using a comparitive method, the rotor moment of inertia was determined as $\underline{3.3 \times 10^{-7} \text{ Kg.m}}$.

Using these parameters in accordance with fig.(5.27), the equivalent circuit per phase of the test machine is as shown in fig.(5.30).

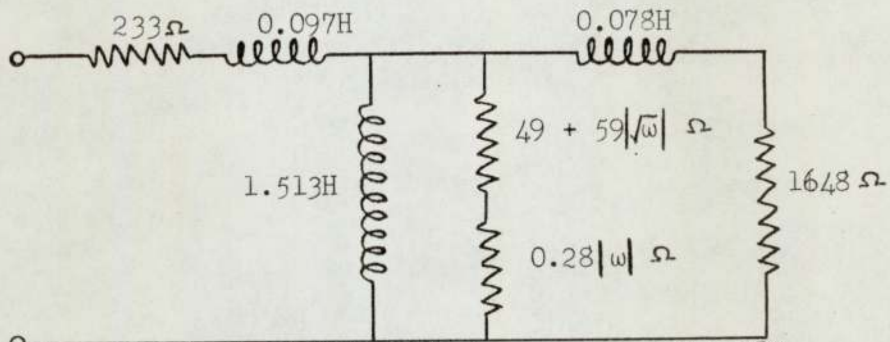

FIG. (5.30). EXPERIMENTALLY DETERMINED EQUIVALENT CIRCUIT per PHASE OF TEST MACHINE.

The non-holonomic primitive of this machine will, therefore, have a rotor with two layers of windings much like a double cage rotor. The one branch, however, has no leakage flux associated with it. The physical nature of this branch will be discussed in chapter VI. This primitive is shown in fig.(5.31).

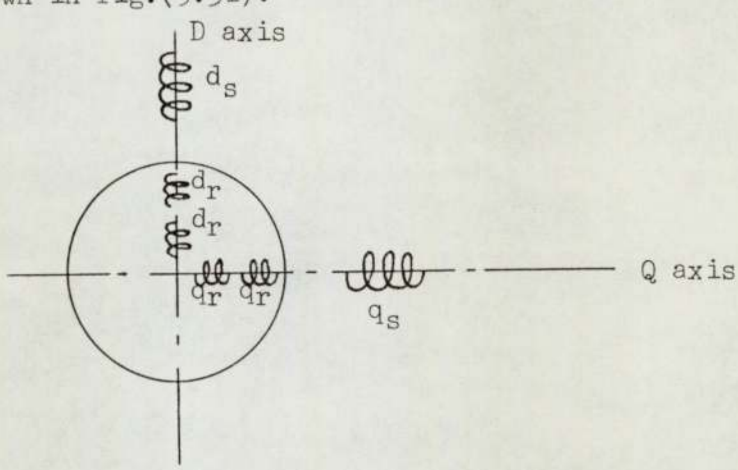

FIG. (5.31). NON-HOLONOMIC PRIMITIVE CORRESPONDING TO FIG. (5.30).

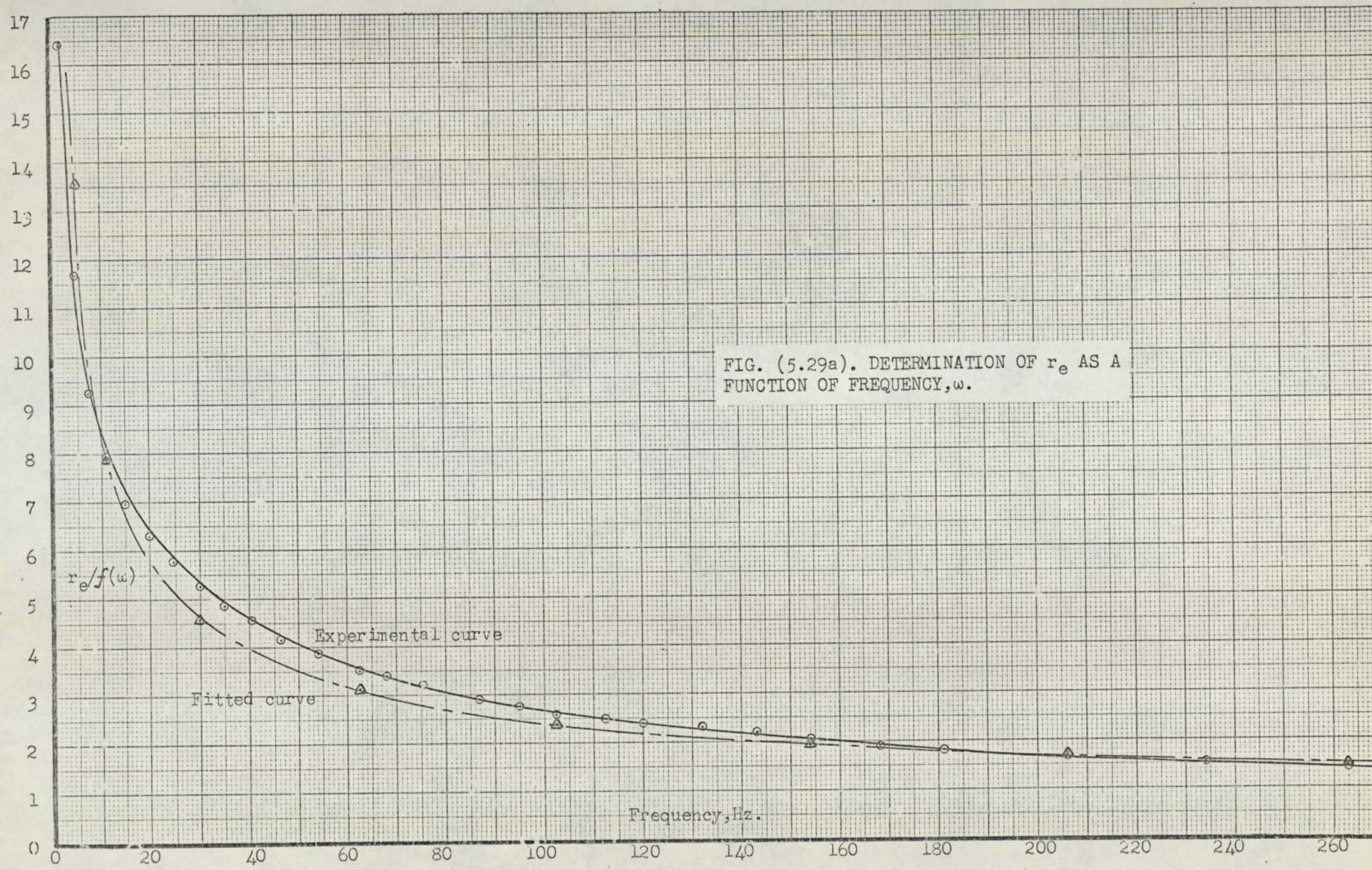

FIG. (5.29a). DETERMINATION OF r_e AS A FUNCTION OF FREQUENCY, ω.

Using the relationships established in section (3) between their elements and the equivalent circuit parameters, the metric, resistance and torque tensors of this model are constructed below in terms of referred values.

$L_{\alpha\beta}$ =

$\alpha \backslash \beta$	d_s	d_{r1}	d_{r2}	q_s	q_{r1}	q_{r2}	t
d_s	1.61	1.51	1.51				
d_{r1}	1.51	1.51	1.51				
d_{r2}	1.51	1.51	1.59				
q_s				1.61	1.51	1.51	
q_{r1}				1.51	1.51	1.51	
q_{r2}				1.51	1.51	1.59	
t							3.3×10^{-7}

(5.9)

$R_{\alpha\beta}$ =

$\alpha \backslash \beta$	d_s	d_{r1}	d_{r2}	q_s	q_{r1}	q_{r2}	t
d_s	233						
d_{r1}		$49+59\sqrt{s\omega}+0.28s\omega$					
d_{r2}			1648				
q_s				233			
q_{r1}					$49+59\sqrt{s\omega}+0.28s\omega$		
q_{r2}						1648	
t							0.0

(5.10)

$G_{\alpha\beta}$ =

$\alpha \backslash \beta$	d_s	d_{r1}	d_{r2}	q_s	q_{r1}	q_{r2}	t
d_s					1.51	1.51	
d_{r1}					1.51	1.51	
d_{r2}					1.51	1.59	
q_s		-1.51	-1.51				
q_{r1}		-1.51	-1.51				
q_{r2}		-1.51	-1.59				
t							

(5.11)

CHAPTER VI

Comparison of Measured and Estimated Impedance Tensors.

21) Estimation of impedance tensor.

The experimental determination of the impedance tensor was carried out at a machine temperature of 113°C. The comparison of the tensors will, therefore, be made at this temperature.

From the calculations made in section (4), the estimated circuit parameters are,

$$R_1 = 164.7 \text{ ohms/phase at } 0^\circ C.$$

Hence at 113°C,

$$R_1 = 164.7(1 + 0.00428 \times 113)$$

$$\text{i.e. } \underline{R_1 = 244 \text{ ohms/phase.}}$$

$$R_2 = 513 \text{ ohms/phase at } 0^\circ C.$$

Hence at 113°C,

$$R_2 = 513(1 + 0.00445 \times 113)$$

$$\text{i.e. } \underline{R_2 = 772 \text{ ohms/phase.}}$$

$$\underline{L_0 = 2.00 \text{ henry;}}$$

$$\underline{L_1 = 0.10 \text{ henry;}}$$

$$\underline{L_2 = 0.071 \text{ henry.}}$$

The friction coefficient F is assumed to be negligible since great care is taken in the manufacturing process to ensure this to be so.

Rotor moment of inertia $\underline{J = 3.3 \times 10^{-7} \text{ Kg.m}^2.}$

As in section (20), using the relationships established in section (3) between their elements and the equivalent circuit parameters, the estimated metric, resistance and torque tensors are constructed below.

$$L_{\alpha\beta} = \begin{array}{c|c|c|c|c|c|} \alpha \backslash \beta & d_s & d_r & q_s & q_r & t \\ \hline d_s & 2.10 & 2.00 & & & \\ \hline d_r & 2.00 & 2.071 & & & \\ \hline q_s & & & 2.10 & 2.00 & \\ \hline q_r & & & 2.00 & 2.071 & \\ \hline t & & & & & 3.3 \times 10^{-7} \\ \hline \end{array} \qquad (6.1)$$

$$R_{\alpha\beta} = \begin{array}{c|c|c|c|c|c|} \alpha \backslash \beta & d_s & d_r & q_s & q_r & t \\ \hline d_s & 244 & & & & \\ \hline d_r & & 772 & & & \\ \hline q_s & & & 244 & & \\ \hline q_r & & & & 772 & \\ \hline t & & & & & 0.0 \\ \hline \end{array} \qquad (6.2)$$

$$G_{\alpha\beta} = \begin{array}{c|c|c|c|c|c|} \alpha \backslash \beta & d_s & d_r & q_s & q_r & t \\ \hline d_s & & & & +2.00 & \\ \hline d_r & & & & +2.071 & \\ \hline q_s & & -2.00 & & & \\ \hline q_r & & -2.071 & & & \\ \hline t & & & & & \\ \hline \end{array} \qquad (6.3)$$

22) Comparison of Tensors.

Before comparing the values of corresponding elements in the set of estimated and measured tensors, cognisance must be made of the difference in their forms in that the estimated tensors appear as 5 x 5 arrays whilst the measured ones appear as 7 x 7 arrays. The reason for this is the presence of the extra branch in the rotor section of the measured equivalent circuit which was required to give the observed form of the impedance per unit frequency locus.

The relationship obtained between rotor frequency and the resistance of this branch, viz: $r_e = 0.28s|\omega| + 49 + 59\sqrt[+]{s|\omega|}$, and the fact that it has no leakage reactance associated with it indicate three things,

a) the branch represents current paths which are not linked by leakage flux; this is witnessed by the constant component of the resistance.

b) the current distribution in these paths is affected to some extent by the flux linking the path; this is witnessed by the term in $s\omega$ in the resistance.

c) the current distribution is also affected by eddy currents as witnessed by the term in $\sqrt{s\omega}$.

These indications lead to the opinion that the first two terms of r_e refer to the actual bars and in particular to that section of them linked by the minimum slot leakage flux. This could well be a further manifestation of the effects of reduced permeability of the rotor iron at the bore surface due to work hardening; this would result in the upper section of the rotor bars being surrounded by iron of a permeability approaching that of air. The last term it is thought refers to currents in the iron between the bars. Such currents are encouraged by the manufacturing process used for the rotors of these machines in that inter-laminar insulation is provided by the bonding material only and this is known to be not fully effective due to "high spot" contacts. In addition, the squirrel cage rotors are centrifugally cast into the already assembled rotor cores resulting in what must be a fairly good contact between bars and laminations.

However, all these terms represent component resistors all of which carry the same current. This, together with the observations just made and the fact that the test machine had skewed rotor slots, strongly suggests the presence of axial interbar currents as shown in fig.(6.1).

Such paths consist of part bar and part iron and would most likely be characterized by a resistance such as that discovered for the additional rotor branch in the experimentally determined equivalent circuit. Furthermore, the currents in these types of paths would tend to be surface currents due to the influence of the iron, particularly at the higher values of rotor frequency.

Obviously, this calls for further investigation under closely controlled manufacturing conditions for the opinions stated to be ratified or otherwise. Further consideration will be given to this in chapter IX.

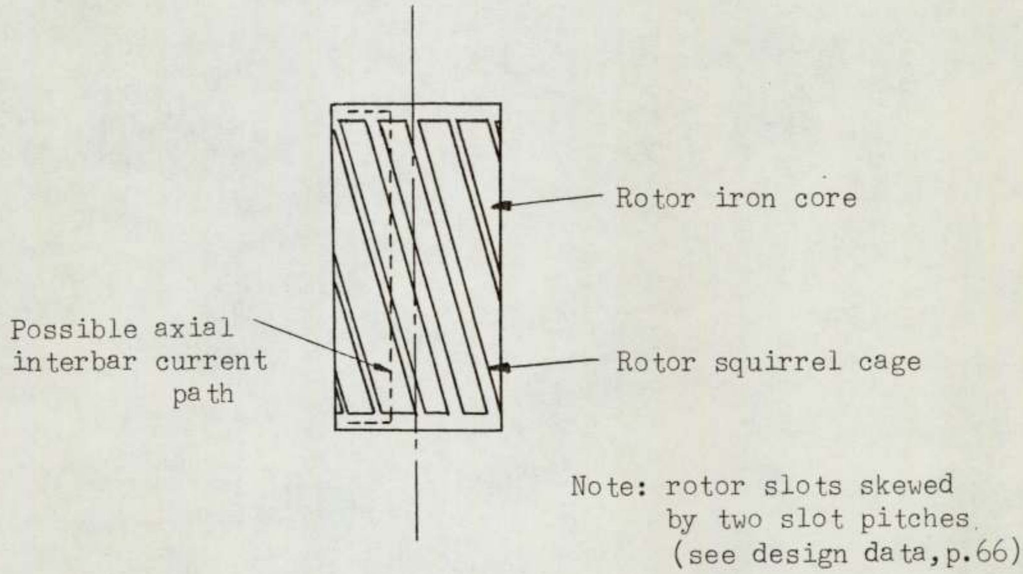

FIG. (6.1). POSSIBLE AXIAL ROTOR CURRENT PATHS.

Consider now the individual tensors:

a) $L\alpha\beta$

In these tensors it is apparent that the estimated inductances are much higher than the measured ones. The reason for this discrepancy has already been mentioned in section (20) where the effect of the manufacturing process on the value of the magnetic air gap was briefly discussed. Thus comparing the values of the mutual inductance $L_{dr\ ds}$ and $L_{qr\ qs}$ with $L_{dr_{'}ds}$ and $L_{qr_{'}qs}$ respectively in the two metric tensors, the estimated value is 2.00 henry and the measured value is 1.51 henry. The estimated figure was obtained by analysis of the machine's magnetic circuit and magnetomotive force waveform; this approach is used in order to allow for the relatively large slot dimension. The result of this analysis gives the magnetising inductance as a function of the effective air gap δ_e, the value of which is obtained from the mechanical gap dimension using the results of Carter's (28) and Binns' (27) work. The same relationship between magnetizing inductance and gap dimension was applied to the determination of the magnetic air gap used in the experimental evaluation of mutual inductance. Consequently, the difference between these two values is due entirely to the difference between the mechanical air gap of 0.05 mm. and the measured magnetic air gap of 0.068 mm.

Remembering that in both of these metric tensors the self inductances are constituted from the magnetizing inductance and the leakage inductance (section (3)) then the difference between the two mutual inductances must affect these self inductances also; this is in addition to the effect of the different air gap dimension on the leakage inductances.

In all these inductances the result of the increased air gap dimension is to decrease their value.

However, reference to section (4) shows that the calculated stator leakage inductance is, with this particular slotting, configuration, little affected by the air gap dimension whereas the calculated rotor leakage inductance is largely dependent upon this value. Thus comparing the calculated values; for the nominal gap dimension of 0.05 mm.,

$L_1 = 0.10$ henry,

$L_2 = 0.071$ henry,

and with the experimentally estimated gap dimension of 0.086 mm.,

$L_1 = 0.097$ henry,

$L_2 = 0.053$ henry.

Consequently, in the elements of the metric tensor the discrepancy in the calculated value of the self inductance L_{ds} and its measured value can be taken as being entirely due to the different value of the magnetizing inductance. On the other hand, the discrepancy in the calculated value of L_{dr} and its measured value is due to difference in both the magnetizing and the leakage inductance. However, in this case also, since the leakage inductance is much smaller than the mutual inductance, the value of L_{dr} can be again considered largely dependent upon the value of this mutual inductance.

In this context the values of the elements of the metric tensor can be misleading.

From what has been said above it might appear that the values of the leakage inductances are, due to their smallness in comparison to the magnetizing inductance, unimportant. Reference to chapter VII will show this not to be the case since the equations for the various currents contain terms such as $(L_{ds} - L_{dsdr})$ which are, in fact, the leakage inductances. It is for this reason that the calculation of the tensor elements L_{ds} and L_{dr} must be made in terms of the mutual inductance and leakage inductance as separate entities. It is for this reason also that the calculation of the leakage inductances is of great importance and it is, therefore, pertinent to consider the method of calculation used in section (4) in the light of the experimental evidence of chapter V insofar as this is possible.

The method used for calculating the leakage inductance is based on the work of Binns (27) which is the first rigorous approach for doubly slotted structures. Thereis,however,an error in his work in that he describes his equations for air gap permeance as being dimensionless. These equations,which are given on page 79 for the stator and on page 91 for the rotor,contain a term $\frac{s_1 s_2 \mu_0}{\delta}$ which is not in fact dimensionless. Binns obtained these equations by a curve fitting process and it has been assumed,therefore,that their form is correct. To overcome the effect of the dimensions in the one term,a scaling factor was introduced to convert from the dimensions used by Binns in his work to those used in this present,or any other,investigation;see introduction to section (4).

With this correction,the value of the stator gap leakage permeance factor Λ_{g1} was calculated and taken to be dependable with the exception of the value used for the air gap as discussed above. The stator slot permeance factor Λ_{s1} was calculated rigorously using the author's own approach. The overhang permeance factor was also obtained using the author's own approach involving a flux plot as opposed to the various "formulae" usually employed. The value of the stator leakage inductance so obtained was taken as the basis for the determination of the experimental parameters. The only indication that can be obtained as to the accuracy of the calculation will come from the comparison of the predicted general performance of the test machine with its measured performance in chapter VIII.

The value of the rotor leakage inductance was similarly calculated but in this case it was subsequently referred to the stator. The method used for referring this value to the stator was developed by the author and is based on the determination of the total inductance of a loop constituted by two adjacent rotor bars. This is in preference to the usual method of determining the inductance per bar and then obtaining an equivalent inductance per phase referred to the stator by applying the relationship obtained between the resistance per bar and the referred rotor resistance per phase. The reason for this is that in the latter method,the mutual coupling between the rotor bars is completely ignored whereas in the former case this mutual coupling is included.

The two values of L_2 so obtained, one for the 0.05mm. airgap and the other for the 0.068mm. airgap, have already been given on page 245. Comparing these with the measured value of 0.078 henry, the value calculated using the mechanical gap differs by -9% from the measured value, whereas the value calculated using the estimated magnetic gap differs by -32%. This suggests that the increased gap should not be used in the leakage permeance calculations but only in the calculation of the magnetising inductance. This is not unreasonable since, as the expression for the total rotor leakage permeance given on page 94 shows, the largest component of the rotor leakage flux is the airgap leakage flux which takes a zig-zag path from the stator bore surface to the rotor bore surface.

By way of further justification of the method developed for obtaining the referred value, had the usual method been employed the two values for L_2 would have been 0.025 henry and 0.018 henry for the 0.05mm. gap and the 0.068mm. gap, respectively. Compared with the measured values these are in error by -68% and -77%, respectively.

The values of rotor moment of inertia compare favourably and require no further comment.

b) $R_{\alpha\beta}$

It is in the measured resistance tensor that the presence of the extra rotor branch is manifest. The estimation of the rotor resistance per phase is based on an analysis given in Trickey's paper.(26) This has been modified by the present author to suit the requirements of the restricted slotting inherent in miniature machines. The method is fully developed in section (4). It does not, however, allow for the presence of current paths of the type which it is thought are associated with new rotor branch in the equivalent circuit. With present knowledge of the effects of the methods of rotor manufacture, it is not possible to make a sensible estimate of the values of the two component resistors in the design stages and, therefore, no comparison can be made. It is, nevertheless, worth noting that the measured resistance of the rotor branch associated with the rotor leakage flux is approximately twice the calculated value. The reliability of the measured values of the resistances of both of the rotor branches wil be assessed from the results of chapter VIII.

The calculated value of the stator resistance per phase turns out to be 4.7% higher than the measured value. Since the estimation of the length of the winding overhang is difficult, this is considered to be a satisfactory comparison.

c) $G_{\alpha\beta}$

The torque tensor is obtained directly from the metric tensor in both cases. No further comments are, therefore, required to those already made concerning the metric tensors.

From the foregoing comparisons it is concluded that the methods proposed for the calculation in the design stages of the stator resistance, stator leakage inductance and rotor leakage inductance yield values close to those indicated by the impedance per unit frequency locus when the mechanical airgap is used. The method employed for the estimation of the magnetising inductance is similarly effective providing the magnetic, as opposed to the simple mechanical, airgap dimension is used. As far as the estimation of the rotor resistance is concerned, in the absence of the results of the further detailed investigation already suggested, it is proposed that, in keeping with what has been observed in this study, the resistance calculated using the method presented in section (4) be doubled and used for the resistance value of the rotor circuit associated with the rotor leakage inductance, and that the resistance of the rotor circuit not associated with this inductance be taken as

$(0.065 + 0.078\sqrt{s|\omega|} + 0.00036|\omega|s)$ x resistance from section(4),

for machines of a similar size to the test machine.

The ultimate efficacy of the measured, and consequently, of the estimated, impedance tensors will become apparent in chapter VIII.

CHAPTER VII.

Calculation of Performance.

23) Equations of Performance and Computer Simulation.

From the analysis carried out in chapter II, substitution of the relationships (5.9), (5.10), (5.11) and the value of the rotor inertia from section (21) into equation (2.5) gives,

$$T = \begin{array}{c|cccccc|} {}_{\alpha}\backslash^{\beta} & d_s & d_{r1} & d_{r2} & q_s & q_{r1} & q_{r2} \\ \hline d_s & & & & & 1.51 & 1.51 \\ d_{r1} & & & & & 1.51 & 1.51 \\ d_{r2} & & & & & 1.51 & 1.59 \\ q_s & & -1.51 & -1.51 & & & \\ q_{r1} & & -1.51 & -1.51 & & & \\ q_{r2} & & -1.51 & -1.59 & & & \\ \hline \end{array} \times \begin{array}{c|c|} \alpha & \\ \hline d_s & i_{ds} \\ d_{r1} & i_{dr1} \\ d_{r2} & i_{dr2} \\ q_s & i_{qs} \\ q_{r1} & i_{qr1} \\ q_{r2} & i_{qr2} \\ \hline \end{array} \times \begin{array}{c|c|} \beta & \\ \hline d_s & i_{ds} \\ d_{r1} & i_{dr1} \\ d_{r2} & i_{dr2} \\ q_s & i_{qs} \\ q_{r1} & i_{qr1} \\ q_{r2} & i_{qr2} \\ \hline \end{array}$$

$$+ 3.3 \times 10^{-7} \times p^2\theta$$

i.e.,

$$\begin{aligned} T = 3.3 \times 10^{-7} \times p^2\theta &- (1.51 i_{qs} + 1.51 i_{qr1} + 1.59 i_{qr2}) i_{dr2} \\ &- (1.51 i_{qs} + 1.51 i_{qr1} + 1.51 i_{qr2}) i_{dr1} \\ &+ (1.51 i_{ds} + 1.51 i_{dr1} + 1.51 i_{dr2}) i_{qr1} \\ &+ (1.51 i_{ds} + 1.51 i_{dr1} + 1.59 i_{dr2}) i_{qr2} \end{aligned} \qquad (7.1)$$

Similarly, substitution into equation (2.7) gives,

$$\begin{array}{c|c|} \beta & \\ \hline d_s & e_{ds} \\ d_{r1} & 0 \\ d_{r2} & 0 \\ q_s & e_{qs} \\ q_{r1} & 0 \\ q_{r2} & 0 \\ \hline \end{array} = \begin{array}{c|cccccc|} {}_{\alpha}\backslash^{\beta} & d_s & d_{r1} & d_{r2} & q_s & q_{r1} & q_{r2} \\ \hline d_s & 233 & & & & & \\ d_{r1} & & 49+(59\sqrt{s\omega}+0.28s\omega) & & & & \\ d_{r2} & & & 1648 & & & \\ q_s & & & & 233 & & \\ q_{r1} & & & & & 49+(59\sqrt{s\omega}+0.28s\omega) & \\ q_{r2} & & & & & & 1648 \\ \hline \end{array} \times \begin{array}{c|c|} \alpha & \\ \hline d_s & i_{ds} \\ d_{r1} & i_{dr1} \\ d_{r2} & i_{dr2} \\ q_s & i_{qs} \\ q_{r1} & i_{qr1} \\ q_{r2} & i_{qr2} \\ \hline \end{array}$$

+ (see over)

$$
\begin{array}{c|cccccc|}
\alpha \backslash \beta & & & & & & \\
\hline
d_s & 1.61 & 1.51 & 1.51 & & & \\
d_{r1} & 1.51 & 1.51 & 1.51 & & & \\
d_{r2} & 1.51 & 1.51 & 1.59 & & & \\
q_s & & & & 1.61 & 1.51 & 1.51 \\
q_{r1} & & & & 1.51 & 1.51 & 1.51 \\
q_{r2} & & & & 1.51 & 1.51 & 1.59 \\
\hline
\end{array}
\quad
\begin{array}{c|c|}
\alpha & \\
\hline
d_s & pi_{ds} \\
d_{r1} & pi_{dr1} \\
d_{r2} & pi_{dr2} \\
\times\ q_s & pi_{qs} \\
q_{r1} & pi_{qr1} \\
q_{r2} & pi_{qr2} \\
\hline
\end{array}
\quad
\begin{array}{c|cccccc|}
\alpha \backslash \beta & & & & & & \\
\hline
d_s & & & & & 1.51 & 1.51 \\
d_{r1} & & & & & 1.51 & 1.51 \\
d_{r2} & & & & & 1.51 & 1.59 \\
-\ q_s & - & 1.51 & -1.51 & & & \\
q_{r1} & - & 1.51 & -1.51 & & & \\
q_{r2} & - & 1.51 & -1.59 & & & \\
\hline
\end{array}
\quad
\begin{array}{c|c|}
\alpha & \\
\hline
d_s & i_{ds} \\
d_{r1} & i_{dr1} \\
d_{r2} & i_{dr2} \\
\times\ q_s & i_{qs} \\
q_{r1} & i_{qr1} \\
q_{r2} & i_{qr2} \\
\hline
\end{array}
\ x p\theta
$$

i.e.,

$$
\begin{aligned}
e_{ds} &= 233i_{ds} + 1.61pi_{ds} + 1.51pi_{dr1} + 1.51pi_{dr2} \\
0 &= (49 + 59\sqrt[+]{s|\omega|} + 0.28s|\omega|)i_{dr1} + 1.51(pi_{ds} + pi_{dr1} + pi_{dr2}) \\
&\qquad + 1.51(i_{qs} + i_{qr1} + i_{qr2})p\theta \\
0 &= 1648i_{dr2} + 1.51(pi_{ds} + pi_{dr1}) + 1.59pi_{dr2} \\
&\qquad + 1.51(i_{qs} + i_{qr1})p\theta + 1.59i_{qr2}p\theta \\
e_{qs} &= 233i_{qs} + 1.61pi_{qs} + 1.51pi_{qr1} + 1.51pi_{qr2} \\
0 &= (49 + 59\sqrt[+]{s|\omega|} + 0.28s|\omega|)i_{qr1} + 1.51(pi_{qs} + pi_{qr1} + pi_{qr2}) \\
&\qquad - 1.51(i_{ds} + i_{dr1} + i_{dr2})p\theta \\
0 &= 1648i_{qr2} + 1.51(pi_{qs} + pi_{qr1}) + 1.59pi_{qr2} \\
&\qquad - 1.51(i_{ds} + i_{dr1})p\theta - 1.59i_{dr2}p\theta
\end{aligned}
\tag{7.2}
$$

Equations (7.1) and (7.2) describe the complete performance of the machine. For computer simulation it is necessary, because of the number of multiplications involved in the solution of these equations, to use a digital computer; the problem lends itself to a continuous system modelling programme.[31] In this, to avoid numerical instability, the equations (7.2) must be reformed into six equations each containing only one term of the form pi, i.e. equation (2.7) needs to be restated as

$$pi^{\alpha} = \frac{1}{L_{\alpha\beta}}\left[e_{\beta} - R_{\alpha\beta}i^{\alpha} + G_{\alpha\beta}i^{\alpha}p\theta\right], \text{writing } i^{\alpha} \text{ for } \dot{x}^{\alpha}. \tag{7.3}$$

Since the index t is omitted in the voltage equation, the tensor $L_{\alpha\beta}$

becomes a bivalent tensor which, from equation (5.9) is seen to be of the compound form

$$\begin{array}{c|c|c|} \alpha\backslash\beta & & \\ \hline & Z_d & 0 \\ \hline & 0 & Z_q \\ \hline \end{array}$$

and its inverse is then

$$\begin{array}{c|c|c|} \alpha\backslash\beta & & \\ \hline & Z_d^{-1} & 0 \\ \hline & 0 & Z_q^{-1} \\ \hline \end{array}$$

Again from equation (5.9), Z_d and Z_q are given by

$$Z_d = \begin{array}{c|c|c|c|} \alpha\backslash\beta & d_s & d_{r1} & d_{r2} \\ \hline d_s & g & l & m \\ \hline d_{r1} & l & h & n \\ \hline d_{r2} & m & n & k \\ \hline \end{array} \qquad \text{and } Z_q = \begin{array}{c|c|c|c|} \alpha\backslash\beta & q_s & q_{r1} & q_{r2} \\ \hline q_s & g & l & m \\ \hline q_{r1} & l & h & n \\ \hline q_{r2} & m & n & k \\ \hline \end{array}$$

in which

$g = L_1 = 1.61$

$h = L_{21} = 1.51$

$k = L_{22} = 1.59$

$m = M_{1,22} = 1.51$

$n = M_{21,22} = 1.51$

$l = M_{1,21} = 1.51$

values referred to stator.
(Suffices: 1, stator winding
21, rotor winding without leakage flux
22, rotor winding with leakage flux.)

Inverting,

$$Z_d^{-1} = \begin{array}{c|c|c|c|} \alpha\backslash\beta & d_s & d_{r1} & d_{r2} \\ \hline d_s & a & d & e \\ \hline d_{r1} & d & b & f \\ \hline d_{r2} & e & f & c \\ \hline \end{array} \times \frac{1}{D}, \qquad Z_q^{-1} = \begin{array}{c|c|c|c|} \alpha\backslash\beta & q_s & q_{r1} & q_{r2} \\ \hline q_s & a & d & e \\ \hline q_{r1} & d & b & f \\ \hline q_{r2} & e & f & c \\ \hline \end{array} \times \frac{1}{D}$$

where

$$\begin{aligned} a &= hk - n^2 \\ b &= gk - m^2 \\ c &= gh - l^2 \\ d &= mn - lk \\ e &= ln - mh \\ f &= ml - gn \end{aligned} \qquad (7.4)$$

and $D = ghk + lnm + mln - gn^2 - kl^2 - hm^2$

Therefore,

$$\frac{1}{L_{\alpha\beta}} = \begin{array}{c|cccccc} {}_{\alpha}\diagdown^{\beta} & d_s & d_{r1} & d_{r2} & q_s & q_{r1} & q_{r2} \\ \hline d_s & a & d & e & & & \\ d_{r1} & d & b & f & & & \\ d_{r2} & e & f & c & & & \\ q_s & & & & a & d & e \\ q_{r1} & & & & d & b & f \\ q_{r2} & & & & e & f & c \end{array} \times \frac{1}{D}$$

In a similar way, let $R_{\alpha\beta}$ and $G_{\alpha\beta}$ (equations (5.10) and (5.11) respectively) be represented algebraically as

$$R_{\alpha\beta} = \begin{array}{c|cccccc} {}_{\alpha}\diagdown^{\beta} & d_s & d_{r1} & d_{r2} & q_s & q_{r1} & q_{r2} \\ \hline d_s & v & & & & & \\ d_{r1} & & w & & & & \\ d_{r2} & & & u & & & \\ q_s & & & & v & & \\ q_{r1} & & & & & w & \\ q_{r2} & & & & & & u \end{array}$$

$$G_{\alpha\beta} = \begin{array}{c|cccccc} {}_{\alpha}\diagdown^{\beta} & d_s & d_{r1} & d_{r2} & q_s & q_{r1} & q_{r2} \\ \hline d_s & & & & & l & m \\ d_{r1} & & & & & h & n \\ d_{r2} & & & & & n & k \\ q_s & & -l & -m & & & \\ q_{r1} & & -h & -n & & & \\ q_{r2} & & -n & -k & & & \end{array}$$

where,

$$v = R_1 = 233$$

$$w = R_{21} = 49 + 59\,{}^{+}\!\sqrt{s|\omega|} + 0.28s|\omega| \quad \text{values referred to stator.}$$

$$u = R_{22} = 1648$$

the other symbols having been already defined.

Then,

$$R_{\alpha\beta}i^{\alpha} = \begin{array}{|c|c|c|c|c|c|} \multicolumn{1}{c}{d_s} & \multicolumn{1}{c}{d_{r1}} & \multicolumn{1}{c}{d_{r2}} & \multicolumn{1}{c}{q_s} & \multicolumn{1}{c}{q_{r1}} & \multicolumn{1}{c}{q_{r2}} \\ \hline v i_{ds} & w i_{dr1} & u i_{dr2} & v i_{qs} & w i_{qr1} & u i_{qr2} \\ \hline \end{array}$$

and

$$G_{\alpha\beta}i^{\alpha}p\theta = \begin{array}{|c|c|c|c|c|c|} \multicolumn{1}{c}{d_s} & \multicolumn{1}{c}{d_{r1}} & \multicolumn{1}{c}{d_{r2}} & \multicolumn{1}{c}{q_s} & \multicolumn{1}{c}{q_{r1}} & \multicolumn{1}{c}{q_{r2}} \\ \hline -(l i_{qs} + h i_{qr1} + n i_{qr2})p\theta & -(m i_{qs} + n i_{qr1} + k i_{qr2})p\theta & & & (l i_{ds} + h i_{dr1} + n i_{dr2})p\theta & (m i_{ds} + n i_{dr1} + k i_{dr2})p\theta \\ \hline \end{array}$$

Remembering that $e_\beta = \begin{array}{cccccc} d_s & d_{r1} & d_{r2} & q_s & q_{r1} & q_{r2} \\ \hline e_{ds} & 0 & 0 & e_{qs} & 0 & 0 \end{array}$ then

$$e_\beta - R_{\alpha\beta} i^\alpha + G_{\alpha\beta} i^\alpha p\theta = \begin{array}{cccccc} d_s & d_{r1} & d_{r2} & q_s & q_{r1} & q_{r2} \\ \hline r & s & t & x & y & z \end{array}$$

where,

$$\begin{aligned} r &= e_{ds} - v i_{ds} \\ s &= -(l i_{qs} + h i_{qr1} + n i_{qr2}) p\theta - w i_{dr1} \\ t &= -(m i_{qs} + n i_{qr1} + k i_{qr2}) p\theta - u i_{dr2} \\ x &= e_{qs} - v i_{qs} \\ y &= (l i_{ds} + h i_{dr1} + n i_{dr2}) p\theta - w i_{qr1} \\ z &= (m i_{ds} + n i_{dr1} + k i_{dr2}) p\theta - u i_{qr2} \end{aligned} \tag{7.5}$$

whence equation (7.3) is

$$p i^\alpha = \frac{1}{D} \times \begin{array}{cccccc} d_s & d_{r1} & d_{r2} & q_s & q_{r1} & q_{r2} \\ \hline ar + ds + et & dr + bs + ft & er + fs + ct & ax + dy + ez & dx + by + fz & ex + fy + cz \end{array} \tag{7.6}$$

For convenience in constructing the computer flow diagram it is helpful to rewrite equation (7.1) in terms of the symbols used above and, for completeness, the friction constant F, which was omitted in equation (7.1), will be included and then made negligibly small in the computer model. Thus,

$$\begin{aligned} T = Fp\theta + Jp^2\theta &- (l i_{qs} + h i_{qr1} + n i_{qr2}) i_{dr1} \\ &- (m i_{qs} + n i_{qr1} + k i_{qr2}) i_{dr2} \\ &+ (l i_{ds} + h i_{dr1} + n i_{dr2}) i_{qr1} \\ &+ (m i_{ds} + n i_{dr1} + k i_{dr2}) i_{qr2} \end{aligned} \tag{7.6a}$$

i.e. $$T = Fp\theta + Jp^2\theta - l(i_{qs} i_{dr1} - i_{ds} i_{qr1}) - m(i_{qs} i_{dr2} - i_{ds} i_{qr2}) \tag{7.7}$$

Using equations (7.5),(7.6) and (7.7) the computer flow diagram for the machine simulation is constructed in terms of the symbols used above and a computer time scaling factor T_s. This diagram is given in fig.(7.1).

The supply voltage equations are

$$e_{ds} = \hat{V}_R \cos\omega t, \quad \text{reference voltage}$$

$$e_{qs} = \hat{V}_C \sin n\omega t, \quad \text{control voltage}$$

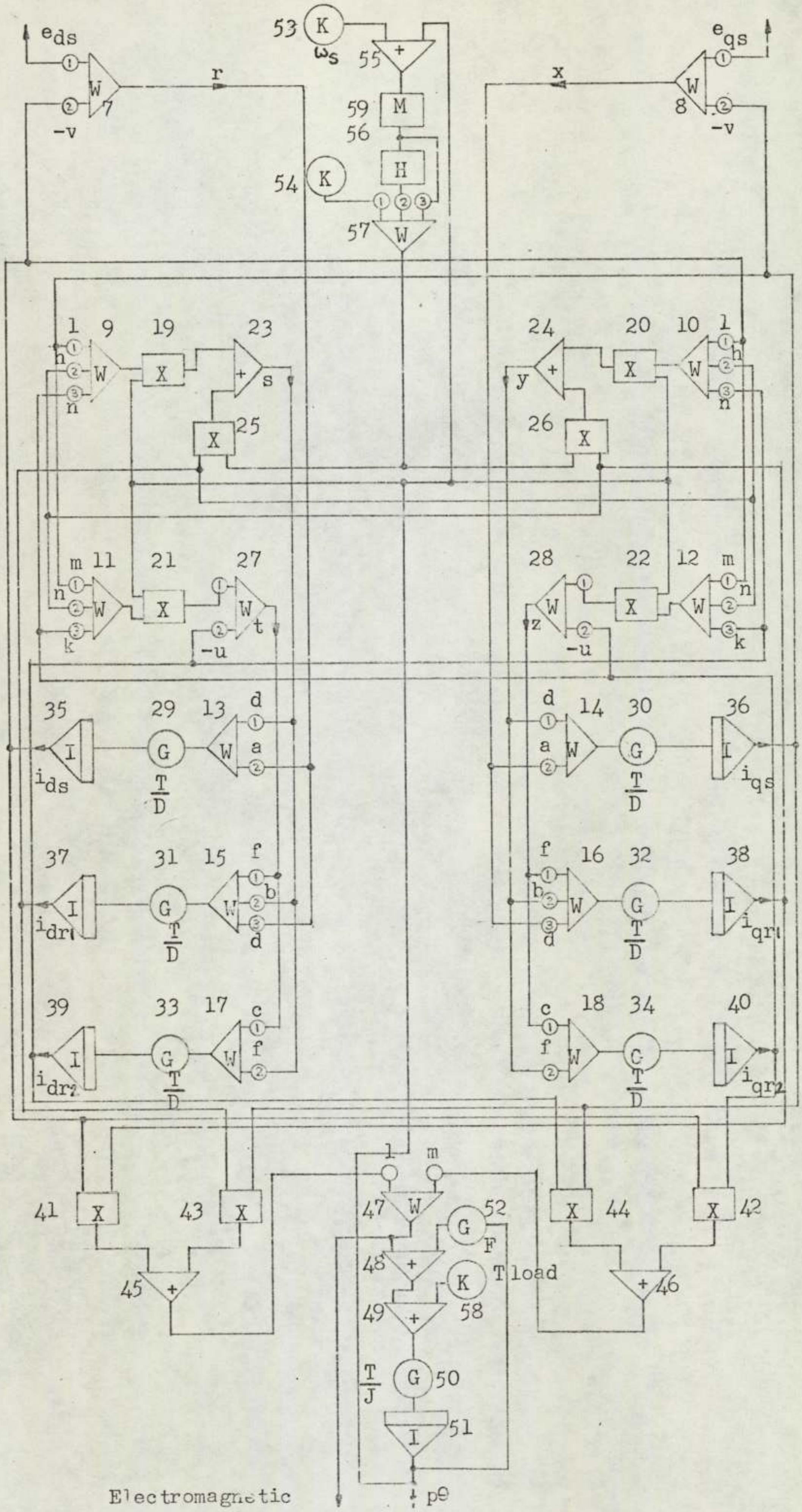

FIG.(7.1). COMPUTER FLOW DIAGRAM FOR MACHINE SIMULATION.

Let $\hat{V}_C = Q\hat{V}_R$ where $0 < Q < 1$.

e_{ds} and e_{qs} are then related by the differential equations

$$p^2 e_{ds} + \omega^2 e_{ds} = 0$$

$$\frac{1}{Q} e_{qs} = -\frac{1}{\omega} p e_{ds} \tag{7.8}$$

The computer flow diagram simulating equations (7.8) and, thereby, the supply system is given in fig.(7.2). To enable the control voltage in the model to be initiated at any desired point in its waveform, a simulated point on wave switch is included in fig.(7.2).

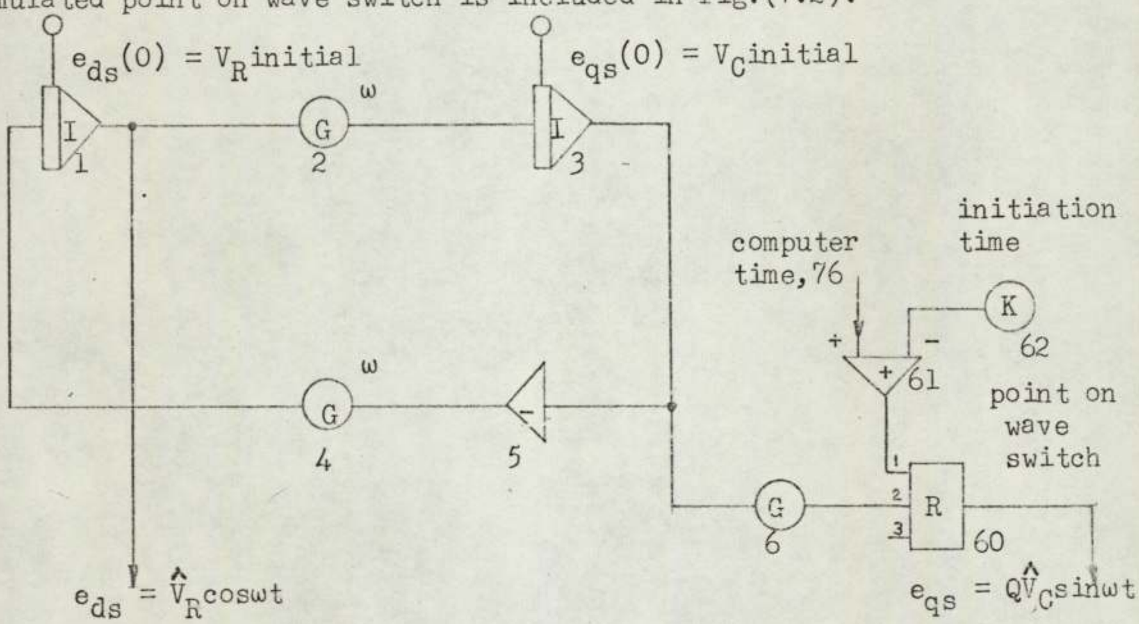

FIG.(7.2). COMPUTER FLOW DIAGRAM FOR SUPPLY SYSTEM SIMULATION.

The computer configuration specification for the flow diagrams is tabulated on the next page and is followed by a table of the initial conditions for a supply frequency of 400 Hz. and a computer time scaling factor of 1000.

KEY:

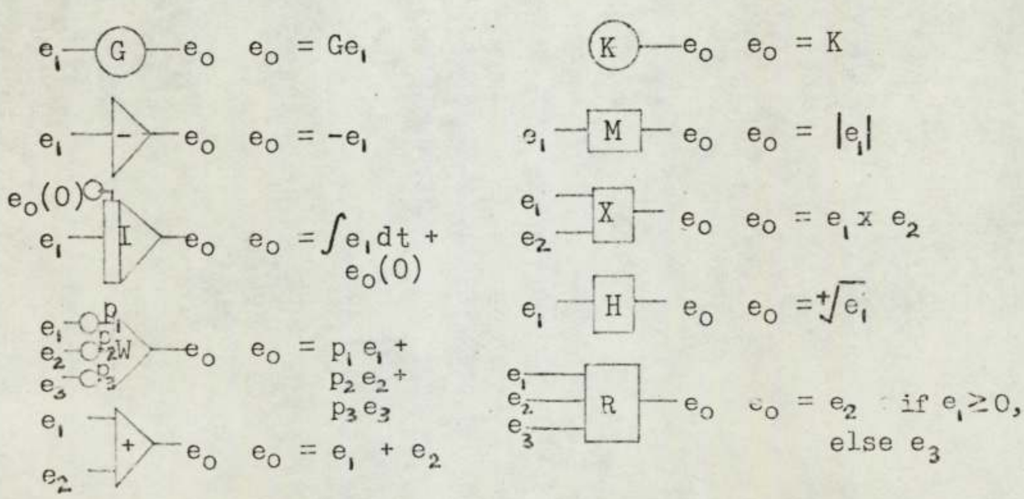

Configuration specification:

Block No.	Type.	Input:1	2	3	Block No.	Type.	Input:1	2	3
1	I	4			32	G	16		
2	G	1			33	G	17		
3	I	2			34	G	18		
4	G	5			35	I	29		
5	-	3			36	I	30		
6	G	3			37	I	31		
7	W	1	35		38	I	32		
8	W	60	36		39	I	33		
9	W	36	38	40	40	I	34		
10	W	35	37	39	41	X	35	38	
11	W	36	38	40	42	X	35	40	
12	W	35	37	39	43	X	37	36	
13	W	23	7		44	X	39	36	
14	W	24	8		45	+	-41	43	
15	W	27	23	7	46	+	-42	44	
16	W	28	24	8	47	W	45	46	
17	W	27	23		48	+	47	-52	
18	W	28	24		49	+	48	58	
19	X	9	51		50	G	49		
20	X	10	51		51	I	50		
21	X	11	51		52	G	51		
22	X	12	51		53	K			
23	+	-19	-25		54	K			
24	+	20	-26		55	+	53	-51	
25	X	57	37		56	H	59		
26	X	57	38		57	W	54	56	59
27	W	21	39		58	K			
28	W	22	40		59	M	55		
29	G	13			60	R	61	6	
30	G	14			61	+	76	-62	
31	G	15			62	K			
					76	computer time.			

Initial conditions:

Block No.	Parameter:1	2	3	Block No.	Parameter:1	2	3
1	V_R initial			34	0.08278		
2	2.514			47	1.51	1.51	
3	V_C initial			50	3035.0		
4	2.514			52	0.1×10^{-5}		
6	Q for test			53	2514.0		
7	1.0	-233.0		54	49.0		
8	1.0	-233.0		57	1.0	59.0	0.28
9	1.51	1.51	1.51	58	0.1×10^{-8}		
10	1.51	1.51	1.51	62	initiation time		
11	1.51	1.51	1.59		for test.		
12	1.51	1.51	1.59				
13	-0.1208	0.1208					
14	-0.1208	0.1208					
15	-0.1510	0.2798	-0.1208				
16	-0.1510	0.2798	-0.1208				
17	0.1510	-0.1510					
18	0.1510	-0.1510					
27	-1.0	-1648.0					
28	1.0	-1648.0					
29	0.08278						
30	0.08278						
31	0.08278						
32	0.08278						
33	0.08278						

24) Steady State Performance.

For economy of computer time this performance is calculated using the steady state representation of the impedance tensor in the form of the equivalent circuit per phase, fig.(7.3), in conjunction with Koopman's (2) method of analysis as outlined in section (1).

Characteristics corresponding to tests a, b, c, d and e, section(13), are determined, sample calculations being given in each case. The results are presented graphically, the measured curve, obtained in section (13), being included for the comparisons in chapter VIII.

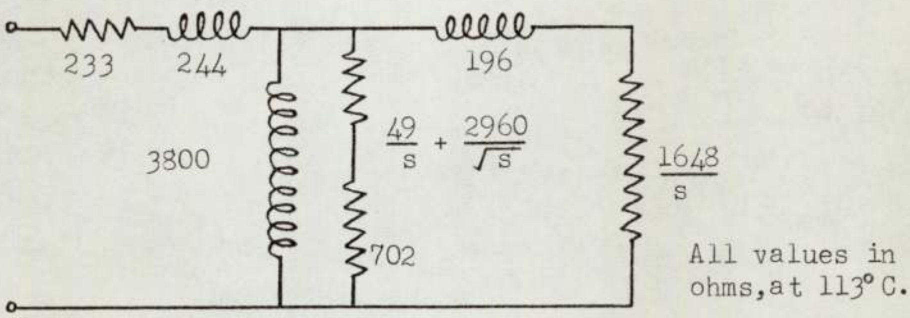

FIG.(7.3). STEADY STATE EQUIVALENT CIRCUIT PER PHASE.

a) Characteristics for balanced rated voltage, rated frequency, variable speed covering slip range 0 - 2.0.

At s = 0.2,

$$\text{total impedance} = 233 + j244\left[\frac{1}{j3800} + \frac{1}{7007} + \frac{1}{8240 + j196}\right]^{-1}$$

$$= 2101 + j2124$$

$$= 2987 \text{ ohms/phase.}$$

$$\text{Phase current} = \frac{117}{2987} = 39.2 \text{ mA.}$$

$$\text{Input power} = 39.2^2 \times 10^{-6} \times 2101 = 3.23 \text{ watts/phase.}$$

$$\text{Stator copper loss} = 39.2^2 \times 10^{-6} \times 233 = 0.357 \text{ watts/phase.}$$

Hence, torque $=(3.23 - 0.357) \times 2$ synchronous watts

$$= 2.29 \times 10^{-3} \text{ Nm.}$$

At s = 1.8,

$$\text{total impedance} = 233 + j244 + \left[\frac{1}{j3800} + \frac{1}{2931} + \frac{1}{915 + j196}\right]^{-1}$$

$$= 880 + j470$$

i.e. total impedance = 997 ohms/phase.

$$\text{Phase current} = \frac{117}{997} = 117.2 \text{ mA.}$$

Input power from source = $117.2^2 \times 10^{-6} \times 880 = 12.1$ watts/phase.

Stator copper loss = $117.2^2 \times 10^{-6} \times 233 = 3.18$ watts/phase.

For slips in excess of 1.0, the rotor power is made up of electrical power form the source and mechanical power from the driving motor. The total power supplied to the rotor is completely dissipated as copper loss since the machine is operating as a brake. Hence,

$$\begin{matrix}\text{(total input power - stator copper loss) +} \\ \text{mechanical input to rotor}\end{matrix} = I_2^2 R_2$$

But the rotor power as indicated by the equivalent circuit is the electrical power input only and is given by $I_2^2 R_2/s$ or,

(total electrical input - stator copper loss).

Hence, the total rotor power is given by

s(total electrical input - stator copper loss)

and is the developed torque in synchronous watts.

In this particular case then,

total rotor power = 1.8(12.1 - 3.18) watts/phase

and developed torque = 2 x 1.8(12.1 - 3.18) synchronous watts

$= 12.8 \times 10^{-3}$ Nm.

Graphs of phase current, total input power and torque as functions of slip are given in figs.(7.4),(7.5) and (7.6), respectively.

b) Characteristics for unbalanced voltage, rated frequency, variable speed covering slip range 0 - 1.0.

Reference phase set at rated voltage 117.0 volts, control phase set at approximately 50% rated voltage, 64.0 volts.

$$\text{Forward sequence voltage, } V_f = \frac{117 + 64}{2} = 90.5 \text{ volts.}$$

$$\text{Backward sequence voltage, } V_b = \frac{117 - 64}{2} = 26.5 \text{ volts}$$

(equations (1.5)&(1.6)).

At forward sequence slip 0.2, from the calculation of the torque for

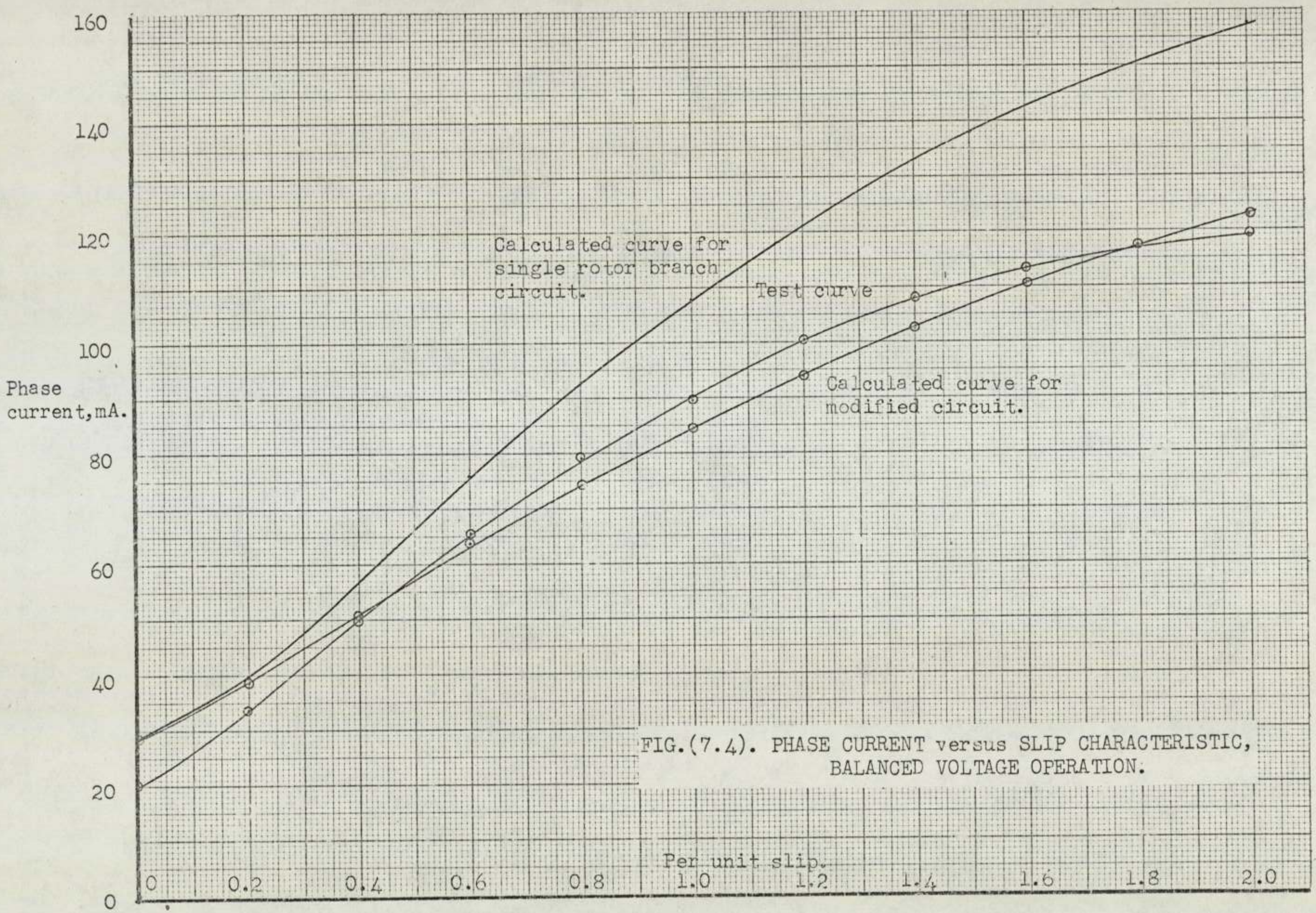

FIG.(7.4). PHASE CURRENT versus SLIP CHARACTERISTIC, BALANCED VOLTAGE OPERATION.

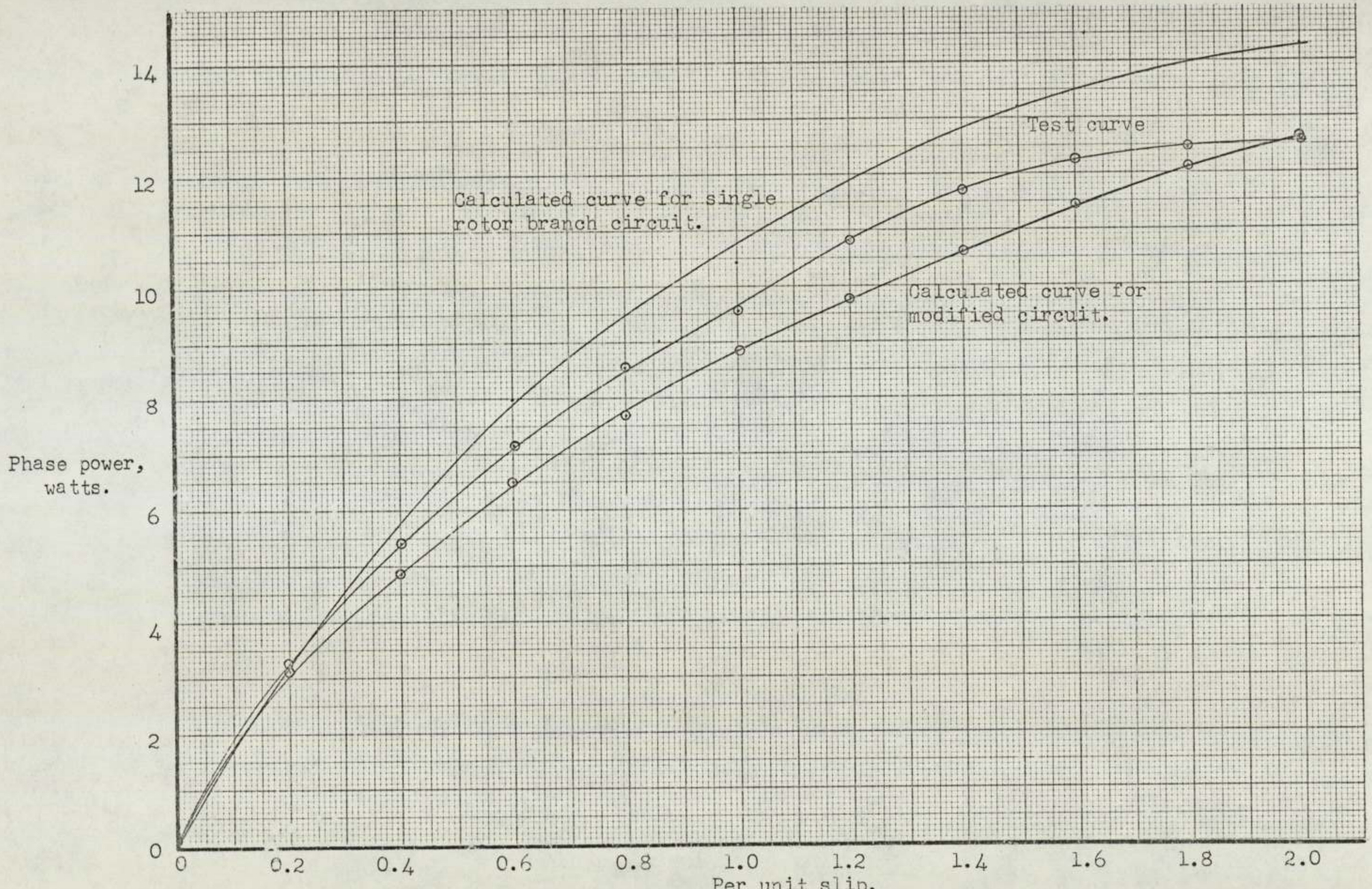

FIG.(7.5). PHASE POWER versus SLIP CHARACTERISTIC, BALANCED VOLTAGE OPERATION.

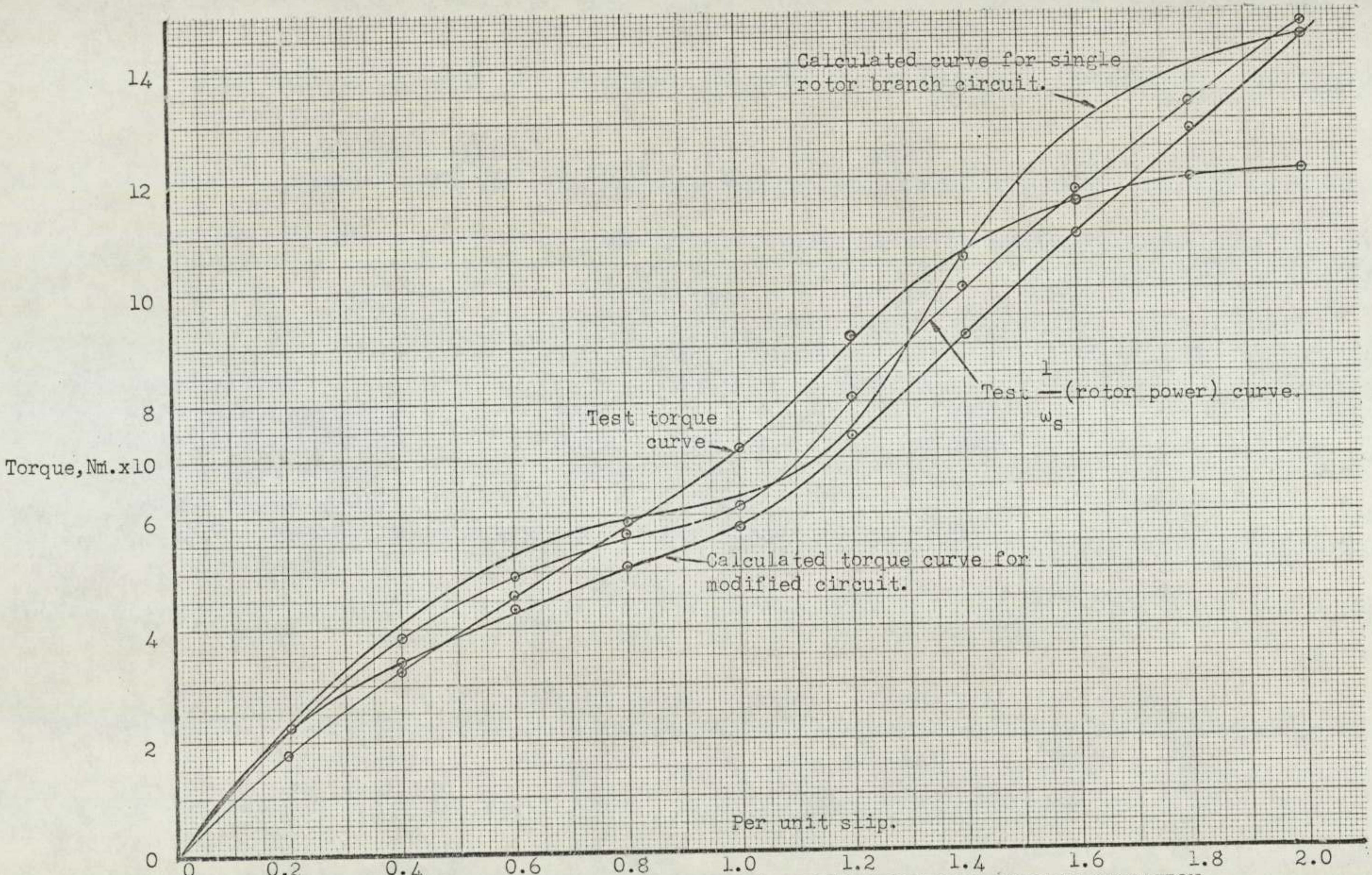

FIG.(7.6). TORQUE versus SLIP CHARACTERISTIC, BALANCED VOLTAGE OPERATION.

balanced voltage operation at slip 0.2,

$$\text{forward torque} = 2.24 \times \left[\frac{90.5}{117.0}\right]^2 \times 10^{-3}$$

$$= 1.34 \times 10^{-3}\,\text{Nm}.$$

Backward sequence slip = (2.0 - 0.2)

Hence from the torque calculated for slip 1.8,balanced voltage operation

$$\text{backward torque} = 12.8 \times \left[\frac{26.5}{117.0}\right]^2 \times 10^{-3} \qquad \text{(equation(1.8))}$$

$$= 0.655 \times 10^{-3}\,\text{Nm}.$$

$$\text{Therefore, net forward torque} = (1.34 - 0.655) \times 10^{-3} \qquad \text{(equation (1.10))}$$

$$= 0.685 \times 10^{-3}\,\text{Nm}.$$

From the current calculated at slip 0.2,balanced voltages,

$$\text{forward sequence current}, I_f = 39.2 \times \frac{V_f}{V_{rated}}\ \text{mA}.$$

$$= 39.2 \times \frac{90.5}{117.0}$$

$$= 30.35\ \text{mA}.$$

and from the impedance calculated at slip 0.2,

forward sequence power factor = 0.704 lag.

i.e. forward sequence current = 30.35(0.704 - j0.71) mA with respect to V_f.

Also,from the current calculated at slip 1.8,balanced voltages,

$$\text{backward sequence current}, I_b = 117.2 \times \frac{V_b}{V_{rated}}\ \text{mA}.$$

$$= 117.2 \times \frac{26.5}{117.0}$$

$$= 26.6\ \text{mA}.$$

and from the impedance calculated at slip 1.8,

backward sequence power factor = 0.883 lag.

i.e. backward sequence current = 26.6(0.883 - j0.469) with respect to V_b.

Hence,reference phase current, $I_R = I_f + I_b$

$$= 30.35(0.704 - j0.71) + 26.6(0.833 - j0.469)$$

$$= 44.85 - j33.99$$

$$= 56.2\ \text{mA}.$$

and the control phase current, $I_C = I_f - I_b$

i.e. $I_C = -2.15 - j9.07$

$= -9.3$ mA. (negative sign indicates a phase angle greater than 90° lag.)

Reference phase power $= V_R I_R \cos \phi_R$

$= 117 \times 44.85 \times 10^{-3}$

$= 5.24$ watts.

Control phase power $= V_C I_C \cos \phi_C$

$= 64 \times -2.65 \times 10^{-3}$

$= -0.17$ watts.

Graphs of torque, control phase and reference phase powers, control phase and reference phase currents as functions of slip are presented in figs.(7.7),(7.8) and (7.9), respectively.

c) Characteristics for the same conditions as (b) but with the control phase voltage set at zero and the winding short circuited.

In this case the processes of calculation are identical to those used for (b), the only difference being in the values of the forward and backward sequence voltages, thus,

$$V_f = \frac{117.0 + 0}{2} = 58.5 \text{ volts}$$

$$V_b = \frac{117.0 - 0}{2} = 58.5 \text{ volts.}$$

Graphs of torque, control phase and reference currents and reference phase power to a base of slip are given in figs.(7.10),(7.11) and (7.12), respectively.

d) Characteristics for a steady speed of 50% synchronous speed, rated reference voltage and variable control voltage covering a range of 0 - 117.0 volts.

For $V_C = 60$ volts,

$$\text{forward sequence voltage} = \frac{117 + 60}{2} = 88.5 \text{ volts}$$

$$\text{backward sequence voltage} = \frac{117 - 60}{2} = 28.5 \text{ volts.}$$

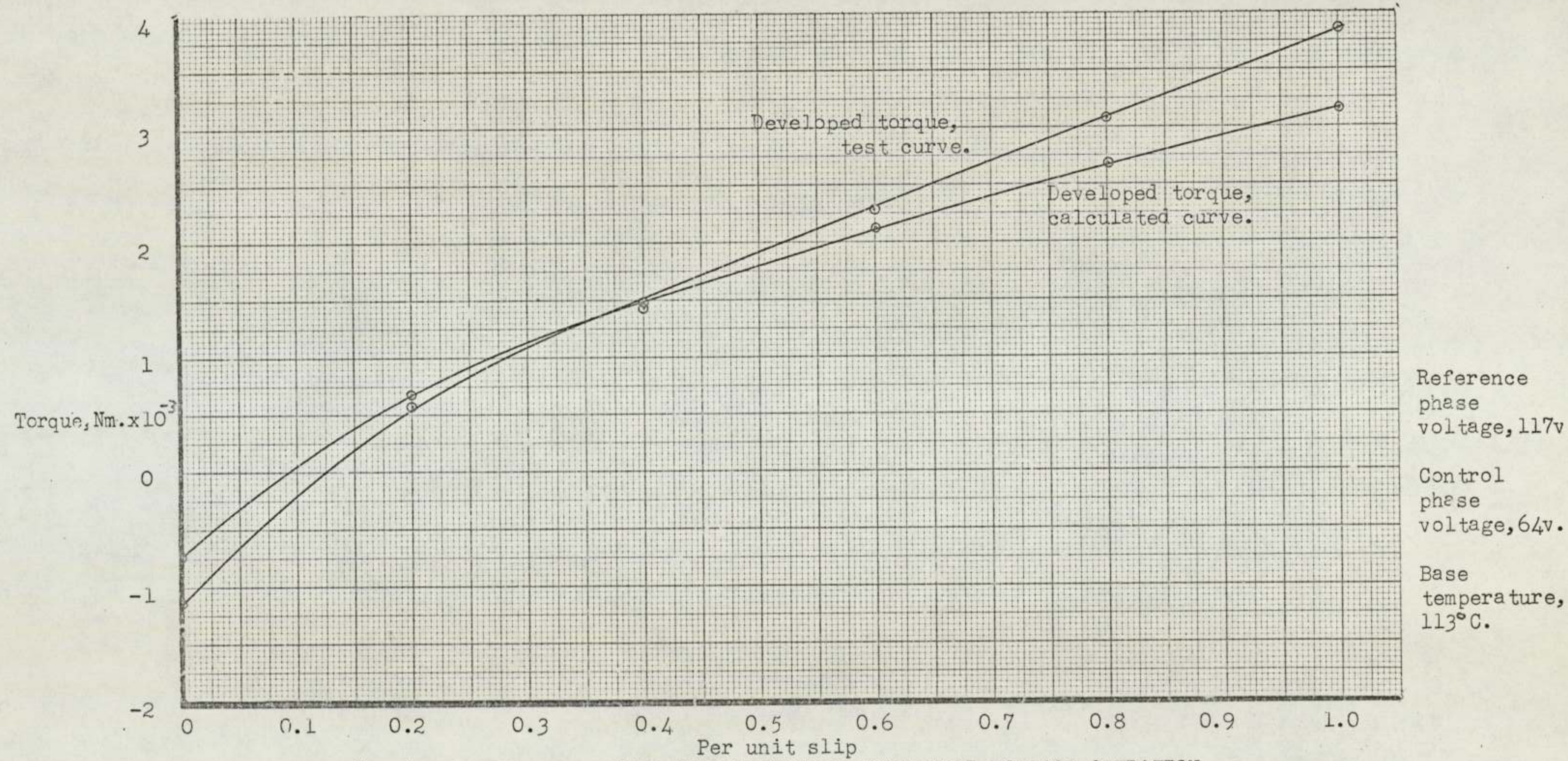

FIG.(7.7). TORQUE versus SLIP CHARACTERISTIC, UNBALANCED VOLTAGE OPERATION.

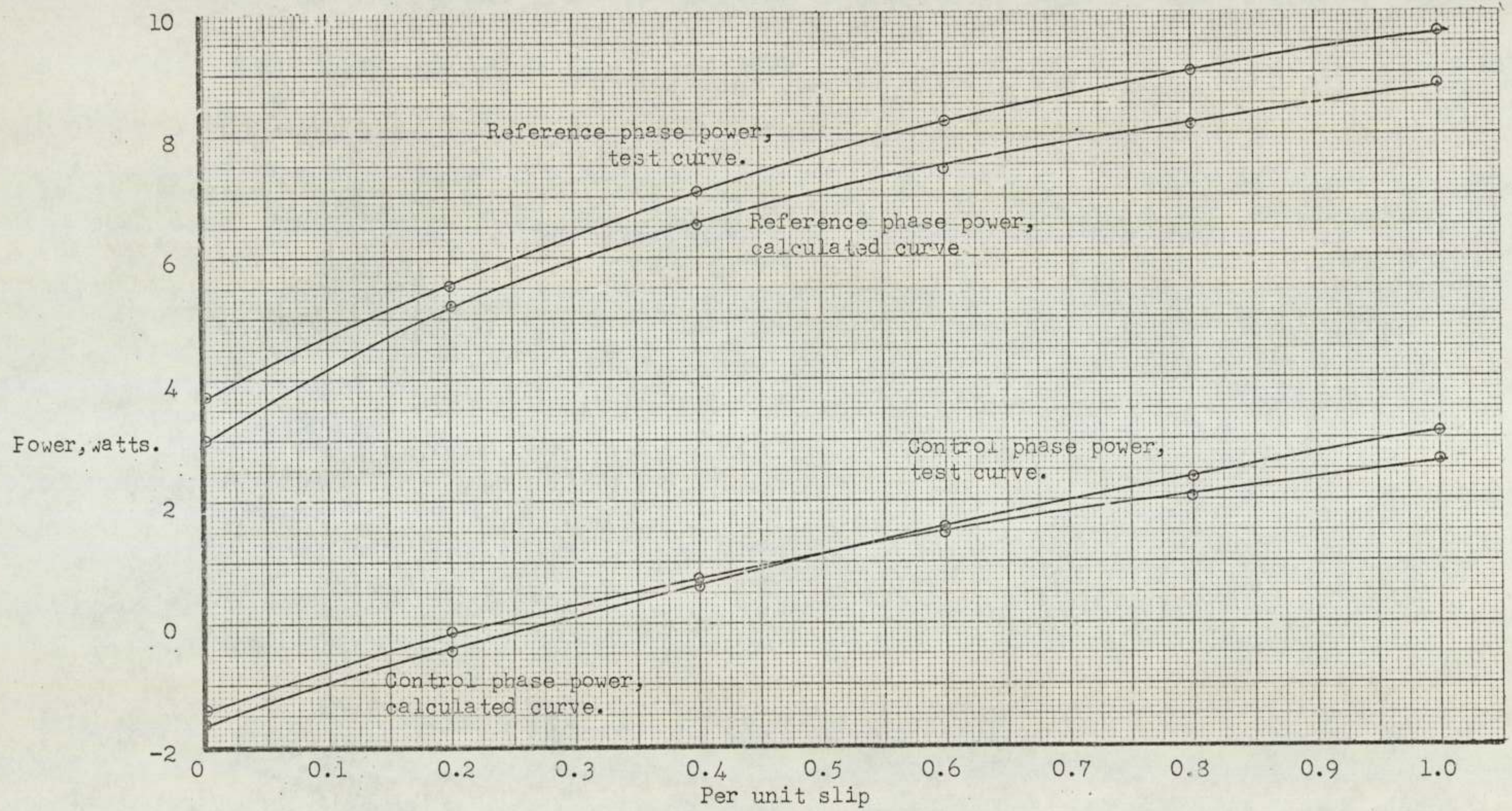

FIG.(7.8). CURRENT versus SLIP CHARACTERISTIC CORRESPONDING TO FIG.(7.7).

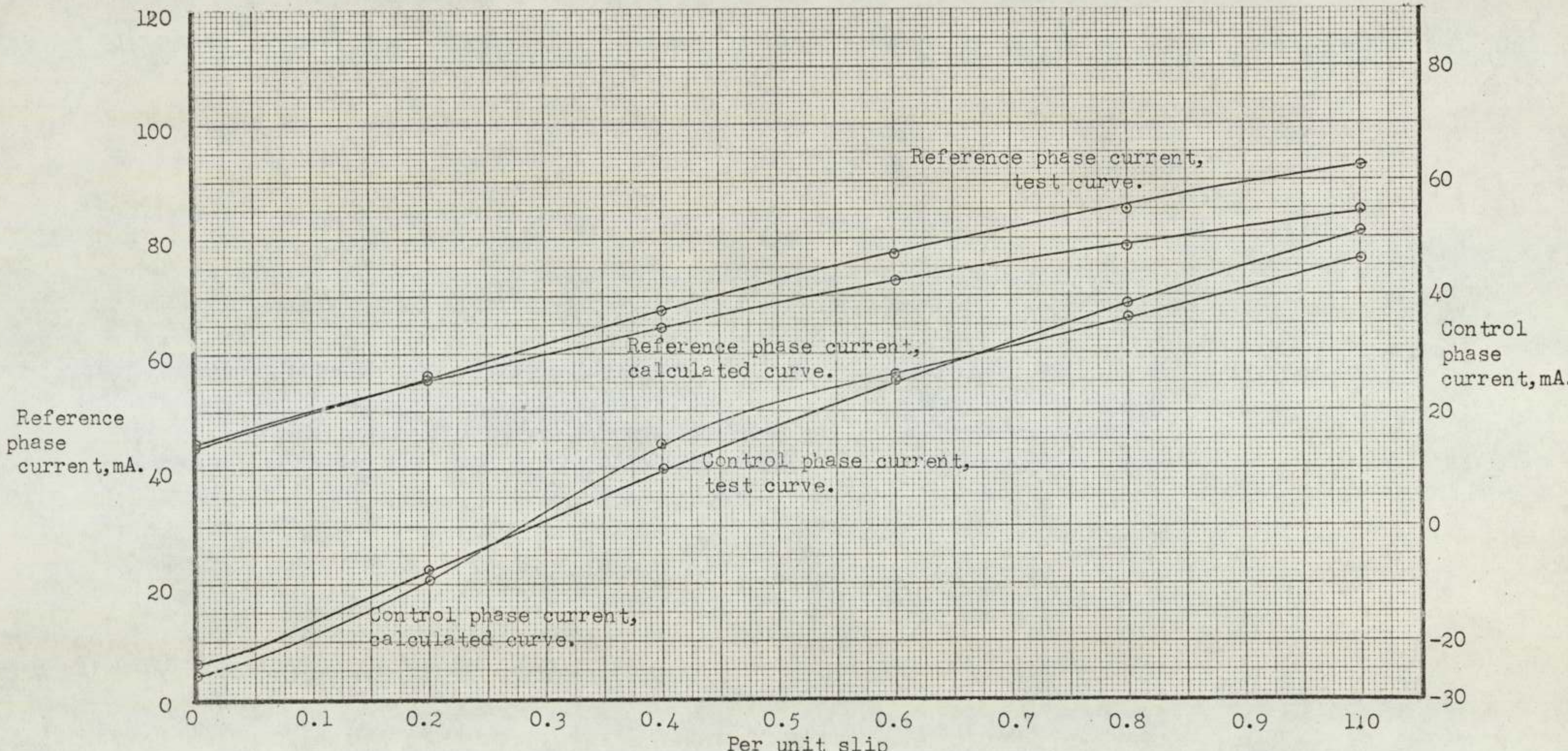

FIG.(7.9). CURRENT versus SLIP CHARACTERISTIC CORRESPONDING TO FIG.(7.7).

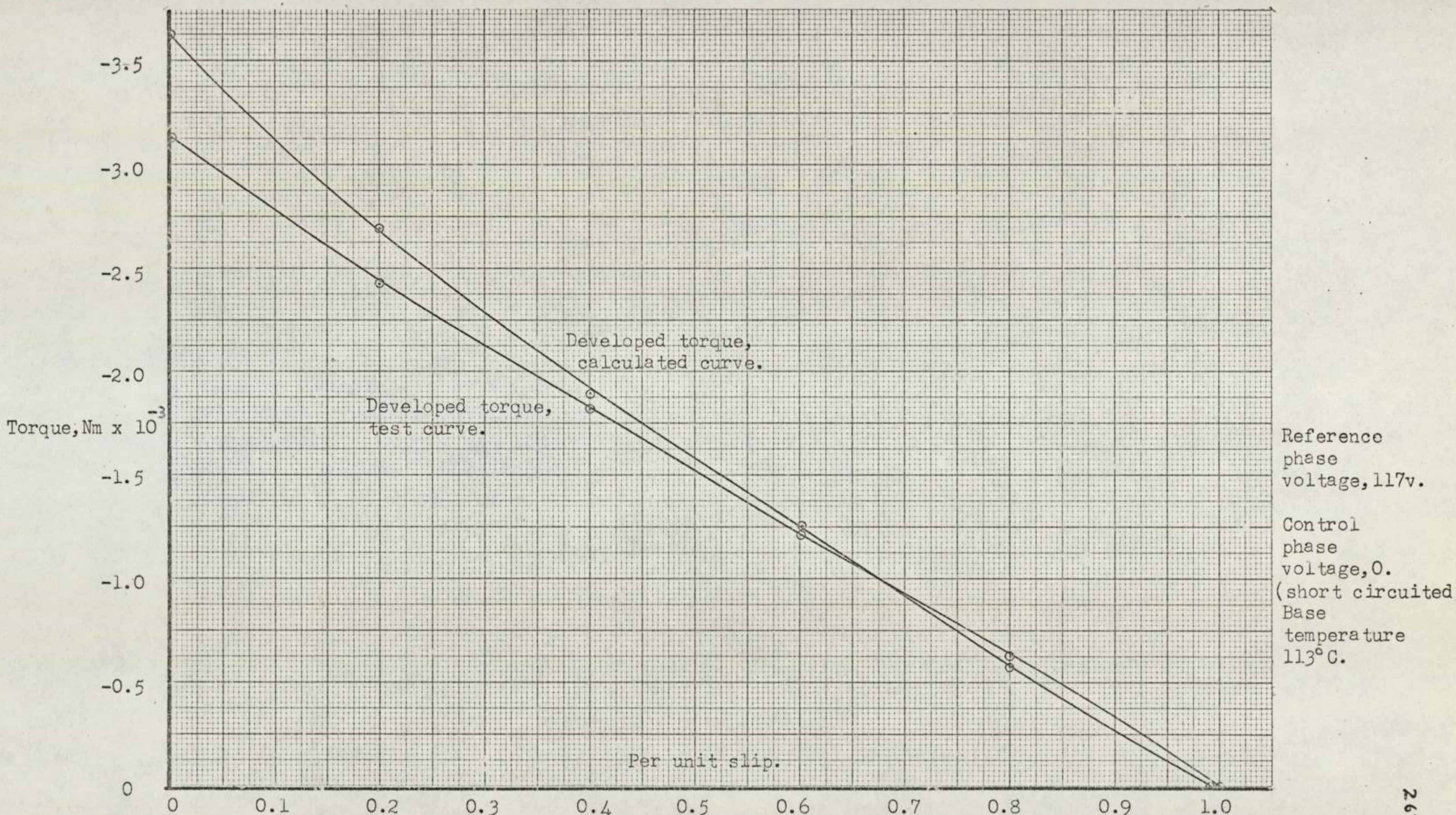

FIG.(7.10). TORQUE versus SLIP CHARACTERISTIC, UNBALANCED VOLTAGE OPERATION.

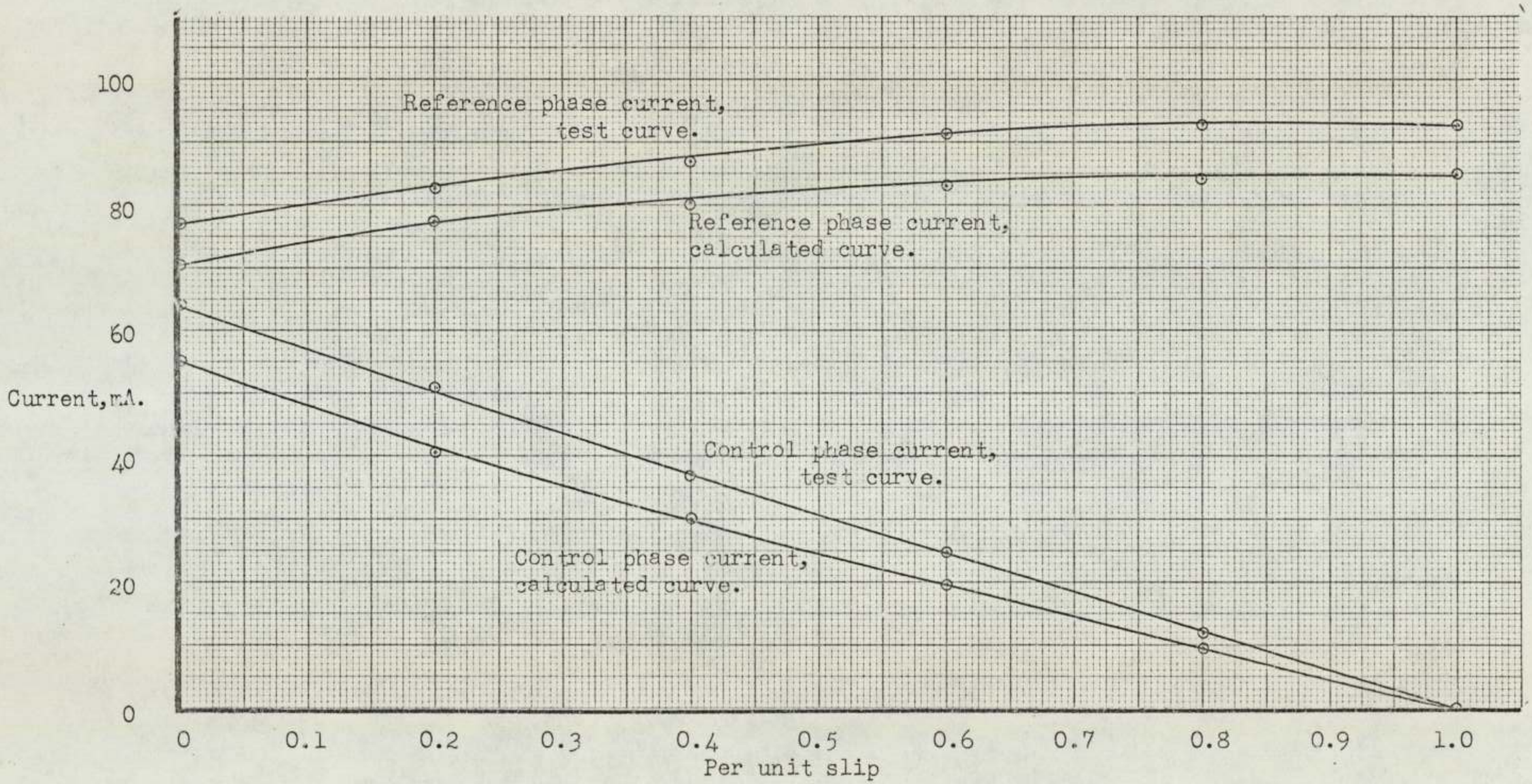

FIG.(7.11). CURRENT versus SLIP CHARACTERISTIC CORRESPONDING TO FIG.(7.10).

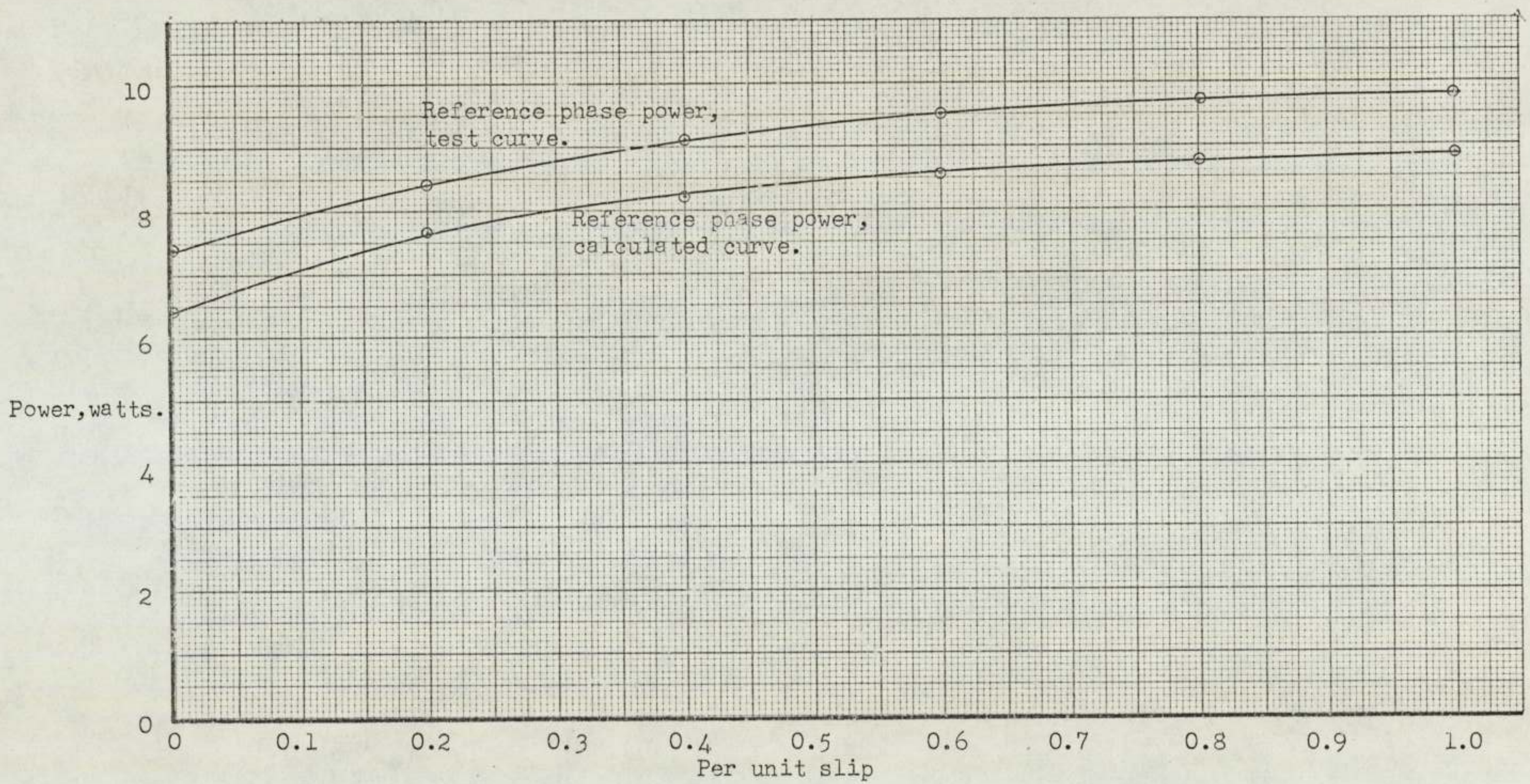

FIG.(7.12). POWER versus SLIP CHARACTERISTIC CORRESPONDING TO FIG.(7.10).

Forward sequence slip = 0.5, backward sequence slip = 1.5.

Therefore, from fig. (7.6),

$$\text{forward sequence torque} = 4.65 \times \left[\frac{88.5}{117.0}\right]^2 \times 10^{-3}$$

$$= 2.6 \times 10^{-3}\ \text{Nm.}$$

$$\text{and backward sequence torque} = 10.05 \times \left[\frac{28.5}{117.0}\right]^2 \times 10^{-3}$$

$$= 0.597 \times 10^{-3}\ \text{Nm.}$$

Hence, net torque $= (2.6 - 0.597) \times 10^{-3}$

$= 2.0 \times 10^{-3}$ Nm.

From fig. (7.4),

$$\text{forward sequence current} = 56.8 \times \frac{88.5}{117.0}\ \text{mA.}$$

$$= 42.9\ \text{mA.}$$

$$\text{and backward sequence current} = 106.5 \times \frac{28.5}{117.0}\ \text{mA.}$$

$$= 25.95\ \text{mA.}$$

From figs. (7.4) & (7.5),

$$\text{forward sequence power factor} = \frac{5.7}{117 \times 56.8 \times 10^{-3}}$$

$$= 0.861\ \text{lag.}$$

$$\text{backward sequence power factor} = \frac{11.05}{117 \times 106.5 \times 10^{-3}}$$

$$= 0.888\ \text{lag.}$$

Therefore, forward sequence current $= 42.9(0.861 - j0.508)$

with respect to V_f

and backward sequence current $= 25.95(0.888 - j0.460)$

with respect to V_b.

Hence, reference phase current $= I_f + I_b$

$= 60.0 - j33.72$ mA

$= 68.6$ mA.

and control phase current $= I_f - I_b$

$= 13.9 - j9.88$ mA

$= 17.1$ mA.

Reference phase power $= V_R I_R \cos\phi_R$

$= 7.01$ watts

Control phase power $= V_C I_C \cos\phi_C$

$= 0.834$ watts

The graphs of torque,reference phase and control phase currents and powers are given in figs.(7.13),(7.14) and (7.15),respectively.

e) Characteristic for zero speed,constant reference phase current and variable control voltage covering the range 0 - 117 volts.

At zero speed,the two phases are electrically independent. Consequently,constant reference phase current is obtained with constant reference phase voltage;this fact is borne out by the test results in fig.(4.16). The calculation procedure is,therefore,exactly the same as that for (d) except that in this case

forward sequence slip = backward sequence slip = 1.0

forward sequence power factor = backward sequence power factor = 0.892 lag.

Torque,control phase current,control phase and reference phase powers as functions of slip are given graphically in figs.(7.16),(7.17) and (7.18), respectively.

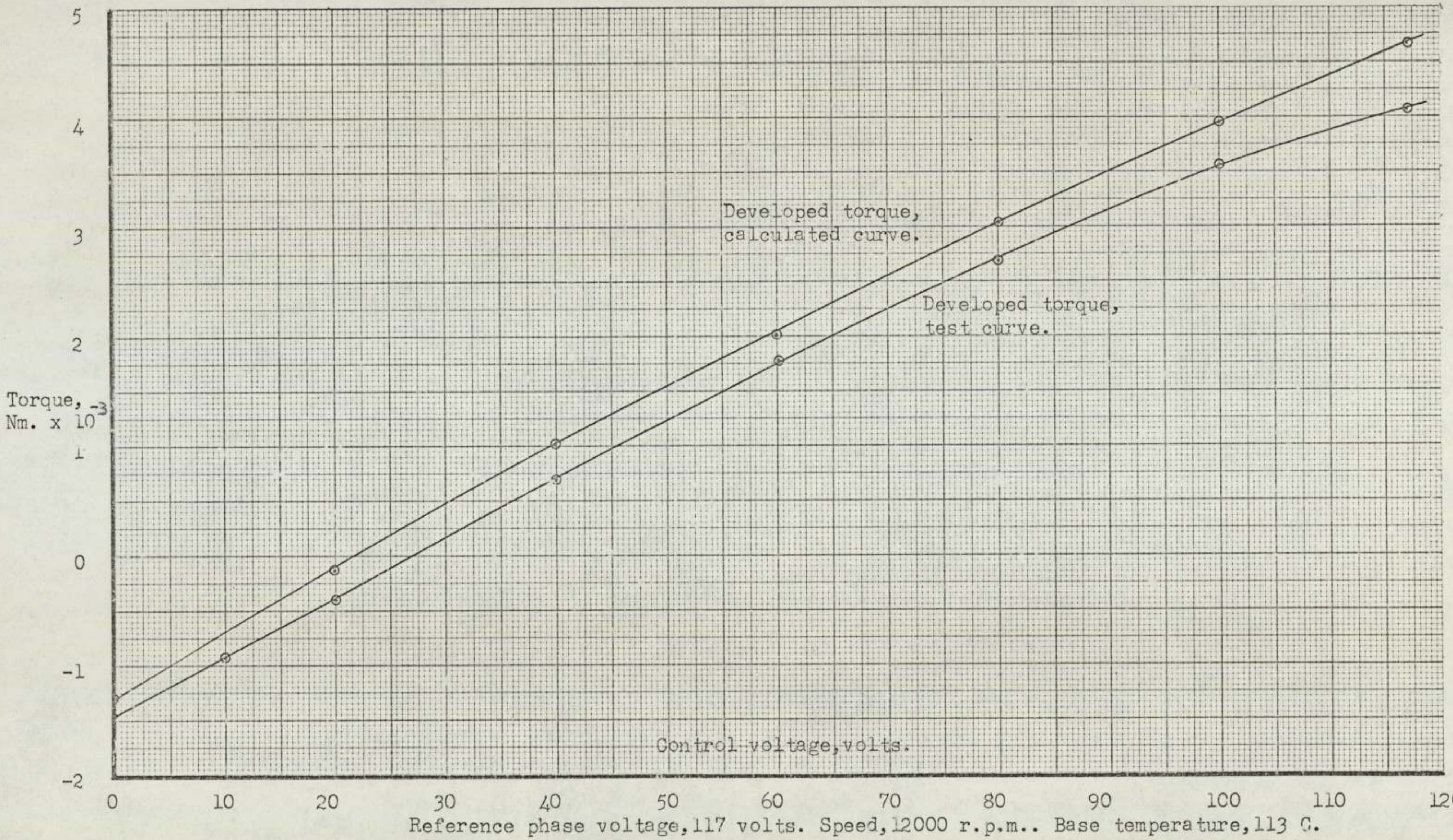

FIG.(7.13). TORQUE versus CONTROL VOLTAGE CHARACTERISTIC AT CONSTANT SPEED.

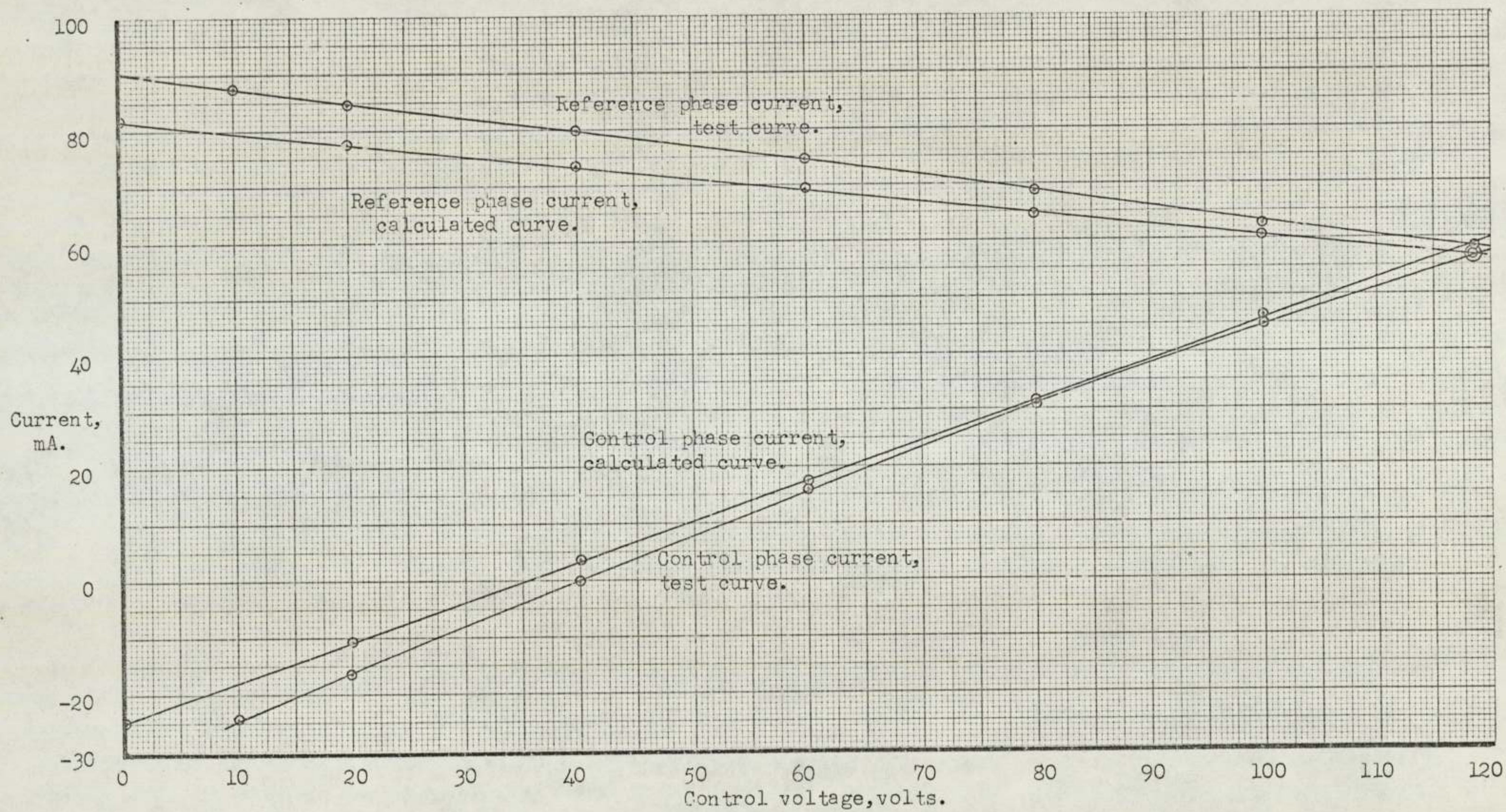

FIG.(7.14). CURRENT versus CONTROL VOLTAGE CHARACTERISTIC CORRESPONDING TO FIG.(7.13).

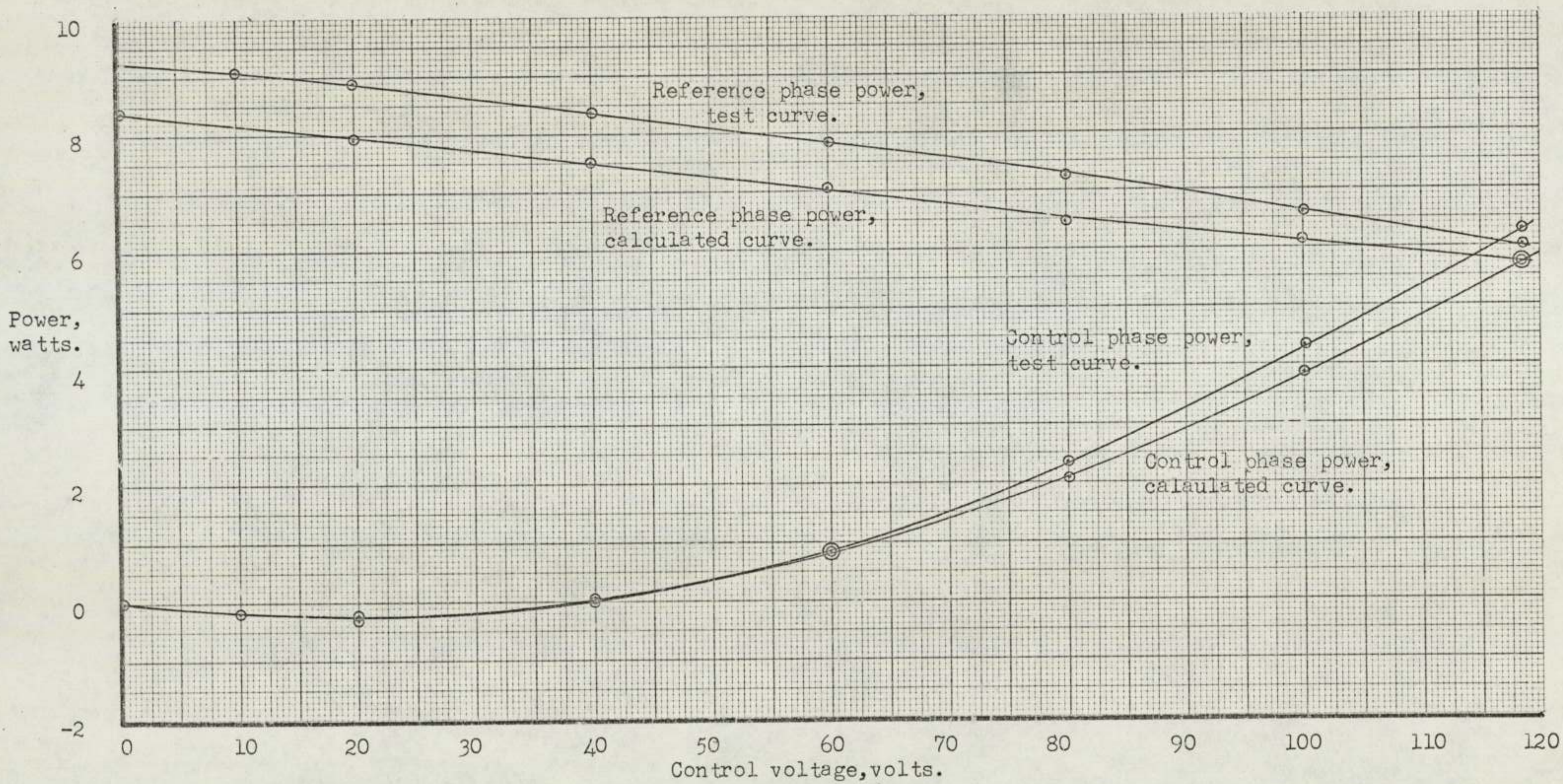

FIG.(7.15). POWER versus CONTROL VOLTAGE CHARACTERISTIC CORRESPONDING TO FIG.(7.13).

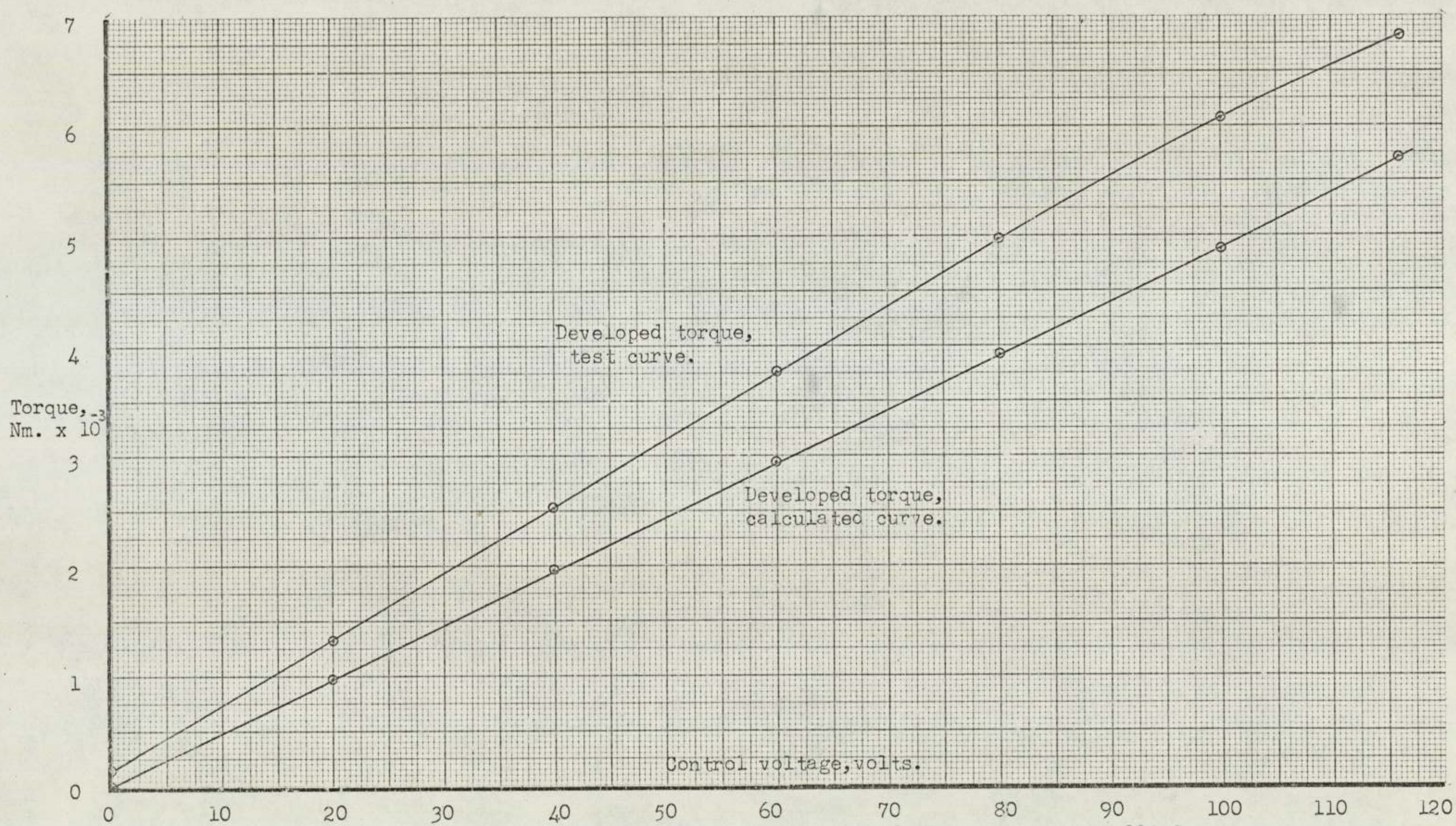

Reference phase voltage, 117 volts. Zero speed. Base temperature 113 C.

FIG. (7.16). TORQUE versus CONTROL VOLTAGE CHARACTERISTIC AT ZERO SPEED.

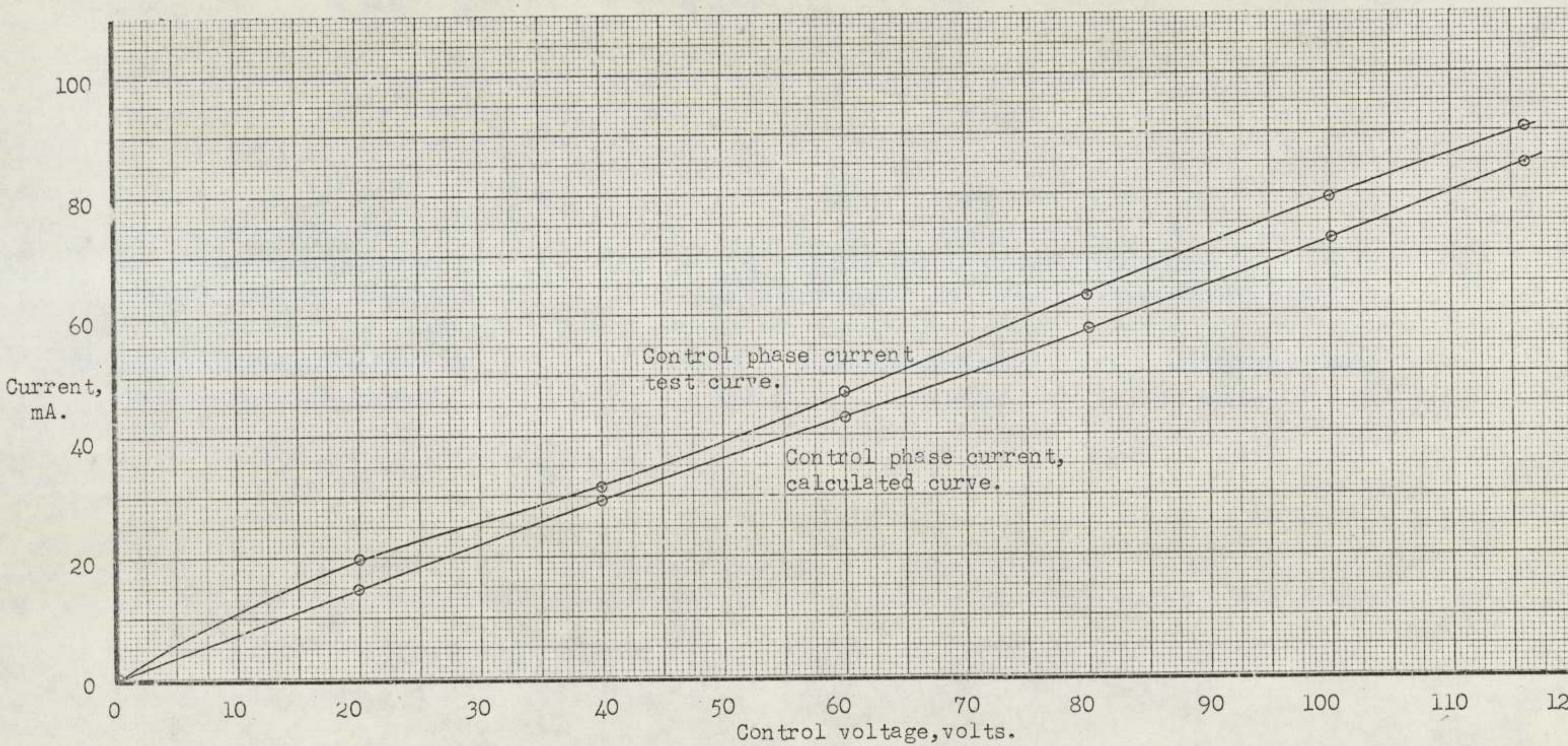

FIG.(7.17). CURRENT versus CONTROL VOLTAGE CHARACTERISTIC CORRESPONDING TO FIG.(7.16).

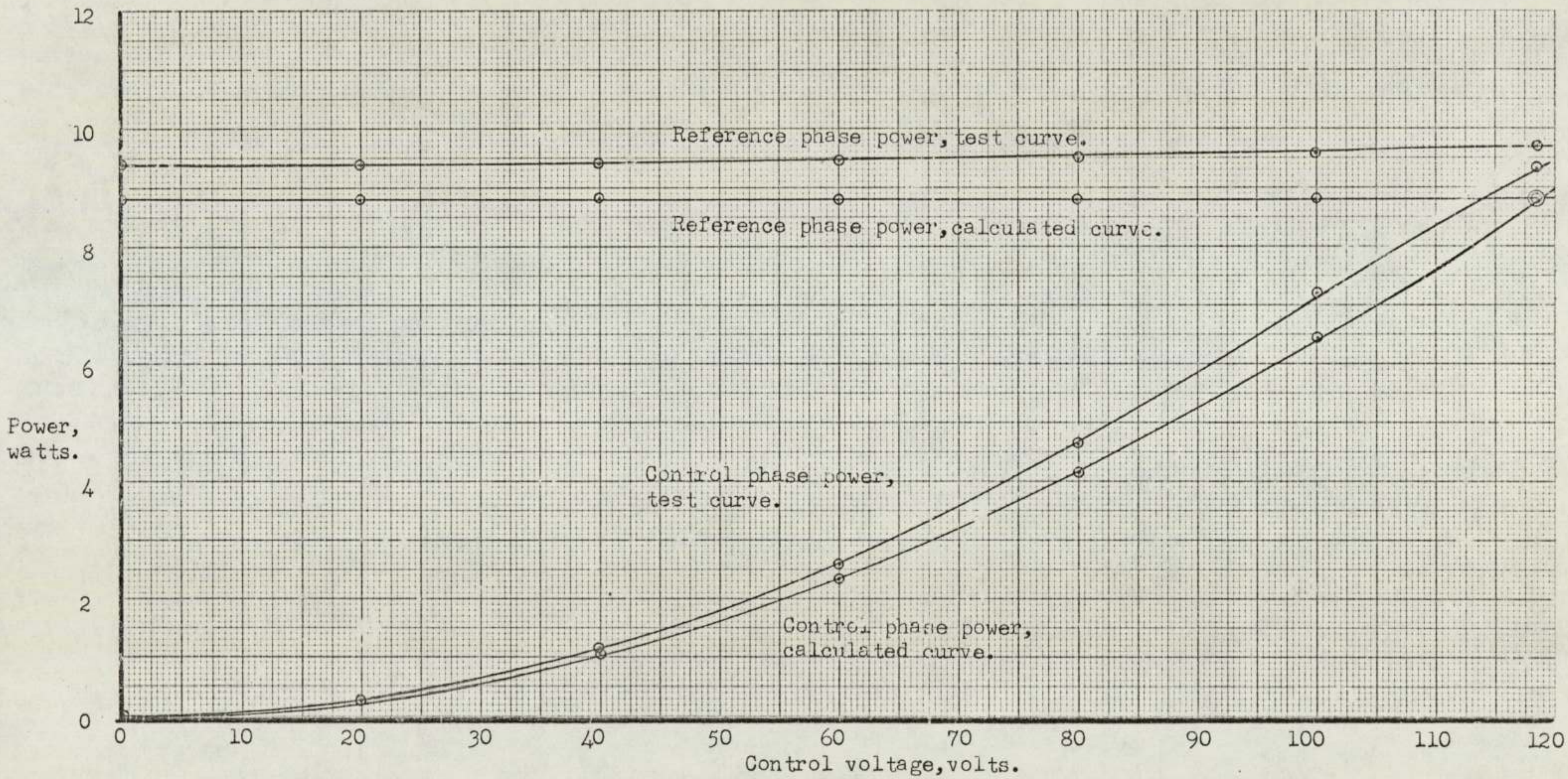

FIG.(7.18). POWER versus CONTROL VOLTAGE CHARACTERISTIC CORRESPONDING TO FIG.(7.16).

25) Dynamic Performance.

The dynamic performance corresponding to each of those measured in section (14) and given in figs.(4.18) and (4.18a) was calculated using the models of fig.(7.1) and fig.(7.2) in conjunction with the continuous system modelling programme on a PDP 9 digital computer. In all cases the torque,control voltage,control current and reference current,as the outputs of blocks 47,6,36 and 35,respectively,were obtained in tabular form and are presented graphically as functions of time in figs.(7.19), (7.20) and (7.20a).

Fig.(7.19) shows the reference phase current and the control phase voltage waveforms relating to figs.(7.20) and (7.20a); these waveforms remained as shown throughout the calculations. Figs.(7.20) and (7.20a) show the developed torque and control phase current during 10 milliseconds from the initiation of the control phase voltage.

To obtain simulated operating conditions identical with those actually used in the tests of section (14) the control phase switch, comprising blocks 60,61 and 62 of fig.(7.2),was set to remain open for 25 ms by giving the constant,block 62, a value of 25. The model was then run for 25 ms and the integrator blocks interrogated. The integrators were then set at these values as initial conditions thereby simulating the actual machine with its reference phase excited at steady state conditions and its control phase quiescent. By setting the value of block 62 to the time interval from the zero to the given initiation points 1 - 10 of fig.(4.17) successively, the model was made to represent the test machine receiving a control voltage signal at different points on the control voltage waveform,as required,balanced and unbalanced supply simulation being obtained by setting the gain of block 6 to 1.0 and 0.5,respectively. This approach was used in order to minimize the integrator round-off errors and to reduce computing time. For comparison in chapter VIII, included on each of the graphs of figs.(7.19),(7.20) and (7.20a) are the corresponding measured characteristics taken from figs.(4.18) and (4.18a).

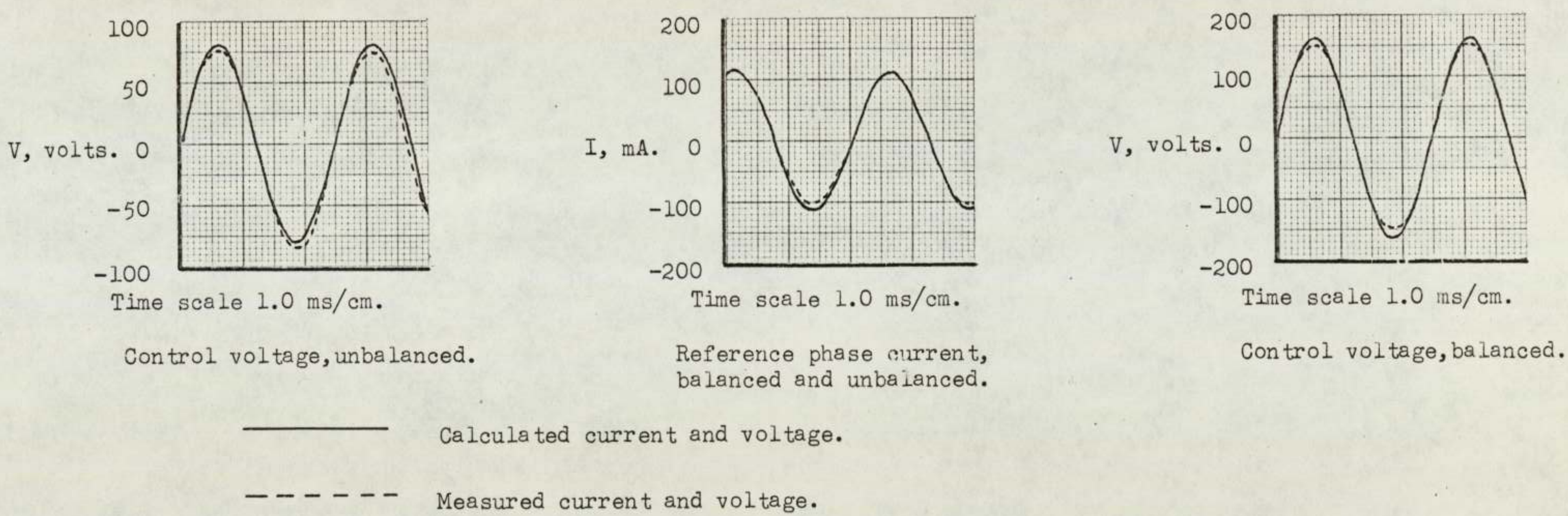

FIG.(7.19). REFERENCE PHASE CURRENT AND CONTROL PHASE VOLTAGE FOR FIGS.(7.20)&(7.20a).

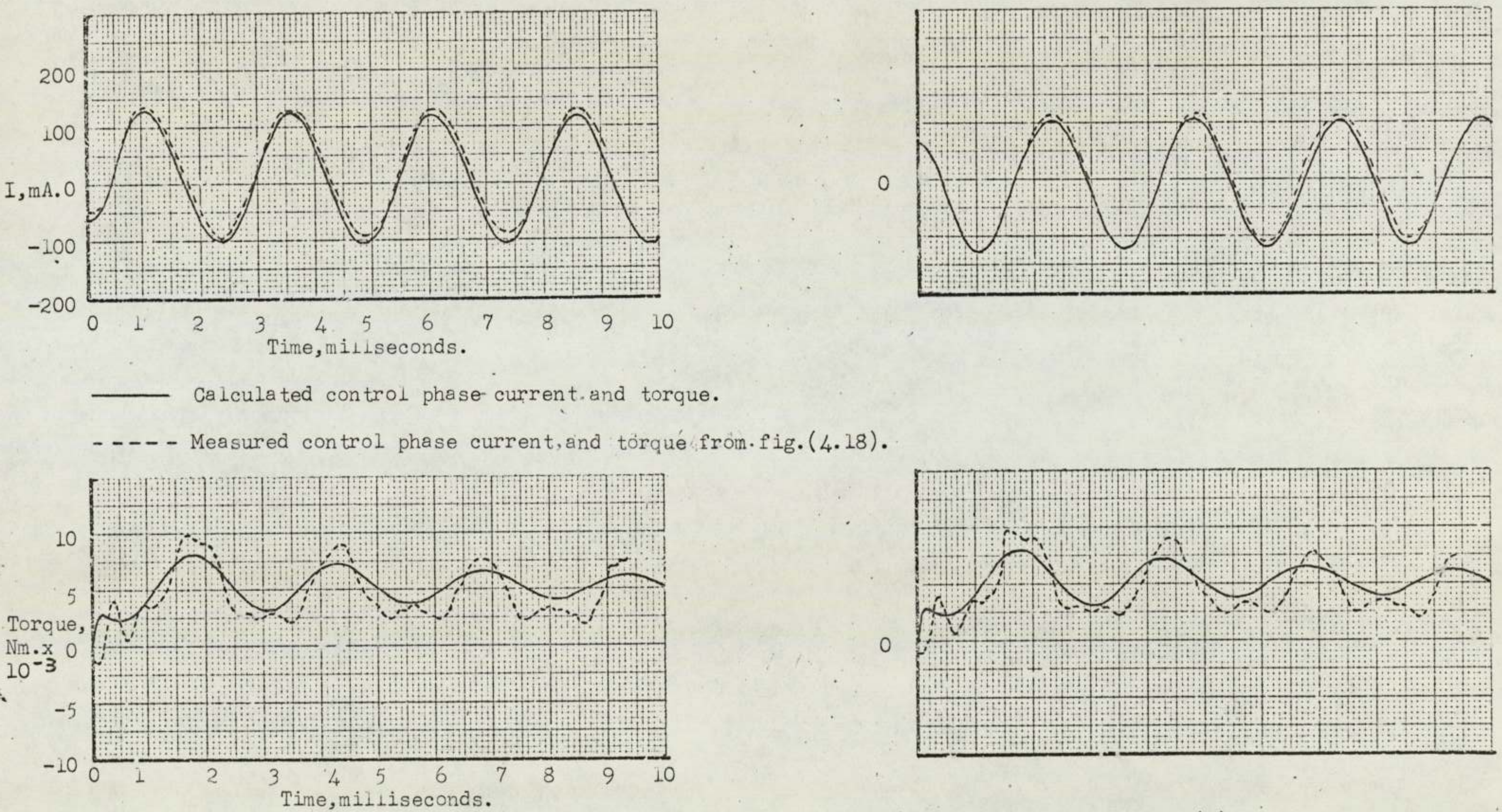

Voltage initiation point (1).
(relates to fig.(4.17))

(2)

Key and scales apply to all graphs in fig.(7.20).

FIG.(7.20). CALCULATED DYNAMIC PERFORMANCE OF TEST MACHINE ON NO LOAD,BALANCED SUPPLY.

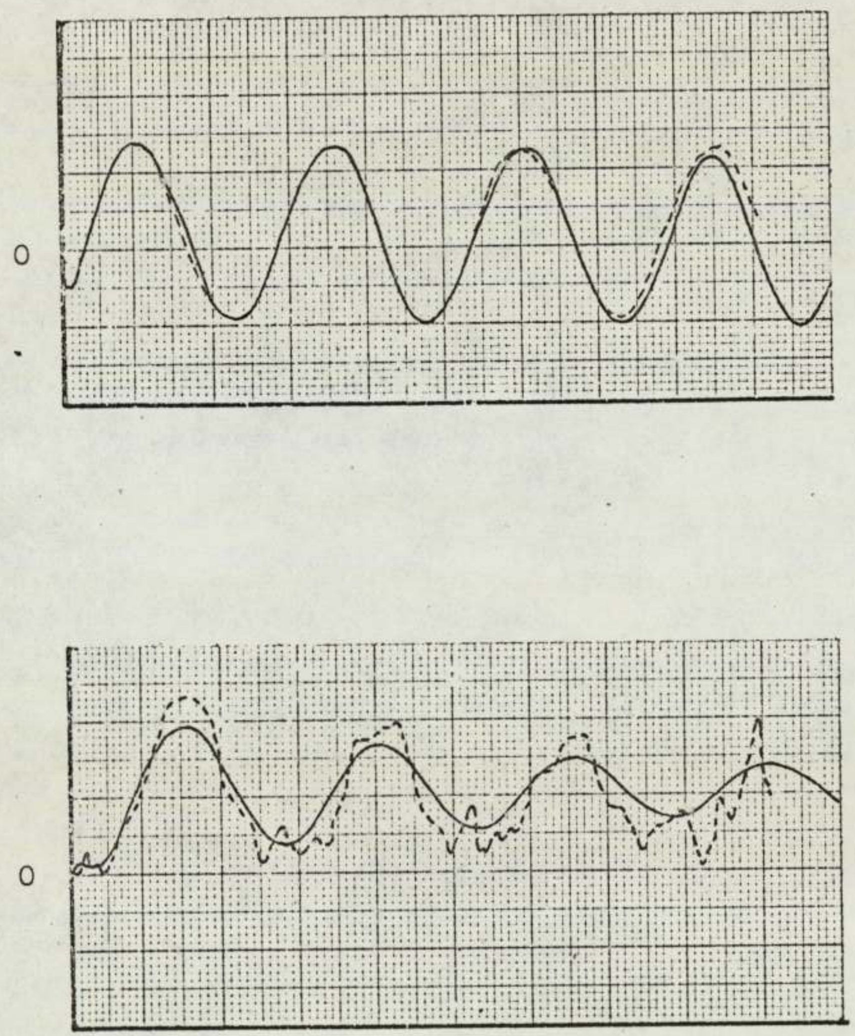

(3)

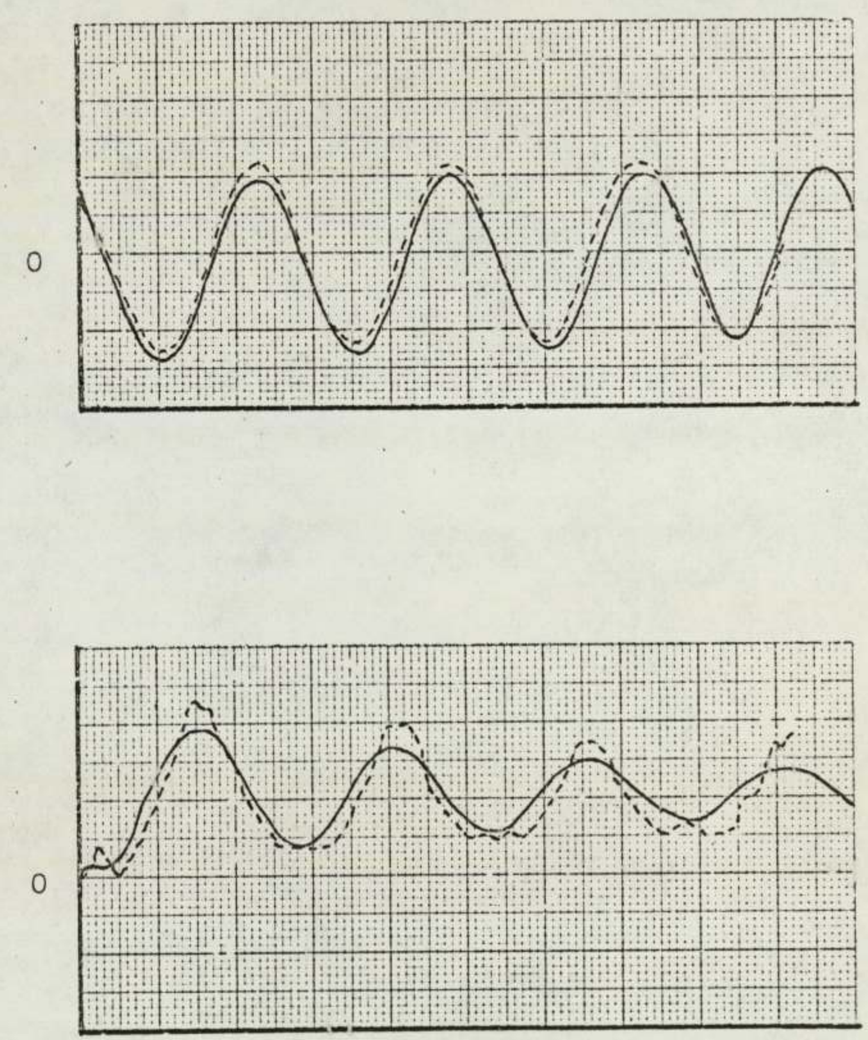

(4)

For scales and key,
see first sheet of figure.

FIG.(7.20).continued.

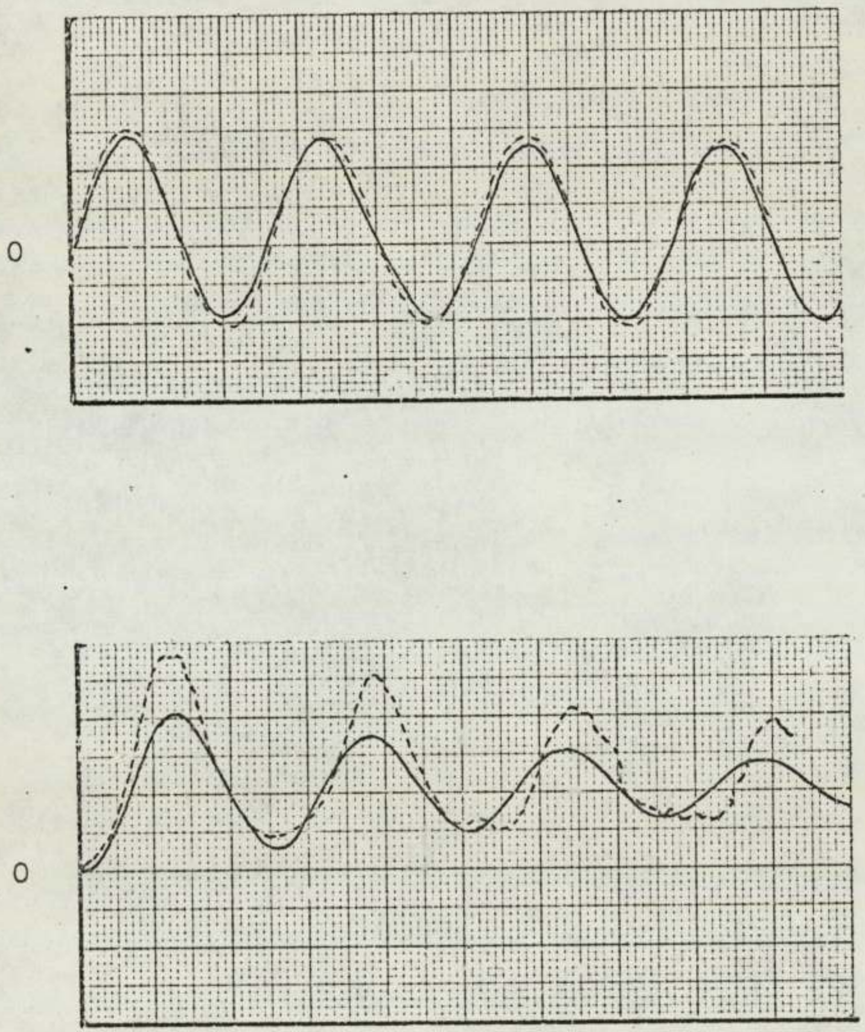

(5)

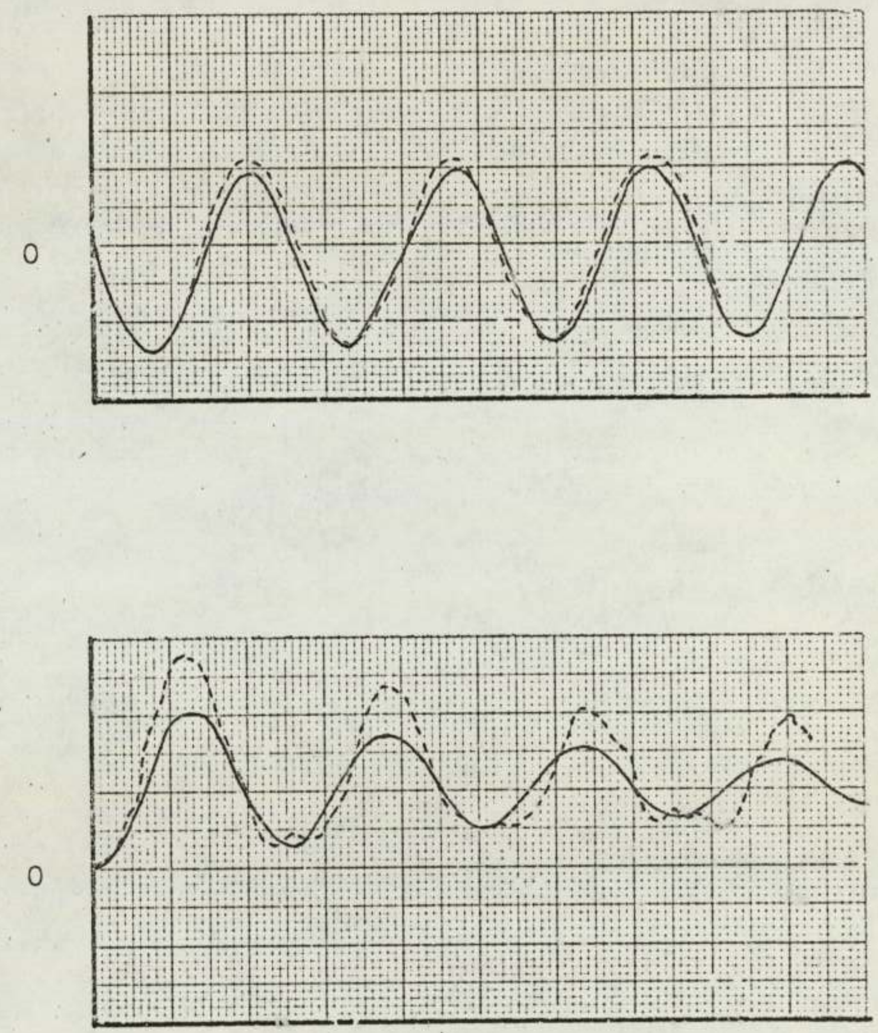

(6)

For scales and key,
see first sheet of figure.

FIG.(7.20).continued.

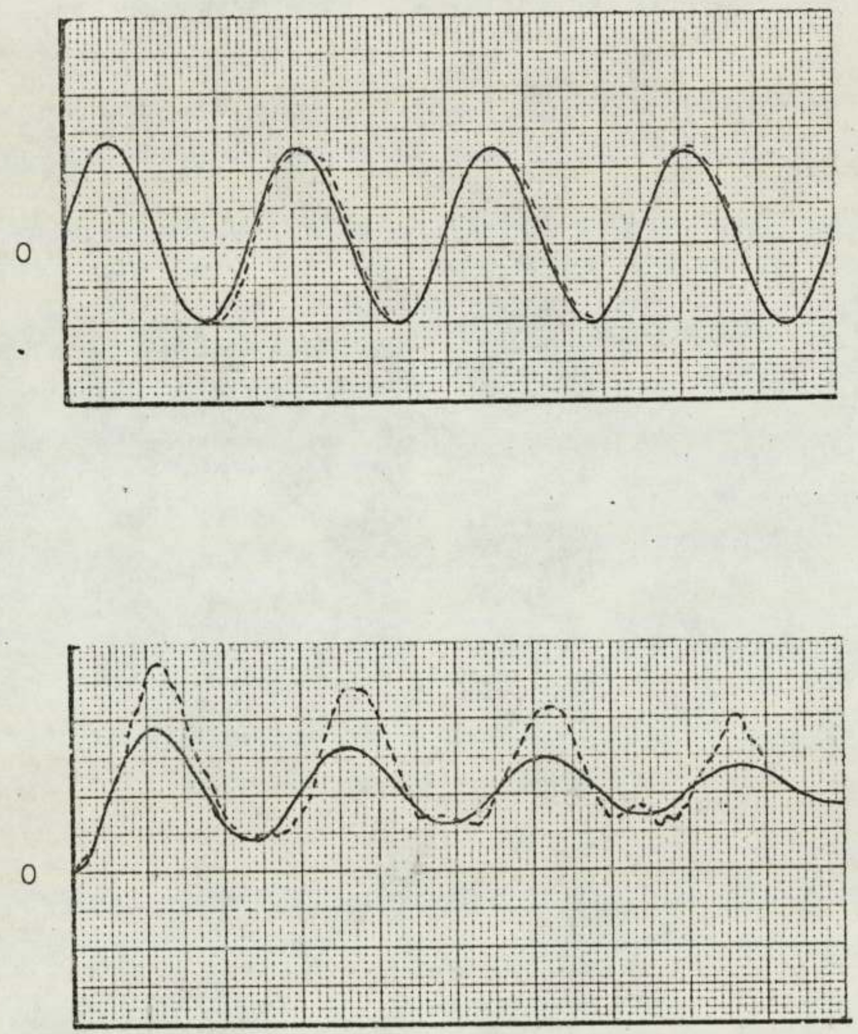

(7)

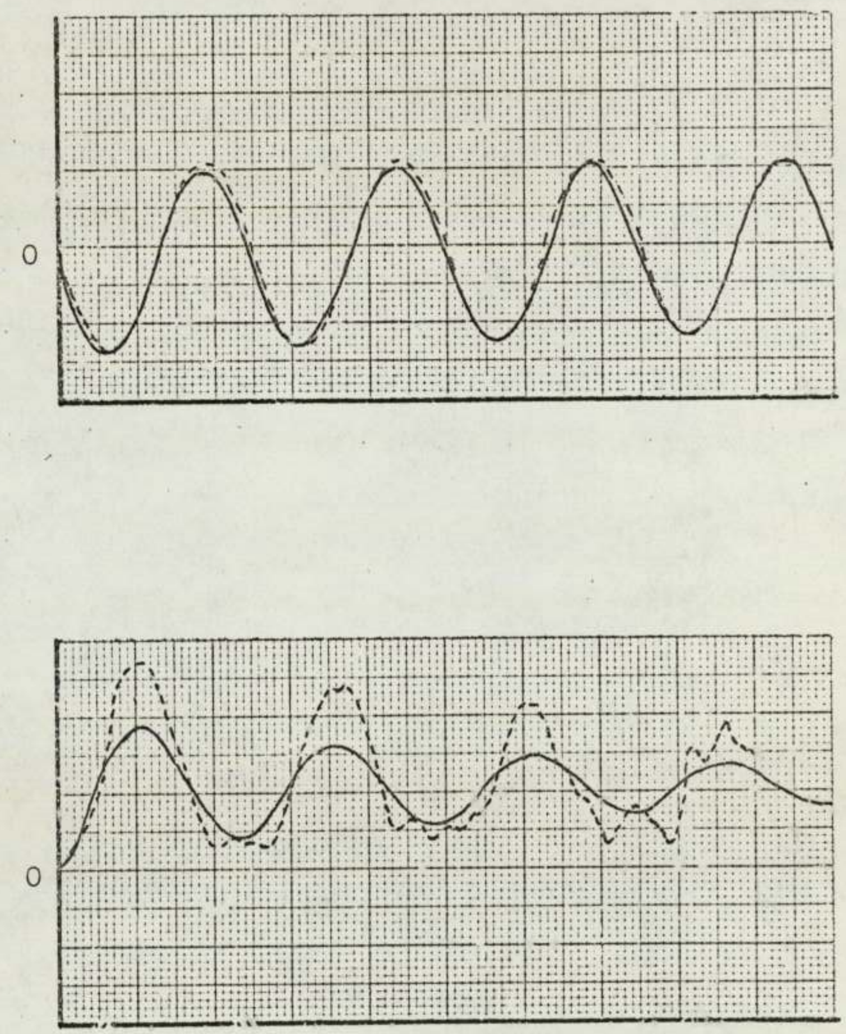

(8)

For scales and key,
see first sheet of figure.

FIG.(7.20). continued.

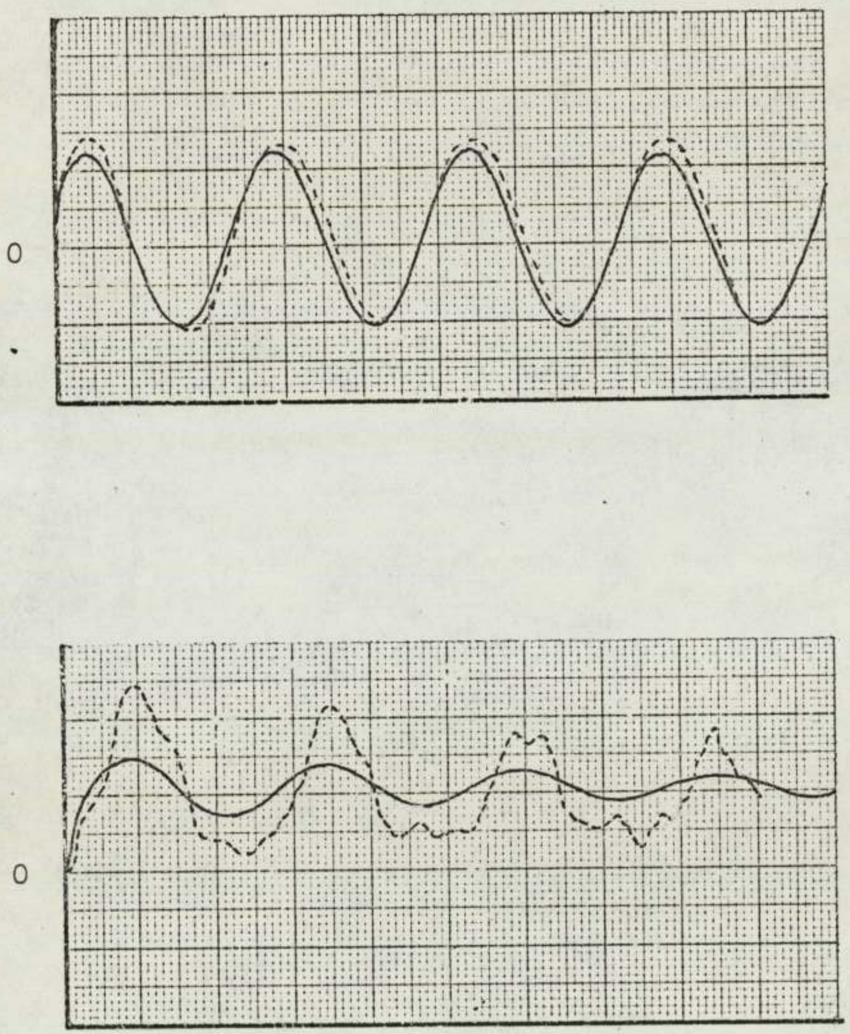

(9)

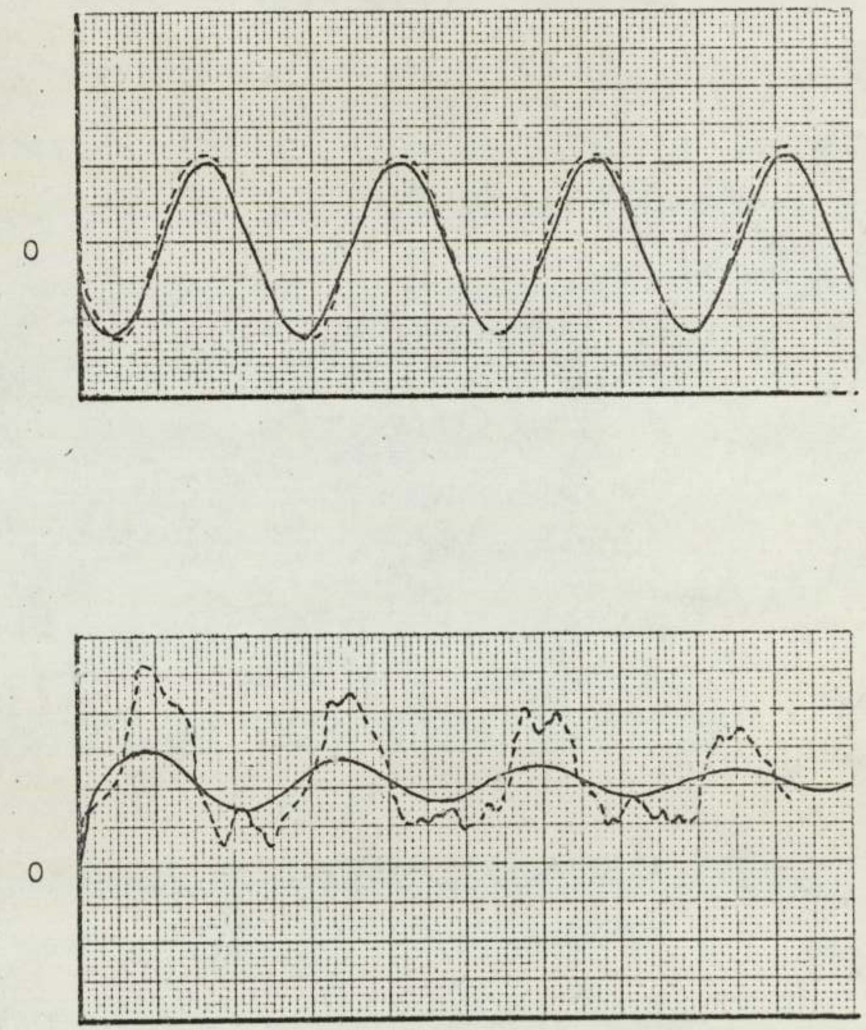

(10)

For scales and key,
see first sheet of figure.

FIG.(7.20). continued.

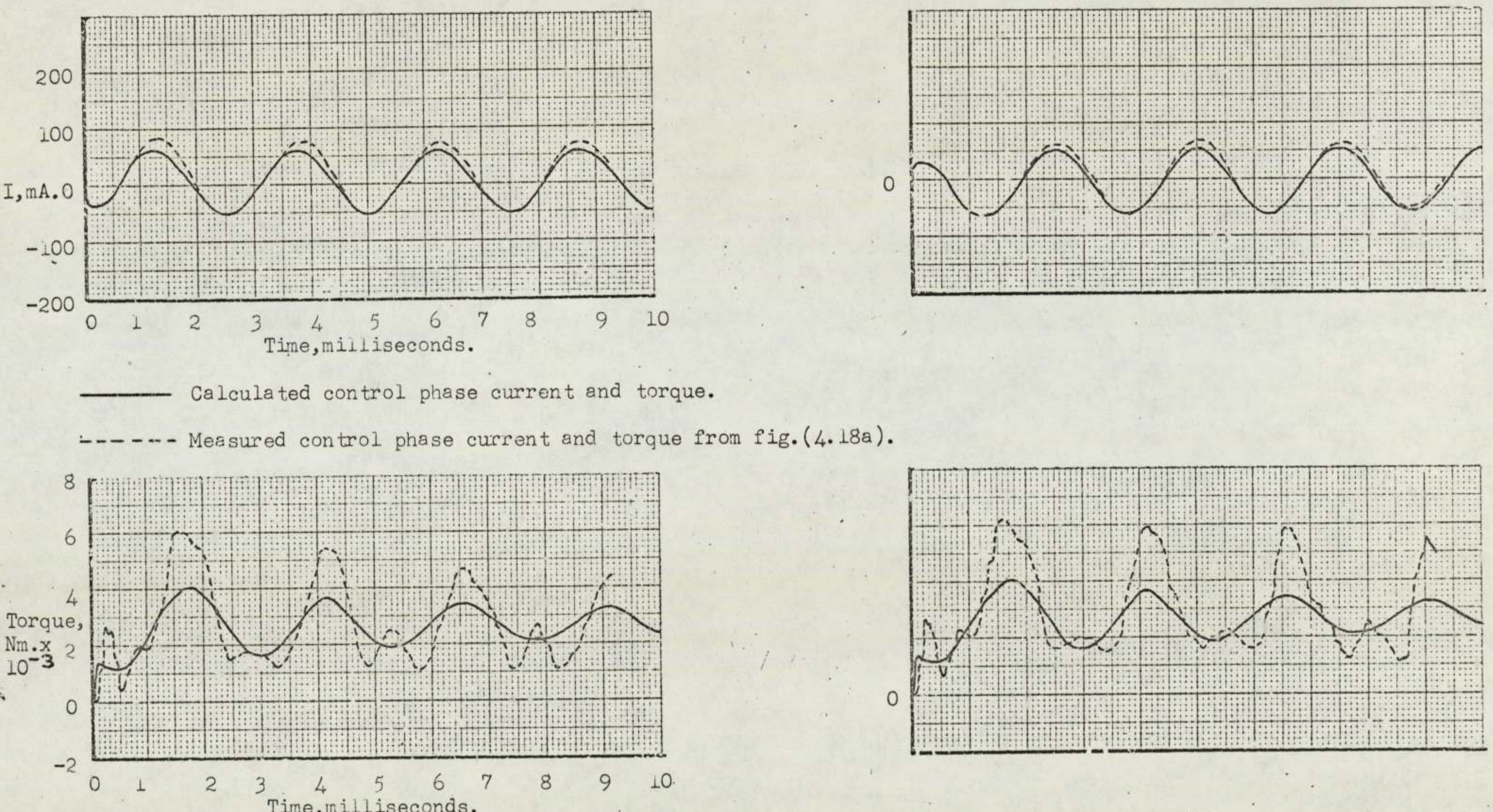

Voltage initiation point (1).
(relates to fig.(4.17)).

(2)

Key and scales apply to all graphs in fig.(7.20a).

FIG.(7.20a). CALCULATED DYNAMIC PERFORMANCE OF TEST MACHINE ON NO LOAD,UNBALANCED SUPPLY.

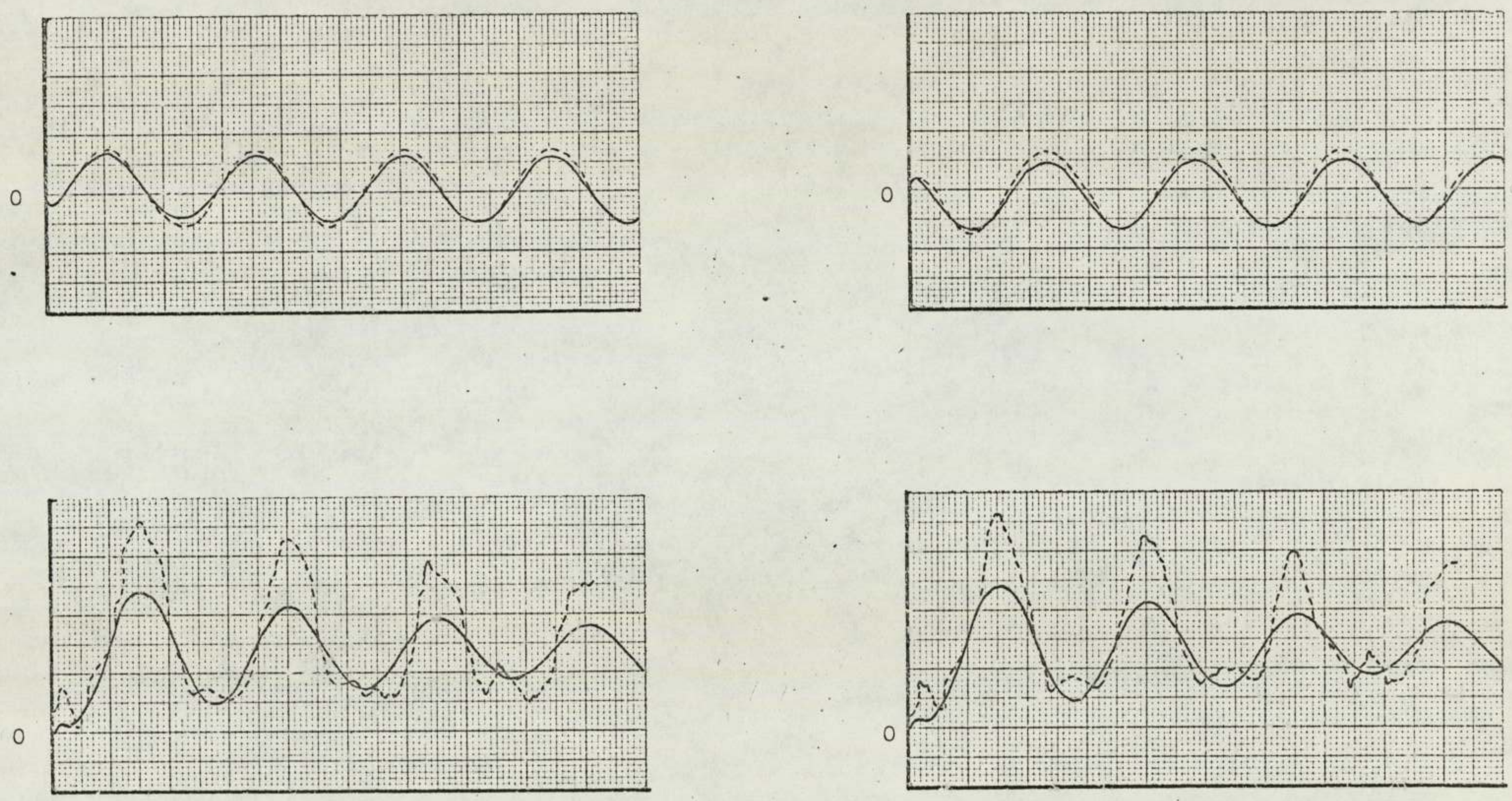

(3) (4)

For scales and key,
see first sheet of figure.

FIG.(7.20a). continued.

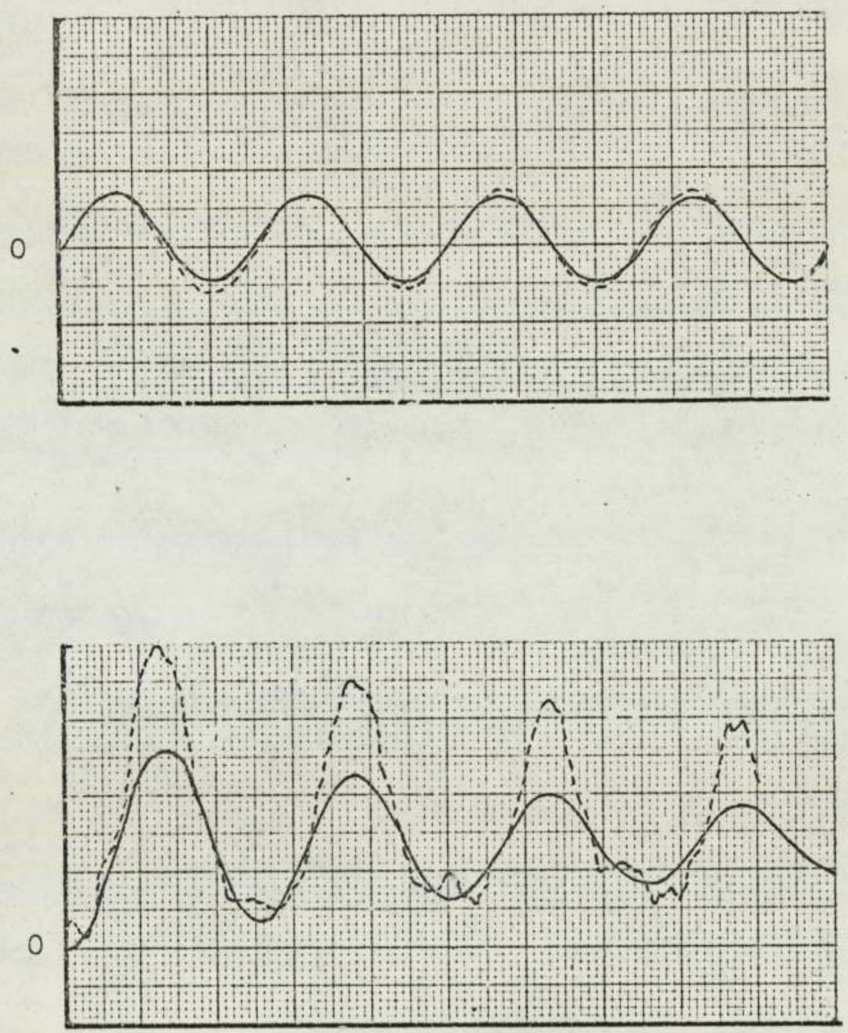

(5)

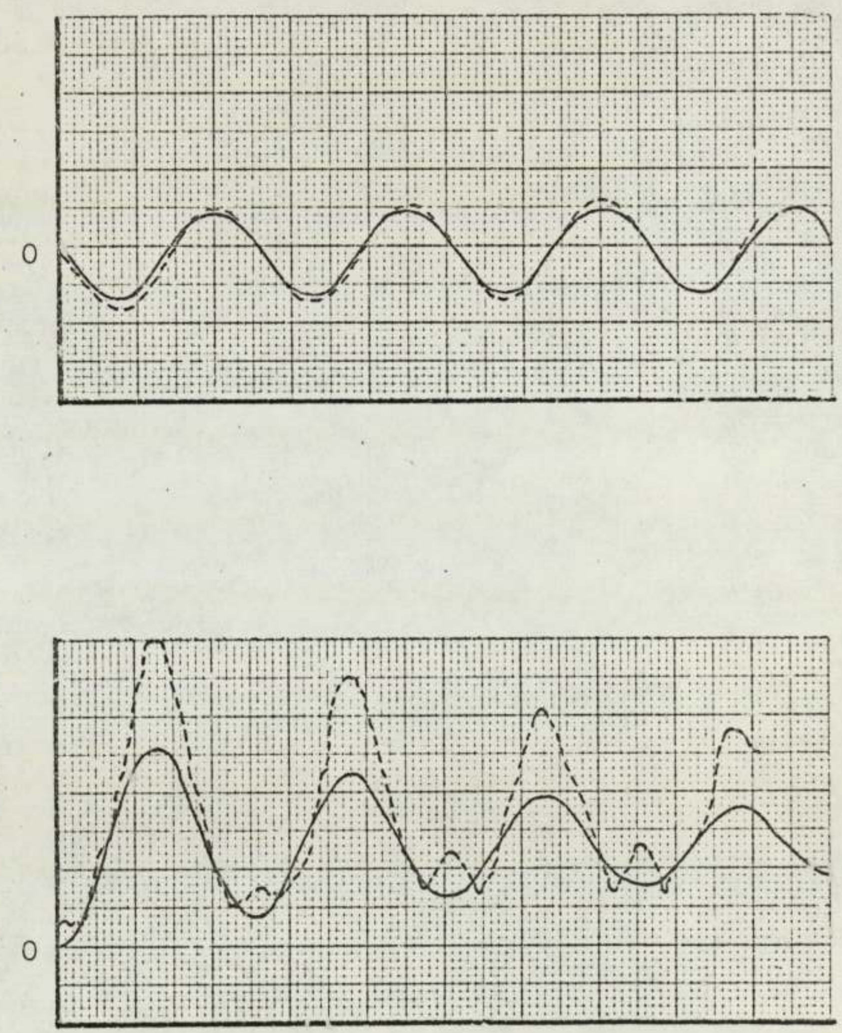

(6)

For scales and key,
see first sheet of figure.

FIG.(7.20a). continued.

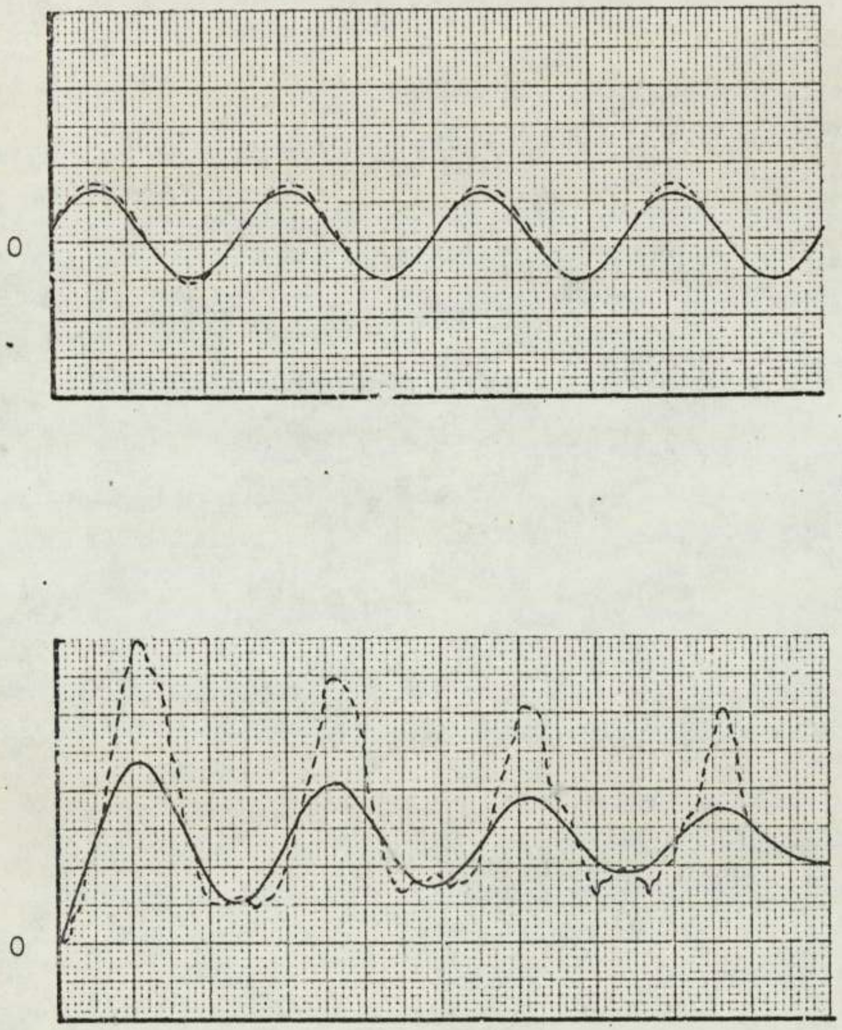

(7)

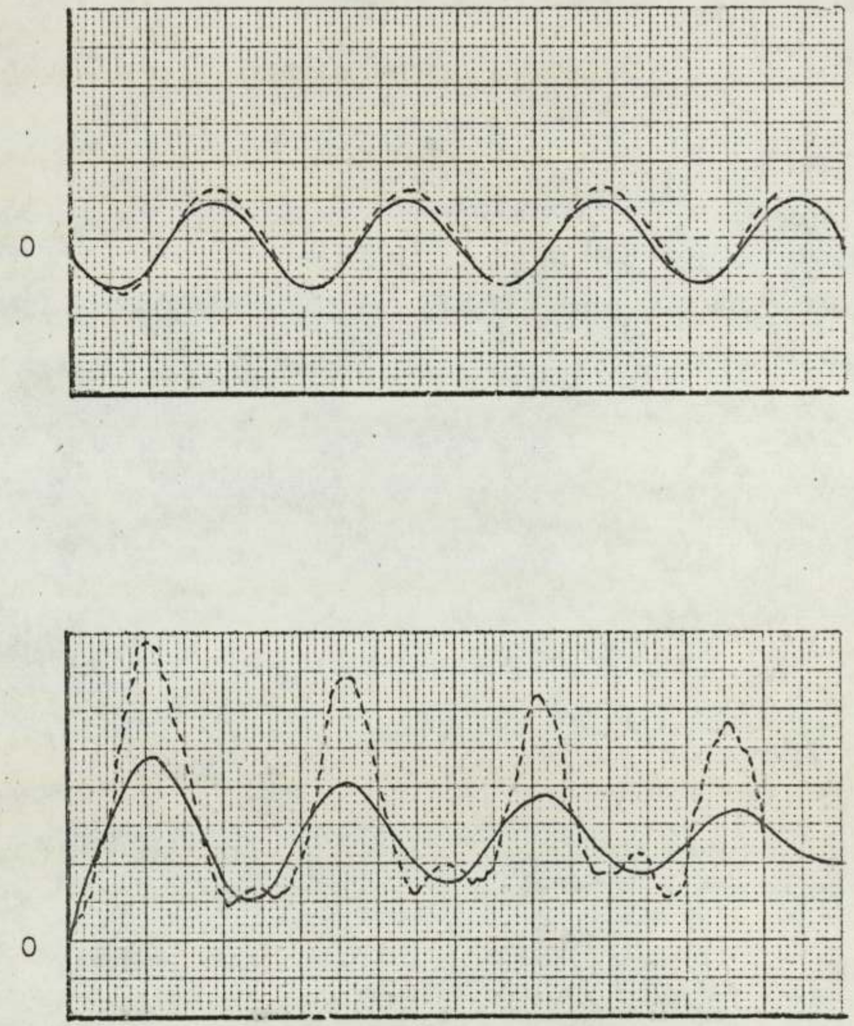

(8)

For scales and key,
see first sheet of figure,

FIG.(7.20a). continued.

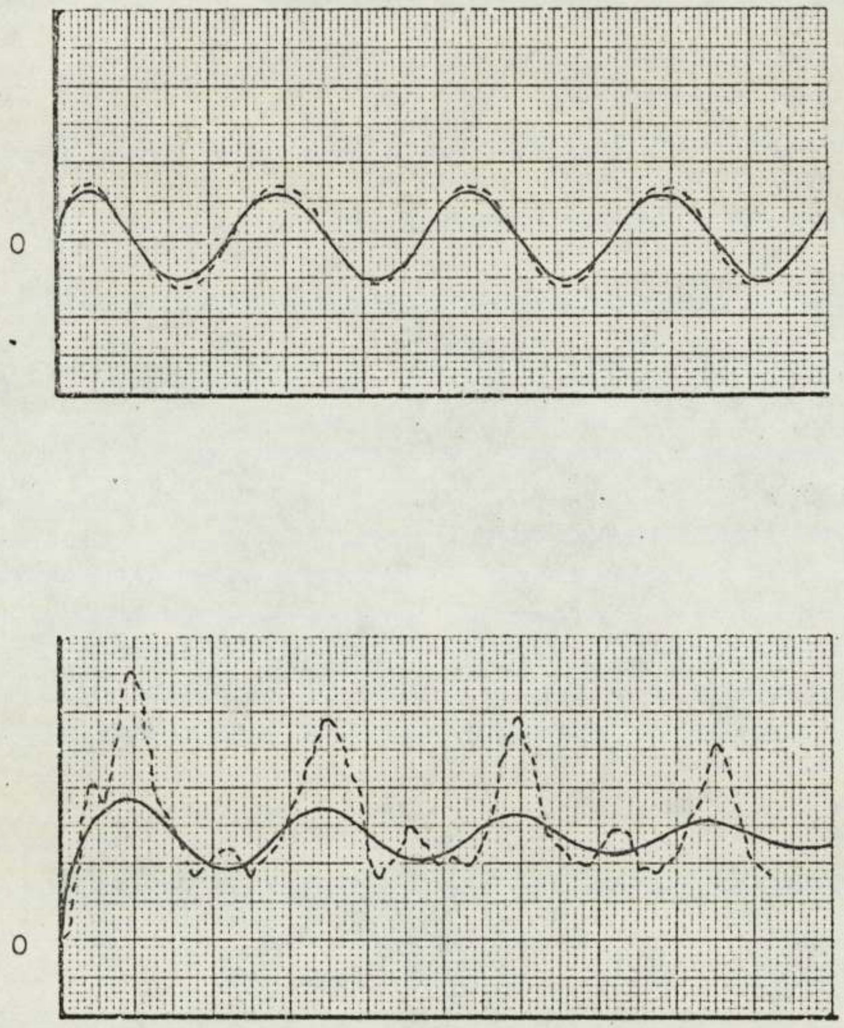

(9)

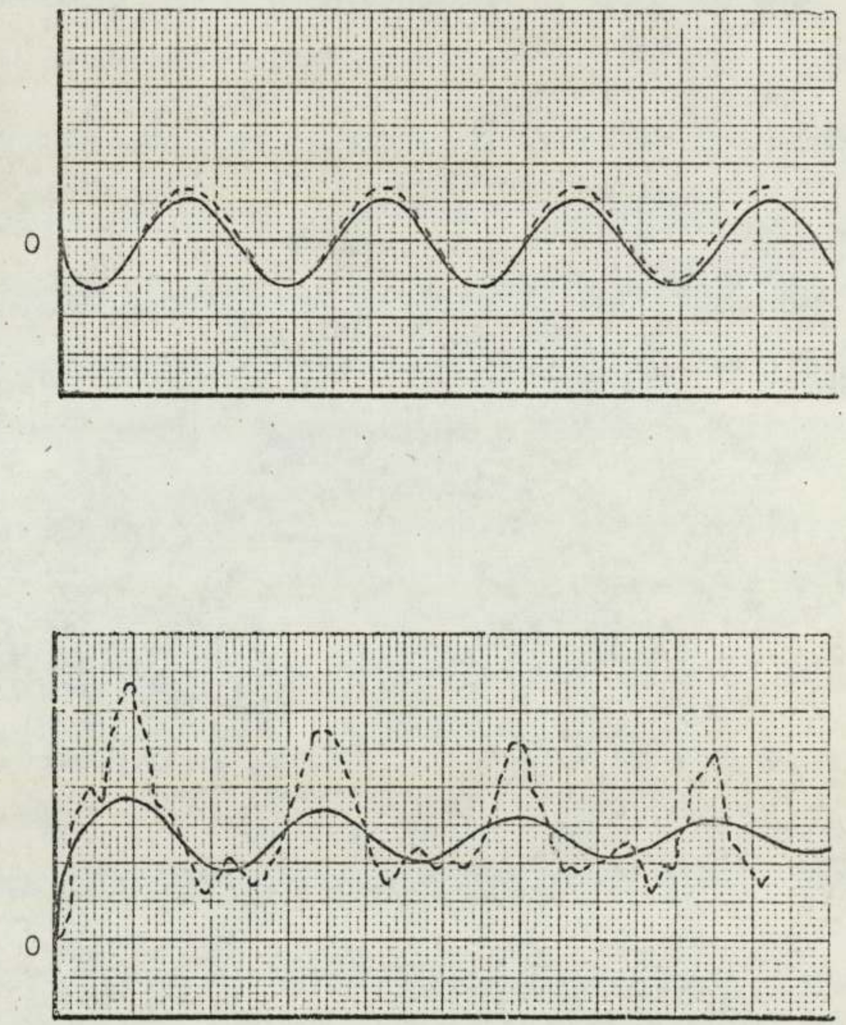

(10)

For scales and key,
see first sheet of figure.

FIG.(7.20a). continued.

CHAPTER VIII.

Comparison of Measured and Calculated Performances.

26) Steady State Performance.

The correlation between the measured and calculated performances under general steady state conditions is largely governed by their correlation under the particular steady state conditions of balanced applied voltages over the extended slip range of 0 to 2.0, providing magnetic saturation of the machine does not occur. Appreciating this fact it may seem superfluous to make a comparison over the whole range of steady state conditions. It was felt, however, that demonstration of the efficacy of the model over the actual working area of a servomotor was essential; it is for this reason that all aspects of performance have been covered.

The assessment of the overall correlation is made a great deal easier, nevertheless, in the light of the foregoing observation since, apart from the effects of magnetic saturation, what is said of the balanced voltage characteristics must, in some degree, apply also to the unbalanced characteristics.

The estimation of the balanced voltage characteristics is greatly influenced by the presence and exact nature of the additional rotor branch in the equivalent circuit and, in the case of the torque characteristics only, by the relationship between the total rotor power and the developed electromagnetic torque. Let it be emphasized at the onset that without this new rotor branch the calculated and measured performances would be much at variance. To reinforce this statement, using a single rotor branch, as is usual, of resistance 772 ohms as estimated in the design calculations, and of leakage reactance 196 ohms, curves of phase current, phase power and torque were calculated, at the correct base temperature, as functions of slip and are included in figs. (7.4), (7.5) and (7.6), respectively. These curves clearly indicate that whilst the calculated characteristics of phase current and phase power for the single branch circuit might be taken as being acceptable over the slip range 0 to 1.0 they are not acceptable over the extended range of 0 to 2.0 which is essential for servosystem application. The modified equivalent circuit, on the other hand, gives a greatly improved correlation which it is proposed is satisfactory over this range.

The measured torque characteristic is clearly affected by the fact that the rotor power and the developed torque are, practically, not directly related. To overcome this the rotor power on test was obtained as (measured input power - stator copper loss + power input from driving motor for slips above 1.0) and a torque determined as $\frac{1}{\omega_s}$(rotor power) is plotted as a function of slip in fig.(7.6). It will be seen that the torque calculated using the new equivalent circuit is more closely related to this curve than that calculated from the conventional circuit; the fact that the measured torque falls away at the higher values of slip in the braking region is to be accounted for by the test machine becoming magnetically non-linear due to the large rotor currents at these slips. It is extremely interesting, however, to see that over a range of slip from 0.7 to 1.6, approximately, the torque given by $\frac{1}{\omega_s}$(rotor power) is less than the measured torque. One would have expected the measured torque to be usually less than that indicated by the rotor power, due to the effects of stray losses. It will be recalled that the results of the variable frequency test, section (18), also indicated a measured torque greater than that given by $\frac{1}{\omega_s}$(rotor power) for which reason the determination of the equivalent circuit parameters was based on the value of rotor power rather than on that of the developed torque since it was argued that the elevated torque figure was due to combined magnetic asymmetries of the stator and the rotor. Such asymmetry could be the result of effective stator ovality, arising from machining damage to the core material, in conjunction with differing bar resistances in the rotor for, in keeping with the observations in section (18), if the stator was excited with direct current no torque due to reluctance would be generated but such a torque would be caused if the rotor were excited at the same time or even independently.

This is borne out by fig.(5.7), section (16), but to further identify the nature of these asymmetries the rotor outside diameter and the stator inside diameter were carefully measured to determine their maximum and minimum values across orthogonal diameters in both cases. The measurements gave for the rotor 0.4963" and 0.4962", and for the stator 0.5007" and 0.5005", i.e. a 0.0001" rotor ovality and a 0.0002" stator ovality resulting in a variation in radial airgap of $\pm$ 0.00015" which, on the basis of the mean radial gap, is a $\pm$ 7% variation. In the light of the findings of section (20) and the subsequent estimation of the magnetic airgap as 0.068 mm. (0.00268") this is a pessimistic figure and, based on the effective gap, assuming uniform depth of magnetic damage round both the stator and rotor bore surfaces, should really be $\pm$ 5.6%. These dimensional variations cannot of themselves account for the observed discrepancy in the stalled torque in the variable frequency test, some other form of rotor asymmetry, such as that already mentioned, must be present. Whether or not this together with the stator ovality is sufficient to cause the difference in torque is difficult to say dogmatically but the likelihood of a completely uniform layer of reduced permeability iron resulting from the bore grinding operation is equally difficult to imagine; to clarify this, further work is obviously necessary and will be given further thought in chapter IX.

Whilst this explains the anomaly of section (18) it does not explain the situation obtaining in fig.(7.6) since the average effect of this torque variation per revolution must be zero. However, the presence of this variation would manifest itself under running conditions as a torque pulsation at a frequency of twice the rotor speed in revolutions per second. In this regard it is convenient to examine now the spectrograms of instantaneous no-load torque taken at no-load speed, i.e. figs.(4.20) and (4.21). These confirm the presence of such a pulsation in that they exhibit oscillations at a frequency between 600 Hz and 700 Hz in both the balanced and unbalanced supply voltage operating modes. This would correspond to a no-load speed of between 18000 and 21000 r.p.m. which is of the correct order for a two pole, 400Hz machine.

The spectrograms do also indicate a pulsation at a frequency between 300 and 350 Hz which suggests that the rotor of the test machine was not concentric with the stator bore for this in conjunction with the uneven bar resistance would result in a torque pulsating at a frequency corresponding directly to the rotor speed in revolutions per second. In addition, torque oscillations at line frequency and twice line frequency are apparent but these will be discussed in the consideration of the dynamic performance.

With the type of dynamometer used in this investigation, a torque pulsation will, since the time constant of the mechanical system is very much longer than that of the electrical system feeding the driving motor, cause a power flow from the driving motor to the rotor of the test machine in order to maintain the torque at its peak value. At slips greater than 1.0 this would occur as an increase in the already existing power flow from the driving motor. This extra power input to the rotor of the test machine will not, of course, make itself apparent on the stator side with the result that the torque calculated from the rotor input power taken as (stator input - stator copper losses) will be lower than that actually measured. This is as observed and constitutes a strong argument in favour of the method of using the rotor power, instead of the measured torque, in the determination of the machine parameters since the effect of this extraneous input is omitted.

Finally, in this consideration of the factors affecting the relationship between predicted and measured torques, it must be remembered that the form of the extra rotor branch in the equivalent circuit was determined by a curve fitting process and found to be a composite resistor. As pointed out in section (22), the exact nature of this branch could only be determined by further experimental work. The statement of this branch as a function of frequency, obtained in section (20), is obviously not precise and, consequently, some error in the predicted performance of the machine must ensue.

With all these factors taken into account, it is claimed that the new representation of the rotor gives a more satisfactory prediction of performance on balanced supply for slips 0 to 2.0 than does the usual configuration.

This being established, the comparison is henceforth restricted to one of measured performance with predicted performance from the improved equivalent circuit. Thus, in figs.(7.7) to (7.12), covering the whole of the steady state performance on unbalanced supply, the degree of correlation is seen to be extremely good. Nevertheless, cognizance must again be taken of the discrepancy between the torque equivalent of rotor power and the measured torque. For this mode of operation it is not possible to determine the rotor power for the measured characteristics without making use of the equivalent circuit parameters. Consequently, curves of developed torque as $\frac{1}{\omega_s}$ (rotor power) cannot be included and the measured torque itself has to be used in the comparison. The analysis of unbalanced performance outlined in section (1) demonstrates that the net torque on unbalanced supply can be taken as the difference between two torques, one at slip s and the other at slip (2 - s). Since the power flow, associated with torque pulsation, from the driving motor increases the developed torque of the test machine in both instances, then in the evaluation of the net torque the effects of this increase will be minimized. Indeed, under the conditions of zero control voltage, when the forward and backward sequence voltages are of equal magnitude, it might be expected that the effect would be altogether nullified if it could be assumed that the increase in the developed torques at s and at (2 - s) were identical. In the region of slip 1.0 this would most likely be true and in this region of slip, therefore, the predicted torque and the measurd torque should have best correspondence; reference to fig.(7.10) proves this to be the case.

At this stage then it may be concluded that the equivalent circuit derived from the mathematical model, which was itself determined from the analysis of the measured impedance per unit frequency locus, is proven to be effective for the prediction of the full range of steady state performance as required for servosystem application whereas the conventional equivalent circuit is not so.

27) Dynamic performance.

In making comparison between the predicted and measured dynamic characteristics, it is observed in the first place that the predicted reference phase current, the balanced and unbalanced control phase voltages, fig.(7.19), show little difference from their measured counterparts except at the peak values where the error is of the order of + 10% to + 20% based on the measured figure. Secondly, the predicted control phase current exhibits a similar error but of the order of $\pm$ 10% in the balanced voltage operation, fig.(7.20), and $\pm$ 20% in the unbalanced voltage operation, fig.(7.20a), again based on the measured figure. Hence, in the dynamic torque characteristics a maximum error of approximately $\pm$ 20% may be expected on thesegrounds. In the actual characteristics, figs.(7.20)&(&.20a), the difference between the predicted and measured curves is in some cases greater than this and appears to be caused by a twice line frequency component manifest in the measured performance only and moreso in the unbalanced than in the balanced voltage operation.

The traces taken of the variation in instantaneous stalled torque for balanced supply voltages at different frequencies during the variable frequency test, fig.(5.14a), also show a twice line frequency component and indicate that it is sensitive in magnitude to the supply frequency in that its amplitude is $\pm$ 0.5 x 10^{-3} Nm. in the region of 20 Hz., decreasing to $\pm$ 0.2 x 10^{-3} Nm. in the region of 100 Hz. and increasing to $\pm$ 2 x 10^{-3} Nm. in the region of 400 Hz., all about an average value of 7 x 10^{-3} Nm..
Furthermore, the spectrograms of the instantaneous no-load torque, figs.(4.20) and (4.21), also indicate a pronounced twice line frequency pulsation as do the traces of the variation in instantaneous stalled torque, fig.(5.9), taken for different positions of the rotor relative to the stator on balanced supply, the latter showing at the same time that the pulsation is

independent of the rotor angular position relative to the stator. All these observations are corroborative and point to a dissimilarity between the stator phase windings as the source of this pulsation. Since the traces of figs.(4.18) and (4.18a) exhibit no transient in the reference phase current it is concluded that the two windings are effectively in space quadrature and are, therefore, correctly distributed. From the fact that the magnitude of the torque pulsation is, as mentioned above, insensitive to rotor position, it is deduced that variation in the effective radial airgap dimension is not responsible for the lack of similarity. The only other feature which could give rise to a difference in inductance between the two phases is the actual manner in which the windings are placed in the machine. The type of winding used in these small two phase machines is a two layer winding in which one phase occupies the whole of the bottom layer whilst the other occupies the whole of the top layer. Thus, although this winding is described as a lap winding it is not so in the strict sense. The slot leakage flux associated with the bottom layer winding will undoubtedly be greater than that associated with the top layer winding although their resistances will be the same since the whole phase winding is former wound and, therefore, both phase windings must have the same length. The distribution of their endwindings will, however, be different so causing the overhang leakage fluxes to differ, again the bottom layer winding having the larger value. It is consequently to be expected then that the inductance coefficient of the one phase will be greater than that of the other and it is this that causes the generation of the twice line frequency torque pulsation. Thus, from equations (2.6) and (7.6a), considering only one of the two rotor circuits, the expression for the electromagnetic torque is

$$T = (li_{qs} + hi_{qr1})i_{dr1} - (l'i_{ds} + hi_{dr1})i_{qr1}$$

where l is the mutual inductance between the d stator phase and the rotor and l' is the mutual inductance between the q stator phase and the rotor. Assuming for simplicity that $|i_{ds}| = |i_{qs}|$ and $|i_{dr1}| = |i_{qr1}|$ and that these currents are sinusoidal functions of time, then, under steady state conditions,

$$T = \hat{I}_s\hat{I}_r\left[\left[l \cos \omega t - h \sin(\omega t + \alpha)\right]\cos(\omega t + \alpha) - \left[l' \sin \omega t + h \cos(\omega t + \alpha)\right] - \sin(\omega t + \alpha)\right]$$

$$= \hat{I}_s\hat{I}_r\left[l \cos \omega t \cos(\omega t + \alpha) + l' \sin \omega t \sin(\omega t + \alpha)\right]$$

$$= \hat{I}_s\hat{I}_r\left[l' \cos \alpha + (l - l')\cos \omega t \cos(\omega t + \alpha)\right]$$

assuming $l > l'$

i.e.

$$T = \hat{I}_s\hat{I}_r\left[l' \cos \alpha + (l - l')(\cos^2 \omega t \cos\alpha - \frac{\sin 2\omega t \sin \alpha}{2})\right]$$

Both of these terms in ωt will generate a torque pulsating at twice line frequency superimposed upon the steady component given $\hat{I}_s\hat{I}_r l \cos \alpha$. A similar expression would apply to the other rotor branch.

It is apparent that, for servosystem application, this particular form of two layer winding should not be used because the high torque pulsations generated thereby will have an adverse effect on the system performance.(33) Such torque pulsations would not be present if the true two layer lap winding was used since for this winding the quadrature and direct axis inductances would be the same.

Because of the importance of these fluctuations in torque it was felt that further experimental evidence in support of the explanations given for their presence was necessary. To this end four more spectrograms were taken and are submitted herewith, viz:

- Fig.(8.1). Torque developed with rotor stationary, reference phase only excited, control phase short circuited.
- Fig.(8.2). Torque developed with rotor stationary, both phases excited from balanced voltage supply.
- Fig.(8.3). Torque developed with rotor stationary, both phases excited from unbalanced voltage supply.
- Fig.(8.4). Background noise with test motor unenergized.

The information contained in these spectrograms and those of figs.(4.20) and (4.21) is summarized in table (8.1) with the exception of the 50 Hz. signal apparent in figs.(8.2) and (8.3) which from fig.(8.4) is seen to be due to pick-up.

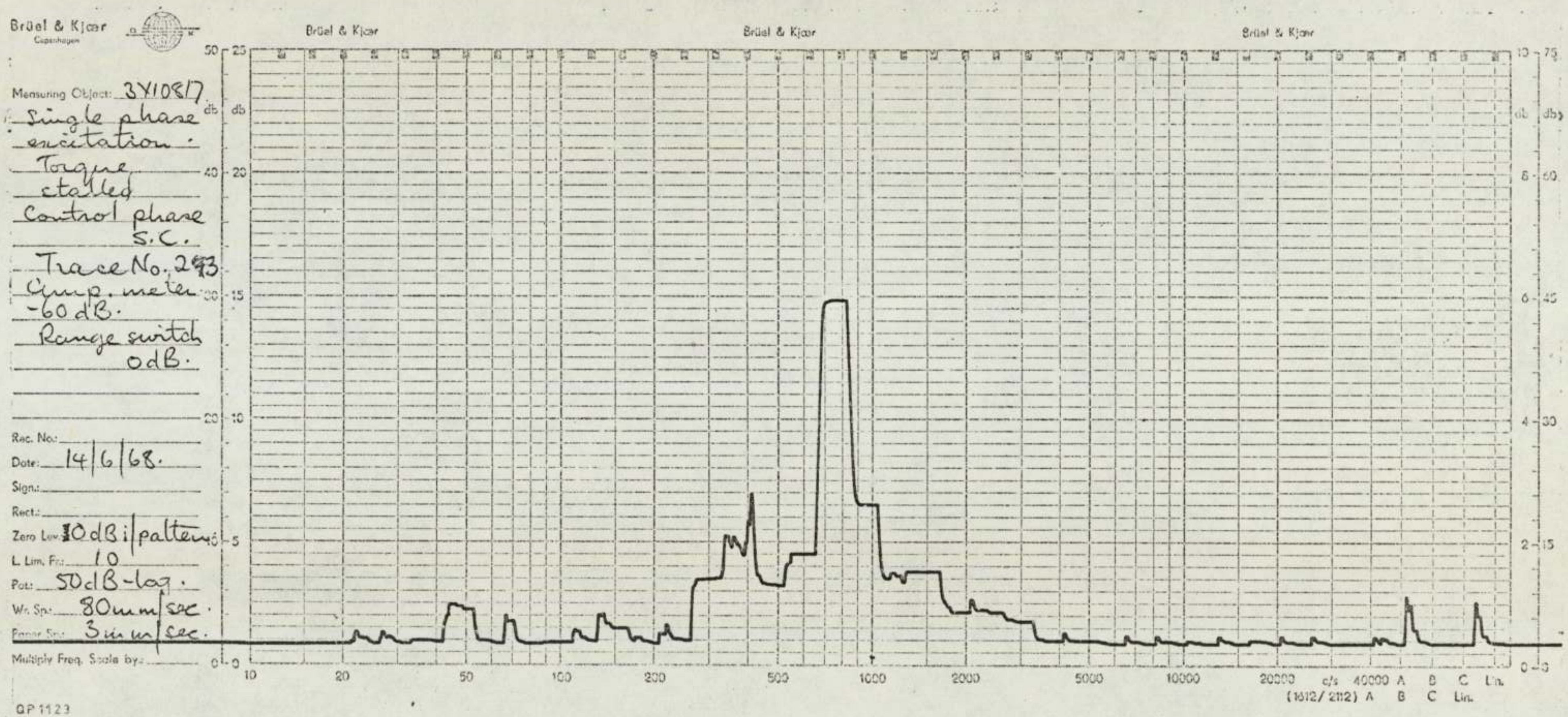

FIG.(8.1). SPECTROGRAM OF NET ACCELEROMETER VOLTAGE, TEST MACHINE STALLED, REFERENCE PHASE ONLY EXCITED.

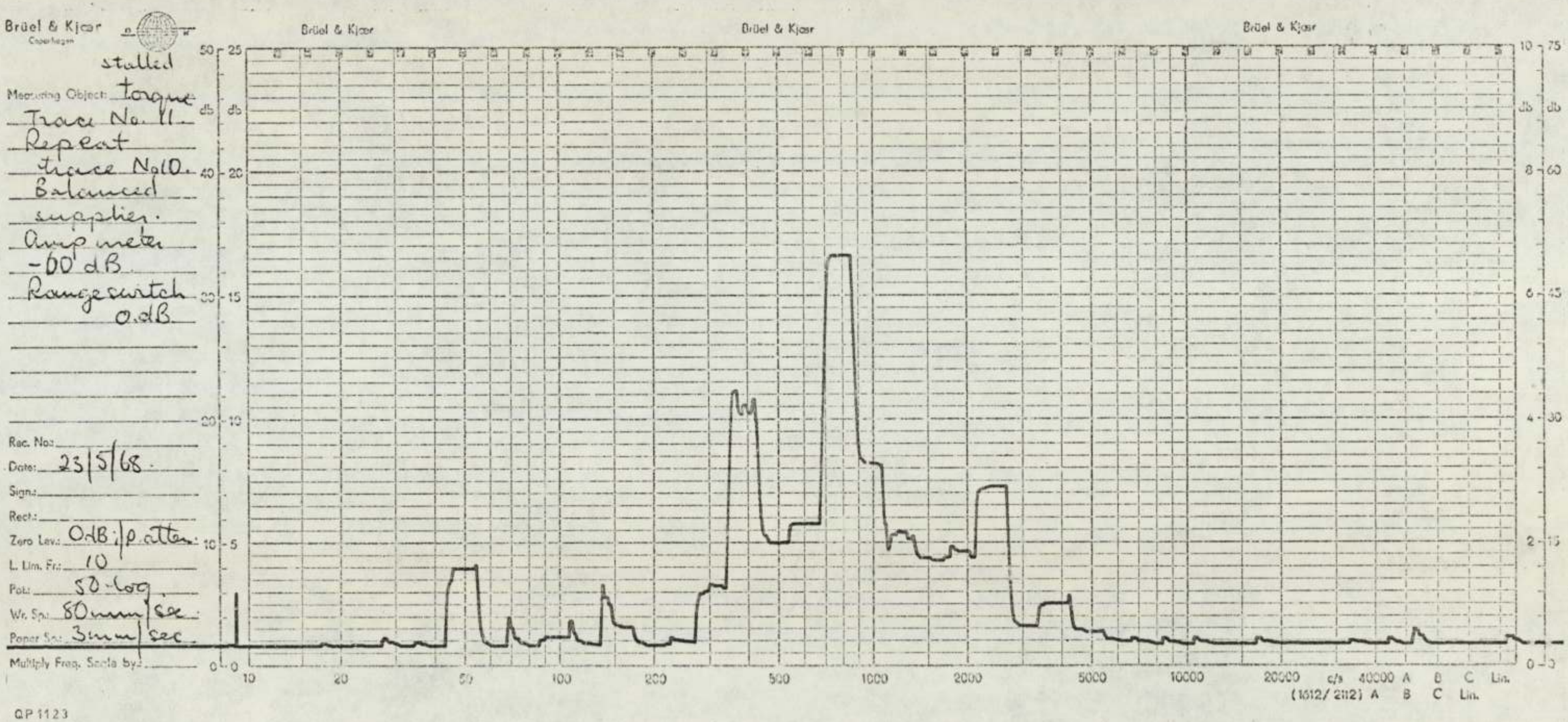

FIG.(8.2). SPECTROGRAM OF NET ACCELEROMETER VOLTAGE, TEST MACHINE STALLED, BALANCED VOLTAGE SUPPLY.

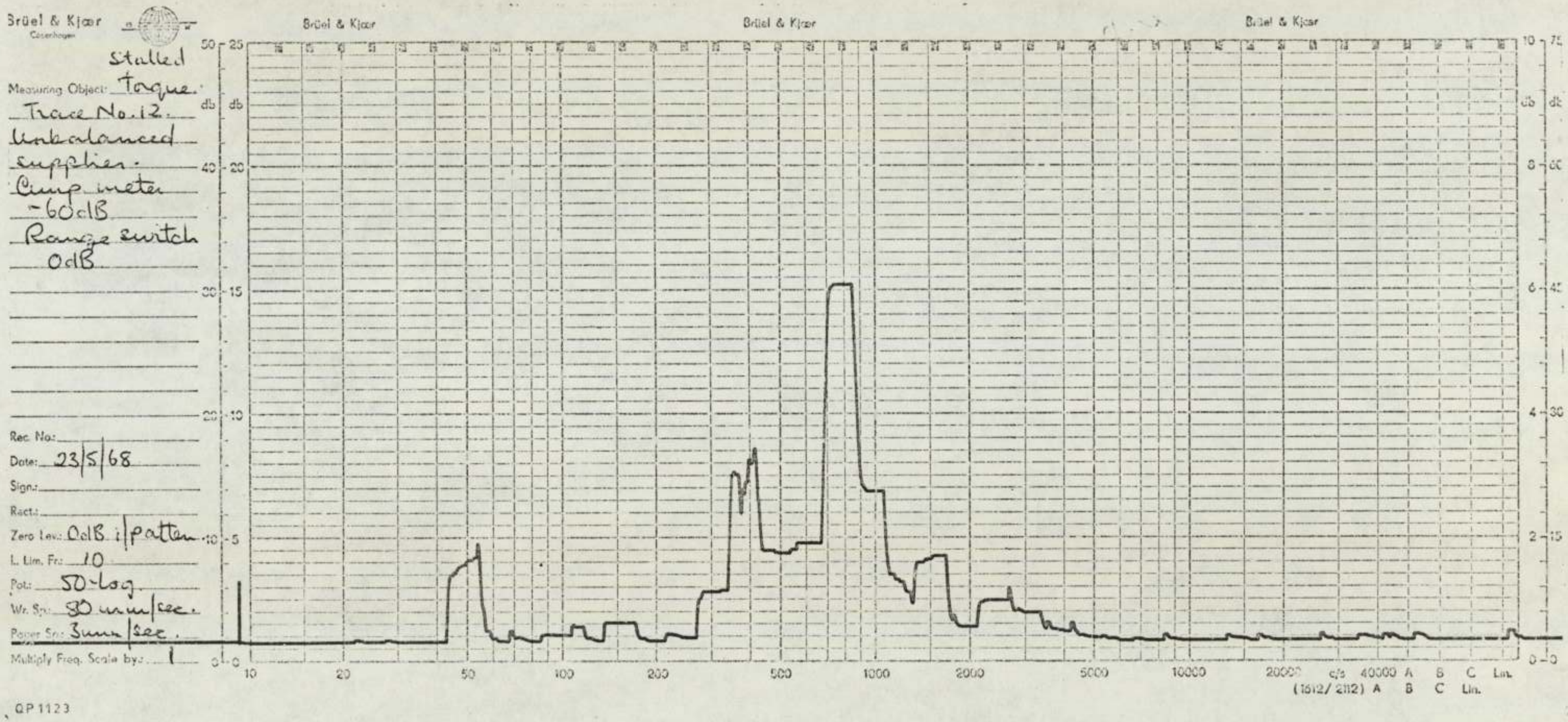

FIG.(8.3). SPECTROGRAM OF NET ACCELEROMETER VOLTAGE, TEST MACHINE STALLED, UNBALANCED VOLTAGE SUPPLY.

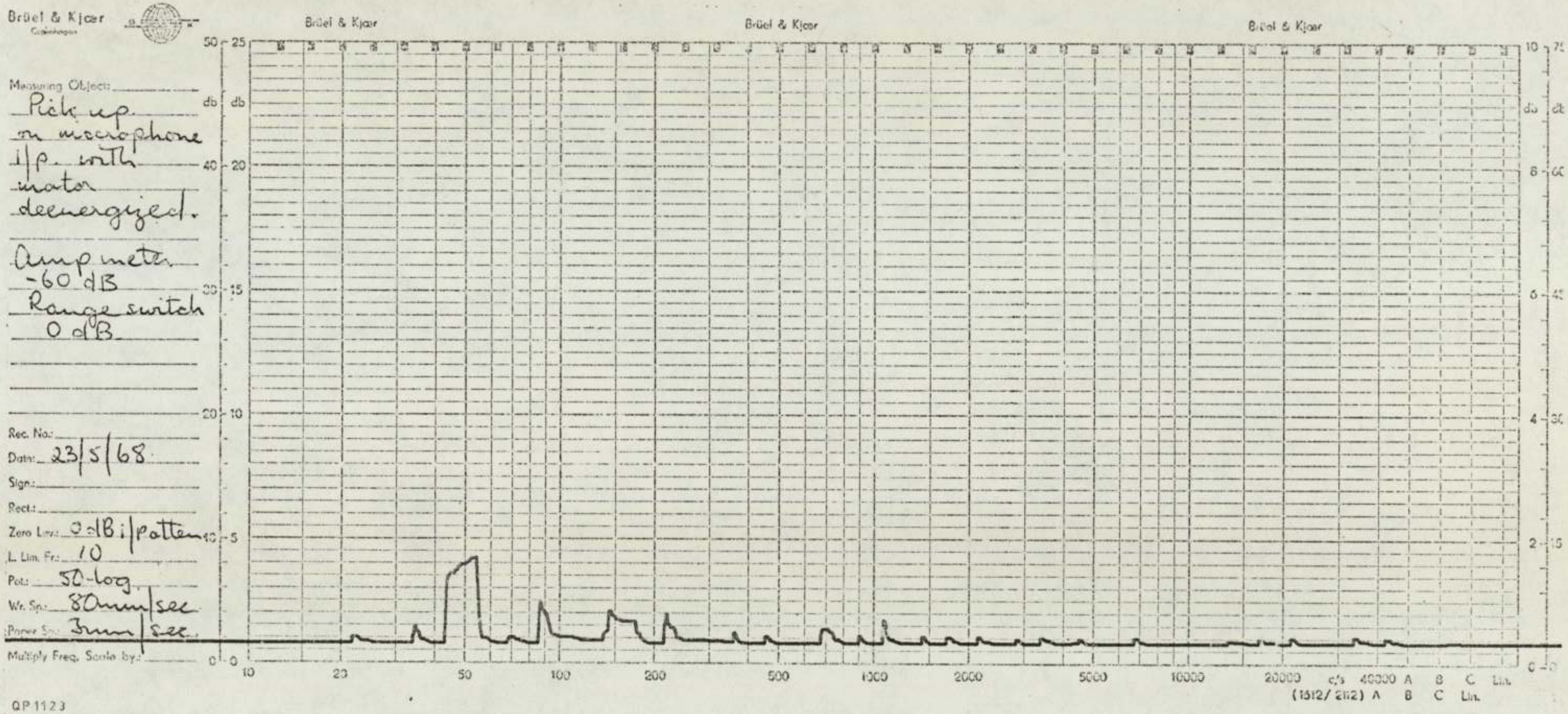

FIG.(8.4). SPECTROGRAM OF NET ACCELEROMETER VOLTAGE DUE TO BACKGROUND NOISE, TEST MACHINE UNENERGIZED.

	Pulsation frequency, Hz.					
	350 .	400 .	700 .	800 .	Random.	
No-load, balanced supply.	-94	-82.8	-90	-69	-65	dB.
No-load, unbalanced supply.	-82.2	-89	-85	-62.5	-65	"
Stalled, balanced supply.	0	-68	0	-77	0	"
Stalled, unbalanced supply.	0	-96	0	-79.5	0	"
single phase.	0	0	0	-79.5	0	"

TABLE (8.1). NET ACCELEROMETER OUTPUT IN dB re 10 volts FOR PROMINENT FREQUENCIES IN OPERATION SPECTROGRAMS.

The principal features of this summary are

a) The presence of a twice line frequency torque pulsation under single phase conditions.

This must be caused by rotor asymmetry. For the particular position of the rotor relative to the stator at which this spectrogram was taken, the rotor asymmetery must haveresulted in a space angle between the magnetic axis of the rotor magneomotive force and the magnetic axis of the stator flux. Thus, a torque given by the expression $k\,\hat{\varnothing}_s\hat{M}_r \sin \omega t \sin(\omega t + \alpha) \sin \theta$ where k is a constant, $\varnothing_s$ is the stator flux, M_r is the rotor magnetomotive force and θ is the space angle, would be generated. This expression can be written in the form

$$\frac{k\,\hat{\varnothing}_s\hat{M}_r \sin\theta}{2}\left[\cos \alpha - \cos(2\omega t + \alpha)\right]$$

which indicates the presence of the twice line frequency component and supports the statement of rotor asymmetery.

b) The absence of the 350 and 700 Hz. pulsations under stalled conditions for both balanced and unbalanced voltages.

This proves that these must be caused by rotor movement and implies stator ovality, unequal rotor bar resistances and lack of concentricity of the rotor with the stator bore.

c) The presence of a line frequency pulsation under stalled and no-load conditions for both balanced and unbalanced voltages.

This particular pulsation,it is thought,is further evidence of the rotor not being concentric with the stator bore for such eccentricity would cause the stator leakage flux pattern to vary as the stator field rotates and this variation would occur only once per revolution of this field,i.e. for the two pole machine,once per cycle.

d) The presence of a twice line frequency pulsation under stalled and no-load conditions for both balanced and unbalanced voltages.

This feature has already been recognized and explained in the no-load operation. Its appearance in the stalled characteristic and its magnitude therein relative to its magnitude in the no-load case, are both in keeping with the explanation already offered.

e) The presence of a relatively high level of random torque fluctuations under running conditions.

The speed of the motor at which these measurements were taken was of the order of 21000 r.p.m.. At this speed the bearings would give rise to noise of this nature. This is a feature which should not be overlooked;in the dynamometer used in this work it will cause extraneous power flow from the driving motor and,when the servomotor is in use in a system,have a bad effect on the system performance.

These observations as a whole emphasize the importance of and the need to control the generation of torque pulsations in the induction servomotor. They further make it clear that such control is possible if due attention is accorded in the manufacturing processes.

Finally,referring again to figs.(7.20) and (7.20a),close examination of these reveals a distinct relationship between the ocurrence of the first peak of torque and the voltage initiation point. This relationship is apparent in both calculated and measured performances. This gives confidence in the dependability of the dynamometer as an instrument for the measurement of dynamic torque which, it will be recalled, was one of the principal requirements in its design specification

The prime object in making these dynamic measurements was to prove the efficacy of the mathematical model obtained from the impedance per unit frequency locus. Bearing in mind what has emerged from the foregoing discussion, it is claimed that the predicted and measured dynamic performances display a satisfactory correlation and that the mathematical model can, therefore, now be accepted as practically proven for the entire range of servosystem use.

CHAPTER IX.

Epilogue.

28) Conclusion.

With the practical proof of the mathematical model and its use now established, the proposed design procedure given in section (3) may be taken as verified since, in the comparison made in section (22) of the impedance tensor obtained using the design calculations with that determined experimentally, the values of the corresponding elements were, with the exception of the rotor resistance, found to be in very close agreement, due regard being given to the effective as opposed to simply the mechanical airgap dimension.

It may seem odd to have approached the verification of the design process indirectly through the use, in the prediction of performance, of the experimental model instead of the one calculated from the design data. The original intention was to employ the latter directly but the discovery that the rotor had to be represented by a multiple circuit, in place of the more usual single circuit, the estimatiom of the parameters of which would constitute a separate investigation, necessitated the indirect approach.

Accepting that the methods of design calculation used in estimating the parameters of the test machine which, as explained in the introduction, was deliberately chosen as a two pole machine to be free from space harmonics, have been substantiated then, since the manner in which these methods were derived was also applied to the derivation of the design methods for estimating the parameters representing the space harmonics in the test machine, these latter methods may too be accepted as substantiated, in part at least. Similar comments apply to the mathematical analysis of performance, the formulation of the machine model and the interpretation of the impedance per unit frequency locus diagram.

Furhtermore, the successful correlation of the measured and predicted characteristics confirms both the design of the equipment used and the validity of the measuring techniques applied in this work. It is believed, therefore, that this equipment and these techniques should be taken as basic to the practical study of miniature machines.

Thus, this investigation has fulfilled the objectives detailed in the introduction (page 7) and thereby contributes to the knowledge of miniature electrical machines in the presentations itemized on page 8.

29) Future Work.

Covering as it does the analysis, design, measurement of performance and manufacture of the machine under investigation, this study brings forth several fields in which further immediate work needs to be done following upon that hereby completed. It is simplest to deal with these under the headings used above, thus

a) Analysis.

Verification, for a test machine with known space harmonics, of the extension of the analysis and the subsequent mathematical model proposed in this thesis.

b) Design.

Verification, for a machine with known space harmonics, of the rotor harmonic resistance and leakage inductance ratios introduced in this thesis.

Detailed investigation into the true nature of the additional rotor circuit discovered in this study and into the mathematical expression of its parameters.

c) Measurement of performance.

Confirmation of the effects of space harmonics on the shape and interpretation of the impedance per unit frequency locus diagram.

Because of the importance of the information at the low frequency extremity of this locus diagram, exploration of methods of obtaining improved accuray of measurement to assist in the extrapolation of the resistance per unit frequency and reactance per unit frequency versus frequency characteristics.

d) Manufacture.

Close study of the effects of machining and general manufacturing stresses on the true magnetic dimensions of miniature machines having nickel-iron alloy cores.

Comparison of performance and cost of production of machines having spark machined bores with those having ground and lapped/honed bores.

Determination of the relationship between the methods of manufacture and the electrical and magnetic nature of the squirrel cage rotor.

Determination of the influence of manufacturing processes on the generation of torque pulsations.

Comparison of squirrel cage motor performance with that of motors constructed with solid rotors made from alloys having different combinations of permeability and conductivity.

Obviously, this programme of work will require close collaboration with industry. Very carefully controlled processes of manufacture must be used if the investigations are to be effective. The proposed studies should, where test motors are necessary, employ machines having spark machined bores and constructed under precise conditions.

If these studies are made, it is confidently expected that improved manufacturing techniques and machines having consistently predictable and improved performances for servosystem application will be the outcome.

Apart from this, the experimental procedures developed in this present study should be applied to other miniature machines intended for servosystem use so that similar mathematical models may be established for them also. It is the considered opinion of the author that such models should be made available by the manufacturers in addition to, or in place of, the usual steady state information offered to the prospective user. It is only in this way that the correct machine for a particular system application can be properly selected.

APPENDIX A

Relationship between frequency distribution and geometry for the impedance per unit frequency locus.

(See chapter V, section 15)

In fig. (5.5), p. 188

$$\frac{P''S''}{O'S''} = \frac{L_t - L_1 - \dfrac{L_oL_2}{L_o + L_2}}{\dfrac{R_t - R_1}{\omega}}$$

From the equivalent circuit of fig. (5.1), p. 186

$$L_t - L_1 = \text{Imaginary}\left[\frac{1}{\dfrac{1}{jL_o} + \dfrac{1}{\dfrac{R_2}{\omega} + jL_2}}\right]$$

$$= \text{Imaginary}\left[\frac{\left(\dfrac{R_2}{\omega} - j(L_o + L_2)\right)\left(jL_o\dfrac{R_2}{\omega} - L_oL_2\right)}{\left(\dfrac{R_2}{\omega}\right)^2 + (L_o + L_2)^2}\right]$$

$$= \frac{L_o\left(\dfrac{R_2}{\omega}\right)^2 + L_oL_2(L_o + L_2)}{\left(\dfrac{R_2}{\omega}\right)^2 + (L_o + L_2)^2}$$

Hence, the numerator of the expression for $\frac{P''S''}{O'S''}$ can be written,

$$\frac{L_o\left(\dfrac{R_2}{\omega}\right)^2 + L_oL_2(L_o + L_2)}{\left(\dfrac{R_2}{\omega}\right)^2 + (L_o + L_2)^2} - \frac{L_oL_2}{L_o + L_2}$$

Substituting $\frac{R_2}{\omega_q}$ for $(L_o + L_2)$, from equation (5.4), in this expression gives,

$$\frac{L_o\left(\dfrac{R_2}{\omega}\right)^2 + L_oL_2\dfrac{R_2}{\omega_q}}{\left(\dfrac{R_2}{\omega}\right)^2 + \left(\dfrac{R_2}{\omega_q}\right)^2} - \frac{L_oL_2}{R_2/\omega_q}$$

i.e.

$$\frac{L_o + \dfrac{L_oL_2\omega}{R_2\omega_q}}{1 + \left(\dfrac{\omega}{\omega_q}\right)^2} - \frac{L_oL_2}{R_2/\omega_q}$$

i.e. $$\frac{\dfrac{R_2 L_0}{\omega_q} + L_0 L_2\left(\dfrac{\omega}{\omega_q}\right)^2 - L_0 L_2\left(1 + \left(\dfrac{\omega}{\omega_q}\right)^2\right)}{\dfrac{R_2}{\omega_q}\left(1 + \left(\dfrac{\omega}{\omega_q}\right)^2\right)}$$

i.e. $$\frac{\dfrac{R_2 L_0}{\omega_q} - L_0 L_2}{\dfrac{R_2}{\omega_q}\left(1 + \left(\dfrac{\omega}{\omega_q}\right)^2\right)}$$

Substituting for L_2 from equation (5.4),p.190 this reduces to

$$\frac{L_0^2 \omega_q}{R_2\left(1 + \left(\dfrac{\omega}{\omega_q}\right)^2\right)}$$

Equation (5.3),p.190 gives the denominator $\frac{R_t - R_1}{\omega}$ of the expression $\frac{P''S''}{O'S''}$

as $$\frac{L_0^2 \dfrac{R_2}{\omega}}{\left(\dfrac{R_2}{\omega}\right)^2 + (L_0 + L_2)^2}$$

which,by substituting $\frac{R_2}{\omega_q}$ for $(L_0 + L_2)$ as above becomes,

$$\frac{L_0^2 \dfrac{R_2}{\omega}}{\left(\dfrac{R_2}{\omega}\right)^2 + \left(\dfrac{R_2}{\omega_q}\right)^2}$$

i.e. $$\frac{L_0^2 \omega}{R_2\left(1 + \left(\dfrac{\omega}{\omega_q}\right)^2\right)}$$

Hence,using these expressions for the numerator and the denominator

$$\frac{P''S''}{O'S''} = \frac{L_0^2 \omega_q}{R_2\left(1 + \left(\dfrac{\omega}{\omega_q}\right)^2\right)} \times \frac{R_2\left(1 + \left(\dfrac{\omega}{\omega_q}\right)^2\right)}{L_0^2 \omega}$$

i.e. $$\frac{P''S''}{O'S''} = \frac{\omega_q}{\omega}$$

APPENDIX B

Equivalent circuit, at standstill, for machine with space harmonics.

(see chapter II, section 3)

Consider the general form of the equivalent circuit, at standstill, in terms of the transformed parameters:

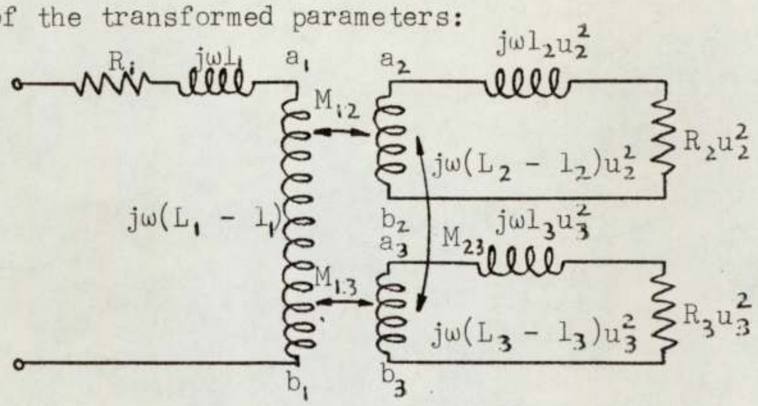

FIG.(B1). GENERAL FORM OF EQUIVALENT CIRCUIT.

In this circuit diagram,

$$j\omega(L_2 - l_2)u_2^2 = j\omega(L_1 - l_1)$$

$$j\omega(L_3 - l_3)u_3^2 = j\omega(L_1 - l_1)$$

whence,

$$M_{12} = (L_1 - l_1)$$

$$M_{13} = (L_1 - l_1)$$

$$M_{23} = (L_1 - l_1)$$

$$M_{32} = (L_1 - l_1)$$

Instantaneously,

$$\begin{aligned} v_{a_1 b_1} &= M_{12} p i_2 + M_{13} p i_3 + (L_1 - l_1) p i_1 \\ &= (L_1 - l_1)(p i_1 + p i_2 + p i_3) \\ v_{a_2 b_2} &= M_{12} p i_1 + M_{23} p i_3 + (L_2 - l_2) u_2^2 p i_2 \\ &= (L_1 - l_1)(p i_1 + p i_2 + p i_3) \\ v_{a_3 b_3} &= M_{13} p i_1 + M_{32} p i_2 + (L_3 - l_3) u_3^2 p i_3 \\ &= (L_1 - l_1)(p i_1 + p i_2 + p i_3) \end{aligned}$$

i.e. $v_{a_1 b_1} = v_{a_2 b_2} = v_{a_3 b_3}$.

Consequently, the above circuit can be redrawn as below in fig.(B2), for which the instantaneous voltage equations are identical to those for the circuit of fig.(B1).

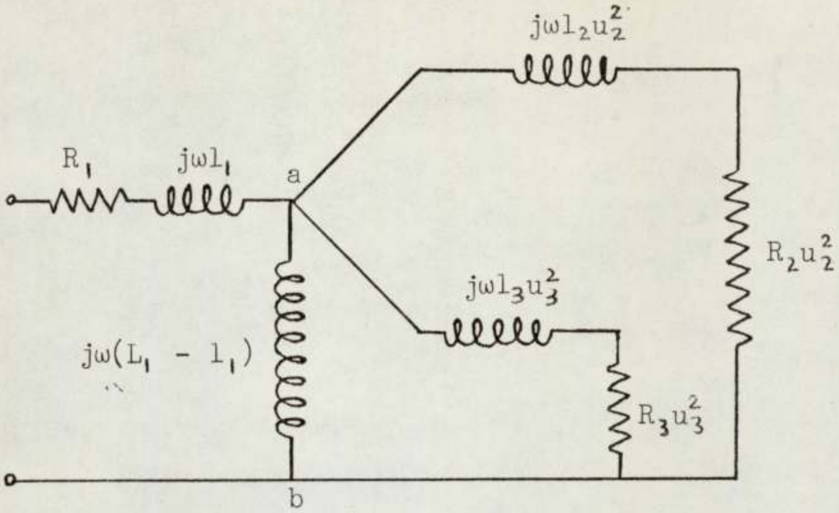

FIG.(B2). SIMPLIFIED FORM OF EQUIVALENT CIRCUIT FOR MACHINE WITH SPACE HARMONICS.

General Symbols Used (unless otherwise stated in text).

θ_i	servosystem input signal.
θ_o	servosystem output signal.
k	servomotor generated torque coefficient.
F	servomotor damping coefficient.
J	moment of inertia of rotor system.
R_1	stator resistance per phase in referred equivalent circuit.
R_2	rotor resistance per phase in referred equivalent circuit.
X_1	stator leakage reactance per phase in referred equivalent circuit.
X_2	rotor leakage reactance per phase in referred equivalent circuit.
X_o	magnetizing reactance per phase in referred equivalent circuit.
R_o	magnetizing resistance per phase in referred equivalent circuit.
$R_{2,n}$	harmonic rotor resistance per phase in referred equivalent circuit.
$L_{1,n}$	harmonic rotor inductance per phase in referred equivalent circuit.
L_o	magnetizing inductance per phase in referred equivalent circuit.
L_1	stator total self inductance per phase in referred equivalent circuit.
L_2	rotor total self inductance per phase in referred equivalent circuit.
l_1	stator leakage inductance per phase in referred equivalent circuit.
l_2	rotor leakage inductance per phase in referred equivalent circuit.
s	rotor per unit slip.
V_R	reference phase applied voltage.
V_C	control phase applied voltage.
ω_s	synchronous speed, radians/sec..
ω_r	rotor instantaneous speed, radians/sec..
ω_{rs}	rotor steady state speed, radians/sec..
T_f	developed torque, forward sequence.
T_b	developed torque, backward sequence.
T_n	developed torque, net value.
T	time constant.
ψ_m	tensor flux conductors.
ϕ_m	tensor flux linkages.
ω	angular frequency of supply.

e_m tensor voltage.

i^n tensor current.

θ rotor angle of rotation,radians.

T_a applied shaft torque.

T_l load torque.

R_{mn} resistance tensor.

L_{mn} metric tensor.

G_{mn} torque tensor.

p differential time operator.

p_n no.pole pairs.

n order of space harmonic.

d_s direct axis stator coil.

q_s quadrature axis stator coil.

d_r direct axis rotor coil,non-holonomic axes.

q_r quadrature axis rotor coil,non-holonomic axes.

r_1 direct axis rotor coil,holonomic axes.

r_2 quadrature axis rotor coil,holonomic axes.

$r_{n,1}$ direct axis harmonic rotor coil,holonomic axes.

$r_{n,2}$ quadrature axis harmonic rotor coil,holonomic axes.

$d_{r,n}$ direct axis harmonic rotor coil,non-holonomic axes.

$q_{r,n}$ quadrature axis harmonic rotor coil,non-holonomic axes.

u rotor/stator transformation ratio.

M mutual inductance between stator and rotor.

L_s stator total self inductance per phase.

L_r rotor total self inductance per phase.

l_s stator leakage inductance perphase.

l_r rotor leakage inductance per phase.

R_s stator resistance per phase.

R_r rotor resistance per phase.

n_1 no.stator slots.

n_2 no.rotor slots.

f supply frequency,Hz..

N_s	synchronous speed, r.p.m..
δ	mechanical radial airgap, mm..
δ_e	effective radial airgap, mm..
q_1	stator slots/pole/phase.
q_2	rotor slots/pole.
c_1	stator conductors/slot.
m	no. stator phases.
α	skew angle (mechanical).
K_p	pitch factor.
K_d	distribution factor.
K_w	winding factor.
k_n	harmonic Fourier coefficient.
$\hat{J}$	peak current density.
ρ	resistivity.
A_r	endring cross-sectional area.
s_w	average slot width.
s_p	average slot pitch.
D_r	effective diameter of endring.
D_b	mean diameter at which bars enter endring.
ID_r	inside diameter of endring.
l_o	active iron axial length.
g_c	airgap extension factor.
g_1	stator gap coefficient.
g_2	rotor gap coefficient.
p_1'	stator slot pitch at bore surface.
p_2'	rotor slot pitch at bore surface.
s_1'	stator slot opening .
s_2'	rotor slot opening.
σ_1	Carter gap coefficient for stator.
σ_2	Carter gap coefficient for rotor.
Λ_g	airgap permeance factor.
Λ_{s1}	stator slot permeance factor.

Λ_{s2} rotor slot permeance factor.

Λ_{h1} stator overhang permeance factor.

Λ_{h2} rotor overhang permeance factor.

t_1' stator tooth top width.

t_2' rotor tooth top width.

μ_o permeability free space.

I_o magnetizing current per phase.

I_1 stator current per phase.

I_2 rotor current per phase referred to stator.

I_R reference phase current.

I_C control phase current.

W_R reference phase power.

W_C control phase power.

BIBLIOGRAPHY.

1) Lauer, Lesnick, Matson.

Servomechanisms Fundamentals. McGraw Hill, 1947.

2) Koopman. R. J. W.

Operating Characteristics of Two Phase Servomotors. A.I.E.E. Trans. Vol.68, 1949.

3) Ward. J.

Motor Elements For Alternating Current Servomechanisms. Electrical Industries Export, July, 1960.

4) Ward. J.

Synchros, Principles and Development. Electrical Industries Export, December, 1961.

5) Steinhacker. M.A., Meserve. W.E.

Two Phase A.C. Servomotor Operation For Varying Phase Angle of Control Winding Applied Voltage. A.I.E.E. Trans. Vol.70, 1951.

6) Hopkin. A.M.

Transient Response of Small Two Phase Induction Motors. A.I.E.E. Trans. Vol.70, 1951.

7) Stanley. H.C.

An Analysis of The Induction Machine. A.I.E.E. Trans. Vol.57, 1938.

8) Brown. L.O.

Transfer Function For a Two Phase Induction Servomotor. A.I.E.E. Trans. Vol.70, 1951.

9) Sobczyk. A.

Stabilization of Carrier Frequency Servomechanisms. Mekhanika. Vols. II & III, 1950.

10) Sadovskii. I.M.

Asynchronous Motors as Control Circuit Elements. Automation and Control, U.S.S.R., No.6. Vol.13, 1952.

11) Titov. V.K.

Transfer Function of Two Phase Asynchronous Motors. Collection of Moscow Technical School, Oborongiz, 1955

12) Mikhail. S.L., Fett. G.H.

Transfer Function of Two Phase Servomotors. A.I.E.E. Trans. Vol.77, 1958.

13) Kutvinov. V.G.

On The Transfer Function of an Asynchronous Two Phase Motor. Automatiom and Control, Vol.20, July, 1959.

14) Shubenko. V.A.

Influences of Transient Processes on Dynamics and Reliability of Induction Motors Operating With Frequent Switching. Report from Urals Polytechnical Inst., Sverdlovsk, U.S.S.R.

15) Vlasov.N.P.

A Method of Obtaining Transfer Functions of Automatic Control Systems Operating on Alternating Current. Automation and Control, Vol.21,No.6,June,1960.

16) Vlasov.N.P.

A Servomechanism With a Two Phase Asynchronous Motor Whose Control Winding is Powered by a Current Generator. Automation and Control, Vol.22,No.5,May,1961.

17) Vlasov.N.P.

The Transfer of a Servosystem With a Two Phase Asynchronous Motor. Automation and Control,Vol.23,No.4,April,1962.

18) Law.J.,Schmitz.N.L.

Transient Response Characteristics of an A.C. Servomotor Excited Non-sinusoidally and Through Non-linear Source Impedances. Trans.A.I.E.E. 1964 & Ph.D. Thesis Univ.Wisconsin,1962.

19) Wilson.D.R.

Method of Obtaining The Transfer Function of a Two Phase Servomotor. Trans.I.E.E.E. Vol.PAS 87,No.1,Jan.1968.

20) Gibbs.W.J.

Tensors in Electrical Machine Theory. Chapman & Hall,1952.

21) Kron.G.

Application of Tensors to The Analysis of Rotating Electrical Machinery. G.E.Review,1942.

22) Kron.G.

Non-Riemannian Dynamics of Rotating Electrical Machinery. Journal of Maths. and Physics,Vol.13,No.2,1934.

23) Kron.G.

Equivalent Circuits of Electrical Machinery. Wiley & Sons,1951.

24) Jakeman.R.G.

Rotating Fields in Polyphase Machines. G.E.C.Journal,Feb.1944.

25) Parker Smith.S.,Barling.W.H.

Calaulation of The Magnetizing Current of Three Phase Motors. Electrician,Oct.1914.

26) Trickey.P.H.

Induction Motor Resistance Ring Width. Electrical Eng.,Feb.1936.

27) Binns.K.J.

Calculation of Some Basic Flux Quantities in Induction and Other Doubly Slotted Electrical Machines. Proc.I.E.E.Vol.III,No.11,1964.

28) Carter.F.W.

The Magnetic Field of The Dynamo-electric Machine. J.I.E.E.Vol.64, 1926.

29) Vitkovitch.

Field Analysis.

30) Wittrick.W.H.

Theory of Symmetrical Crossed Flexure Pivots. Australian Journal Scientific Research, Vol.1, 1948, A.

31) Lawrenson.P.J. et al.

Transient Performances of Reluctance Machines. Proc.I.E.E. Vol.118, No.6, 1971.

32) Binns.K.J., Hindmarsh.R., Short.B.P.

Effect of Skewing Slots on Flux Distribution in Induction Machines. Proc.I.E.E. Vol.118, No.3/4, 1971.

33) Ejiri.M.

Torque Variation and Rotor Vibration in The Two Phase Servomotor. Report of Central Research Lab., Hitachi Ltd., Japan.

34) Stein.W.A., Thaler.G.J.

Evaluating The Effect of Non-linearity in a Two Phase Servomotor. Trans.A.I.E.E. Vol.73, pt.II, 1955.

35) International Electrotechnical Commission.

Report on The Measurement of Temperature Rise by The Method of Superposition. Technical Committee No.2, Sept.1966.

36) Alger P.L.

Nature of Polyphase Induction Machines. Wiley and Sons, 1951.


3 HOLES EQUALLY SPACED No. 56 DRILL.
SECTION ON AA.
THIS DIAMETER TO BE MACHINED SIZE FOR SIZE WITH BALL RACE BORE DIAMETER.
ITEM 4/3. DRIVING HEAD ROTOR. ONE OFF MILD STEEL. (2x FULL SIZE)
3 HOLES EQUALLY SPACED DRILL & TAP 10 BA.
THIS BORE TO BE MACHINED SIZE FOR SIZE WITH O.D. ROTOR ITEM 3/4
ITEM 5/3. DRIVING HEAD PULLEY. ONE OFF MILD STEEL. (2x FULL SIZE)
ITEM 0/1. DRIVING HEAD GENERAL ARRANGEMENT. (2x FULL SIZE)
ITEM 6/3. GRUB SCREWS FOR ITEM 3/5. THREE OFF MILD STEEL. (4x FULL SIZE)
DRILL 1/8" WHIT. CLEARANCE.
4 HOLES EQUALLY SPACED 1 1/8" P.C.D. No. 51 DRILL.
OIL HOLE 1/16" DIA.
4 HOLES DRILL & TAP 10 BA. 1 1/8" P.C.D.
ITEM 2/3. DRIVING HEAD END PLATES. TWO OFF ALUMINIUM-MANGANESE ALLOY. (2x FULL SIZE)
NOTES:-
ITEM 7/3. FIXING SCREWS FOR ITEM 3/2. 3/16" x 10 BA. CHEESE HEAD. EIGHT OFF. MILD STEEL.
ITEM 3/3. DRIVING HEAD BEARING. ONE OFF HOFFMANN S3 CODE. Hoedi GRADE 0. HIGH SPEED CAGE, OIL LUBRICATED.
ITEM 1/3. DRIVING HEAD BRACKET. ONE OFF ALUMINIUM-MANGANESE ALLOY. (2x FULL SIZE)
LATERAL MOVEMENT OF SUPPORT ABOUT CROSS-SLIDE DATUM ± 3/8"
DATUM
ITEM 14/1. DRIVING MOTOR SUPPORT. GENERAL ARRANGEMENT. (FULL SIZE)
3 HOLES EQUALLY SPACED DRILL 6 BA. CLEARANCE 2 1/8" P.C.D.
3 HOLES DRILL 6 BA. CLEARANCE & COUNTERSINK.
ITEM 8/3. DRIVING MOTOR SUPPORT END PLATES. TWO OFF ALUMINIUM-MANGANESE ALLOY. (FULL SIZE)
6 HOLES DRILL & TAP 6 BA. x 3/8" DEEP.
1/8" WHIT. CLEARANCE.
ITEM 9/3. DRIVING MOTOR SUPPORT SOLE PLATE. ONE OFF ALUMINIUM-MANGANESE ALLOY. (FULL SIZE)
ITEM 10/3. DRIVING MOTOR SUPPORT CROSS-SLIDE. ONE OFF MILD STEEL. (FULL SIZE)
DRILL 1/8" WHIT. CLEARANCE.
NOTE:- ITEM 11/3. FIXING SCREWS. 6 OFF 6 B.A. x 1/4" COUNTERSUNK HEADS. MILD STEEL.
DRG. No. 3.
COMPONENT DETAILS.
PRECISION TORQUE DYNAMOMETER.
COLLEGE OF ADVANCED TECHNOLOGY, BIRMINGHAM
DEPT. OF ELEC. ENG.
2/12/1963.